



VCU

Virginia Commonwealth University
VCU Scholars Compass

Theses and Dissertations


Graduate School

2016

USING SEMIPHYSIOLOGICALLY-BASED PHARMACOKINETIC (SEMI-PBPK) MODELING TO EXPLORE THE IMPACT OF DIFFERENCES BETWEEN THE INTRAVENOUS (IV) AND ORAL (PO) ROUTE OF ADMINISTRATION ON THE MAGNITUDE AND TIME COURSE OF CYP3A-MEDIATED METABOLIC DRUG-DRUG INTERACTIONS (DDI) USING MIDAZOLAM (MDZ) AS PROTOTYPICAL SUBSTRATE AND FLUCONAZOLE (FLZ) AND ERYTHROMYCIN (ERY) AS PROTOTYPICAL INHIBITORS

Mengyao Li
VCU

Follow this and additional works at: <https://scholarscompass.vcu.edu/etd>

 Part of the [Other Pharmacy and Pharmaceutical Sciences Commons](#), and the [Pharmaceutics and Drug Design Commons](#)

© The Author

Downloaded from

<https://scholarscompass.vcu.edu/etd/4402>

This Dissertation is brought to you for free and open access by the Graduate School at VCU Scholars Compass. It has been accepted for inclusion in Theses and Dissertations by an authorized administrator of VCU Scholars Compass. For more information, please contact libcompass@vcu.edu.

©Mengyao Li 2016
All Rights Reserved

USING SEMIPHYSIOLOGICALLY-BASED PHARMACOKINETIC (SEMI-PBPK)
MODELING TO EXPLORE THE IMPACT OF DIFFERENCES BETWEEN THE
INTRAVENOUS (IV) AND ORAL (PO) ROUTE OF ADMINISTRATION ON THE
MAGNITUDE AND TIME COURSE OF CYP3A-MEDIATED METABOLIC DRUG-DRUG
INTERACTIONS (DDI) USING MIDAZOLAM (MDZ) AS PROTOTYPICAL SUBSTRATE
AND FLUCONAZOLE (FLZ) AND ERYTHROMYCIN (ERY)
AS PROTOTYPICAL INHIBITORS

A dissertation submitted in partial fulfillment of the requirements for the degree of Doctor of
philosophy at Virginia Commonwealth University.

By

Mengyao Li, M.S.
Peking University Health Science Center, China, 2012

Director: Jürgen Venitz, M.D., Ph.D.
Professor, Department of Pharmaceutics
School of Pharmacy

Virginia Commonwealth University
Richmond, Virginia
July 2016

ACKNOWLEDGEMENTS

First and foremost, I would like to express my sincere gratitude to my advisor Dr. Jürgen Venitz, for giving me the opportunity to pursue Ph.D. under his guidance. His enthusiasm in teaching and science, breadth of knowledge and continuous support and patience have helped me acquire more skills and confidence in my research, and even life. I sincerely appreciate his time and efforts in training me, and allowing me to pursue two internships during my Ph.D. studies.

I would also like to thank my advisory committee members, Dr. Peter Byron, Dr. Patricia W. Slattum, Dr. Douglas Boudinot and Dr. Joseph Grillo, for their constructive inputs on my dissertation project.

A special thank to Dr. Ping Zhao for answering my questions about PBPK and giving me hands on training of Simcyp[®]. Dr. David Z. D'Argenio for answering my questions about ADAPT. Dr. Phillip Gerk for answering my questions about enzyme kinetics. Dr. Susanna Wu-Pong for her mentoring during Broadening Experiences for Scientific Training (BEST) program. All faculties in School of Pharmacy for their help in my coursework. Keyetta, Laura and Shakim for their kindly help with anything I needed.

I would like to thank VCU alumni and my old lab-mates, Apoorva and Gopichand, who played significant roles in guiding me professionally and their valuable suggestions during my tenure as a graduate student and beyond. Vijay, Angela, Satjit, and Lokesh, for their constructive inputs on my future career development.

A special thank to my current lab mate, Bishoy, who is a closest friend and helped me a lot in my research and life. My good friends, Xiangyin, Hebing, Emmanuel, Xiaomeng, Xiaolei, Meng, Liang, Yao, Chengyue, Zhonghui, Clara, who provided me consistent support and helped me relaxed throughout this process. Thanks to Omar, Anuja, Neha and all other friends and colleagues, each one of whom have made my experience at VCU memorable.

Last but not the least, thanks to my dear family members, who have been very supportive and eager for me to finish up, and my boy friend, Chenyue, who always cheers me up and encourages me to overcome all the problems emerged in my life.

TABLE OF CONTENTS

LIST OF TABLES	viii
LIST OF FIGURES	xi
LIST OF ABBREVIATIONS	xviii
ABSTRACT	xxvii
1 INTRODUCTION	1
1.1 Clinical significance of drug-drug interaction (DDI)	1
1.2 Strategies to assess metabolic DDI	3
1.3 Use of Physiologically-based pharmacokinetic (PBPK) modeling in quantitative assessment of DDI	7
1.4 Mechanism of metabolic inhibition	9
1.5 Known/suspected differences in DDI between IV and PO routes of administration and clinical significance of exploring routes of administration impact on DDI	14
1.6 Selection of prototypical drug metabolism enzyme (DME): CYP3A	17
1.7 Selection of prototypical CYP3A substrate: MDZ	18
1.7.1 Metabolites of MDZ	21
1.8 Selection of prototypical CYP3AI: Fluconazole (FLZ) and Erythromycin (ERY)	22
1.8.1 FLZ	22
1.8.2 ERY	24
2 HYPOTHESIS, SPECIFIC AIMS AND OVERALL STRATEGIES	27
2.1 Hypothesis	27
2.2 Specific Aims	27
2.3 Overall strategy	28
3 QUANTITATIVE META-ANALYSIS OF MDZ PK AFTER IV/PO ADMINISTRATION WITHOUT AND WITH IV/PO CYP3AI	30
3.1 Background and Objective	30
3.2 Methods	31

3.2.1	Data collection	31
3.2.2	PK dose-proportionality assessment	32
3.2.3	Estimation of secondary PK parameters in the absence of CYP3AI	33
3.2.4	Estimation of inhibitory effect on hepatic and intestinal metabolism by CYP3AI	39
3.2.5	Dose/concentration-dependent inhibition of FLZ	39
3.3	Results and Discussion	42
3.3.1	Data collection	42
3.3.2	PK dose-proportionality assessment	44
3.3.3	Estimation of PK exposure metrics and parameters in absence of CYP3AI	48
3.3.4	Estimation of inhibitory effect on hepatic and intestinal metabolism of CYP3AI	54
3.3.5	Dose/concentration dependent inhibition by FLZ	63
3.4	Conclusions	67
4	SEMI-PBPK MODELING OF IV/PO FLZ	69
4.1	Background and Objectives	69
4.1.1	Selection of CYP3AI	69
4.1.2	FLZ PK information and simulation strategies	69
4.1.3	Objectives	71
4.2	Methods	71
4.2.1	Development of FLZ semi-PBPK model	71
4.2.2	Model qualification and predictions	80
4.2.3	Sensitivity Analysis	80
4.3	Results and Discussion	81
4.3.1	Model evaluation	81
4.3.2	Model Predictions	85
4.4	Conclusions	88
5	SEMI-PBPK MODELING OF IV/PO MDZ	89
5.1	Background and Objectives	89
5.1.1	MDZ PK information	89
5.1.2	Available validation studies and simulation strategies	90
5.1.3	Objectives	91
5.2	Methods	91
5.2.1	Development of MDZ semi-PBPK model	91
5.2.2	Model qualification and predictions	102

5.2.3	Sensitivity Analysis	102
5.3	Results and Discussion	103
5.3.1	Model evaluation	103
5.3.2	Model Predictions	111
5.4	Conclusions	115
6	SEMI-PBPK MODELING OF METABOLIC INHIBITION BETWEEN IV/PO FLZ AND IV/PO MDZ	116
6.1	Background and Objectives	116
6.1.1	Available DDI studies	116
6.1.2	FLZ inhibitory information and simulation strategies	116
6.1.3	Objectives	118
6.2	Methods	119
6.2.1	Development of MDZ-FLZ DDI PBPK model	119
6.2.2	Model qualification and predictions	123
6.2.3	Sensitivity Analysis	123
6.2.4	Simulations of route-dependent DDI with various administration time intervals	124
6.2.5	Simulations of route-dependent DDI with various FLZ doses	124
6.2.6	Simulation of route-dependent DDI between CYP3A substrates and CYP3AIs	125
6.3	Results and Discussion	127
6.3.1	Model evaluation	127
6.3.2	Model Predictions	139
6.4	Conclusions	157
7	SEMI-PBPK MODELING OF IV/PO ERY	160
7.1	Background and Objectives	160
7.1.1	Selection of CYP3AI	160
7.1.2	ERY PK information and simulation strategies	160
7.1.3	Objectives	162
7.2	Methods	163
7.2.1	ERY PK meta-analysis	163
7.2.2	Saturable plasma protein binding model of ERY	163
7.2.3	Development of ERY semi-PBPK model	165
7.2.4	Model qualification and predictions	184
7.3	Results and Discussion	186

7.3.1	Meta-analysis of ERY PK studies	186
7.3.2	Meta-analysis of ERY and MDZ DDI studies	188
7.3.3	Saturable plasma protein binding model	189
7.3.4	Dose proportionality assessment	192
7.3.5	ERY semi-PBPK model after single IV administration	198
7.3.6	ERY semi-PBPK model after single/repeat- PO doses (ERY base enteric-coated tablet formulation)	211
7.3.7	ERY semi-PBPK model after single/repeat- PO doses (ERY stearate salt tablet formulation)	224
7.4	Conclusions	234
8	SEMI-PBPK MODELING OF METABOLIC INHIBITION BETWEEN IV/PO ERY AND IV/PO MDZ	236
8.1	Background and Objectives	236
8.1.1	Available DDI studies	236
8.1.2	ERY MBI information and simulation strategies	237
8.1.3	Objectives	238
8.2	Methods	239
8.2.1	Development of MDZ-ERY DDI PBPK model	239
8.2.2	Model qualification and predictions	246
8.2.3	Sensitivity Analyses	247
8.2.4	Simulations of route-dependent DDI with various administration time intervals	248
8.2.5	Assessment of linearity of MBI by ERY	249
8.2.6	Simulations of route-dependent DDI with various single doses of ERY	249
8.2.7	Simulations of route-dependent DDI with different dosing intervals of ERY	250
8.2.8	Simulation of route-dependent DDI between CYP3A substrates and CYP3AIs	251
8.3	Results and Discussion	252
8.3.1	Model evaluation	252
8.3.2	Model Predictions	276
8.4	Conclusions	306
9	OVERALL CONCLUSIONS, LIMITATIONS AND FUTURE DIRECTIONS	309
9.1	Overall Conclusions	309
9.1.1	Substrate properties	310
9.1.2	CYP3AI properties	311

9.2	Limitations and Future Directions	319
LIST OF REFERENCES		322
APPENDICES		336
A.MDZ META-ANALYSIS		336
A.1	Summary of MDZ meta-analysis after IV administration in absence of CYP3AI	337
A.2	Summary of MDZ meta-analysis after PO administration in absence of inhibitors	341
A.3	Summary of MDZ meta-analysis after IV administration in presence of CYP3AI	345
A.4	Summary of MDZ meta-analysis after PO administration in presence of CYP3AI	350
B.SENSITIVITY ANALYSIS OF FLZ		354
C.ESTIMATION OF V_B^{MDZ}, V_{P1}^{MDZ}, V_{P2}^{MDZ}, Q_2^{MDZ} AND Q_3^{MDZ}		365
D.SENSITIVITY ANALYSIS OF MDZ		370
E.SENSITIVITY ANALYSIS OF MDZ IN PRESENCE OF FLZ		377
F.ESTIMATION OF SATURABLE (SPECIFIC) PLASMA PROTEIN BINDING PARAMETERS OF ERY		393
F.1.	Control profile of hyperbolic binding model (using ADAPT)	393
F.2.	Control profile of Sigmoidal binding model (using ADAPT)	394
F.3.	In-vitro total binding data digitized from Detta et al. (Dette et al., 1982)	395
F.4.	In-vitro non-specific binding data digitized from Detta et al. (Dette et al., 1982)	395
G.ESTIMATION OF $V_{B,U}^{ERY}$, $V_{P,U}^{ERY}$ AND $Q_{2,U}^{ERY}$		396
H.ERY META-ANALYSIS		402
H.1.	Meta-analysis of IV ERY studies	402
H.2.	Meta-analysis of PO ERY studies	405
I.META-ANALYSIS OF MDZ AND ERY DDI STUDIES		412
J.ESTIMATION OF UNBOUND ERY RENAL CLEARANCE AFTER IV ADMINISTRATION		416
J.1.	Assumptions	416
J.2.	Predictability assessment of empirical hyperbolic renal clearance model	416
K.SENSITIVITY ANALYSIS OF DDI BETWEEN MDZ AND EC ERY FOR STUDY 28		418
L.SENSITIVITY ANALYSIS OF DDI BETWEEN MDZ AND SS ERY FOR STUDY 603		436
VITA		451

LIST OF TABLES

Table 3.1 Composition of AUCPOmet formed by pre-systemic GI/hepatic and systemic hepatic metabolism.....	37
Table 3.2 Summary of power model fit of exposure metrics vs dose plots.....	47
Table 3.3 Summary of linear regression of exposure metric vs dose plots.	48
Table 3.4 Descriptive statistics of important PK endpoints in absence of CYP3AI across studies.	51
Table 3.5 Exposure metrics and PK parameter estimates of 1'-OH-MDZ in absence of CYP3AI.	52
Table 3.6 Exposure metrics and PK parameter estimates of 1'-OH-MDZ in presence of CYP3AI.	60
Table 3.7 Summary of dose/concentration-dependent inhibition model of FLZ estimated from study 21.....	64
Table 3.8 Summary of extraction ratios and FLZ concentrations in various compartments.....	67
Table 4.1 Semi-PBPK FLZ model parameters.	78
Table 4.2 Values of parameters used in sensitivity analysis.....	81
Table 4.3 Comparison of reported and PBPK model-predicted FLZ plasma (blood) exposure metrics.....	83
Table 4.4 Sensitivity analysis heat-map results for semi-PBPK IV FLZ model.	85
4.5 Sensitivity analysis heat-map results for semi-PBPK PO FLZ model	85
Table 5.1 Initial semi-PBPK MDZ model parameters.....	100
Table 5.2 Values of parameters used in sensitivity analysis.....	103

Table 5.3 Comparison of reported and semi-PBPK model-predicted MDZ plasma exposure metrics in the absence FLZ using initial model (study 21) and adjusted model (study 103 and 26) parameters.....	109
Table 5.4 Adjusted semi-PBPK MDZ model parameters.....	109
Table 5.5 Sensitivity analysis heat-map results for semi-PBPK IV/PO MDZ model.	111
Table 6.1 Initial Semi-PBPK MDZ - FLZ DDI model parameters.	121
Table 6.2 Adjusted semi-PBPK MDZ model parameters.....	122
Table 6.3 Values of parameters used in sensitivity analysis.....	124
Table 6.4 Parameter modifications for hypothetical drugs, based on FLZ and MDZ individual semi-PBPK models.	126
Table 6.5 Comparison of reported and semi-PBPK model-predicted MDZ plasma exposure metrics in the absence/presence of IV/PO FLZ using initial model (study 21) and adjusted model (study 103 and 26) parameters.....	136
Table 6.6 Sensitivity analysis heat-map results for semi-PBPK MDZ and FLZ DDI model....	139
Table 7.1 Initial semi-PBPK ERY model parameters.	181
Table 7.2 Parameter estimates of two saturable plasma protein binding models.	190
Table 7.3 Summary of power model fit for total ERY plasma AUC vs dose plots.....	193
Table 7.4 Parameter estimates of power model fit using unbound ERY concentrations.	194
Table 7.5 Unbound PK parameters of IV ERY in study 611.....	196
Table 7.6 Comparison of reported and PBPK model-predicted ERY plasma exposure metrics and clearances.	203
Table 7.7 Comparison of reported and semi-PBPK (“MBI”) model-predicted PO EC ERY plasma exposure metrics and accumulation ratios using PO ERY model (study 620, 623, 626) and adjusted model (study 629) parameters.....	218
Table 7.8 Comparison of reported and semi-PBPK (“MBI” or “No MBI”) model-predicted accumulation ratio of $AUC_{0-\tau}$ after PO ERY EC or SS formulation.	219
Table 7.9 Adjusted semi-PBPK ERY model parameters.....	219
Table 7.10 Comparison of reported and semi-PBPK (“MBI”) model-predicted PO SS ERY plasma exposure metrics and accumulation ratios using PO ERY model parameters.	229
Table 8.1 MDZ and ERY initial semi-PBPK DDI model parameters.....	240

Table 8.2 Values of parameters used in sensitivity analysis.....	248
Table 8.3 Parameter modifications for hypothetical drugs, based on ERY and MDZ individual semi-PBPK models.....	252
Table 8.4 Comparison of reported and semi-PBPK model-predicted MDZ plasma exposure metrics and F_{oral} in the absence and presence of PO (EC/SS) ERY, as well as (inhibited/uninhibited) $AUC_{0-\infty}^{MDZ}$ ratio using PO ERY semi-PBPK model parameters ($v_{max,hep-3A}^{ERY} = 800 \mu\text{g}/\text{min}/\text{kg}$, $v_{max,bile}^{ERY} = 0.5 \mu\text{g}/\text{min}/\text{kg}$) with adjustments in study 28 and 603 (see Table 8.5).....	255
Table 8.5 Adjusted semi-PBPK DDI (MDZ+ERY) model parameters for study 28 and 603. .	265
Table 8.6 Sensitivity analysis heat-map results for semi-PBPK MDZ and ERY EC DDI model under dosing regimen in study 28.....	274
Table 8.7 Sensitivity analysis heat-map results for semi-PBPK MDZ and ERY SS DDI model under dosing regimen in study 603.....	275

LIST OF FIGURES

Figure 1.1 Probability of potential drug interactions.....	2
Figure 1.2 Metabolism-Based Drug-Drug Interaction Studies – Decision Tree (FDA, 2012).....	5
Figure 1.3 Using a PBPK model to explore drug-drug interaction potential between a substrate drug and an interacting drug (FDA, 2012).....	9
Figure 1.4 Scheme of competitive inhibition.....	10
Figure 1.5 Scheme of noncompetitive inhibition.....	11
Figure 1.6 Scheme of MBI.....	12
Figure 1.7 Scheme of disposition processes a drug has experienced after IV and PO administration.	15
Figure 1.8 Structure of MDZ.	19
Figure 1.9 Equilibrium between closed-ring and open-ring form of MDZ (Ranbaxy Pharmaceuticals Inc., 2013).....	20
Figure 1.10 pH-dependence of open-ring form MDZ in water (Ranbaxy Pharmaceuticals Inc., 2013).	20
Figure 1.11 Structure of metabolites of MDZ.	22
Figure 1.12 Structure of FLZ.	24
Figure 1.13 Structure of ERY.	26
Figure 3.1 Equations and assumptions used in estimating secondary PK parameters for MDZ after IV administration.....	35
Figure 3.2 Equations and assumptions used in estimating secondary PK parameters for MDZ after PO administration.....	36
Figure 3.3 Scheme of MDZ pre-systemic metabolism.	37

Figure 3.4 Dose proportionality assessment.....	46
Figure 3.5 Comparison of pre-systemic hepatic and GI metabolism of MDZ in absence of CYP3A1.....	50
Figure 3.6 Comparison of pre-systemic hepatic and intestinal formation of 1'-OH-MDZ.....	53
Figure 3.7 Evaluation of hepatic inhibitory effect of CYP3A1.....	55
Figure 3.8 Evaluation of intestinal/overall pre-systemic inhibitory effect of CYP3A1.....	57
Figure 3.9 Evaluation of inhibitory effect of CYP3A1.....	59
Figure 3.10 Evaluation of inhibitory effect of CYP3A1 on MDZ and 1'-OH-MDZ exposures..	62
Figure 3.11 Dose/concentration-dependent inhibition of FLZ.....	65
Figure 4.1 Semi-PBPK model scheme for the disposition of FLZ after IV administration.....	72
Figure 4.2 Semi-PBPK model scheme for the disposition of FLZ after PO administration.....	76
Figure 4.3 Observed and PBPK model-predicted FLZ PK profiles.....	83
Figure 4.4 Model predicted FLZ concentrations in different compartments.....	87
Figure 5.1 Semi-PBPK model scheme for the disposition of MDZ after IV administration.....	92
Figure 5.2 Semi-PBPK model scheme for the disposition of MDZ after PO administration.....	97
Figure 5.3 Observed and PBPK-model simulated MDZ PK profiles in study 21.....	104
Figure 5.4 Observed and PBPK-model simulated MDZ PK profiles in study 103.....	105
Figure 5.5 Observed and PBPK-model simulated MDZ PK profiles in study 26.....	107
Figure 5.6 Model predicted MDZ concentrations in different compartments.....	114
Figure 6.1 Semi-PBPK model scheme of MDZ in presence of FLZ.....	120
Figure 6.2 Simulated DDI dosing scheme between FLZ and MDZ.....	124
Figure 6.3 Observed and PBPK model-simulated MDZ PK profiles in study 21.....	128
Figure 6.4 Semi-PBPK model-predicted FLZ unbound hepatic and GW concentration – time profiles in study 21.....	130
Figure 6.5 Observed and PBPK model ($v_{\max, \text{hep}}^{\text{MDZ}}$ adjusted) - simulated MDZ PK profiles for study 103.....	132

Figure 6.6 Observed and PBPK model (f_{villi} adjusted) - simulated MDZ PK profiles for study 26.	135
Figure 6.7 Semi-PBPK model predicted FLZ unbound hepatic and GW concentration – time profiles for study 26.	137
Figure 6.8 MDZ AUCR by 400 mg IV 1-hour infusion or PO FLZ administered at various time intervals before 1 mg IV/3 mg PO MDZ.	141
Figure 6.9 Plots of FLZ unbound concentrations and relative CYP3A activity under 400 mg IV 1-hour-infusion or PO FLZ.	143
Figure 6.10 Ratio of MDZ AUCR by PO FLZ and by IV 1-hour infusion FLZ after various FLZ single doses.	144
Figure 6.11 MDZ AUCR by 400 mg IV 1-hour infusion or PO 3AIX1 administered at various time intervals before 1 mg IV/3 mg PO MDZ.	146
Figure 6.12 Plots of 3AIX1 unbound concentrations and relative CYP3A activity under 400 mg IV 1-hour infusion or PO 3AIX1.	147
Figure 6.13 MDZ AUCR by 400 mg IV 1-hour infusion or PO 3AIX2 administered at various time intervals before 1 mg IV/3 mg PO MDZ.	149
Figure 6.14 Plots of 3AIX2 unbound concentrations and relative CYP3A activity in presence of 400 mg IV 1-hour infusion or PO 3AIX2.	150
Figure 6.15 Unbound plasma concentration of 400 mg IV 1-hour infusion and PO administration of 3AIX2 and FLZ on Cartesian and semi-log plots.	151
Figure 6.16 MDZ AUCR by 400 mg IV 1-hour infusion or PO 3AIX3 administered at various time intervals before 1 mg IV/3 mg PO MDZ.	152
Figure 6.17 Plots of 3AIX3 unbound concentrations and relative CYP3A activity in presence of 400 mg IV 1-hour infusion or PO 3AIX3.	153
Figure 6.18 3ASX1 AUCR by 400 mg (IV: 1-hour infusion or PO) FLZ administered at various time intervals before 1 mg IV/3 mg PO 3ASX1.	154
Figure 6.19 3ASX2 AUCR by 400 mg (IV: 1-hour infusion or PO) FLZ administered at various time intervals before 1 mg IV/3 mg PO 3ASX2.	156
Figure 6.20 3ASX2 AUCR by 400 mg (IV: 1-hour infusion or PO) 3AIX2 administered at various time intervals before 1 mg IV/3 mg PO 3ASX2.	157
Figure 7.1 Binding of [14 C]-ERY to human serum as a function of unbound ERY concentration.	165
Figure 7.2 Semi-PBPK model scheme for the disposition of ERY after IV administration.	167

Figure 7.3 Semi-PBPK model scheme for the disposition of ERY after PO administration.....	175
Figure 7.4 Systemic exposure after the same oral single dose and formulation of ERY.	188
Figure 7.5 Diagnostic plots of two saturable plasma protein binding models.....	191
Figure 7.6 Relationship between f_u^{ERY} and total plasma ERY concentration.....	191
Figure 7.7 Dose proportionality assessment after single dose IV ERY and PO EC ERY (total AUC versus dose).	192
Figure 7.8. Figure 7.8 Dose proportionality assessment after single dose IV ERY and PO EC ERY (unbound AUC versus dose).....	194
Figure 7.9 Estimation of F_{oral}^{ERY} at different ERY dose.....	197
Figure 7.10 Observed and model-predicted ERY PK profiles after IV administration.....	202
Figure 7.11 Model-predicted and observed total (unbound + bound) ERY clearances versus dose.	204
Figure 7.12 Model-predicted unbound hepatic ERY concentrations after various IV dose over 15-min infusion relative to $K_{m,bile}^{ERY}$, $K_{m,hep-3A}^{ERY}$ and K_I^{ERY} on Cartesian and semi-log scales.	206
Figure 7.13 Model predicted contribution of different elimination pathways after various IV ERY dose in study 611.	208
Figure 7.14 Time course of intrinsic hepatic clearances and hepatic extraction ratio at different doses in study 611.....	210
Figure 7.15 Observed and model-predicted ERY PK profiles after PO EC administration in study 620 (Cartesian and semi-log scales).....	212
Figure 7.16 Observed and model-predicted ERY PK profiles after PO EC administration.....	215
Figure 7.17 Observed and model-predicted ERY PK profiles after PO EC administration in study 629 (Cartesian and semi-log plots).....	217
Figure 7.18 Model - predicted F_{oral}^{ERY} and different contribution of F_{oral}^{ERY} (F_{abs}^{ERY} , F_{hep}^{ERY} and F_{GI}^{ERY}) versus PO EC ERY dose (125 mg, 250 mg, 500 mg, 1000 mg).....	221
Figure 7.19 Model-predicted unbound ERY concentrations in liver and GW mucosa after 125mg, 250mg, 500mg, 1000mg single PO EC ERY dose relative to $K_{m,bile}^{ERY}$, $K_{m,hep-3A}^{ERY}$ ($K_{m,GW-3A}^{ERY}$) and K_I^{ERY}	223
Figure 7.20 Observed and model-predicted ERY PK profiles after PO SS administration.	228

Figure 7.21 Model - predicted F_{oral}^{ERY} and different contribution of F_{oral}^{ERY} (F_{abs}^{ERY} , F_{hep}^{ERY} and F_{GI}^{ERY}) versus PO SS ERY dose (125 mg, 250 mg, 500 mg, 1000 mg).....	231
Figure 7.22 Model-predicted unbound ERY concentrations in liver and GW mucosa after 125mg, 250mg, 500mg, 1000mg single PO EC ERY dose relative to $K_{m,bile}^{ERY}$, $K_{m,hep-3A}^{ERY}$ ($K_{m,GW-3A}^{ERY}$) and K_I^{ERY}	233
Figure 8.1 Semi-PBPK model scheme of MDZ in presence of ERY.....	243
Figure 8.2 Simulated DDI dosing scheme between ERY and MDZ.....	249
Figure 8.3 Observed and model-predicted MDZ PK profiles after 0.05 mg/kg IV injection over 2 min (Cartesian and semi-log scales) ($v_{max,hep}^{MDZ} = 305067 \mu\text{g}/\text{min}/\text{kg}$).....	254
Figure 8.4 Observed and model-predicted MDZ PK profiles after 0.05 mg/kg IV injection over 2 min (Cartesian and semi-log scales) ($v_{max,hep}^{MDZ} = 170,000 \mu\text{g}/\text{min}/\text{kg}$).....	254
Figure 8.5 Observed and model-predicted MDZ PK profiles after 15 mg PO MDZ (Cartesian and semi-log scales) ($v_{max,hep}^{MDZ} = 170,000 \mu\text{g}/\text{min}/\text{kg}$, $k_{GL}^{MDZ} = 0.05 \text{ min}^{-1}$).....	257
Figure 8.6 Observed and model-predicted MDZ PK profiles after 15 mg PO MDZ (Cartesian and semi-log scales) ($v_{max,hep}^{MDZ} = 170,000 \mu\text{g}/\text{min}/\text{kg}$, $k_{GL}^{MDZ} = 0.03 \text{ min}^{-1}$).....	257
Figure 8.7 Observed and model-predicted IV MDZ (0.05mg/kg) PK profiles in presence of EC ERY (500 mg TID for 7 days, IV MDZ was administered 2 hours after the 2 nd ERY dose on the 6 th day) on Cartesian and semi-log scales.....	259
Figure 8.8 Semi-PBPK model-predicted ERY plasma concentration – time profile.....	260
Figure 8.9 Observed and model-predicted IV MDZ (0.05mg/kg) PK profiles in presence of EC ERY (500mg TID for 7 days, IV MDZ was administered 2 hours after the 2 nd ERY dose on the 6 th day) on Cartesian and semi-log scales.....	261
Figure 8.10 Semi-PBPK model - predicted unbound hepatic and blood concentration – time profiles for ERY and relative hepatic CYP3A activity for study 28.....	262
Figure 8.11 Observed and model-predicted PK profiles after 15 mg PO MDZ in presence of EC ERY (500 mg TID for 7 days; PO MDZ was administered 2 hours after the 2 nd ERY dose on the 6 th day) on Cartesian and semi-log scales.....	263
Figure 8.12 Semi-PBPK model-predicted ERY unbound hepatic/GW mucosa/blood concentration – time profiles and relative hepatic/GW CYP3A activity for study 28.....	264
Figure 8.13 Observed and model-predicted MDZ PK profiles after 5 mg PO administration (Cartesian and semi-log scales) ($v_{max,hep}^{MDZ} = 305,067 \mu\text{g}/\text{min}/\text{kg}$, $k_{GL}^{MDZ} = 0.05 \text{ min}^{-1}$, $f_{villi} = 2.2$).....	266

Figure 8.14 Observed and model-predicted MDZ PK profiles after 5 mg PO administration (Cartesian and semi-log scales) ($v_{\max, \text{hep}}^{\text{MDZ}} = 170,000 \mu\text{g}/\text{min}/\text{kg}$, $k_{\text{GL}}^{\text{MDZ}} = 0.03 \text{ min}^{-1}$, $f_{\text{villi}} = 5.0$).	266
Figure 8.15 Observed and model-predicted 2.5 mg PO MDZ PK profiles (profiles scaled to 5 mg MDZ dose) in presence of SS ERY (200mg QID for 2, 4 or 7 days).	268
Figure 8.16 Semi-PBPK model predicted ERY unbound hepatic/GW mucosa/blood concentration – time profiles and relative hepatic/GW CYP3A activity in study 603.	271
Figure 8.17 MDZ AUCR by 1,000 mg ERY IV (as 15-min infusion) or PO (EC) administration followed by MDZ (IV: 1 mg; PO 3 mg) at various time intervals.	278
Figure 8.18 MDZ AUCR by 1,000 mg ERY IV (as 15-min infusion) or PO (SS) administration followed by MDZ (IV: 1 mg; PO 3 mg) at various time intervals.	278
Figure 8.19 Plots of unbound hepatic/GW concentrations for ERY and relative CYP3A activity profiles after a single dose of ERY (1,000 mg; IV: 15-min infusion, PO: EC).	279
Figure 8.20 Plots of unbound hepatic/GW concentrations for ERY and relative CYP3A activity profiles after a single dose of ERY (1,000 mg; IV: 15-min infusion, PO: SS).	280
Figure 8.21 $F_{\text{oral}}^{\text{MDZ}}$ in presence of ERY (1,000 mg; IV: 15-min infusion, PO: EC/SS) administered at various time intervals before 1 mg IV/3 mg PO MDZ.	282
Figure 8.22 Hepatic/GW extraction ratio of MDZ in presence of ERY (1,000 mg; IV: 15-min infusion, PO: EC/SS) administered at various time intervals before 1 mg IV/3 mg PO MDZ.	283
Figure 8.23 Relationship between apparent inactivation rate constant of ERY ($k_{\text{inact, app}}^{\text{ERY}}$) and unbound ERY tissue (liver or GW) concentrations after 1,000 mg ERY (IV 15min-infusion, PO: EC/SS).	284
Figure 8.24 Ratio of MDZ AUCR by ERY (IV: 15-min infusion, PO: EC) after various ERY single dose.	287
Figure 8.25 Relative CYP3A activity after various single doses of IV 15min infusion or PO EC ERY.	288
Figure 8.26 Plots of ERY unbound concentrations and relative CYP3A activity after 10,000 mg and 1,000 mg ERY (IV: 15min infusion, PO: EC).	289
Figure 8.27 AUCR of MDZ in presence of single dose PO EC ERY 250 mg/500 mg/1,000 mg or multiple doses PO EC ERY 250 mg QID/500 mg BID/1,000 mg QD (same daily dose).	292
Figure 8.28 Unbound ERY concentration after PO EC 250 mg QID, 500 mg BID and 1,000 mg QD.	293

Figure 8.29 Relative CYP3A activity after PO EC ERY single dose (250 mg / 500 mg/ 1,000 mg) or multiple doses (250 mg QID/ 500 mg BID/ 1,000mg QD).....	294
Figure 8.30 (Steady-state) accumulation ratio (R _{ss}) of ERY unbound hepatic/GW mucosa concentration, and inhibited hepatic/GW CYP3A after 250 mg QID / 500 mg BID / 1,000 mg QD PO EC ERY.	295
Figure 8.31 AUCR of MDZ in presence of single dose PO SS ERY 250 mg/500 mg/1,000 mg or multiple doses PO SS ERY 250 mg QID/500 mg BID/1,000 mg QD (same daily dose).	297
Figure 8.32 Unbound ERY concentration after PO SS 250 mg QID, 500 mg BID and 1,000 mg QD.....	298
Figure 8.33 Relative CYP3A activity after PO SS ERY single dose (250 mg / 500 mg/ 1,000 mg) or multiple doses (250 mg QID/ 500 mg BID/ 1,000mg QD).....	299
Figure 8.34 (Steady-state) accumulation ratio (R _{ss}) of ERY unbound hepatic/GW mucosa concentration, and inhibited hepatic/GW CYP3A after 250 mg QID / 500 mg BID / 1,000 mg QD PO SS ERY.	300
Figure 8.35 MDZ AUCR by 3AIX4 (1,000 mg; IV: 15-min infusion, or PO) administered at various time intervals before 1 mg IV/3 mg PO MDZ.	302
Figure 8.36 Plots of 3AIX4 unbound concentrations and relative CYP3A activity under 1,000 mg IV 15-min infusion or PO 3AIX4.	303
Figure 8.37 3ASX1 AUCR by 1,000 mg ERY (IV: 15-min infusion or PO) administered at various time intervals before (1 mg IV/3 mg PO) 3ASX1.	304
Figure 8.38 3ASX2 AUCR by 1,000 mg ERY (IV: 15-min infusion or PO) administered at various time intervals before (1 mg IV/3 mg PO) 3ASX2.	306
Figure 9.1 Proposed decision tree to determine the impact of route of administration (IV/PO) on the metabolic inhibitory DDI for the victim drug.....	311
Figure 9.2 Proposed decision tree to determine the impact of route of administration (IV/PO) on the DDI for perpetrator drug (based on F _{oral}).	316
Figure 9.3 Proposed decision tree to determine the impact of route of administration (IV/PO) on the DDI for perpetrator drug (based on mechanism of inhibition).....	318

LIST OF ABBREVIATIONS

1'-OH-MDZ	1-hydroxy-midazolam
3AIX1	A hypothetical low F_{oral} and long $t_{1/2}$ non-competitive CYP3AI, derived from FLZ semi-PBPK model
3AIX2	A hypothetical high F_{oral} and short $t_{1/2}$ non-competitive CYP3AI, derived from FLZ semi-PBPK model
3AIX3	A hypothetical low F_{oral} and short $t_{1/2}$ non-competitive CYP3AI, derived from FLZ semi-PBPK model
3AIX4	A hypothetical high F_{oral} and short $t_{1/2}$ mechanism-based CYP3AI, derived from ERY semi-PBPK model
3ASX1	A hypothetical CYP3A substrate with GW metabolism removed, derived from MDZ semi-PBPK model
3ASX2	A hypothetical CYP3A substrate with GW metabolism removed and hepatic metabolism decreased, derived from MDZ semi-PBPK model
4-OH-MDZ	4-hydroxy-midazolam
AAG	α -acid glycoprotein
ABX	Antibiotics
ADE	Adverse drug event
ADME	Absorption, distribution, metabolism and excretion
ANOVA	Analysis of variance

AUC	Area under the curve
AUCR	AUC increase ratio
B:P	Blood-to-plasma partitioning ratio
BCS	Biopharmaceutical Classification System
BID	Twice daily
BL	Body length (height)
B_{\max}	Binding capacity of specific (AAG) binding to ERY
BSA	Body surface area
BW	Body weight
Caco-2	Human colonic carcinoma cell line
$C_{\text{bo-ns}}$	Non-specific bound ERY concentration
$C_{\text{bo-total}}$	Total (specific + non-specific) bound ERY concentration
CI _s	Confidence interval
$CL_{\text{gf,u}}$	Unbound glomerular filtration clearance
CL_{GW}	Gut wall clearance
CL_{hep}	Hepatic clearance
$CL_{\text{int,GW}}$	Intrinsic gut wall clearance
$CL_{\text{int,hep}}$	Intrinsic hepatic clearance
$CL_{\text{int,hep-3A}}$	Intrinsic hepatic CYP3A clearance
$CL_{\text{int,hep-bile}}$	Intrinsic biliary excretion clearance

CL_{others}	Other clearance
$CL_{\text{ra,u}}$	Unbound tubular reabsorption clearance
CL_{ren}	Renal clearance
$CL_{\text{ren,u}}$	Unbound renal clearance
$CL_{\text{tot,b}}$	Total blood clearance
$CL_{\text{tot,p}}$	Total plasam clearance
$CL_{\text{ts,u}}$	Unbound tubular secretion clearance
c_{max}	Peak concentration
c_{min}	Trough concentration
CV	Coefficient of variance
CYP3A	Cytochrome P450 3A subfamily
CYP3AI	CYP3A inhibitors
CYPs	Cytochrome P450s
DDI	Drug-drug interaction
DME	Drug metabolism enzyme
DTZ	Diltiazem
E	Enzyme
E_0	Baseline CYP3A activity in liver or gut wall
EBT	Erythromycin breath test
EC	Enteric-coated tablet formulation of ERY

ED_{50}	Dose that requires to produce 50% tubular reabsorption
EHC	Enterohepatic Circulation
EI	Enzyme-inhibitor complex
EI'	Reactive enzyme-inhibitor intermediate
EMA	European Medicines Agency
ER_{GI}	Gastrointestinal extraction ratio
ER_{hep}	Hepatic extraction ratio
ER_{presys}	Overall presystemic extraction ratio
ERY	Erythromycin
ES	Enzyme-substrate complex
ESI	Enzyme-substrate-inhibitor complex
F_{abs}	Fraction of PO dose absorbed from gut lumen
FDA	Food and Drug Administration
f_e	Fraction of renal clearance relative to total clearance after IV administration
F_{GI}	Fraction of absorbed dose that reaches portal vein, escaping first-pass GW metabolism
f_{HA}	Fraction of hepatic artery to total hepatic blood flow
F_{hep}	Fraction of drug absorbed into portal vein that escaping hepatic pre-systemic metabolism
f_{hep-3A}	Fraction of hepatic CYP3A clearance relative to total clearance after IV administration

$f_{\text{hep-bile}}$	Fraction of biliary excretion relative to total clearance after IV administration
FLZ	Fluconazole
f^{met}	Fraction of IV MDZ dose that converted to 1'-OH-MDZ
f_m^{CYP3A}	Ratio of CYP3A metabolic clearance of a drug to its total clearance after IV administration
F_{oral}	Oral bioavailability
$F_{\text{oral}}^{\text{met}}$	Apparent oral bioavailability of 1'-OH-MDZ after PO MDZ
f_{pv}	Fraction of the components of portal vein that contain drug
f_u	Fraction unbound
f_{villi}	IVIVE scaling factor and IIV adjusting factor
GC-MS	Gas chromatography mass spectrometry
GFJ	Grape fruit juice
GI	Gastrointestinal
GIT	Gastrointestinal tract
GW	Gut wall
HLM	Human liver microsomes
HPLC	High performance liquid chromatography
IC_{50}	Concentration of inhibitor to produce half of maximum inhibition
IIV	Inter-individual variability
IND	Investigational New Drug

IV	Intravenous
IVIVE	<i>In vitro-in vivo</i> extrapolation
k_a	Absorption rate constant
$K_{b,50}$	Binding affinity of ERY to AAG
k_{deg}	First-order degradation rate of CYP3A
k_e	Elimination rate constant
k_{GL}	Absorption rate constant from gut lumen to gut wall
K_i (K_I)	Binding affinity of inhibitor to the target enzyme (inhibitory potency)
k_{in}	Enzyme synthesis rate constant
k_{inact}	Maximum enzyme inactivation rate constant
K_m	Binding affinity of substrate
k_{obs}	Observed inactivation rate constant
K_p	Partition coefficient between tissue and blood
LC-MS	Liquid chromatography–mass spectrometry
LLOQ	Lowest limit of quantification
m	Slope of non-specific binding of ERY linear regression
M&S	Modeling and Simulation
MBI	Mechanism-based inhibition/inhibitor
MDZ	Midazolam
Met	Metabolite

MR	Metabolic ratio
MRP2	Multidrug resistance-associated protein 2
MW	Molecular weight
n	Hill coefficient in Sigmoidal binding model
NDA	New Drug Application
nd-ERY	N-demethyl-erythromycin
P	Product
$P_{app\ A-B}$	Apical-to-basolateral apparent permeability
$P_{app\ B-A}$	Basolateral-to-apical apparent permeability
PBPK	Physiologically-based pharmacokinetic
PC	Parent compound
PD	Pharmacodynamics
P_{eff}	Effective permeability
P-gp	P-glycoprotein
PI	Protease inhibitor
PK	Pharmacokinetic
pKa	Acid dissociation constant
PO	Oral
q12h	every 12 hours

Q_2	Trans-departmental clearance between central and shallow peripheral compartments
Q_3	Trans-departmental clearance between central and deep peripheral compartments
q6h	every 6 hours
q8h	every 8 hours
QD	Once daily
Q_{en}	Enterocyte blood flow
Q_{HA}	Hepatic artery blood flow
Q_{hep}	Hepatic blood flow
Q_{HV}	Hepatic portal vein blood flow
Q_{villi}	Villous blood flow
R_0	zero-order synthesis rate of CYP3A
RSE	Relative standard error
Rss	Steady-state accumulation ratio
S	Substrate
SAD	Single escalating dose
SD	Standard deviation
semi-PBPK	Semiphysiologically-based pharmacokinetic
SS	Stearate salt formulation of ERY
$t_{1/2}$	Half-life

t_{\max}	Time to reach c_{\max}
UGT	glucuronosyltransferase
$V_{d_{cc}}$	Central compartmental volume of distribution
$V_{d_{ss}}$	Steady-state volume of distribution
V_{GW}	Volume of gut wall
V_{hep}	Volume of liver
v_{\max}	Maximum metabolizing velocity
V_{PV}	Volume of portal vein

ABSTRACT

USING SEMIPHYSIOLOGICALLY-BASED PHARMACOKINETIC (SEMI-PBPK) MODELING TO EXPLORE THE IMPACT OF DIFFERENCES BETWEEN THE INTRAVENOUS (IV) AND ORAL (PO) ROUTE OF ADMINISTRATION ON THE MAGNITUDE AND TIME COURSE OF CYP3A-MEDIATED METABOLIC DRUG-DRUG INTERACTIONS (DDI) USING MIDAZOLAM (MDZ) AS PROTOTYPICAL SUBSTRATE AND FLUCONAZOLE (FLZ) AND ERYTHROMYCIN (ERY) AS PROTOTYPICAL INHIBITORS

By: Mengyao Li, M.S.

A dissertation submitted in partial fulfillment of the requirements for the degree of Doctor of philosophy at Virginia Commonwealth University.

Virginia Commonwealth University, 2016

Director: Jürgen Venitz, M.D., Ph.D.
Professor, Department of Pharmaceutics, School of Pharmacy

The purpose of the project was to investigate the impact of IV and PO routes difference for MDZ, a prototypical CYP3A substrate, and two CYP3A inhibitors (CYP3AI) -FLZ and ERY-, on the magnitude and time course of their inhibitory metabolic DDI.

Individual semi-PBPK models for MDZ, FLZ and ERY were developed and validated separately, using pharmacokinetic (PK) parameters from clinical/*in-vitro* studies and published physiological parameters. Subsequently, DDI sub-models between MDZ and CYP3AIs incorporated non-competitive and mechanism-based inhibition (MBI) for FLZ and ERY,

respectively, on hepatic and gut wall (GW) CYP3A metabolism of MDZ, using available *in-vitro/in-vivo* information. Model-simulated MDZ PK profiles were compared with observed data from available clinical PK and DDI studies, by visual predictive check and exposure metrics comparison. DDI magnitude and time course for CYP3AI (IV vs. PO) followed by MDZ (IV vs. PO) at various time points were predicted by the validated semi-PBPK-DDI models. Two hypothetical CYP3A substrates and four CYP3AI (derived from MDZ, FLZ and ERY, with GW metabolism removed, hepatic metabolism reduced, or oral bioavailability (F_{oral}) and/or elimination half-life ($t_{1/2}$) modified) were also simulated to generalize conclusions.

The final semi-PBPK-DDI models predict well the PK profiles for IV/PO MDZ in absence/presence of IV/PO CYP3AI, with deviations between model-predicted and observed exposure metrics within 30%. Prospective simulations demonstrate that:

- 1) CYP3A substrates, *e.g.*, MDZ, are consistently more sensitive to metabolic inhibition after PO than after IV administration, due to pre-systemic hepatic and/or GW metabolism. For substrates without GW metabolism and limited hepatic metabolism, only a marginal route difference for substrate administration is observed.
- 2) For high- F_{oral} CYP3AIs, *e.g.*, FLZ, no inhibitor IV-PO route DDI differences are expected, unless they are given simultaneously with PO MDZ.
- 3) For low- F_{oral} CYP3AIs, *e.g.*, ERY, greater inhibition is expected after IV than after PO administration for IV MDZ, but is difficult to predict for PO MDZ.
- 4) In addition to F_{oral} and plasma $t_{1/2}$ of CYP3AIs, the DDI onset, peak and duration are determined by their oral absorption rate and by the resulting hepatic and/or GW concentration profiles relative to K_i for noncompetitive CYP3AIs, but by CYP3A kinetics (synthesis, degradation rate) for MBI CYP3AIs.

CHAPTER 1

1 INTRODUCTION

1.1 Clinical significance of drug-drug interaction (DDI)

By definition, drug-drug interaction (DDI) occurs when a drug (“victim” drug)’s clinical efficacy or toxicity is affected by the co-administration of another drug (“perpetrator” drug). This could result from the pharmacokinetics (when plasma concentration is affected, through absorption, distribution, metabolism and excretion (ADME) processes) of the victim drug or its metabolites; and/or from the impact on pharmacodynamics, when changes in drug action occur in the area of target receptors (Pleuvry, 2005).

DDI remains an important issue in clinical practice and is most commonly observed in the elderly population due to polypharmacy. The incidence and extent of DDI may increase as the number of drugs prescribed increases, as is illustrated by **Figure 1.1** (Delafuente, 2003).

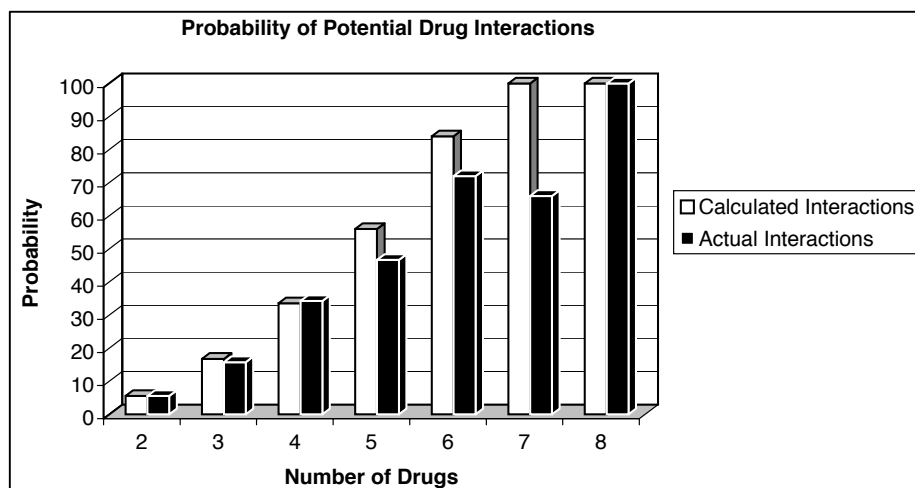


Figure 1.1 Probability of potential drug interactions.

The open bars are model calculated probabilities of having a drug-drug interaction. The solid bars are observed interactions identified in patients.

If not being taken care of appropriately, DDI can result in severe adverse drug events (ADEs), due to toxicity or lack of efficacy. ADEs are reported to be the 4th leading cause of death in the US, with more than 2,216,000 serious ADEs reported in hospitalized patients which caused more than 100,000 deaths yearly (FAERS Reporting by Patient Outcomes by Year, 2015). Moura et al. (2009) estimated the cost of drug-related morbidity and mortality annually is \$136 billion, which is more than the total cost of cardiovascular or diabetic care in the US. A 2-fold greater mean length of stay, cost and mortality have been reported for hospitalized patients suffered from ADEs compared to patients without ADEs (Sultana et al., 2013). According to the study by Agrawal et al. (2009), DDI represent 3-5% of all in-hospital medication errors, and DDI is also an important cause of patient visits to emergency departments (Ray et al., 2010). Despite the modest overall incidence of ADEs caused by DDI, the consequences of DDI is usually severe, which in most cases lead to hospitalization (Mirošević Skvrce et al., 2011). Some DDIs have led to life-threatening ADEs during treatment, resulting in restrictions in the prescription of drugs or even withdrawal of drugs from the market. This brought huge economic consequences for the

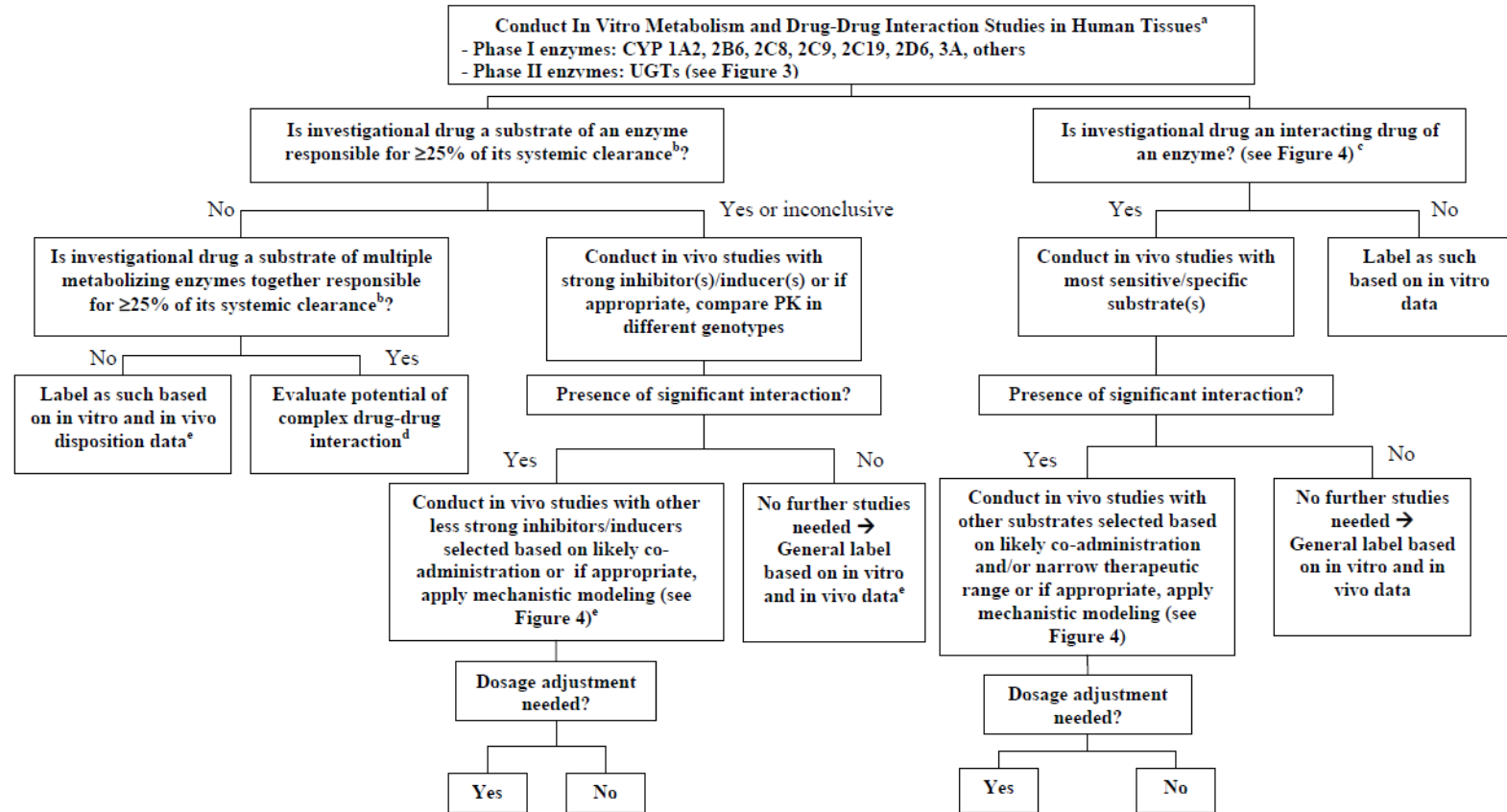
pharmaceutical industry and the loss from the marketplace of effective drugs. For example, concurrent administration of terfenadine and cytochrome P450 3A (CYP3A) inhibitors, such as ketoconazole, itraconazole, erythromycin, has resulted in fatal arrhythmia (torsades de pointes), and led to the withdrawal of terfenadine (Seldane[®]) from US market in 1998 (Seldane (Rxlist)). Cisapride (Propulsid[®]) had been discontinued in the US in 2000, due to ventricular arrhythmias caused by co-administration of CYP3A inhibitors (Michalets & Williams, 2000). Cerivastatin (Lipobay[®]) was withdrawn from the US market in 2001, due to rhabdomyolysis that leads to kidney failure in patients. This risk was caused by inhibition of cerivastatin's uptake into liver and hepatic metabolic clearance by gemfibrozil and its metabolite gemfibrozil glucuronide (Furberg & Pitt, 2001).

The topic of DDI has received a great deal of recent attention from regulatory, scientific and health care communities worldwide, and due to a large number of drugs introduced annually (45 novel drug approval for 2015 in the US (Novel drug approval for 2015), pharmaceutical companies should investigate the interactions between a presumably new drug and other drugs during drug development process, as part of an adequate assessment of drug's safety and effectiveness (FDA, 2012). The US Food and Drug Administration (FDA) and European Medicines Agency (EMA) have both published guidelines on the investigation of drug interactions, and the main focus of these guidance is pharmacokinetic drug interactions (European Medicines Agency, 2012; FDA, 2012)

1.2 Strategies to assess metabolic DDI

Metabolic DDI, caused by the inhibition and/or induction of cytochrome P450s (CYPs), are the major components of DDIs. The general strategy to assess metabolic DDI is to begin with *in-*

vitro studies to determine whether a drug is a substrate, inhibitor, or inducer of metabolic enzymes. The results of *in-vitro* studies, along with clinical pharmacokinetic (PK) data, may help with ruling out the need for additional *in-vivo* studies, or providing a proper design of clinical trials using a modeling and simulation (M&S) approach (FDA, 2012). If potential DDI is possible between investigational agent and other drugs, *in-vivo* clinical studies should be conducted to determine clinical recommendations for the DDI. *In-vivo* animal DDI studies may also be conducted during exploratory drug development process. However, final DDI recommendations should be based on results from *in-vitro* human enzymes, or *in-vivo* studies performed in humans (European Medicines Agency, 2012). A decision tree from FDA for metabolism-based DDI studies was demonstrated in **Figure 1.2** (FDA, 2012).



^a Other Phase I enzymes (CYP and non-CYP) are discussed in section IV.A.1.a.

^b Results from in vitro enzyme phenotyping experiments, human pharmacokinetic studies such as an intravenous study, a mass-balance study, and pharmacokinetic studies in which renal/biliary clearances are determined can be evaluated together to determine the percent contribution of enzyme to overall in vivo drug elimination in humans.

^c See Figure 4 for calculation of R values and cutoff values. Sponsor may conduct an in vivo cocktail study in humans (Reference: *Clinical Pharmacology and Therapeutics*, 81: 298-304, 2007). See section V.C.3.

^d See section V.C.4 for evaluation of complex drug interactions.

^e Additional population pharmacokinetic analysis may assist the overall evaluation of the investigational new drug as a substrate.

Figure 1.2 Metabolism-Based Drug-Drug Interaction Studies – Decision Tree (FDA, 2012).

In the *in-vitro* studies, if the investigational drug is a possible victim for any metabolic inhibition or induction, the need for *in-vivo* DDI studies are determined by quantitative measurement of the contribution of one specific enzyme or multiple metabolic enzymes to the overall systemic clearance of the drug. If the investigational drug is a possible perpetrator, the decision to conduct *in-vivo* study or not should be based on quantitative analysis of both *in-vitro* and clinical PK data, by using a variety of models (i.e. basic models, mechanistic static models, PBPK models, *etc.*).

In the *in-vivo* studies, if the investigational drug is a possible victim for any metabolic DDI, *in-vivo* studies should start with a strong inhibitor/inducer of the targeted enzyme. If the results from the study with strong inhibitors/inducers indicate positive interactions, the impact of a less strong inhibitor/inducer should be evaluated. Generally, crossover designs in which same subjects receive victim drug in the absence and presence of perpetrator are more efficient. Dose of the substrate and interacting drug should maximize the possibility of DDI, thus the maximum planned or approved dose and shortened dosing interval of the interacting drug should be used. Sequence of administration and the time interval between dosing of substrate and inhibitor/inducer should also be chosen to maximize the DDI effect, depending on mechanism of DDIs. Other factors, such as safety, objectives of the studies, genetic polymorphism of targeted enzymes, clinical relevant usage, PK and pharmacodynamic (PD) characteristics, *etc.*, can also affect the selection of study design. Simulations (e.g., by PBPK models) can provide valuable insight into optimizing the study design. In most scenarios, *in-vivo* DDI studies can be performed in healthy volunteers, however, patient population may be used for the sake of safety considerations in healthy volunteers, or the intention to evaluate PD endpoints.

In terms of route of administration, generally, the route of administration should be the one planned for clinical use. However, DDI studies may need to be conducted on multiple routes of administration, if more than one route is being developed. The changes in PK parameters are generally used to assess clinical significance of DDI, such as change in area-under-the-curve (AUC), peak plasma concentration (C_{max}) and time to peak concentration (t_{max}). DDI study results should be reported as 90% confidence intervals (CIs) of the geometric mean ratio of the observed PK measures of substrate with and without inhibitor/inducer. When the 90% CIs of the ratios fall entirely within the equivalence range of 80%-125%, no DDI effect can be claimed; otherwise, dosing recommendations should be provided based on clinical significance of the DDI.

1.3 Use of Physiologically-based pharmacokinetic (PBPK) modeling in quantitative assessment of DDI

To better inform clinical design and optimize dosing regimen for individual patients, physiologically-based pharmacokinetic (PBPK) models have increasingly been employed during drug discovery and development process (Huang & Rowland, 2012). A public workshop entitled “Application of Physiologically-based Pharmacokinetic (PBPK) Modeling to Support Dose Selection” was held by FDA on Mar 10, 2014, to discuss the role of PBPK in drug development and regulation (Wagner et al., 2015). Between 2008 and 2013, the US FDA received 84 IND/NDA (Investigational New Drug/ New Drug Application) submissions containing PBPK modeling approaches (Zhao et al., 2011). Of these, 60% are related to the predictions of DDI (Zhao et al., 2011)..

According to FDA drug interactions guidance, ‘PBPK is a useful tool that can help sponsors (1) better design drug-drug interaction studies, dedicated trials and population pharmacokinetic

studies, and (2) quantitatively predict the magnitude of drug-drug interactions in various clinical situations' (FDA, 2012). Compared with conventional compartmental models, it integrates system-dependent parameters (based on physiological knowledge) and drug-dependent parameters (factors that influence ADME processes of the drug) into the description of PK, which offers clear advantages in certain situations. First, PBPK model can be used to simulate the dynamics of drug interactions after various doses, routes of administration or dosing intervals between victim and perpetrator drugs, and to evaluate the necessity for additional *in-vivo* studies. Second, it assumes a particular mechanism of drug interactions based on *in vitro-in vivo* extrapolation (IVIVE), which can be used to investigate the magnitude and time course of drug exposure in the tissues of interest. In addition, it can incorporate multiple patient intrinsic (*e.g.*, age, gender, genetics, *etc.*) and/or extrinsic (*e.g.*, organ dysfunction, *etc.*) factors into the prediction of patient-specific drug exposures, and allow the dosing recommendation or study design for specific population. The overall workflow and input information for a PBPK model to simulate a DDI study is demonstrated in **Figure 1.3** (modified from Zhao et al. (2011)). Instead of traditional whole-body PBPK models, semiphysiologically-based pharmacokinetic (semi-PBPK) models, which lump together body tissues that are not of interest, are more often utilized, to reduce the dimensionality and complexity of whole-body PBPK model (Cao & Jusko, 2012), but still allows the investigation of DDI at drug interaction sites (tissues).

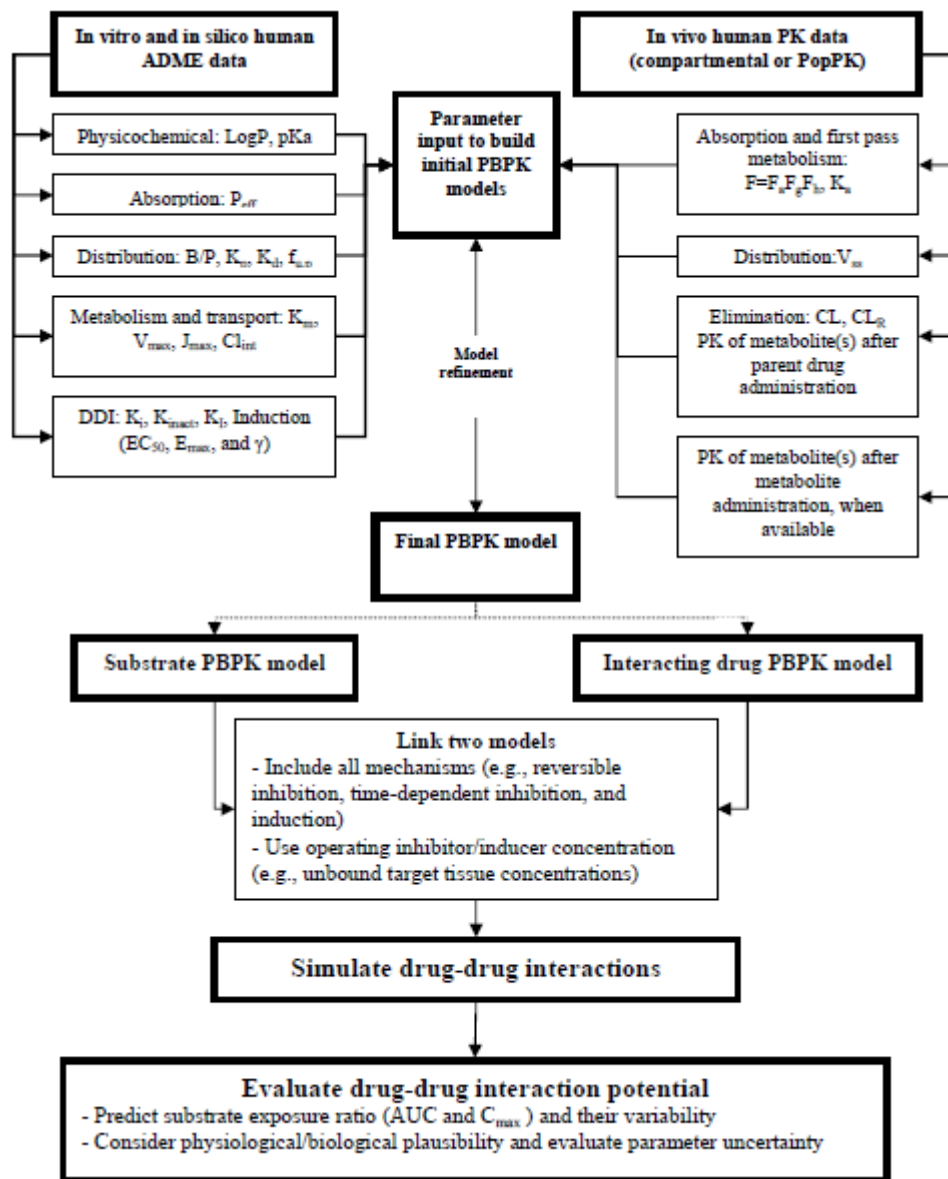


Figure 1.3 Using a PBPK model to explore drug-drug interaction potential between a substrate drug and an interacting drug (FDA, 2012).

1.4 Mechanism of metabolic inhibition

Metabolic inhibition is a major component of DDI. During PBPK modeling process, different types of metabolic inhibition models should be applied at interaction sites (hepatocytes, enterocytes, *etc.*), according to mechanism of metabolic inhibition, *in-vitro* enzyme inhibitory

information, and unbound target tissue concentrations of perpetrator drug. Mechanisms and corresponding models used in different types of metabolic inhibition are discussed below, with focus on competitive, noncompetitive and mechanism-based inhibition (MBI).

As to competitive inhibition, inhibitor and the substrate compete for the same enzyme active site, which prevents binding of substrate to it metabolic enzyme. It is usually a reversible inhibition, and the inhibitory effect can be overcome by increasing substrate concentration. Apparent binding affinity of substrate (K_m') depends on unbound concentration of inhibitor ($[I]_u$) and binding affinity of inhibitor to the target enzyme (K_I), and can be expressed as equation (1.1). Therefore, competitive inhibitor will decrease binding affinity of substrate (K_m), but has no effect on maximum metabolizing velocity (v_{max}).

$$K_m' = K_m \cdot \left(1 + \frac{[I]_u}{K_I}\right) \quad (1.1)$$

A scheme of competitive inhibition is shown in **Figure 1.4** (Inhibition of Enzyme Activity, class handout).

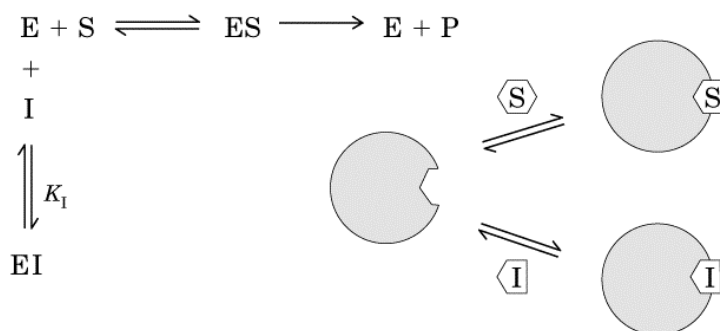


Figure 1.4 Scheme of competitive inhibition.

E = enzyme, S = substrate, ES = enzyme-substrate complex, EI = enzyme-inhibitor complex, P = product, I = competitive inhibitor.

As to non-competitive inhibition, inhibitor can bind to both substrate and enzyme-substrate complex with equal affinity (if not equal, it is call mixed inhibition) and to a different site with

substrate. However, when both the substrate and inhibitor are bound to the enzyme, this enzyme-substrate-inhibitor complex cannot form product and can only be converted back to ES or EI. The inhibitor is not necessarily structurally similar to substrate, so it does not affect K_m of substrate. However, since ES has a different fate (binding to inhibitor) other than forming product, the maximum velocity to produce the product (v_{max}) is decreased, and the extent of decrease is determined by $[I]_u$ and noncompetitive binding affinity to the enzyme or ES (K_i , assuming same binding affinity to enzyme as to ES), shown in equation (1.2). This inhibition is also reversible inhibition.

$$v'_{max} = v_{max} / (1 + \frac{[I]_u}{K_i}) \quad (1.2)$$

v_{max}' is the apparent v_{max} in presence of noncompetitive inhibitor.

A scheme of non-competitive inhibition is shown in **Figure 1.5**. (Inhibition of Enzyme Activity, class handout)

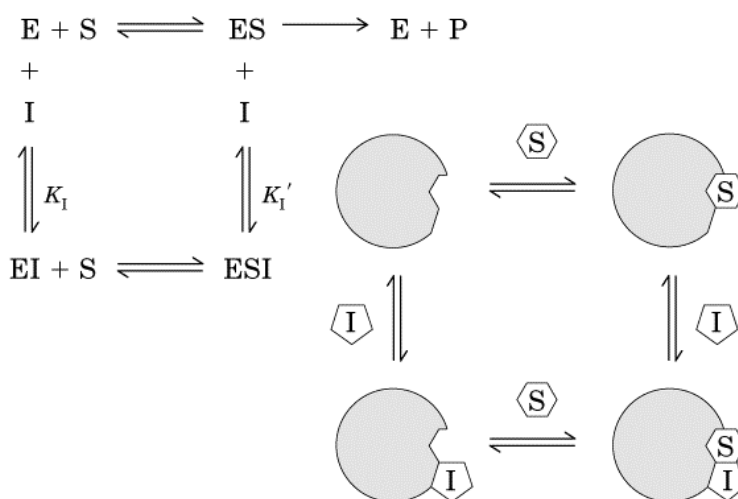


Figure 1.5 Scheme of noncompetitive inhibition.

I = non-competitive inhibitor, ESI = enzyme-substrate-inhibitor complex, K_i = affinity of noncompetitive inhibitor to enzyme, K_i' = affinity of noncompetitive inhibitor to enzyme-substrate complex (might be equal to K_i or not, if not, which is called mixed inhibition).

MBI is a form of irreversible enzyme inhibition. The inhibitor chemically resembles the substrate and binds to the active site in the same way as substrate binds. EI is then catalyzed to a reactive intermediate that could either be metabolized to product of inhibitor, or (more importantly) covalently bind to a moiety in the enzyme active site, resulting in chemical modification and inactivation of the enzyme protein (Yang et al., 2005). Since MBI is associated with irreversible loss of enzyme function and it takes time to synthesis new enzyme before activity is restored, it can typically cause hepatotoxicity and should be avoided in drug development. Due to the loss of enzyme activity, v_{max} is decreased by MBI, and K_m does not change. A scheme of MBI is shown in **Figure 1.6** (Rowland & Tozer, 2011; Yang et al., 2005).

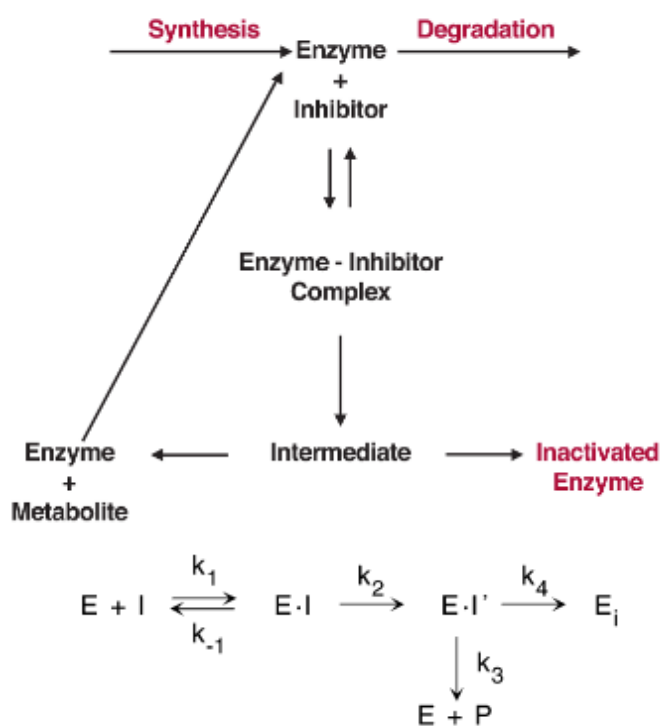


Figure 1.6 Scheme of MBI

$E \cdot I'$ is the reactive enzyme-inhibitor intermediate, E_i is the inactivated enzyme, P is metabolite of MBI inhibitor. k_1 and k_{-1} represents association and disassociation constants between inhibitor and enzyme, k_2 is catalytic activity of EI to form $E \cdot I'$, k_3 is the catalytic activity to form metabolite of MBI inhibitor, k_4 is catalytic activity of enzyme inactivation.

To incorporate MBI in a PBPK model, a published PBPK model (Quinney et al., 2010) of DDI between MDZ and clarithromycin, which is a CYP3A MBI, is introduced here. At steady state, the amount of active CYP3A enzyme (E_0) available in the liver or intestinal wall is determined by a zero-order synthesis rate (R_0) and first-order degradation rate (k_{deg}) of enzyme. The rate of change of active enzyme (dE_t/dt) in the absence of a CYP3A MBI is given by equation (1.3)

$$\frac{dE_t}{dt} = R_0 - k_{deg} \times E_0 \quad (1.3)$$

At steady state (equation 1.4),

$$R_0 = k_{deg} \times E_0 \quad (1.4)$$

E_0 is the baseline (at time 0) amount of active CYP3A.

In the presence of a MBI, the degradation rate of enzyme is increased by an inactivation rate constant, k_{obs} (equation 1.5),

$$\text{Rate of inactivation} = k_{obs} \times E_{(t)} = \frac{k_{inact} \times I_t}{K_I + I_t} \times E_{(t)} \quad (1.5)$$

k_{inact} is the maximum rate of enzyme inactivation, K_I is the dissociation rate constant of the inhibitor, and I_t is the unbound concentration of inhibitor at the enzyme site at time t . k_{inact} and K_I can be described by k_2 , k_3 and k_4 , shown in equation (1.6-1.7), which were mathematically derived in Tatsunami et al. (1981):

$$k_{inact} = \frac{k_2 k_4}{k_2 + k_3 + k_4} \quad (1.6)$$

$$K_I = \frac{k_{-1} + k_2}{k_1} \frac{k_2 k_4}{k_2 + k_3 + k_4} \quad (1.7)$$

The rate of change of CYP3A in response to inactivation can be described by equation (1.8),

$$\frac{dE_{(t)}}{dt} = R_0 - k_{deg} \times E_{(t)} - \frac{k_{inact} \times I_t}{K_I + I_t} \times E_{(t)} \quad (1.8)$$

$E_{(t)}$ is the amount of active CYP3A enzyme present at time t .

At time = t , GW and hepatic clearance of MDZ should be corrected by a factor of $E_{(t),GW}/E_{0,GW}$ and $E_{(t),hep}/E_{0,hep}$, where subscript GW and hep represent GW and hepatic CYP3A enzyme, respectively. Among these parameters, R_0 and k_{deg} can be estimated from *in-vivo* experiments measuring CYP3A recovery following enzyme MBI or inducer administration. K_I and k_{inact} can be obtained from *in-vitro* inhibitory studies.

1.5 Known/suspected differences in DDI between IV and PO routes of administration and clinical significance of exploring routes of administration impact on DDI

Different routes of administration of victim/perpetrator could have a different magnitude and/or time course for DDI. As is mentioned in FDA drug interactions guidance, the route of administration chosen for a metabolic DDI study is very important, and the possibility of formulation differences in the DDI potential should be considered when extrapolating interaction study results across formulations. Generally, the route of administration should be the one planned for clinical use, and ‘if multiple routes are being developed, the need for metabolic interaction studies by each route depends on the expected mechanisms of interaction and the similarity of corresponding concentration-time profiles for parent drug and metabolites’ (FDA, 2012).

The two commonly used routes, intravenous (IV) and oral (PO) routes of administration, are chosen as routes of interest in this project, because in contrast to IV administration, drugs can undergo absorption and/or pre-systemic clearance after PO administration. **Figure 1.7** illustrates the physiological processes a drug has experienced after IV and PO administration. After IV administration, drug is injected into systemic blood, distributes into tissues through artery blood flows and eliminates by systemic hepatic clearance (CL_{hep}) and/or other clearances (CL_{other}),

such as renal clearance (CL_{ren}). After PO administration, drug gets into gut lumen first, and only the soluble and permeable drug (F_{abs}) can be absorbed into GW enterocytes. Within enterocytes, if possible, a fraction of drug could be metabolized by GW enzymes, and the rest of drug which survives from this pre-systemic GW metabolism ($F_{abs} \cdot F_{GI}$) permeates into portal vein. Drug in portal vein is then brought into liver through portal vein blood flow, and liver can pre-systemically metabolize and/or excrete a portion of drug, and the rest reaches systemic circulation ($F_{abs} \cdot F_{GI} \cdot F_{hep}$). The final fraction of drug gets absorbed into systemic circulation is oral bioavailability (F_{oral}), which is a product of F_{abs} , F_{GI} and F_{hep} . After it reaches systemic circulation, the drug behaves the same as after IV administration.

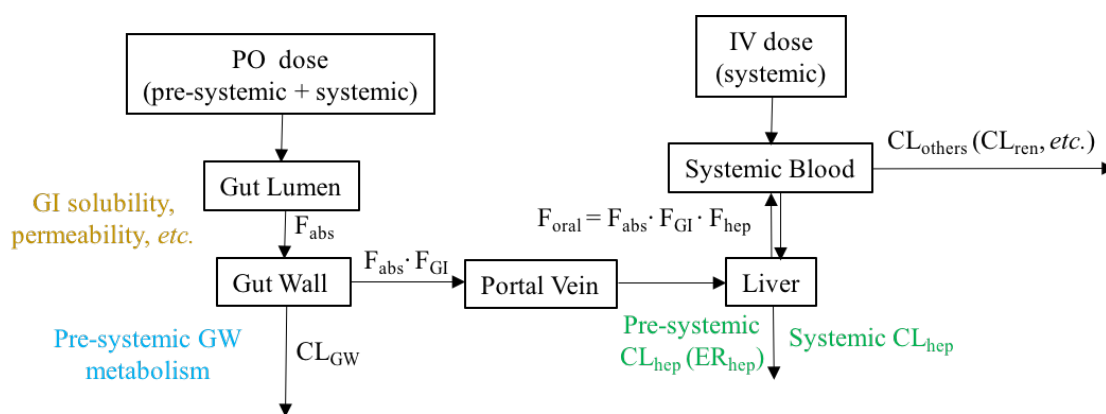


Figure 1.7 Scheme of disposition processes a drug has experienced after IV and PO administration.

F_{abs} is the fraction of PO dose absorbed from gut lumen, F_{GI} is the fraction of absorbed drug that reaches portal vein, escaping first-pass GW metabolism. F_{hep} is the fraction of drug absorbed into portal vein that escaping hepatic pre-systemic clearance. ER_{hep} is hepatic extraction ratio. CL_{GW} is GW clearance

Several clinical DDI studies (Gorski et al., 1998; Kharasch et al. 2005; Kupferschmidt et al. 1995; Olkkola et al., 1993; Olkkola et al., 1996; Tsunoda et al., 1999) have investigated the impact of route of administration of MDZ, a typically used CYP3A substrate, on its inhibitory DDI by other CYP3A inhibitors (e.g. ketoconazole, itraconazole, fluconazole, erythromycin,

clarithromycin, *etc.*), and concluded that PO MDZ exposure is increased more by CYP3A inhibitors (CYP3AI) than IV MDZ exposure, mainly due to pre-systemic hepatic and GW inhibition. However, all the CYP3AI used in these studies were administered as PO administration. In terms of route of administration impact of perpetrator drugs, Ahonen *et al.* conducted a three-phase crossover study, to investigate 400mg IV 1 hour-infusion and PO FLZ's inhibitory effect on PO MDZ. Their conclusions are the AUC_{0-3} and peak concentration (c_{max}) of MDZ were significantly higher after PO than after IV 1 hour-infusion FLZ, however, $AUC_{0-\infty}$ of MDZ were not statistically significant between different FLZ routes (Ahonen *et al.*, 1997). Another study performed by Palkama *et al.* (1998) demonstrated that both IV 1 hour-infusion and PO 400mg FLZ result in the same inhibitory extent to IV alfentanil exposure, which is another CYP3A substrate. Nevertheless, no others were found to investigate route difference of perpetrator drugs on DDI outcome, and even for FLZ, route of administration impact of FLZ was not tested when IV MDZ or PO alfentanil was administered.

The impact of routes of administration difference on the magnitude and time course of DDI outcome depends on the dynamic PK profiles of both victim and perpetrator drugs at the sites of drug-drug interaction, as well as the expected mechanism and potency of interaction. Dynamic PK profiles of either victim or perpetrator are determined by three factors: patient-specific (*e.g.*, age, gender, genetics, ethnicity, *etc.*), drug-specific (*e.g.*, F_{oral} , elimination half-life, mechanism and potency of interaction, *etc.*) and dosing regimen-specific (*e.g.*, dose, administration sequence/interval between perpetrator and victim, formulation, *etc.*) characteristics. In this research, the aim is to investigate the impact of routes of administration of both victim and perpetrator drugs on the magnitude and time course of metabolic DDI using semi-PBPK M&S. This may be beneficial to comprehensively assessing key factors that determine DDI differences,

and at which scenario the interaction study results can be extrapolated between different routes of administration without additional *in-vivo* DDI studies.

1.6 Selection of prototypical drug metabolism enzyme (DME): CYP3A

CYP3A is the most important enzyme of the cytochrome P450 superfamily because of its abundance in the liver and intestine and its ability to metabolize more than half of therapeutic compounds that undergo oxidation. (Tsunoda et al., 1999) The CYP3A subfamily primarily consists of three known isoforms in humans – CYP3A4, CYP3A5 and CYP3A7 and CYP3A43 (Isoherranen et al., 2008). Among adults, CYP3A4 is the dominant CYP3A enzyme in liver and small intestine. CYP3A5 is also found in adult liver and small intestine (Daly, 2006), and other organs, like kidney, colon and peripheral blood (Janardan et al., 1996), but its expression is clearly polymorphic. CYP3A7 is the major fetal liver CYP3A enzyme, although in rare cases, CYP3A7 mRNA has also been detected in adults (Williams et al., 2002). CYP3A43 has revealed a much lower catalytic activity, which is unlikely to contribute much to the metabolic clearance of CYP3A substrate (Daly, 2006).

A number of different polymorphisms, which lead to complete absence of CYP3A5 expression, are now known, with the CYP3A5*3 allele being by far the most common, and additional rare polymorphisms including CYP3A5*6 and CYP3A5*7 (Daly, 2006). In different populations, CYP3A5*3 has different distribution, with a frequency of 85-95% in Caucasians, 60-73% in Asians and 27-50% in African Americans (Miao et al., 2009). CYP3A5*1 allele is the wild type of CYP3A5, and subjects who possess at least one copy of CYP3A5*1 allele do express CYP3A5 (Daly, 2006). Ethnicity also affect the expression of CYP3A5*1 allele, with African-Americans more commonly expressed CYP3A5 enzymes (more than 50%) than

Caucasians (10-20%) (Jonge et al., 2013). According to Lown et al. (1994), CYP3A4 and CYP3A5 are independently regulated in liver and small intestine. Some CYP3A inhibitors (ketoconazole (Shirasaka et al., 2013), itraconazole (Yu et al., 2004), fluconazole (Yang et al., 2012), *etc.*) are more potent inhibitors to CYP3A4 than CYP3A5.

The activity of CYP3A can be influenced by many factors, like age, gender, hormones, and DDI, and all these factors can cause difficulty in the therapeutic use of CYP3A substrates. In addition, expression of CYP3A is independently regulated in intestine and liver (Tsunoda et al., 1999), so it is likely that these factors may differently modulate intestinal and hepatic CYP3A activity. Therefore a practical *in-vivo* probe method that characterizes and quantitates both intestinal and hepatic CYP3A activity would be useful.

1.7 Selection of prototypical CYP3A substrate: MDZ

MDZ is a commonly used CYP3A *in-vivo* probe substrate, which is a short acting benzodiazepine used for conscious sedation. MDZ can be administered both intravenously and orally, which allows both hepatic and intestinal metabolism investigation. Several PK properties make MDZ an attractive *in-vivo* probe for CYP3A. It has a short half-life ($t_{1/2}$), 1.8-6.4 h, and can be rapidly eliminated exclusively by CYP3A to one predominant metabolite (1'-hydroxymidazolam, 1'-OH-MDZ) with negligible renal elimination and limited P-glycoprotein (P-gp) modulation (Baxter Healthcare Corporation.; Tolle-Sander et al., 2003). More importantly, a large number of clinical DDI studies were conducted using IV or PO MDZ as a victim drug, and CYP3AI as perpetrators (see **Chapter 3**), providing diverse choices of CYP3AI (different mechanism of interaction, different PK properties, *etc.*) to make comparisons among them. In addition, several studies have compared inhibitory effect of PO CYP3AI (e.g., ketoconazole

(Chien et al., 2006), diltiazem (Zhang et al., 2009), clarithromycin (Quinney et al., 2010), voriconazole (Frechen et al., 2013), *etc.*) on MDZ after IV/PO administration by using semi-PBPK models. Although research objectives were different in these publications, their model skeletons can be used as the basis of our MDZ PBPK model.

MDZ has a molecular weight (MW) of 325.77 g/mol, and the structure is shown in **Figure 1.8**. Due to its low solubility when $\text{pH} > 4$ (Midazolam SciFinder Report), MDZ hydrochloride is formulated in sterile water for IV injection and syrup or tablet for PO administration. Each mL contains MDZ hydrochloride equivalent to 1-5 mg MDZ in sterile water for injection (Baxter Healthcare Corporation.), and contains 2 mg MDZ in syrup (Ranbaxy Pharmaceuticals Inc., 2013). Under the acidic conditions required to solubilize MDZ in the product, MDZ is present as an equilibrium mixture (shown in **Figure 1.9**) of the closed-ring form and an open-ring structure. The amount of open-ring form is dependent upon the pH of the solution. At the specified pH of sterile water for injection ($\text{pH} = 2.5 - 3.7$) and syrup ($\text{pH} = 3.1 - 3.3$), the solution may contain up to about 25% and 40 %, respectively, of the open-ring compound. At the physiological conditions under which the product is absorbed (pH of 5 to 8) into the systemic circulation, any open-ring form present reverts to the physiologically active, lipophilic, closed-ring form (MDZ), as shown in **Figure 1.10**.

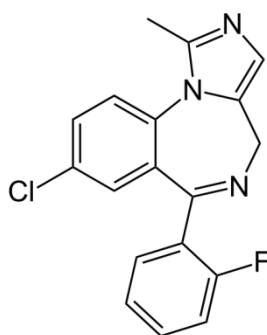


Figure 1.8 Structure of MDZ.

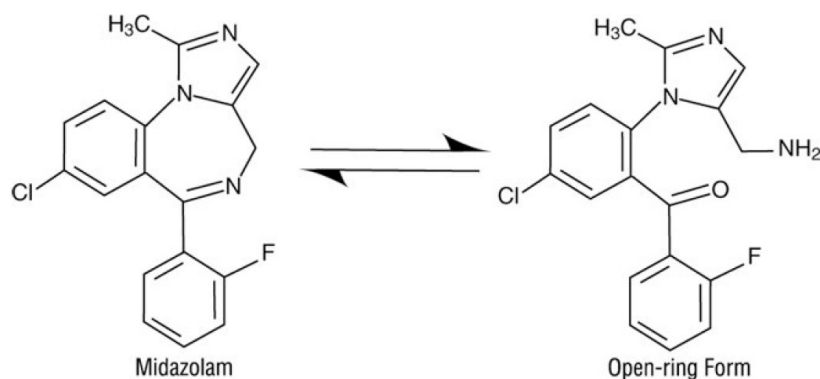


Figure 1.9 Equilibrium between closed-ring and open-ring form of MDZ (Ranbaxy Pharmaceuticals Inc., 2013).

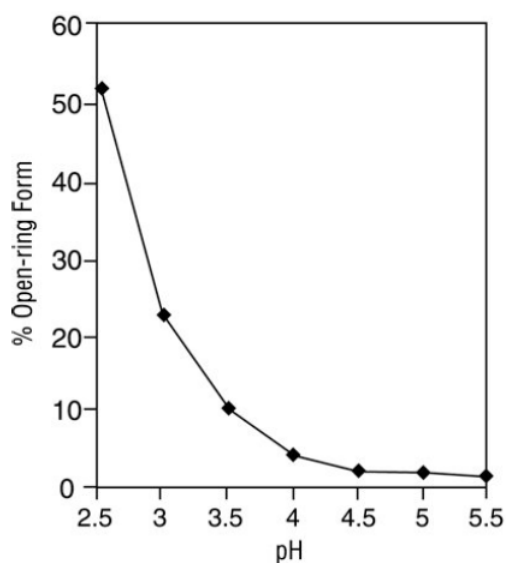


Figure 1.10 pH-dependence of open-ring form MDZ in water (Ranbaxy Pharmaceuticals Inc., 2013).

MDZ is lipophilic (LogP = 3.78 (Midazolam SciFinder Report)) and highly plasma protein bound (97%), and the steady-state volume of distribution ($V_{d_{ss}}$) ranges from 1.0-3.1 L/kg (Midazolam Hydrochloride – Injection FDA Label). After IV administration, the urinary recovery of its metabolite (1'-OH-MDZ), as its glucuronide, accounts for at least 70% of an administered dose (Thummel et al., 1996). Formation of two minor metabolites, 4-hydroxymidazolam (4-OH-MDZ) and 1', 4-dihydroxymidazolam, are also catalyzed by CYP3A

and together, as glucuronide conjugates, comprise another 4%-6% of an administered dose (Thummel et al., 1996). Recent *in-vitro* (Hyland et al., 2009; Klieber et al., 2008) and *in-vivo* (Hyland et al., 2009) studies demonstrate that MDZ can also be metabolized directly by glucuronosyltransferase (UGT) and the glucuronide MDZ accounts for 1%-2% of total dose. After IV administration, MDZ can be only metabolized by hepatic CYP3A through systemic clearance; while after PO administration, it is rapidly and completely dissolved and permeates into intestinal epithelium (Heizmann et al., 1983) (BCS Class 1 drug (Wu & Benet, 2005)), and then subject to substantial intestinal and hepatic first-pass metabolism, before reaching systemic circulation (Ranbaxy Pharmaceuticals Inc., 2013). CYP3AI can inhibit all the three pathways (pre-systemic intestinal/hepatic metabolism, systemic hepatic metabolism), but the inhibitory extent on intestinal and hepatic CYP3A activity might be different.

1.7.1 Metabolites of MDZ

1'-OH-MDZ and 4-OH-MDZ are the primary metabolites of MDZ, which are converted subsequently to N- and O-glucuronides by UGT (Yang et al., 2012). Their molecular weight is 341.77 g/mol, with the structures shown in **Figure 1.11 a-b**. 1'-OH-MDZ has a larger total clearance than MDZ (680 ± 19 ml/min vs. 523 ± 31 ml/min) (Mandema et al., 1992); the plasma protein binding of 1'-OH-MDZ is 90%, and $V_{d_{ss}}$ is 54 ± 4 L (Mandema et al., 1992). *In-vivo* studies in humans suggest that 1'-OH-MDZ is at least as potent as the parent compound and may contribute to the net pharmacologic activity of MDZ (Mandema et al., 1992). *In-vitro* studies have demonstrated that the affinities of 1'- and 4-OH-MDZ for the benzodiazepine receptor are approximately 20% and 7%, respectively, relative to MDZ (Mandema et al., 1992). It is reported that relatively high concentration of 1'-OH-MDZ was observed after PO administration of MDZ,

and can shift the concentration-effect relationship of MDZ based on reaction time measurements more to the left than IV route (Mandema et al., 1992). The formation of 1'-OH-MDZ had the characteristics of substrate-inhibition kinetics when tested with recombinantly expressed CYP3A4, and its formation can be inhibited by CYP3AI, like fluconazole, to a greater extent than 4-OH-MDZ, resulting in a metabolic switch to 4-OH-MDZ pathway (Yang et al., 2012).

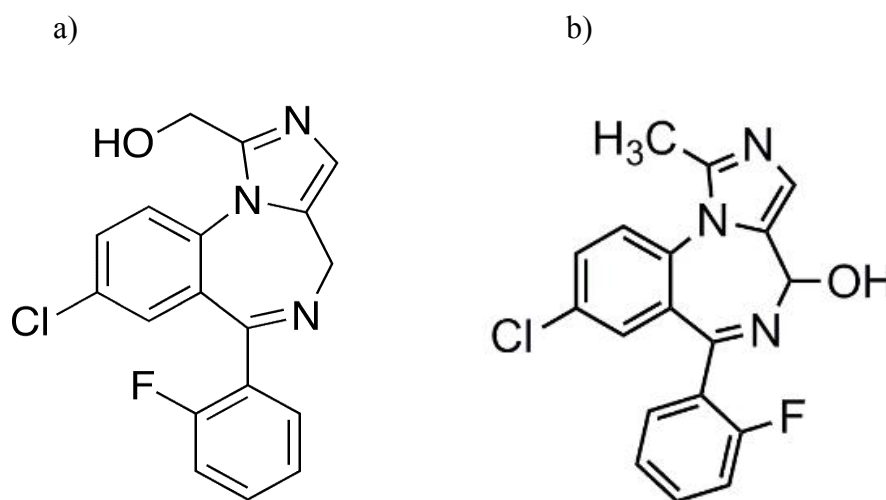


Figure 1.11 Structure of metabolites of MDZ.

Structure of metabolites of MDZ. a) 1'-OH-MDZ. b) 4-OH-MDZ.

1.8 Selection of prototypical CYP3AI: Fluconazole (FLZ) and Erythromycin (ERY)

1.8.1 FLZ

FLZ is an azole antifungal drug, which can be administered by both IV and PO administration clinically. This is the only CYP3AI that clinical DDI studies of both IV and PO FLZ are available (Ahonen et al., 1997), using MDZ as victim drug, which allows us to validate DDI semi-PBPK model between IV perpetrator and victim drug. “Validate” or “Validation” throughout the dissertation indicates that the semi-PBPK models were verified and sometimes

optimized, if necessary, by observed clinical studies, and in other literatures, “qualification” or “calibration” might be used to indicate the same meaning.

FLZ has a MW of 306.27 g/mol, and the structure is shown in **Figure 1.12**. FLZ is sparingly soluble at pH range of 3-8 (solubility = 0.98 g/L at pH of 3; solubility \approx 0.30 g/L at pH = 4-8). FLZ is formulated as sterile solution for IV injection, and as power (for suspension) or tablet for PO administration. IV FLZ injection solution is usually formulated in a sodium chloride or dextrose diluent, and each mL contains 2 mg of FLZ and 9 mg of sodium chloride or 56 mg of dextrose, hydrous. PO FLZ tablets and suspension are formulated with several inactive ingredients, as details listed in DIFLUCAN label (Pfizer, 2011). The PK properties of FLZ are similar following IV and PO administration, with F_{oral} above 90% (Humphrey et al., 1985; Pfizer, 2011; Washton, 1989), which is defined as BCS Class 1 drug (Lindenberg et al., 2004). It is less lipophilic ($\log P = 0.4$ (DrugBank Fluconazole)), and low plasma protein bound (11%-12%) (Humphrey et al., 1985), and $V_{d_{ss}}$ is about 0.7 L/kg in humans (Humphrey et al., 1985; Carrasco-Portugal & Flores-Murrieta, 2007); the ratio of distribution to different tissues is near to 1 (Carrasco-Portugal & Flores-Murrieta, 2007). FLZ is cleared primarily by renal excretion, and approximately 70% (Humphrey et al., 1985; Ripa et al., 1993; Sobue et al., 2004; Washton, 1989) of the administered dose appear in the urine as unchanged drug. About 11% of the dose is excreted in the urine as metabolites and only two metabolites are present in detectable quantities, a glucuronide conjugate of unchanged FLZ and a FLZ N-oxide, which account for 6.5 and 2.0% of an administered dose (Brammer et al., 1991; Pfizer, 2011). Renal clearance is reported to be 0.2ml/min/kg on average (Ripa et al., 1993; Sobue et al., 2004), and all non-renal pathways are assumed to be hepatic metabolism. The mean terminal plasma elimination $t_{1/2}$ ranges from 22 to 37 hours, indicating its prolonged inhibitory effect on hepatic and intestinal CYP3A. It is a less

profound (moderate) CYP3AI (Kharasch et al., 2005; Drug Interactions & Labeling Drug Development and Drug Interactions Table of Substrates, Inhibitors and Inducers), which can non-competitively inhibit hepatic and intestinal CYP3A (Gibbs et al., 1999; Isoherranen et al., 2008), with comparable K_i^{FLZ} to human intestinal and hepatic microsomes ($10.7 \pm 4.2 \mu\text{M}$ and $10.4 \pm 2.9 \mu\text{M}$, respectively) (Isoherranen et al., 2008).

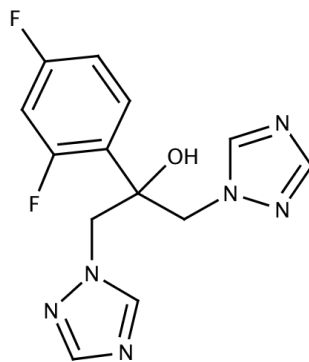


Figure 1.12 Structure of FLZ.

1.8.2 ERY

ERY is a macrolide antibiotic which is active against gram-positive bacteria and some gram-negative bacteria (Hospira, 2013). It can be administered both intravenously and orally, and different oral dosage forms are available, such as enteric coated tablet, ERY stearate, ERY ethylsuccinate, to avoid its degradation by gastric acid. It is a commonly used mechanism-based CYP3AI, and metabolites of ERY has no clinical significant CYP3AI (Zhang, 2007), if any, could largely increase the complexity of DDI semi-PBPK model between ERY and MDZ.

ERY has a MW of 733.94 g/mol, and the structure is shown in **Figure 1.13**. It is a basic and less lipophilic drug ($\text{pK}_a = 8.8$, $\log P = 0.8$ (DrugBank Erythromycin; Erythromycin Scifinder Report)), with very high solubility across physiologically relevant pH (solubility $> 73 \text{ g/L}$ at pH 1-8). ERY is known to exhibit a predominant binding to α_1 -acid glycoprotein (AAG) at

therapeutic relevant concentrations, and to albumin at higher than therapeutic concentrations (Dette & Knothe, 1986) ($f_u = 0.31$ after 500mg IV ERY *in-vivo* (Suarez et al.)), resulting in increasing Vd_{ss} with dose (Austin et al., 1980). Vd_{ss} at 125mg IV ERY is 0.47L/kg (Austin et al., 1980), still larger than blood volume, indicating that ERY is well distributed in the body. Tissue levels (e.g. liver, spleen, kidneys, and lungs) are generally higher than serum levels and persist longer (Suarez et al.). After IV administration, ERY unbound hepatic clearance is similar to hepatic blood flow (Q_{hep}) (Barre et al., 1987), indicating its high hepatic extraction ratio (ER_{hep}). It is partially metabolized by CYP3A to its major metabolite N-demethyl-erythromycin (nd-ERY). Integration of CO_2 flux to time infinity, measured in Erythromycin breath test (EBT), demonstrated that only up to 1/3 of ERY is metabolized by CYP3A at low dose (Rivory et al., 2001). As a substrate for P-gp and MRP2 (Kurnik et al., 2006) (K_m unknown), mean bile levels of ERY were approximately 10 times higher than corresponding serum concentration 1 h after I.V. ERY (Chelvan et al., 1997) in human, indirectly indicating that biliary excretion might be a major route of elimination of ERY. Only 2-15% of unchanged ERY is observed in urine, depending on dose. $t_{1/2}$ of ERY is about 1.5-2 hours (Austin et al., 1980). After PO administration, F_{oral} of ERY is quite variable (18%-45%) (Somogyi et al., 1995), and due to extensively hydrolysis by gastric acid, enteric-coated tablets or pellets, less soluble salts and pro-drugs are adopted as dosage forms. It is a BCS Class 3 drug (Heizmann et al., 1983), and pre-systemic intestinal/hepatic CYP3A metabolism and biliary excretion may also prevent the absorption of ERY into systemic circulation. ERY can inhibit CYP3A by irreversibly binding, resulting in MBI of CYP3A. K_I^{ERY} and k_{inact}^{ERY} measured in *in-vitro* experiments (Ito et al., 2003; McConn et al., 2004; Rowland et al., 2011; Xu et al., 2009; Yamano et al., 2001; Yates et al., 2012; Zhang et al., 2009; Zhang et al., 2010; Ping et al., 2005) using human liver microsomes

(HLM) were highly variable, with K_I^{ERY} ranged from 1.48 – 109 μM and k_{inact}^{ERY} ranged from 0.017 – 0.066 min^{-1} .

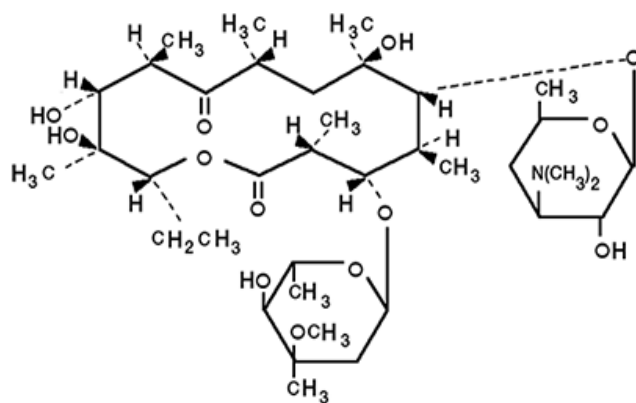


Figure 1.13 Structure of ERY.

CHAPTER 2

2 HYPOTHESIS, SPECIFIC AIMS AND OVERALL STRATEGIES

2.1 Hypothesis

The route of administration (IV vs PO) for MDZ, a prototypical CYP3A substrate, and prototypical CYP3AI will affect the magnitude and time course of their metabolic DDI, due to different sites of metabolic interaction (*i.e.*, liver, GW). The DDI depends on the PK characteristics of the CYP3AI (F_{oral} , dose/time-dependent PK, *etc.*), mechanism and potency of inhibition, dosing regimen (dose, single vs. repeat- dosing, different formulations, *etc.*) and administration time interval between MDZ and CYP3AI.

2.2 Specific Aims

The overall objective of this research is to explore the impact of differences between IV and PO route of administration for both victim drugs (MDZ and hypothetical substrates) and perpetrator drugs (CYP3AI) on the magnitude and time course of CYP3A-mediated metabolic DDI (*i.e.*, plasma concentration-time profile and exposure metrics (c_{max} , t_{max} , AUC)). To accomplish this objective, the specific aims are as follows:

- 1) Assess the contribution of intestinal and hepatic CYP3A metabolism to the PK of MDZ after IV and PO administration in humans. In addition, compare the inhibitory effect of various CYP3AI on the hepatic and intestinal metabolism of MDZ by conducting an exhaustive

literature search and a quantitative meta-analysis. Select CYP3AI of interest for further PBPK modeling.

- 2) Build and validate a semi-PBPK model for MDZ, to predict its plasma, hepatic and GW concentrations after IV or PO administration.
- 3) Build and validate a semi-PBPK model for FLZ (a highly oral bioavailable, noncompetitive CYP3AI), to predict its plasma, hepatic and GW concentrations after IV or PO administration.
- 4) Build and validate a semi-PBPK metabolic inhibition model between MDZ and FLZ. Assess route-dependent DDI profiles by simulations (IV MDZ and IV FLZ, IV MDZ and PO.FLZ, PO MDZ and IV FLZ, PO MDZ and PO FLZ)
- 5) Build and validate a semi-PBPK model for ERY (a relatively poorly orally bioavailable, mechanism-based CYP3AI), to predict its dose-/time-dependent PK, and predict its plasma, hepatic and GW concentrations after IV or PO administration
- 6) Build and validate a semi-PBPK metabolic inhibition model between MDZ and ERY. Assess route-dependent DDI by simulations (IV MDZ and IV ERY, IV MDZ and PO ERY, PO MDZ and IV ERY, PO MDZ and PO ERY)
- 7) Generate hypothetical MDZ-like substrates and FLZ- (ERY-) like CYP3AI by changing key PK properties and compare their route-dependent DDI profiles

2.3 Overall strategy

In order to accomplish the specific aims and test the research hypothesis, the following steps were followed:

- a. Extensive literature search and quantitative meta-analysis were carried out to collect human PK information for both MDZ and the selected CYP3AI (*i.e.*, FLZ and ERY) after

IV and PO administration.

- b. The semi-PBPK models for MDZ and CYP3AI were developed separately based on compiled clinical PK information and physiological parameters from the literature. Models were validated by clinical PK profiles after IV and PO administration for each drug, and sensitivity analyses were performed to optimize model parameters and identify key parameters.
- c. The drug interaction models between MDZ and CYP3AI for GW and liver CYP3A were established from *in-vitro* studies and were subsequently validated by clinical DDI studies. Sensitivity analyses were performed to identify key model parameters.
- d. Final DDI semi-PBPK models were used to investigate impact of route of administration for MDZ and CYP3AI at different clinical scenarios (*i.e.*, various doses, different administration time interval, formulation, *etc.*). A series of hypothetical drugs were also simulated to come up with general (proposed) rules regarding route-dependent DDI.

CHAPTER 3

3 QUANTITATIVE META-ANALYSIS OF MDZ PK AFTER IV/PO ADMINISTRATION WITHOUT AND WITH IV/PO CYP3AI

3.1 Background and Objective

MDZ is a prototypical CYP3A substrate, with negligible renal clearance and P-gp modulation (Baxter Healthcare Corporation; Tolle-Sander et al., 2003). Due to the abundance of CYP3A in small intestine and liver, MDZ could be metabolized by both intestinal and hepatic CYP3A enzyme. Intestinal CYP3A metabolism of MDZ is generally assumed to occur during first-pass metabolism only, thus, IV MDZ is only cleared by systemic hepatic CYP3A metabolism, whereas PO MDZ is exposed to both intestinal and hepatic pre-systemic metabolism, as well as systemic hepatic clearance. It will be of interest to assess the contribution of intestinal and hepatic CYP3A to the overall metabolic clearance of MDZ.

In presence of CYP3AI, pre-systemic intestinal/hepatic metabolism and systemic hepatic metabolism may be inhibited to different extent, due to the mechanism, potency, and PK profiles of CYP3AI. More specifically, a study by Kharasch *et al.* (2005) investigated the dose-dependent CYP3A inhibition by FLZ, in which 12 subjects received IV or PO MDZ in absence or presence of single dose of 100, 200, or 400 mg PO FLZ. Dose/concentration-dependent inhibition of FLZ on IV/PO MDZ could be determined through this study. Furthermore, Ahonen *et al* (1997) performed a double-dummy, randomized, 3-way cross-over study in 9 healthy volunteers, in

which subjects were dosed with PO MDZ in absence or presence of either IV or PO FLZ. This study can be used to compare the route-dependent inhibitory effect on intestinal and hepatic metabolism of MDZ.

In addition, MDZ is mainly metabolized to 1'-OH-MDZ, with urinary recovery of 1'-OH-MDZ, as its glucuronide, accounts for at least 70% of an IV MDZ dose. (Thummel et al., 1996) Therefore, the formation of 1'-OH-MDZ by pre-systemic intestinal and pre-systemic/systemic hepatic CYP3A can also implicate their contribution to MDZ clearance, as well as the inhibitory effect on GW and hepatic CYP3A.

The major objectives of this chapter were to:

- a. Assess the contribution of intestinal and hepatic CYP3A to the overall metabolic clearance of MDZ and systemic/pre-systemic formation of 1'-OH-MDZ
- b. Compare the effects of various CYP3AI on PK of MDZ and formation of 1'-OH-MDZ
- c. Determine the dose/concentration-dependent inhibition of PO FLZ
- d. Investigate the route-dependent inhibitory effect on intestinal and hepatic metabolism of IV/PO FLZ.

3.2 Methods

3.2.1 Data collection

An extensive literature search was carried out in PubMed, to search for any MDZ PK studies with CYP3AI in humans. MDZ was to have been administered both intravenously and orally, and plasma exposures (their means and standard deviations (SD)) after IV and PO administration should be well estimated and provided for both control and inhibitor treatment groups. Due to the age-related decline in the metabolism of MDZ (Dundee et al., 1985), studies in the elderly (age >

60 years) were excluded from the final database. There is also evidence showing that Japanese have significantly lower systemic clearance of MDZ than Caucasians (Ozawa et al., 2004); thus one study in the Asian population was also excluded. All studies were to have been conducted in healthy volunteers without any co-medications, except women who may have used oral contraceptives. All the exposure metrics (AUC, c_{max} , *etc.*), demographics, study design (dose, sample size, sampling time, *etc.*) and bio-analytical (LLOQ, assay method, *etc.*) information for both MDZ and 1'-OH-MDZ were extracted from the studies.

3.2.2 PK dose-proportionality assessment

Most secondary PK parameters are derived and interpreted based on the assumption of linear PK. Therefore, it is necessary to determine dose-proportionality of both MDZ and 1'-OH-MDZ. Mean plasma exposures of MDZ and 1'-OH-MDZ were plotted against their corresponding MDZ dose after IV and PO administration on log scales. A power model ($y = ax^b$) was then fit the data; an exponent value of 1 indicates dose-proportional PK. 95% CI of the exponent, b, was generated by JMP Pro 9.0 (SAS, Cary, NC) to assess if there was significant deviation from 1 ($p < 0.05$).

According to several clinical studies (Yang et al., 2012; Mandema et al., 1992), 1'-OH-MDZ is an active metabolite of MDZ, presumably equally potent as MDZ. Estimation of metabolic ratio (MR) is a method to evaluate the exposure of metabolite relative to the parent compound (MDZ). The equation to calculate MR is as follows,

$$MR = \frac{AUC^{met}}{AUC^{MDZ}} \cdot \left(\frac{MW^{MDZ}}{MW^{met}} \right) \quad (3.1)$$

MW^{MDZ} is the molecular weight of MDZ, 325.78 g/mol; MW^{met} is the molecular weight of 1'-OH-MDZ, 341.77 g/mol; AUC^{met} is AUC of 1'-OH-MDZ. In some studies, AUC ratio between MDZ and 1'-OH-MDZ was provided instead of AUC^{met} , thus AUC^{met} was calculated

accordingly. Furthermore, one-way analysis of variance (ANOVA) was used to compare MR across various doses. Finally, AUC^{met} was plotted against AUC^{MDZ} , after both IV and PO routes, to detect nonlinear formation or elimination of 1'-OH-MDZ. Superscripts 'MDZ' and 'met' refer to MDZ and 1'-OH-MDZ, respectively; subscripts 'IV' and 'PO' refer to different route of administration of MDZ. If not mentioned otherwise, AUC refers to AUC from time 0 to infinitive.

3.2.3 Estimation of secondary PK parameters in the absence of CYP3AI

In all of the following equations, it is assumed that MDZ and 1'-OH-MDZ follow dose-proportional PK within corresponding IV and PO MDZ dose ranges.

3.2.3.1 MDZ (parent compound)

The algorithms of estimating secondary PK parameters for IV and PO MDZ in absence of CYP3AI are presented in **Figure 3.1** and **Figure 3.2**, respectively.

After IV administration of MDZ, total plasma clearance ($CL_{tot,p}^{MDZ}$) was calculated by administered dose ($Dose_{IV}^{MDZ}$) and AUC after IV MDZ (AUC_{IV}^{MDZ}) as follows:

$$CL_{tot,p}^{MDZ} = \frac{Dose_{IV}^{MDZ}}{AUC_{IV}^{MDZ}} \quad (3.2)$$

A value of 0.86 (Chien et al., 2006) was used as blood to plasma partitioning ratio ($B:P^{MDZ}$), in order to convert $CL_{tot,p}^{MDZ}$ to total blood clearance ($CL_{tot,b}^{MDZ}$). Since MDZ is exclusively metabolized by CYP3A and has negligible renal clearance, hepatic extraction ratio (ER_{hep}^{MDZ}) was then calculated as follows:

$$ER_{hep}^{MDZ} = \frac{CL_{tot,b}^{MDZ}}{Q_{hep}} \quad (3.3)$$

where Q_{hep} is hepatic blood flow, fixed at 21.4 mL/min/kg (Tsunoda et al., 1999). The fraction of MDZ dose absorbed into portal vein that escapes liver pre-systemic metabolism (F_{hep})

was then estimated by equation (3.4):

$$F_{\text{hep}}^{\text{MDZ}} = 1 - ER_{\text{hep}}^{\text{MDZ}} \quad (3.4)$$

Hepatic intrinsic clearance ($CL_{\text{int,hep}}^{\text{MDZ}}$), after f_u^{MDZ} correction, was estimated by equation (3.5), assuming that MDZ is in equilibrium between hepatocytes and venous outflow (well-stirred model):

$$f_u^{\text{MDZ}} \cdot CL_{\text{int,hep}}^{\text{MDZ}} = \frac{Q_{\text{hep}} \cdot CL_{\text{tot,b}}^{\text{MDZ}}}{Q_{\text{hep}} - CL_{\text{tot,b}}^{\text{MDZ}}} \quad (3.5)$$

After PO administration of MDZ, the oral bioavailability of MDZ ($F_{\text{oral}}^{\text{MDZ}}$) was estimated as follows, assuming dose-proportional PK:

$$F_{\text{oral}}^{\text{MDZ}} = \frac{AUC_{\text{IV}}^{\text{MDZ}} / \text{Dose}_{\text{IV}}^{\text{MDZ}}}{AUC_{\text{PO}}^{\text{MDZ}} / \text{Dose}_{\text{PO}}^{\text{MDZ}}} \quad (3.6)$$

The overall pre-systemic extraction ratio ($ER_{\text{presys}}^{\text{MDZ}}$) was determined by equation (3.7):

$$ER_{\text{presys}}^{\text{MDZ}} = 1 - F_{\text{oral}}^{\text{MDZ}} \quad (3.7)$$

Under the assumption that $CL_{\text{int,hep}}^{\text{MDZ}}$ and Q_{hep} remain the same for systemic and pre-systemic metabolism, the fraction of MDZ dose that reaches portal vein ($F_{\text{abs}}^{\text{MDZ}} \cdot F_{\text{GI}}^{\text{MDZ}}$) was calculated as follows:

$$F_{\text{abs}}^{\text{MDZ}} \cdot F_{\text{GI}}^{\text{MDZ}} = \frac{F_{\text{oral}}^{\text{MDZ}}}{F_{\text{hep}}^{\text{MDZ}}} = \frac{F_{\text{oral}}^{\text{MDZ}}}{1 - ER_{\text{hep}}^{\text{MDZ}}} \quad (3.8)$$

$F_{\text{abs}}^{\text{MDZ}}$ is the fraction of MDZ dose absorbed from gut lumen, and $F_{\text{GI}}^{\text{MDZ}}$ is the fraction of absorbed MDZ dose that reaches portal vein, escaping first-pass GI wall metabolism.

Based on the BCS class (Wu & Benet, 2005) and physicochemical properties (Andersin, 1991) of MDZ, MDZ is a BCS class 1 drug, ($F_{\text{abs}}^{\text{MDZ}} > 90\%$), with high solubility (soluble in 250 ml or less of aqueous media over a pH range of 1–7.5 at 37°C (Wu & Benet, 2005)) and high permeability (the extent of the absorption (parent drug plus metabolites) in humans is determined to be $\geq 90\%$ of an administered dose based on a mass balance determination or in comparison to

an intravenous reference dose (Wu & Benet, 2005)). Therefore, F_{abs}^{MDZ} is assumed to be 100%.

The pre-systemic gastrointestinal extraction ratio (ER_{GI}^{MDZ}) was then calculated by equation

(3.9):

$$ER_{GI}^{MDZ} = 1 - F_{GI}^{MDZ} \quad (3.9)$$

ER_{presys}^{MDZ} versus ER_{hep}^{MDZ} , ER_{GI}^{MDZ} versus ER_{hep}^{MDZ} and ER_{presys}^{MDZ} versus ER_{GI}^{MDZ} were plotted to compare the pre-systemic hepatic and intestinal CYP3A metabolism of MDZ. JMP Pro 9.0 (SAS, Cary, NC) was used to estimate the correlation coefficient between the two variables in each comparison pair, and if the correlation coefficient (r) was larger than 0.9, linear regression was conducted for the two variables.

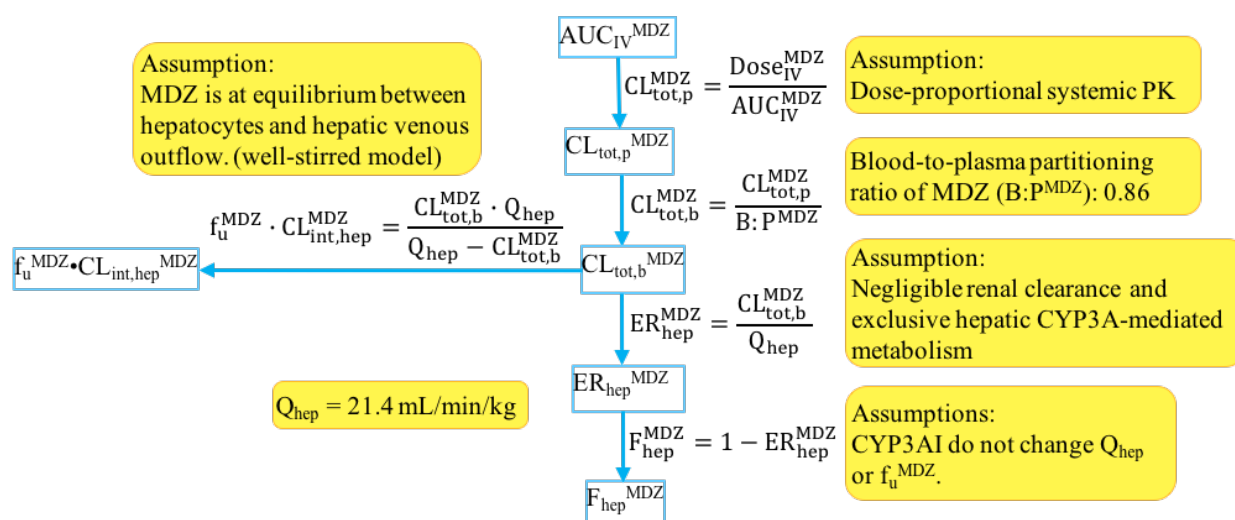


Figure 3.1 Equations and assumptions used in estimating secondary PK parameters for MDZ after IV administration.

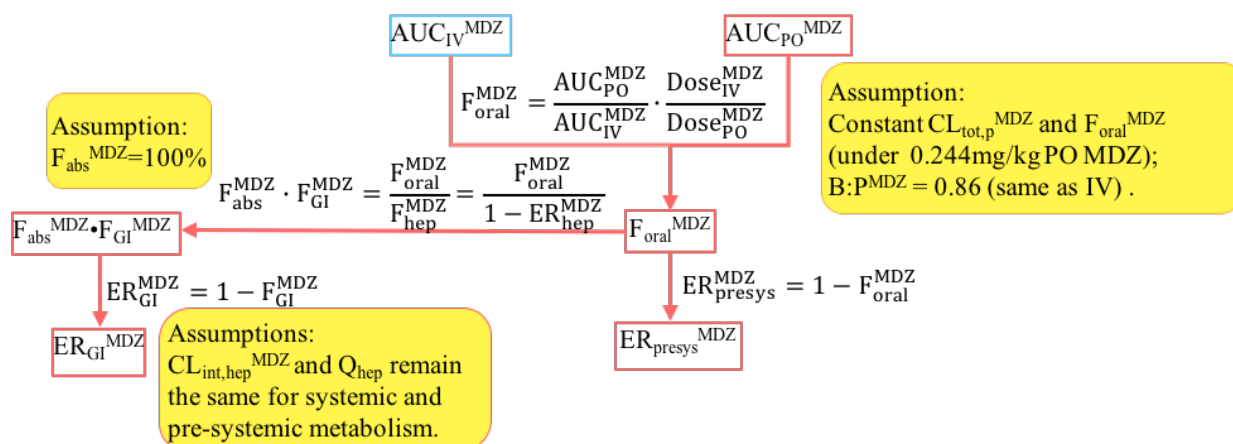


Figure 3.2 Equations and assumptions used in estimating secondary PK parameters for MDZ after PO administration.

3.2.3.2 1-hydroxy-midazolam (1'-OH-MDZ, metabolite)

Using the corresponding AUC^{met} information, F_{oral}^{met} (apparent oral bioavailability of 1'-OH-MDZ after PO MDZ) was estimated as follows:

$$F_{oral}^{met} = \frac{AUC_{PO}^{met}/Dose_{PO}^{MDZ}}{AUC_{IV}^{met}/Dose_{IV}^{MDZ}} \quad (3.10)$$

Combining equation (3.1), (3.6) and (3.10), we can obtain:

$$\frac{F_{oral}^{met}}{F_{oral}^{MDZ}} = \frac{MR_{PO}}{MR_{IV}} \quad (3.11)$$

MR_{IV} and MR_{PO} are the metabolic ratio after IV and PO MDZ, respectively. If F_{oral}^{met} is greater than F_{oral}^{MDZ} ($MR_{PO}/MR_{IV} > 1$), it indicates that formation of 1'-OH-MDZ also occurs pre-systemically.

AUC of 1'-OH-MDZ after IV MDZ (AUC_{IV}^{met}) can be estimated as follows:

$$AUC_{IV}^{met} = \frac{Dose_{IV}^{MDZ} \cdot (\frac{MW^{met}}{MW^{MDZ}}) \cdot f^{met}}{CL_{tot,p}^{met}} \quad (3.12)$$

f^{met} is the fraction of IV MDZ dose that converted to 1'-OH-MDZ, $CL_{tot,p}^{met}$ is the total plasma clearance of 1'-OH-MDZ after IV 1'-OH-MDZ.

Likewise, AUC^{met} after PO administration of MDZ that formed by systemic metabolism (AUC_{sys}^{met}) can be estimated as follows, under the major assumption that both f^{met} and $CL_{tot,p}^{met}$ remain the same after IV and PO routes of MDZ.

$$AUC_{sys}^{met} = \frac{Dose_{PO}^{MDZ} \cdot F_{oral}^{MDZ} \cdot \left(\frac{MW_{met}}{MW_{pc}}\right) \cdot f^{met}}{CL_{tot,p}^{met}} \quad (3.13)$$

Thus, AUC_{sys}^{met} can then be derived as

$$AUC_{sys}^{met} = AUC_{IV}^{met} \cdot \left(\frac{Dose_{PO}^{MDZ}}{Dose_{IV}^{MDZ}}\right) \cdot F_{oral}^{MDZ} \quad (3.14)$$

AUC^{met} formed pre-systemically (AUC_{presys}^{met}) can be estimated from AUC_{PO}^{met} as follows:

$$AUC_{presys}^{met} = AUC_{PO}^{met} - AUC_{sys}^{met} \quad (3.15)$$

To separate AUC^{met} formed pre-systemically by liver and GW, **Figure 3.3** and **Table 3.1** illustrates the estimation methods.

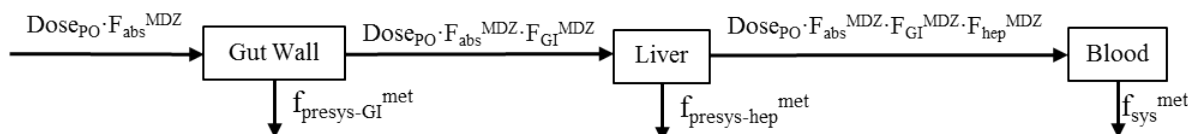


Figure 3.3 Scheme of MDZ pre-systemic metabolism.

$f_{presys-GI}^{met}$, $f_{presys-hep}^{met}$ and f_{sys}^{met} are corresponding f^{met} of pre-systemic GI metabolism, pre-systemic hepatic metabolism and systemic clearance.

Table 3.1 Composition of AUC_{PO}^{met} formed by pre-systemic GI/hepatic and systemic hepatic metabolism.

Composition	Fraction of PO MDZ dose left in the compartment	Fraction converted to 1'-OH-MDZ	AUC_{PO}^{met} of 1'-OH-MDZ formed
Gut lumen	$1 - F_{abs}^{MDZ}$	0	0
Pre-systemic GW	$1 - F_{GI}^{MDZ}$	$f_{presys-GI}^{met}$	$Dose \cdot F_{abs}^{MDZ} \cdot (1 - F_{GI}^{MDZ}) \cdot f_{presys-GI}^{met} / CL_{tot,p}^{met}$
Pre-systemic Liver	$F_{abs}^{MDZ} \cdot F_{GI}^{MDZ} \cdot (1 - F_{hep}^{MDZ})$	$f_{presys-hep}^{met}$	$Dose \cdot F_{abs}^{MDZ} \cdot F_{GI}^{MDZ} \cdot (1 - F_{hep}^{MDZ}) \cdot f_{presys-hep}^{met} / CL_{tot,p}^{met}$
Systemic Liver	$F_{abs}^{MDZ} \cdot F_{GI}^{MDZ} \cdot F_{hep}^{MDZ}$	f_{sys}^{met}	$Dose \cdot F_{abs}^{MDZ} \cdot F_{GI}^{MDZ} \cdot F_{hep}^{MDZ} \cdot f_{sys}^{met} / CL_{tot,p}^{met}$

$f_{\text{presys-GI}}^{\text{met}}$, $f_{\text{presys-hep}}^{\text{met}}$ and $f_{\text{sys}}^{\text{met}}$ are assumed to be the same, referred as f^{met} . $CL_{\text{tot,p}}^{\text{met}}$ is also presumed to be the same for pre-systemic GW metabolism, pre-systemic hepatic metabolism and systemic metabolism. However, it is likely that due to the different enzyme expression/activity (CYP3A or UGT) and/or different drug permeability into the liver and GW, f^{met} and/or $CL_{\text{tot,p}}^{\text{met}}$ for GW metabolism and pre-/systemic hepatic metabolism may be quite different.

Based on equations (3.12), (3.14) and **Table 3.1**, AUC^{met} after PO administration of MDZ that is formed by pre-systemic hepatic metabolism ($AUC_{\text{presys-hep}}^{\text{met}}$) was estimated as follows:

$$AUC_{\text{presys-hep}}^{\text{met}} = AUC_{\text{sys}}^{\text{met}} \cdot \frac{F_{\text{abs}}^{\text{MDZ}} \cdot F_{\text{GI}}^{\text{MDZ}} \cdot (1 - F_{\text{hep}}^{\text{MDZ}})}{F_{\text{oral}}^{\text{MDZ}}} \quad (3.15)$$

AUC^{met} after PO administration of MDZ that formed by pre-systemic GW metabolism ($AUC_{\text{presys-GI}}^{\text{met}}$) was estimated as equation (3.16):

$$AUC_{\text{presys-GI}}^{\text{met}} = AUC_{\text{presys}}^{\text{met}} - AUC_{\text{presys-hep}}^{\text{met}} \quad (3.16)$$

Furthermore, AUC^{met} after PO administration of MDZ that formed by hepatic (pre-systemic + systemic) metabolism ($AUC_{\text{hep}}^{\text{met}}$) can be estimated as follows:

$$AUC_{\text{hep}}^{\text{met}} = AUC_{\text{sys}}^{\text{met}} \cdot \frac{F_{\text{abs}}^{\text{MDZ}} \cdot F_{\text{GI}}^{\text{MDZ}}}{F_{\text{oral}}^{\text{MDZ}}} \quad (3.17)$$

Meanwhile, based on equation (3.1) and (3.12), MR_{IV} can be calculated as follows,

$$MR_{\text{IV}} = \frac{f^{\text{met}} \cdot CL_{\text{tot,p}}^{\text{MDZ}}}{CL_{\text{tot,p}}^{\text{met}}} \quad (3.18)$$

$AUC_{\text{presys}}^{\text{met}}$ versus $AUC_{\text{presys-hep}}^{\text{met}}$, $AUC_{\text{presys-GI}}^{\text{met}}$ versus $AUC_{\text{presys-hep}}^{\text{met}}$ and $AUC_{\text{presys}}^{\text{met}}$ versus $AUC_{\text{presys-hep}}^{\text{met}}$ were plotted to compare the pre-systemic hepatic and intestinal formation of 1'-OH-MDZ. The correlation coefficient between the two variables in each comparison pair was estimated by JMP Pro 9.0 (SAS, Cary, NC), and if the correlation coefficient (r) was larger than 0.9, linear regression was conducted for the two variables.

3.2.4 Estimation of inhibitory effect on hepatic and intestinal metabolism by CYP3AI

Secondary parameters in presence of inhibitors: $ER_{\text{hep}(i)}^{\text{MDZ}}$, $ER_{\text{GI}(i)}^{\text{MDZ}}$, $ER_{\text{presys}(i)}^{\text{MDZ}}$, $CL_{\text{int,hep}(i)}^{\text{MDZ}}$, $F_{\text{oral}(i)}^{\text{MDZ}}$, $F_{\text{GI}(i)}^{\text{MDZ}}$ and $F_{\text{hep}(i)}^{\text{MDZ}}$ were estimated by using the method in **Section 3.2.3.1**, assuming that Q_{hep} , f_u^{MDZ} and $F_{\text{abs}}^{\text{MDZ}}$ remain the same after co-administration of CYP3AI. $MR_{(i)}$, $F_{\text{oral}(i)}^{\text{met}}$, $AUC_{\text{sys}(i)}^{\text{met}}$, $AUC_{\text{presys}(i)}^{\text{met}}$, $AUC_{\text{presys-hep}(i)}^{\text{met}}$, $AUC_{\text{presys-GI}(i)}^{\text{met}}$ and $AUC_{\text{hep}(i)}^{\text{met}}$ were calculated by the method in **Section 3.2.3.2**, assuming fraction unbound of 1'-OH-MDZ (f_u^{met}) remains the same in the presence of CYP3AI. The subscript (i) refers to the corresponding parameter in the presence of CYP3AI. The ratios of $ER_{\text{hep}(i)}^{\text{MDZ}}$, $CL_{\text{int,hep}(i)}^{\text{MDZ}}$, $F_{\text{oral}(i)}^{\text{MDZ}}$, $F_{\text{GI}(i)}^{\text{MDZ}}$, $AUC_{(i)}^{\text{met}}$ and $MR_{(i)}$ over baseline values, in absence of inhibitor, (indicated as “inhibition ratio” for $ER_{\text{hep}}^{\text{MDZ}}$, $CL_{\text{int,hep}}^{\text{MDZ}}$, AUC^{met} and $MR_{(i)}$, and “relative change” for $F_{\text{oral}(i)}^{\text{MDZ}}$ and $F_{\text{GI}(i)}^{\text{MDZ}}$ were plotted against the baseline values. The correlation coefficient between the two variables was estimated by JMP Pro 9.0 (SAS, Cary, NC), and $p < 0.05$ was considered as significantly correlated.

3.2.5 Dose/concentration-dependent inhibition of FLZ

Dose/concentration-dependent inhibition on intestinal and hepatic MDZ metabolism was determined by the data from Kharasch *et al* (2005) (study 21) and Ahonen *et al* (1997) (study 103), both using FLZ as CYP3AI.

In study 21, twelve volunteers were enrolled in a randomized 4-way crossover study, separated by at least 2 weeks between each session. They received single dose of 0, 100, 200, or 400 mg PO FLZ, followed 2 hour later by 1mg IV MDZ; the next day, they received the same dose of FLZ, followed by 3 mg PO MDZ. Plasma concentrations of MDZ after IV and PO administration were both determined up to 8 h. $CL_{\text{int,hep}}^{\text{MDZ}}$, $ER_{\text{hep}}^{\text{MDZ}}$ and $ER_{\text{GI}}^{\text{MDZ}}$ were then calculated using the method in **Section 3.2.3.1** for control and FLZ treatment groups, and the

inhibition ratios of $CL_{int,hep}^{MDZ}$, ER_{hep}^{MDZ} and ER_{GI}^{MDZ} were plotted against FLZ exposure metrics (FLZ dose, $c_{max-lumen}^{FLZ}$, c_{max-GI}^{FLZ} and $c_{max,u-hep}^{FLZ}$).

$c_{max-lumen}^{FLZ}$ is the maximal concentration of FLZ in the gut lumen (apical side of GW). It was calculated as follows, assuming FLZ was dissolved in 250 ml aqueous media.

$$c_{max-lumen}^{FLZ} = \frac{Dose_{PO}^{FLZ}}{250} \quad (3.19)$$

c_{max-GI}^{FLZ} is the maximal concentration of FLZ in the enterocytes. It was calculated by equation (3.20) (FDA, 2012):

$$c_{max-GI}^{FLZ} = \frac{F_{abs}^{FLZ} \cdot k_a^{FLZ} \cdot Dose_{PO}^{FLZ}}{Q_{en}} \quad (3.20)$$

Q_{en} is the enterocyte blood flow, which is 4.3 mL/min/kg (FDA, 2012). F_{abs}^{FLZ} was assumed to be 100%, due to its BCS class 1 (Lindenberg et al., 2004; World Health Organization, 2005) property. A value of 1.28 h⁻¹ was used for FLZ absorption rate constant (k_a^{FLZ}) (Olkkola et al., 1996).

$c_{max,u-hep}^{FLZ}$ is the maximal FLZ concentration in the hepatocyte, which was calculated as follows (FDA, 2012),

$$c_{max,u-hep}^{FLZ} = f_u^{FLZ} \cdot \left(c_{max,u}^{FLZ} + k_a^{FLZ} \cdot F_{abs}^{FLZ} \cdot F_{GI}^{FLZ} \cdot \frac{Dose_{PO}^{FLZ}}{Q_{hep}} \right) \quad (3.21)$$

Q_{hep} was fixed at 21.4 mL/min/kg (Tsunoda et al., 1999), F_{abs}^{FLZ} and F_{GI}^{FLZ} were both assumed to be 100%. f_u^{FLZ} is 0.88, based on the experiment from Ripa *et al.* (1993) (K T Olkkola et al., 1996). $c_{max,u}^{FLZ}$ is the maximal unbound blood/plasma concentration of FLZ, which was calculated by equations (3.22) - (3.24) (Dhillon & Gill, (2006)), assuming FLZ follows 1-compartmental body model with first-order elimination (Humphrey et al., 1985):

$$c_{max,u}^{FLZ} = \frac{f_u^{FLZ} \cdot F_{oral}^{FLZ} \cdot Dose_{PO}^{FLZ} \cdot e^{-k_e^{FLZ} \cdot t_{max}^{FLZ}}}{Vd^{FLZ}} \quad (3.22)$$

$$t_{\max}^{\text{FLZ}} = \frac{\ln(k_a^{\text{FLZ}}) - \ln(k_e^{\text{FLZ}})}{k_a^{\text{FLZ}} - k_e^{\text{FLZ}}} \quad (3.23)$$

$$k_e^{\text{FLZ}} = \frac{0.693}{t_{1/2}^{\text{FLZ}}} \quad (3.24)$$

$F_{\text{oral}}^{\text{FLZ}}$ is assumed to be 100%, due to its high oral bioavailability (> 90%) (Ripa et al., 1993); $t_{1/2}^{\text{FLZ}}$ was set at 30 h; V_d^{FLZ} is 0.7 L/kg (Olkkola et al., 1996), and 70 kg was used for body weight. FLZ plasma concentration was assumed to be the same as blood concentration ($B:P^{\text{FLZ}} = 1.0$) (Ervin & Houston, 1994).

Nonlinear regression using a hyperbolic model ($y = \frac{1}{\frac{x}{x_{50}^{\text{FLZ}}} + 1}$) was performed for each relationship using Scientist v2.0 (Micromath®, MO) to estimate D_{50}^{FLZ} , $c_{\max\text{-lumen},50}^{\text{FLZ}}$, $c_{\max\text{-GI},50}^{\text{FLZ}}$ and $c_{\max,u\text{-hep},50}^{\text{FLZ}}$ (X represents dose, $c_{\max\text{-lumen}}^{\text{FLZ}}$, $c_{\max\text{-GI}}^{\text{FLZ}}$, $c_{\max\text{-hep}}^{\text{FLZ}}$, respectively), assuming the mechanism of inhibition of FLZ on MDZ is non-competitive inhibition (Gibbs et al., 1999) (reduce v_{\max} and has no effect on K_m of CYP3A), and the maximum inhibition on both hepatic and GI metabolism is 100%.

In study 103, a double-dummy, randomized, 3-way cross-over study was performed in 9 healthy volunteers. The subjects were given PO FLZ 400 mg and IV saline within 60 min; PO placebo and IV FLZ 400 mg; or PO placebo and IV saline. An oral dose of 7.5 mg midazolam was ingested 60 min after oral intake of FLZ or placebo (at the end of the corresponding infusion). Plasma concentrations of MDZ, 1'-OH-MDZ and FLZ were determined for up to 17 h. This study can be used to compare the inhibitory effect on intestinal and hepatic metabolism of IV and PO FLZ. However, MDZ was not administered intravenously in the study. In order to calculate $CL_{\text{int,hep}}^{\text{MDZ}}$, $ER_{\text{hep}}^{\text{MDZ}}$ and $ER_{\text{GI}}^{\text{MDZ}}$ for this study, the value for $ER_{\text{hep}}^{\text{MDZ}}$ from Palkama *et al.* (Palkama et al., 1999) was used, because these two studies ingested similar MDZ doses and achieved similar $AUC_{\text{PO}}^{\text{MDZ}}$ after PO MDZ in the control group. Therefore, subjects in these two

studies were likely to have similar CYP3A activity in the absence of CYP3AI. To estimate secondary parameters in presence of FLZ in study 103, inhibition ratio of $ER_{\text{hep}}^{\text{MDZ}}$ was assumed to be the same after PO FLZ as in study 21, due to the same PO FLZ dose administered in the two studies. Inhibition ratio of $ER_{\text{hep}}^{\text{MDZ}}$ after IV FLZ was predicted by the hyperbolic model between $ER_{\text{hep}(i)}^{\text{MDZ}}/ER_{\text{hep}}^{\text{MDZ}}$ and $c_{\text{max,u-hep}}^{\text{FLZ}}$, supposing that $c_{\text{max,u-hep}}^{\text{FLZ}}$ after IV FLZ was comparable with plasma $c_{\text{max,u}}^{\text{FLZ}}$, which was reported in study 103. $ER_{\text{GI}(i)}^{\text{MDZ}}$ as well as its inhibition ratio was calculated by method in **section 3.2.3.1**, and $c_{\text{max-GI}}^{\text{FLZ}}$ was predicted by the developed hyperbolic model ($ER_{\text{GI}(i)}^{\text{MDZ}}/ER_{\text{GI}}^{\text{MDZ}}$ vs. $c_{\text{max-GI}}^{\text{FLZ}}$) based on calculated $ER_{\text{GI}(i)}^{\text{MDZ}}/ER_{\text{GI}}^{\text{MDZ}}$.

3.3 Results and Discussion

3.3.1 Data collection

A total of 20 studies with 242 healthy volunteers were included in the final database, with 127 males and 91 females. Each study was assigned a study ID number. Gender information was not available for study 23 (Garg et al., 2012). Study 1 (Vieira et al., 2012), study 8 (Zhang et al., 2009), study 11 (Krishna et al., 2009), study 16 (Palkama et al., 1999), 17 (Tsunoda et al., 1999), study 18 (Gorski et al., 1998), study 20 (Kirby et al., 2011), study 21 (Kharasch et al., 2005), study 22 (Kharasch et al., 2004), study 23 (Garg et al., 2012), study 25 (Saari et al., 2006), study 26 (Olkkola et al., 1996), study 28 (Olkkola et al., 1993) and study 30 (Kupferschmidt et al., 1995) provided AUC^{MDZ} in the absence and presence of CYP3AI after IV and PO administration of MDZ. Studies 16 (Palkama et al., 1999), 25 (Saari et al., 2006) and 30 (Kupferschmidt et al., 1995) also provided AUC^{met} . Study 23 (Garg et al., 2012) provided only AUC^{met} after PO MDZ for the control and inhibitor treatment groups. Studies 201 (Mandema et al., 1992), 202

(Thummel et al., 1996), 203 (Fetzner et al., 2011) and 204 (Link et al., 2008) provided AUC^{MDZ} and AUC^{met} without CYP3AI after IV and PO MDZ. Study 103 (Ahonen et al., 1997) was included to compare the inhibitory effect on intestinal and hepatic metabolism of IV and PO CYP3AI, but only AUC^{MDZ} and AUC^{met} after PO MDZ for control and inhibitor (FLZ) treatment groups were given. Study 158 (Yang et al., 2012) was another study using PO FLZ as the CYP3AI, and provided AUC^{met} after MDZ IV route both in the absence and presence of FLZ.

IV doses of MDZ ranged from 0.005 mg/kg to 0.1 mg/kg, and PO doses ranged from 0.025 mg/kg to 0.244 mg/kg. Age ranged from 20 to 46 years, and body weight ranged from 56 to 100 kg, with four studies not providing that information. Studies 18 (Gorski et al., 1998) and 20 (Kirby et al., 2011) were both conducted in 16 volunteers: 1 Asian, 1 African Americans, and 14 Caucasians. We assume that the only Asian in both studies had no large influence on the mean AUC^{MDZ} and AUC^{met} of the whole study population, and kept these two studies in the final database. Study 158 performed in African Americans due to their higher rate of CYP3A5*1/*1 expression, but no major / clinically important differences in CYP3A activity is known to be present between African Americans and Caucasians (Wandel et al., 2000). All other studies were conducted in Caucasians, with 15 studies not providing ethnicity information. The CYP3AI used in these studies can be divided into five categories: antifungal azoles (ketoconazole, fluconazole, itraconazole, voriconazole, and posaconazole), macrolide antibiotic (telithromycin, clarithromycin, troleandomycin and erythromycin), HIV protease inhibitor (saquinavir, telaprevir, ritonavir, nelfinavir) and others (diltiazem and grapefruit juice). FLZ was administered by both IV and PO routes, while all other CYP3AI were only given by PO route. Other relevant PK, demographic, study design and sample analysis information for both MDZ and 1'-OH-MDZ was summarized in **Appendices A**.

3.3.2 PK dose-proportionality assessment

Figures 3.4 (a-c) illustrates the dose-proportionality of MDZ and 1'-OH-MDZ. The parameter estimates for the power model and their 95% CIs were summarized in **Table 3.2**. Power model fit MDZ and 1'-OH-MDZ exposure metrics well, with $r^2 > 0.8$; however, c_{\max} of metabolite is poorly characterized by the model, with a lower r^2 value and wider 95% CIs of the estimated exponent. Possible explanations could be small sample sizes, narrow dose range, and large variability with regard to the formation and elimination of 1'-OH-MDZ in the studies that reported c_{\max}^{met} . PO exposure metrics exhibits inferior fit than IV exposures, either because PO is a more complex process physiologically (i.e. involved with absorption and first-pass metabolism) than IV, or because PO studies have narrower dose range than IV studies. MDZ follows dose-proportional PK within the respective IV and PO dose ranges, however, 1'-OH-MDZ follows apparent infra-proportional PK after IV route of MDZ. The possible explanations might be presumably saturable plasma protein binding (increased $CL_{\text{tot,p}}^{\text{met}}$), or presumably saturable 1'-OH-MDZ formation, resulting in a metabolic switch to non-1'-OH-MDZ pathways (decrease in f^{met}). However, none of these explanations are consistent with the dose-proportional PK of 1'-OH-MDZ after PO route of MDZ. The mean MR_{IV} is 0.13 (range: 0.08-0.18), and mean of MR_{PO} is 0.39 (range: 0.29-0.52), suggesting that there is first-pass formation of metabolite during absorption process. MR is not significantly different among doses, and the AUC^{met} vs. AUC^{MDZ} relationship is well fit by a linear model (**Figure 3.4c**), both of which indicate dose-proportional PK of 1'-OH-MDZ pathway. Therefore, the infra-proportional PK for $AUC_{\text{IV}}^{\text{met}}$ vs. $\text{Dose}_{\text{IV}}^{\text{MDZ}}$ is likely to be an artifact, due to large inter-study variability (e.g. subjects in study 201 had higher $CL_{\text{tot,p}}^{\text{MDZ}}$ than other studies). Overall, both MDZ and 1'-OH-MDZ follow dose-proportional PK across the IV MDZ doses ranging from 0.005 mg/kg - 0.1 mg/kg, and PO doses ranging from

0.025 mg/kg to 0.244 mg/kg. This allows the use and interpretation of the secondary PK parameters.

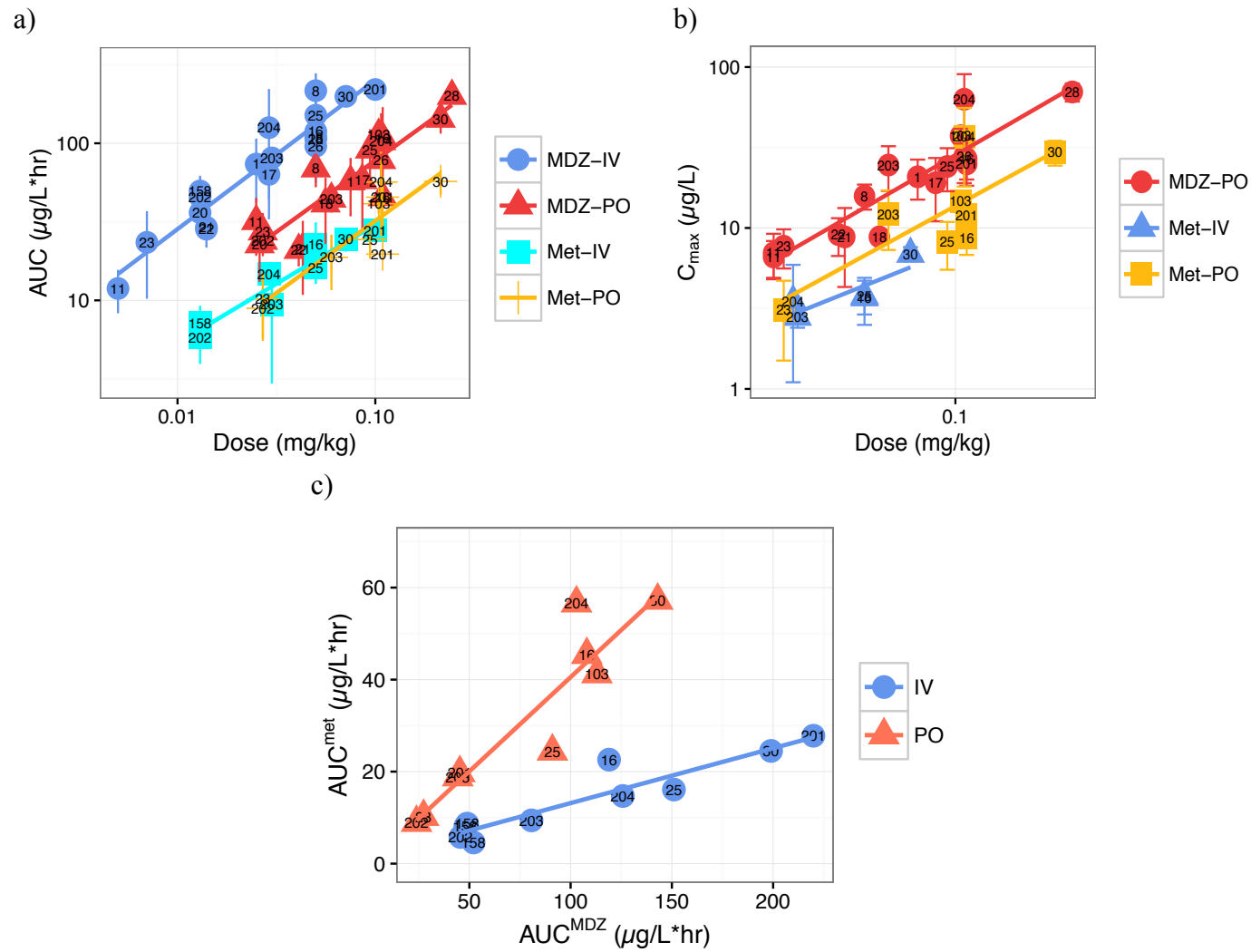


Figure 3.4 Dose proportionality assessment.

The colored lines represent fits by power (a-b) or linear model (c), and symbols represent the observed values. Values are expressed as mean \pm SD. The number inside each point is the study ID.

Table 3.2 Summary of power model fit of exposure metrics vs dose plots.

No. of studies (n)	Dependent Variable	Independent variable	Dose range (mg/kg)	Power coefficient	95% CI of power	Intercept	r ²
19	AUC _{IV} ^{MDZ}	Dose _{IV} ^{MDZ}	0.005-0.100	0.95	0.80, 1.10	3.35	0.904
19	AUC _{PO} ^{MDZ}	Dose _{PO} ^{MDZ}	0.025-0.244	0.91	0.70, 1.13	2.80	0.806
8	AUC _{IV} ^{met}	Dose _{IV} ^{MDZ}	0.013-0.100	0.76	0.59, 0.95	2.24	0.913
9	AUC _{PO} ^{met}	Dose _{PO} ^{MDZ}	0.027-0.214	0.92	0.58, 1.26	2.42	0.805
17	C _{max-PO} ^{MDZ}	Dose _{PO} ^{MDZ}	0.025-0.244	1.08	0.84, 1.32	2.54	0.847
5	C _{max-IV} ^{met}	Dose _{IV} ^{MDZ}	0.029-0.071	0.75	0.22, 1.28	1.62	0.726
8	C _{max-PO} ^{met}	Dose _{PO} ^{MDZ}	0.027-0.214	1.02	0.37, 1.67	2.16	0.623

After dose-proportional PK was ascertained, linear regression was then performed for AUC_{IV}^{MDZ} vs Dose_{IV}^{MDZ}, AUC_{PO}^{MDZ} vs Dose_{PO}^{MDZ}, AUC_{IV}^{met} vs Dose_{IV}^{met}, AUC_{PO}^{met} vs Dose_{PO}^{met}, AUC_{IV}^{met} vs AUC_{IV}^{MDZ} and AUC_{PO}^{met} vs AUC_{PO}^{MDZ} plots, and the respective slopes (summarized in **Table 3.3**) can translate into important secondary PK parameters, namely CL_{tot,p}^{MDZ}, F_{oral}^{MDZ}, etc. Across studies, CL_{tot,p}^{MDZ} is estimated as 7.04 ml/min/kg, which is far less than liver blood flow (21.4 ml/min/kg), suggesting liver blood flow doesn't limit the metabolism of MDZ in the liver. F_{oral}^{MDZ} is estimated as 31.6% from CL_{tot,p}^{MDZ} and CL_{tot,p}^{MDZ}/F_{oral}^{MDZ}. However as for 1'-OH-MDZ, CL_{tot,p}^{met}/f^{met} is larger than CL_{tot,p}^{met}/(f^{met}·F_{oral}^{MDZ}), implicating F_{oral}^{MDZ} larger than 1, which is not possible. The reason might be poor goodness of fit of AUC_{IV}^{met} vs Dose_{IV}^{MDZ} and AUC_{PO}^{met} vs Dose_{PO}^{MDZ} plots, reflected by large 95% CIs of estimated slopes.

Another way to estimate CL_{tot,p}^{MDZ}, CL_{tot,p}^{MDZ}/F_{oral}^{MDZ}, CL_{tot,p}^{met}/f^{met} and CL_{tot,p}^{met}/(f^{met}·F_{oral}^{MDZ}) is to calculate weighted mean and SD across studies, with sample size used as weighting factor for each study (presented in **Table 3.3**). Weighted mean values for CL_{tot,p}^{MDZ}, CL_{tot,p}^{MDZ}/F_{oral}^{MDZ}, MR_{IV}, MR_{PO} estimations are close to the slopes, whereas mean CL_{tot,p}^{met}/f^{met} and CL_{tot,p}^{met}/(f^{met}·F_{oral}^{MDZ}) are less than their slope estimates, suggesting that some studies with higher CL_{tot,p}^{met}/f^{met} and CL_{tot,p}^{met}/(f^{met}·F_{oral}^{MDZ}) might have small sample size, and

bias the slope estimates. Conjugated 1'-OH-MDZ in urine accounts for ~70%^{20,25} of PO MDZ, and 69.3%²⁰ after IV MDZ. If we assume a constant f^{met} of 70% in all the studies, $CL_{\text{tot,p}}^{\text{met}}$ should be 24.6 mL/min/kg, which is very close to Q_{hep} (21.4mL/min/kg (Tsunoda et al., 1999)), indicating that Q_{hep} may be the rate-limiting step for the elimination of metabolite, and 1'-OH-MDZ is a very high ER_{hep} drug by itself. F_{oral} of MDZ is estimated as 68.9% from $CL_{\text{tot,p}}^{\text{met}}/f^{\text{met}}$ and $CL_{\text{tot,p}}^{\text{met}}/(f^{\text{met}} \cdot F_{\text{oral}}^{\text{MDZ}})$, which is much higher than that estimated from $CL_{\text{tot,p}}^{\text{MDZ}}$ and $CL_{\text{tot,p}}^{\text{MDZ}}/F_{\text{oral}}^{\text{MDZ}}$. This is more likely due to the large inter-study variability of $CL_{\text{tot,p}}^{\text{met}}$, f^{met} and/or $F_{\text{oral}}^{\text{MDZ}}$, although different $CL_{\text{tot,p}}^{\text{met}}$ and/or f^{met} after IV or PO MDZ may also explain this. MR_{PO} is significantly larger than MR_{IV} ($p < 0.0001$), implying that more 1'-OH-MDZ is formed pre-systemically than systemically.

Table 3.3 Summary of linear regression of exposure metric vs dose plots.

No. of studies (n)	Dependent Variable	Independent variable	Slope (units)	Unit corrected slope	95% CI of slope	Intercept	r ²	Weighted Mean (SD)
19	$AUC_{\text{IV}}^{\text{MDZ}}$	$Dose_{\text{IV}}^{\text{MDZ}}$	$CL_{\text{tot,p}}^{\text{MDZ}}$ (mL/min/kg)	7.04	5.71, 9.20	11.4	0.811	6.1 (1.5)
19	$AUC_{\text{PO}}^{\text{MDZ}}$	$Dose_{\text{PO}}^{\text{MDZ}}$	$CL_{\text{tot,p}}^{\text{MDZ}}/F_{\text{oral}}^{\text{MDZ}}$ (mL/min/kg)	22.3	18.7, 27.7	5.37	0.862	21.0 (7.2)
8	$AUC_{\text{IV}}^{\text{met}}$	$Dose_{\text{IV}}^{\text{MDZ}}$	$CL_{\text{tot,p}}^{\text{met}}/f^{\text{met}}$ (mL/min/kg)	64.1	49.3, 91.8	4.45	0.880	35.2 (10.3)
9	$AUC_{\text{PO}}^{\text{met}}$	$Dose_{\text{PO}}^{\text{MDZ}}$	$CL_{\text{tot,p}}^{\text{met}}/(f^{\text{met}} \cdot F_{\text{oral}}^{\text{MDZ}})$ (mL/min/kg)	60.8	39.3, 134.8	5.49	0.654	51.1 (18.0)
8	$AUC_{\text{IV}}^{\text{met}}$	$AUC_{\text{IV}}^{\text{MDZ}}$	MR_{IV}	0.12	0.09, 0.15	1.23	0.872	0.10 (0.02)
9	$AUC_{\text{PO}}^{\text{met}}$	$AUC_{\text{PO}}^{\text{MDZ}}$	MR_{PO}	0.41	0.28, 0.54	-0.42	0.860	0.38 (0.06)

3.3.3 Estimation of PK exposure metrics and parameters in absence of CYP3AI

3.3.3.1 MDZ (parent compound)

Figure 3.5a shows that in absence of CYP3AI, MDZ is a low to intermediate $ER_{\text{hep}}^{\text{MDZ}}$ drug (21%-47%). $ER_{\text{presys}}^{\text{MDZ}}$ has wider range (41%-78%) than $ER_{\text{hep}}^{\text{MDZ}}$, and consistently exceeds $ER_{\text{hep}}^{\text{MDZ}}$ (except one arm in study 11(Krishna et al., 2009)), suggesting the presence of intestinal

metabolism of MDZ. There is no correlation between these variables, indicating high inter-study variability of the intestinal metabolism, which is independent of the variability in hepatic metabolism. Study 11 was performed in 12 healthy volunteers, with 6 subjects in each arm. No extraordinary study design or demographic information could be found; and therefore, the absence of GW metabolism in arm 1 might be caused by some factors that were not mentioned in the study, such as dietary habits, or genetic polymorphism of CYP3A.

ER_{GI}^{MDZ} has a much wider range (0%-73%) than ER_{hep} , and there is no correlation between these two variables (**Figure 3.5b**), confirming the fact that intestinal and hepatic CYP3A metabolism are independently regulated (Tsunoda et al., 1999). The reasons for the higher inter-study variability of intestinal than hepatic metabolism may be due to different dietary habits across study (Won et al. 2013). The mean ER_{GI}^{MDZ} estimate (51%) is much greater than the mean ER_{hep}^{MDZ} value (32%), indicating larger intestinal first-pass than hepatic first pass metabolism of MDZ on average.

In **Figure 3.5c**, the relationship between ER_{presys}^{MDZ} and ER_{GI}^{MDZ} is fit well by a linear model ($r^2 = 0.91$). Therefore, 91% of the variability in ER_{presys}^{MDZ} can be explained by the variability of ER_{GI}^{MDZ} , in other words, the higher range of ER_{presys}^{MDZ} is primarily due to the high variability of intestinal metabolism of MDZ, rather than hepatic metabolism.

Descriptive statistics of important PK parameters (ER_{hep}^{MDZ} , $CL_{int,hep}^{MDZ}$, F_{oral}^{MDZ} , ER_{GI}^{MDZ}) are summarized in **Table 3.4**

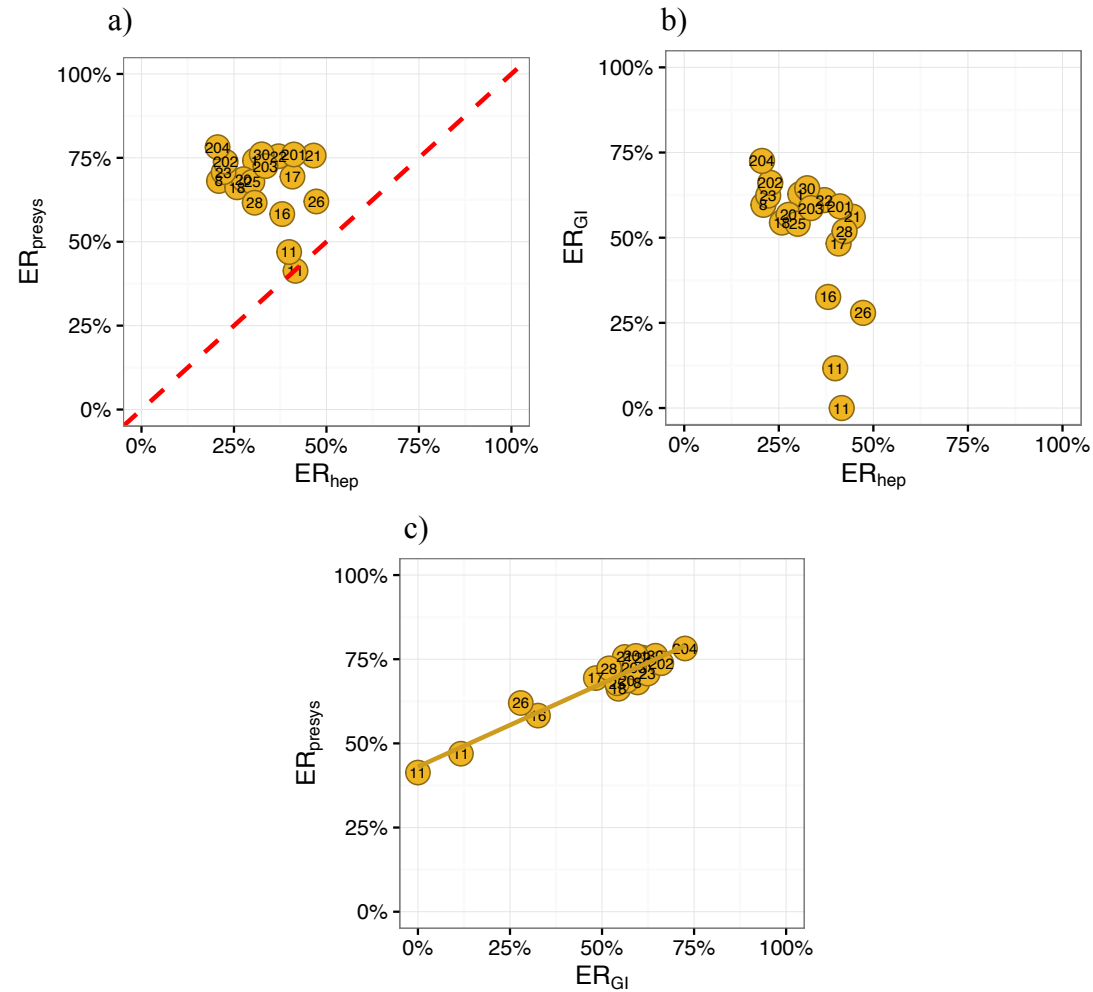


Figure 3.5 Comparison of pre-systemic hepatic and GI metabolism of MDZ in absence of CYP3A1.

a) Relationship between ER_{presys}^{MDZ} and ER_{hep}^{MDZ} . b) Relationship between ER_{GI}^{MDZ} and ER_{hep}^{MDZ} . c) Relationship between ER_{presys}^{MDZ} and ER_{GI}^{MDZ} . The red dashed line in **Figure 3.5a** is the line of identity. The yellow solid line in **Figure 3.5c** is the linear model fit for the data ($y = 0.49x + 0.43$, $r^2 = 0.91$). The number inside each point is study ID.

Table 3.4 Descriptive statistics of important PK endpoints in absence of CYP3AI across studies.

Endpoints	No. of Studies	Mean	SD	Minimum	Median	Maximum
$ER_{\text{hep}}^{\text{MDZ}}$	19	33%	9%	21%	33%	47%
$CL_{\text{int,hep}}^{\text{MDZ}}$ (ml/min)	19	10.8	4.3	4.6	9.9	19.2
$F_{\text{oral}}^{\text{MDZ}}$	18	32%	10%	22%	29%	59%
$ER_{\text{GI}}^{\text{MDZ}}$	18	51%	19%	0%	57%	73%

3.3.3.2 1'-OH-MDZ (metabolite)

All the secondary parameter estimates using AUC^{met} are presented in **Table 3.5**. $F_{\text{oral}}^{\text{met}}$ in all the studies are 2-3 fold higher than $F_{\text{oral}}^{\text{MDZ}}$, indicating that 1'-OH-MDZ formed pre-systemically exceeds that formed systemically. **Figure 3.6a** demonstrates that $AUC_{\text{presys-hep}}^{\text{met}}$ in all studies are less than the corresponding $AUC_{\text{presys}}^{\text{met}}$, confirming that 1'-OH-MDZ is also formed by intestinal metabolism. These two terms are not correlated with each other. **Figure 3.6b** also illustrates the independently regulated formation of 1'-OH-MDZ by hepatic and intestinal CYP3A metabolisms, and 1'-OH-MDZ formed by GW metabolism exceeds that formed by pre-systemic hepatic metabolism. In **Figure 3.6c**, all the points are close to the line of identity, suggesting that most 1'-OH-MDZ is formed by GW instead of the liver pre-systemically. Linear regression characterizes the relationship well ($r^2 = 0.96$); thus, 96% of the change in $AUC_{\text{presys}}^{\text{met}}$ is due to the change in $AUC_{\text{presys-GI}}^{\text{met}}$.

All the conclusions obtained from the metabolite estimations agree well with the conclusions from MDZ estimations. However, all of them are based on an important assumption that $f_{\text{presys-GI}}^{\text{met}}$, $f_{\text{presys-hep}}^{\text{met}}$ and $f_{\text{sys-hep}}^{\text{met}}$ are the same, indicated as f^{met} .

Table 3.5 Exposure metrics and PK parameter estimates of 1'-OH-MDZ in absence of CYP3A1.

Study ID	F _{oral} ^{met}	F _{oral} ^{MDZ}	AUC _{PO} ^{met} [µg/L*hrs]	MR _{PO}	AUC _{sys} ^{met} [µg/L*hrs]	AUC _{presys} ^{met} [µg/L*hrs]	AUC _{presys-hep} ^{met} [µg/L*hrs]	AUC _{presys-GI} ^{met} [µg/L*hrs]	AUC _{hep} ^{met} [µg/L*hrs]
16	92%	42%	45.4	0.40	20.5	24.8	9.7	15.2	30.2
25	81%	32%	24.4	0.29	9.7	14.7	3.3	11.4	13.0
30	78%	24%	57.2	0.40	17.6	39.6	6.6	33.0	24.2
201	65%	24%	19.7	0.41	7.3	12.4	3.9	8.6	11.1
202	77%	26%	8.9	0.36	3.0	5.9	0.9	5.0	3.9
203	100%	27%	18.8	0.41	5.2	13.7	2.0	11.6	7.2
204	103%	22%	56.6	0.52	12.0	44.6	2.5	42.1	14.5

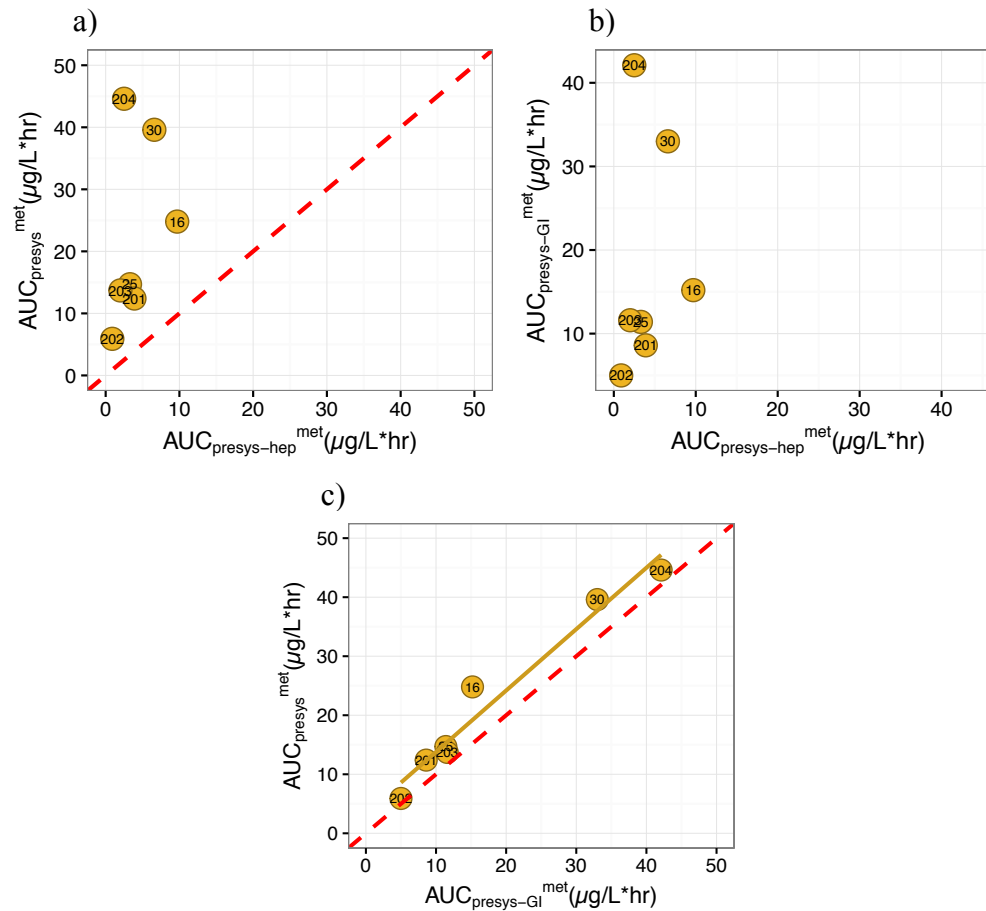


Figure 3.6 Comparison of pre-systemic hepatic and intestinal formation of 1'-OH-MDZ.

a) Relationship between AUC_{presys}^{met} and $AUC_{presys-hep}^{met}$. b) Relationship between $AUC_{presys-GI}^{met}$ and $AUC_{presys-hep}^{met}$. c) Relationship between AUC_{presys}^{met} and $AUC_{presys-GI}^{met}$. The red dash lines in **Figure 3.6a** and **3.6c** are the line of identity. The yellow solid line in **Figure 3.6c** is the linear model fit for the data ($y = 1.04x + 3.39$, $r^2 = 0.96$). The number inside each point is the study ID.

3.3.4 Estimation of inhibitory effect on hepatic and intestinal metabolism of CYP3AI

3.3.4.1 MDZ (parent compound)

To investigate the inhibitory effect on systemic MDZ metabolism, $ER_{\text{hep}}^{\text{MDZ}}$ and $CL_{\text{int,hep}}^{\text{MDZ}}$ in presence of CYP3AI are plotted against baseline $ER_{\text{hep}}^{\text{MDZ}}$ and $CL_{\text{int,hep}}^{\text{MDZ}}$ respectively in **Figure 3.7a-b**. Inhibitors consistently reduce hepatic metabolism of MDZ in all the studies, resulting in reduction in $ER_{\text{hep}}^{\text{MDZ}}$ and $CL_{\text{int,hep}}^{\text{MDZ}}$ by between 4% and 96%. Study 30 (Kupferschmidt et al., 1995) only has 4% reduction in $ER_{\text{hep}}^{\text{MDZ}}$, because the inhibitor used was PO grapefruit juice (GFJ), which is a selective intestinal CYP3AI (Kupferschmidt et al., 1995). PO GFJ is also a known P-gp substrate, making it difficult to reach the liver and affect hepatic metabolism. $ER_{\text{hep}}^{\text{MDZ}}$ and $CL_{\text{int,hep}}^{\text{MDZ}}$ in presence of inhibitors are not correlated with their corresponding values without inhibitor, probably because the inhibitors used in the various studies have different potency, mechanism of inhibition and dosing regimen, leading to large inter-study variability.

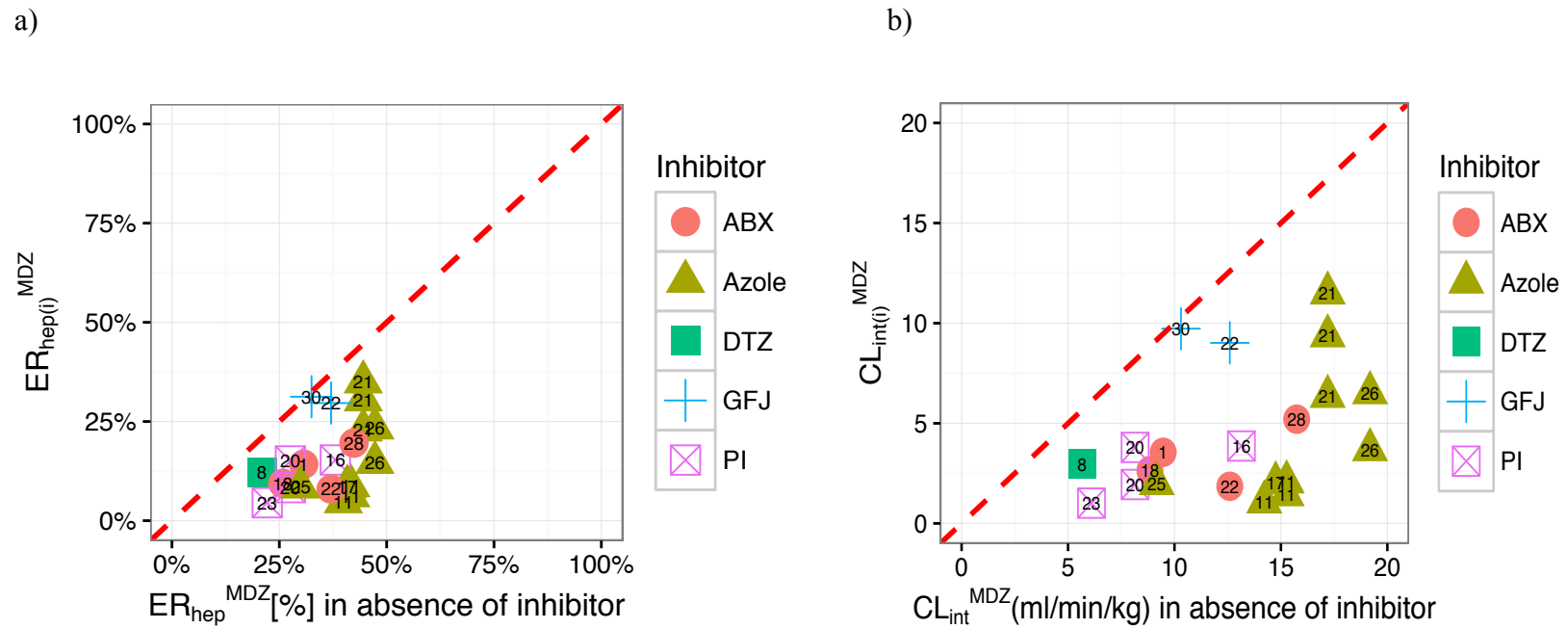


Figure 3.7 Evaluation of hepatic inhibitory effect of CYP3A1.

a) Relationship between $ER_{hep(i)}^{MDZ}$ and baseline ER_{hep}^{MDZ} . b) Relationship between $CL_{int,hep(i)}^{MDZ}$ and baseline $CL_{int,hep}^{MDZ}$. The red dashed lines are the lines of identity. The number inside each point is the study ID.

Relative change in F_{GI}^{MDZ} and F_{oral}^{MDZ} were then plotted against baseline F_{GI}^{MDZ} and F_{oral}^{MDZ} , to assess the inhibitory effect on intestinal metabolism as well as overall pre-systemic extraction. Inhibitors consistently decreased intestinal metabolism in most studies (except study 11), leading to an increase of F_{GI}^{MDZ} by 38% to 132%, as well as an increase in F_{oral}^{MDZ} by 46% to 248%. The degree of increase in F_{GI}^{MDZ} or F_{oral}^{MDZ} is negatively correlated with F_{GI}^{MDZ} ($r = -0.83$, $n = 21$, $p < 0.0001$, **Figure 3.8a**) or F_{oral}^{MDZ} ($r = -0.64$, $n = 21$, $p = 0.0011$, **Figure 3.8b**) without CYP3AI, respectively; thus, subjects with lower baseline F_{GI}^{MDZ} (and lower F_{oral}^{MDZ}) are more sensitive to CYP3A inhibition, and CYP3AI can decrease the inter-study variability of intestinal bioavailability and overall oral bioavailability.

Study 11 is an outlier, suggesting a slight induction in GW metabolism. This might be owing to two reasons: subjects in study 11 had higher F_{oral}^{MDZ} (59%) in the control group, thus CYP3AI may have fewer enzymes to act on. Furthermore, the CYP3AI (400 mg QD ketoconazole and 200 mg/400 mg BID posaconazole) were administered for 7 days, which may have started to induce CYP3A enzyme. Other outliers such as study 21 (100 mg PO FLZ), 22 (single dose PO GFJ) and 30 (double dose PO GFJ) had low F_{oral}^{MDZ} values in their control groups, but were also less sensitive to their corresponding inhibitors. This is likely because - besides CYP3A activity in the control group - the inhibitory effect is also determined by potency, mechanism of action and dosing regimen of the inhibitors. Studies 22 and 30 used less potent CYP3A inhibitor (GFJ), and study 21 used a moderate CYP3A inhibitor (FLZ) with a low single dose, which may make them appear as outliers.

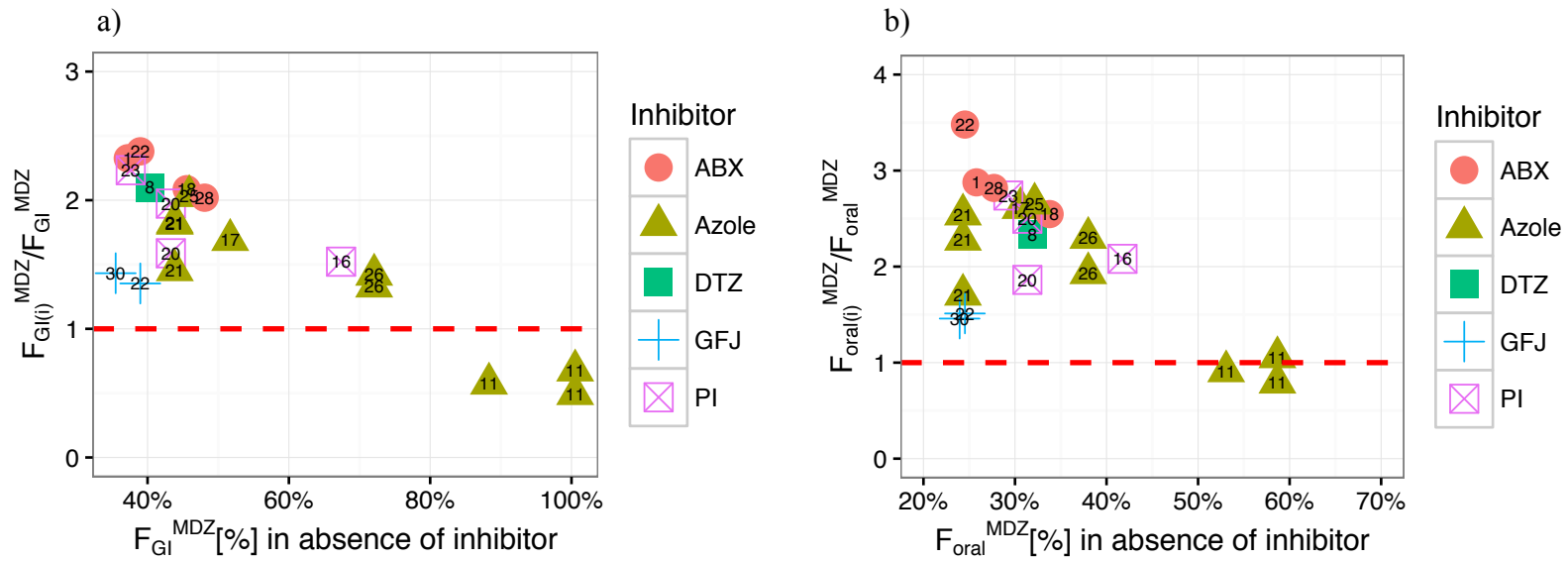


Figure 3.8 Evaluation of intestinal/overall pre-systemic inhibitory effect of CYP3A1.

a) Relationship between $F_{GI(i)}^{MDZ}$ and baseline F_{GI}^{MDZ} . b) Relationship between $F_{oral(i)}^{MDZ}$ and baseline F_{oral}^{MDZ} . The red dashed lines are horizontal lines with intercept of 1. The number inside each point is the study ID.

Relative change in $F_{\text{oral}}^{\text{MDZ}}$ is plotted against relative change in $F_{\text{GI}}^{\text{MDZ}}$ in **Figure 3.9a**, to assess the contribution of GW metabolism inhibition to the overall pre-systemic inhibition. The reason to use $F_{\text{oral}}^{\text{MDZ}}$ and $F_{\text{GI}}^{\text{MDZ}}$, instead of $ER_{\text{presys}}^{\text{MDZ}}$ and $ER_{\text{GI}}^{\text{MDZ}}$ is that the estimation process of $F_{\text{oral}}^{\text{MDZ}}$ and $F_{\text{GI}}^{\text{MDZ}}$ includes fewer assumptions than $ER_{\text{presys}}^{\text{MDZ}}$ and $ER_{\text{GI}}^{\text{MDZ}}$ (**section 3.2.3.1**), thus it is more accurate to use the two bioavailability terms, instead of extraction ratios. The relationship between increase in $F_{\text{oral}}^{\text{MDZ}}$ and increase in $F_{\text{GI}}^{\text{MDZ}}$ can be fit well by a linear model ($y = 1.21x + 0.17$, $r^2 = 0.87$), suggesting that the variability of increase in $F_{\text{oral}}^{\text{MDZ}}$ can mainly be explained by the increase in $F_{\text{GI}}^{\text{MDZ}}$, and the average increase in $F_{\text{hep}}^{\text{MDZ}}$ is 21%, as is indicated by the slope.

After excluding study 11, the change in $ER_{\text{GI}}^{\text{MDZ}}$ is positively correlated with the change in $ER_{\text{hep}}^{\text{MDZ}}$ ($r = 0.78$, $n = 18$, $p < 0.0001$, **Figure 3.9b**), illustrating that inhibitory effect on hepatic and intestinal metabolism of a specific CYP3AI are highly associated, regardless of its potency, mechanism of inhibition and dosing regimen.

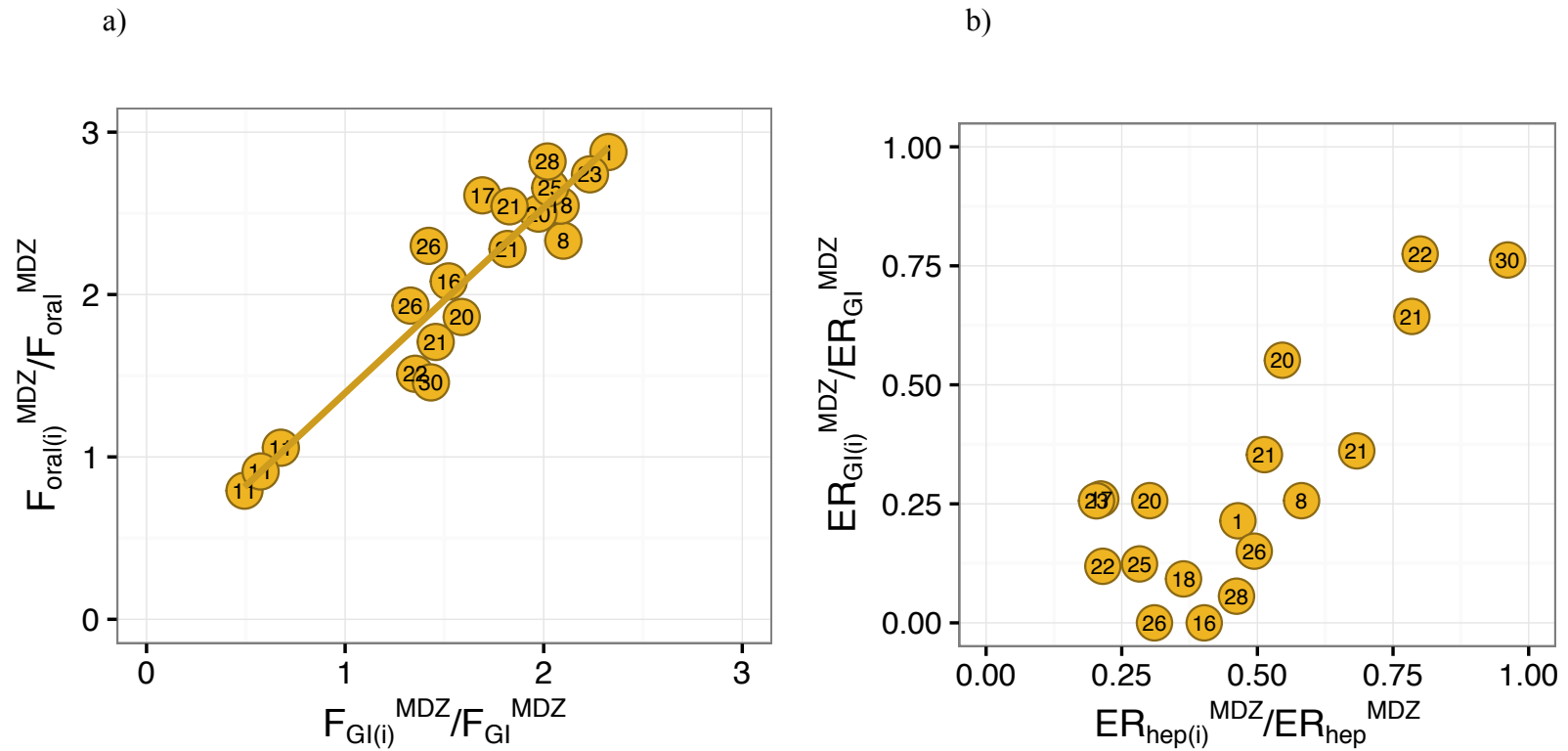


Figure 3.9 Evaluation of inhibitory effect of CYP3A1.

a) Relationship between relative change in $F_{\text{oral}(i)}^{\text{MDZ}}$ and $F_{\text{GI}(i)}^{\text{MDZ}}$. b) Relationship between inhibitory ratio of $ER_{\text{GI}(i)}^{\text{MDZ}}$ and $ER_{\text{hep}(i)}^{\text{MDZ}}$. The yellow solid line in **Figure 3.9a** is the linear model fit the the data. The number inside each point is the study ID.

3.3.4.2 1'-OH-MDZ (metabolite)

All the estimates by using $AUC_{(i)}^{met}$ are exhibited in **Table 3.6**. $F_{oral(i)}^{met}$ in study 16 (Palkama et al., 1999) (voriconazole was used as the CYP3AI) is the same as $F_{oral(i)}^{MDZ}$, indicating no 1'-OH-MDZ formed by pre-systemic metabolism in this study. However, ER_{presys}^{MDZ} in presence of voriconazole is 13%, suggesting that other pre-systemic pathways, like 4-OH-MDZ or 1,4-dihydroxymidazolam, might contribute to the first-pass metabolism in study 16. In study 25 and 30, $F_{oral(i)}^{met}$ are greater than $F_{oral(i)}^{MDZ}$, suggesting that 1'-OH-MDZ can be formed pre-systemically in this two studies.

Table 3.6 Exposure metrics and PK parameter estimates of 1'-OH-MDZ in presence of CYP3AI.

Study ID	$F_{oral(i)}^{met}$	$F_{oral(i)}^{MDZ}$	$AUC_{PO(i)}^{met}$ [$\mu\text{g/L*hrs}$]	$MR_{PO(i)}$	$AUC_{sys(i)}^{met}$ [$\mu\text{g/L*hrs}$]	$AUC_{presys(i)}^{met}$ [$\mu\text{g/L*hrs}$]	$AUC_{presys-hep(i)}^{met}$ [$\mu\text{g/L*hrs}$]	$AUC_{presys-GI(i)}^{met}$ [$\mu\text{g/L*hrs}$]	$AUC_{hep(i)}^{met}$ [$\mu\text{g/L*hrs}$]
16	0.87	87%	44.7	0.08	44.7	0.00			44.7
25	1.20	85%	60.8	0.07	43.2	17.6	3.33	14.2	46.6
30	0.95	35%	74.6	0.32	27.4	47.2	9.78	37.5	37.1

Inhibition ratio of AUC^{met} is plotted against AUC^{met} without inhibitor after IV and PO routes of MDZ in **Figure 3.10a**. In the presence of CYP3AI, AUC_{IV}^{met} in all the studies were higher than the control group; while AUC_{PO}^{met} change differently across studies. When MDZ is administered intravenously, AUC_{IV}^{met} can be estimated by equation 3.12:

$$AUC_{IV}^{met} = \frac{Dose_{IV}^{MDZ} \cdot \left(\frac{MW^{met}}{MW^{MDZ}}\right) \cdot f^{met}}{CL_{tot,p}^{met}}$$

In the presence of CYP3AI, assuming inhibitor has no inhibitory effect on $CL_{tot,p}^{met}$,

$$AUC_{IV(i)}^{met} = \frac{Dose_{IV}^{MDZ} \cdot \left(\frac{MW^{met}}{MW^{MDZ}}\right) \cdot f_{(i)}^{met}}{CL_{tot,p}^{met}} \quad (3.25)$$

In all the studies, $AUC_{IV(i)}^{met}$ were greater than AUC_{IV}^{met} , translating into an increase $f_{(i)}^{met}$ after IV MDZ, which could not be explained with current assumptions. Hence $CL_{tot,p}^{met}$ might also be affected by CYP3AI. Nevertheless 1'-OH-MDZ is primarily cleared by glucuronidation, which is unlikely to be inhibited by the inhibitors used in these studies. More investigation is required to explore the underlying reasons of this finding.

The change in AUC_{PO}^{met} is the combined effect on F_{oral}^{MDZ} , f_{PO}^{met} and $CL_{tot,p}^{met}$ by CYP3AI. Only two studies (study 25 and 30) provided both AUC^{met} information after IV and PO administration of MDZ; thus, it is hard to draw valid conclusions regarding inhibitors' effect on F_{oral}^{MDZ} , f_{PO}^{met} and $CL_{tot,p}^{met}$.

According to **Figure 3.10b**, the fold change in AUC^{MDZ} is consistently larger than fold change in AUC^{met} after both IV and PO MDZ, which implies that MR declines after co-administration with inhibitors. By the same token, the change in MR is an integrated outcome of the changes in f^{met} , $CL_{tot,p}^{MDZ}$ and $CL_{tot,p}^{met}$, and more evidence is required to evaluate inhibitors' effect on the three terms. Only three studies (study 16, 25, 30) are available to calculate all the derived AUC^{met} , including study 30 which used GFJ, a less potent inhibitor. Hence it is difficult to explore any correlation between AUC^{met} in presence of CYP3AI and AUC^{met} in the control groups.

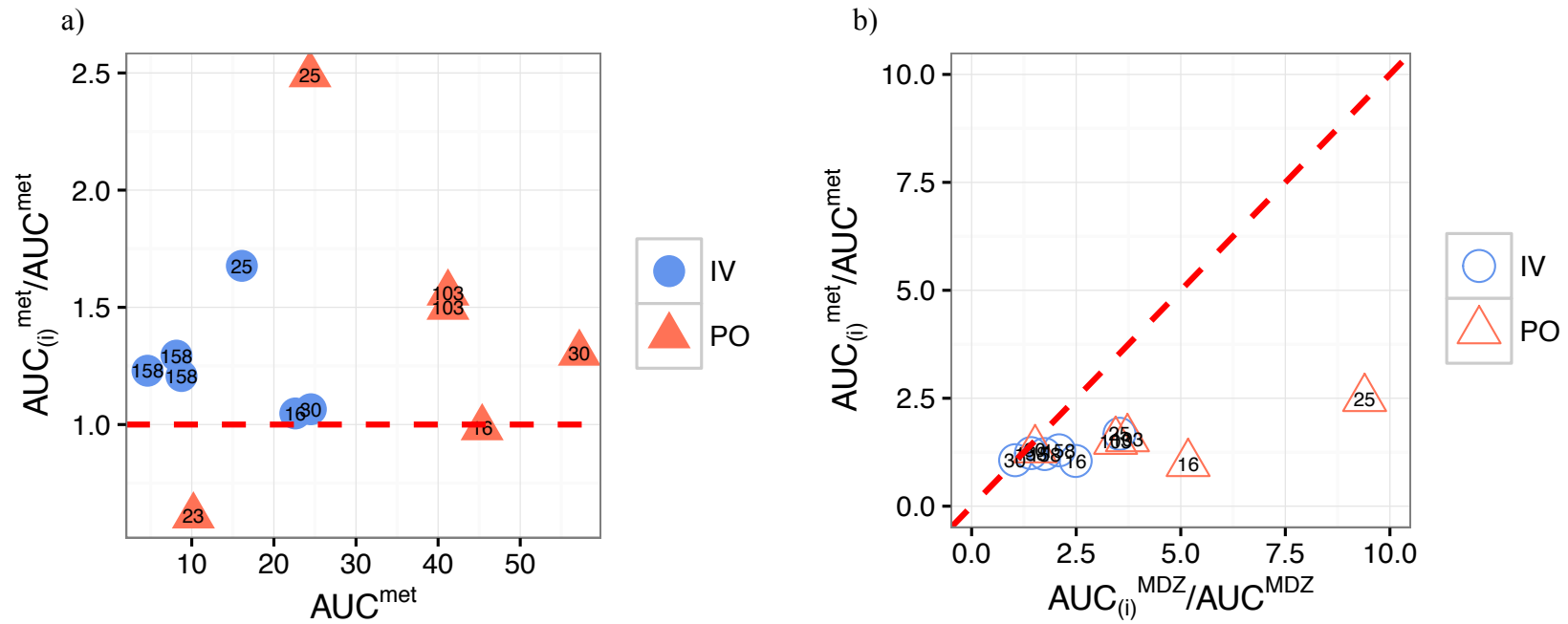


Figure 3.10 Evaluation of inhibitory effect of CYP3AI on MDZ and 1'-OH-MDZ exposures.

The red dash line in **Figure 3.10a** is a horizontal line with the intercept of 1. The dash line in **Figure 3.10b** is the line of identity. The number inside each point is the study ID.

3.3.5 Dose/concentration dependent inhibition by FLZ

X_{50} (estimates and 95% CIs) for different models are summarized in **Table 3.7**, and the predicted and observed profiles are shown in **Figure 3.11a-f**. **Figures 3.11a-c** demonstrates the change of inhibition ratio of $CL_{int,hep}^{MDZ}$, ER_{hep}^{MDZ} and ER_{GI}^{MDZ} versus PO FLZ dose, estimated from study 21. With single increasing dose, FLZ shows stronger inhibition on both hepatic and GI metabolism, while the inhibitory effect on intestinal metabolism is saturated more easily than hepatic metabolism (D_{50}^{FLZ} for ER_{hep}^{MDZ} inhibition = 426mg; D_{50}^{FLZ} for ER_{GI}^{MDZ} inhibition = 209mg). r^2 for $ER_{hep(i)}^{MDZ}/ER_{hep}^{MDZ}$ vs $Dose^{FLZ}$ regression is larger than $ER_{GI(i)}^{MDZ}/ER_{GI}^{MDZ}$ vs $Dose^{FLZ}$, indicating that a hyperbolic model might not be enough to describe relationship between $ER_{GI(i)}^{MDZ}/ER_{GI}^{MDZ}$ vs $Dose^{FLZ}$. It is possible that inhibition ratio on ER_{GI}^{MDZ} is more sensitive to FLZ dose, and may be better characterized by a sigmoidal model.

Figures 3.11d-f demonstrates the fold change of ER_{hep}^{MDZ} and ER_{GI}^{MDZ} with PO FLZ versus maximal FLZ unbound hepatic concentration ($c_{max,u-hep}^{FLZ}$), maximal FLZ gut lumen concentration ($c_{max-lumen}^{FLZ}$) or maximal FLZ GI concentration (c_{max-GI}^{FLZ}). These models are more physiologically based. If complete inhibition is assumed in both hepatic and intestinal metabolism, IC_{50} (concentration of inhibitor to produce half of maximum inhibition) can be estimated by non-linear regression with hyperbolic models. $c_{max,u-hep,50}^{FLZ}$ and $c_{max-GI,50}^{FLZ}$ are estimated to be 10.22 mg/L and 14.94 mg/L, which are in the same magnitude with K_i obtained in some *in-vitro* studies using FLZ to inhibition MDZ metabolism in liver and intestine microsomes: $K_{i,hep}^{FLZ} = 0.4 - 8.2$ mg/L (1.27-25 μ M (Galetin et al., 2005; Gibbs et al., 1999; Isoherranen et al., 2008; von Moltke et al., 1996; Yang et al., 2012)); $K_{i,GW}^{FLZ} = 3.3$ mg/L (10.4 μ M (Gibbs et al., 1999)). However $c_{max-lumen,50}^{FLZ}$ is estimated to be 836 mg/L, much higher than $K_{i,GW}^{FLZ}$, confirming that CYP3A is located intra-cellularly in the enterocytes. Hepatic

CYP3A is almost equally sensitive to the inhibitory effect of FLZ as GW CYP3A, suggested by tissue IC₅₀ estimations, whereas GW CYP3A is more sensitive to metabolic inhibition than hepatic CYP3A supported by FLZ dose models.

Table 3.7 Summary of dose/concentration-dependent inhibition model of FLZ estimated from study 21.

Independent variable		Dependent variable	X ₅₀ ¹	95% CI	r ²
Dose ^{FLZ} [mg]		CL _{int,hep(i)} ^{MDZ} /CL _{int,hep} ^{MDZ}	285	253-317	0.996
		ER _{hep(i)} ^{MDZ} /ER _{hep} ^{MDZ}	426	378-474	0.997
		ER _{GI(i)} ^{MDZ} /ER _{GI} ^{MDZ}	209	129-291	0.968
c _{max,u} ^{FLZ}	c _{max,u-hep} ^{FLZ} [mg/L]	ER _{hep(i)} ^{MDZ} /ER _{hep} ^{MDZ}	10.22	9.05-10.51	0.997
	c _{max-lumen} ^{FLZ} [mg/L]	ER _{GI(i)} ^{MDZ} /ER _{GI} ^{MDZ}	836	516-1164	0.968
	c _{max-GI} ^{FLZ} [mg/L]	ER _{GI(i)} ^{MDZ} /ER _{GI} ^{MDZ}	14.91	9.14-20.68	0.968

¹ Represents D₅₀^{FLZ} (mg), c_{max,u-hep,50}^{FLZ} (mg/L) c_{max-lumen,50}^{FLZ} (mg/L) c_{max-GI,50}^{FLZ} (mg/L) in different models

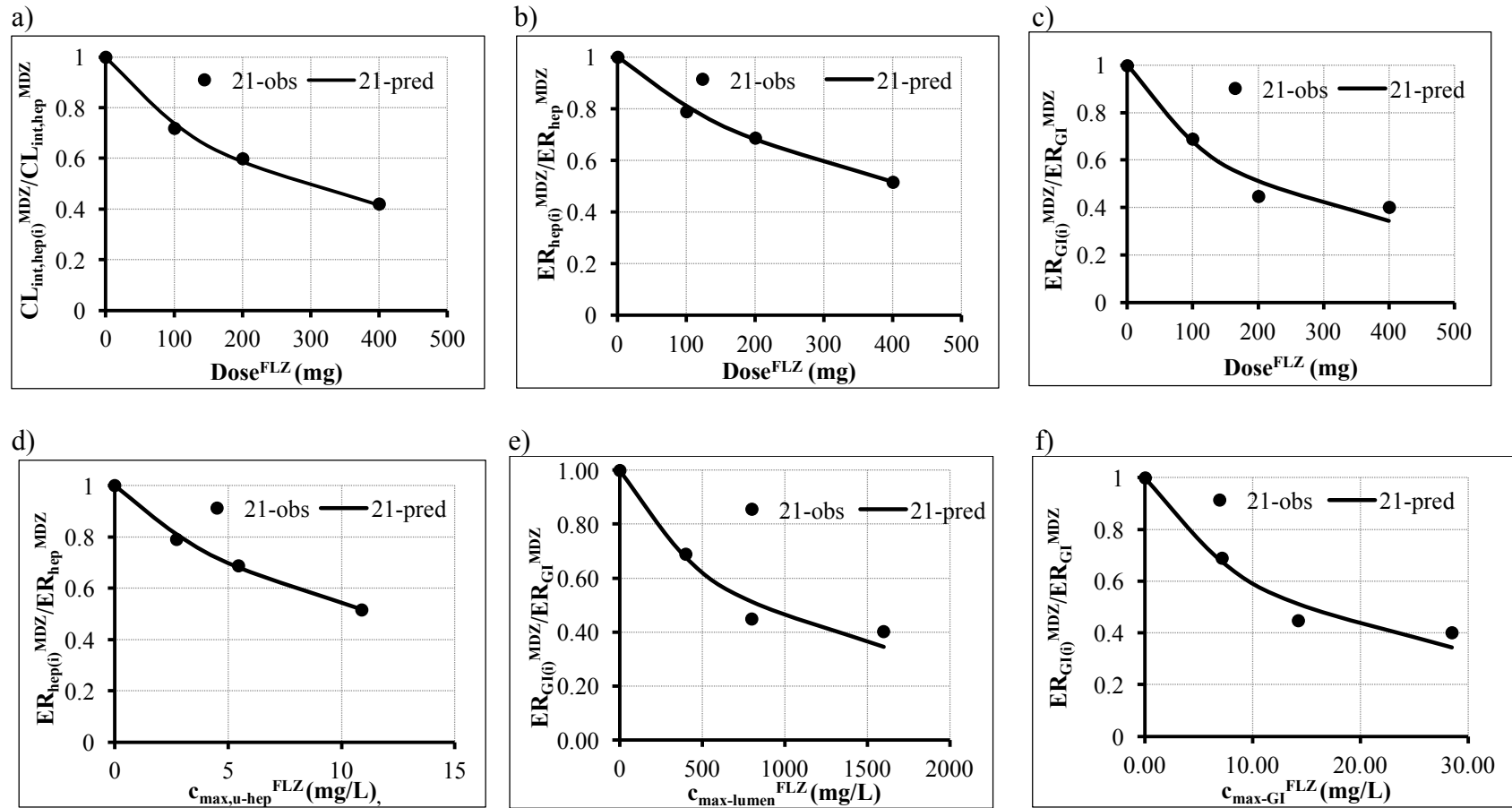


Figure 3.11 Dose/concentration-dependent inhibition of FLZ.

a) Relationship between $CL_{int,hep}^{MDZ} / CL_{int,hep}^{MDZ}$ inhibition ratio and single PO FLZ dose. b) Relationship between $ER_{hep}^{MDZ} / ER_{hep}^{MDZ}$ inhibition ratio and single PO FLZ dose. c) Relationship between $ER_{GI}^{MDZ} / ER_{GI}^{MDZ}$ inhibition ratio and single PO FLZ dose. d) Relationship between $ER_{hep}^{MDZ} / ER_{hep}^{MDZ}$ inhibition ratio and $c_{max,u-hep}^{FLZ}$. e) Relationship between $ER_{GI}^{MDZ} / ER_{GI}^{MDZ}$ inhibition ratio and $c_{max-lumen}^{FLZ}$. f) Relationship between $ER_{GI}^{MDZ} / ER_{GI}^{MDZ}$ inhibition ratio and c_{max-GI}^{FLZ} . The symbols are the observed values in study 21, the solid lines are the predicted profiles in study 21.

$ER_{\text{hep}}^{\text{MDZ}}$ and $ER_{\text{GI}}^{\text{MDZ}}$ in absence/presence of FLZ in study 21 and 103, along with the predicted maximum inhibitory concentration in liver and gut are demonstrated in **Table 3.8**. The calculated $c_{\text{max,u}}^{\text{FLZ}}$ (6.67 $\mu\text{g/mL}$) after oral dose of 400 mg in study 21 is comparable to the observed $c_{\text{max,u}}^{\text{FLZ}}$ (7.22 $\mu\text{g/mL}$) in study 103, confirming the validity of parameters used in calculating $c_{\text{max,u}}^{\text{FLZ}}$. Observed $c_{\text{max,u}}^{\text{FLZ}}$ after IV (7.39 $\mu\text{g/mL}$) and PO FLZ (7.22 $\mu\text{g/mL}$) are quite similar, due to the rapid absorption rate and high F_{oral} of FLZ.

Inhibitory effect on GW metabolism after 400 mg PO FLZ in study 103 is lower than study 21, probably because study 103 had higher baseline F_{GI} (48%) than study 21 (36%), resulting in less intestinal CYP3A available to be inhibited (less sensitive to inhibitors). Both IV and PO FLZ can inhibit hepatic and GW metabolism, while IV FLZ demonstrates less inhibition on hepatic and intestinal metabolism than PO FLZ at the same dose, mainly because it gets into the enterocytes and hepatocytes through systemic circulation rather than absorption through gut lumen or portal vein blood flow, hence concentration in the GW and liver should be lower after IV administration.

To compare $c_{\text{max,u-hep}}^{\text{FLZ}}$ and $c_{\text{max-GI}}^{\text{FLZ}}$ after IV and PO FLZ, IV FLZ has slightly lower $c_{\text{max,u-hep}}^{\text{FLZ}}$ than PO FLZ (7.22 vs. 9.59 $\mu\text{g/mL}$), and a larger difference is found in $c_{\text{max-GI}}^{\text{FLZ}}$ (16.14 $\mu\text{g/mL}$ vs. 28.44 $\mu\text{g/mL}$) between IV and PO FLZ. $c_{\text{max-GI}}^{\text{FLZ}}$ is much higher than $c_{\text{max,u-hep}}^{\text{FLZ}}$ and calculated $c_{\text{max,u}}^{\text{FLZ}}$ (6.77 $\mu\text{g/mL}$) after PO FLZ in study 21, whereas $c_{\text{max,u-hep}}^{\text{FLZ}}$ and $c_{\text{max,u}}^{\text{FLZ}}$ are comparable, because liver is highly a perfused organ, compared with gut, leading to more rapid concentration equilibrium between liver and blood. After IV FLZ, we assumed that $c_{\text{max,u-hep}}^{\text{FLZ}}$ and $c_{\text{max,u}}^{\text{FLZ}}$ are the same in our previous calculation, because more than 90% FLZ gets absorbed into systemic circulation, indicating a very limited hepatic first pass metabolism. Estimated $c_{\text{max-GI}}^{\text{FLZ}}$ after IV FLZ is higher than $c_{\text{max,u}}^{\text{FLZ}}$, may be due to a high partitioning ratio of FLZ into

GW.

Table 3.8 Summary of extraction ratios and FLZ concentrations in various compartments.

Parameters	Study 21 (400 mg PO FLZ)	Study 103 (400 mg IV FLZ)	Study 103 (400 mg PO FLZ)
$ER_{\text{hep}(i)}/ER_{\text{hep}}$	0.52	0.62	0.52 ¹
$ER_{\text{GI}(i)}/ER_{\text{GI}}$	0.34	0.53	0.42
$c_{\text{max},u}^{\text{FLZ}}$	6.77	7.39 ²	7.22 ²
$c_{\text{max},u\text{-hep}}^{\text{FLZ}}$	9.59	7.39 ³	9.59 ⁴
$c_{\text{max-GI}}^{\text{FLZ}}$	28.44	16.14	28.44 ⁴

¹ Assumed to be the same as study 21

² Observed $c_{\text{max}}^{\text{FLZ}}$ in study 103, corrected by f_u^{FLZ} ($f_u^{\text{FLZ}} = 0.88$ (Olkola et al., 1996))

³ Assumed to be the same as $c_{\text{max},u}^{\text{FLZ}}$ after IV FLZ in study 103

⁴ Assumed to be the same as study 21

3.4 Conclusions

In conclusion, both MDZ and 1'-OH-MDZ follow dose-proportional PK within the respective IV and PO MDZ dose range in our database. MDZ is a low to intermediate $ER_{\text{hep}}^{\text{MDZ}}$ drug. Intestinal metabolism exists for MDZ during first pass metabolism, and 1'-OH-MDZ gets formed more in the GW than in the liver pre-systemically. High variability of intestinal metabolism is the main source of the high variability in $F_{\text{oral}}^{\text{MDZ}}$ of MDZ in the absence and presence of CYP3AI. CYP3AI can inhibit hepatic and intestinal metabolism, hence decrease $CL_{\text{int,hep}}^{\text{MDZ}}$, $ER_{\text{hep}}^{\text{MDZ}}$ and $ER_{\text{GI}}^{\text{MDZ}}$. Subjects with lower $F_{\text{GI}}^{\text{MDZ}}$ (and lower $F_{\text{oral}}^{\text{MDZ}}$) are more sensitive to the inhibitors, thus inhibitors can decrease the variability of $F_{\text{GI}}^{\text{MDZ}}$ and $F_{\text{oral}}^{\text{MDZ}}$. On average, $F_{\text{hep}}^{\text{MDZ}}$ shows a 21% increase due to pre-systemic, metabolic DDI. CYP3AI can increase $AUC_{\text{IV}}^{\text{met}}$, but the effect on $AUC_{\text{PO}}^{\text{met}}$ varies among studies. MRs after both IV and PO routes of MDZ go down in all the studies. Owing to limited studies and unexplained MR decrease for 1'-OH-MDZ, only DDI on parent compound (MDZ) is considered for further PBPK modeling.

With single increasing dose, FLZ demonstrates stronger inhibition on both hepatic and intestinal metabolism, however hepatic CYP3A is less sensitive to the inhibitory effect of FLZ than GW CYP3A when using the dose model, and equally sensitive when using the inhibitory concentration models. Both IV and PO FLZ inhibit hepatic and GW metabolism of MDZ, and concentration of FLZ is lower after IV route than PO both in the liver and small intestine, leading to less inhibition on $ER_{\text{hep}}^{\text{MDZ}}$ and $ER_{\text{GI}}^{\text{MDZ}}$ after IV FLZ. Representative CYP3AI will be selected based on the analysis above, and PBPK models will be developed to characterize the magnitude and time course of DDI between MDZ and CYP3AI.

CHAPTER 4

4 SEMI-PBPK MODELING OF IV/PO FLZ

4.1 Background and Objectives

4.1.1 Selection of CYP3AI

Based on the quantitative meta-analysis discussed in **Chapter 3**, study 103 (Ahonen et al., 1997) is the only *in-vivo* DDI study that administered CYP3AI – FLZ both IV and PO concomitant with MDZ. The CYP3AI in other studies within the final database were all dosed orally. As a consequence, study 103 is the only choice to validate MDZ PK profiles after both IV and PO inhibitors, and FLZ is the selected CYP3AI. Besides study 103, study 21(Kharasch et al., 2005) and study 26 (Olkola et al., 1996) were another two *in-vivo* DDI studies between MDZ and FLZ, however, only study 103 provided FLZ plasma concentration-time profile along with MDZ profiles, while the other two studies only reported MDZ profiles. Therefore, study 103 is a key reference to validate semi-PBPK model of FLZ.

4.1.2 FLZ PK information and simulation strategies

Clinically, FLZ is a triazole antifungal agent, available as tablets or suspension for oral administration, or as a sterile solution for IV administration (Pfizer, 2011). The general dosing regimen of FLZ is 200 - 800 mg loading dose and 200 – 800 mg maintenance dosing once daily, with duration and dosage depending on location and severity of infection (Fluconazole .

Lexi.com). IV and PO formulations have the same recommended dose, indicating its high $F_{\text{oral}}^{\text{FLZ}}$ (> 90%) (Humphrey et al., 1985; Pfizer, 2011; Washton, 1989). Dose proportional PK is established between 50 and 400mg single oral dose range (Pfizer, 2011). After IV administration, FLZ is well-characterized by a 1-compartmental body model (Humphrey et al., 1985), with reported $V_{d_{ss}}$ about 0.7 L/kg in humans (Humphrey et al., 1985; Carrasco-Portugal & Flores-Murrieta, 2007). It is cleared primarily by renal excretion, with approximately 70% (Humphrey et al., 1985; Ripa et al., 1993; Sobue et al., 2004; Washton, 1989) of the administered dose appear in the urine as unchanged drug, and all non-renal pathways are assumed to be hepatic metabolism (Humphrey et al., 1985). The mean terminal plasma elimination half-life ($t_{1/2}^{\text{FLZ}}$) ranges from 22 to 37 hours, indicating its prolonged inhibitory effect on hepatic and intestinal metabolism of MDZ. It is a less profound (moderate) CYP3AI (Kharasch et al., 2005; Drug Interactions & Labeling Drug Development and Drug Interactions Table of Substrates, Inhibitors and Inducers), which can non-competitively inhibit hepatic and intestinal CYP3A (Gibbs et al., 1999; Isoherranen et al., 2008). After PO administration, it is well absorbed into GW (BCS class 1 drug (World Health Organization, 2005)), and first-pass metabolism is very limited.

Besides study 103, FLZ plasma concentration-time profiles were available in several other clinical studies, making it easy to validate its concentration in plasma (blood) compartment of the semi-PBPK model. However, inhibition on CYP3A occurs in the enterocytes and hepatocytes, so it is more important to characterize FLZ PK profiles in liver and GW, which cannot be validated through any study in human. In this case, sensitivity analysis was used to detect key PK/physiological parameters in the semi-PBPK model, that could influence FLZ exposure in liver and GW considerably, to facilitate future DDI model optimization.

4.1.3 Objectives

The major objectives of the chapter were to:

- a. Develop a semi-PBPK model of FLZ to describe its PK profiles in human after IV and PO administration
- b. Validate the model using plasma concentration-time profiles in clinical FLZ PK studies, and identify pivotal PK/physiological parameters that determine FLZ exposure in liver and GW by sensitivity analysis
- c. Predict hepatic and intestinal concentration – time profiles of FLZ using the validated semi-PBPK model

4.2 Methods

4.2.1 Development of FLZ semi-PBPK model

4.2.1.1 FLZ semi-PBPK model after IV administration

A semi-PBPK model for IV FLZ was developed, based on the reported PK and physiological parameters (**Table 4.1**). A conventional one-compartmental body model with additional compartments for GW, portal vein, and liver was built, and showed in **Figure 4.1**. Since no saturable protein binding was observed for FLZ, the semi-PBPK model was developed based on total (unbound + bound) FLZ mass transfer. After IV administration, FLZ is injected directly into the systemic circulation and distributes into GW and liver through the superior mesenteric artery and hepatic artery, with the blood flow of villous blood flow (Q_{villi}) (Yang et al., 2007) and hepatic artery blood flow (Q_{HA}). Q_{villi} was chosen instead of total mesenteric artery blood flow or intestinal mucosa blood flow, because the metabolic CYP enzymes are located at the villous tips

(Watkins, 1997; Yang et al., 2007). Portal vein flow (Q_{PV}) is formed by the confluence of the superior mesenteric and splenic veins, and also receives blood from the inferior mesenteric gastric, and cystic veins (Abboud et al., 2009). Drug distributed to portal vein from other veins can be regarded as directly distributed from central compartment, with the blood flow of $Q_{PV} - Q_{villi}$. An additional scaling factor (f_{PV}) is added, to adjust for the components of portal vein that contain drug. f_{PV} was set at 1 for initial model simulation, and sensitivity analysis was conducted for f_{PV} on FLZ concentrations (see section 4.2.3). The hepatic vein supplies blood flow from liver to systemic blood with blood flow of Q_{hep} . FLZ can be eliminated from the body through renal elimination and hepatic metabolism, with the respective clearance of CL_{ren}^{FLZ} and $f_u^{FLZ} \cdot CL_{int,hep}^{FLZ}$.

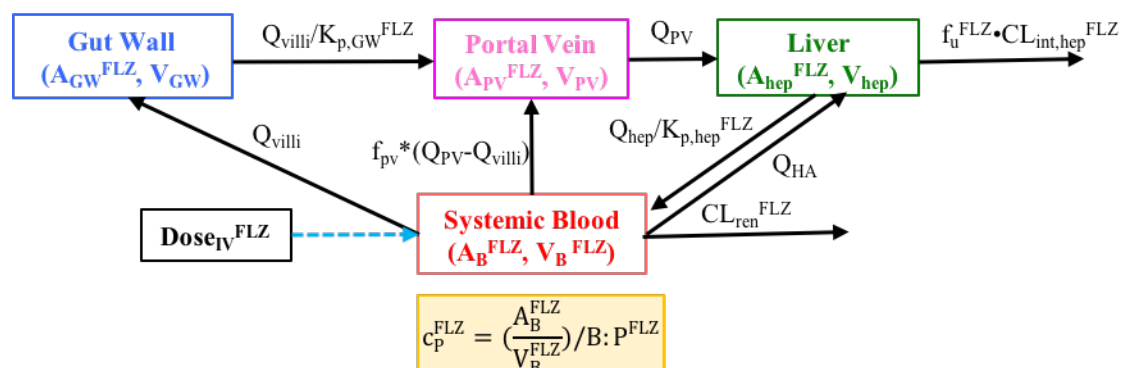


Figure 4.1 Semi-PBPK model scheme for the disposition of FLZ after IV administration.

1) Differential equations:

Based on the model above, differential equations for total (unbound + bound) FLZ mass transfer between compartments were expressed as equations (4.1) to (4.4):

$$\frac{dA_B^{FLZ}(t)}{dt} = k_0^{FLZ} + \left(\frac{C_{hep}^{FLZ}}{K_{p,hep}^{FLZ}} \right) \cdot Q_{hep} - c_B^{FLZ} \cdot CL_{ren}^{FLZ} - c_B^{FLZ} \cdot f_{PV} \cdot (Q_{PV} - Q_{villi}) - c_B^{FLZ} \cdot Q_{HA} - c_B^{FLZ} \cdot Q_{villi}$$

$$\text{when } t = 0, A_B^{FLZ}(0) = 0; \text{ when } t = t_{inf}, A_B^{FLZ}(t_{inf}) = Dose_{IV}^{FLZ} \quad (4.1)$$

$$\frac{dA_{GW}^{FLZ}(t)}{dt} = c_B^{FLZ} \cdot Q_{villi} - \left(\frac{C_{GW}^{FLZ}}{K_{p,GW}^{FLZ}} \right) \cdot Q_{villi}$$

$$\text{when } t = 0, A_{GW}^{FLZ}(0) = 0 \quad (4.2)$$

$$\frac{dA_{PV}^{FLZ}(t)}{dt} = c_B^{FLZ} \cdot f_{PV} \cdot (Q_{PV} - Q_{villi}) + \left(\frac{C_{GW}^{FLZ}}{K_{p,GW}^{FLZ}} \right) \cdot Q_{villi} - c_{PV}^{FLZ} \cdot Q_{PV}$$

$$\text{when } t = 0, A_{PV}^{FLZ}(0) = 0 \quad (4.3)$$

$$\frac{dA_{hep}^{FLZ}(t)}{dt} = c_B^{FLZ} \cdot Q_{HA} + c_{PV}^{FLZ} \cdot Q_{PV} - \left(\frac{C_{hep}^{FLZ}}{K_{p,hep}^{FLZ}} \right) \cdot Q_{hep} - c_{hep}^{FLZ} \cdot f_u^{FLZ} \cdot CL_{int,hep}^{FLZ}$$

$$\text{when } t = 0, A_{hep}^{FLZ}(0) = 0 \quad (4.4)$$

A_B^{FLZ} , A_{GW}^{FLZ} , A_{PV}^{FLZ} and A_{hep}^{FLZ} are the amounts of drug in central, GW, portal vein and liver compartments, respectively; c_B^{FLZ} , c_{GW}^{FLZ} , c_{PV}^{FLZ} , c_{hep}^{FLZ} are drug concentrations in central, GW, portal vein and liver compartments, calculated by dividing amount (A) by the respective compartment volume: V_B^{FLZ} , V_{GW} , V_{PV} and V_{hep} , which are FLZ volume of blood compartment, volume of GW, portal vein and liver. In most FLZ IV studies, FLZ was administered as IV infusion, hence an infusion rate k_0^{FLZ} was introduced in equation (4.1) as a dose input rate, and initial amounts for all the four compartments are 0.

2) Volume of distributions

The volume of blood compartment of FLZ (V_B^{FLZ}) should be:

$$V_B^{FLZ} = Vd_{ss}^{FLZ} - K_{p,hep}^{FLZ} \cdot V_{hep} - V_{PV} - K_{p,GW}^{FLZ} \cdot V_{GW} \quad (4.5)$$

Vd_{ss}^{FLZ} is the observed steady-state volume of distribution of FLZ from literature (0.7 L/kg) (Humphrey et al., 1985).

V_{GW} is the volume of GW epithelium, which can be estimated as equation (4.6), assuming small intestine is a cylinder and V_{GW} is the volume of the surface for this cylinder with a certain thickness:

$$V_{GW} = \pi(R + t)^2L - \pi R^2L \quad (4.6)$$

R (= 1.75cm) (Fenneteau et al. 2010) is the mean radius of gut lumen, t (= 3mm) (Fleischer et al., 1981) is the mean thickness of GW, and L (= 680cm) (Fenneteau et al., 2010) is the total small intestine length. Therefore, the calculated V_{GW} is 2.43 L.

V_{hep} was estimated by equation (4.7 - 4.8) (Heinemann et al., 1999; Kan & Hopkins, 1979) (Heinemann et al., 1999):

$$V_{hep} \text{ (ml)} = 1072.8 \cdot BSA(m^2) - 345.7 \quad (4.7)$$

$$BSA(m^2) = BW(kg)^{0.425} \times BL(cm)^{0.725} \times 0.007184 \quad (4.8)$$

BSA is body surface area, BW is mean body weight and BL is mean body length (height).

Mean body weight is set as 72kg, and average height is assumed to be 170cm.

V_{PV} is the portal vein volume extracted from literature (Ito et al., 2003).

3) Partition coefficient between blood and tissue (K_p)

$K_{p,GW}^{FLZ}$ and $K_{p,hep}^{FLZ}$ are the GW-to-blood partition coefficient and liver-to-blood partition coefficient, which were set to 1 (Carrasco-Portugal & Flores-Murrieta, 2007).

4) Blood flows (Q)

Q_{hep} was set as 21.4ml/min/kg (Tsunoda et al., 1999). Q_{PV} and Q_{HA} are the portal vein blood flow and hepatic artery blood flow, which represent 75% and 25% of Q_{hep} , respectively. Q_{villi} is 4.3ml/min/kg, according to literature (Yang et al., 2007).

5) Clearance

$f_u^{\text{FLZ}} \cdot \text{CL}_{\text{int,hep}}^{\text{FLZ}}$ can be calculated by equation (4.9)

$$f_u^{\text{FLZ}} \cdot \text{CL}_{\text{int,hep}}^{\text{FLZ}} = \frac{\text{CL}_{\text{hep}}^{\text{FLZ}} \cdot Q_{\text{hep}}}{Q_{\text{hep}} - \text{CL}_{\text{hep}}^{\text{FLZ}}} \quad (4.9)$$

Assuming all non-renal clearance is hepatic clearance, $\text{CL}_{\text{hep}}^{\text{FLZ}}$ should be $(\text{CL}_{\text{tot,p}}^{\text{FLZ}} - \text{CL}_{\text{ren}}^{\text{FLZ}})$. $\text{CL}_{\text{tot,p}}^{\text{FLZ}}$ and $\text{CL}_{\text{ren}}^{\text{FLZ}}$ were extracted from literatures (Ripa et al., 1993; Sobue et al., 2004).

6) Fraction unbound and blood-to-plasma partitioning ratio

Due to limited information, fraction unbound of FLZ (f_u^{FLZ}) was assumed to be time/concentration independent, and f_u^{FLZ} in plasma, hepatocyte and enterocyte were assumed to be the same, which is 0.88 (Humphrey et al., 1985). Blood-to-plasma partitioning ratio of FLZ ($B:P^{\text{FLZ}}$) was assumed to be 1.0 (Ervin & Houston, 1994)

4.2.1.2 FLZ semi-PBPK model after PO administration

A semi-PBPK model for PO FLZ (**Figure 4.2**) was developed based on the reported PK and physiological parameters (**Table 4.1**). A conventional one-compartmental body model with additional compartments for gut lumen, GW, portal vein, and liver was developed, by adding an absorption compartment (gut lumen) to the IV model.

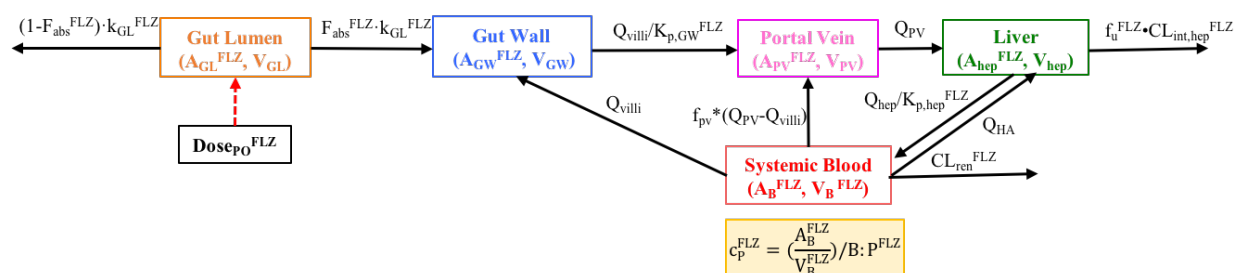


Figure 4.2 Semi-PBPK model scheme for the disposition of FLZ after PO administration.

After PO administration, FLZ is dissolved in the gut lumen first, and a fraction of drug (F_{abs}^{FLZ}) permeates through the GW, with a first order absorption rate k_{GL}^{FLZ} . Since FLZ is a BCS class 1 drug (World Health Organization, 2005), with high solubility and high permeability, it is reasonable to assume $F_{abs}^{FLZ} = 100\%$, and drug transporters have little effect on its absorption. Due to the high observed F_{oral}^{FLZ} and low GW and hepatic first-pass effect of FLZ, drug permeating into the GW is assumed to be the rate-limiting step of its oral absorption; hence, k_{GL}^{FLZ} is equal to k_a^{FLZ} , which was reported in literature (Ripa et al., 1993). V_{GL} is the same as the volume of water a patient would take to administer the drug, which was set to be 250 ml (FDA, 2012). Assuming no drug gets metabolized in the GW, FLZ is carried into portal vein with blood flow of Q_{villi} , and reaches the liver via Q_{PV} . Before getting into the systemic blood compartment, FLZ can be metabolized by liver pre-systemically with the clearance of $f_u^{FLZ} \cdot CL_{int, hep}^{FLZ}$. Once it gets into the systemic blood, the disposition is the same as IV administration.

Based on the model scheme, differential equations for mass transfer between compartments are expressed as equations (4.10) to (4.14):

$$\frac{dA_{GL}^{FLZ}(t)}{dt} = -c_{GL}^{FLZ} \cdot V_{GL} \cdot F_{abs}^{FLZ} \cdot k_{GL}^{FLZ} - c_{GL}^{FLZ} \cdot V_{GL} \cdot (1 - F_{abs}^{FLZ}) \cdot k_{GL}^{FLZ}$$

when $t = 0$, $A_{GL}^{FLZ}(0) = Dose_{PO}^{FLZ}$ (4.10)

$$\frac{dA_{GW}^{FLZ}(t)}{dt} = c_{GL}^{FLZ} \cdot V_{GL} \cdot F_{abs}^{FLZ} \cdot k_{GL}^{FLZ} + c_B^{FLZ} \cdot Q_{villi} - \left(\frac{c_{GW}^{FLZ}}{K_{p,GW}^{FLZ}} \right) \cdot Q_{villi}$$

when $t = 0$, $A_{GW}^{FLZ}(0) = 0$ (4.11)

$$\frac{dA_{PV}^{FLZ}(t)}{dt} = c_B^{FLZ} \cdot f_{PV} \cdot (Q_{PV} - Q_{villi}) + \left(\frac{c_{GW}^{FLZ}}{K_{p,GW}^{FLZ}} \right) \cdot Q_{villi} - c_{PV}^{FLZ} \cdot Q_{PV}$$

when $t = 0$, $A_{PV}^{FLZ}(0) = 0$ (4.12)

$$\frac{dA_{hep}^{FLZ}(t)}{dt} = c_B^{FLZ} \cdot Q_{HA} + c_{PV}^{FLZ} \cdot Q_{PV} - \left(\frac{C_{hep}^{FLZ}}{K_{p,hep}^{FLZ}} \right) \cdot Q_{hep} - c_{hep}^{FLZ} \cdot f_u^{FLZ} \cdot CL_{int,hep}^{FLZ}$$

when $t = 0$, $A_{hep}^{FLZ}(0) = 0$ (4.13)

$$\begin{aligned} \frac{dA_B^{FLZ}(t)}{dt} = & k_0^{FLZ} + \left(\frac{C_{hep}^{FLZ}}{K_{p,hep}^{FLZ}} \right) \cdot Q_{hep} - c_B^{FLZ} \cdot CL_{ren}^{FLZ} - c_B^{FLZ} \cdot f_{PV} \cdot (Q_{PV} - Q_{villi}) - c_B^{FLZ} \cdot Q_{HA} \\ & - c_B^{FLZ} \cdot Q_{villi} \end{aligned}$$

when $t = 0$, $A_B^{FLZ}(0) = 0$ (4.14)

A_{GL}^{FLZ} and C_{GL}^{FLZ} are the amount and concentration of drug in gut lumen compartment, and C_{GL}^{FLZ} is calculated by dividing A_{GL}^{FLZ} by V_{GL} .

4.2.1.3 Model parameters and assumptions

Model parameters used in semi-PBPK models of IV/PO FLZ were summarized in Table 4.1.

Table 4.1 Semi-PBPK FLZ model parameters.

Parameter	Definition	Value	Source
Physiological parameters			
V_{GL} (ml/kg)	Volume of gut lumen	3.57	Assumed to be 250ml (USA Food and Drug Administration, 2012)
V_{GW} (ml/kg)	Volume of GW	33.6	Calculated by equation (4.6), assumed to be the surface of gut lumen cylinder
V_{PV} (ml/kg)	Volume of portal vein	0.97	Unknown methods (Ito et al., 2003)
V_{hep} (ml/kg)	Volume of liver	22.5	Calculated by equation (4.7) and (4.8)
Q_{villi} (ml/min/kg)	Villous blood flow	4.30	<i>In-vivo</i> experiment (Yang et al., 2007)
Q_{hep} (ml/min/kg)	Hepatic blood flow	21.4	<i>In-vivo</i> experiment (Tsunoda et al., 1999)
f_{HA}	Fraction of hepatic artery to total hepatic blood flow	0.25	(Eipel et al., 2010) (Q_{HA} was calculated as $f_{HA} \cdot Q_{hep}$; Q_{PV} was calculated as $(1 - f_{HA}) \cdot Q_{hep}$)
f_{PV}	Fraction of the components of portal vein that contain drug	1.00	A correction factor that can be adjusted according to simulation results.
FLZ PK Parameters			
V_B^{FLZ} (ml/kg)	Volume of systemic blood compartment	641	Calculated by equation (4.5) (Carrasco-Portugal & Flores-Murrieta, 2007; Humphrey et al., 1985)
f_u^{FLZ}	Fraction unbound of FLZ in hepatocytes and enterocytes	0.88	Assumed to be the same as fraction unbound in plasma (Humphrey et al., 1985)
$K_{p,GW}^{FLZ}$	GW-to-blood partition coefficient	1	Assumed to be 1 (Carrasco-Portugal & Flores-Murrieta, 2007)
$K_{p,hep}^{FLZ}$	Liver-to-blood partition coefficient	1	Assumed to be 1 (Carrasco-Portugal & Flores-Murrieta, 2007)
$CL_{int,hep}^{FLZ}$ (ml/min/kg)	Hepatic intrinsic clearance	0.11	Calculated by equation (4.9)
CL_{ren}^{FLZ} (ml/min/kg)	Renal clearance	0.2	<i>In-vivo</i> experiment (Ripa et al., 1993; Sobue et al., 2004)
$B:P^{FLZ}$	Blood to plasma partitioning ratio	1	(Ervine & Houston, 1994)
k_{GL}^{FLZ} (min^{-1})	Absorption rate constant from gut lumen to GW	0.0213	Assumed to be k_a^{FLZ} from <i>in-vivo</i> experiment (Ripa et al., 1993)
F_{abs}^{FLZ}	Fraction of FLZ absorbed from gut lumen	100%	BCS Class 1 drug (Lindenberg et al., 2004)

The assumptions made in FLZ semi-PBPK modeling included:

- 1) FLZ is virtually instantaneously and homogeneously distributed across the body after IV administration. (i.e. follows a 1-compartmental body model) (Humphrey et al., 1985)
- 2) Perfusion (blood flow) is the rate-limiting step for FLZ distribution, rather than tissue uptake.
- 3) All non-renal clearance of FLZ is due to hepatic clearance (i.e., other elimination pathways, such as GW metabolism, are negligible).
- 4) Negligible, if any, drug transporter effect involved in GI absorption of FLZ.
- 5) FLZ follows dose-proportional PK at relevant dose range after IV/PO administration.
- 6) Partition coefficient (K_p) for GW and liver are 1 (Carrasco-Portugal & Flores-Murrieta, 2007), and are constant at simulated concentrations.
- 7) FLZ plasma concentration is assumed to be the same as blood concentration (Ervine & Houston, 1994).
- 8) Fraction unbound of FLZ in the blood, liver and GW are assumed to be the same.
- 9) FLZ is rapidly dissolved in gut lumen, and completely absorbed from gut lumen ($F_{abs}^{FLZ} = 100\%$).
- 10) FLZ follows 1st-order diffusion across GW, and this process is the rate-limiting step of its absorption.
- 11) MDZ has no effect on FLZ PK.

4.2.2 Model qualification and predictions

IV and PO FLZ semi-PBPK model were validated using the observed mean PK profiles from study 103 (Ahonen et al., 1997), and other FLZ clinical PK studies, based on a comprehensive literature search of FLZ clinical PK studies after IV and PO administration. In study 103, FLZ was administered as 400 mg 1 hour IV infusion and 400 mg PO; concentrations in all the other studies were normalized to 400 mg dose. Concentrations in all compartments were simulated using Simbiology (MATLAB, 2015a), and the predicted exposure metrics were summarized and compared to reported values. The most commonly used criteria of prediction acceptance: predicted exposure metrics are within 0.5 to 2-fold of observed, were used to assess performance of FLZ semi-PBPK model. FLZ concentrations in all compartments were then simulated using the validated semi-PBPK model, in order to compare tissue concentration-time profiles after different route of administration.

4.2.3 Sensitivity Analysis

Sensitivity analyses were performed to provide information of specific parameters that the model predictions are most sensitive to. Parameters (i.e. f_{pv} , $K_{p,GW}^{FLZ}$, $K_{p,hep}^{FLZ}$, $CL_{int,hep}^{FLZ}$, CL_{ren}^{FLZ} , and k_{GL}^{FLZ}) that are uncertain/highly variable and/or expected to affect FLZ blood/hepatic/GW exposures the most were selected to perform sensitivity analysis. All parameters (except f_{pv} , which was simulated at 0.0, 0.5 and 1.0) were increased and decreased by 2-fold relative to their original values (overall-fold change in values = 4 - fold), as showed in **Table 4.2**, and the respective unbound blood/hepatic/GW concentration - time profiles were predicted under 400 mg 1 hour IV infusion or PO FLZ, as a representative of the dosing regimen in study 103, as well as the most commonly used daily dosing regimen of FLZ. Exposure metrics (AUC, c_{max} , t_{max}) of FLZ in blood, liver and GW were identified and the sensitivity to each

parameter was assessed by dividing respective exposure metrics simulated at the upper limit by that simulated at the lower limit.

Table 4.2 Values of parameters used in sensitivity analysis.

Parameter Name	Initial Value	Lower/Upper Sensitivity Limits
f_{pv}	1.0	0; 1.0
$K_{p,hep}^{FLZ}$	1.0	0.5; 2
$K_{p,GW}^{FLZ}$	1.0	0.5; 2
$CL_{int,hep}^{FLZ}$ (ml/min/kg)	0.1	0.05; 0.2
CL_{ren}^{FLZ} (ml/min/kg)	0.2	0.1; 0.4
k_{GL}^{FLZ} (min^{-1})	0.0213	0.0106; 0.0426

4.3 Results and Discussion

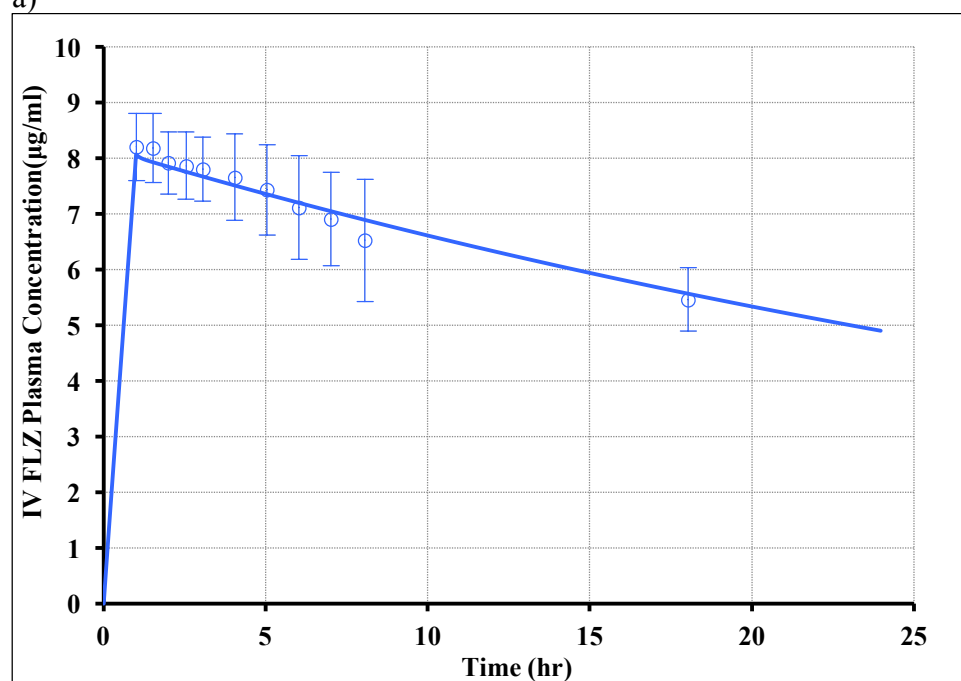
4.3.1 Model evaluation

4.3.1.1 Predictive performance check

Semi-PBPK model after IV FLZ was validated using the observed mean PK profile from study 103 (Ahonen et al., 1997), and mean plasma concentrations digitized from studies 103 (Ahonen et al., 1997), 301 (Humphrey et al., 1985), 308 (Jovanovid et al., 2005), 309 (Porta et al., 2005), 310 (Zimmermann et al., 1994) and 311 (Yeates et al., 1995) were utilized to validate PO FLZ model. Based on the assumption of dose-proportional PK, each concentration-time profile digitized from the literatures was corrected by the dose of study 103, which is 400 mg. Since IV FLZ was administered with different infusion times in different studies, observed profiles in other IV FLZ PK studies cannot be conveniently normalized to 400 mg dose, and as AUC after IV FLZ has small inter-study variability (<10%), (because FLZ is primarily renal-cleared, and is not a potent substrate to any transporters in the kidney), only study 103, which is

a DDI study between MDZ and FLZ, was used to validate semi-PBPK model of FLZ after IV administration. **Figure 4.3a** demonstrates that the final PBPK model of FLZ can adequately predict FLZ plasma concentration after 1 hour IV infusion, with all simulated values within \pm SD of the observed mean data. For PO FLZ (50 - 800 mg), the model can predict all observed exposure metrics within roughly 50% deviations (**Table 4.3**), with observed PK profiles evenly spread throughout the entire simulated PK profile. Differences in analytical methods, sampling strategies, subjects' demographics may account for the variation among studies.

a)



b)

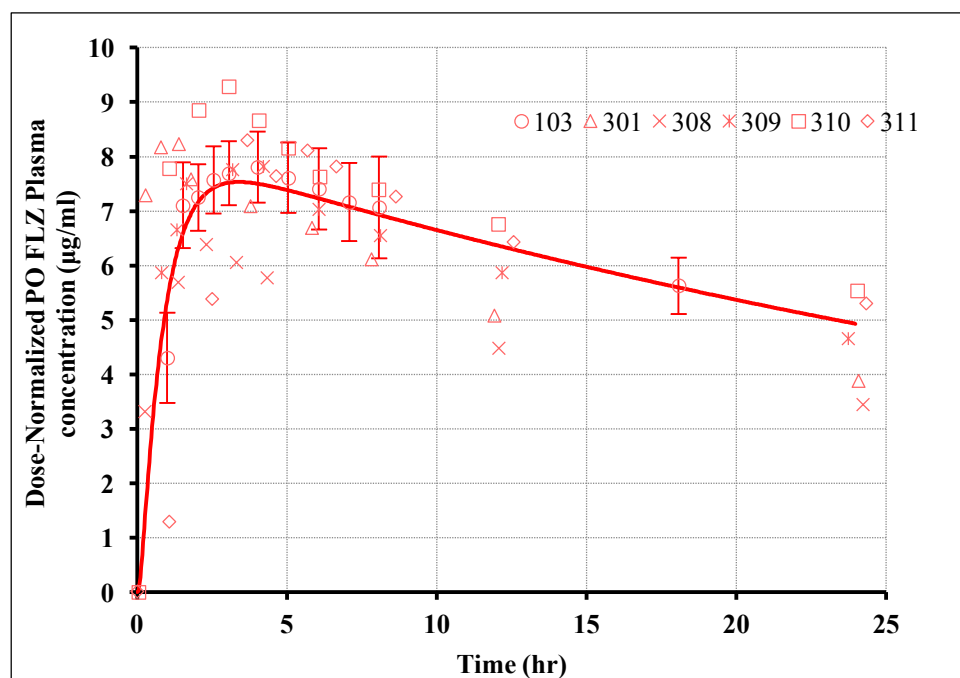


Figure 4.3 Observed and PBPK model-predicted FLZ PK profiles.

a) PK profile of 400 mg FLZ administered after 1 hour IV infusion. b) PK profiles of 400 mg PO FLZ. The solid lines reflect the predicted PK profiles. The circles and bars are observed means and SD values from study 103. Other symbols are observed mean values from different studies (indicated by study ID).

Table 4.3 Comparison of reported and PBPK model-predicted FLZ plasma (blood) exposure metrics.

Deviations of AUC and c_{\max} are marked as bold.

Validation study	Route	Reported Mean AUC ($\mu\text{g/ml}\cdot\text{hr}$)	Predicted Mean AUC ($\mu\text{g/ml}\cdot\text{hr}$)	Deviation (%)	Reported Mean c_{\max} ($\mu\text{g/ml}$)	Predicted Mean c_{\max} ($\mu\text{g/ml}$)	Deviation (%)	Reported Mean t_{\max} (hr)	Predicted Mean t_{\max} (hr)
103	IV (0-18h)	118 ± 7.5	114	3%	8.4 ± 0.6	8.1	-3%	1	1
301	PO (0- ∞)	239	370	55%				~1	3.4
308	PO (0- ∞)	293	370	26%	7.1	8.1	14%	2.37	3.4
309	PO (0- ∞)	345	370	7%	8.2	8.1	-2%	3	3.4
310	PO (0- ∞)	452	370	-18%	9.4	8.1	-14%	3.08	3.4
311	PO (0- ∞)	456	370	-19%	9.4	8.1	-14%	3.08	3.4
103	PO (0-18h)	121 ± 9.5	113	-7%	8.2 ± 0.6	7.5	-9%	4	3.4

4.3.1.2 Sensitivity analysis

The -fold change in unbound blood/hepatic/GW $\text{AUC}_{0-\infty}$, c_{\max} and t_{\max} were calculated by dividing respective exposure metrics simulated at the upper limit by that simulated at the lower limit (Table 4.4 and Table 4.5). A greater than 2-fold or less than 0.5-fold change was

highlighted as bold, indicating the corresponding exposure was sensitive to that parameter. After IV FLZ, CL_{ren}^{FLZ} substantially affects the AUC in all the three compartments, because FLZ is primarily (67%) eliminated through kidney in the model, and hepatic and GW concentrations mimics the decline of blood concentration at pseudo steady-state. $K_{p,hep}^{FLZ}$ and $K_{p,GW}^{FLZ}$ are pivotal parameters determining hepatic and GW concentrations, respectively, albeit no big effect on blood concentration. Increasing f_{pv} can significantly increase drug exposure in the liver, mainly because more drugs got into the liver through portal vein, resulting in slightly reduction in blood AUC (19%) as well. After PO FLZ, most parameters affect corresponding exposure metrics with the same trend as IV FLZ, but a larger f_{pv} drastically prolongs t_{max} of hepatic concentration. This is within expectation because a greater f_{pv} triggers a faster input of drug into liver compartment systemically, and even if the drug has been mostly absorbed, the rapid systemic input can still sustain drug levels in the liver for a while, which delays its t_{max} in the liver. k_{GL}^{FLZ} has no influence on AUC, but can alter t_{max} in all the compartments and c_{max} in GW considerably. The more impact of hepatic t_{max} (~10-fold difference with lower and upper limit of k_{GL}^{FLZ}) than GW t_{max} (~2-fold difference with lower and upper limit of k_{GL}^{FLZ}) is presumably because systemic input of FLZ into liver (through both hepatic artery and portal vein) is pretty fast, which can maintain drug levels and prolong t_{max} quite a bit (similar as f_{pv} 's effect), if k_{GL}^{FLZ} is not fast enough. On the other hand, systemic input of FLZ into GW through Q_{villi} can barely impact t_{max} of c_{GW}^{FLZ} , due to the slow input rate (i.e. Q_{villi}) and the rapid output rate (i.e. Q_{PV}). However, in MDZ and FLZ DDI studies (Ahonen et al., 1997; Kharasch et al., 2005; Olkkola et al., 1996), MDZ was administered 1-2 hours after the administration of FLZ, thus the change in t_{max} might not be clinical significant. FLZ PK profiles in all sensitivity analyses are presented in

Appendices B.

Table 4.4 Sensitivity analysis heat-map results for semi-PBPK IV FLZ model.

(More solid green indicates smaller value; more solid red indicates larger value)

Parameter	-Fold Change	-Fold change in blood exposure metrics			-Fold change in hepatic exposure metrics			-Fold change in GW exposure metrics		
		AUC _{0-∞}	c _{max}	t _{max}	AUC _{0-∞}	c _{max}	t _{max}	AUC _{0-∞}	c _{max}	t _{max}
f _{pV} ^{FLZ}	0-1	0.81	0.98	1.00	1.79	2.17	0.90	0.81	0.98	0.95
K _{p,hep} ^{FLZ}	4	0.61	0.95	1.00	2.42	3.73	0.97	0.61	0.94	0.95
K _{p,GW} ^{FLZ}	4	1.00	0.95	1.00	1.00	0.92	1.17	3.99	3.66	1.50
CL _{int,hep} ^{FLZ}	4	0.61	0.99	1.00	0.61	0.98	0.96	0.61	0.99	1.00
CL _{ren} ^{FLZ}	4	0.43	0.99	1.00	0.43	0.98	0.92	0.43	0.98	0.96

4.5 Sensitivity analysis heat-map results for semi-PBPK PO FLZ model .

(More solid green indicates smaller value; more solid red indicates larger value)

Parameter	-Fold Change	-Fold change in blood exposure metrics			-Fold change in hepatic exposure metrics			-Fold change in GW exposure metrics		
		AUC _{0-∞}	c _{max}	t _{max}	AUC _{0-∞}	c _{max}	t _{max}	AUC _{0-∞}	c _{max}	t _{max}
f _{pV} ^{FLZ}	0-1	0.81	0.97	0.96	1.77	1.64	5.69	0.82	1.00	1.01
K _{p,hep} ^{FLZ}	4	0.61	0.91	0.97	2.42	3.67	0.89	0.63	0.99	0.95
K _{p,GW} ^{FLZ}	4	1.00	0.93	1.13	1.00	0.93	1.05	3.99	2.97	1.50
CL _{int,hep} ^{FLZ}	4	0.61	0.96	0.88	0.61	0.96	0.84	0.63	1.00	1.00
CL _{ren} ^{FLZ}	4	0.43	0.99	1.00	0.43	0.98	0.92	0.43	0.98	0.96
k _{GL} ^{FLZ}	4	1.00	1.09	0.37	1.00	1.23	0.09	1.00	2.79	0.51

4.3.2 Model Predictions

Model predicted FLZ concentrations for all the compartments after 400 mg 1 hour IV infusion or PO FLZ are showed in **Figure 4.4a-b**. After IV administration, GW, portal vein and liver concentration almost mimic the blood concentrations, due to rapid equilibrium among all the compartments. As a consequence, FLZ is instantaneously and homogenously distributed throughout the whole body tissue, which follows one-compartment body model. This is in agreement with the conclusion from other FLZ clinical PK study (Humphrey et al., 1985).

After PO administration, drug in gut lumen is fully absorbed after 7.5 hours. c_{max} of GW, portal vein, liver and systemic blood are sequentially achieved, at 0.3 hour, 2.23 hours, 2.63 hours and 3.23 hours, respectively, which is in consistent with the oral absorption order of FLZ.

After around 4 hours, the distribution of FLZ has reached pseudo steady-state, and concentrations of all the compartments decline at the same rate.

To compare GW and liver concentration after IV and PO administration (**Figure 4.4c**), FLZ unbound hepatic concentrations are almost superimposable, although marginal difference is observed during the first 2 hours. GW concentration after PO FLZ is much higher than IV FLZ during the first 4 hours, but no difference is found after 4 hours. As a result, it is expected that PO FLZ would have greater inhibition on MDZ GW metabolism than IV FLZ, while no significant difference could be found as to hepatic metabolism inhibition. However, the inhibitory effect is also determined by the dynamic concentration of MDZ after IV and PO administration, as well as the inhibitory potency of FLZ on hepatic and GW CYP3A.

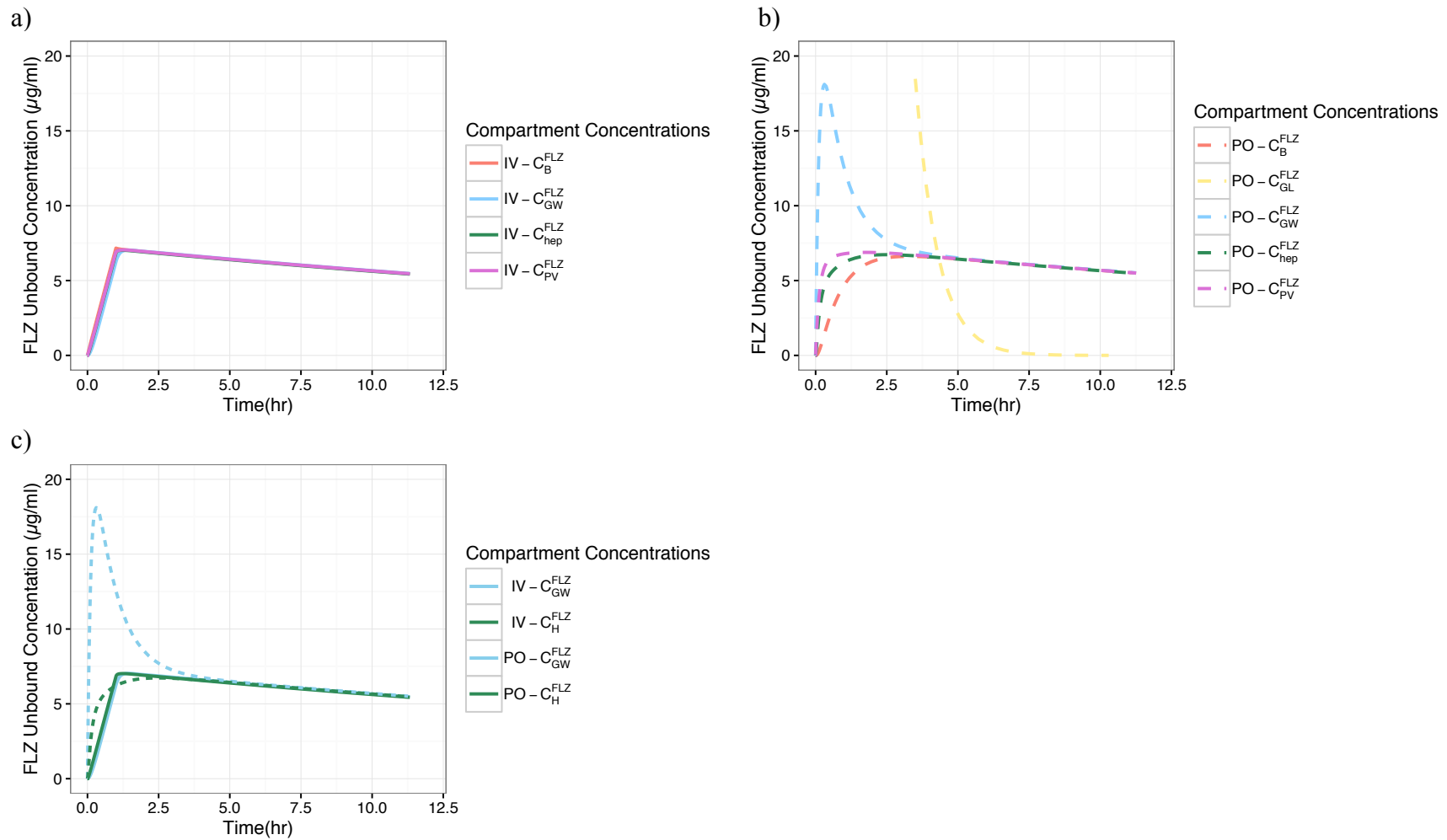


Figure 4.4 Model predicted FLZ concentrations in different compartments.

a) FLZ unbound concentration – time profiles after 400 mg 1 hour IV infusion FLZ. b) FLZ unbound concentration – time profiles after 400 mg PO FLZ. c) FLZ unbound hepatic and GW concentration – time profiles.

4.4 Conclusions

A FLZ semi-PBPK model was developed to describe its clinical PK after IV and PO administration. The model was validated by several clinical PK studies of FLZ, and plasma concentration – time profiles can be characterized well by the model, after dose correction. Formal parameter sensitivity analyses were conducted for six key/uncertain model parameters, and CL_{ren}^{FLZ} is the only influential parameter on FLZ plasma concentration after both IV and PO administration, while k_{GL}^{FLZ} can only affect t_{max} after PO FLZ. In addition to CL_{ren}^{FLZ} and k_{GL}^{FLZ} , hepatic and GW FLZ concentrations are also sensitive to f_{pv} , $K_{p,hep}^{FLZ}$ and $K_{p,GW}^{FLZ}$. Since CL_{ren}^{FLZ} and k_{GL}^{FLZ} are supported by FLZ clinical PK literatures, f_{pv} and $K_{p,hep}^{FLZ}$ and $K_{p,GW}^{FLZ}$ are the pivotal parameters affecting c_{hep}^{FLZ} and c_{GW}^{FLZ} , which may require further optimization once MDZ and FLZ DDI model is built. GW concentration after PO FLZ is much higher than that after IV infusion FLZ, indicating that FLZ may be expected to have greater inhibition on GW metabolism of MDZ after PO than IV infusion administration. Hepatic FLZ concentration doesn't have much difference between IV and PO administration, suggesting no route difference of FLZ on hepatic metabolism of MDZ.

CHAPTER 5

5 SEMI-PBPK MODELING OF IV/PO MDZ

5.1 Background and Objectives

5.1.1 MDZ PK information

Clinically, MDZ is a short-acting benzodiazepine, indicated for preoperative sedation/amnesia/anxiolysis for adults after IV or intramuscular injection, or oral syrup for pediatric patients (Baxter Healthcare Corporation; Ranbaxy Pharmaceuticals Inc., 2013). From **Chapter 3**, dose proportional PK was established between 0.005 mg/kg - 0.1 mg/kg after IV MDZ and between 0.025 mg/kg - 0.244 mg/kg after PO MDZ. After IV administration, MDZ was well-characterized by a 3-compartmental body model in study 21 (Kharasch et al., 2005b), and rapidly eliminated by hepatic CYP3A metabolism exclusively, with negligible renal elimination (Baxter Healthcare Corporation; Tolle-Sander et al., 2003). It has a short half-life ($t_{1/2}^{\text{MDZ}}$) of 1.8-6.4 hours, and a high plasma protein binding ($f_u^{\text{MDZ}} = 0.03$ (Baxter Healthcare Corporation)). After PO administration, it is well absorbed into GW (BCS class 1 drug (Wu & Benet, 2005)), and sequentially subject to extensive pre-systemic GW and hepatic CYP3A metabolism before reaching systemic circulation.

5.1.2 Available validation studies and simulation strategies

Based on the quantitative meta-analysis discussed in **Chapter 3**, study 21 (Kharasch et al., 2005), study 26 (Olkola et al., 1996) and study 103 (Ahonen et al., 1997) are the three clinical studies to assess DDI between MDZ and FLZ in our final database. Therefore, MDZ semi-PBPK model should be validated by the observed MDZ plasma concentration – time profiles in absence of FLZ in the three studies.

In study 21, twelve volunteers were enrolled in a randomized 4-way crossover study, separated by at least 2 weeks between each session. They received single dose of 0, 100, 200, or 400 mg PO FLZ, followed 2 hours later by 1mg IV MDZ; the next day, they received the same dose of placebo or FLZ, followed by 3 mg PO MDZ. Plasma concentrations of MDZ after IV and PO administration were both determined up to 8 h by LC-MS (LLOQ = 0.1ng/ml).

In study 103, a double-dummy, randomized, 3-way cross-over study was performed in 9 healthy volunteers. The subjects were given 7.5 mg PO MDZ 1 hour after placebo, IV 400mg FLZ over 1-hour infusion or PO 400 mg FLZ. Plasma concentrations of MDZ and FLZ were determined for up to 17 h by HPLC (LLOQ = 1ng/ml).

In study 26, a double-blind, randomized, 3-phase cross-over study was conducted in 12 healthy volunteers (7 males and 5 females). The subjects were given orally, once daily either placebo or FLZ 400 mg on the first day and then 200 mg daily for 5 days. On the first day of pretreatment, 7.5 mg of PO MDZ was ingested 2 hours after the first dose of placebo or FLZ. IV MDZ 0.05 mg/kg, was administered over 2 min injection on the 4th day of pretreatment. The third dose, 7.5 mg of PO MDZ was ingested on the 6th day. MDZ was always administered 2 hours after placebo or FLZ doses. Plasma concentrations of MDZ were determined for up to 17 h by gas chromatography (LLOQ = 0.1ng/ml).

After model qualification by the three studies, sensitivity analyses were performed to detect key PK/physiological parameters in MDZ semi-PBPK model that could influence MDZ plasma exposures the most, to facilitate future DDI model optimization.

5.1.3 Objectives

The major objectives of the chapter were to:

- a. Develop a semi-PBPK model of MDZ to describe its PK profiles in human after IV and PO administration
- b. Validate the model using plasma concentration-time profiles in clinical DDI studies (without FLZ group), and identify pivotal PK/physiological parameters that determine MDZ plasma exposure metrics by sensitivity analysis
- c. Predict tissue (*e.g.* hepatic, GW) concentration – time profiles of MDZ using the validated semi-PBPK model

5.2 Methods

5.2.1 Development of MDZ semi-PBPK model

5.2.1.1 MDZ semi-PBPK model after IV administration

A semi-PBPK model for IV MDZ was built based on the reported *in-vitro* metabolic information, PK and physiological parameters (**Table 5.1**). A conventional three-compartmental body model with additional compartments for GW serosa, portal vein, and liver was developed, and showed in **Figure 5.1**. This model is similar to the FLZ semi-PBPK model (**see Chapter 4, Section 4.2.1**), with the following differences: (1) After IV administration, MDZ is injected directly into the systemic circulation, and assumed to distribute to a rapidly equilibrating

“shallow” peripheral compartment (Peripheral Cpt-1) and a slowly equilibrating “deep” peripheral compartment (Peripheral Cpt-2), with the inter-compartmental clearance of Q_2^{MDZ} to Peripheral Cpt-1 and Q_3^{MDZ} to Peripheral Cpt-2, except GW, portal vein and liver, as tissues of interest. (2) MDZ has negligible renal elimination, and hepatic intrinsic clearance is expressed as $V_{max,hep}^{MDZ}/K_{m,hep}^{MDZ}$. (3) In terms of GW metabolism, after scaling from *in-vitro* metabolic study to *in-vivo* intrinsic clearance of unbound MDZ (Paine et al., 1997), intrinsic GW clearance ($CL_{int,GW}^{MDZ}$) is only 1.3% of $CL_{int,hep}^{MDZ}$, confirming the assumption of negligible GW metabolism of MDZ after IV administration. Hence, hepatic clearance is assumed to be the only elimination pathway after IV MDZ.

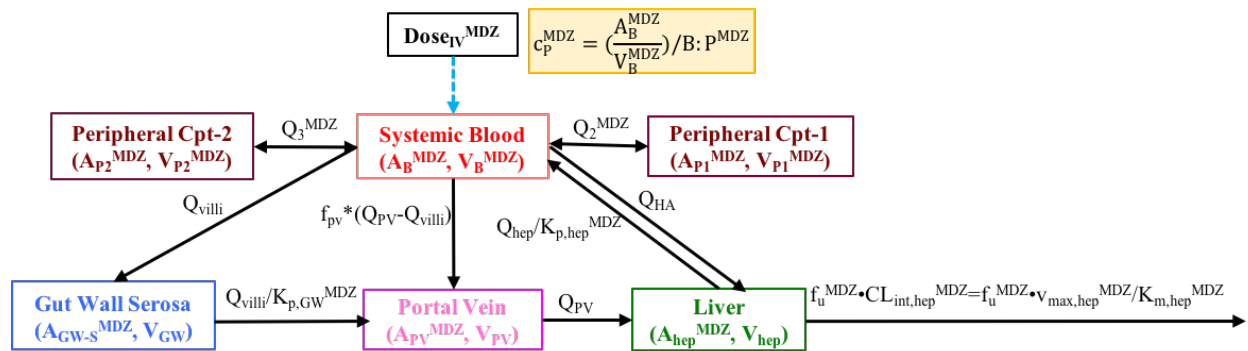


Figure 5.1 Semi-PBPK model scheme for the disposition of MDZ after IV administration.

1) Differential equations:

Based on the model above, differential equations for total (unbound + bound) MDZ mass transfer between compartments were expressed as equations (5.1) to (5.6):

$$\frac{dA_B^{MDZ}(t)}{dt} = k_0^{MDZ} + c_{P1}^{MDZ} \cdot Q_2^{MDZ} + c_{P2}^{MDZ} \cdot Q_3^{MDZ} + \left(\frac{C_{hep}^{MDZ}}{K_{p,hep}^{MDZ}} \right) \cdot Q_{hep} - c_B^{MDZ} \cdot f_{PV} \cdot (Q_{PV} - Q_{villi}) - c_B^{MDZ} \cdot Q_{HA} - c_B^{MDZ} \cdot Q_{villi} - c_B^{MDZ} \cdot Q_2^{MDZ} - c_B^{MDZ} \cdot Q_3^{MDZ}$$

when $t = 0$, $A_B^{MDZ}(0) = 0$; when $t = 2$ min, $A_B^{MDZ}(2) = Dose_{IV}^{MDZ}$ (5.1)

$$\frac{dA_{P1}^{MDZ}(t)}{dt} = c_B^{MDZ} \cdot Q_2^{MDZ} - c_{P2}^{MDZ} \cdot Q_2^{MDZ}$$

$$\text{when } t = 0, A_{P1}^{\text{MDZ}}(0) = 0 \quad (5.2)$$

$$\frac{dA_{P2}^{\text{MDZ}}(t)}{dt} = c_B^{\text{MDZ}} \cdot Q_3^{\text{MDZ}} - c_{P2}^{\text{MDZ}} \cdot Q_3^{\text{MDZ}}$$

$$\text{when } t = 0, A_{P2}^{\text{MDZ}}(0) = 0 \quad (5.3)$$

$$\frac{dA_{\text{GW-S}}^{\text{MDZ}}(t)}{dt} = c_B^{\text{MDZ}} \cdot Q_{\text{villi}} - \left(\frac{c_{\text{GW-S}}^{\text{MDZ}}}{K_{p,\text{GW}}^{\text{MDZ}}} \right) \cdot Q_{\text{villi}}$$

$$\text{when } t = 0, A_{\text{GW-S}}^{\text{MDZ}}(0) = 0 \quad (5.4)$$

$$\frac{dA_{\text{PV}}^{\text{MDZ}}(t)}{dt} = c_B^{\text{MDZ}} \cdot f_{\text{PV}} \cdot (Q_{\text{PV}} - Q_{\text{villi}}) + \left(\frac{c_{\text{GW-S}}^{\text{MDZ}}}{K_{p,\text{GW}}^{\text{MDZ}}} \right) \cdot Q_{\text{villi}} - c_{\text{PV}}^{\text{MDZ}} \cdot Q_{\text{PV}}$$

$$\text{when } t = 0, A_{\text{PV}}^{\text{MDZ}}(0) = 0 \quad (5.5)$$

$$\frac{dA_{\text{hep}}^{\text{MDZ}}(t)}{dt} = c_B^{\text{MDZ}} \cdot Q_{\text{HA}} + c_{\text{PV}}^{\text{MDZ}} \cdot Q_{\text{PV}} - \left(\frac{c_{\text{hep}}^{\text{MDZ}}}{K_{p,\text{hep}}^{\text{MDZ}}} \right) \cdot Q_{\text{hep}} - c_{\text{hep}}^{\text{MDZ}} \cdot f_u^{\text{MDZ}} \cdot V_{\text{max,hep}}^{\text{MDZ}} / K_{m,\text{hep}}^{\text{MDZ}}$$

$$\text{when } t = 0, A_{\text{hep}}^{\text{MDZ}}(0) = 0 \quad (5.6)$$

A_B^{MDZ} , A_{P1}^{MDZ} , A_{P2}^{MDZ} , $A_{\text{GW-S}}^{\text{MDZ}}$, $A_{\text{PV}}^{\text{MDZ}}$ and $A_{\text{hep}}^{\text{MDZ}}$ are the amounts of drug in central, shallow peripheral, deep peripheral, GW serosa, portal vein and liver compartments, respectively; c_B^{MDZ} , c_{P1}^{MDZ} , c_{P2}^{MDZ} , $c_{\text{GW-S}}^{\text{MDZ}}$, $c_{\text{PV}}^{\text{MDZ}}$, $c_{\text{hep}}^{\text{MDZ}}$ are drug concentrations in central, shallow peripheral, deep peripheral, GW serosa, portal vein and liver compartments, calculated by dividing amount (A) by the respective compartment volume: V_B^{MDZ} , V_{P1}^{MDZ} , V_{P2}^{MDZ} , V_{GW} , V_{PV} and V_{hep} , which are MDZ volume of central, shallow peripheral, deep peripheral compartments, volume of GW, portal vein and liver. IV bolus is assumed to be a 2-min IV infusion, thus an infusion rate k_0^{MDZ} was introduced in equation (5.1) as a dose input rate, and initial amounts for all the six compartments are 0.

2) Volume of distributions and inter-departmental clearance

Systemic blood compartment volume of distribution (V_B^{MDZ}), shallow peripheral compartment volume of distribution (V_{P1}^{MDZ}), deep peripheral compartment volume of

distribution (V_{p2}^{MDZ}), Q_2^{MDZ} and Q_3^{MDZ} were estimated from the digitized plasma concentration – time data of MDZ in absence of FLZ in study 21 (Kharasch et al., 2005b), with a traditional three-compartmental body model (See **Appendix C**).

V_{GW} , V_{hep} and V_{PV} were used the same values as FLZ semi-PBPK model (see **Chapter 4, section 4.2.1.3**).

3) Partition coefficient between blood and tissue (K_p)

$K_{p,GW}^{MDZ}$ and $K_{p,hep}^{MDZ}$ are the GW-to-blood partition coefficient and liver-to-blood partition coefficient, which are 1.12 and 1.09 (Björkman et al., 2001), respectively.

4) Blood flows (Q)

Q_{hep} , Q_{PV} , Q_{HA} and Q_{villi} were used the same values as FLZ semi-PBPK model (see **Chapter 4, section 4.2.1.3**)

5) Clearance

Since MDZ follows dose-proportional PK under 0.1 mg/kg after IV MDZ, and under 0.224 mg/kg after PO MDZ (according to **Chapter 3**), $CL_{int,hep}^{MDZ}$ can be represented as $v_{max,hep}^{MDZ}/K_{m,hep}^{MDZ}$. $K_{m,hep}^{MDZ}$ was set as *in-vitro* K_m of human liver microsomes from 4 donors by measuring the formation rate of 1'-OH-MDZ (Thummel et al., 1996). $v_{max,hep}^{MDZ}$ was quite variable across *in-vitro* metabolic studies, hence $CL_{int,hep}^{MDZ}$ was calculated by equation (5.7) using study 21.

$$CL_{int,hep}^{MDZ} = \left(\frac{CL_{hep}^{MDZ} \cdot Q_{hep}}{Q_{hep} - CL_{hep}^{MDZ}} \right) / f_u^{MDZ} \quad (5.7)$$

CL_{hep}^{MDZ} is the systemic hepatic clearance (corrected by blood-to-plasma partitioning ratio of MDZ) estimated from study 21 using non-compartmental analysis, assuming system hepatic clearance is the only elimination pathway after IV MDZ. f_u^{MDZ} is the fraction unbound of MDZ in hepatocytes. $v_{max,hep}^{MDZ}$ was then calculated by equation (5.8),

$$V_{\max, \text{hep}}^{\text{MDZ}} = \text{CL}_{\text{int, hep}}^{\text{MDZ}} \cdot K_{\text{m, hep}}^{\text{MDZ}} \quad (5.8)$$

6) Fraction unbound and blood-to-plasma partitioning ratio

Due to limited information, fraction unbound of MDZ (f_u^{MDZ}) was assumed to be time/concentration independent, and f_u^{MDZ} in plasma and hepatocytes were assumed to be the same, which is 0.03 (Gandhi et al., 2012). Blood-to-plasma partitioning ratio of MDZ ($B:P^{\text{MDZ}}$) was set as 0.86 (Ervine & Houston, 1994).

Body weight was set as the mean body weight (70kg) of subjects in study 21.

5.2.1.2 MDZ semi-PBPK model after PO administration

A semi-PBPK model for PO MDZ (**Figure 5.2**) was built based on the reported *in-vitro* metabolic information, PK and physiological parameters (**Table 5.1**). A conventional three-compartmental body model with additional compartments for gut lumen, GW mucosa, GW serosa, portal vein, and liver was developed, by adding two absorptive compartments (gut lumen and GW mucosa) to the IV model. After PO administration, MDZ is dissolved in the gut lumen first, and a fraction of drug ($F_{\text{abs}}^{\text{MDZ}}$) permeates through GW, with a first order absorption rate $k_{\text{GL}}^{\text{MDZ}}$. Since MDZ is a BCS class 1 drug (Wu & Benet, 2005), with high solubility across the whole gastrointestinal tract pH range and high permeability, it is reasonable to assume that $F_{\text{abs}}^{\text{MDZ}} = 100\%$, and drug transporters have little effect on its absorption (Tolle-Sander et al., 2003). Due to the rapid diffusion of MDZ into GW, portal vein and liver, permeating into the GW was assumed to be the rate-limiting step of its oral absorption, and $k_{\text{GL}}^{\text{MDZ}} \approx k_a^{\text{MDZ}}$ (k_a^{MDZ} was the observed oral absorption rate constant of MDZ reported in literatures (Johnson et al., 2002; Kato et al., 2008). Once it is permeated into GW through mucosa side, MDZ can be metabolized by GW CYP3A enzymes located at the villous tips (Yang et al., 2007; Watkins, 1997). Pre-systemic GW extraction is much higher than systemic GW extraction, due to the

negligible protein binding ($f_{u,GW-M}^{MDZ} = 1.0$) and potential higher concentrations at the mucosal side of intestinal epithelium. To calculate pre-systemic GW intrinsic clearance ($CL_{int,GW}^{MDZ}$), $V_{max,GW}^{MDZ}$ and $K_{m,GW}^{MDZ}$ values were extrapolated from *in-vitro* metabolic study (Thummel et al., 1996). f_{villi} was added as an *in vitro – in vivo* scaling factor, as well as an adjustment of the real functional GW CYP3A (drugs may not diffuse to certain regions of GW, or oxygen may not be sufficient, inter-individual variability, etc.). Sensitivity analysis was conducted to f_{villi} on MDZ plasma concentrations (See **section 5.2.3**). In addition, the potential high concentration of MDZ at GW mucosa may lead to saturable GW metabolism, therefore, $CL_{int,GW}^{MDZ}$ was expressed as a Michaelis-Menten equation format (5.9)

$$CL_{int,GW}^{MDZ} = \frac{f_{villi} \cdot V_{max,GW}^{MDZ}}{K_{m,GW}^{MDZ} + f_{u,GW-M}^{MDZ} \cdot C_{GW-M}^{MDZ}} \quad (5.9)$$

Furthermore, a transit rate constant (k_T) from mucosa to serosa was added to connect the two sides of GW, and set as Q_{villi}/V_{GW} , to keep the outflow from mucosa to serosa of intestinal epithelium constant to be Q_{villi} . MDZ is then carried into portal vein with blood flow of Q_{villi} , and reaches liver via portal vein. Before getting into the systemic blood compartment, it can be metabolized by liver pre-systemically. Once it gets into the systemic blood, the disposition is the same as IV administration.

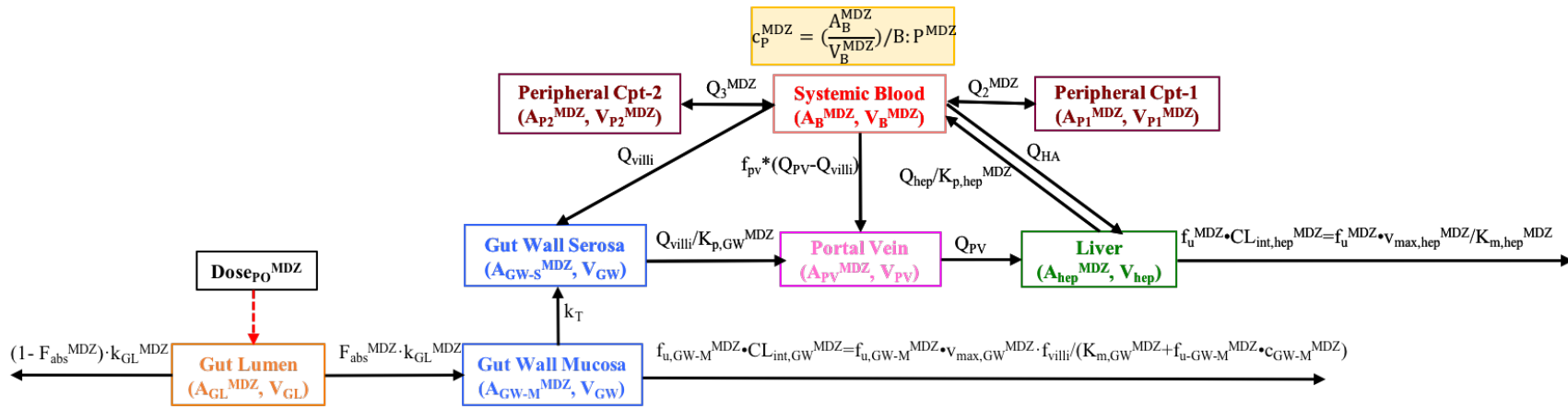


Figure 5.2 Semi-PBPK model scheme for the disposition of MDZ after PO administration.

Based on the model scheme, differential equations for mass transfer between compartments were expressed as equations (5.10) to (5.17):

$$\frac{dA_{GL}^{MDZ}(t)}{dt} = -c_{GL}^{MDZ} \cdot V_{GL} \cdot F_{abs}^{MDZ} \cdot k_{GL}^{MDZ} - c_{GL}^{MDZ} \cdot V_{GL} \cdot (1 - F_{abs}^{MDZ}) \cdot k_{GL}^{MDZ}$$

when $t = 0$, $A_{GL}^{MDZ}(0) = Dose_{PO}^{MDZ}$ (5.10)

$$\frac{dA_{GW-M}^{MDZ}(t)}{dt} = c_{GL}^{MDZ} \cdot V_{GL} \cdot F_{abs}^{MDZ} \cdot k_{GL}^{MDZ} - c_{GW-M}^{MDZ} \cdot V_{GW} \cdot k_T - f_{u,GW-M}^{MDZ} \cdot c_{GW-M}^{MDZ} \cdot f_{villi}$$

$$\cdot v_{max,GW} / (K_{m,GW} + f_{u,GW-M}^{MDZ} \cdot c_{GW-M}^{MDZ})$$

when $t = 0$, $A_{GW-M}^{MDZ}(0) = 0$ (5.11)

$$\frac{dA_{GW-S}^{MDZ}(t)}{dt} = c_{GW-M}^{MDZ} \cdot V_{GW} \cdot k_T + c_B^{MDZ} \cdot Q_{villi} - \left(\frac{c_{GW-S}^{MDZ}}{K_{p,GW}^{MDZ}} \right) \cdot Q_{villi}$$

when $t = 0$, $A_{GW-S}^{MDZ}(0) = 0$ (5.12)

$$\frac{dA_{PV}^{MDZ}(t)}{dt} = c_B^{MDZ} \cdot f_{PV} \cdot (Q_{PV} - Q_{villi}) + \left(\frac{c_{GW-S}^{MDZ}}{K_{p,GW}^{MDZ}} \right) \cdot Q_{villi} - c_{PV}^{MDZ} \cdot Q_{PV}$$

when $t = 0$, $A_{PV}^{MDZ}(0) = 0$ (5.13)

$$\frac{dA_{hep}^{MDZ}(t)}{dt} = c_B^{MDZ} \cdot Q_{HA} + c_{PV}^{MDZ} \cdot Q_{PV} - \left(\frac{c_{hep}^{MDZ}}{K_{p,hep}^{MDZ}} \right) \cdot Q_{hep} - c_{hep}^{MDZ} \cdot f_u^{MDZ} \cdot v_{max,hep} / K_{m,hep}^{MDZ}$$

when $t = 0$, $A_{hep}^{MDZ}(0) = 0$ (5.14)

$$\frac{dA_B^{MDZ}(t)}{dt} = c_{P1}^{MDZ} \cdot Q_2^{MDZ} + c_{P2}^{MDZ} \cdot Q_3^{MDZ} + \left(\frac{c_{hep}^{MDZ}}{K_{p,hep}^{MDZ}} \right) \cdot Q_{hep} - c_B^{MDZ} \cdot f_{PV} \cdot (Q_{PV} - Q_{villi})$$

$$- c_B^{MDZ} \cdot Q_{HA} - c_B^{MDZ} \cdot Q_{villi} - c_B^{MDZ} \cdot Q_2^{MDZ} - c_B^{MDZ} \cdot Q_3^{MDZ}$$

when $t = 0$, $A_B(0) = 0$ (5.15)

$$\frac{dA_{P1}^{MDZ}(t)}{dt} = c_B^{MDZ} \cdot Q_2^{MDZ} - c_{P2}^{MDZ} \cdot Q_2^{MDZ}$$

$$\text{when } t = 0, A_{P1}^{\text{MDZ}}(0) = 0 \quad (5.16)$$

$$\frac{dA_{P2}^{\text{MDZ}}(t)}{dt} = c_B^{\text{MDZ}} \cdot Q_3^{\text{MDZ}} - c_{P2}^{\text{MDZ}} \cdot Q_3^{\text{MDZ}}$$

$$\text{when } t = 0, A_{P2}^{\text{MDZ}}(0) = 0 \quad (5.17)$$

A_{GL}^{MDZ} and A_{GW-M}^{MDZ} are the amounts of drug in gut lumen and GW mucosa, respectively; C_{GL}^{MDZ} and C_{GW-M}^{MDZ} are drug concentrations in gut lumen and GW mucosa, calculated by dividing amount (A) by the respective compartment volume: V_{GL} and V_{GW} . Volume of both GW mucosa and serosa were assumed to be the same as V_{GW} .

5.2.1.3 Model parameters and assumptions

Initial model parameters used in semi-PBPK models of IV/PO MDZ are summarized in **Table 5.1**. Physiological parameters were the same as FLZ semi-PBPK model, except for adding $f_{\text{villi}} \cdot v_{\text{max,hep}}^{\text{MDZ}}$ and f_{villi} , representing hepatic CYP3A capacity and scaling factor for GW CYP3A capacity, were adjusted during model qualification processes, which were discussed in **section 5.3.1.1**.

Table 5.1 Initial semi-PBPK MDZ model parameters.

Parameter	Definition	Value	Source
Physiological parameters			
V_{GL} (ml/kg)	Volume of gut lumen	3.57	Assumed to be 250ml (FDA, 2012)
V_{GW} (ml/kg)	Volume of GW	33.6	Calculated by equation (4.6), assumed to be the surface of gut lumen cylinder
V_{PV} (ml/kg)	Volume of portal vein	0.97	Unknown methods (Ito et al., 2003)
V_{hep} (ml/kg)	Volume of liver	22.5	Calculated by equation (4.7) and (4.8)
Q_{villi} (ml/min/kg)	Villous blood flow	4.30	<i>In-vivo</i> experiment (Yang et al., 2007)
Q_{hep} (ml/min/kg)	Hepatic blood flow	21.4	<i>In-vivo</i> experiment (Tsunoda et al., 1999)
f_{HA}	Fraction of hepatic artery to total hepatic blood flow	0.25	(Eipel et al., 2010) (Q_{HA} was calculated as $f_{HA} \cdot Q_{hep}$; Q_{PV} was calculated as $(1-f_{HA}) \cdot Q_{hep}$)
f_{PV}	Fraction of the components of portal vein that contain drug	1.00	A correction factor that can be adjusted according to simulation results.
$l_{F_{villi}}$	IVIVE scaling factor and IIV adjusting factor	2.2	Optimized with data from study 21
MDZ PK Parameters			
V_B^{MDZ} (ml/kg)	Volume of systemic blood compartment	140.4	See Appendices C
V_{P1}^{MDZ} (ml/kg)	Volume of shallow peripheral compartment	313.7	See Appendices C
V_{P2}^{MDZ} (ml/kg)	Volume of deep peripheral compartment	531.4	See Appendices C
Q_2^{MDZ} (min ⁻¹)	Inter-compartmental clearance between central and peripheral cpt-1	55.27	See Appendices C
Q_3^{MDZ} (min ⁻¹)	Inter-compartmental clearance between central and peripheral cpt-2	7.25	See Appendices C
f_u^{MDZ}	Fraction unbound of MDZ	0.03	Assume to be the same in plasma and hepatocytes (Gandhi et al., 2012)
$f_{u,GW-M}^{MDZ}$	Fraction unbound at mucosal side of intestinal epithelium	1.0	Assumed to be negligible bound
$V_{max,GW}^{MDZ}$ (ng/min/kg)	GW CYP3A capacity to metabolize MDZ	3357.6	<i>In-vitro</i> experiment (Thummel et al., 1996)
$K_{m,GW}^{MDZ}$ (ng/ml)	GW CYP3A affinity of metabolizing MDZ	1173	<i>In-vitro</i> experiment (Thummel et al., 1996) (3.6 μ M)
$l_{V_{max,hep}^{MDZ}}$ (ng/min/kg)	Hepatic CYP3A capacity to metabolize MDZ	3050 ⁶⁷	<i>In-vivo</i> experiment, calculated from equation (5.7-5.8), using data from study 21
$K_{m,hep}$ (ng/ml)	Hepatic CYP3A affinity of metabolizing MDZ	880	<i>In-vitro</i> experiment (Thummel et al., 1996) (2.7 μ M)
$K_{p,GW}^{MDZ}$	GW-to-blood partition coefficient	1.12	Scaled from rats K_p (Björkman et al., 2001)
$K_{p,hep}^{MDZ}$	Liver-to-blood partition coefficient	1.09	Scaled from rats K_p (Björkman et al., 2001)
$B:P^{MDZ}$	Blood-to-plasma partitioning ratio	0.86	(Ervin & Houston, 1994)
k_{GL}^{MDZ} (min ⁻¹)	Absorption rate constant from gut lumen to GW	0.05	<i>In-vivo</i> experiment (Johnson et al., 2002; Kato et al., 2008), assumed to be k_a^{MDZ}
k_T (min ⁻¹)	Transit rate from mucosal to serosal side of intestinal epithelium	0.13	Assumed, calculated from Q_{villi}/V_{GW}
F_{abs}^{MDZ}	Fraction of MDZ absorbed from gut lumen	100%	BCS Class 1 drug (Wu & Benet, 2005)

¹Parameter values were adjusted in study 103 and 26.

The assumptions made in MDZ semi-PBPK modeling included:

- 1) MDZ follows a three-compartmental body disposition model (except GW, portal vein, liver) after IV administration (based on observed PK profile in study 21).
- 2) Perfusion (blood flow) is the rate-limiting step for MDZ tissue distribution, rather than tissue uptake.
- 3) Renal clearance of MDZ is negligible.
- 4) Negligible drug transporter effect, if any, on MDZ PK.
- 5) CYP3A is the only elimination pathway in GW and liver (metabolic fraction by CYP3A is 0.93 (Quinney et al., 2010; Zhang et al., 2009)), and the formation of other metabolites (besides 1'-OH-MDZ) is negligible.
- 6) MDZ is at equilibrium between hepatocytes and hepatic venous outflow (well-stirred model).
- 7) Partition coefficient (K_p) for GW and liver are constant.
- 8) No/negligible GW metabolism occurs after IV MDZ.
- 9) MDZ's binding to hepatic proteins is assumed to be the same as plasma protein binding; protein binding at mucosal side of intestinal epithelium is negligible.
- 10) MDZ is rapidly dissolved in gut lumen, and completely absorbed from gut lumen.
($F_{abs}^{MDZ}=100\%$)
- 11) MDZ follows 1st-order diffusion across GW, and this process is the rate-limiting step of its oral absorption. ($k_{GL}^{MDZ} \approx k_a^{MDZ}$)
- 12) GW compartment is divided into mucosal side and serosal side; volumes of the two compartments are both V_{GW} , and the transit rate (k_T) from mucosa to serosa is Q_{villi}/V_{GW} .
- 13) MDZ follows dose-proportional PK at relevant dose range. ($CL_{int,hep}^{MDZ}$ can be represented by $v_{max,hep}/K_{m,hep}$)

5.2.2 Model qualification and predictions

Model simulated MDZ plasma concentration-time profiles were compared with observed profiles in absence of FLZ from study 21 (Kharasch et al., 2005), study 103 (Ahonen et al., 1997) and study 26 (Olkola et al., 1996), to assess model validity by predictive visual check and exposure metrics comparison. Since some parameters (i.e. $v_{\max, \text{hep}}^{\text{MDZ}}$ and f_{villi} , discussed later) were optimized in different MDZ PK studies - due to the large inter-study variability of hepatic and GW CYP3A-, a more stringent acceptance criterion: predicted exposure metrics are $\pm 30\%$ of observed, were used to assess performance of MDZ semi-PBPK model. Plasma concentrations were simulated using Simbiology (MATLAB, 2015a), and the predicted exposure metrics were summarized and compared to reported values. MDZ concentrations in all compartments were simulated using the semi-PBPK model, in order to compare tissue concentration-time profiles after different route of administration.

5.2.3 Sensitivity Analysis

Formal sensitivity analyses were conducted by altering the values for 8 key semi-PBPK model parameters (f_{pv} , $v_{\max, \text{hep}}^{\text{MDZ}}$, $K_{\text{p, hep}}^{\text{MDZ}}$, $K_{\text{p, GW}}^{\text{MDZ}}$, Q_2^{MDZ} , Q_3^{MDZ} , f_{villi} and $k_{\text{GL}}^{\text{MDZ}}$), to assess their significance on MDZ systemic plasma exposures in absence of FLZ. All parameters (except f_{pv} , which was simulated at 0.0, 0.5 and 1.0) were increased and decreased by 2-fold relative to their original values (overall-fold change in values = 4 - fold), as showed in **Table 5.2**, and the respective plasma concentration - time profiles were predicted under 1 mg IV bolus MDZ over 2 min or 3 mg PO MDZ, as a representative of the dosing regimen in study 21. Plasma exposure metrics (AUC, c_{\max} , t_{\max}) were identified, and the sensitivity to each parameter was assessed by dividing respective exposure metrics simulated at the upper limit by that simulated at the lower limit.

Table 5.2 Values of parameters used in sensitivity analysis.

Parameter Name	Initial Value	Lower/Upper Sensitivity Limits
f_{pv}	1.0	0; 1.0
$v_{max,hep}^{MDZ}$ (ng/min/kg)	305067	152534; 610134
$K_{p,hep}^{MDZ}$	1.09	0.55; 2.18
$K_{p,GW}^{MDZ}$	1.12	0.56; 2.24
Q_2^{MDZ} (ml/min/kg)	55.3	27.7; 110.6
Q_3^{MDZ} (ml/min/kg)	7.25	3.63; 14.5
f_{villi}	2.2	1.1; 4.4
k_{GL}^{MDZ} (min ⁻¹)	0.05	0.025; 0.1

5.3 Results and Disucssion

5.3.1 Model evaluation

5.3.1.1 Predictive performance check

The observed and model-predicted MDZ PK profiles for study 21 are showed in **Figure 5.3a-b** and the comparison of observed and model simulated exposure metrics are summarized in **Table 5.3**. **Figure 5.3a-b** demonstrate that the model can predict MDZ PK profiles well after both IV and PO administration in study 21, with all predicted values superimposable with observed data. Deviations (%) of $AUC_{0-\infty}$ and c_{max} are all less than 30%, which is a pre-defined cut-off of precise prediction, and t_{max} difference was quite minimal.

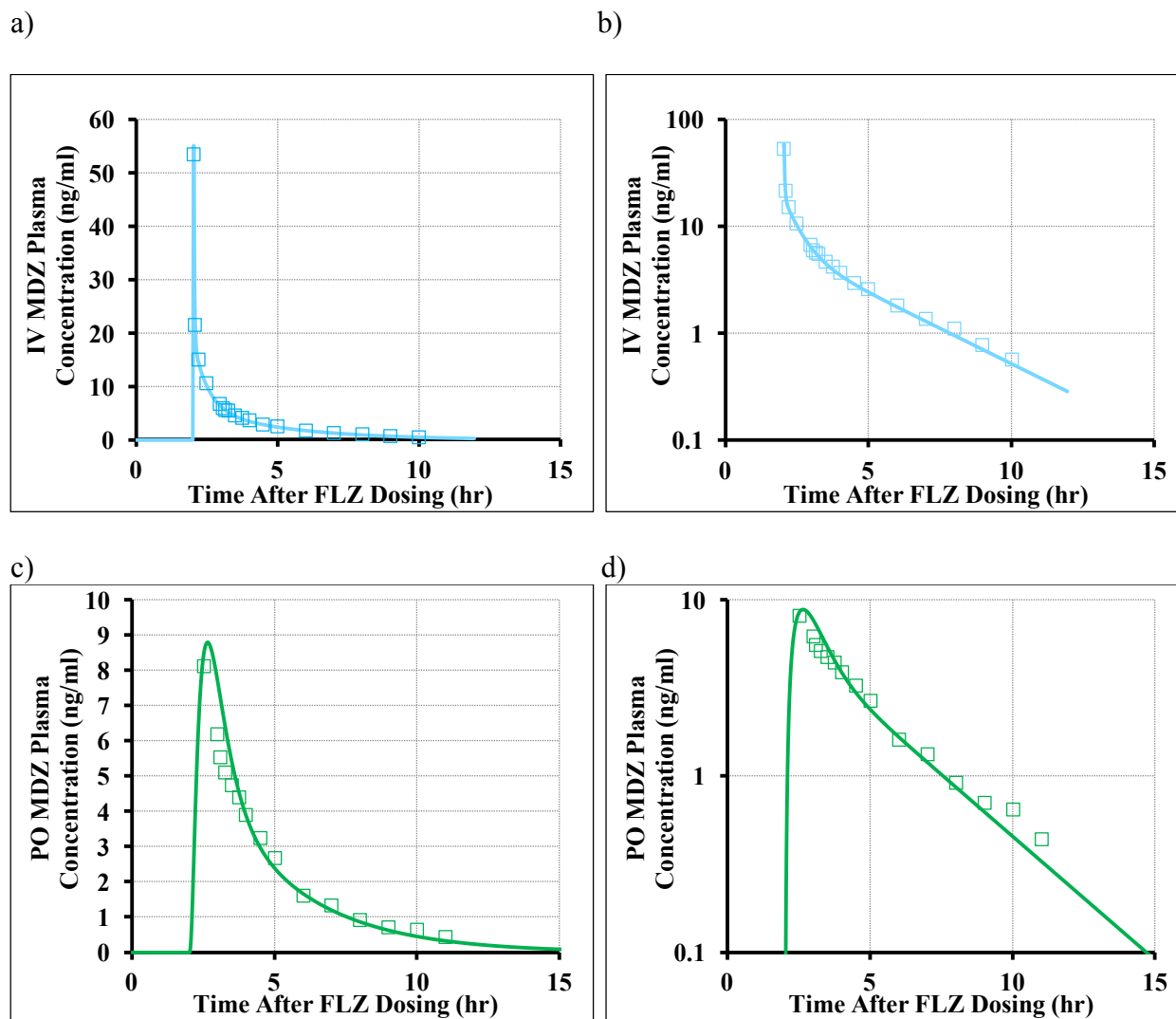
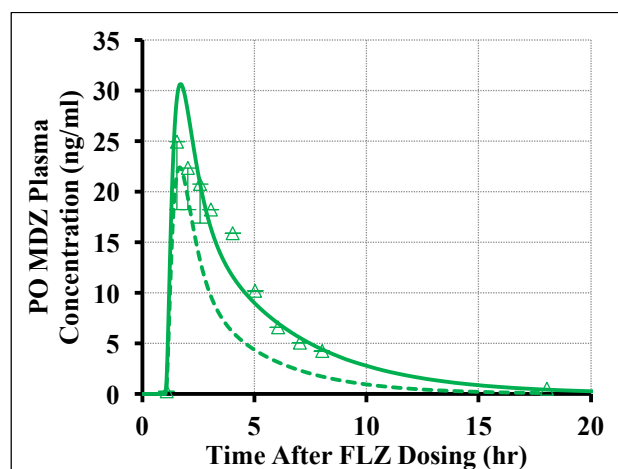


Figure 5.3 Observed and PBPK-model simulated MDZ PK profiles in study 21.

a-b) IV MDZ 1 mg (0.014mg/kg) in the absence of FLZ (Cartesian and semi-log plots). c-d) PO MDZ 3mg (0.043mg/kg) in the absence of FLZ (Cartesian and semi-log plots). The solid lines reflect the predicted PK profiles. The symbols are reported mean concentrations in study 21.

For study 103, all the parameters were originally assumed to be the same with study 21. However, the predicted terminal slope was apparently steeper than the observed slope (**Figure 5.4, dashed lines**), resulting in under-estimation of MDZ $AUC_{0-\infty}$ by 51%. Since MDZ was only administered orally in study 103, $CL_{int,hep}^{MDZ}$ cannot be estimated through observed data. As a result, $v_{max,hep}^{MDZ}$ was optimized based on visual inspection of the terminal slope, and a value of 170,000ng/min/kg was finally chosen to simulate PK profiles in study 103. This adjustment is within the 4.2-fold inter-study variability of $CL_{int,hep}^{MDZ}$, as characterized in **Chapter 3, section 3.3.3.1**. After changing $v_{max,hep}^{MDZ}$, the adjusted PBPK model predicts MDZ PK profile reasonably well (shown in **Figure 5.4**), with deviations (%) of $AUC_{0-\infty}$ and c_{max} less than 30%, and marginal t_{max} difference (see **Table 5.3**).

a)



b)

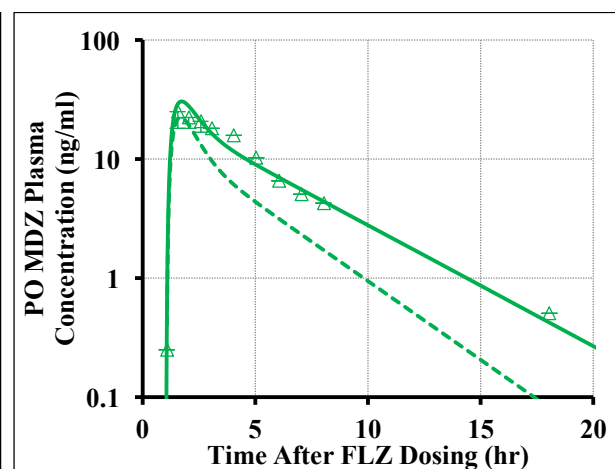


Figure 5.4 Observed and PBPK-model simulated MDZ PK profiles in study 103.

a) PO MDZ 7.5 mg (0.104mg/kg) in the absence of FLZ (Cartesian plot) b) PO MDZ 7.5 mg (0.104mg/kg) in the absence of FLZ (Semi-log plot). The dashed lines reflect the predicted PK profiles without $v_{max,hep}^{FLZ}$ adjustment. The solid lines reflect the predicted PK profiles after $v_{max,hep}^{MDZ}$ adjustment. The symbols and bars are reported mean concentrations and SD in study 103 if available.

For study 26, all the parameters were originally assumed to be the same with study 21. IV MDZ PK profile (**Figure 5.5a-b**) can be well characterized by the original model parameters, however, after PO MDZ, the predicted concentrations (including c_{\max}) were consistently lower than observed values (**Figure 5.5c-f, dashed lines**), resulting in underestimation of PO MDZ $AUC_{0-\infty}$ by 32% and 41% compared with MDZ exposure on day 1 and day 6, respectively. Therefore, f_{villi} (adjusting intestinal CYP3A capacity) for study 26 was changed to 1.45 from original value of 2.2, based on ER_{GI} calculation for study 21 ($ER_{\text{GI}} = 56\%$) and 26 ($ER_{\text{GI}} = 37\%$) in **Chapter 3**. After changing f_{villi} , the adjusted PBPK model predicts PO MDZ PK profiles much better than before (shown in **Figure 5.5**), and $AUC_{0-\infty}$ and c_{\max} deviations are all less than 30% after adjustment (see **Table 5.3**).

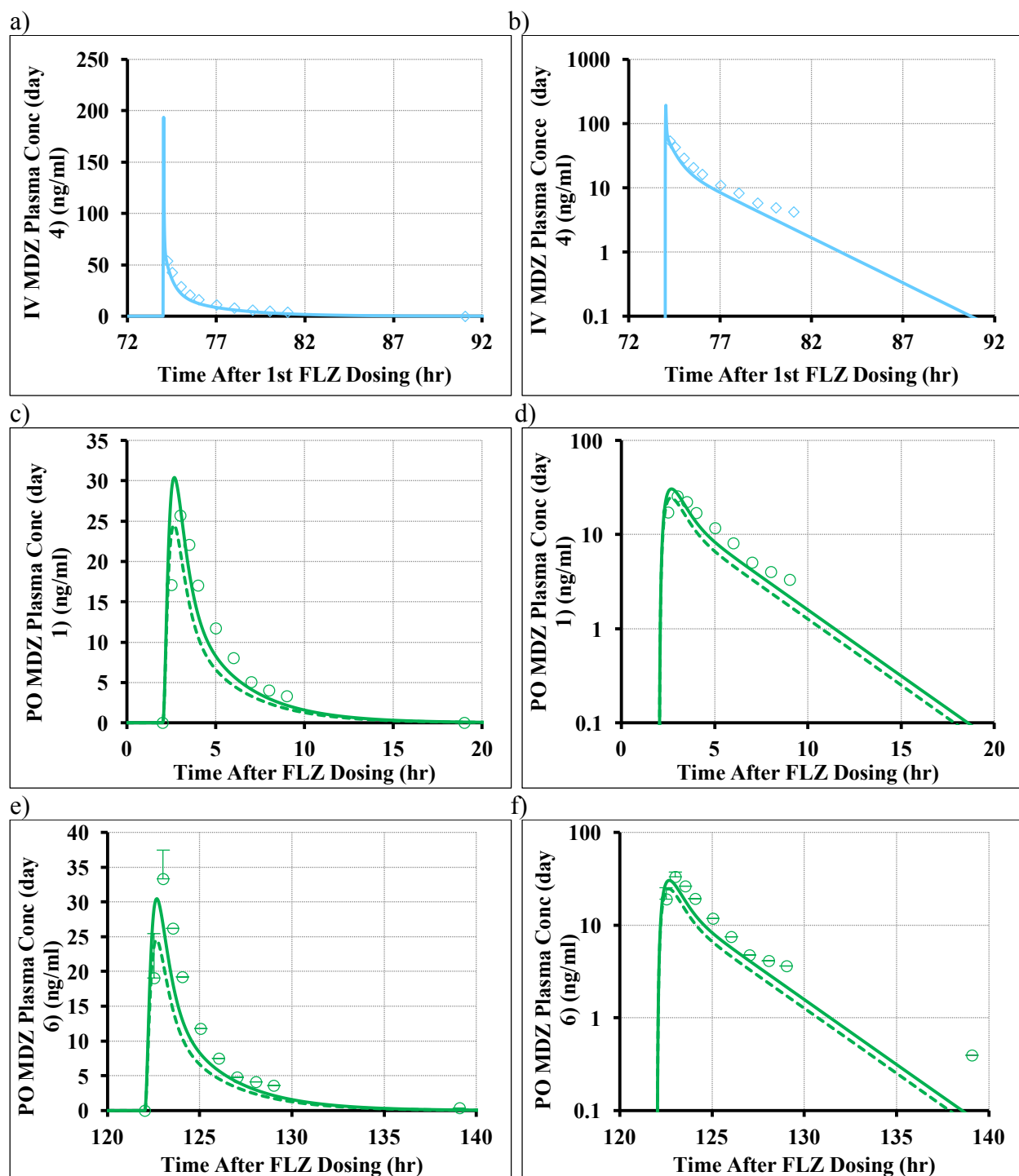


Figure 5.5 Observed and PBPK-model simulated MDZ PK profiles in study 26.

a-b) IV bolus (over 2 min) MDZ 0.05 mg/kg in absence of FLZ administered on day 4 (Cartesian and semi-log plots). c-d) PO MDZ 7.5 mg (0.107 mg/kg) in absence of FLZ administered on day 1 (Cartesian and semi-log plots). e-f) PO MDZ 7.5 mg (0.107 mg/kg) in absence of FLZ administered on day 6 (Cartesian and semi-log plots). The dashed lines reflect predicted PK profiles without f_{villi} adjustment. The solid lines reflect predicted PK profiles after f_{villi} adjustment. The symbols and bars are reported mean concentrations and SD in study 26.

Predictive performance checks for all the three studies after adjustments suggest that the semi-PBPK model for IV or PO MDZ in the absence FLZ predicts the reported data from three clinical studies well, confirming the validity of this model and model parameters. Adjusted parameter values were presented in **Table 5.4**.

Table 5.3 Comparison of reported and semi-PBPK model-predicted MDZ plasma exposure metrics in the absence FLZ using initial model (study 21) and adjusted model (study 103 and 26) parameters.

Deviations greater than 30% were marked as bold.

Study ID	Route & Dose (MDZ)	Reported Mean AUC _{0-∞} (ng/ml*hr)	Predicted AUC _{0-∞} (ng/ml*hr)	Deviation (%)	Reported Mean C _{max} (ng/ml)	Predicted C _{max} (ng/ml)	Deviation (%)	Start from MDZ was administered	
								Reported Mean t _{max} (hr)	Predicted t _{max} (hr)
21	IV (0.014mg/kg)	29.8	27.6	-7%	53.5	55.1	3%		
21	PO (0.043mg/kg)	24.0	23.0	-4%	8.1	9.1	12%	0.77	0.67
103	PO (0.104mg/kg) V _{max,hep} ^{MDZ} not adjusted	113	55.8	-51%	24.9	22.4	-10%	0.55	0.67
103	PO (0.104mg/kg) V _{max,hep} ^{MDZ} adjusted	113	106.3	-6%	24.9	30.6	23%	0.55	0.73
26	IV (0.05mg/kg)	117.0	96.7	-17%					
26	PO (0.107mg/kg) day 1; day 6 f _{villi} not adjusted	87.0; 101.3	59.3	-32%; -41%	25.7; 33.3	23.1	-10%; -30%	1; 1	0.67
26	PO (0.107mg/kg) day 1; day 6 f _{villi} adjusted	87.0; 101.3	76.2	-12%; -25%	25.7; 33.3	30.4	19%; -9%	1; 1	0.7

Table 5.4 Adjusted semi-PBPK MDZ model parameters.

Parameter	Definition	Value	Source
f _{villi}	IVIVE scaling factor and IIV adjusting factor	1.45	Value used for study 26 based on difference in ER _{GI} ^{MDZ} between study 21 and 26
V _{max,hep} ^{MDZ} (ng/min/kg)	Hepatic CYP3A capacity to metabolize MDZ	170000	Value used for study 103 based on terminal slope optimization

5.3.1.2 Sensitivity analysis

The -fold change in plasma $AUC_{0-\infty}$, c_{max} and t_{max} were calculated by dividing plasma exposure metrics simulated at the upper limit of a certain parameter by that simulated at the lower limit (**Table 5.5**). A greater than 2-fold or less than 0.5-fold change was marked as bold, indicating the corresponding exposure is sensitive to that parameter. After IV MDZ, f_{pv} , $v_{max,hep}^{MDZ}$ and $K_{p,hep}^{MDZ}$ substantially affect MDZ AUC, because IV MDZ is exclusively metabolized in the liver, and all the three parameters influence MDZ hepatic concentration and/or hepatic clearance considerably. Increasing f_{pv} and $K_{p,hep}^{MDZ}$ increases drug exposure in the liver, resulting in more drug got metabolized, while increasing $v_{max,hep}^{MDZ}$ accelerates hepatic metabolism, also leading to more drug gets cleared. After PO MDZ, increasing f_{pv} , $v_{max,hep}^{MDZ}$ and $K_{p,hep}^{MDZ}$ also significantly decreases MDZ exposures, as a consequence, both AUC and c_{max} are reduced. AUC is altered to the same extent by f_{pv} after PO MDZ as that after IV MDZ, because f_{pv} can only affect drug input into the liver systemically. However, PO MDZ AUC and c_{max} are more sensitive to $K_{p,hep}^{MDZ}$ and $v_{max,hep}^{MDZ}$ than IV MDZ, because both parameters play a role in pre-systemic hepatic metabolism as well. f_{villi} potentially affects GW CYP3A capacity, and a higher f_{villi} exerts greater intestinal CYP3A metabolism of MDZ, and produces a lower AUC and c_{max} . MDZ plasma PK profiles for all sensitivity analyses are presented in **Appendices D**.

Table 5.5 Sensitivity analysis heat-map results for semi-PBPK IV/PO MDZ model.
(More solid green indicates smaller value; more solid red indicates larger value)

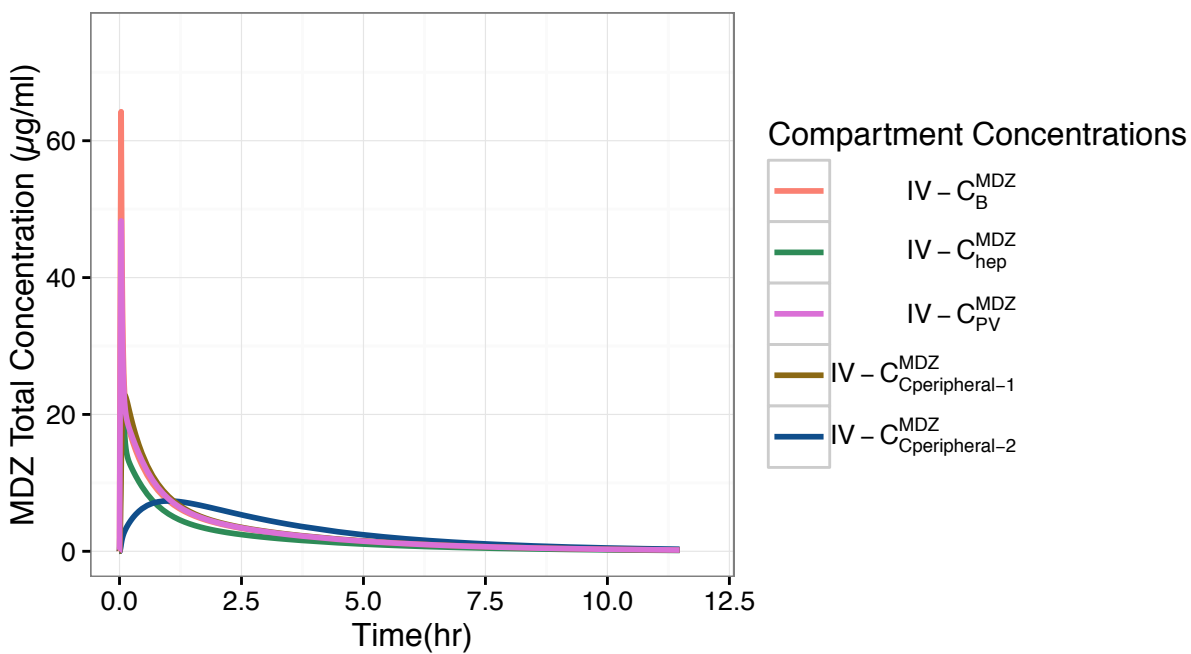
MDZ Sensitivity Analysis		1 mg IV MDZ			3 mg PO MDZ		
		-Fold change in plasma exposure metrics			-Fold change in plasma exposure metrics		
Parameter	-Fold Change	AUC _{0-∞}	c _{max}	t _{max}	AUC _{0-∞}	c _{max}	t _{max}
f _{pV} ^{MDZ}	0-1	0.45	0.96	1.00	0.45	0.84	0.85
v _{max,hep} ^{MDZ}	4	0.41	0.99	1.00	0.25	0.49	0.79
K _{p,hep} ^{MDZ}	4	0.41	0.97	1.00	0.25	0.49	0.92
K _{p,GW} ^{MDZ}	4	1.00	1.00	1.00	1.00	0.83	1.44
Q ₂ ^{MDZ}	4	1.00	0.72	1.00	1.00	1.01	1.20
Q ₃ ^{MDZ}	4	1.00	0.94	1.00	1.00	0.79	0.91
f _{villi} ^{MDZ}	4	-	-	-	0.44	0.44	0.91
k _{GL} ^{MDZ}	4	-	-	-	1.05	1.65	0.52

5.3.2 Model Predictions

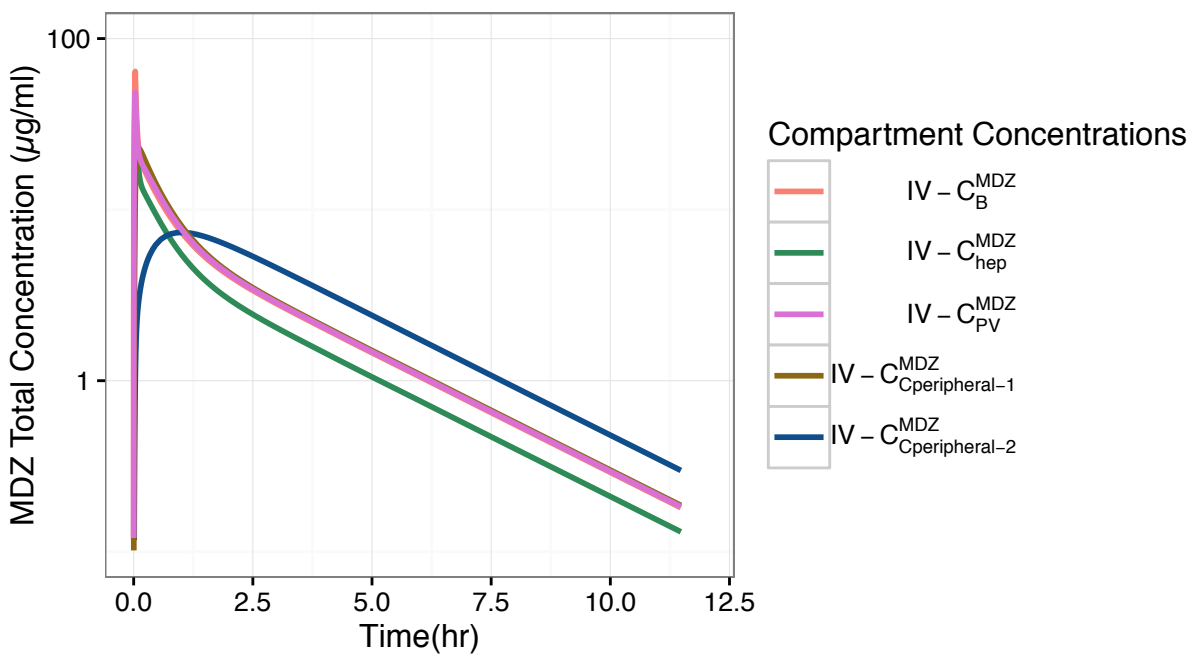
Model predicted MDZ concentrations after 1 mg IV bolus (over 2 min) and 3 mg PO administration for all the compartments are demonstrated in **Figure 5.5a-d**. After IV administration, pseudo steady-state is reached 2 hours after administration, with concentrations in all compartments declined at the same rate. Portal vein and shallow peripheral compartment concentrations are overlapped with blood concentrations, due to rapid equilibrium among the three compartments. Hepatic concentration profile mimics blood concentration profile, with lower concentrations at the terminal phase, making MDZ continuously transfer from blood to the liver, and get cleared by the liver. There is an obvious rising phase of the deep peripheral compartment concentration profile, due to the slow distribution to this compartment, and the concentration difference between deep peripheral compartment and blood is the driving force of its redistribution. A clear three-phase profile is exhibited in **Figure 5.5b** for all compartments, except deep peripheral compartment. Since MDZ GW compartment is separated to mucosa and serosa, and GW metabolism is only assumed to occur after PO MDZ in mucosa compartment, C_{GW-M}^{MDZ} profile is only plotted after PO MDZ.

After PO administration, drug concentration in gut lumen peaks at time 0 (not shown due to extremely high level), and MDZ is quickly absorbed into GW mucosa with a rate constant of k_{GL}^{MDZ} . c_{GW-M}^{MDZ} has much higher peak (~150 ng/ml) than other tissue concentrations, except c_{GL}^{MDZ} , primarily because extensive GW metabolism removes MDZ pre-systemically quite a bit. Afterwards, MDZ is transited into GW serosa, carried into liver through portal vein and reached systemic circulation via hepatic vein. c_{max} of GW mucosa, portal vein, liver and systemic blood are sequentially achieved, at 0.12 hour, 0.35 hour, 0.35 hour and 0.65 hour, respectively, which is in consistent with the oral absorption order of MDZ. Once the drug reaches systemic circulation, the disposition profiles mimics PK profiles after IV administration. Pseudo steady-state is achieved at around 3 hours after PO administration, when concentrations in blood, hepatic, portal vein and two peripheral compartments decline at the same rate. Nevertheless, drug in gut lumen and GW mucosa compartments drop faster than other compartments, because MDZ PBPK model assumes no equilibrium between GW mucosa and systemic circulation, and k_{GL}^{MDZ} , which determines the decline of c_{GW-M}^{MDZ} concentration, is faster than elimination rate constant (k_e) of MDZ (~0.004 min⁻¹)

a)



b)



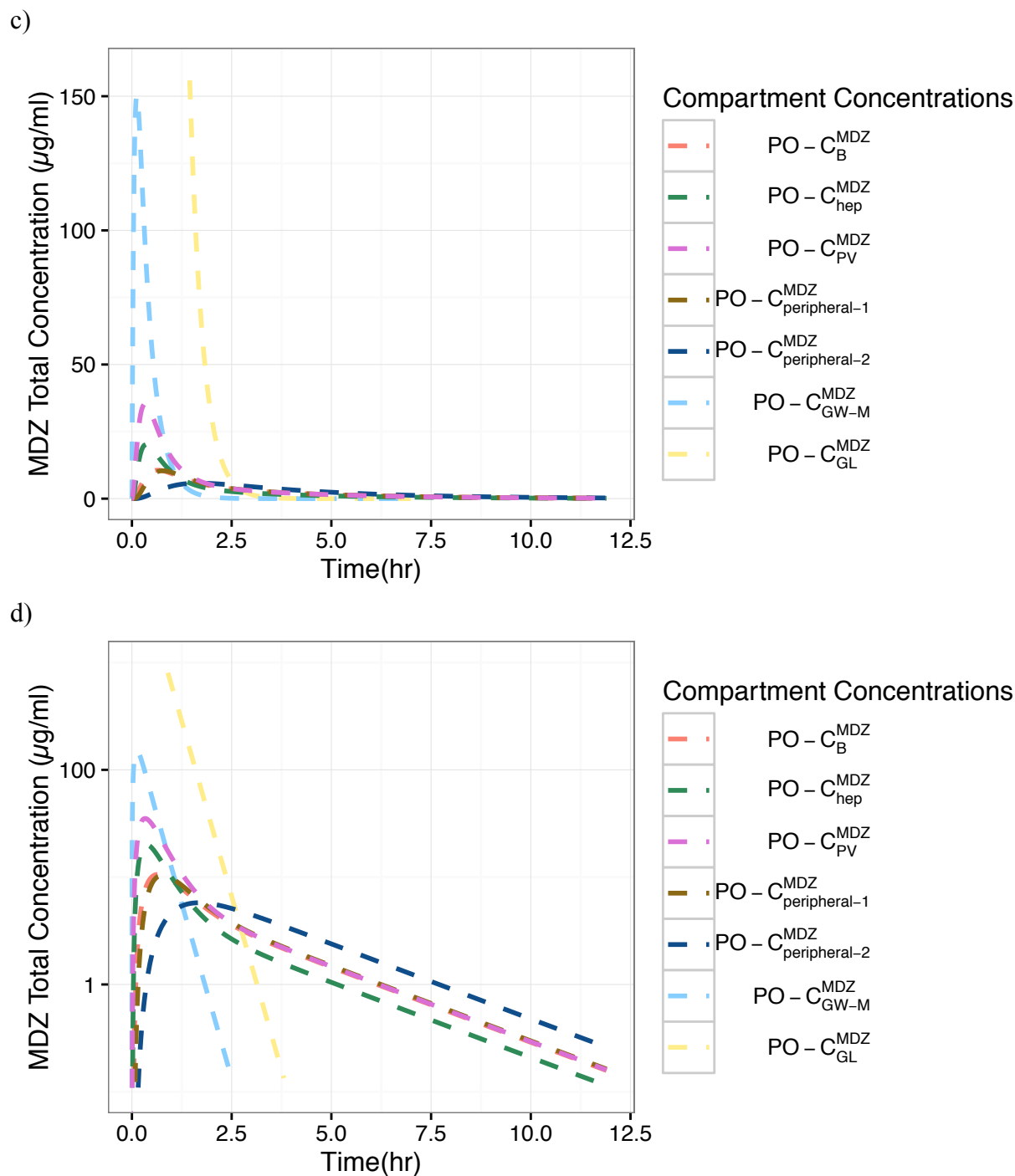


Figure 5.6 Model predicted MDZ concentrations in different compartments.

a) MDZ total concentration – time profiles after 1 mg IV bolus (over 2min) MDZ on linear scale.
 b) MDZ total concentration – time profiles after 1 mg IV bolus (over 2min) MDZ on semi-log scale.
 c) MDZ total concentration – time profiles after 3 mg PO MDZ on linear scale.
 d) MDZ total concentration – time profiles after 3 mg PO MDZ on semi-log scale.

5.4 Conclusions

A semi-PBPK model was developed to describe MDZ clinical PK profiles after IV and PO administration. The model was validated by MDZ plasma concentration – time profiles in absence of FLZ in three clinical DDI studies between MDZ and FLZ. After reasonable adjustments on $v_{\max, \text{hep}}^{\text{MDZ}}$ and f_{villi} (representing hepatic CYP3A capacity and the scaling factor of intestinal CYP3A capacity), plasma concentration – time profiles of MDZ in all the three studies can be characterized well by the model, with all predicted $\text{AUC}_{0-\infty}$ and c_{\max} within 30% of observed, and minimal difference in t_{\max} . Formal parameter sensitivity analyses were conducted for eight key/uncertain model parameters, and f_{pv} , $K_{\text{p, hep}}^{\text{MDZ}}$ and $v_{\max, \text{hep}}^{\text{MDZ}}$, which considerably affect hepatic drug levels/clearance, are the pivotal parameters determining both IV and PO MDZ exposure metrics, indicating the important contribution of hepatic metabolism to the disposition of MDZ after both IV and PO administration. Exposure metrics after PO MDZ is also sensitive to f_{villi} , suggesting that PO MDZ is also subject to extensive pre-systemic GW metabolism. As a result, f_{pv} , $K_{\text{p, hep}}^{\text{MDZ}}$, $K_{\text{p, GW}}^{\text{MDZ}}$, $v_{\max, \text{hep}}^{\text{MDZ}}$ and f_{villi} are the most sensitive parameters affecting plasma concentrations of MDZ, which may require further optimization once MDZ and FLZ DDI model is built. Concentrations in all tissues reach pseudo steady-state around 2 hours after IV administration, and around 3 hours after PO administration. Due to the unidirectional transfer from GW mucosa to serosa, as assumed in model structure, no distribution equilibrium is obtained at pseudo steady-state between GW mucosa and systemic circulation, thus GW mucosa concentrations decline much faster than other compartments at the terminal phase, governed by absorption rate constant ($k_{\text{GL}}^{\text{MDZ}}$).

CHAPTER 6

6 SEMI-PBPK MODELING OF METABOLIC INHIBITION BETWEEN IV/PO FLZ AND IV/PO MDZ

6.1 Background and Objectives

6.1.1 Available DDI studies

As mentioned in **Chapter 3**, study 103 (Ahonen et al., 1997) is the only *in-vivo* DDI study in our final database that administered CYP3AI – FLZ both IV and PO concomitantly with MDZ, assessing the impact of route of administration of CYP3AI. As a result, the CYP3AI used in study 103, FLZ, was selected as one of the inhibitors of interest, and other MDZ and FLZ DDI studies (study 21(Kharasch et al., 2005) and study 26 (Olkola et al., 1996)), together with study 103 were used to validate MDZ - FLZ PBPK DDI model, by comparing the observed IV/PO MDZ plasma concentration – time profiles in presence of IV/PO single- and repeat- doses FLZ to corresponding model predicted profiles.

6.1.2 FLZ inhibitory information and simulation strategies

FLZ is a less profound (moderate) CYP3AI (Kharasch et al., 2005; Drug Interactions & Labeling Drug Development and Drug Interactions Table of Substrates, Inhibitors and Inducers) which can non-competitively inhibit hepatic and intestinal CYP3A (Gibbs et al., 1999; Isoherranen et al., 2008), with comparable K_i to human intestinal and hepatic microsomes (10.7

$\pm 4.2 \mu\text{M}$ and $10.4 \pm 2.9 \mu\text{M}$, respectively) (Isoherranen et al., 2008). After IV MDZ, hepatic CYP3A metabolism is assumed to be the only elimination pathway of MDZ, thus magnitude and time course of DDI are determined by FLZ unbound hepatic concentration over time, relative to K_i of FLZ on hepatic CYP3A ($K_{i,\text{hep}}^{\text{FLZ}}$). After PO administration, MDZ is subject to both GW and hepatic metabolism pre-systemically, as well as systemic hepatic clearance. Hence, unbound FLZ concentration – time profiles in both GW and liver, relative to $K_{i,\text{GW}}^{\text{FLZ}}$ and $K_{i,\text{hep}}^{\text{FLZ}}$, respectively, govern the magnitude and time course of FLZ inhibition. Due to the high $F_{\text{oral}}^{\text{FLZ}}$ (> 90%) of FLZ (Humphrey et al., 1985; Pfizer, 2011; Washton, 1989), IV and PO FLZ have similar hepatic concentration profiles, suggesting similar inhibitory effects on hepatic metabolism. Nevertheless, GW concentrations after PO FLZ are higher than that after IV FLZ, during the first 4 hours (discussed in **Chapter 4**), potentially leading to greater GW inhibition after PO FLZ. Furthermore, FLZ has a long terminal plasma elimination half-life ($t_{1/2}^{\text{FLZ}}$), ranging from 22 to 37 hours, indicating its prolonged inhibitory effect on hepatic and intestinal CYP3A.

Meanwhile, the impact of route of administration for either MDZ or FLZ is also affected by dose, administration time interval between FLZ and MDZ, as well as inhibitory potency of FLZ to intestinal/hepatic CYP3A. To explore these factors, simulations were performed to assess dose and time-dependency of route difference in DDI, by varying IV/PO FLZ single dose and administration time interval between FLZ and MDZ, to better understand route-dependent DDI in multiple clinical scenarios. Sensitivity analyses were also performed on key PK/physiological parameters in the MDZ - FLZ DDI semi-PBPK model, to identify pivotal parameters that determine MDZ exposure metrics in presence FLZ.

Finally, several hypothetical CYP3AIs and CYP3A substrates were created based on FLZ

and MDZ individual semi-PBPK models, to assess the impact of F_{oral} and $t_{1/2}$ for a noncompetitive CYP3AI and hepatic/GW metabolism for a CYP3A substrate on the magnitude and time course of route-dependent DDI.

6.1.3 Objectives

The major objectives of the chapter were to:

- a. Develop a semi-PBPK DDI model between MDZ and FLZ, to describe IV/PO MDZ PK profiles in presence of IV/PO FLZ.
- b. Validate the model using MDZ plasma concentration-time profiles (with co-administration of FLZ) in clinical DDI studies, and identify pivotal PK/physiological parameters that determine MDZ plasma exposure metrics in presence of FLZ by sensitivity analyses
- c. Assess impact of route of administration for MDZ and FLZ on the magnitude and time course of their metabolic DDI after various administration time intervals between the two drugs
- d. Predict profiles of FLZ concentrations and relative CYP3A activity levels in GW and liver
- e. Assess impact of route of administration for MDZ and FLZ on the magnitude and time course of their metabolic DDI after various single dose of FLZ
- f. Explore route-dependent DDI between MDZ and several hypothetical CYP3AIs that have low F_{oral} and/or short $t_{1/2}$ and between two hypothetical CYP3A substrates with hepatic/GW metabolism reduced/removed and FLZ

6.2 Methods

6.2.1 Development of MDZ-FLZ DDI PBPK model

A semi-PBPK model for MDZ in presence of FLZ was built based on the reported *in-vitro* metabolic inhibitory information and the previously presented FLZ semi-PBPK and MDZ semi-PBPK models (**Figure 6.1**). Metabolic inhibition parameters, along with previously discussed MDZ (initial and adjusted) and FLZ model parameters were summarized in **Table 6.1** and **Table 6.2**. In presence of IV/PO FLZ, unbound FLZ in liver and GW non-competitively (Isoherranen et al., 2008; Gibbs et al., 1999) inhibit hepatic and intestinal intrinsic clearance of MDZ, decreasing $V_{\max, \text{hep}}^{\text{MDZ}}$ and $V_{\max, \text{GW}}^{\text{MDZ}}$ by $1/(1+f_u^{\text{FLZ}} \cdot c_{\text{hep}}^{\text{FLZ}}/K_{i, \text{hep}}^{\text{FLZ}})$ and $1/(1+f_u^{\text{FLZ}} \cdot c_{\text{GW}}^{\text{FLZ}}/K_{i, \text{GW}}^{\text{FLZ}})$, respectively, and the corresponding differential equations for MDZ hepatic and GW mucosa mass transfer were expressed as equations (6.1) and (6.2):

$$\begin{aligned} \frac{dA_{\text{hep}}^{\text{MDZ}}(t)}{dt} &= c_B^{\text{MDZ}} \cdot Q_{\text{HA}} + c_{\text{PV}}^{\text{MDZ}} \cdot Q_{\text{PV}} - \left(\frac{c_{\text{hep}}^{\text{MDZ}}}{K_{\text{p, hep}}^{\text{MDZ}}} \right) \cdot Q_{\text{hep}} - c_{\text{hep}}^{\text{MDZ}} \\ &\quad \cdot f_u^{\text{MDZ}} \cdot v_{\max, \text{hep}}^{\text{MDZ}} / \left(1 + f_u^{\text{FLZ}} \cdot \frac{c_{\text{hep}}^{\text{FLZ}}}{K_{i, \text{hep}}^{\text{FLZ}}} \right) / K_{\text{m, hep}}^{\text{MDZ}} \\ &\quad \text{when } t = 0, A_{\text{hep}}^{\text{MDZ}}(0) = 0 \end{aligned} \quad (6.1)$$

$$\begin{aligned} \frac{dA_{\text{GW-M}}^{\text{MDZ}}(t)}{dt} &= c_{\text{GL}}^{\text{MDZ}} \cdot V_{\text{GL}} \cdot F_{\text{abs}}^{\text{MDZ}} \cdot k_{\text{GL}}^{\text{MDZ}} - c_{\text{GW-M}}^{\text{MDZ}} \cdot V_{\text{GW}} \cdot k_{\text{T}} - f_{\text{u, GW-M}}^{\text{MDZ}} \cdot c_{\text{GW-M}}^{\text{MDZ}} \cdot f_{\text{villi}} \\ &\quad \cdot v_{\max, \text{GW}}^{\text{MDZ}} / \left(1 + f_u^{\text{FLZ}} \cdot \frac{c_{\text{GW}}^{\text{FLZ}}}{K_{i, \text{GW}}^{\text{FLZ}}} \right) / \left(K_{\text{m, GW}}^{\text{MDZ}} + f_{\text{u, GW-M}}^{\text{MDZ}} \cdot c_{\text{GW-M}}^{\text{MDZ}} \right) \\ &\quad \text{when } t = 0, A_{\text{GW-M}}^{\text{MDZ}}(0) = 0 \end{aligned} \quad (6.2)$$

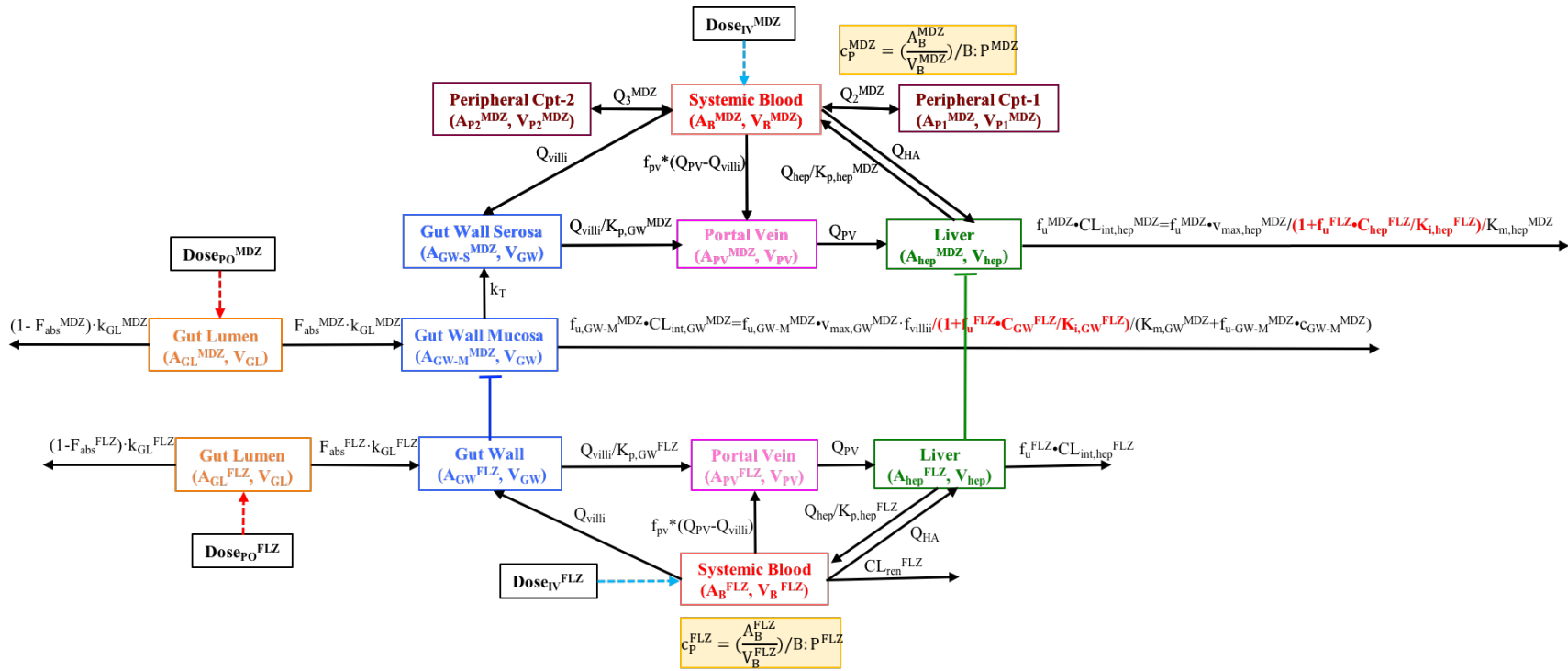


Figure 6.1 Semi-PBPK model scheme of MDZ in presence of FLZ.

Table 6.1 Initial Semi-PBPK MDZ - FLZ DDI model parameters.

Parameter	Definition	Value	Source
Physiological parameters			
V_{GL} (ml/kg)	Volume of gut lumen	3.57	Assumed to be 250ml (FDA, 2012)
V_{GW} (ml/kg)	Volume of GW	33.6	Calculated by equation (4.6), assumed to be the surface of gut lumen cylinder
V_{PV} (ml/kg)	Volume of portal vein	0.97	Unknown methods (Ito et al., 2003)
V_{hep} (ml/kg)	Volume of liver	22.5	Calculated by equation (4.7) and (4.8)
Q_{villi} (ml/min/kg)	Villous blood flow	4.30	<i>In-vivo</i> experiment (Yang et al., 2007)
Q_{hep} (ml/min/kg)	Hepatic blood flow	21.4	<i>In-vivo</i> experiment (Tsunoda et al., 1999)
f_{HA}	Fraction of hepatic artery to total hepatic blood flow	0.25	(Eipel et al., 2010) (Q_{HA} was calculated as $f_{HA} \cdot Q_{hep}$; Q_{PV} was calculated as $(1-f_{HA}) \cdot Q_{hep}$)
f_{PV}	Fraction of the components of portal vein that contain drug	1.00	A correction factor that can be adjusted according to simulation results.
* f_{villi}	IVIVE scaling factor and IIV adjusting factor	2.2	Optimized with data from study 21
FLZ PK Parameters			
V_B^{FLZ} (ml/kg)	Volume of systemic blood compartment	641	Calculated by equation (4.5) (Carrasco-Portugal & Flores-Murrieta, 2007; Humphrey et al., 1985)
f_u^{FLZ}	Fraction unbound of FLZ in hepatocytes and enterocytes	0.88	Assumed to be the same as fraction unbound in plasma (Humphrey et al., 1985)
$K_{p,GW}^{FLZ}$	GW-to-blood partition coefficient	1	Assumed to be 1 (Carrasco-Portugal & Flores-Murrieta, 2007)
$K_{p,hep}^{FLZ}$	Liver-to-blood partition coefficient	1	Assumed to be 1 (Carrasco-Portugal & Flores-Murrieta, 2007)
$CL_{int,hep}^{FLZ}$ (ml/min/kg)	Hepatic intrinsic clearance	0.11	Calculated by equation (4.9)
CL_{ren}^{FLZ} (ml/min/kg)	Renal clearance	0.2	<i>In-vivo</i> experiment (Ripa et al., 1993; Sobue et al., 2004)
$B:P^{FLZ}$	Blood to plasma partitioning ratio	1	(Ervine & Houston, 1994)
k_{GL}^{FLZ} (min^{-1})	Absorption rate constant from gut lumen to GW	0.0213	Assumed to be k_a^{FLZ} from <i>in-vivo</i> experiment (Ripa et al., 1993)
F_{abs}^{FLZ}	Fraction of FLZ absorbed from gut lumen	100%	BCS class 1 drug (Lindenberg et al., 2004)
MDZ PK Parameters			
V_B^{MDZ} (ml/kg)	Volume of systemic blood compartment	140.4	See Appendices C
V_{P1}^{MDZ} (ml/kg)	Volume of shallow peripheral compartment	313.7	See Appendices C
V_{P2}^{MDZ} (ml/kg)	Volume of deep peripheral compartment	531.4	See Appendices C
Q_2^{MDZ} (min^{-1})	Inter-compartmental clearance between central and peripheral cpt-1	55.27	See Appendices C
Q_3^{MDZ} (min^{-1})	Inter-compartmental clearance between central and peripheral cpt-2	7.25	See Appendices C
f_u^{MDZ}	Fraction unbound of MDZ	0.03	Assume to be the same in plasma and hepatocytes (Gandhi et al., 2012)
$f_{u,GW-M}^{MDZ}$	Fraction unbound at mucosal side of intestinal epithelium	1.0	Assumed to be negligible bound
$V_{max,GW}^{MDZ}$	GW CYP3A capacity to metabolize	3357.6	<i>In-vitro</i> experiment (Thummel et al., 1996)

(ng/min/kg)	MDZ		
$K_{m,GW}^{MDZ}$	GW CYP3A affinity of metabolizing MDZ	1173	<i>In-vitro</i> experiment (Thummel et al., 1996) (3.6 μ M)
(ng/ml)	MDZ		
$V_{max,hep}^{MDZ}$	Hepatic CYP3A capacity to metabolize MDZ	305067	<i>In-vivo</i> experiment, calculated from equation (5.7)-(5.8), using data from study 21
(ng/min/kg)			
$K_{m,hep}$ (ng/ml)	Hepatic CYP3A affinity of metabolizing MDZ	880	<i>In-vitro</i> experiment (Thummel et al., 1996) (2.7 μ M)
$K_{p,GW}^{MDZ}$	GW-to-blood partition coefficient	1.12	Scaled from rat K_p (Björkman et al., 2001)
$K_{p,hep}^{MDZ}$	Liver-to-blood partition coefficient	1.09	Scaled from rat K_p (Björkman et al., 2001)
$B:P^{MDZ}$	Blood-to-plasma partitioning ratio	0.86	(Ervine & Houston, 1994)
k_{GL}^{MDZ} (min ⁻¹)	Absorption rate constant from gut lumen to GW	0.05	<i>In-vivo</i> experiment (Johnson et al., 2002; Kato et al., 2008), assumed to be k_a^{MDZ}
k_T (min ⁻¹)	Transit rate from mucosal to serosal side of intestinal epithelium	0.13	Assumed, calculated from Q_{villi}/V_{GW}
F_{abs}^{MDZ}	Fraction of MDZ absorbed from gut lumen	100%	BCS class 1 drug (Wu & Benet, 2005)
DDI Parameters (Noncompetitive inhibition)			
$K_{i,GW}^{FLZ}$ (ng/ml)	FLZ inhibitory potency on GW CYP3A	3182	<i>In-vitro</i> experiment (Gibbs et al., 1999) (10 μ M)
$K_{i,hep}^{FLZ}$ (ng/ml)	FLZ inhibitory potency on hepatic CYP3A	3829	<i>In-vitro</i> experiment (Isoherranen et al., 2008; Gibbs et al., 1999) (12.5 μ M)

*Parameter values were adjusted in study 103 and study 26.

Table 6.2 Adjusted semi-PBPK MDZ model parameters.

Parameter	Definition	Value	Source
f_{villi}	IVIVE scaling factor and IIV adjusting factor	1.45	Value used for study 26 based on difference in ER_{GI}^{MDZ} between study 21 and 26
$V_{max,hep}^{MDZ}$ (ng/min/kg)	Hepatic CYP3A capacity to metabolize MDZ	170000	Value used for study 103 based on terminal slope optimization

Besides the assumptions mentioned in **Chapter 4** and **Chapter 5**, two additional assumptions were made during the DDI modeling processes, which were:

- 1) Noncompetitive inhibition by FLZ is assumed for both GW and liver CYP3A.
- 2) Negligible CYP3A5 is expressed in both hepatic and intestinal CYP3A. ($K_{i,hep}^{MDZ}$ and $K_{i,GW}^{MDZ}$ are in respective to CYP3A4 inhibition only).

6.2.2 Model qualification and predictions

Model simulated MDZ plasma concentration-time profiles in presence of FLZ were compared with observed profiles from study 21 (Kharasch et al., 2005), study 103 (Ahonen et al., 1997) and study 26 (Olkola et al., 1996), to assess model validity by predictive visual check and exposure metrics comparison. Since some parameters (i.e. $v_{\max, \text{hep}}^{\text{MDZ}}$ and f_{villi}) were optimized in different MDZ and FLZ DDI studies - due to the large inter-study variability of hepatic and GW CYP3A-, a more stringent acceptance criterion: predicted exposure metrics are $\pm 30\%$ of observed, were used to assess performance of MDZ and FLZ DDI semi-PBPK model. Plasma concentrations were simulated using Simbiology (MATLAB, 2015a), and the predicted exposure metrics were summarized and compared to reported values. FLZ GW and liver concentrations, as well as relative intestinal and hepatic CYP3A activity levels were also simulated, to better interpret the impact of route difference for FLZ.

6.2.3 Sensitivity Analysis

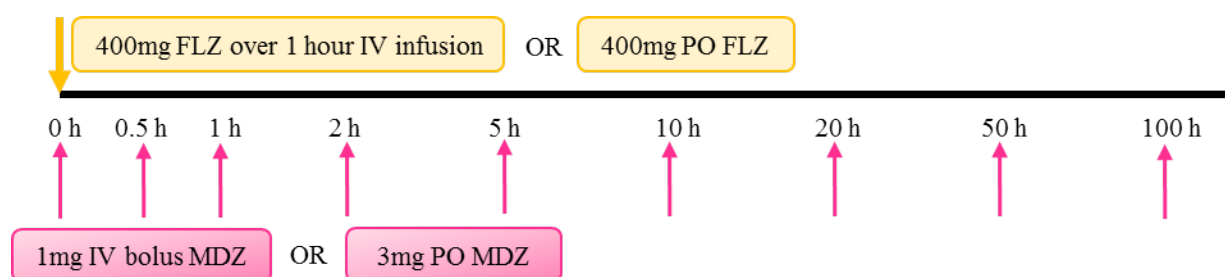
Formal sensitivity analyses were conducted by altering the values for 10 key PBPK model parameters (f_{pV} , $v_{\max, \text{hep}}^{\text{MDZ}}$, $K_{\text{p, hep}}^{\text{MDZ}}$, $K_{\text{p, GW}}^{\text{MDZ}}$, $K_{\text{p, hep}}^{\text{FLZ}}$, $K_{\text{p, GW}}^{\text{FLZ}}$, $K_{\text{i, hep}}^{\text{FLZ}}$, $K_{\text{i, GW}}^{\text{FLZ}}$, f_{villi} and $k_{\text{GL}}^{\text{MDZ}}$), to assess their significance on MDZ systemic plasma exposures in presence of FLZ. All parameters (except f_{pV} , which was simulated at 0.0, 0.5 and 1.0) were increased and decreased by 2-fold relative to their original values (overall-fold change in values = 4 - fold), as shown in **Table 6.3**, and the respective plasma concentration - time profiles were predicted under 1 mg IV bolus MDZ over 2 min or 3 mg PO MDZ, administered 2 hours after 400 mg 1 hour IV infusion or PO FLZ. Plasma exposure metrics ($\text{AUC}_{0-\infty}$, c_{\max} , t_{\max}) were estimated, and the sensitivity to each parameter was assessed by dividing respective exposure metrics simulated at the upper limit by that simulated at the lower limit.

Table 6.3 Values of parameters used in sensitivity analysis.

Parameter Name	Initial Value	Lower/Upper Sensitivity Limits
f_{pv}	1.0	0; 1.0
$v_{max,hep}^{MDZ}$ (ng/min/kg)	305067	152534; 610134
$K_{p,hep}^{MDZ}$	1.09	0.55; 2.18
$K_{p,GW}^{MDZ}$	1.12	0.56; 2.24
$K_{p,hep}^{FLZ}$	1.0	0.5; 2
$K_{p,GW}^{FLZ}$	1.0	0.5; 2
$K_{i,hep}^{FLZ}$ (ng/ml)	3829 (10 μ M)	1915; 7658
$K_{i,GW}^{FLZ}$ (ng/ml)	3182 (12.5 μ M)	1591; 6364
f_{villi}	2.2	1.1; 4.4
k_{GL}^{MDZ} (min ⁻¹)	0.05	0.025; 0.1

6.2.4 Simulations of route-dependent DDI with various administration time intervals

To investigate impact of route difference of MDZ and FLZ at different administration time intervals between the two drugs, as well as explore the duration of FLZ inhibition, semi-PBPK model of MDZ in presence of FLZ (using initial model parameters in **Table 6.1**) was employed to simulate MDZ PK profiles after 400mg FLZ as IV-1hr-infusion, and PO administered at 0, 0.5, 1, 2, 5, 10, 20, 50, 100 hours before 1 mg IV MDZ or 3 mg PO MDZ was given. Simulated DDI dosing scheme is illustrated in **Figure 6.2**. $AUC_{0-\infty}$ increase ratio (AUCR) of MDZ for each scenario was calculated to assess the extent of inhibition.

**Figure 6.2 Simulated DDI dosing scheme between FLZ and MDZ.**

6.2.5 Simulations of route-dependent DDI with various FLZ doses

To investigate impact of FLZ dose on the route-dependent DDI between the two drugs, MDZ $AUC_{0-\infty}$ after 1 mg IV or 3 mg PO administration concurrent with (administration time interval =

0) a series of SAD of FLZ (40 mg, 80 mg, 200 mg, 400 mg, 800 mg, 2,000 mg, 4,000 mg) administered either as 1-hour IV infusion or orally were simulated. AUCR of MDZ for each scenario was calculated, and FLZ route difference was assessed to be the ratio of MDZ AUCR by PO FLZ and that by IV FLZ.

6.2.6 Simulation of route-dependent DDI between CYP3A substrates and CYP3AIs

FLZ is a high $F_{\text{oral}}^{\text{FLZ}}$ (> 90%) and long $t_{1/2}^{\text{FLZ}}$ (~30%) noncompetitive CYP3AI, which are two important PK characteristics that would determine its route of administration impact on MDZ metabolic inhibition. Semi-PBPK models for three hypothetical drugs (3AIX1, 3AIX2, 3AIX3) were developed based on the semi-PBPK model for FLZ, with modification of $F_{\text{abs}}^{\text{FLZ}}$ and/or $CL_{\text{ren}}^{\text{FLZ}}$, to generate low F_{oral} and/or short $t_{1/2}$ CYP3AI. $F_{\text{abs}}^{\text{FLZ}}$ was decreased from 1.0 to 0.1, to generate a low F_{oral} drug (3AIX1), clinically could due to its low solubility, low permeability and/or degradation in gut lumen. As to 3AIX2, $CL_{\text{ren}}^{\text{FLZ}}$ was increased from 0.2 ml/min/kg to 3 ml/min/kg, which shortened elimination $t_{1/2}$ to almost 1/10 of FLZ ($CL_{\text{int}}^{\text{FLZ}}$ was not adjusted to avoid change in first-pass metabolism or F_{oral}). Furthermore, a drug with low F_{oral} and short $t_{1/2}$ was created by changing both $F_{\text{oral}}^{\text{FLZ}}$ and $CL_{\text{ren}}^{\text{FLZ}}$.

With respect to MDZ, route different of IV/PO MDZ is primarily due to existence of pre-systemic hepatic/GW metabolism after PO (but not IV) MDZ, and as discussed in **Chapter 4**, PO FLZ has higher GW concentration than the same dose of IV infusion FLZ, whereas hepatic FLZ concentration doesn't have much route difference. Hence it is of interest to investigate route difference for both substrate and inhibitor when the substrate doesn't have GW metabolism. A CYP3A substrate without GW metabolism (3ASX1) was derived from MDZ PBPK model, by setting f_{villi} , the parameter to adjust GW CYP3A activity, to 0. Actually based on quantitative

meta-analysis in **Chapter 3**, ER_{GI}^{MDZ} has very large inter-study variability, and the derived ER_{GI}^{MDZ} in study 11 (Krishna et al., 2009) was 0, proving the clinical relevance of making this hypothetical CYP3A substrate.

Furthermore, a second CYP3A substrate (3ASX2) was generated by setting f_{villi} to 0 (no GW metabolism), along with decreasing $v_{max,hep}^{MDZ}$ by 5-fold, to create a high F_{oral} ($F_{oral} = 89\%$) CYP3A substrate with limited first pass effect.

All other PBPK parameters, including metabolic inhibitory potency and IV/PO doses, for the five hypothetical drugs (3AIX1/2/3, 3ASX1/2) remained unchanged from their original drugs, and changes were summarized in **Table 6.4**.

Table 6.4 Parameter modifications for hypothetical drugs, based on FLZ and MDZ individual semi-PBPK models.

(MDZ initial model parameters were used.)

CYP3AI	F_{oral}	$t_{1/2}$	Mechanism of DDI	Change
FLZ	> 90%	~30 hrs	Noncompetitive	-
3AIX1	~10 %	~30 hrs	Noncompetitive	Change F_{abs}^{FLZ} from 1.0 to 0.1
3AIX2	> 90%	~3 hrs	Noncompetitive	Change CL_{ren}^{FLZ} from 0.2ml/min/kg to 3ml/min/kg
3AIX3	~10%	~3 hrs	Noncompetitive	Change F_{abs}^{FLZ} from 1.0 to 0.1 and change CL_{ren}^{FLZ} from 0.2ml/min/kg to 3ml/min/kg
CYP3A Substrate	F_{oral}	ER_{hep}	ER_{GI}	Change
MDZ	0.28	0.40 ($t_{1/2}$: ~2.5 hrs)	0.52	-
3ASX1	0.60	0.40 ($t_{1/2}$: ~2.5 hrs)	0	Change f_{villi} from 2.2 to 0.0.
3ASX2	0.89	0.11 ($t_{1/2}$: ~9 hrs)	0	Change $v_{max,hep}^{MDZ}$ from 305067 $\mu\text{g}/\text{min}/\text{kg}$ to 61013.4 $\mu\text{g}/\text{min}/\text{kg}$ and change f_{villi} from 2.2 to 0.0.

The route impact on metabolic DDI between MDZ (IV: 1 mg, PO: 3 mg) and 3AIX1/2/3 (400 mg IV-1 hours-infusion and PO) and between 3ASX1/2 (same dose as MDZ) and FLZ (400 mg IV-1 hour-infusion and PO) were investigated by simulating the -fold $AUC_{0-\infty}^{substrate}$ increase by CYP3AI at varying time intervals between single-dose substrate and CYP3AI administration (same strategy as **Figure 6.2**). Since 3ASX2 has a longer plasma $t_{1/2}$ than MDZ and 3ASX1, different magnitude of DDI may be expected between short and long $t_{1/2}$ CYP3AI. Therefore, the

same simulation strategy (as **Figure 6.2**) was used to predict magnitude and time course of DDI between 3ASX2 and 3AIX2. Unbound GW and hepatic concentrations of 3AIX1/3AIX2/3AIX3, as well as relative hepatic and intestinal CYP3A levels in presence of three hypothetical CYP3AIs were also simulated, to better interpret the route-dependent DDI between MDZ and the three drugs.

6.3 Results and Discussion

6.3.1 Model evaluation

6.3.1.1 Predictive performance check

6.3.1.1.1 Study 21

The observed and model-predicted MDZ PK profiles in absence/presence of FLZ in study 21 were showed in **Figure 6.3a-d** and comparison of observed and model simulated exposure metrics was summarized in **Table 6.5**. **Figure 6.3a-d** demonstrate that the model captures MDZ observed profiles in presence of FLZ well after both IV and PO MDZ, with all predicted values superimposable with observed data. From **Table 6.5**, deviations (%) of $AUC_{0-\infty}$ and c_{max} are all less than 30%, which is a pre-defined cut-off of precise prediction. In addition, F_{oral} in absence/presence of FLZ and AUCR in presence of FLZ can also be well characterized in all scenarios, indicating that no apparent bias is observed in model predictions.

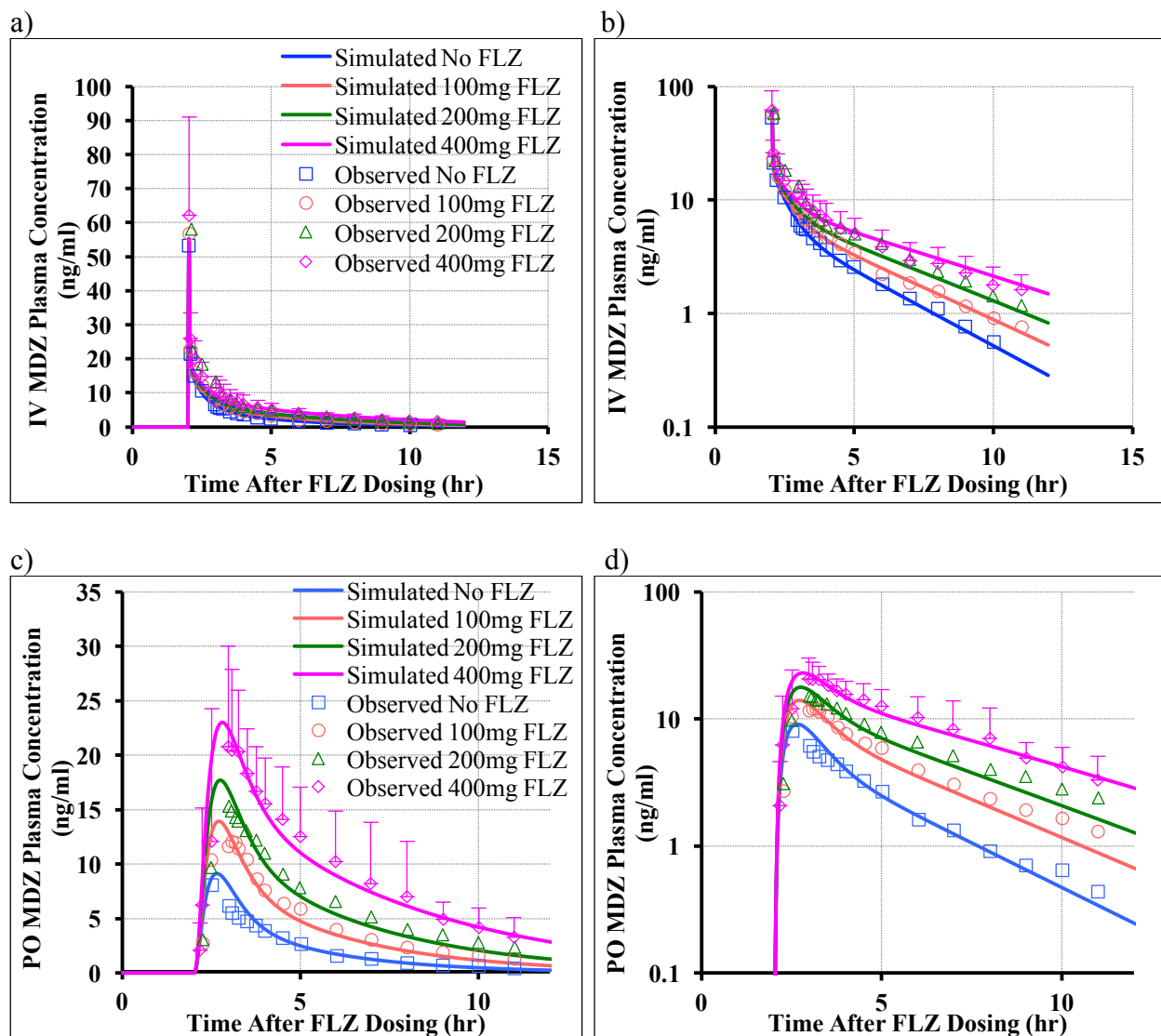


Figure 6.3 Observed and PBPK model-simulated MDZ PK profiles in study 21.

a-b) IV MDZ 1 mg administered 2 hours after placebo, 100, 200, 400 mg PO FLZ (Cartesian plots and semi-log plots). c-d) PO MDZ 3 mg administered 2 hours after placebo, 100, 200, 400 mg PO FLZ (Cartesian plots and semi-log plots). The solid lines reflect the predicted PK profiles. The symbols and bars are reported means and SD values (if available).

In study 21, FLZ was administered 100 mg, 200 mg or 400 mg orally for two consecutive days, and the predicted unbound hepatic and GW concentrations relative to $K_{i,hep}^{FLZ}$ and $K_{i,GW}^{FLZ}$ are plotted in **Figure 6.4a-b**. FLZ concentrations in liver and GW increase proportionally with dose, and concentrations at the highest dose (400 mg PO FLZ) exceed respective K_i values for more than 50 hours. Accumulation of hepatic and GW concentrations at the end of the first dose are 1.53 – fold for all dose levels, which are estimated as the ratio of c_{min}^{FLZ} after 2nd dose and c_{min}^{FLZ} after 1st dose.

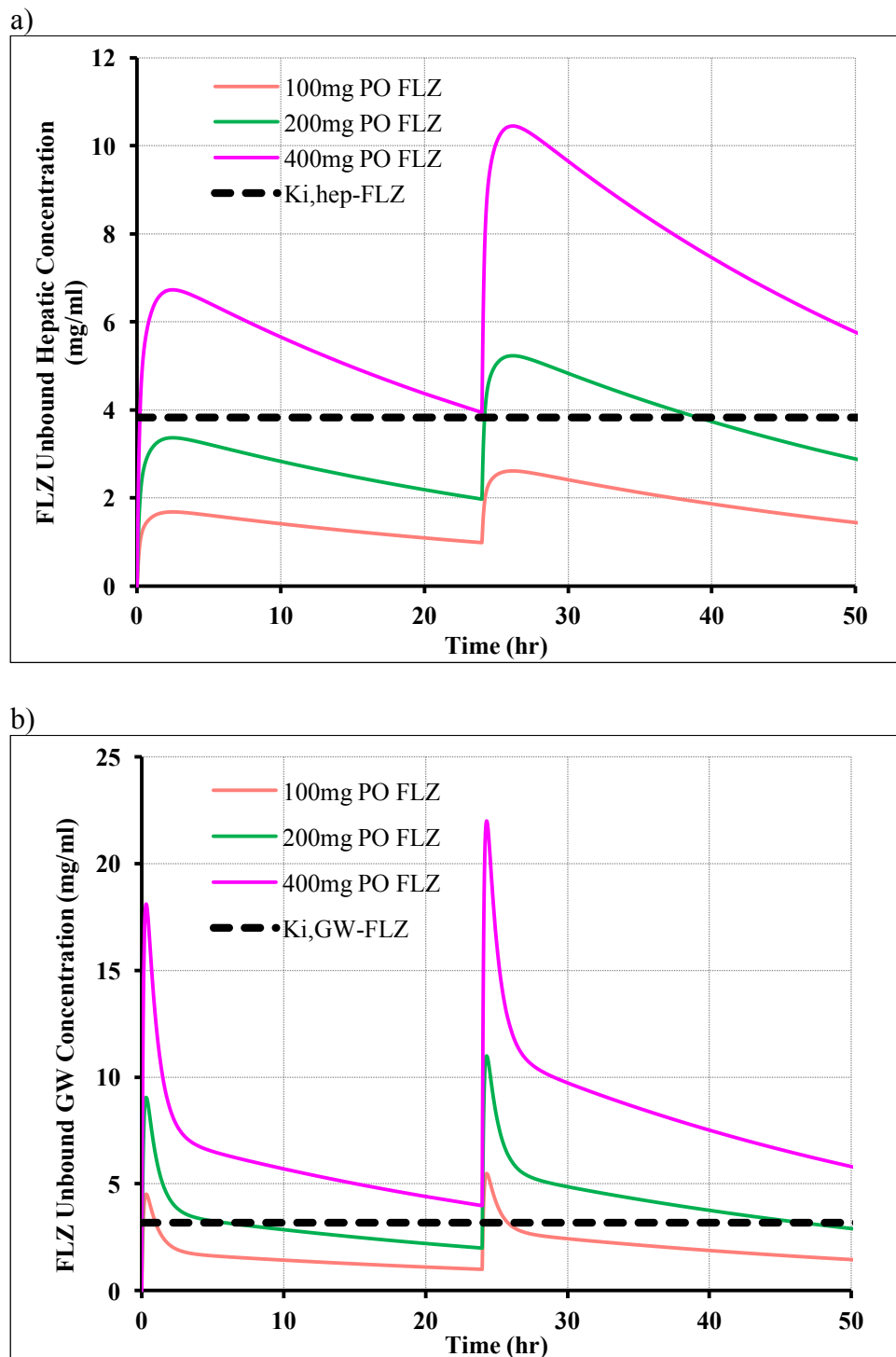


Figure 6.4 Semi-PBPK model-predicted FLZ unbound hepatic and GW concentration – time profiles in study 21.

a) FLZ unbound hepatic concentration – time profiles after 100 mg, 200 mg, and 400 mg PO FLZ once daily for 2 days. b) FLZ unbound GW concentration – time profiles after 100 mg, 200 mg, and 400 mg PO FLZ once daily for 2 days.

6.3.1.1.2 Study 103

For study 103, after changing $v_{\max, \text{hep}}^{\text{MDZ}}$, the adjusted PBPK model predicts MDZ PK profiles in absence/presence of FLZ reasonably well (shown in **Figure 6.5**), with deviations (%) of $\text{AUC}_{0-\infty}$ and c_{\max} less than 30% (see **Table 6.5**). However, even after adjustment, c_{\max}^{MDZ} in presence of IV FLZ is beyond mean \pm SD of the observed data, which may be due to inter-study variability related to GW metabolism, DDI parameters ($K_{i, \text{hep}}^{\text{FLZ}}$, $K_{i, \text{GW}}^{\text{FLZ}}$), and/or differences in subject demographics, analytical method or sampling strategy. The PBPK model over-estimates MDZ AUCR in presence of IV or PO FLZ by 22% and 29%, respectively, possibly owing to slight misspecification of distribution parameters (*i.e.* $V_{\text{P1}}^{\text{MDZ}}$, $V_{\text{P2}}^{\text{MDZ}}$, Q_2^{MDZ} , Q_3^{MDZ}) for study 103. Hepatic and GW FLZ concentration and CYP3A levels were predicted and discussed in **section 6.3.2.1**.

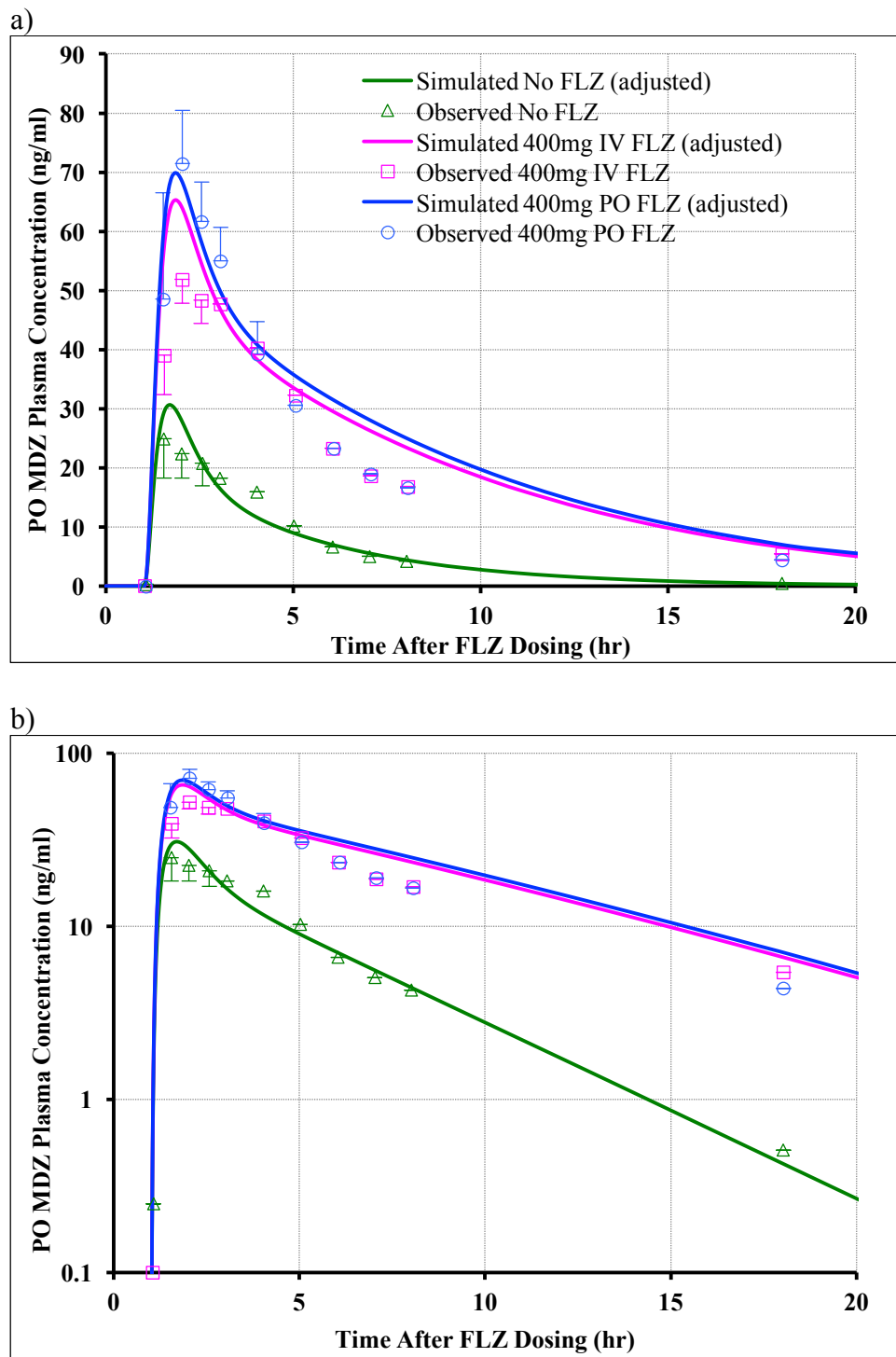


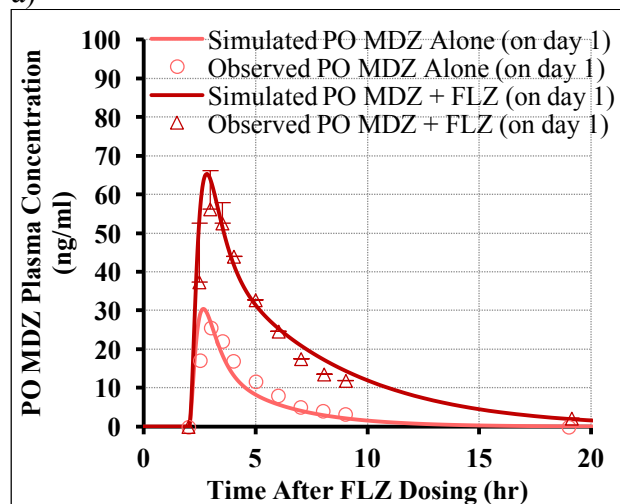
Figure 6.5 Observed and PBPK model ($v_{\max, \text{hep}}^{\text{MDZ}}$ adjusted) - simulated MDZ PK profiles for study 103.

a-b) PO MDZ 7.5 mg administered 1 hour after placebo, 400 mg IV 1-hour infusion, 400 mg PO FLZ on Cartesian and semi-log plots. The solid lines reflect predicted PK profiles. The symbols and bars are reported means and SD values (if available).

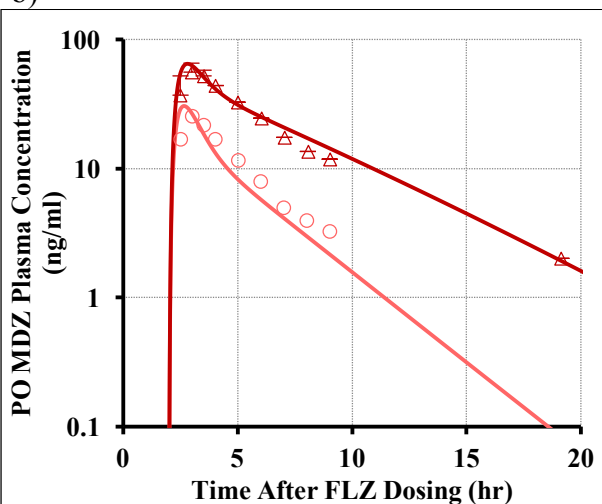
6.3.1.1.3 Study 26

Similarly, for study 26, after changing f_{villi} , the adjusted PBPK model adequately describes MDZ PK profiles in control and single-/repeat-doses FLZ groups (shown in **Figure 6.6**). Deviations (%) of all exposure metrics, as well as F_{oral} and AUCR are within 30%, except c_{max} and AUCR when PO MDZ was administered on the 6th day of FLZ dose (**Table 6.5**). The reason for the poor predictions could be that all the $AUC_{0-\infty}$ of MDZ in absence of FLZ is still underestimated, even with f_{villi} adjustment. Also, observed PO MDZ $AUC_{0-\infty}$ administered on 6th day is 16% higher than that administered on 1st day, ultimately resulting in over-prediction of AUCR after repeat- FLZ doses to a greater extent. The model predictions may be improved by tweaking f_{villi} even more, or changing $v_{max,hep}^{MDZ}$, however, further adjustment is not considered necessary, given the adequate prediction accuracy in most scenarios.

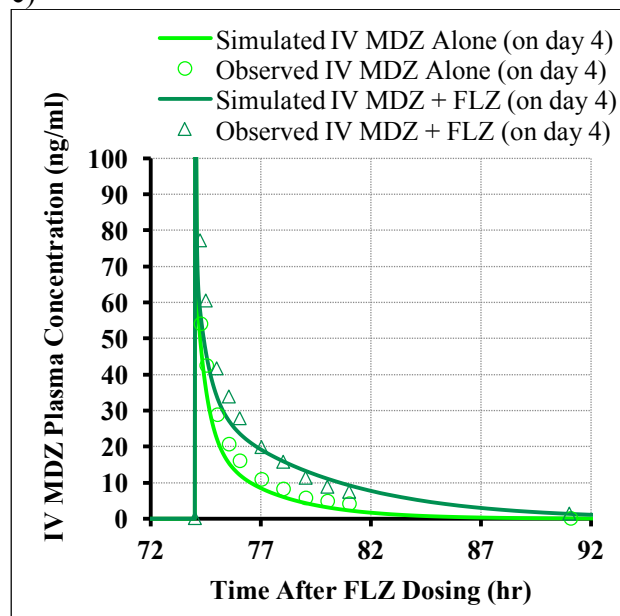
a)



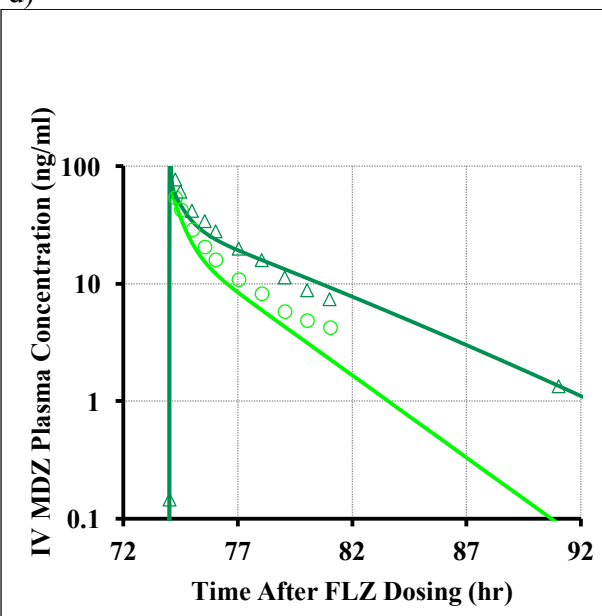
b)



c)



d)



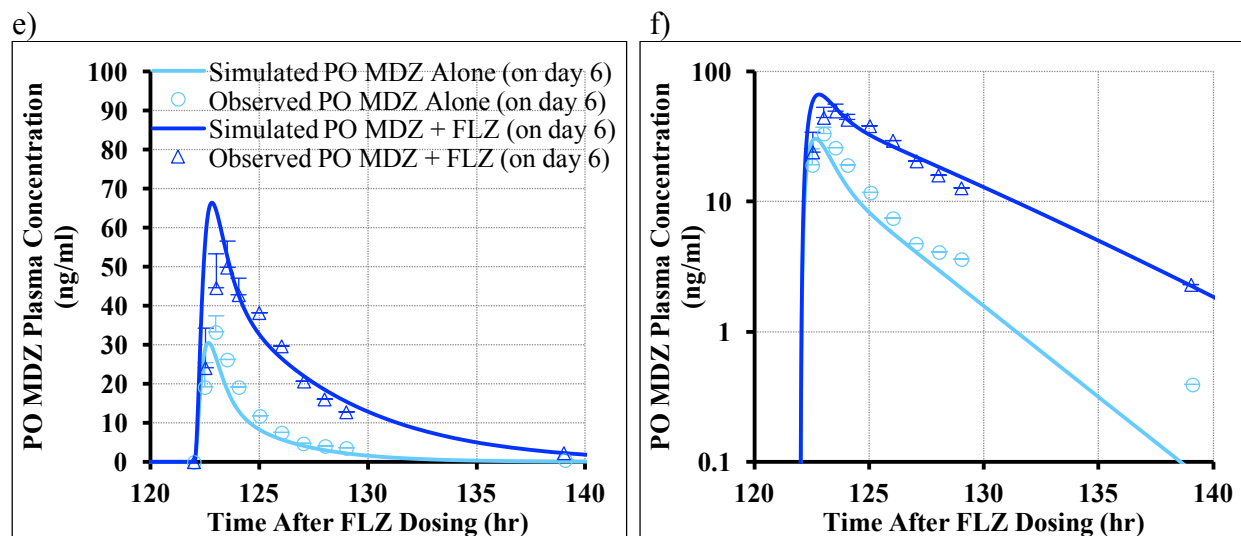


Figure 6.6 Observed and PBPK model (f_{villi} adjusted) - simulated MDZ PK profiles for study 26.

Placebo or PO FLZ was administered 400 mg on the 1st day and then 200 mg daily for 5 days. a-b) PO MDZ 7.5 mg administered 2 hours after the 1st dose of placebo or FLZ (Cartesian plots and semi-log plots). c-d) IV MDZ 0.05mg/kg administered 2 hours after the 4th dose of placebo or FLZ. e-f) PO MDZ 7.5 mg administered 2 hours after the 6th dose of placebo or FLZ. The solid lines reflect predicted PK profiles. The symbols and bars are reported means and SD values (if available).

Table 6.5 Comparison of reported and semi-PBPK model-predicted MDZ plasma exposure metrics in the absence/presence of IV/PO FLZ using initial model (study 21) and adjusted model (study 103 and 26) parameters.

(Deviation greater than 30% were marked as bold.)

Study ID	MDZ	FLZ	Deviation (%)			
			AUC _{0-∞} (ng/ml•hr)	C _{max} (ng/ml)	F _{oral}	AUCR
21	IV: 1mg	-	-7%	3%		
21	IV: 1mg	PO Single Dose: 100mg	-9%	-3%		-2%
21	IV: 1mg	PO Single Dose: 200mg	-10%	-3%		-3%
21	IV: 1mg	PO Single Dose: 400mg	-4%	-11%		4%
21	PO: 3mg	-	-4%	12%	3%	
21	PO: 3mg	PO Multiple Doses: 100mg (2 days)	-9%	16%	0%	-5%
21	PO: 3mg	PO Multiple Doses: 200mg (2 days)	-10%	16%	0%	-6%
21	PO: 3mg	PO Multiple Doses: 400mg (2 days)	2%	11%	7%	7%
103	PO: 7.5mg (Adjust v _{max,hep} ^{MDZ})	-	-6%	23%		
103	PO: 7.5mg (Adjust v _{max,hep} ^{MDZ})	IV 1-hr infusion: 400mg	14%	26%		22%
103	PO: 7.5mg (Adjust v _{max,hep} ^{MDZ})	PO Single Dose: 400mg	21%	-2%		29%
26	IV: 0.05mg/kg	-	-17%			
26	IV: 0.05mg/kg	PO Multiple Doses (day 1: PO 400mg; day 2-4: PO 200mg)	-3%			18%
26	PO: 7.5mg (Adjust f _{villi})	-	-12%	19%		
26	PO: 7.5mg (Adjust f _{villi})	PO Single Dose: 400mg	3%	16%		18%
26	PO: 7.5mg (Adjust f _{villi})	-	-25%	-9%		
26	PO: 7.5mg (Adjust f _{villi})	PO Multiple Doses (day 1: PO 400mg; day 2-6: PO 200mg)	6%	33%		41%

In study 26, FLZ was administered 400 mg on the first day and then 200 mg daily for 5 days, and the predicted unbound hepatic and GW concentrations relative to $K_{i,\text{hep}}^{\text{FLZ}}$ and $K_{i,\text{GW}}^{\text{FLZ}}$ are plotted in **Figure 6.7a-b**. Since loading dose (400 mg) doubles from maintenance dose (200 mg daily), $c_{\text{hep}}^{\text{FLZ}}$ and $c_{\text{GW}}^{\text{FLZ}}$ reach steady-state almost after the first dose, with all concentrations exceeding respective K_i values for more than 140 hours. Although $c_{\text{max,GW}}^{\text{FLZ}}$ after the first dose is ~50% higher than $c_{\text{max,GW}}^{\text{FLZ}}$ of the following doses, it quickly drops to a similar level, and as MDZ is administered 2 hours after FLZ, the 50% higher $c_{\text{max,GW}}^{\text{FLZ}}$ after loading dose would not translate into any difference in inhibitory effect after single- or repeat-doses FLZ.

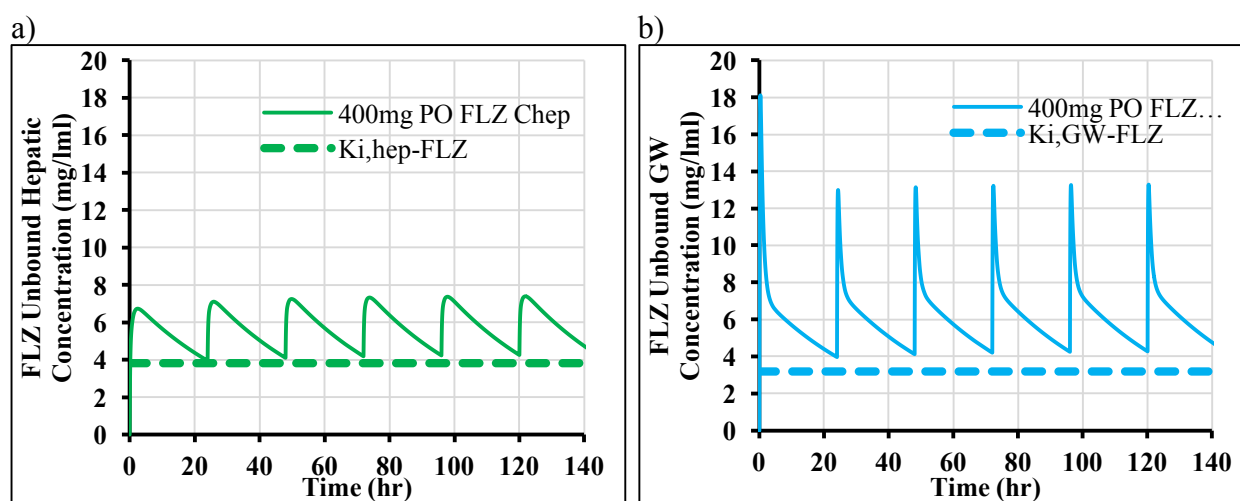


Figure 6.7 Semi-PBPK model predicted FLZ unbound hepatic and GW concentration – time profiles for study 26.

PO FLZ was administered 400 mg on the first day and then 200 mg daily for 5 days. a) FLZ unbound hepatic concentration – time profile. b) FLZ unbound GW concentration – time profile.

Predictive performance checks for all the three studies after adjustments suggest that the semi-PBPK model for IV or PO MDZ in the absence/presence of IV or PO FLZ predicts the reported data from three clinical studies well, confirming the validity of this model and model parameters.

6.3.1.2 Sensitivity analysis

The -fold change in plasma $AUC_{0-\infty}$, c_{max} and t_{max} were calculated by dividing plasma exposure metrics simulated at the upper limit of a certain parameter by that simulated at the lower limit (**Table 6.6**). A greater than 2-fold or less than 0.5-fold change was highlighted in bold, indicating the corresponding exposure is sensitive to that parameter. With the co-administration of IV or PO FLZ, exposure metrics of IV MDZ are substantially affected by f_{pv} , $V_{max,hep}^{MDZ}$ and $K_{p,hep}^{MDZ}$, the same parameters as IV MDZ without FLZ, because hepatic metabolism is the only source of MDZ elimination after IV administration, no matter FLZ is given or not, and all the three parameters influence MDZ hepatic concentration and/or hepatic clearance considerably. Increasing f_{pv} amplifies both MDZ and FLZ exposures in the liver, resulting in more MDZ metabolism and more enzymes inhibition by FLZ. $K_{p,hep}^{MDZ}$ and $V_{max,hep}^{MDZ}$ only affect MDZ; larger values of both parameters would lead to higher MDZ metabolism in the liver and less systemic exposure. After PO MDZ, besides f_{pv} , $V_{max,hep}^{MDZ}$ and $K_{p,hep}^{MDZ}$, which play essential roles in both pre-systemic and systemic hepatic metabolism, $K_{p,hep}^{FLZ}$ and $K_{i,hep}^{FLZ}$ are also pivotal parameters, regardless of FLZ routes. A larger $K_{p,hep}^{FLZ}$ value reflects higher FLZ hepatic concentrations and greater inhibition on MDZ hepatic metabolism, eventually resulting in higher MDZ systemic exposure. Increased $K_{i,hep}^{FLZ}$ reduces FLZ inhibitory potency to hepatic CYP3A, so that MDZ hepatic metabolism is less inhibited. $K_{p,GW}^{FLZ}$ and $K_{i,GW}^{FLZ}$ also affect MDZ systemic exposure to the same direction as $K_{p,hep}^{FLZ}$ and $K_{i,hep}^{FLZ}$, but to a less extent, due to the fact that $K_{p,hep}^{FLZ}$ and $K_{i,hep}^{FLZ}$ influence both pre-systemic and systemic MDZ clearance, while $K_{p,GW}^{FLZ}$ and $K_{i,GW}^{FLZ}$ only alter MDZ first pass GW metabolism. Under non-competitive inhibition, MDZ systemic exposure is actually affected by the ratios between $K_{i,hep}^{FLZ}$ and $K_{p,hep}^{FLZ}$ ($K_{i,hep}^{FLZ}/K_{p,hep}^{FLZ}$) and between $K_{i,GW}^{FLZ}$ and

$K_{p,GW}^{FLZ}$ ($K_{i,GW}^{FLZ}/K_{p,GW}^{FLZ}$), instead of a single parameter. Hence, even if some parameters used in the model (i.e., $K_{p,hep}^{FLZ}$ and $K_{p,GW}^{FLZ}$) may not be qualified clinically, the two ratios $K_{i,hep}^{FLZ}/K_{p,hep}^{FLZ}$ and $K_{i,GW}^{FLZ}/K_{p,GW}^{FLZ}$ were indirectly validated by MDZ and FLZ DDI studies.

No FLZ route difference in the metabolic DDI sensitivity analysis is observed, probably because there is a dosing lag-time between the two drugs (MDZ was administered 2 hours after FLZ). MDZ plasma PK profiles in presence of IV/PO FLZ for all sensitivity analyses are presented in **Appendices E**.

Table 6.6 Sensitivity analysis heat-map results for semi-PBPK MDZ and FLZ DDI model. (More solid green indicates smaller value; more solid red indicates larger value)

FLZ+MDZ Sensitivity Analysis (IV MDZ)		400mg 1hr IV infusion FLZ + 1 mg IV MDZ (2hr later)			400mg PO FLZ + 1 mg IV MDZ (2hr later)		
Parameter -Fold Change		-Fold change in plasma exposure metrics			-Fold change in plasma exposure metrics		
		AUC _{0-∞}	c _{max}	t _{max}	AUC _{0-∞}	c _{max}	t _{max}
f _{pV} ^{MDZ}	0-1	0.48	0.96	1.00	0.48	0.96	1.00
V _{max,hep} ^{MDZ}	4	0.34	1.00	1.00	0.34	1.00	1.00
K _{p,hep} ^{MDZ}	4	0.34	0.97	1.00	0.34	0.97	1.00
K _{p,GW} ^{MDZ}	4	1.00	1.00	1.00	1.00	1.00	1.00
K _{p,hep} ^{FLZ}	4	1.82	1.00	1.00	1.82	1.00	1.00
K _{i,hep} ^{FLZ}	4	0.51	1.00	1.00	0.51	1.00	1.00
FLZ+MDZ Sensitivity Analysis (PO MDZ)		400mg 1hr IV infusion FLZ + 3 mg PO MDZ (2hr later)			400mg PO FLZ + 3 mg PO MDZ (2hr later)		
Parameter Fold Change		-Fold change in plasma exposure metrics			-Fold change in plasma exposure metrics		
		AUC _{0-∞}	c _{max}	t _{max}	AUC _{0-∞}	c _{max}	t _{max}
f _{pV} ^{MDZ}	0-1	0.48	0.90	0.97	0.48	0.90	0.98
V _{max,hep} ^{MDZ}	4	0.27	0.67	0.94	0.27	0.67	0.94
K _{p,hep} ^{MDZ}	4	0.27	0.65	0.98	0.27	0.65	0.95
K _{p,GW} ^{MDZ}	4	0.99	0.86	1.12	0.99	0.86	1.11
K _{p,hep} ^{FLZ}	4	2.03	1.24	1.02	2.04	1.24	1.02
K _{p,GW} ^{FLZ}	4	1.25	1.27	1.03	1.26	1.27	1.03
K _{i,hep} ^{FLZ}	4	0.45	0.79	0.99	0.45	0.79	0.98
K _{i,GW} ^{FLZ}	4	0.76	0.77	0.97	0.77	0.77	0.97
f _{villi} ^{MDZ}	4	0.65	0.66	0.99	0.67	0.68	0.96
k _{GL} ^{MDZ}	4	1.04	1.48	0.83	1.05	1.48	0.82

6.3.2 Model Predictions

6.3.2.1 Simulation of route-dependent DDI between MDZ and FLZ after various administration time intervals

AUCR for each scenario was calculated to assess the extent of inhibition, and was plotted against administration interval time shown in **Figure 6.8**. After IV MDZ, no apparent difference is found among IV 1-hour infusion and PO FLZ at all time intervals. Within 5 hours, both routes of FLZ increase AUC^{MDZ} by 2-fold, and the inhibition lasts for more than 100 hours. However, after PO MDZ, PO FLZ has 62% more increase in AUC^{MDZ} than the same dose of IV infusion FLZ, when simultaneously administered with MDZ. With increasing delay in MDZ administration, the route difference is gradually reduced, and no route difference is demonstrated after 5 hours. The short duration of route difference is because FLZ has very high F_{oral} ($> 90\%$) and can be absorbed into systemic circulation quite fast, leading to similar drug levels after IV and PO administration. Regardless of route, FLZ increases AUC^{MDZ} more for PO MDZ than for IV MDZ, because pre-systemic hepatic and GW metabolism is inhibited after PO MDZ but not IV MDZ. Inhibition of CYP3A metabolism by FLZ fades after >100 hours, due to the long terminal $t_{1/2}$ of FLZ in plasma.

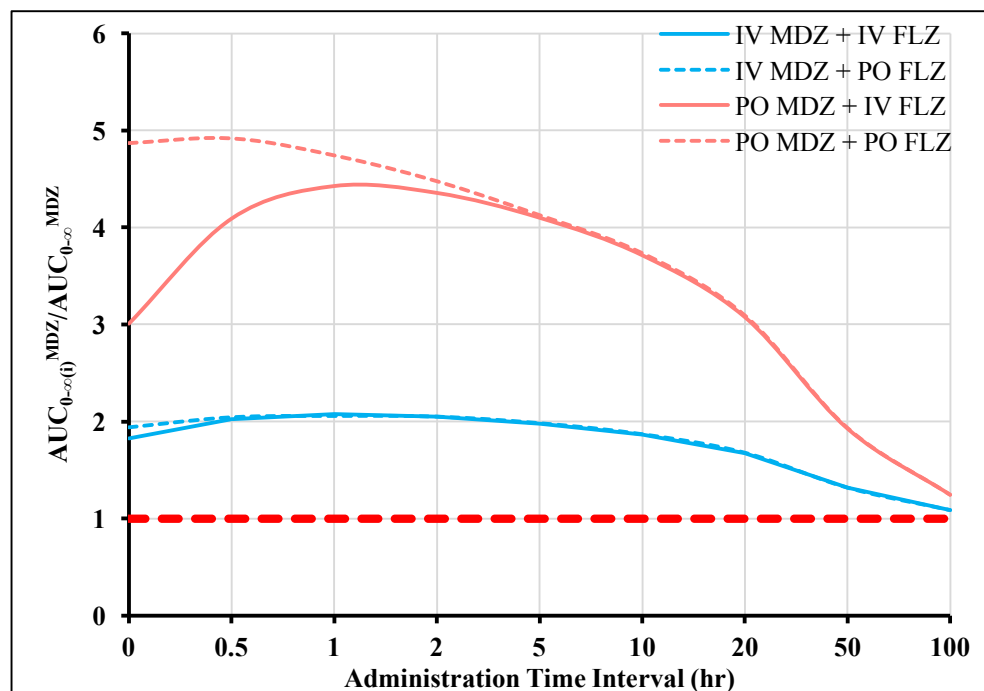


Figure 6.8 MDZ AUCR by 400 mg IV 1-hour infusion or PO FLZ administered at various time intervals before 1 mg IV/3 mg PO MDZ.

Red dash line indicates no inhibition on MDZ exposure.

To better interpret impact of route of administration of FLZ, plots of FLZ concentration and relative CYP3A activity levels in GW and liver were simulated (**Figure 6.9**), based on the dosing regimen of 400 mg IV 1-hour infusion or PO FLZ. Unbound hepatic and GW concentrations exceed relative K_i values for 25 and 30 hours, respectively, resulting in ~65% maximal inhibition on hepatic CYP3A at $c_{\max,u,\text{hep}}^{\text{FLZ}}$, and 70% after IV FLZ and 85% inhibition after PO FLZ on GW CYP3A at $c_{\max,u,\text{GW}}^{\text{FLZ}}$. No apparent route difference is observed with respect to hepatic CYP3A inhibition, reflecting marginal FLZ route difference when MDZ is dosed intravenously. GW concentration after PO FLZ is much higher than IV FLZ during the first 1-2 hours, but no difference is found after 5 hours, indicating stronger inhibition on GW CYP3A after PO than IV FLZ when PO MDZ is dosed simultaneously with FLZ, but no route difference when they are dosed 5 hours apart. Inhibitory effect lasts for more than 100 hours, as both hepatic and GW CYP3A are inhibited by more than 10% at 100 hours administration interval.

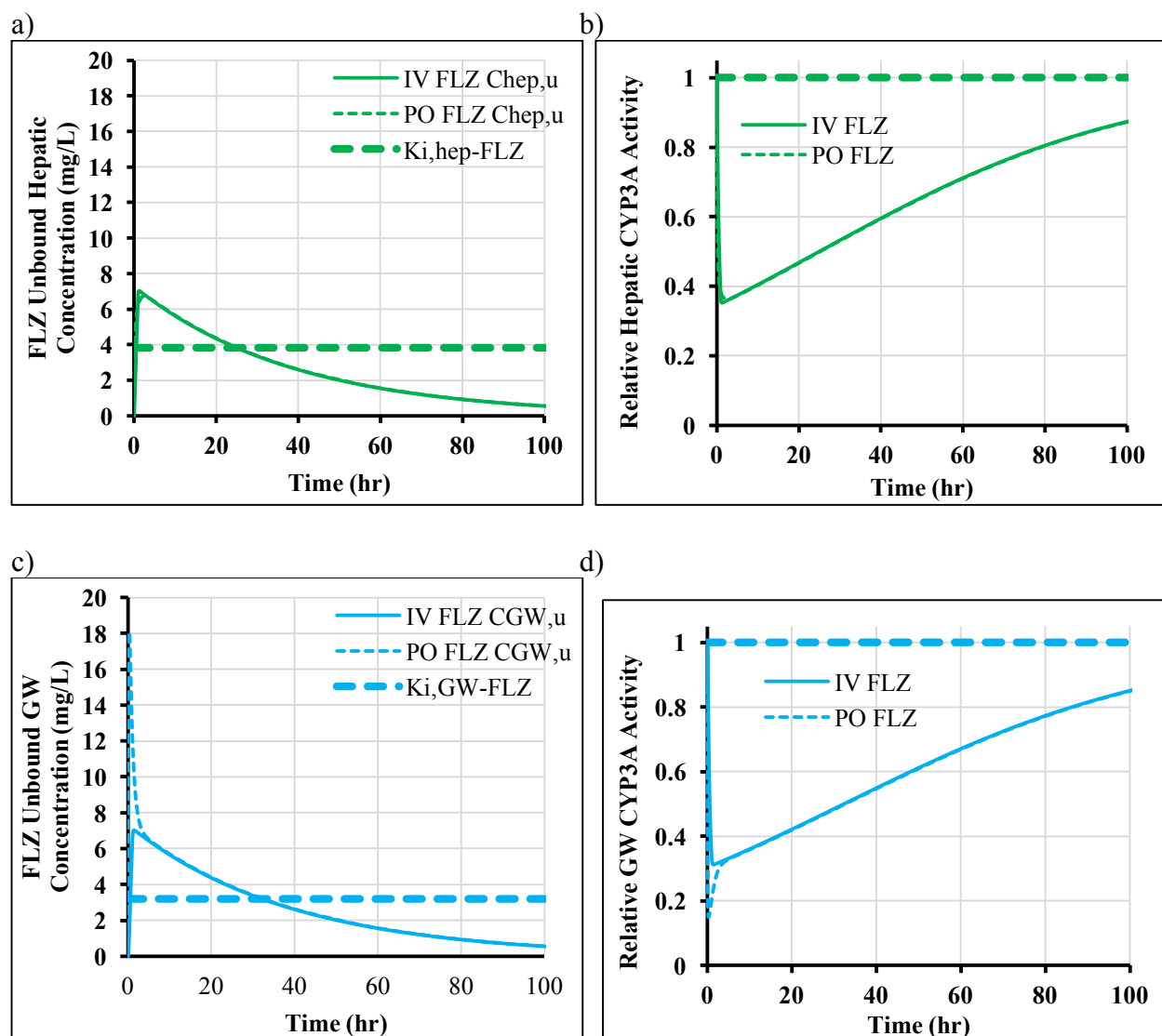


Figure 6.9 Plots of FLZ unbound concentrations and relative CYP3A activity under 400 mg IV 1-hour-infusion or PO FLZ.

a) FLZ unbound hepatic concentration – time profiles. b) Relative hepatic CYP3A activity in presence of FLZ. c) FLZ unbound GW concentration – time profiles. d) Relative GW CYP3A activity in presence of FLZ. Dash lines in a) and c) represent $K_{i,hep}^{FLZ}$ and $K_{i,GW}^{FLZ}$ values. Dash lines in b) and d) represent no change in hepatic and GW CYP3A activity.

6.3.2.2 Simulation of route-dependent DDI between MDZ and FLZ after various single dose of FLZ

To compare impact of FLZ route of administration on DDI after various FLZ dose, ratio of MDZ AUCR after PO FLZ and after IV FLZ were plotted against FLZ single dose (**Figure 6.10**). After IV MDZ, no apparent route difference (< 10%) of FLZ is observed, due to similar FLZ hepatic concentration profiles after IV or PO administration across doses. After PO MDZ, route difference – FLZ dose profile appears to be a “bell” shape curve: at both low end (40 mg) and high end (4000 mg) FLZ doses, slight route differences are demonstrated (~20%), while maximal route difference occurs at middle dose (400 mg). This is because at very low dose, both IV and PO FLZ have likely trivial inhibition on hepatic and GW CYP3A, while at very high dose, both routes completely inhibit hepatic and GW CYP3A. It is at the middle dose, when FLZ GW concentration is close to $K_{i,GW}^{FLZ}$, that the GW concentration difference of FLZ translates into the largest GW CYP3A inhibition difference.

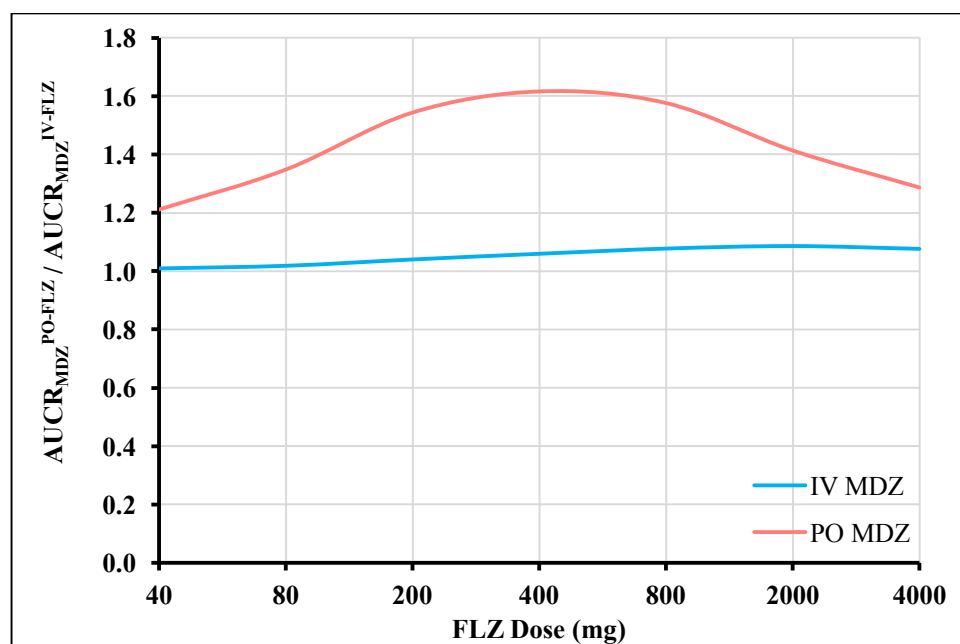


Figure 6.10 Ratio of MDZ AUCR by PO FLZ and by IV 1-hour infusion FLZ after various FLZ single doses.

6.3.2.3 Simulation of route-dependent DDI between MDZ and hypothetical CYP3AI and between hypothetical CYP3A substrates and ERY

6.3.2.3.1 Route-dependent DDI between MDZ and 3AIX1/2/3

To change FLZ to a low F_{oral} CYP3AI (3AIX1), $F_{\text{abs}}^{\text{FLZ}}$ was decreased from 1.0 to 0.1. MDZ AUC in presence of IV/PO 3AIX1 with different administration time interval were simulated, and AUCR of MDZ for each scenario is plotted against administration interval time shown in **Figure 6.11**. Plots of 3AIX1 concentration and relative CYP3A levels in GW and liver were simulated (**Figure 6.12**), based on the dosing regimen of 400 mg IV 1-hour infusion or PO 3AIX1. From **Figure 6.12**, due to the low F_{oral} of 3AIX1, IV 3AIX1 has much higher hepatic and GW concentrations than PO 3AIX1, producing more inhibition of CYP3A in liver and GW, regardless of MDZ route. Consequently, IV 3AIX1 consistently yields higher AUCR than PO 3AIX1, as is demonstrated in **Figure 6.11**. The DDI (peak 4.5-fold) lasts for up to one week, due to the long $t_{1/2}$ of 3AIX1 at pseudo steady-state (same as FLZ). In terms of MDZ route difference, PO MDZ is consistently more sensitive to the metabolism inhibition than IV MDZ, in line with the conclusions from MDZ and FLZ DDI simulations.

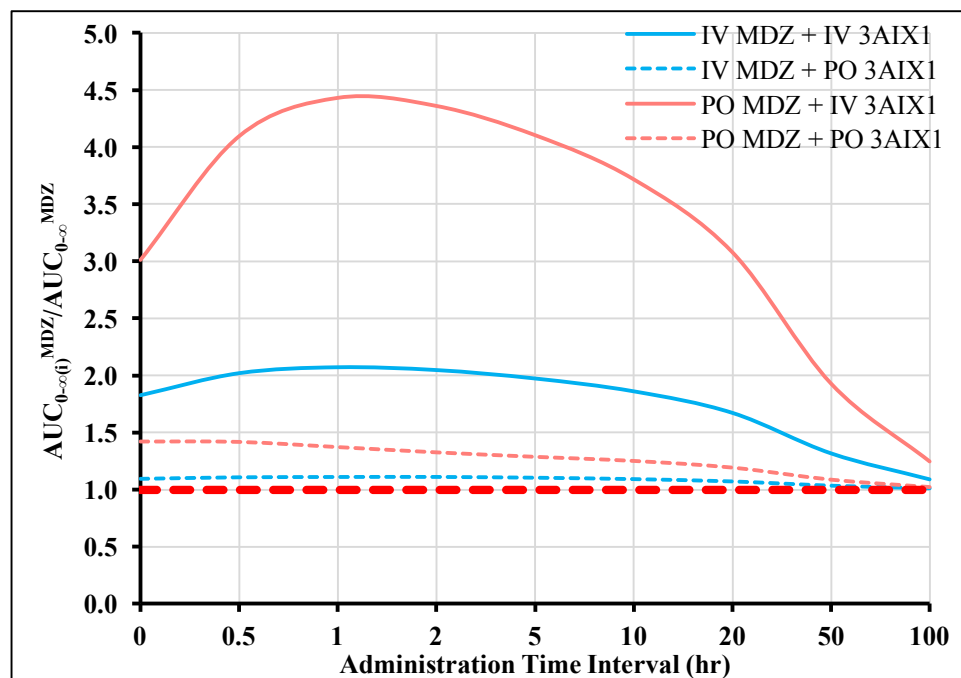


Figure 6.11 MDZ AUCR by 400 mg IV 1-hour infusion or PO 3AIX1 administered at various time intervals before 1 mg IV/3 mg PO MDZ.
Red dash line indicates no inhibition on MDZ exposure.

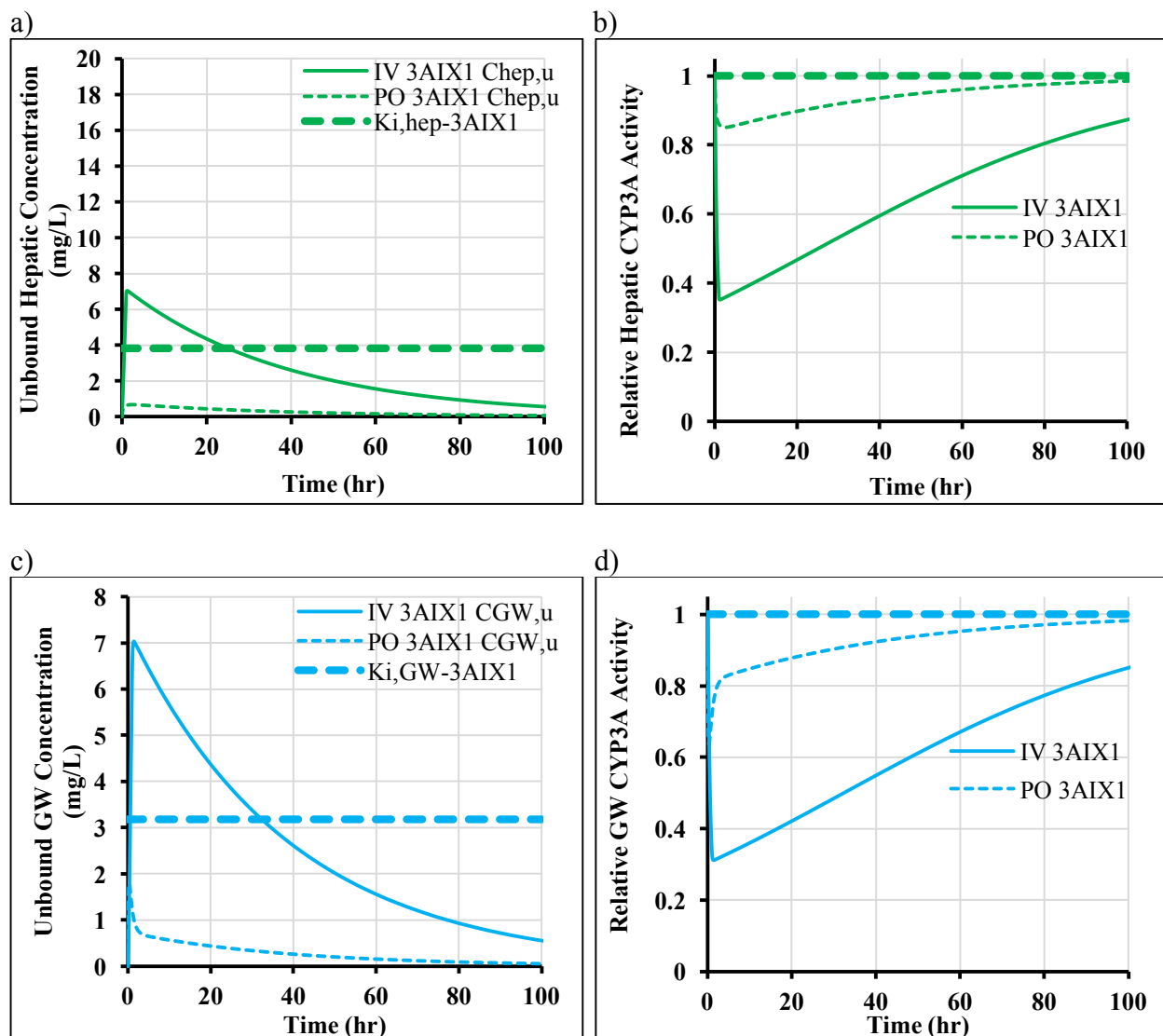


Figure 6.12 Plots of 3AIX1 unbound concentrations and relative CYP3A activity under 400 mg IV 1-hour infusion or PO 3AIX1.

a) 3AIX1 unbound hepatic concentration – time profiles. b) Relative hepatic CYP3A activity in presence of 3AIX1. c) 3AIX1 unbound GW concentration – time profiles. d) Relative GW CYP3A activity in presence of 3AIX1. Dash lines in a) and c) represent $K_{i, hep}^{3AIX1}$ and $K_{i, GW}^{3AIX1}$ values. Dash lines in b) and d) represent no change in hepatic and GW CYP3A activity.

To change FLZ to a short $t_{1/2}$ CYP3AI (3AIX2), CL_{ren}^{FLZ} was increased from 0.2 ml/min/kg to 3 ml/min/kg, which shortens elimination $t_{1/2}$ of this drug to $\sim 1/10$ of FLZ (CL_{int}^{FLZ} was not adjusted to avoid change in first-pass metabolism and F_{oral}). MDZ AUC in presence of IV/PO 3AIX2 with different administration time interval were simulated, and AUCR of MDZ for each scenario is plotted against administration interval time shown in **Figure 6.13**. Plots of 3AIX2 concentration and relative CYP3A levels in GW and liver were simulated (**Figure 6.14**), based on the dosing regimen of 400 mg IV 1-hour infusion or PO 3AIX2.

Only a small (<10%) route difference of 3AIX2 is observed after IV MDZ, given similar 3AIX2 hepatic concentration after both routes (**Figure 6.14 a-b**). However, after PO MDZ, PO administration of 3AIX2 results in a 68% higher (3.8- vs. 2.3-fold) DDI than IV, only when both drugs are administered simultaneously - primarily caused by higher GW concentrations after PO than IV administration during the first 1-2 hours. With increasing delay in MDZ administration, the route difference gradually reduces, but consistently exists. This is confirmed by the slightly higher hepatic and GW 3AIX2 concentration after PO administration than after IV infusion. To explain the sustained concentration difference, plasma concentrations of 3AIX2 after both routes were compared with FLZ plasma concentrations (**Figure 6.15**), because concentrations in both tissues (liver and GW) are driven by plasma concentrations after absorption. From **Figure 6.15b**, both FLZ and 3AIX2 are completely absorbed within 4 hours, as IV and PO concentrations decline at the same rate after 4 hours, indicating the only process going on after 4 hours is elimination (1 – compartmental body model drug). As to FLZ, IV and PO FLZ profiles intercross exactly at 4 hours, so that no concentration difference is observed afterwards. However, with respect to 3AIX2, due its faster elimination, intersection of IV and PO profiles occurs earlier than 4 hours (~ 2.3 hours), and after 2.3 hours, absorption process has not completed yet, leading

to shallower declining rate after PO 3AIX2 than IV 3AIX2 from 2.3 to 4 hours. Eventually at 4 hours, 3AIX2 has higher concentration after PO administration than after IV administration, and the concentration difference between routes consistently exists throughout the entire terminal phase (after 4 hours). Due to the short $t_{1/2}$ of 3AIX2, inhibition on hepatic and GW CYP3A only last for 20 hours, which is much shorter than inhibitory duration of FLZ. Regardless of route, 3AIX2 increases AUC^{MDZ} more for PO MDZ than for IV MDZ, because pre-systemic hepatic and GW metabolism are inhibited after PO MDZ but not IV MDZ.

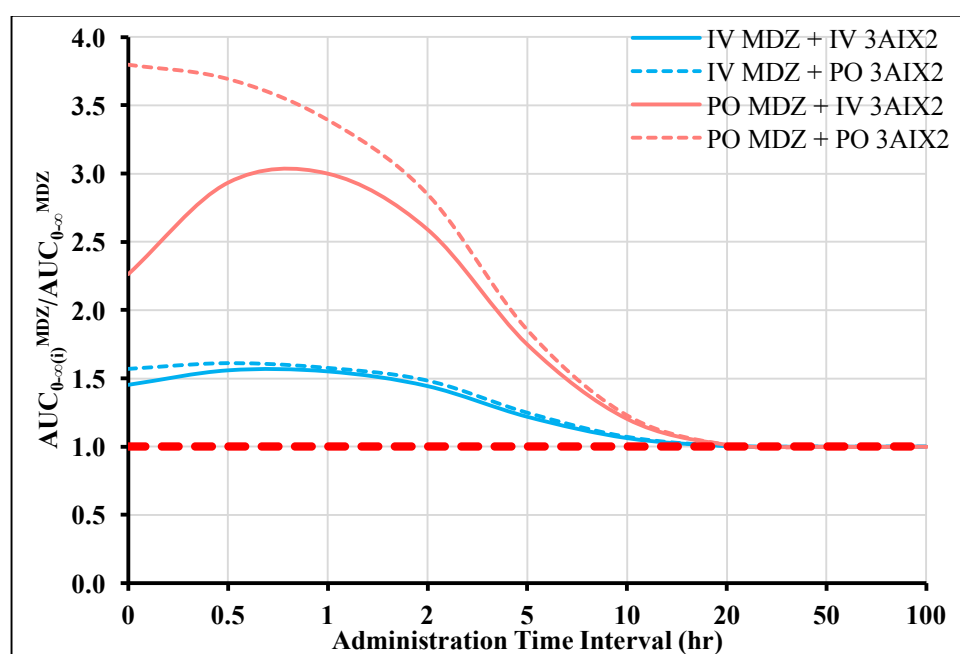


Figure 6.13 MDZ AUCR by 400 mg IV 1-hour infusion or PO 3AIX2 administered at various time intervals before 1 mg IV/3 mg PO MDZ.
Red dash line indicates no inhibition on MDZ exposure.

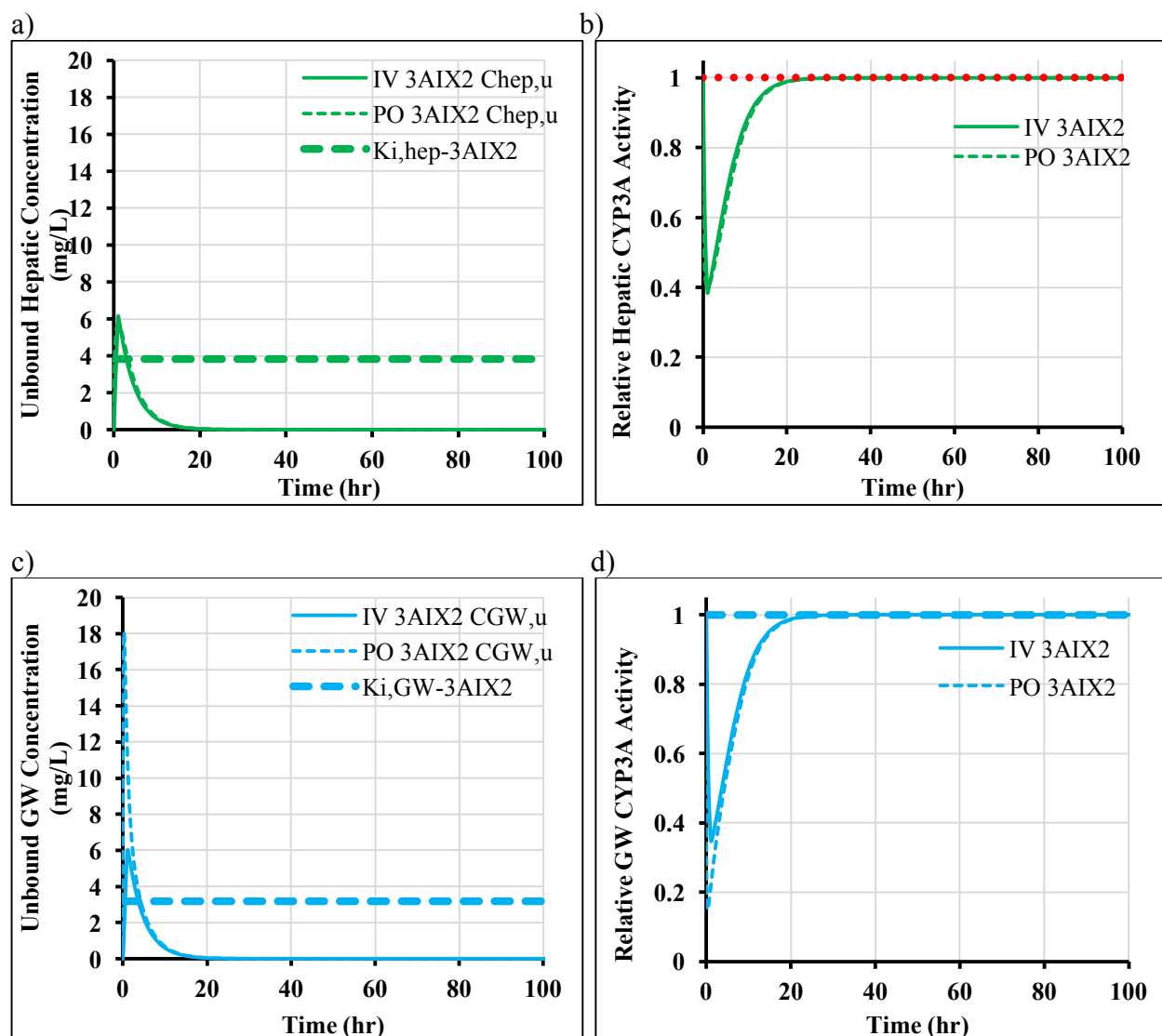
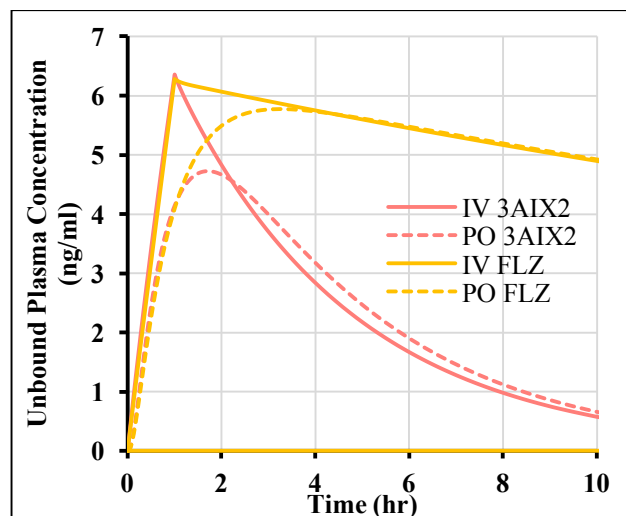


Figure 6.14 Plots of 3AIX2 unbound concentrations and relative CYP3A activity in presence of 400 mg IV 1-hour infusion or PO 3AIX2.

a) 3AIX2 unbound hepatic concentration – time profiles. b) Relative hepatic CYP3A activity in presence of 3AIX2. c) 3AIX2 unbound GW concentration – time profiles. d) Relative GW CYP3A activity in presence of 3AIX2. Dash lines in a) and c) represent $K_{i,hep}^{3AIX2}$ and $K_{i,GW}^{3AIX2}$ values. Dash lines in b) and d) represent no change in hepatic and GW CYP3A activity.

a)



b)

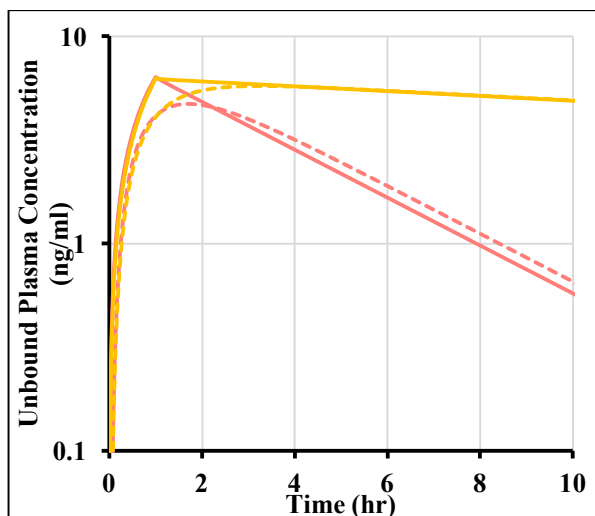


Figure 6.15 Unbound plasma concentration of 400 mg IV 1-hour infusion and PO administration of 3AIX2 and FLZ on Cartesian and semi-log plots.

To change FLZ to a low F_{oral} and short $t_{1/2}$ CYP3AI (3AIX3), both $F_{\text{abs}}^{\text{FLZ}}$ and $CL_{\text{ren}}^{\text{FLZ}}$ were adjusted, with $F_{\text{abs}}^{\text{FLZ}}$ decreasing from 1.0 to 0.1 and $CL_{\text{ren}}^{\text{FLZ}}$ increasing from 0.2 ml/min/kg to 3.0 ml/min/kg. MDZ AUC in presence of IV/PO 3AIX3 with different administration time interval were simulated, and AUCR of MDZ for each scenario is plotted against administration interval time shown in **Figure 6.16**. Plots of 3AIX3 concentration and relative CYP3A levels in GW and liver were simulated (**Figure 6.17**), based on the dosing regimen of 400 mg IV 1-hour infusion or PO 3AIX3. From **Figure 6.17**, due to the low F_{oral} of 3AIX3, IV 3AIX3 has much higher hepatic and GW concentrations than PO 3AIX3, leading to more inhibition of CYP3A in liver and GW, regardless of MDZ route. Consequently, IV 3AIX3 consistently yields higher AUCR than PO 3AIX3, as is demonstrated in **Figure 6.16**. Due to the short $t_{1/2}$ of 3AIX3, inhibition on hepatic and GW CYP3A only last for 20 hours, which is much shorter than inhibitory duration of FLZ. Regardless of route, 3AIX3 increases AUC^{MDZ} more for PO MDZ than for IV MDZ, because of the inhibition on pre-systemic hepatic and GW metabolism.

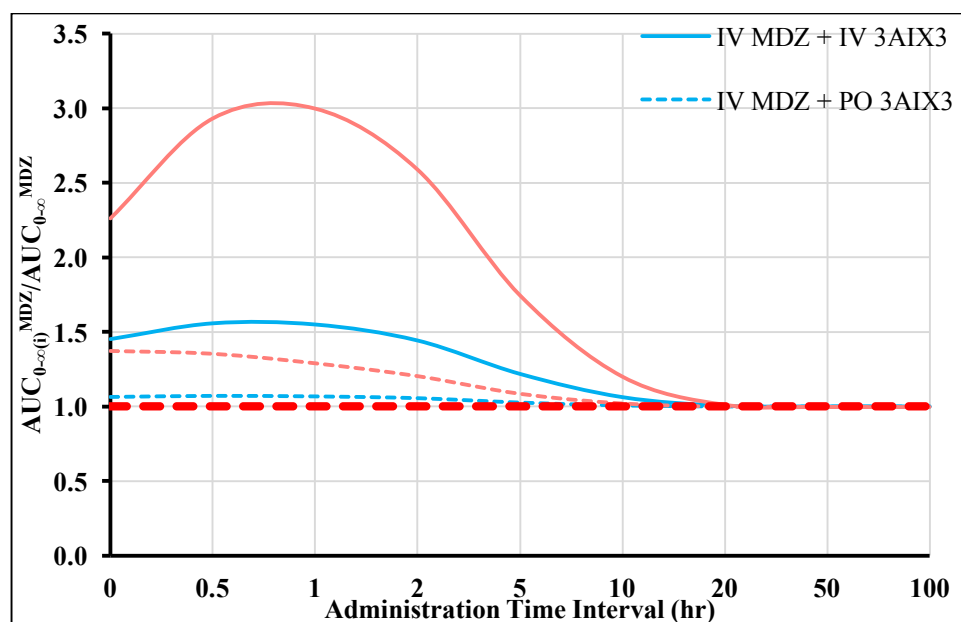


Figure 6.16 MDZ AUCR by 400 mg IV 1-hour infusion or PO 3AIX3 administered at various time intervals before 1 mg IV/3 mg PO MDZ. Red dash line indicates no inhibition on MDZ exposure.

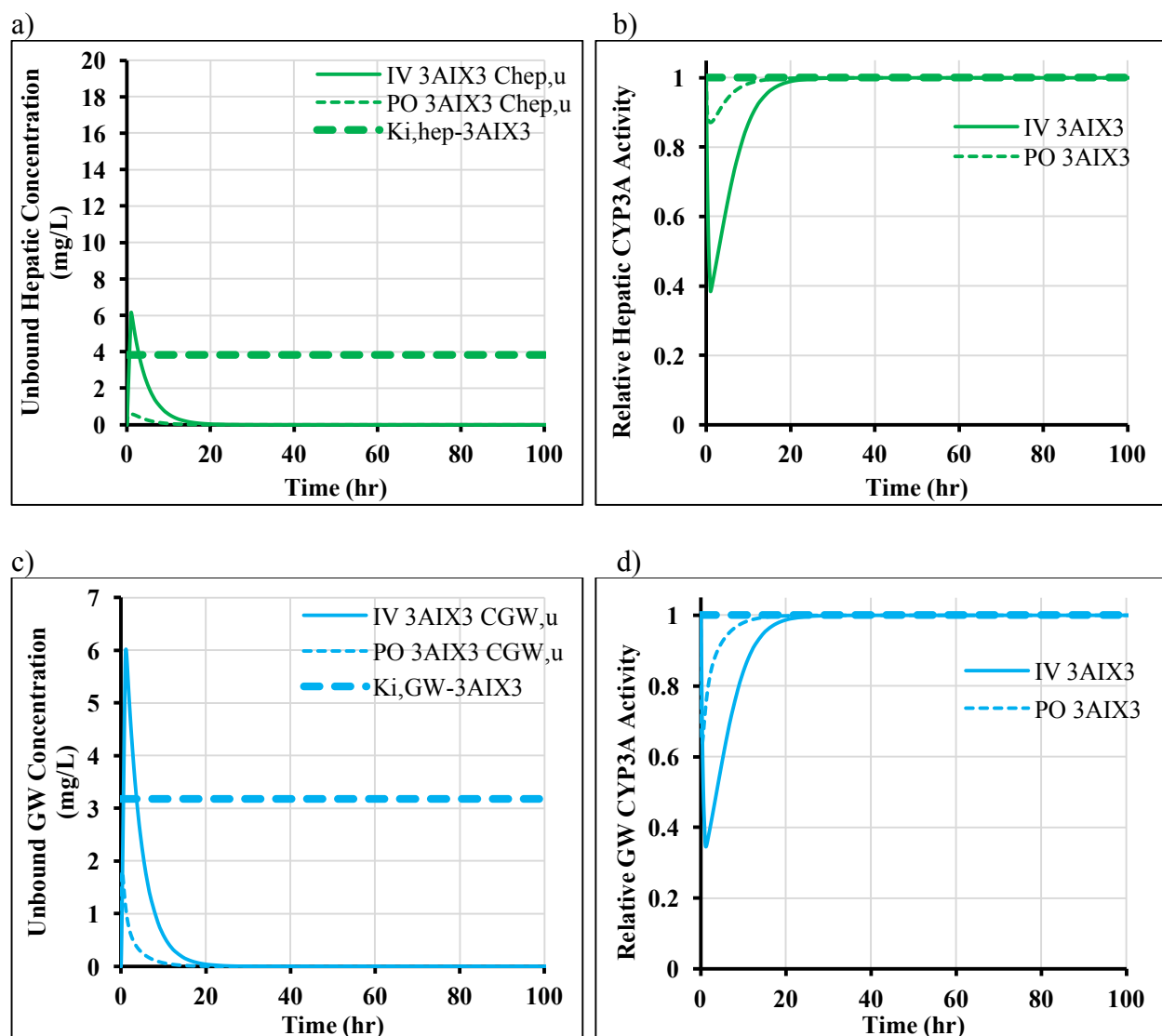


Figure 6.17 Plots of 3AIX3 unbound concentrations and relative CYP3A activity in presence of 400 mg IV 1-hour infusion or PO 3AIX3.

a) 3AIX3 unbound hepatic concentration – time profiles. b) Relative hepatic CYP3A activity in presence of 3AIX3. c) 3AIX3 unbound GW concentration – time profiles. d) Relative GW CYP3A activity in presence of 3AIX3. Dash lines in a) and c) represent $K_{i,hep}^{3AIX3}$ and $K_{i,GW}^{3AIX3}$ values. Dash lines in b) and d) represent no change in hepatic and GW CYP3A activity.

6.3.2.3.2 Route-dependent DDI between 3ASX1/2 and FLZ

Subsequently, two CYP3A substrate (3ASX1: no GW metabolism; 3ASX2: no GW metabolism and decreased hepatic metabolism) were derived from MDZ PBPK model. 3ASX1/2 AUC in presence of 400 mg IV 1-hour infusion or PO FLZ with different administration time interval were simulated, and AUCR of 3ASX1/2 for each scenario is plotted against administration interval time shown in **Figure 6.18** and **Figure 6.19**.

From **Figure 6.18**, PO 3ASX1 is consistently more sensitive to metabolic inhibition than IV 3ASX1, due to the existence of pre-systemic hepatic metabolism after PO administration. However, the impact of the FLZ administration route is the same regardless of 3ASX1 route, as metabolic DDI is limited to hepatic metabolism of 3ASX1 (no GW metabolism).

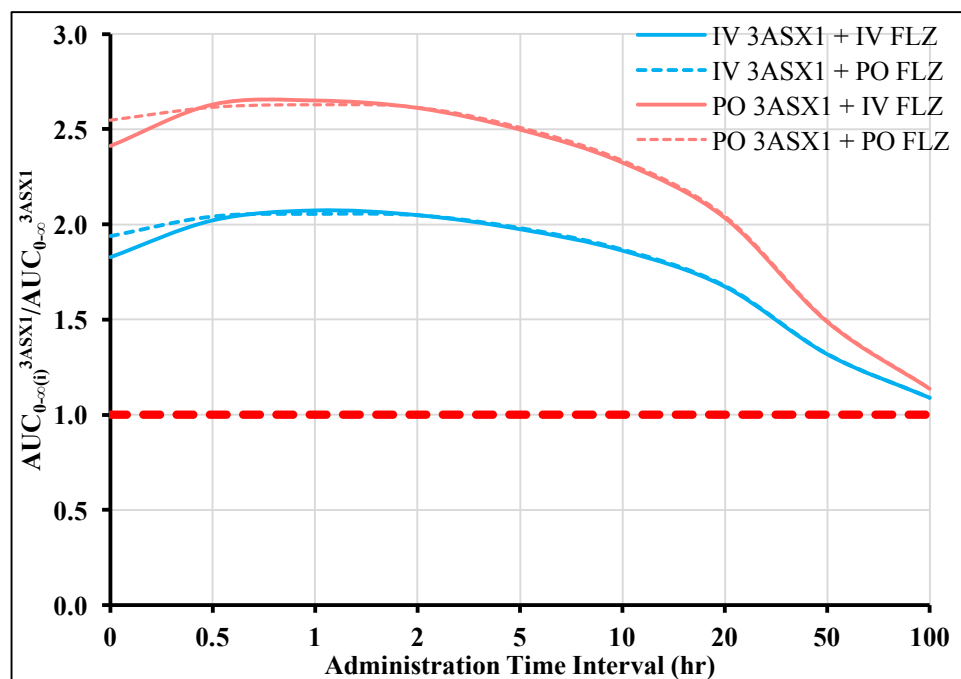


Figure 6.18 3ASX1 AUCR by 400 mg (IV: 1-hour infusion or PO) FLZ administered at various time intervals before 1 mg IV/3 mg PO 3ASX1. Red dash line indicates no inhibition on 3ASX1 exposure.

From **Figure 6.19**, no clinical significant IV-PO route difference (<10%) of 3ASX2 is observed, due to limited pre-systemic hepatic extraction ($ER_{\text{hep}}^{3\text{ASX}2} = 0.11$) and no GW metabolism. The impact of the FLZ administration route is the same regardless of 3ASX2 route, as metabolic DDI is limited to hepatic metabolism of 3ASX2 (no GW metabolism). To compare **Figure 6.18** and **Figure 6.19**, maximal DDI between PO 3ASX2 and FLZ is smaller than maximal DDI between PO 3ASX1 and FLZ, because 3ASX1 has lower F_{oral} than 3ASX2, and more potential to increase F_{oral} in presence of FLZ. IV 3ASX2 can be inhibited slightly more than IV 3ASX1, because as a very low ER_{hep} drug ($ER_{\text{hep}} = 0.11$), the decrease in its CL_{hep} is almost the same as the decrease in its $CL_{\text{int,hep}}$ (by FLZ), given the limited influence of Q_{hep} on its CL_{hep} . However, 3ASX1 has higher ER_{hep} ($ER_{\text{hep}} = 0.40$) than 3ASX2, and Q_{hep} will have larger impact on its CL_{hep} , resulting in less decrease in CL_{hep} than decrease in its $CL_{\text{int,hep}}$. Hence, the smaller the ER_{hep} , the greater extent of inhibition should be observed in CL_{hep} of the substrate, and the closer the decrease in CL_{hep} to the decrease in $CL_{\text{int,hep}}$. If a high ER_{hep} (> 0.7) substrate is used, given the same FLZ dose, marginal increase in AUC should be observed, because for a high ER_{hep} drug, CL_{hep} is not dependent on $CL_{\text{int,hep}}$, but on Q_{hep} .

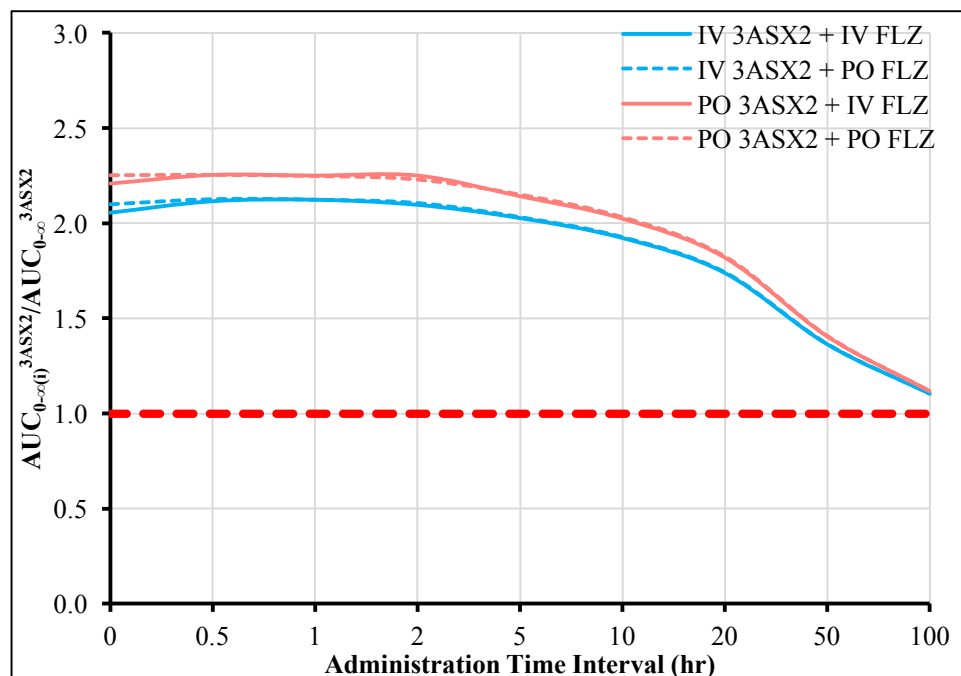


Figure 6.19 3ASX2 AUCR by 400 mg (IV: 1-hour infusion or PO) FLZ administered at various time intervals before 1 mg IV/3 mg PO 3ASX2.

Red dash line indicates no inhibition on 3ASX1 exposure.

6.3.2.3.3 Route-dependent DDI between 3ASX2 and 3AIX2

AUCR of 3ASX2 in presence of 400 mg IV 1-hour infusion or PO FLZ with different administration time intervals was demonstrated in **Figure 6.20**. No clinical significant IV-PO route difference (<10%) of 3ASX2 is observed, due to its limited re-systemic hepatic extraction ratio and no GW metabolism. Duration of DDI is less than 10 hours, due to the short plasma $t_{1/2}$ of 3AIX2. To compare **Figure 6.19** and **Figure 6.20**, AUCR of 3ASX2 is much lower in presence of 3AIX2 (AUCR range: 1.34 – 1.42) than FLZ (AUCR range: 2.10 – 2.25), because 3AIX2 produces shorter duration of DDI, and the terminal phase of 3ASX2's plasma concentration – time profiles is less inhibited. Therefore, DDI magnitude is also affected by $t_{1/2}$ of CYP3AI, relative to $t_{1/2}$ of CYP3A substrate.

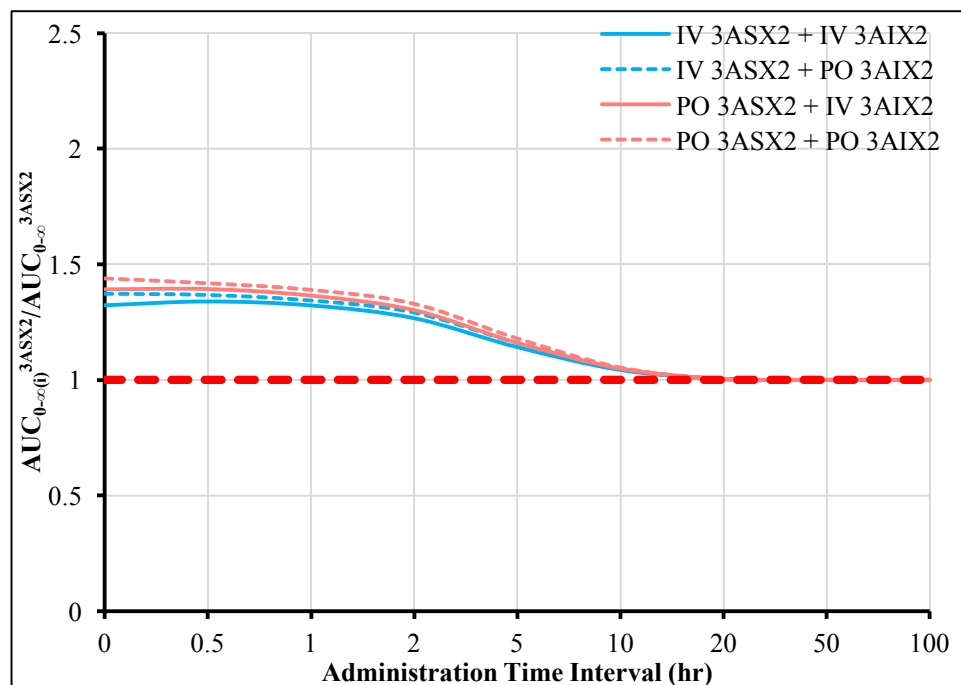


Figure 6.20 3ASX2 AUCR by 400 mg (IV: 1-hour infusion or PO) 3AIX2 administered at various time intervals before 1 mg IV/3 mg PO 3ASX2.
Red dash line indicates no inhibition on 3ASX2 exposure.

6.4 Conclusions

A semi-PBPK DDI model was developed to describe IV/PO MDZ clinical PK profiles in presence of IV/PO FLZ. The model was validated by MDZ plasma concentration – time profiles and exposure metrics in presence of FLZ in three clinical DDI studies. All the observed profiles are captured well by the model (with adjustment on $v_{\max, \text{hep}}^{\text{MDZ}}$ and f_{villi} in study 103 and study 26, respectively), with deviations (%) of exposure metrics less than $\pm 30\%$ in most scenarios. Formal parameter sensitivity analyses were conducted for ten key/uncertain model parameters, and f_{pv} , $K_{\text{p, hep}}^{\text{MDZ}}$ and $v_{\max, \text{hep}}^{\text{MDZ}}$, which considerably affect hepatic drug levels/clearance, are the pivotal parameters determining both IV and PO MDZ exposure metrics in presence of FLZ. Exposure metrics of PO MDZ in presence of FLZ is also sensitive to $K_{\text{p, hep}}^{\text{FLZ}}$ and $K_{\text{i, hep}}^{\text{FLZ}}$, regardless of FLZ routes. No FLZ route difference in the metabolic DDI sensitivity analysis is observed,

probably because there is a dosing lag-time between the two drugs (MDZ was administered 2 hours after FLZ). As a result, f_{pv} , $K_{p,hep}^{MDZ}$, $v_{max,hep}^{MDZ}$, $K_{p,hep}^{FLZ}$ and $K_{i,hep}^{FLZ}$ are the most sensitive parameters affecting plasma concentrations of MDZ in presence of FLZ, and may be tweaked when the predicted profile cannot adequately describe observed data. Given the accurate predictions with the current parameter sets, no additional adjustments are considered at this point.

Using the semi-PBPK DDI model, simulations were performed to assess impact of route of administration for both MDZ and FLZ on their metabolic DDI, after different administration time intervals between the two drugs. After IV MDZ, no apparent FLZ route difference is found, while after PO MDZ, PO FLZ has more inhibition on GW metabolism than IV infusion FLZ, when the two drugs are dosed simultaneously. With increasing delay in MDZ administration, route difference of FLZ gradually reduces, and no route difference is found after 5 hours.

Maximal inhibition on hepatic and GW CYP3A occur when FLZ concentration in liver and GW peak, and metabolic inhibition lasts for more than 100 hours, due to the long terminal $t_{1/2}$ of FLZ in plasma. Regardless of route, PO MDZ is more sensitive to metabolic inhibition of FLZ than IV MDZ.

Furthermore, a series of FLZ doses were simulated simultaneously administered with IV/PO MDZ, to compare FLZ route difference across doses. After IV MDZ, no apparent route difference (< 10%) of FLZ is detected across doses. After PO MDZ, only a slight FLZ route difference is observed at the lowest and the highest simulated FLZ dose, while the middle dose (400 mg) has the largest route difference, which is caused by the relationship between hepatic and GW FLZ concentrations relative to the corresponding K_i values.

Three hypothetical CYP3AIs (3AIX1/2/3) with F_{oral} and/or $t_{1/2}$ modified from FLZ semi-PBPK model, and two hypothetical CYP3A substrates with hepatic or GW metabolism reduced

or removed from MDZ semi-PBPK model (3ASX1/2) were also simulated to generalize conclusions. For DDI between MDZ and 3AIX1/2/3, when decreasing F_{abs}^{FLZ} by 10 fold (3AIX1/3), IV FLZ consistently has greater inhibition than PO FLZ, regardless of administration time intervals, although clinically, PO dose is usually adjusted to match systemic exposure after IV dose. When shortening $t_{1/2}^{FLZ}$ by ~ 10 fold (3AIX2/3), FLZ inhibition only lasts less than 20 hours, indicating that duration of inhibition is determined by pseudo steady-state plasma $t_{1/2}$ of CYP3AI for non-competitive inhibition. For DDI between 3ASX1 and FLZ, PO 3ASX1 was still be inhibited more than IV 3ASX1, but the route effects of FLZ are the same no matter how 3ASX1 is given. For DDI between 3ASX2 and FLZ, marginal route difference of 3ASX2 is observed, due to its limited hepatic first-pass metabolism (low ER_{hep}^{3ASX2}). DDI magnitude between 3ASX2 and 3AIX2 is much less than that between 3ASX2 and FLZ, suggesting that extent of DDI is also affected by $t_{1/2}$ of CYP3AI, relative to $t_{1/2}$ of CYP3A substrate.

CHAPTER 7

7 SEMI-PBPK MODELING OF IV/PO ERY

7.1 Background and Objectives

7.1.1 Selection of CYP3AI

From **Chapter 6**, the route difference for MDZ and FLZ metabolic DDI is only evident when the two drugs are administered simultaneously, due to the high F_{oral} of FLZ. However, if another CYP3AI has a low F_{oral} , a marked difference of CYP3AI exposure after IV/PO administration is expected, leading to larger route differences, even when MDZ is dosed with longer delay time after CYP3AI. In contrast to FLZ, a second CYP3AI should meet three criteria: 1) CYP3AI can be clinically administered as both IV and PO administration, and its PK profiles in clinical studies after both routes should be accessible; 2) F_{oral} is relatively low; 3) no inhibitory metabolites are formed, otherwise the interpretation of DDI results would be more complicated and model modification and additional model parameters would be required. After a preliminary screening of all the CYP3AI in the final meta-analysis database (**Chapter 3**), erythromycin (ERY) was chosen as a desirable inhibitor.

7.1.2 ERY PK information and simulation strategies

ERY is a macrolide antibiotic, and has widespread clinical use in various infections.

According to Erythromycin (Systemic) Lexi.com, IV ERY is usually administered as the form of

lactobionate salt, with 15-20 mg/kg/day equivalent base divided every 6 hours (q6h) and a maximum dose of 4 g daily. PO ERY can be administered either as enteric-coated base or salt or ester form, with 250 mg q6h, or 500 mg every 12 hours (q12h), and dosage may be increased up to 4 g per day according to the severity of the infection (Arbor Pharmaceuticals, 2013). Oral bioavailability of ERY is relatively low and quite variable (18% - 45%) (Somogyi et al., 1995), because of several reasons. Firstly, it is extensively hydrolyzed by gastric acid, thus, various approaches, such as ERY base enteric-coated tablets, ERY stearate salts or ERY ethylsuccinate, have been adopted to improve its $F_{\text{oral}}^{\text{ERY}}$ (Somogyi et al., 1995). Secondly, it is classified as BCS class 3 (Heizmann et al., 1983) drug, which is identified as a potent P-gp substrate in Caco-2 cells (Lin et al., 2011; Nožini et al., 2010; Schuetz et al., 1998). However, since ERY concentration (50 μM) used in these *in-vitro* studies was much lower than clinical relevant gut lumen concentration of ERY, assuming it is dissolved in 250 ml aqueous liquid in gut lumen, P-gp may be saturated at clinical dose. Last but not least, it is metabolized by CYP3A in both small intestine and liver, and can be excreted unchanged into bile. $CL_{\text{hep,u}}^{\text{ERY}}$ was reported to be 98.6 L/hr (Barre et al., 1987), indicating its high hepatic extraction ratio as unbound drug. Once absorbed into systemic circulation, ERY can be characterized by a 2 –compartmental body model (Hall et al., 1982; Parsons & David, 1980), and exhibits a predominant binding to AAG at therapeutic relevant concentrations, and to albumin at higher than therapeutic concentrations (Dette & Knothe, 1986), resulting in increasing $V_{\text{d}_{\text{ss}}}$ with dose (Austin et al., 1980). It is partly cleared by CYP3A to its major metabolite N-demethyl-erythromycin (nd-ERY) and also excreted primarily unchanged in bile (Frassetto et al. 2007). Nd-ERY is considerably less microbiologically active than the parent compound (Austin et al., 1980), and its exposure is 4% and 12%, respectively, of parent drug exposure after IV and PO administration of ERY (Sun et

al., 2010), indicating its negligible role in pharmacological effect. Only 2-15% of unchanged ERY is observed in urine, depending on dose (Austin et al. 1981), and elimination $t_{1/2}$ of ERY is about 1.5-2 hours (Austin et al., 1980). *In-vitro* metabolic study (Xu et al., 2009) showed that ERY can inhibit CYP3A by irreversible binding, resulting in MBI of CYP3A.

ERY clinical PK studies after IV and PO administration were searched, to look for appropriate studies to validate semi-PBPK model after IV and PO ERY. Once the model was qualified by clinical PK profiles, ERY hepatic and GW concentrations was simulated via the semi-PBPK model after different dosing regimen, to forecast impact of ERY administration route on its metabolic inhibition on MDZ.

7.1.3 Objectives

The major objectives of the chapter were to:

- a. Search for ERY clinical PK studies and look for appropriate studies to validate semi-PBPK model of ERY
- b. Develop a semi-PBPK model of ERY to describe its PK profiles in human after IV and PO administration
- c. Validate the model using ERY plasma concentration-time profiles in clinical PK studies
- d. Predict concentration – time profiles of ERY and relative CYP3A activity levels change in liver and GW using the validated semi-PBPK model

7.2 Methods

7.2.1 ERY PK meta-analysis

An extensive literature search was carried out in PubMed, to search for any ERY PK studies in absence or presence of MDZ. ERY was to have been administered either intravenously or orally, and plasma exposures (their means and SD) after IV or PO administration should be well estimated and provided, or could be calculated based on the provided information. All studies were to have been conducted in healthy volunteers without any co-medications, except women who may have used oral contraceptives. All the exposure metrics (AUC^{ERY} , c_{max}^{ERY} , *etc.*), PK information (f_u^{ERY} , CL_{tot}^{ERY} , CL_{ren}^{ERY} *etc.*), PK parameters estimated by compartmental analysis (k_a , k_{12} , k_{21} , V_1 , V_2 , *etc.*), demographics, dosing regimen design (dose, formulation, sample size, sampling time, *etc.*) and bio-analytical (LLOQ, assay method, *etc.*) information for both ERY and MDZ were extracted from the studies.

7.2.2 Saturable plasma protein binding model of ERY

Austin *et al.* (Austin et al., 1980) conducted a SAD study of IV infusion ERY lactobionate (equivalent to 125 mg, 250 mg, 500 mg and 900 mg ERY base), and plasma and urinary concentrations were measured by bioassay using *Sarcina lutea*. Based on parameters estimated by two-compartment models, central compartment volume of distribution ($V_{d_{cc}}$) and $V_{d_{ss}}$ increased with dose, implying potential saturable plasma protein binding. In addition, Dette *et al.* (Dette et al., 1982) characterized *in-vitro* binding profiles of ERY to human serum as a function of unbound ERY concentration. Total protein binding and non-specific binding (albumin, *etc.*) of ERY were measured by *in-vitro* equilibrium dialysis, and specific binding (presumably AAG binding) was obtained by subtraction of non-specific binding from total binding. Results (**Figure 7.1**) demonstrated that with increasing free ERY concentration, bound

ERY concentration increased less than proportionally: specific (AAG) binding profile exhibited a hyperbolic curve and non-specific binding profile showed a straight line, and the highest concentration in Austin *et al.* study ($\sim 12 \mu\text{M}$) fell into the plateau part of specific binding curve. As a result, a mathematical model could be generated to predict fraction unbound of ERY (f_u^{ERY}) in plasma at various concentrations, and assess dose-proportionality of ERY PK after correcting by plasma protein binding. Two models were tried to characterize specific (AAG) binding profile: a hyperbolic model and a sigmoidal model. A straight line started from origin ($y = mx$) was used to describe non-specific binding profile. Total bound concentration ($C_{\text{bo-total}}$) was then expressed as a hyperbolic/linear model (equation (7.1)) and a sigmoidal/linear model (equation (7.2)):

$$C_{\text{bo-total}} = \frac{B_{\text{max}} \cdot C_u}{K_{b,50} + C_u} + m \cdot C_u \quad (7.1) - \text{Model 1}$$

$$C_{\text{bo-total}} = \frac{B_{\text{max}} \cdot C_u^n}{K_{b,50}^n + C_u^n} + m \cdot C_u \quad (7.2) - \text{Model 2}$$

B_{max} is the binding capacity of specific (AAG) binding, $K_{b,50}$ is the binding affinity of ERY to AAG, m is the slope of non-specific binding linear regression, n is the hill coefficient in sigmoidal model, and c_u is unbound ERY concentration. Only observed total binding and non-specific binding profiles were digitized from Dette *et al.* (Dette et al., 1982), because specific binding profile was the subtraction of the two, which was not measured data. A linear regression was performed to fit non-specific binding profile, and m was estimated and fixed in future modeling process, due to parameter identification issues when estimating all parameters together. Afterwards, the two models were separately employed to fit digitized total binding profile, and a better model (based on visual predictive check and statistical report) was selected to depict saturable plasma protein binding in ERY semi-PBPK model. All modeling was implemented by ADAPT 5 (Argenio et al., 2009) (BMSR Biomedical Simulations Resource, available at

<https://bmsr.usc.edu/software/adapt/>), with control profiles and observed data summarized in

Appendices F.

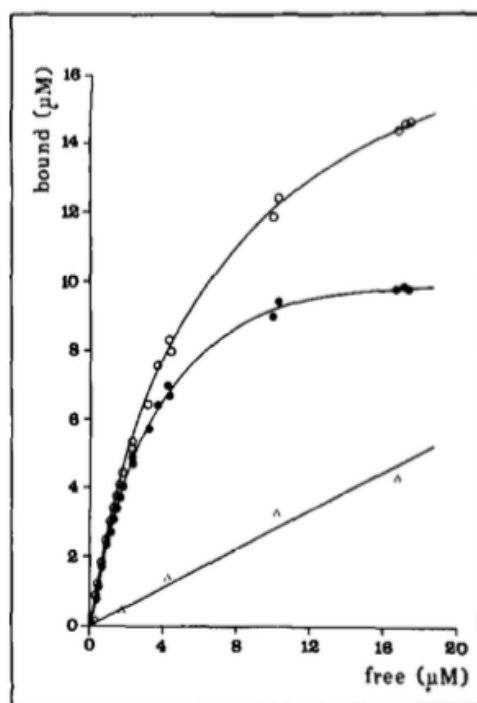


Figure 7.1 Binding of [^{14}C]-ERY to human serum as a function of unbound ERY concentration.

Open circles represent total bound profile (specific + non-specific), open triangles represent non-specific bound profile, solid circles represent specific bound profile, which were calculated by subtraction of nonspecific from total bound profile.

7.2.3 Development of ERY semi-PBPK model

7.2.3.1 ERY semi-PBPK model after single IV administration

Semi-PBPK model for IV ERY was developed based on the reported *in-vitro* metabolic information, PK and physiological parameters (**Table 7.1**). Since model development was based on results from **section 7.3.1 - 7.3.3**, it is suggested to read these three sections first, before start reading this part. A conventional two-compartmental body model with additional compartments for GW serosa, portal vein, and liver was developed, and showed in **Figure 7.2**. Since saturable

plasma protein binding of ERY was demonstrated after single ascending IV dose of ERY, the semi-PBPK model was developed using unbound ERY mass transfer. The predicted unbound concentration in blood was converted to total concentration in plasma, by dividing f_u^{ERY} at corresponding unbound concentration, and a constant $B:P^{\text{ERY}}$, in model validation. This model is similar to the FLZ semi-PBPK model (see Chapter 4, Section 4.2.1), with the following differences: (1) After IV administration, ERY is injected directly into systemic circulation, and assumed to be distributed to a peripheral compartment (Peripheral Cpt) with the inter-compartmental clearance ($Q_{2,u}^{\text{ERY}}$), except GW serosa, portal vein and liver, as tissues of interest. (2) Unbound renal clearance of ERY ($CL_{\text{ren},u}^{\text{ERY}}$) increases with dose, so that an empirical hyperbolic equation was applied to describe dose-dependent $CL_{\text{ren},u}^{\text{ERY}}$ (3) Hepatic intrinsic clearance was expressed as addition of two Michaelis – Menten equations, to characterize hepatic CYP3A metabolism and biliary excretion, respectively. As to CYP3A metabolism pathway, specifically, a CYP3A MBI model was introduced to delineate auto-inhibition of ERY on its own metabolism. (4) With respect to GW metabolism, after scaling from *in-vitro* metabolic study to *in-vivo* intrinsic clearance of unbound ERY (Paine et al., 1997), intrinsic GW clearance ($CL_{\text{int,GW}}^{\text{ERY}}$) was only 1.3% of $CL_{\text{int,hep-3A}}^{\text{ERY}}$, thus GW metabolism of ERY after IV administration is assumed to be negligible.

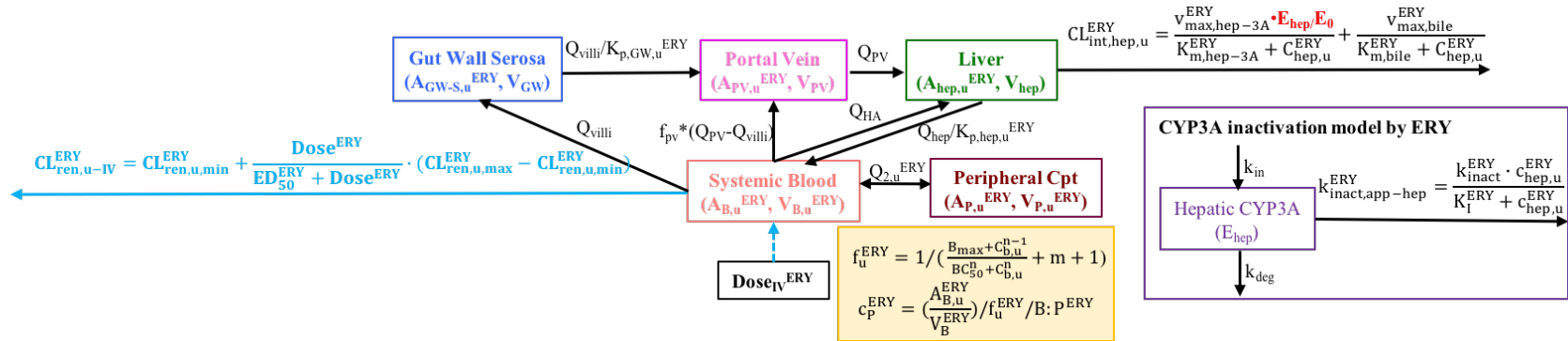


Figure 7.2 Semi-PBPK model scheme for the disposition of ERY after IV administration.

1) Differential equations:

Based on the model above, differential equations for unbound ERY mass transfer between compartments were expressed as equations (7.1) to (7.6):

$$\begin{aligned} \frac{dA_{B,u}^{ERY}(t)}{dt} = & k_0^{ERY} + c_{hep,u}^{ERY} \cdot \frac{Q_{hep}}{K_{p,u,hep}^{ERY}} + c_{P,u}^{ERY} \cdot Q_{2,u}^{ERY} - c_{B,u}^{ERY} \\ & \cdot \left(CL_{ren,u,min}^{ERY} + \frac{Dose_{IV}^{ERY}}{ED_{50}^{ERY} + Dose_{IV}^{ERY}} \cdot (CL_{ren,u,max}^{ERY} - CL_{ren,u,min}^{ERY}) \right) - c_{B,u}^{ERY} \cdot Q_{villi} \\ & - c_{B,u}^{ERY} \cdot f_{PV} \cdot (Q_{PV} - Q_{villi}) - c_{B,u}^{ERY} \cdot Q_{HA} - c_{B,u}^{ERY} \cdot Q_{2,u}^{ERY} \end{aligned}$$

when $t = 0$, $A_B^{ERY}(0) = 0$; when $t = t_{inf}$, $A_{B,u}^{ERY}(t_{inf}) = Dose_{IV}^{ERY}$ (7.1)

$$\frac{dA_{p,u}^{ERY}(t)}{dt} = c_{B,u}^{ERY} \cdot Q_{2,u}^{ERY} - c_{P,u}^{ERY} \cdot Q_{2,u}^{ERY}$$

when $t = 0$, $A_{p,u}^{ERY}(0) = 0$ (7.2)

$$\frac{dA_{GW-S,u}^{ERY}(t)}{dt} = c_{B,u}^{ERY} \cdot Q_{villi} - c_{GW-S,u}^{ERY} \cdot \frac{Q_{villi}}{K_{p,u,GW}^{ERY}}$$

when $t = 0$, $A_{GW-S,u}^{ERY}(0) = 0$ (7.3)

$$\frac{dA_{PV,u}^{ERY}(t)}{dt} = c_{GW-S,u}^{ERY} \cdot \frac{Q_{villi}}{K_{p,u,GW}^{ERY}} + c_{B,u}^{ERY} \cdot f_{PV} \cdot (Q_{PV} - Q_{villi}) - c_{PV,u}^{ERY} \cdot Q_{PV}$$

when $t = 0$, $A_{PV,u}^{ERY}(0) = 0$ (7.4)

$$\begin{aligned} \frac{dA_{hep,u}^{ERY}(t)}{dt} = & c_{B,u}^{ERY} \cdot Q_{HA} + c_{PV,u}^{ERY} \cdot Q_{PV} - c_{hep,u}^{ERY} \cdot \frac{Q_{hep}}{K_{p,u,hep}^{ERY}} - c_{hep,u}^{ERY} \\ & \cdot \left(\frac{v_{max,hep-3A}^{ERY} \cdot \frac{E_{hep}}{E_0}}{K_{m,hep-3A}^{ERY} + c_{hep,u}^{ERY}} + \frac{v_{max,bile}^{ERY}}{K_{m,bile}^{ERY} + c_{hep,u}^{ERY}} \right) \end{aligned}$$

when $t = 0$, $A_{hep,u}^{ERY}(0) = 0$ (7.5)

$$\frac{dE_{\text{hep}}(t)}{dt} = k_{\text{in}} - E_{\text{hep}} \cdot k_{\text{deg}} - E_{\text{hep}} \cdot \left(\frac{k_{\text{inact}}^{\text{ERY}} \cdot c_{\text{hep,u}}^{\text{ERY}}}{K_{\text{I}}^{\text{ERY}} + c_{\text{hep,u}}^{\text{ERY}}} \right)$$

when $t = 0$, $E_{\text{hep}}(0) = 1$ (7.6)

$A_{\text{B,u}}^{\text{ERY}}$, $A_{\text{P,u}}^{\text{ERY}}$, $A_{\text{GW-S,u}}^{\text{ERY}}$, $A_{\text{PV,u}}^{\text{ERY}}$ and $A_{\text{hep,u}}^{\text{ERY}}$ are the amounts of unbound ERY in central, peripheral, GW serosa, portal vein and liver compartments, respectively; $c_{\text{B,u}}^{\text{ERY}}$, $c_{\text{P,u}}^{\text{ERY}}$, $c_{\text{GW-S}}^{\text{ERY}}$, $c_{\text{PV}}^{\text{ERY}}$, $c_{\text{hep}}^{\text{ERY}}$ are unbound drug concentrations in central, peripheral, GW serosa, portal vein and liver compartments, calculated by dividing amount (A) by the respective compartment volume: $V_{\text{B,u}}^{\text{ERY}}$, $V_{\text{P,u}}^{\text{ERY}}$, V_{GW} , V_{PV} and V_{hep} , which are unbound ERY volume of central and peripheral compartments, volume of GW, portal vein and liver. In most ERY IV studies, ERY was administered as IV infusion, so an infusion rate k_0^{ERY} was introduced in equation (7.1) as a dose input rate, and initial amount for all the five tissue compartments (equation 7.1-7.5) were 0. In terms of CYP3A activity, E_0 (assumed to be 1) is baseline CYP3A activity without ERY, which is determined by a zero-order synthesis rate (k_{in}) and a first-order degradation rate (k_{deg}) of CYP3A enzyme. E_{hep} is relative hepatic CYP3A level changed with time. $k_{\text{inact}}^{\text{ERY}}$ is the maximum rate of enzyme inactivation by ERY and $K_{\text{I}}^{\text{ERY}}$ is the ERY inhibitory potency on CYP3A.

2) Volume of distributions and inter-compartmental clearance

Unbound central compartment volume of distribution ($V_{\text{B,u}}^{\text{ERY}}$), unbound peripheral compartment volume of distribution ($V_{\text{P,u}}^{\text{ERY}}$) and inter-compartmental clearance ($Q_{2,\text{u}}^{\text{ERY}}$) were estimated from digitized plasma concentration – time profiles of ERY in study 611 (Austin et al., 1980), with a traditional two-compartmental body model (See **Appendices G**).

V_{GW} , V_{hep} and V_{PV} were used the same values as FLZ semi-PBPK model (see **Chapter 4, section 4.2.1.3**).

3) Partition coefficient between blood and tissue (K_{p})

$K_{p,hep,u}^{ERY}$ is the liver-to-blood partition coefficient of unbound ERY, reported as 2.71 (Ahmad, 2007). $K_{p,GW,u}^{ERY}$ is GW-to-blood partition coefficient of unbound ERY, assumed to be the same as $K_{p,hep,u}^{ERY}$.

4) Blood flows (Q)

Q_{hep} , Q_{PV} , Q_{HA} and Q_{villi} were used the same values as FLZ semi-PBPK model (see **Chapter 4, section 4.2.1.3**)

5) Clearance

Hepatic clearance of ERY includes two parts: CYP3A metabolism and biliary excretion. According to an *in-vitro* metabolic kinetics study (Riley & Howbrook, 1998) using human liver microsomes (HML) to characterize Michaelis-Menten parameters of ERY N-demethylation, $v_{max,hep-3A}^{ERY}$ and $K_{m,hep-3A}^{ERY}$ were reported as 345 ± 13 pmol/min/mg and 88 ± 10 μ M. After IVIVE of $v_{max,hep-3A}^{ERY}$ by equation (7.7), $v_{max,hep-3A}^{ERY}$ *in-vivo* was estimated to be 285 μ g/min/kg, which was used as initial parameter value, and optimized in future modeling processes.

$$v_{max,hep-3A}^{ERY} \text{ in vivo} = v_{max,hep-3A}^{ERY} \text{ in vitro} \cdot \frac{52.5\text{mg protein}}{\text{g liver}} \cdot \frac{1500\text{g liver}}{70 \text{ kg body weight}} \quad (7.7)$$

As for biliary excretion, no $v_{max,bile}^{ERY}$ or $K_{m,bile}^{ERY}$ values were reported in any literature. As a result, values for $v_{max,hep-3A}^{ERY}$, $v_{max,bile}^{ERY}$ and $K_{m,bile}^{ERY}$ were optimized together, to finalize a parameter set that could characterize observed PK profiles across doses (125 – 900 mg single dose) in study 611. Since ERY has a very short plasma elimination $t_{1/2}$ (1.5 – 2 hrs), enterohepatic circulation (EHC) of ERY would not contribute significantly to its total systemic exposure (no clinical data was found), and as a potent P-gp substrate, ERY could be effectively pumped out of GW during EHC phase. Therefore, EHC of ERY was assumed to be negligible in this model.

As mentioned in **section 7.3.3**, unbound ERY renal clearance after IV administration ($CL_{ren,u-IV}^{ERY}$) increased with dose in study 611, indicating potential saturable reabsorption. An empirical hyperbolic equation was applied to describe the relationship between ERY dose and $CL_{ren,u-IV}^{ERY}$, shown in equation (7.8)

$$CL_{ren,u-IV}^{ERY} = CL_{ren,u,min}^{ERY} + \frac{Dose^{ERY}}{ED_{50}^{ERY} + Dose^{ERY}} \cdot (CL_{ren,u,max}^{ERY} - CL_{ren,u,min}^{ERY}) \quad (7.8)$$

Since it was impossible to estimate all the parameters (*i.e.* $CL_{ren,u,min}^{ERY}$, $CL_{ren,u,max}^{ERY}$ and ED_{50}^{ERY}) based on $CL_{ren,u}^{ERY}$ at only four dose levels, parameter optimizations were performed based on visual inspection, and residual at each dose level was calculated to assess predictability of equation (7.8). Ultimately, $CL_{ren,u,min}^{ERY}$ and $CL_{ren,u,max}^{ERY}$ were optimized to be 0.5 ml/min/kg and 3.5 ml/min/kg, and ED_{50}^{ERY} was set at 475 mg.

Assumptions and predictability of empirical hyperbolic model were discussed in **Appendices**

J.

6) Fraction unbound and blood-to-plasma partitioning ratio

Relationship between f_u^{ERY} and $c_{b,u}^{ERY}$ was expressed as equation (7.24) (see **section 7.3.2**). Each $c_{b,u}^{ERY}$ was converted to total plasma concentration by dividing corresponding f_u^{ERY} and B:P^{ERY} (set at 0.85 (Ahmad, 2007)).

7) Auto-inhibition on hepatic CYP3A metabolism

Since all IV ERY PK studies were single dose studies, auto-inhibition of CYP3A by ERY was not evident in these studies. However, in ERY and MDZ DDI studies, ERY was given orally after repeat- doses, which may exhibit substantial auto-inhibition characteristics. To keep systemic disposition model structure after IV and PO ERY the same, auto-inhibition on hepatic CYP3A metabolism was also incorporated in IV ERY semi-PBPK model, and detailed enzyme

turnover model was discussed in **section 7.2.3.2**.

Body weight throughout the model was set as the median body weight (67kg) of subjects in study 611.

7.2.3.2 ERY semi-PBPK model after single/repeat- PO doses (ERY base enteric-coated tablet formulation)

7.2.3.2.1 Semi-PBPK model

A semi-PBPK model for PO ERY after enteric-coated tablet (EC) formulation (**Figure 7.3**) was built based on the reported *in-vitro* metabolic information, PK and physiological parameters (**Table 7.1**). A conventional two-compartmental body model with additional compartments for gut lumen, absorptive transit compartments, GW mucosa, GW serosa, portal vein, and liver was developed, by adding several absorptive compartments (gut lumen, absorptive transit compartments and GW mucosa) to the IV model.

After PO administration of ERY EC base, ERY was dissolved in the intestinal lumen, and a fraction of drug (F_{abs}^{ERY}) could permeate into GW mucosa. To determine the role of acid hydrolysis on GI absorption of ERY, Somogyi et al. (1995) conducted a clinical PK study, in which six healthy subjects received ERY as a 240 mg IV dose, a 250 mg PO solution administered via endoscope directly into the duodenum and bypassing the stomach, and an EC 250 mg capsule. After calculating F_{GI}^{ERY} and $F_{abs}^{ERY} \cdot F_{GI}^{ERY}$ by using the method in **Chapter 3, Figure 3.2**, assuming that F_{abs}^{ERY} after duodenum injection was 100%, F_{abs}^{ERY} after PO EC ERY was estimated to be 0.88.

Before ERY was absorbed into GW, a number of transit compartments were added to characterize an observed lag-time of ERY appearance in plasma after PO EC administration. Physiologically, transit compartments represented slow disintegration, dissolution or intestinal

transit of ERY before absorption into GW, and number of transit compartments was optimized based on observed lag-time of its plasma concentration-time profile ($n = 7$ was used in PO EC ERY model).

Although ERY is identified a BCS class 3 (Heizmann et al., 1983) drug due to its high solubility within clinical relevant pH and low permeability as a potent P-gp substrate (Lin et al., 2011; Nožini et al., 2010; Schuetz et al., 1998), P-gp is likely to be saturated at clinical relevant dose, potentially making it an apparent BCS class 1 drug, if gastric acid degradation is not considered. Hence it is reasonable to assume that permeating into the GW is the rate-limiting step of its oral absorption, and $k_{GL}^{ERY} \approx k_a^{ERY}$ (k_a^{ERY} was the observed first-order oral absorption rate constant of ERY reported in literature (Josefsson et al., 1982)).

Once it is permeated into GW through mucosa side, ERY can be metabolized by GW CYP3A enzymes located at the villous tips (Yang et al., 2007; Watkins, 1997). Pre-systemic GW extraction is higher than systemic GW extraction, due to the negligible protein binding ($f_{u,GW-M}^{ERY} = 1.0$) and potential higher concentrations at the mucosal side of intestinal epithelium. To calculate unbound pre-systemic GW intrinsic clearance ($CL_{int,GW,u}^{ERY}$), $V_{max,GW-3A}^{ERY}$ was extrapolated from *in-vitro* metabolic study (Thummel et al., 1996) and $K_{m,GW-3A}^{ERY}$ was assumed to be the same as $K_{m,hep-3A}^{ERY}$. f_{villi} was also added and used the same value as MDZ semi-PBPK model, which is an adjusting factor for GW CYP3A activity.

Furthermore, a transit rate constant (k_T) from mucosa to serosa was added to connect the two sides of GW, and set as Q_{villi}/V_{GW} , to keep the outflow from mucosa to serosa of intestinal epithelium constant to be Q_{villi} .

ERY is then carried into portal vein with blood flow of Q_{villi} , and reaches liver via portal vein. Before getting into the systemic blood compartment, it can be metabolized or excreted by

CYP3A and bile pre-systemically. Once it gets into the systemic blood, the disposition is the same as IV administration.

With respect to renal clearance, Josefsson *et al.* (1982) conducted a SAD study (study 620) of PO EC ERY within the dose range of 250 mg to 1000 mg, and measured renal clearance in addition to systemic exposure. After corrected by average f_u^{ERY} (f_u^{ERY} at $c_{max}^{ERY}/2$) at each dose, $CL_{ren,u}^{ERY}$ was almost constant with dose, which cannot be predicted by the empirical hyperbolic model after IV ERY. This could probably due to lower systemic concentration after PO administration, given its low F_{oral}^{ERY} , leading to less saturation of tubular reabsorption, or the narrower dose range (250 mg -1000 mg) after PO administration than IV administration (125 mg – 900 mg). As a result, a constant $CL_{ren,u-PO}^{ERY}$ (average of measured $CL_{ren,u}^{ERY}$ at three dose levels) was used in PO EC ERY semi-PBPK model. Although this may cause inconsistency between ERY semi-PBPK models after difference routes of administration, the influence of renal clearance on ERY PK is limited, due to its minor contribution (2-15%) to total ERY clearance after IV administration.

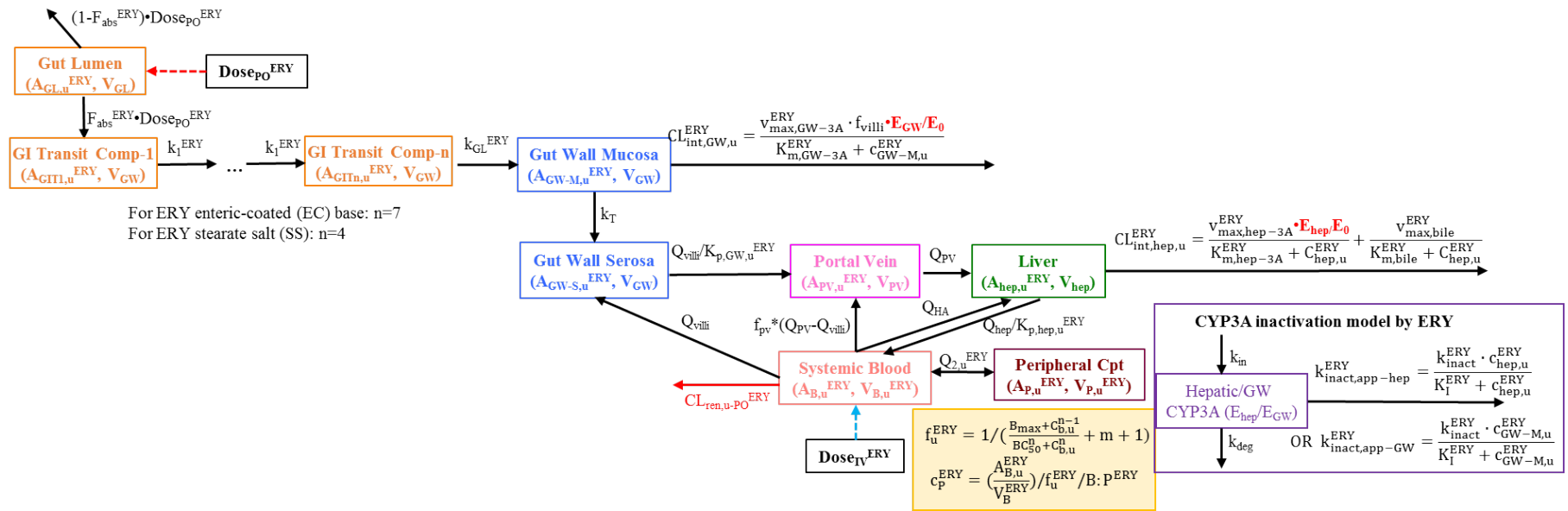


Figure 7.3 Semi-PBPK model scheme for the disposition of ERY after PO administration.

Based on the model scheme, differential equations for mass transfer between compartments were expressed as equations (7.9) to (7.19):

$$\frac{dA_{GL,u}^{ERY}(t)}{dt} = -c_{GL,u}^{ERY} \cdot V_{GL} \cdot F_{abs}^{ERY} - c_{GL,u}^{ERY} \cdot V_{GL} \cdot (1 - F_{abs}^{ERY})$$

when $t = 0$, $A_{GL,u}^{ERY}(0) = Dose_{po}^{ERY}$ (7.9)

$$\frac{dA_{GIT1,u}^{ERY}(t)}{dt} = c_{GL,u}^{ERY} \cdot V_{GL} \cdot F_{abs}^{ERY} - A_{GIT1,u}^{ERY} \cdot k_1^{ERY}$$

when $t = 0$, $A_{GIT1,u}^{ERY}(0) = 0$ (7.10)

...

$$\frac{dA_{GITn,u}^{ERY}(t)}{dt} = A_{GIT(n-1),u}^{ERY} \cdot k_1^{ERY} - A_{GITn,u}^{ERY} \cdot k_1^{ERY}$$

when $t = 0$, $A_{GITn,u}^{ERY}(0) = 0$ (7.11)

$$\frac{dA_{GW-M,u}^{ERY}(t)}{dt} = A_{GITn,u}^{ERY} \cdot k_{GL}^{ERY} - c_{GW-M,u}^{ERY} \cdot V_{GW} \cdot k_T - c_{GW-M,u}^{ERY} \cdot (f_{villi} \cdot v_{max,GW-3A}^{MDZ} \cdot \frac{E_{GW}}{E_0})$$

$$/ (K_{m,GW-3A}^{ERY} + c_{GW-M,u}^{ERY})$$

when $t = 0$, $A_{GW-M,u}^{ERY}(0) = 0$ (7.12)

$$\frac{dA_{GW-S,u}^{ERY}(t)}{dt} = c_{GW-M,u}^{ERY} \cdot V_{GW} \cdot k_T + c_{B,u}^{ERY} \cdot Q_{villi} - \left(\frac{c_{GW-S,u}^{ERY}}{K_{p,GW,u}^{ERY}} \right) \cdot Q_{villi}$$

when $t = 0$, $A_{GW-S,u}^{ERY}(0) = 0$ (7.13)

$$\frac{dA_{PV,u}^{ERY}(t)}{dt} = c_{GW-S,u}^{ERY} \cdot \frac{Q_{villi}}{K_{p,u,GW}^{ERY}} + c_{B,u}^{ERY} \cdot f_{PV} \cdot (Q_{PV} - Q_{villi}) - c_{PV,u}^{ERY} \cdot Q_{PV}$$

when $t = 0$, $A_{PV,u}^{ERY}(0) = 0$ (7.14)

$$\frac{dA_{\text{hep},u}^{\text{ERY}}(t)}{dt} = c_{\text{B},u}^{\text{ERY}} \cdot Q_{\text{HA}} + c_{\text{PV},u}^{\text{ERY}} \cdot Q_{\text{PV}} - c_{\text{hep},u}^{\text{ERY}} \cdot \frac{Q_{\text{hep}}}{K_{\text{p},u,\text{hep}}^{\text{ERY}}} - c_{\text{hep},u}^{\text{ERY}} \cdot \left(\frac{V_{\text{max,hep-3A}}^{\text{ERY}} \cdot \frac{E_{\text{hep}}}{E_0}}{K_{\text{m,hep-3A}}^{\text{ERY}} + c_{\text{hep},u}^{\text{ERY}}} + \frac{V_{\text{max,bile}}^{\text{ERY}}}{K_{\text{m,bile}}^{\text{ERY}} + c_{\text{hep},u}^{\text{ERY}}} \right)$$

$$\text{when } t = 0, A_{\text{hep},u}^{\text{ERY}}(0) = 0 \quad (7.15)$$

$$\frac{dA_{\text{B},u}^{\text{ERY}}(t)}{dt} = c_{\text{hep},u}^{\text{ERY}} \cdot \frac{Q_{\text{hep}}}{K_{\text{p},u,\text{hep}}^{\text{ERY}}} + c_{\text{P},u}^{\text{ERY}} \cdot Q_{2,u}^{\text{ERY}} - c_{\text{B},u}^{\text{ERY}} \cdot \text{Cl}_{\text{ren},u-\text{PO}}^{\text{ERY}} - c_{\text{B},u}^{\text{ERY}} \cdot Q_{\text{villi}} - c_{\text{B},u}^{\text{ERY}} \cdot f_{\text{PV}} \cdot (Q_{\text{PV}} - Q_{\text{villi}}) - c_{\text{B},u}^{\text{ERY}} \cdot Q_{\text{HA}} - c_{\text{B},u}^{\text{ERY}} \cdot Q_{2,u}^{\text{ERY}}$$

$$\text{when } t = 0, A_{\text{B}}^{\text{ERY}}(0) = 0 \quad (7.16)$$

$$\frac{dA_{\text{p},u}^{\text{ERY}}(t)}{dt} = c_{\text{B},u}^{\text{ERY}} \cdot Q_{2,u}^{\text{ERY}} - c_{\text{P},u}^{\text{ERY}} \cdot Q_{2,u}^{\text{ERY}}$$

$$\text{when } t = 0, A_{\text{p},u}^{\text{ERY}}(0) = 0 \quad (7.17)$$

$$\frac{dE_{\text{GW}}(t)}{dt} = k_{\text{in}} - E_{\text{GW}} \cdot k_{\text{deg}} - E_{\text{GW}} \cdot \left(\frac{k_{\text{inact}}^{\text{ERY}} \cdot c_{\text{GW-M},u}^{\text{ERY}}}{K_{\text{I,hep}}^{\text{ERY}} + c_{\text{GW-M},u}^{\text{ERY}}} \right)$$

$$\text{when } t = 0, E_{\text{GW}}(0) = 1 \quad (7.18)$$

$$\frac{dE_{\text{hep}}(t)}{dt} = k_{\text{in}} - E_{\text{hep}} \cdot k_{\text{deg}} - E_{\text{hep}} \cdot \left(\frac{k_{\text{inact}}^{\text{ERY}} \cdot c_{\text{hep},u}^{\text{ERY}}}{K_{\text{I,hep}}^{\text{ERY}} + c_{\text{hep},u}^{\text{ERY}}} \right)$$

$$\text{when } t = 0, E_{\text{hep}}(0) = 1 \quad (7.19)$$

where $A_{\text{GL},u}^{\text{ERY}}$, $A_{\text{GIT1},u}^{\text{ERY}}$, ..., $A_{\text{GITn},u}^{\text{ERY}}$ and $A_{\text{GW-M},u}^{\text{ERY}}$ are the amounts of unbound ERY in gut lumen, first GI transit compartment, ... nth GI transit compartment and GW mucosa, respectively; $c_{\text{GL},u}^{\text{ERY}}$ and $c_{\text{GW-M},u}^{\text{ERY}}$ are unbound concentrations in gut lumen and GW mucosa, calculated by dividing amount (A) by the respective compartment volume: V_{GL} and V_{GW} . Initial amount for all the compartments are 0, except for gut lumen, which is $\text{Dose}_{\text{PO}}^{\text{ERY}}$.

7.2.3.2.2 Auto-inhibition model

After multiple PO ERY, several studies (Birkett et al., 1990; McDonald et al., 1977; Miglioli et al., 1990) found that accumulation ratios at steady-state after PO ERY (EC and other formulations) were all higher than 2, when dosing interval was about 3-4 $t_{1/2}$. This cannot be purely explained by PK nonlinearity, as discussed in **section 7.3.3**. Furthermore, Danan et al. (1981) and Larrey et al. (1983) demonstrated that ERY induced its own CYP3A – mediated transformation into metabolite, which formed an inactive 456-nm absorbing complex with the Fe (II) of CYP3A in rats and humans. All these evidence confirmed that ERY can inhibit its own CYP3A metabolism through MBI. In our semi-PBPK model, auto-inhibition was incorporated with respect to both GW and hepatic metabolism.

In absence of ERY, hepatic or GW CYP3A level was determined by a zero-order synthesis rate (k_{in}) and first-order degradation rate (k_{deg}), which can be expressed as equation (7.20).

$$\frac{dE(t)}{dt} = k_{in} - E \cdot k_{deg} \quad (7.20)$$

E represents hepatic or GW CYP3A level. At steady-state, $dE(t)/dt = 0$; thus,

$$k_{in} = E \cdot k_{deg} \quad (7.21)$$

Assuming E at baseline (E_0) is 100%, numerically, k_{in} is equal to k_{deg} .

In presence of ERY, the degradation rate of enzyme is increased by an apparent inactivation rate constant, $k_{inact,app}^{ERY}$, which is a function of k_{inact}^{ERY} , K_I^{ERY} , and ERY unbound concentration in liver and GW mucosa, respectively (equation 7.22 and 7.23), assuming that k_{inact}^{ERY} and K_I^{ERY} are the same in hepatic and intestinal CYP3A inhibition.

$$k_{inact,app-hep}^{ERY} = \frac{k_{inact}^{ERY} \times c_{hep,u}^{ERY}}{K_I^{ERY} + c_{hep,u}^{ERY}} \quad (7.22)$$

$$k_{inact,app-GW}^{ERY} = \frac{k_{inact}^{ERY} \times c_{GW-M,u}^{ERY}}{K_I^{ERY} + c_{GW-M,u}^{ERY}} \quad (7.23)$$

Equation (7.18) and (7.19) calculated relative GW (E_{GW}) and hepatic (E_{hep}) levels change over time, and $v_{max,GW-3A}^{ERY}$ and $v_{max,hep-3A}^{ERY}$ were corrected by E_{GW}/E_0 and E_{hep}/E_0 , to reflect corresponding v_{max} change over time in presence of ERY. In terms of parameter values, k_{deg} was reported to be highly variable estimated by different *in-vitro* and *in-vivo* methods, between 8×10^{-5} and 1.15×10^{-3} (CYP3A degradation $t_{1/2}$ ranges from 10 hours to 144 hours) (Rowland Yeo et al., 2011; Wang, 2010; Yang et al., 2008). Therefore, k_{deg} was optimized between 8×10^{-5} and $1.15 \times 10^{-3} \text{ min}^{-1}$, to find a value that could provide good predictions for all ERY PK studies that used for model validation. K_I^{ERY} and k_{inact}^{ERY} were also variably reported in several *in-vitro* inhibitory studies (Ito et al., 2003; McConn et al., 2004; Rowland Yeo et al., 2011; Xu et al., 2009; Yamano et al., 2001; Yates et al., 2012; Zhang et al., 2009; Zhang et al., 2010; Ping Zhao et al., 2005), with K_I^{ERY} ranged from 1.48 – 109 μM and k_{inact}^{ERY} ranged from 0.017 – 0.066 min^{-1} . Finally, k_{inact}^{ERY} was set at 0.0375 min^{-1} (Rowland Yeo et al., 2011) (value used in Simcyp® Erythromycin model) and K_I^{ERY} was optimized in model validation, due to its large variability.

7.2.3.3 ERY semi-PBPK model after single/repeat- PO doses (ERY stearate salt tablet formulation)

Semi-PBPK model for PO ERY after ERY stearate salt (SS) formulation (**Figure 7.3**) was developed based on model for EC formulation, with several changes. 1) SS is reported to be less oral bioavailable than EC (Josefsson et al., 1982; McDonald et al., 1977; Mannisto et al., 1988), and in study 620 by Josefsson et al., both 500 mg ERY EC and SS formulations were administered to the same subjects, and mean reported $AUC_{0-\infty}^{ERY}$ after EC and SS formulations were 11.2 $\text{mg/L}\cdot\text{hr}$ and 7.5 $\text{mg/L}\cdot\text{hr}$, respectively. Assuming difference in AUC was completely caused by F_{abs}^{ERY} of the two formulations, F_{abs}^{ERY} for EC (0.88) was corrected by the AUC ratio

of SS and EC, to come up with F_{abs}^{ERY} for SS (0.59). 2) Number of transit compartments was optimized by plasma concentration – time profiles of ERY after SS formulation ($n = 4$ was used in PO SS ERY model). Number of transit compartment for SS model was less than that for EC model, indicating that ERY in EC formulation requires longer disintegration/dissolution time than in SS. 3) Absorption rate constant k_{GL}^{ERY} of SS was reported to be less than k_{GL}^{ERY} of EC (Iliopoulou et al., 1982), either due to inter-study variability, or because ERY SS may be absorbed into GW as both ERY base and ERY SS format, leading to a lower permeability.

Since only two ERY PO formulations (EC and SS) were administered in MDZ and ERY DDI studies, PBPK models for other ERY PO formulations were not developed.

7.2.3.4 Model parameters and assumptions

Initial model parameters used in semi-PBPK models of IV/PO ERY were summarized in **Table 7.1**. Physiological parameters were the same as MDZ semi-PBPK model. $v_{max,hep-3A}^{ERY}$, $v_{max,bile}^{ERY}$ and F_{abs}^{ERY} (EC) were further adjusted during model qualification for PO ERY model, discussed in **section 7.3.5**.

Table 7.1 Initial semi-PBPK ERY model parameters.

Parameter	Definition	Value	Source
Physiological parameters			
V_{GL} (ml/kg)	Volume of gut lumen	3.57	Assumed to be 250ml (FDA, 2012)
V_{GW} (ml/kg)	Volume of GW	33.6	Calculated by equation (4.6), assumed to be the surface of gut lumen cylinder
V_{PV} (ml/kg)	Volume of portal vein	0.97	Unknown methods (Ito et al., 2003)
V_{hep} (ml/kg)	Volume of liver	22.5	Calculated by equation (4.7) and (4.8)
Q_{villi} (ml/min/kg)	Villous blood flow	4.30	<i>In-vivo</i> experiment (Yang et al., 2007)
Q_{hep} (ml/min/kg)	Hepatic blood flow	21.4	<i>In-vivo</i> experiment (Tsunoda et al., 1999)
f_{HA}	Fraction of hepatic artery to total hepatic blood flow	0.25	(Eipel et al., 2010) (Q_{HA} was calculated as $f_{HA} \cdot Q_{hep}$; Q_{PV} was calculated as $(1 - f_{HA}) \cdot Q_{hep}$)
f_{PV}	Fraction of the components of portal vein that contain drug	1.00	A correction factor that can be adjusted according to simulation results.
f_{villi}	IVIVE scaling factor and IIV adjusting factor	2.2	Optimized with data from study 21
ERY PK Parameters (Systemic Disposition)			
$V_{B,u}^{ERY}$ (mL/kg)	Unbound volume of central compartment	479	See Appendices G
$V_{P,u}^{ERY}$ (mL/kg)	Unbound volume of peripheral compartment	1853	See Appendices G
$Q_{2,u}$ (ml/min/kg)	Inter-compartmental clearance	34.1	See Appendices G
$CL_{ren,u,min}^{ERY}$ (ml/min/kg)	Minimal unbound renal clearance after IV ERY	0.5	Optimized by empiric hyperbolic model
$CL_{ren,u,max}^{ERY}$ (ml/min/kg)	Maximal unbound renal clearance after IV ERY	3.5	Optimized by empiric hyperbolic model
ED_{50}^{ERY} (mg)	Dose of IV ERY that requires to produce 50% tubular reabsorption	475	Optimized by empiric hyperbolic model
$CL_{ren,u-PO}^{ERY}$ (ml/min/kg)	ERY unbound renal clearance after PO ERY	2.65	Average of CL_{ren}^{ERY} reported at 250, 500, 1000mg dose (Josefsson et al., 1982) (corrected by average f_u^{ERY} and $B:P^{ERY}$)
$V_{max,hep-3A}^{ERY}$ (μ g/min/kg)	Capacity of hepatic CYP3A to metabolize ERY	900	Optimized by regimen 2 in study 611 (Austin et al., 1980)
$K_{m,hep-3A}^{ERY}$ (μ g/ml)	Affinity of hepatic CYP3A to metabolize ERY	64.6	<i>In-vitro</i> study (88 μ M) (Riley & Howbrook, 1998)
$V_{max,bile}^{ERY}$ (μ g/min/kg)	Capacity of ERY biliary excretion	10	Optimized by regimen 2 in study 611 (Austin et al., 1980)
$K_{m,bile}^{ERY}$ (μ g/ml)	Affinity to drug transporter that is responsible for biliary excretion	0.1	Optimized by regimen 2 in study 611 (Austin et al., 1980)
$K_{p,hep,u}^{ERY}$	liver-to-blood partition coefficient of unbound drug	2.71	(Ahmad, 2007)
$K_{p,GW,u}^{MDZ}$	GW-to-blood partition coefficient of unbound drug	2.71	Assumed to be the same as $K_{p,hep,u}^{ERY}$
$B:P^{ERY}$	Blood-to-plasma partitioning ratio	0.85	(Ahmad, 2007)
B_{max} (mg/L)	Binding capacity to AAG	8.15	See section 7.3.2 (11.1 μ M)
$K_{b,50}$ (mg/L)	Binding affinity to AAG	2.14	See section 7.3.2 (2.92 μ M)
n	Hill coefficient of AAG binding	1.32	See section 7.3.2
m	Slope of non-specific binding	0.265	See section 7.3.2
ERY PK Parameters (Oral Absorption)			
F_{abs}^{ERY} (EC)	Fraction of ERY EC absorbed from gut lumen	0.88	Estimated from study 624 (Somogyi et al., 1995)
k_{GL}^{ERY} (min^{-1})	Absorption rate constant of EC from last transit	0.06	Assume to be k_a^{ERY} in study 620

(EC)	compartment to GW		(Josefsson et al., 1982)
F_{abs}^{ERY} (SS)	Fraction of ERY SS absorbed from gut lumen	0.59	Relative bioavailability between EC and SS in study 620 (Josefsson et al., 1982)
k_{GL}^{ERY} (min ⁻¹) (SS)	Absorption rate constant of SS from last transit compartment to GW	0.018	Assume to be k_a^{ERY} in study 618 (Iliopoulou et al., 1982)
ERY PK Parameters (Auto-inhibition model on CYP3A)			
k_{deg} (min ⁻¹)	CYP3A degradation rate constant	0.0008	Optimized between $t_{1/2}$ of 10 -144 hours (Rowland Yeo et al., 2011; Wang, 2010; Yang et al., 2008) ($t_{1/2}$ = 14 hours) ²⁶
k_{inact}^{ERY} (min ⁻¹)	ERY maximum rate of inactivation on CYP3A	0.0375	
K_I^{ERY} (mg/L)	ERY inhibitory potency on CYP3A	30	Optimized between 1 - 80 mg/L (1.48 – 109 μ M) (Ito et al., 2003; McConn et al., 2004; Rowland Yeo et al., 2011; Xu et al., 2009; Yamano et al., 2001; Yates et al., 2012; Zhang et al., 2009; Zhang et al., 2010; Ping Zhao et al., 2005)

¹ Parameter values were adjusted in PO ERY model.

² Parameter value was adjusted in study 629.

The assumptions made in semi-PBPK IV/PO ERY model included:

- 1) ERY follows two-compartmental body model (except for GW, portal vein, liver) after IV administration.
- 2) Perfusion (blood flow) is the rate-limiting step for ERY tissue distribution, rather than tissue uptake.
- 3) Tubular reabsorption of ERY follows Michaelis-Menten kinetics with dose (saturated with increasing dose).
- 4) Glomerular filtration and tubular secretion of ERY are constant across doses, and them in total is 3.5 ml/min/kg ($CL_{ren,u,max}^{ERY}$).
- 5) At very low dose, when tubular reabsorption is not saturated, unbound renal clearance of ERY is 0.5 ml/min/kg ($CL_{ren,umin}^{ERY}$).
- 6) ERY is in equilibrium between hepatocytes and venous outflow (well-stirred model).
- 7) Partition coefficient (K_p) for GW and liver are the same, and remain constant at simulated

concentration.

- 8) Negligible GW metabolism occurs after IV ERY.
- 9) Although ERY is a BCS Class 3 drug, it behaves like a BCS Class 1 drug after clinical relevant PO dose, and P-gp in enterocytes is saturated at clinical relevant concentration. Therefore, loss of ERY in gut lumen is due to gastric acid degradation, and F_{abs}^{ERY} after duodenum ERY injection is 100%.
- 10) Different systemic exposure between EC and SS after the same dose of ERY is mainly owing to gastric acid degradation difference, and F_{abs}^{ERY} for SS can be calculated based on its relative bioavailability to EC formulation.
- 11) ERY follows 1st-order diffusion across GW, and this process is the rate-limiting step of its oral absorption. ($k_{GL}^{ERY} \approx k_a^{ERY}$)
- 12) GW compartment is divided into mucosal side and serosal side; volumes of the two compartments are both V_{GW} , and the transit rate (k_T) from mucosa to serosa is Q_{villi}/V_{GW} .
- 13) With respect to ERY GW metabolism, $K_{m,GW-3A}^{ERY}$ was assumed to be the same as $K_{m,hep-3A}^{ERY}$.
- 14) Baseline CYP3A level is determined by a zero-order synthesis rate (k_{in}) and a first-order degradation rate (k_{deg}), and hepatic and GW CYP3A have the same synthesis and degradation rate constants.
- 15) ERY can inhibit its own GW and hepatic metabolism by MBI, and maximal inactivation rate constant (k_{inact}^{ERY}) and inhibitory potency (K_I^{ERY}) are the same for hepatic and intestinal CYP3A inhibition.
- 16) MDZ has no effect on ERY PK.

7.2.4 Model qualification and predictions

As for IV ERY semi-PBPK model, uncertain model parameters (*i.e.*, $v_{\max, \text{hep-3A}}^{\text{ERY}}$, $v_{\max, \text{bile}}^{\text{ERY}}$ and $K_{\text{m, bile}}^{\text{ERY}}$) were optimized by study 611, because this is the only SAD study after IV ERY, which can validate the model across doses, regardless of inter-study variability. In study 611, two IV dosage regimens were administered. Regimen 1 consisted of the administration of 250 mg (base equivalent) of ERY lactobionate infused over 3min. Regimen 2 was to administer 125, 250, 500 and 900 mg (base equivalent) ERY lactobionate infused over 15min. 24 healthy volunteers (12 males, 12 females, aged 17-23) participated in regimen 1, and 5 healthy volunteers were included in regimen 2. Blood and urinary samples were collected over time, and a bioassay using *Sarcina lutea* organism was applied to measure total ERY concentrations in both plasma and urine. Since nonlinear PK was observed for ERY, observed PK profiles after regimen 2 were used to optimize $v_{\max, \text{hep-3A}}^{\text{ERY}}$, $v_{\max, \text{bile}}^{\text{ERY}}$ and $K_{\text{m, bile}}^{\text{ERY}}$, and regimen 1 in study 611, as well as studies 612 (Barre et al., 1987), 613 (Parsons & David, 1980), 616 (Sun et al., 2010) and 624 (Somogyi et al., 1995) were used to externally validate the model by visual predictive check and exposure metrics comparison.

As for PO EC ERY semi-PBPK model, number of transit compartments and uncertain parameters ($v_{\max, \text{hep-3A}}^{\text{ERY}}$, $v_{\max, \text{bile}}^{\text{ERY}}$, number of transit compartments) were further tweaked by study 620 (Josefsson et al., 1982), the only SAD study after PO EC ERY, given the potential large inter-study variability of $v_{\max, \text{hep-3A}}^{\text{ERY}}$ and $v_{\max, \text{bile}}^{\text{ERY}}$. In study 620, ERY EC base was administered to 24 healthy males, with single oral dose of 250, 500, or 1000 mg. The subjects also received a film-coated ERY stearate tablet (equivalent to 500 mg base). Blood and urinary samples were collected over time, and a bioassay using *Micrococcus lutea* organism was applied to measure total ERY concentrations in both serum and urine. In addition, PO ERY EC model

was externally validated by several multiple doses ERY EC PK studies (studies 623 (Birkett et al., 1990), 626 (McDonald et al., 1977), 629 (Yakatan et al., 1985)), in which plasma concentration – time profiles after both single and multiple ERY EC doses were compared with predicted profiles by visual predictive check and exposure metrics comparison. To test the necessity of incorporating ERY auto-inhibition into its semi-PBPK model, predicted profiles in absence/presence of auto-inhibition in hepatic and GW metabolism were both compared with observed data.

As for PO SS ERY semi-PBPK model, number of transit compartments was further adjusted by study 604 (Carls et al., 2014), the only SAD study after PO SS ERY. In study 604, ERY SS tablet was administered to 16 healthy volunteers (two dose groups, 250 mg and 1000 mg base equivalent dose, with n = 8), and a microdose of MDZ (3µg PO) was administered 1 hour after ERY dosing. Both ERY and MDZ plasma concentrations were measured by LC-MS. Since only PK profiles for ERY were provided (partial AUC of MDZ between 2 – 4 hours), study 604 was used to validate PO ERY SS model only, instead of MDZ and ERY DDI model. Besides study 604, PO ERY SS model was externally validated by several multiple doses ERY SS PK studies (studies 615 (Triggs & Ashley, 1978), 626 (McDonald et al., 1977), 627 (Mather et al., 1981) and 625(Miglioli et al., 1990)), in which plasma concentration – time profiles after both single and multiple ERY SS doses were compared with predicted profiles by visual predictive check and exposure metrics comparison. To test the necessity of incorporating ERY auto-inhibition into the PBPK model, predicted profiles in absence/presence of auto-inhibition in hepatic and GW metabolism were both compared with observed data.

The most commonly used criteria of prediction acceptance: predicted exposure metrics are within 0.5 to 2-fold of observed, were used to assess performance of ERY semi-PBPK model

after IV and two PO formulations.

ERY concentrations in liver and GW mucosa were simulated and compared after different routes of administration at different dose levels, and additional simulations were conducted to interpret consequences of nonlinear PK and auto-inhibition. All M&S were implemented in Simbiology (MATLAB, 2015a), if not otherwise mentioned.

To make more clinical relevant conclusions, sensitivity analysis and simulation of hepatic/GW CYP3A activity levels vs. time were performed under ERY dosing regimen in DDI studies, and will be discussed in **Chapter 8**.

7.3 Results and Discussion

7.3.1 Meta-analysis of ERY PK studies

A total of 7 IV studies with 95 healthy volunteers and 21 PO studies with 269 healthy volunteers were included in the final database. Each study was assigned a study ID number. In IV studies, 55 subjects were males, 34 subjects were females, and gender information was not provided in study 613 (Parsons & David, 1980). In PO studies, 170 subjects were males, 75 subjects were females, and gender information was not available in study 620 (Josefsson et al., 1982) and study 632 (Benardi et al., 1988). Age ranged from 19 to 55 years in IV studies, and from 18 - 51 years in PO studies. As to dosing regimen, IV ERY were all administered after single dose, ranged from 125 mg to 1344 mg. PO ERY were administered as both single- and repeat- doses, with single PO dose ranged from 250 mg to 1000 mg, and repeat- PO doses (studies 615 (Triggs & Ashley, 1978), 623 (Birkett et al., 1990), 626 (McDonald et al., 1977), 627 (Mather et al., 1981), 629 (Yakatan et al., 1985), 614 (Malmberg, 1979), 618 (Iliopoulou et al., 1982) and 625 (Miglioli et al., 1990)) ranged from 1000 mg to 2000 mg daily dose (different

dosing interval). Formulations used in IV studies were mostly ERY lactobionate salt, except for study 616 (Sun et al., 2010) and study 617 (Lappin et al., 2006) (formulation was not mentioned in the two studies). Formulations used in PO studies were ERY salts (stearate salt, piopionate salt), ERY base enteric-coated tablet, ERY base capsules containing enteric-coated pellets, and ERY ethylsuccinate ester.

To investigate inter-study variability of different formulations, studies using the same dose and formulation were identified, and reported $AUC_{0-\infty}^{ERY}$ in these studies were compared and plotted in **Figure 7.4**. In studies 620, 623, 626 and 629, ERY were all administered as 250 mg single oral ERY base in an EC tablet, and their reported mean AUCs ranged by 3.8 fold, with SD overlapped with each other. In studies 604, 615, 626 and 627, ERY were all administered as 250 mg single oral ERY SS in tablet, and their reported mean AUCs ranged by 2.2 fold. In studies 604 and 625, ERY were both administered as 1000 mg single oral ERY SS in tablet, and their reported mean AUCs ranged by 1.9 fold. No demographic, study design or analytical assay difference could explain the exposure metrics variability among the studies. Overall, **Figure 7.4** indicates that inter-study variability exists for both EC ERY base formulation and ERY SS formulation after PO administration, and EC demonstrates higher variability than SS.

Bioassay using microbiological activity to quantify ERY concentrations was applied in most studies, except for study 616, 617, 604 (Carls et al., 2014), and 623 (Birkett et al., 1990), in which HPLC was used. Bioassay measures total microbiologically active moieties, including both ERY and its active metabolite nd-ERY, while HPLC specifically measures ERY base. Due to less microbiological activity and negligible serum exposure of nd-ERY, measurements obtained by bioassay demonstrated similar exposures as HPLC measurements in studies using same IV or PO dose and formulations (*e.g.*, study 611 vs. study 616; study 623 vs. study 620).

However, given the large inter-study variability of ERY PK, especially after PO EC formulation, it was still difficult to compare the two analytical methods, so that cautions were taken when comparing results from different analytical measurements. Detailed PK, demographic, study design and sample analysis information for all ERY IV and PO studies were summarized in **Appendices H**.

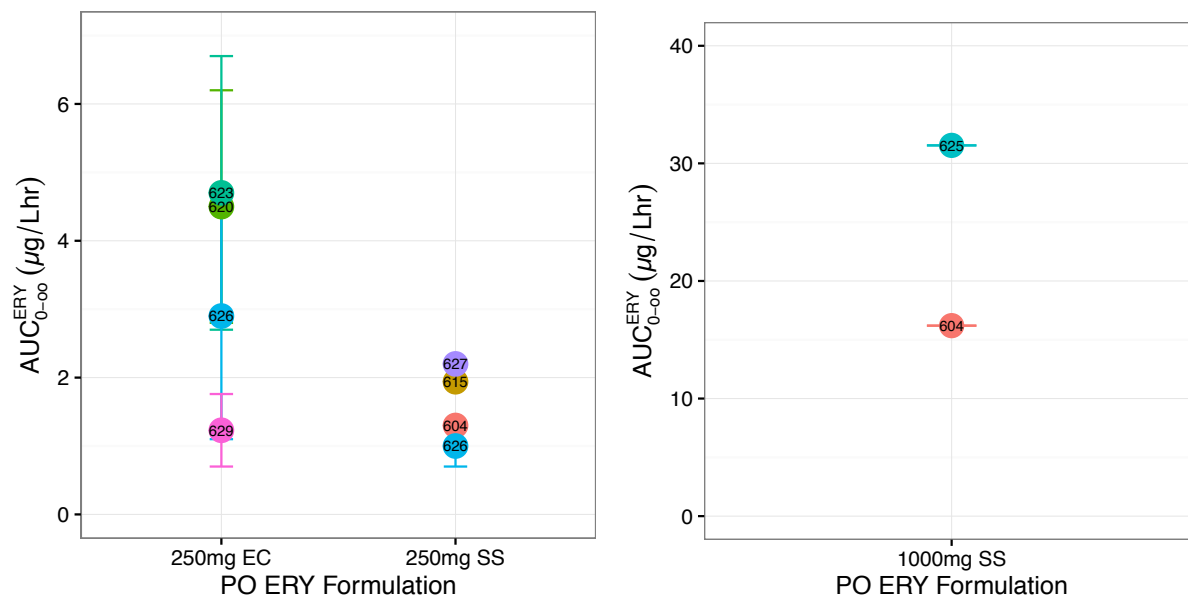


Figure 7.4 Systemic exposure after the same oral single dose and formulation of ERY. a) $AUC_{0-\infty}^{ERY}$ after single 250 mg oral EC tablet containing ERY base or oral tablet containing ERY SS. b) $AUC_{0-\infty}^{ERY}$ after single 1000 mg oral tablet containing ERY SS. The symbols and bars are reported mean AUC and SD in each study (if available). The number inside each symbol is the study ID.

7.3.2 Meta-analysis of ERY and MDZ DDI studies

MDZ and ERY were co-administered in 4 studies (study 28 (Olkola et al., 1993), study 601 (Zimmermann et al., 1996), study 603 (Okudaira et al., 2007) and study 604 (Carls et al., 2014)), with 38 healthy volunteers included in total. Subjects in all the studies experienced overnight fast before drug administration, thus food effect didn't need to be considered in future modeling process, and only ERY PK profiles measured in fasted subjects were used for ERY semi-PBPK

model validations. ERY was administered as repeat- oral doses in all the four DDI studies, and no IV ERY was co-administered with MDZ in any clinical DDI study. Study 601 was excluded from the final database, because it didn't mention ERY formulation, which is an important factor influencing ERY's PK profile. Study 604 was the only study providing both MDZ and ERY PK information: it provided ERY PK profiles after single SS 250 mg and 1000 mg doses, while only partial MDZ AUC (AUC measured between 2 – 4 hours after MDZ administration) was given. Therefore, study 604 was only used to validate PO ERY SS model, instead of MDZ and ERY DDI model. Eventually, MDZ and ERY DDI semi-PBPK model could only be validated by study 28 and study 603. Study 28 administered both IV and PO MDZ with placebo or 500mg PO EC ERY every 8 hours (q8h) for 7 days. Study 603 administered PO MDZ after various time course of PO SS ERY (2 days, 4 days, 7 days). Hence, PO ERY semi-PBPK model was only developed for ERY EC base formulation (short for "EC") and ERY SS formulation (short for "SS"). Detailed PK, demographic, study design and sample analysis information for both ERY and MDZ were summarized in **Appendices I**.

7.3.3 Saturable plasma protein binding model

Parameter estimates and diagnostic plots of two models are demonstrated in **Table 7.2** and **Figure 7.5**. From **Table 7.2** and **Figure 7.5**, both the two models predict observed binding profiles well, with small CV% for all parameters. f_u^{ERY} is then plotted against total (unbound + bound) ERY concentrations (**Figure 7.6**), to facilitate conversion between total and unbound concentrations. From **Figure 7.6**, model 1 (hyperbolic/linear model) underestimates f_u^{ERY} at low concentrations, while model 2 (sigmoidal/linear model) perfectly characterizes entire observed binding profile. f_u^{ERY} is around 0.5 originally, and gradually decreases to 0.28 (lowest value) at the total plasma concentration range of 1.5 – 6.5mg/L, and then increases back to 0.55 at around

27 mg/L. This is in agreement with reported f_u^{ERY} of 0.27 - 0.31 in most studies (Barre et al., 1987; Sun et al., 2010). The higher f_u^{ERY} at very low concentration may be because ERY can bind to other unknown high affinity (higher than AAG) low capacity plasma protein (globulin, fibrinogen, *etc.*) at very low concentration. As a conclusion, sigmoidal/linear model was further used in ERY semi-PBPK model, to transform between unbound and total ERY concentrations. f_u^{ERY} can be estimated by equation (7.24).

$$f_u^{ERY} = 1 / \left(\frac{B_{max} + C_{b,u}^{n-1}}{K_{b,50}^n + C_{b,u}^n} + m + 1 \right) \quad (7.24)$$

where $c_{b,u}$ is unbound blood concentration of ERY (predicted value of concentration in systemic blood compartment in ERY semi-PBPK model).

Table 7.2 Parameter estimates of two saturable plasma protein binding models.

Model	Parameter	Estimate	RSE (CV%)
1	B_{max} (μ M)	12.9	2.61
	K_m (μ M)	4.18	6.26
	M^1	0.265	9.43
2	B_{max} (μ M)	11.1	1.84
	K_m (μ M)	2.92	4.06
	n	1.32	3.67
	M^1	0.265	9.43

¹ m was fixed when estimating B_{max} , $K_{b,50}$ and n. Relative standard error (RSE) of m was estimated in linear regression.

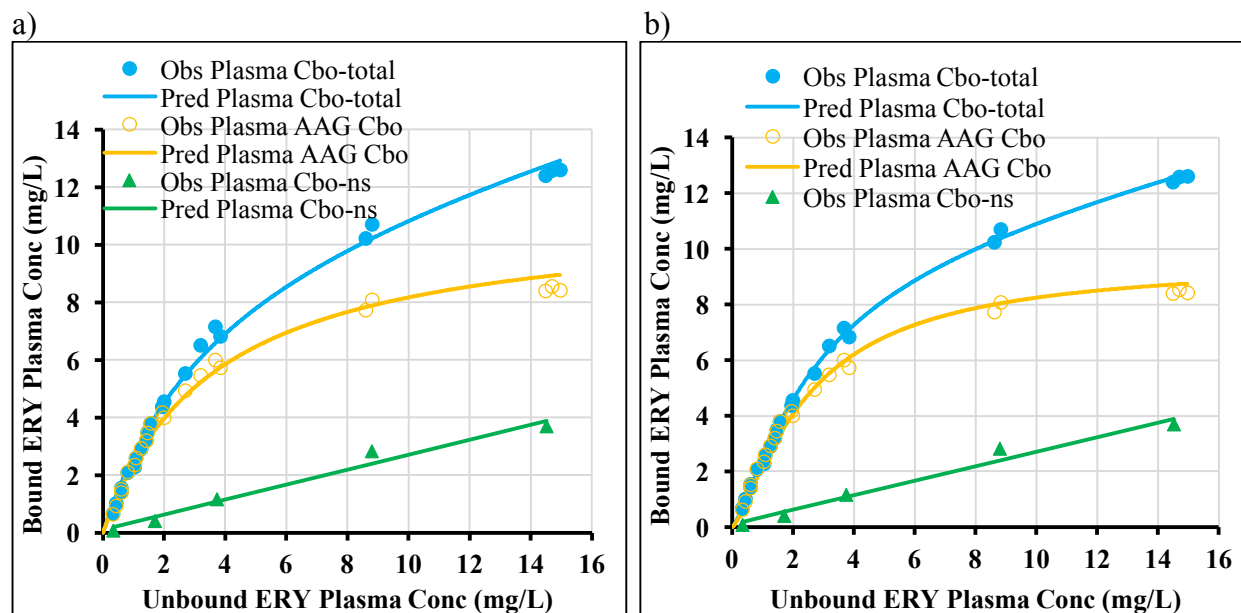


Figure 7.5 Diagnostic plots of two saturable plasma protein binding models.

a) Hyperbolic/linear model. b) Sigmoidal/linear model. $C_{bo-total}$ is ERY total bound concentration, AAG C_{bo} is ERY AAG bound concentration, C_{bo-ns} is ERY non-specific bound concentration

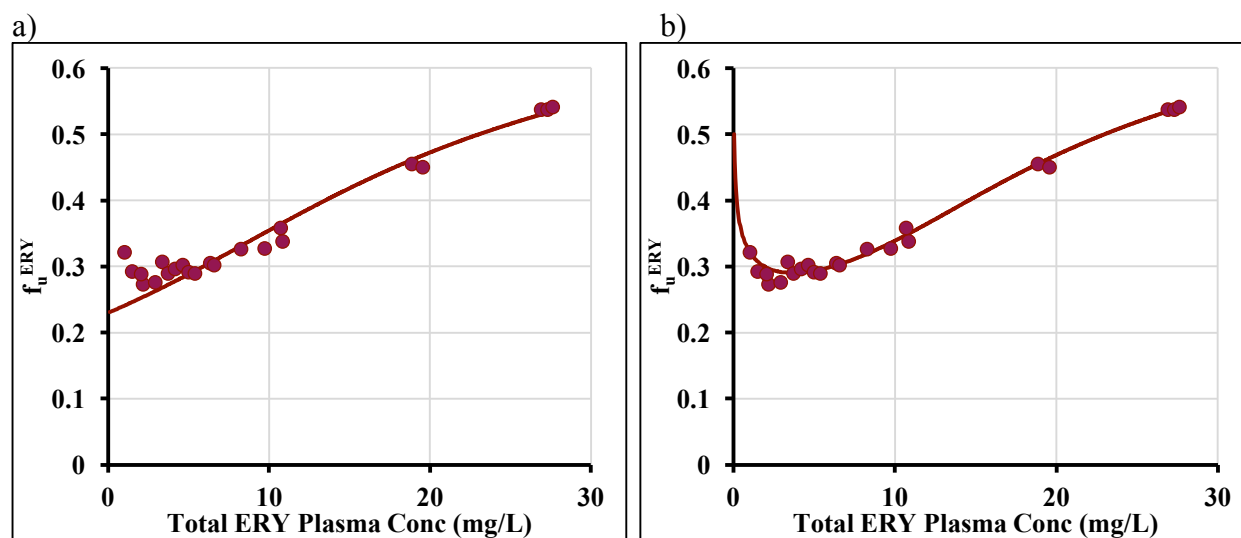


Figure 7.6 Relationship between f_u^{ERY} and total plasma ERY concentration.

a) Hyperbolic/linear model. b) Sigmoidal/linear model. Symbols reflect observed data, and lines reflect predicted profiles.

7.3.4 Dose proportionality assessment

Due to large inter-study variability of ERY PK, dose proportionality assessment was performed only in SAD studies: study 611 after IV ERY and study 620 after PO EC ERY. PO SS ERY was administered only as 250 mg and 1000 mg single dose in study 604; thus, dose proportionality was not assessed in SS. Mean plasma $AUC_{0-\infty}$ of total (unbound + bound) ERY is plotted against ERY dose after 15-min IV infusion (regimen 2 in study 611) and PO EC administration (study 620). A power model ($y = ax^b$) was used to fit the data; an exponent value of 1 indicates dose-proportional PK. 95% CIs of the exponent, b , was generated by JMP Pro 9.0 (SAS, Cary, NC) to assess if there was significant deviation from 1 ($p < 0.05$). **Figure 7.7** illustrates the dose-proportionality of IV and PO EC ERY. Parameter estimates for the power model and their 95% CIs are summarized in **Table 7.3**.

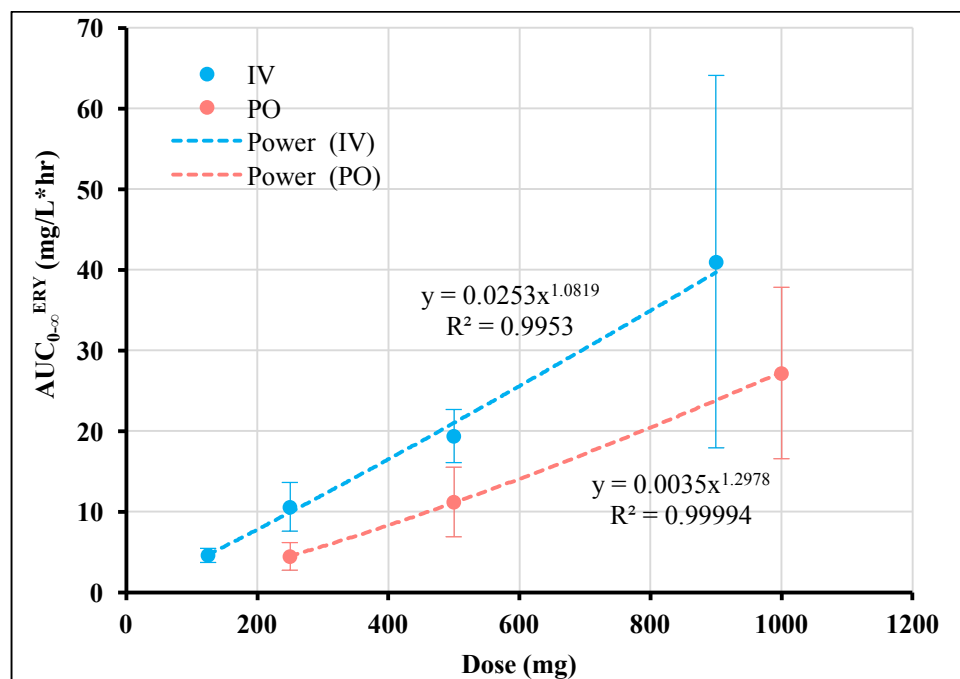


Figure 7.7 Dose proportionality assessment after single dose IV ERY and PO EC ERY (total AUC versus dose).

The dashed lines represent fits by power model, and symbols and bars represent the observed mean \pm SD.

Table 7.3 Summary of power model fit for total ERY plasma AUC vs dose plots.

ERY Route	Dose (mg)	AUC _{0-∞} ^{ERY} (mg/L*hr)	SD of AUC _{0-∞} ^{ERY} (mg/L*hr)	Power coefficient	95% CI of power	r ²
IV (Study 611)	125	4.6	0.9	1.08	(0.98, 1.18)	0.995
	250	10.6	3			
	500	19.4	3.3			
	900	41	23.1			
PO EC (Study 620)	250	4.5	1.7	1.30	(1.28, 1.32)	0.999
	500	11.2	4.3			
	1000	27.2	10.6			

From **Figure 7.7** and **Table 7.3**, AUC after PO EC ERY is consistently lower than AUC after IV ERY at the same dose, indicating its relative low $F_{\text{oral}}^{\text{ERY}}$ after PO EC formulation. Power models fit both IV and PO EC dose-proportionality well, with $r^2 > 0.99$ in both cases. Power coefficient and 95% CIs of power indicate that total (unbound + bound) ERY follows dose-proportional PK after IV administration and supra-proportional PK after PO EC ERY. However, since saturable plasma protein binding was observed within the dose range of study 611, which could lead to infra-proportional PK of ERY, unbound ERY AUC was calculated, to further investigate ERY PK nonlinearities without the influence of plasma protein binding. Total ERY AUC was corrected by average f_u^{ERY} (referred as f_u^{ERY} at $c_{\text{max}}^{\text{ERY}}/2$) at each dose, to generate unbound ERY AUC (AUC_u), and dose proportionality was assessed again using AUC_u and dose, demonstrated in **Figure 7.8** and **Table 7.4**. After f_u^{ERY} correction, ERY exhibits supra-proportional PK after both IV and PO administration, and the exponents of IV and PO power models are similar, with overlapped 95% CIs.

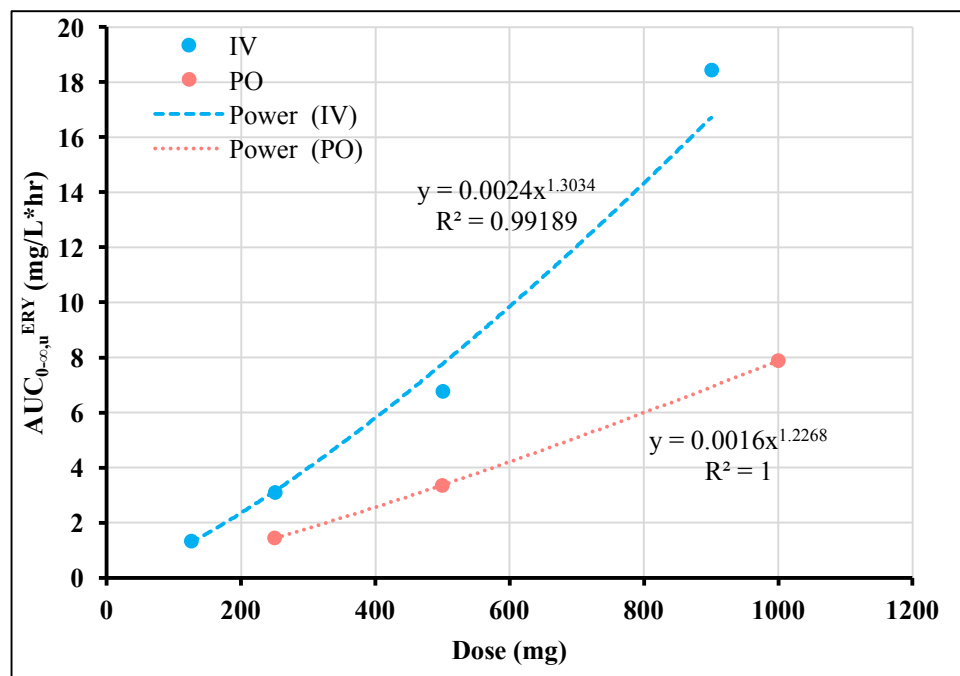


Figure 7.8. Figure 7.8 Dose proportionality assessment after single dose IV ERY and PO EC ERY (unbound AUC versus dose).

The dashed lines represent fits by power models, and symbols represent the observed values.

Table 7.4 Parameter estimates of power model fit using unbound ERY concentrations.

ERY Route	Dose (mg)	Total plasma AUC _{0-∞} ^{ERY} (mg/L*hr)	Average f _u ^{ERY}	Unbound plasma AUC _{0-∞,u} ^{ERY} (mg/L*hr)	Power coefficient	95% CI of power	r ²
IV (Study 611)	125	4.6	0.29	1.3	1.30	(1.13, 1.48)	0.992
	250	10.6	0.29	3.1			
	500	19.4	0.35	6.8			
	900	41	0.45	18.4			
PO (Study 611)	250	4.5	0.32	1.4	1.23	(1.19, 1.26)	0.999
	500	11.2	0.3	3.4			
	1000	27.2	0.29	7.9			

In study 611, central compartment volume of distribution ($V_{d_{cc}}$), steady-state volume of distribution ($V_{d_{ss}}$), total clearance ($CL_{tot,p}^{ERY}$) and renal clearance (CL_{ren}^{ERY}) were also provided, and non-renal clearance ($CL_{nonren,p}^{ERY}$) could be calculated by subtracting CL_{ren}^{ERY} from $CL_{tot,p}^{ERY}$. All the volumes and clearances were corrected by average f_u^{ERY} (referred as f_u^{ERY} at $c_{max}^{ERY}/2$), as shown in **Table 7.5**. Before f_u^{ERY} correction, $V_{d_{cc}}$ and $V_{d_{ss}}$ tend to increase with dose, while after converted to unbound volumes ($V_{d_{cc,u}}$ and $V_{d_{ss,u}}$), no obvious trend is found regarding the two volumes, confirming the existence of saturable plasma protein binding in study 611. After f_u^{ERY} correction on the three clearances, unbound renal clearance ($CL_{ren,u}^{ERY}$) increases with dose, indicating potential saturable tubular reabsorption. Meanwhile, both unbound total plasma clearance ($CL_{tot,u}^{ERY}$) and unbound non-renal clearance ($CL_{nonren,u}^{ERY}$) decrease with dose, suggesting the existence of saturable N-demethylation by CYP3A and/or saturable biliary excretion. Due to the high $K_{m,hep-3A}^{ERY}$ (64.6mg/L) reported by Riley et al. (Riley & Howbrook, 1998), CYP3A metabolism of ERY is not likely to be saturable within the concentrations in study 611, and saturable biliary excretion is the only plausible explanation of supra-proportional PK after IV ERY. There are no publications reported the contribution of CYP3A metabolism and biliary excretion to the total hepatic clearance of ERY. However, biliary excretion of ERY had been studied following parenteral administration in 23 patients, including 9 patients underwent duodenoscopy, who were administered 300 mg IV ERY, 4 patients with partial or complete obstruction of bile ducts, who were given 300 mg IV ERY, and 10 patients underwent cholangiopancreatography, who were administered 100mg intramuscular (IM) ERY (Chelvan et al., 1979). It was found that mean bile levels of ERY were approximately ten times higher than corresponding serum concentration 1 hour after IV and IM injection, implying potential high accumulation of ERY in bile after IV administration. In addition, Rivory *et al.*

(Rivory et al., 2001) integrated $^{14}\text{CO}_2$ flux as a function of time to infinity in an erythromycin breath test (EBT), in which 3-4 μCi of [^{14}C] ERY was administered after IV injection. The authors mentioned that the integration of $^{14}\text{CO}_2$ flux actually produces an estimate of the fraction of ERY that is metabolized by CYP3A, and was only 6-33%, according to their result, implying that only up to 1/3 of ERY is metabolized by CYP3A. This proves that biliary excretion may play a key role in hepatic clearance of ERY after IV administration, and it is highly likely that biliary excretion was saturated across the dose ranges in study 611 and study 620. As a P-gp and OATP1A4 (in rat) substrate, saturation of either of them could result in decreased $\text{CL}_{\text{nonren,u}}^{\text{ERY}}$ with dose. In rat hepatocytes, K_m of OATP1A4 is 53mg/L (no human study available), higher than clinical relevant levels, so OATP1A4 is not likely to cause saturation of biliary excretion in human, and P-gp-mediated biliary excretion is the most likely source of supra-proportional PK of unbound ERY after IV administration.

Table 7.5 Unbound PK parameters of IV ERY in study 611.

Dose mg	Average f_u^{ERY}	$\text{Vd}_{\text{cc,u}}^{\text{ERY}}$ ml/kg	$\text{Vd}_{\text{ss,u}}^{\text{ERY}}$ ml/kg	$\text{CL}_{\text{tot,p,u}}^{\text{ERY}}$ ml/min/kg	$\text{CL}_{\text{ren,u}}^{\text{ERY}}$ ml/min/kg	$\text{CL}_{\text{nonren,u}}^{\text{ERY}}$ ml/min/kg
125	0.29	506	1620	23.0	1.2	21.8
250	0.29	907	1970	23.5	1.1	22.4
500	0.35	787	2870	17.2	1.8	15.4
900	0.45	994	2434	13.9	2.3	11.6

For nonlinear PK drug, F_{oral} cannot be easily estimated as dose-corrected AUC ratio. Instead, ERY F_{oral} was roughly estimated by ratio of the corresponding IV and PO doses that produce the same unbound AUC, assuming that same drug exposure results in the same extent of nonlinearity. The method was illustrated in **Figure 7.9**. Since AUC_u after 125 mg IV ERY (in study 611) and AUC_u after 250 mg PO EC ERY (in study 620) were almost the same, $F_{\text{oral}}^{\text{ERY}}$ at 250 mg PO EC ERY can be estimated as $125\text{mg}/250\text{mg} = 50\%$. Likewise, AUC_u after 250 mg IV ERY (in study 611) and AUC_u after 500 mg PO EC ERY (in study 620) were almost the

same, thus $F_{\text{oral}}^{\text{ERY}}$ at 500 mg PO EC ERY can be estimated as $250\text{mg}/500\text{mg} = 50\%$. AUC_u after 492 mg IV ERY (in study 611) and AUC_u after 1000 mg PO EC ERY (in study 620) were almost the same, thus $F_{\text{oral}}^{\text{ERY}}$ at 1000 mg PO EC ERY can be estimated as $492\text{mg}/1000\text{mg} = 49\%$. As a result, $F_{\text{oral}}^{\text{ERY}}$ at different doses were almost constant in study 620, indicating that supra-proportional PK after PO administration is more likely owing to systemic saturable metabolism/biliary excretion.

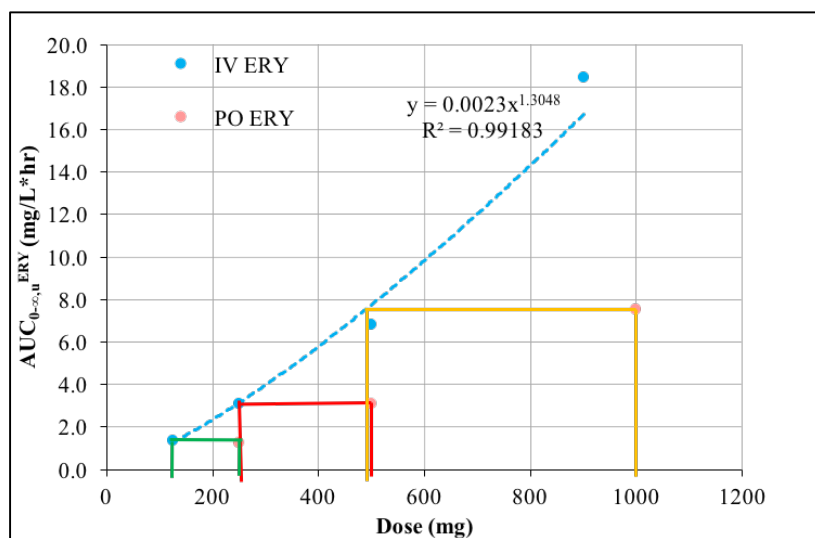


Figure 7.9 Estimation of $F_{\text{oral}}^{\text{ERY}}$ at different ERY dose.

$F_{\text{oral}}^{\text{ERY}}$ was calculated by ratio of the corresponding IV and PO doses, that produce the same unbound AUC (dose indicated by the same colors). A power model fit was performed on IV $AUC_{0-\infty,u}^{\text{ERY}}$ versus dose data, and IV dose that could produce the same AUC_u as 1000mg PO ERY was calculated based on power model ($AUC_u = 0.0023 \cdot \text{Dose}_{\text{IV}}^{1.3048}$), which was estimated to be 492 mg.

Overall, after IV ERY, there are four partially offsetting sources of nonlinearities involved in the systemic disposition of ERY across clinical dose range: saturable plasma protein binding and saturable renal tubular reabsorption result in infra-proportional PK; saturable biliary excretion and potential saturable CYP3A metabolism (higher than clinical dose) result in supra-proportional PK. The apparent dose-proportionality of total AUC and slight supra-proportionality of unbound AUC reflect the overall net effects of the four sources. After PO

administration, $F_{\text{oral}}^{\text{ERY}}$ is almost constant with dose, indicating that supra-proportional PK after PO administration is more likely owing to systemic saturable metabolism/biliary excretion.

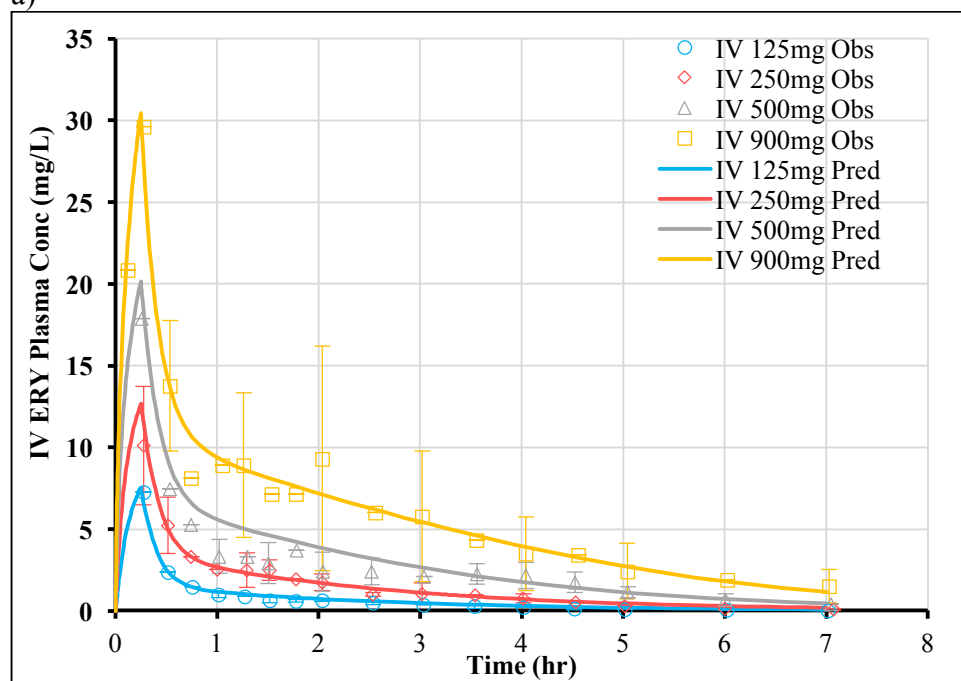
7.3.5 ERY semi-PBPK model after single IV administration

7.3.5.1 Predictive performance check

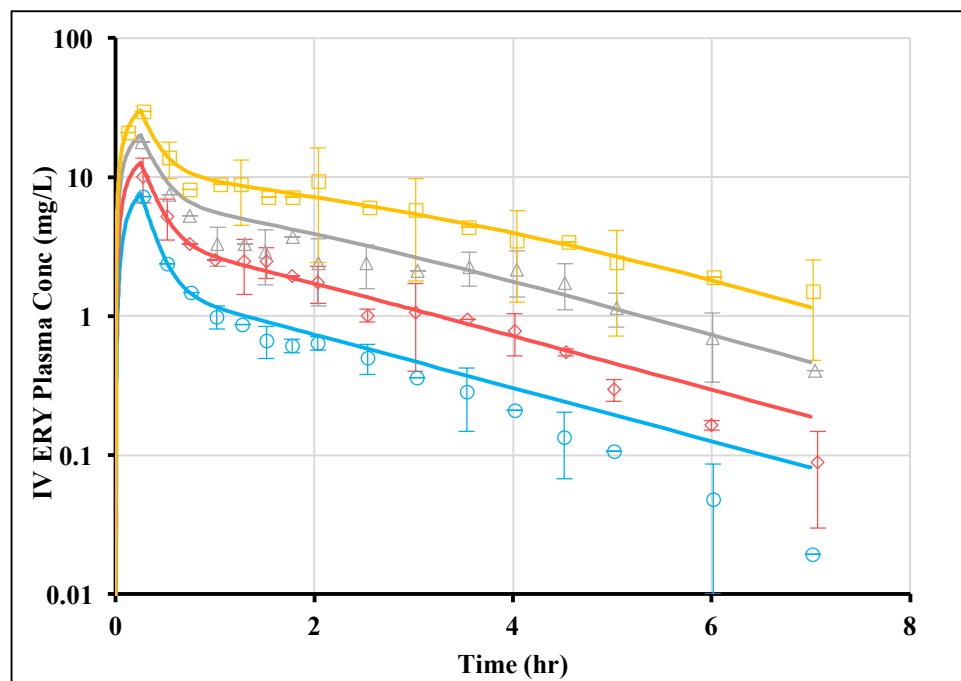
After optimization of $v_{\text{max,hep-3A}}^{\text{ERY}}$, $v_{\text{max,bile}}^{\text{ERY}}$ and $K_{\text{m,bile}}^{\text{ERY}}$, the observed and model-predicted ERY PK profiles after IV administration are demonstrated in **Figure 7.10** and the comparison of observed and model simulated exposure metrics are summarized in **Table 7.6**. From **Figure 7.10a-b**, the current parameters predict IV ERY PK profiles across doses (regimen 2 of study 611) well, with all predicted profiles superimposable with observed data, except at the low dose (125 mg and 250 mg), terminal slopes of predicted profiles appear to be shallower than observed. However, after repeated “try and error” processes to tweak $v_{\text{max,hep-3A}}^{\text{ERY}}$, $v_{\text{max,bile}}^{\text{ERY}}$ and $K_{\text{m,bile}}^{\text{ERY}}$, a perfect description across doses cannot be obtained. Also, external validation by study 616 (125 mg IV ERY, **Figure 7.10e-f**) and study 624 (240 mg IV ERY, **Figure 7.10g-h**) demonstrated perfect match between observed and predicted data, confirming the validity of IV ERY PBPK model at low doses. In studies 612 and 613, although some discrepancies were demonstrated between predicted and observed profiles (**Figure 7.10i-l**), simulation results can be easily improved by adjusting systemic distribution parameters (*i.e.*, $V_{\text{B,u}}^{\text{ERY}}$ and/or $V_{\text{P,u}}^{\text{ERY}}$) in study 612 and hepatic clearance parameters (*i.e.*, $v_{\text{max,hep-3A}}^{\text{ERY}}$ and/or $v_{\text{max,bile}}^{\text{ERY}}$) in study 613, explained as inter-study variability. Deviations (%) of $\text{AUC}_{0-\infty}^{\text{ERY}}$ and various clearances are mostly less than 50%, except for f_e^{ERY} at 250 mg IV ERY and AUC of study 612. There is a huge discrepancy between reported f_e^{ERY} and $\text{CL}_{\text{ren,p}}^{\text{ERY}}$ of 250mg ERY over 15min IV infusion (regimen 2) and over 3min IV infusion (regimen 1), indicating large inter-individual variability on f_e^{ERY} and $\text{CL}_{\text{ren,p}}^{\text{ERY}}$. The current model balances predictive deviations of $\text{CL}_{\text{ren,p}}^{\text{ERY}}$ for the

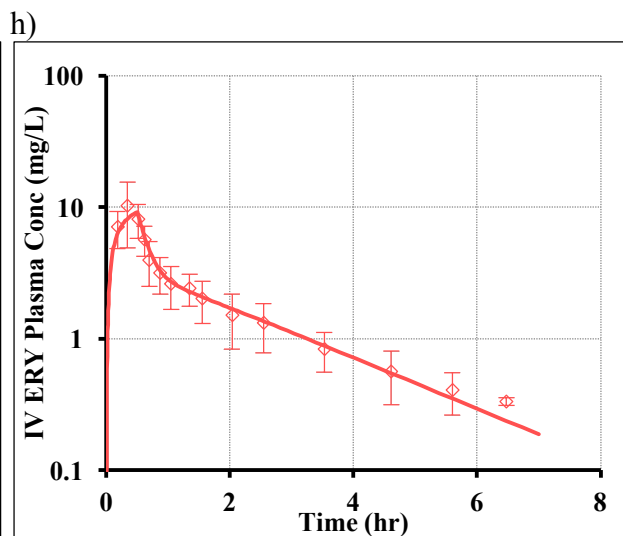
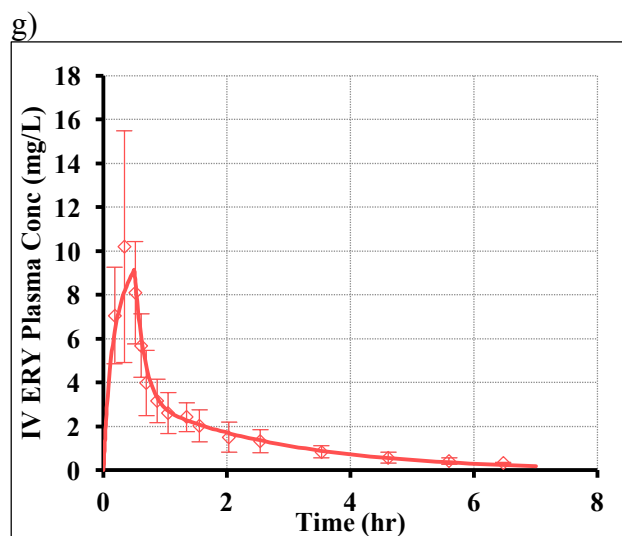
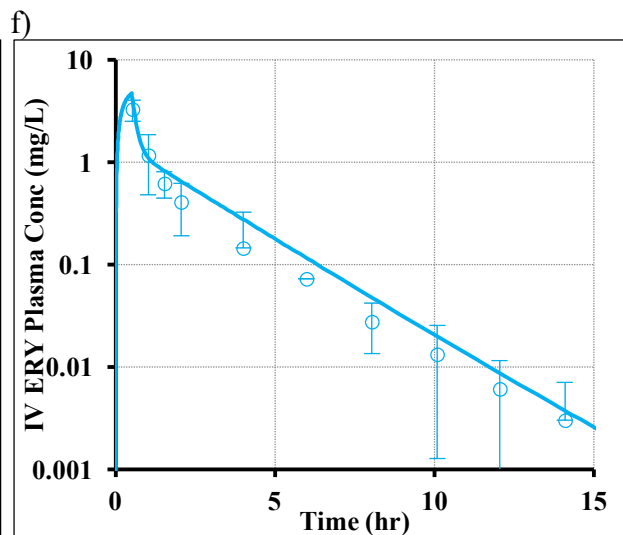
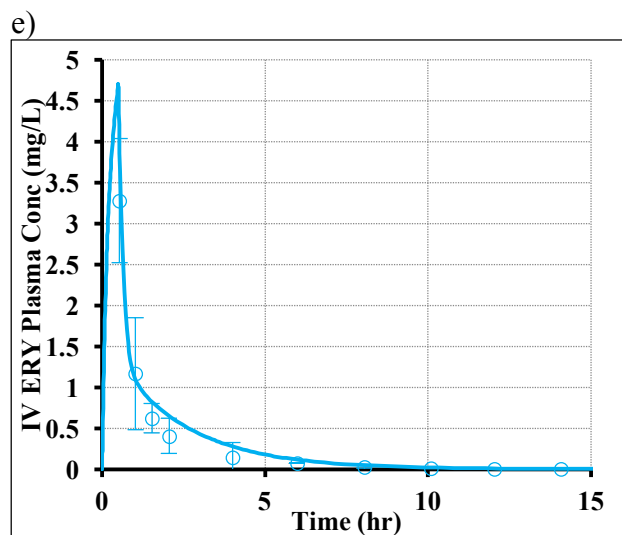
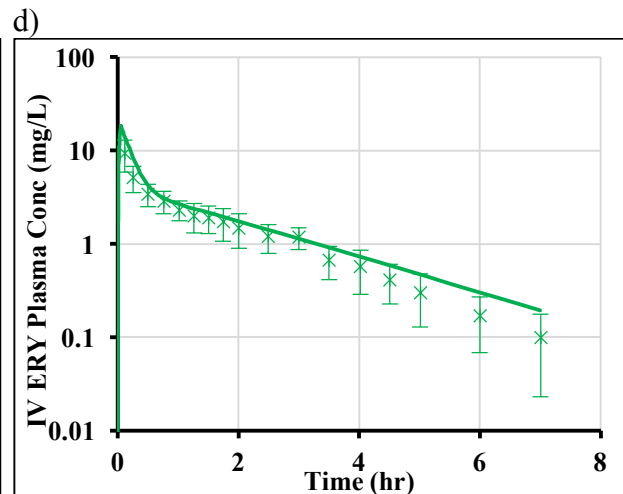
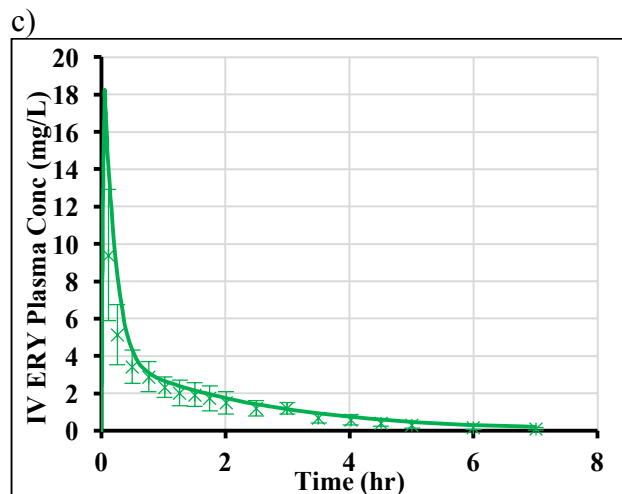
two regimens in study 611, with predicted $CL_{ren,p}^{ERY}$ overestimates observed value in regimen 2 by 48%, and underestimates observed in regimen 1 by 50%. Even at the highest dose (900 – 1344 mg ERY), only a slight plateau could be observed before terminal decline on semi-log plots (**Figure 7.10b, I**), probably because at high doses, CYP3A N-demethylation pathway becomes the predominant elimination pathway, which is not easy to saturate at clinical relevant concentrations. This occurs quite often clinically, when a drug has parallel elimination pathways.

a)



b)





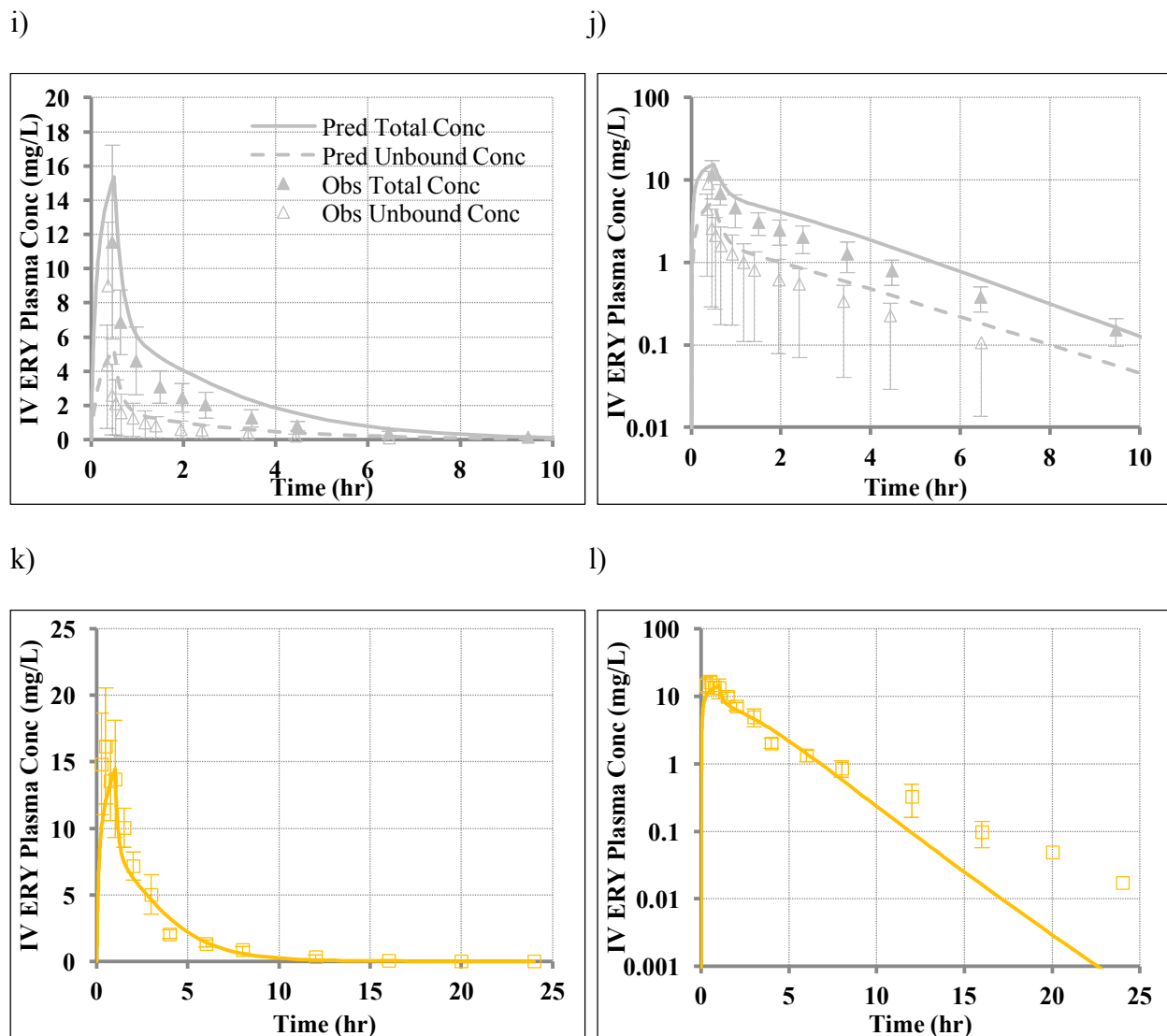


Figure 7.10 Observed and model-predicted ERY PK profiles after IV administration.

a-b) PK profiles after 125 mg, 250 mg, 500 mg or 900 mg IV ERY over 15 min infusion (regimen 2) in study 611 (Cartesian and semi-log plots) c-d) PK profiles after 250 mg IV ERY over 3 min infusion (regimen 1) in study 611 (Cartesian and semi-log plots) e-f) PK profiles after 125 mg IV ERY over 30 min infusion in study 616 (Cartesian and semi-log plots) g-h) PK profiles after 240 mg IV ERY over 30 min infusion in study 624 (Cartesian and semi-log plots) i-j) PK profiles after 500 mg IV ERY over 30 min infusion in study 612 (Cartesian and semi-log plots). Both unbound and total ERY plasma concentrations were reported. k-l) PK profiles after 2g ERY lactobionate (equivalent to 1344 mg IV ERY base) over 1-hour infusion in study 613 (Cartesian and semi-log plots). The solid lines are predicted PK profiles. The symbols and bars are observed means and SD values (if available).

Table 7.6 Comparison of reported and PBPK model-predicted ERY plasma exposure metrics and clearances.

Deviations greater than 50% were marked as bold.

Study ID	Dose (mg)	Time of infusion (min)	Deviation (%)				
			$AUC_{0-\infty}^{ERY}$	$CL_{tot,p}^{ERY}$ (ml/min/kg)	f_e^{ERY}	$CL_{ren,p}^{ERY}$ (ml/min/kg)	$CL_{nonren,p}^{ERY}$ (ml/min/kg)
611	125 (R2)	15	15%	-13%	3%	-10%	-13%
611	250 (R2)	15	15%	-13%	70%	48%	-16%
611	500 (R2)	15	21%	-17%	11%	-9%	-18%
611	900 (R2)	15	-4%	4%	-13%	-9%	7%
611	250 (R1)	3	38%	-27%	-31%	-50%	-24%
616	125	30	38%				
624	240	30	-4%				
612	500	30	59%				
613	1344	60	-14%				

Observed and model predicted total (unbound + bound) ERY clearances in study 611 (regimen 2) are plotted against IV ERY dose (**Figure 7.11**). Although some discrepancies are demonstrated between predicted and observed clearances, the overall trends in all the three clearances are characterized well by the model, and residuals across doses are balanced around 0.

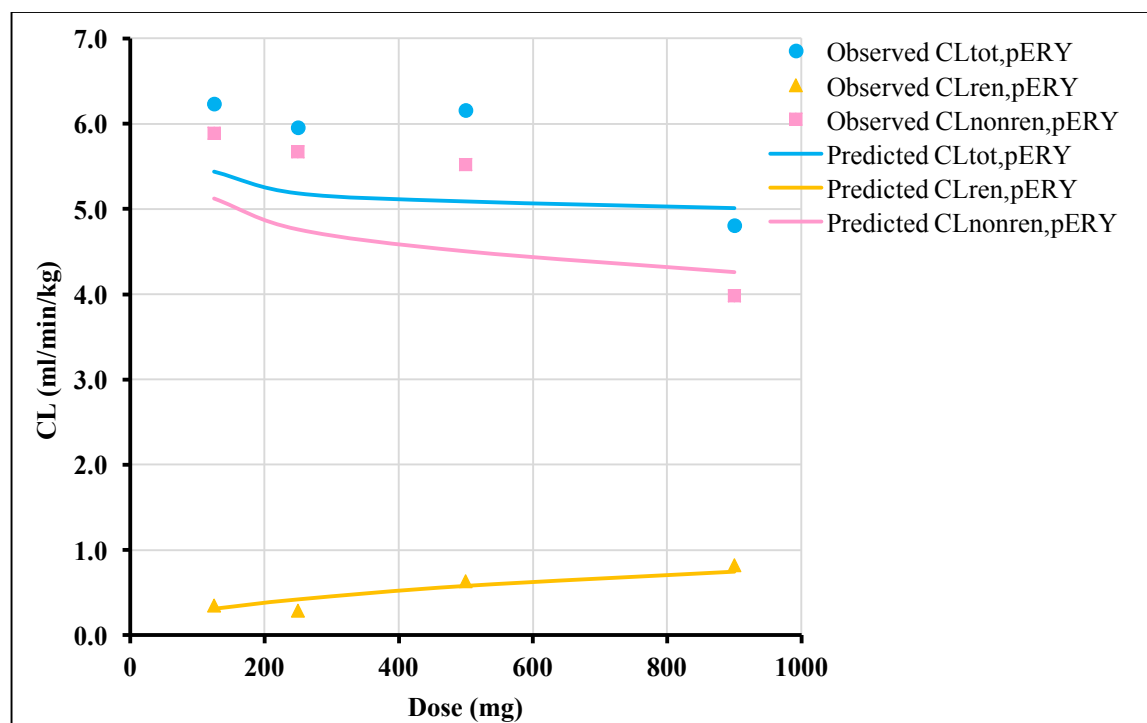


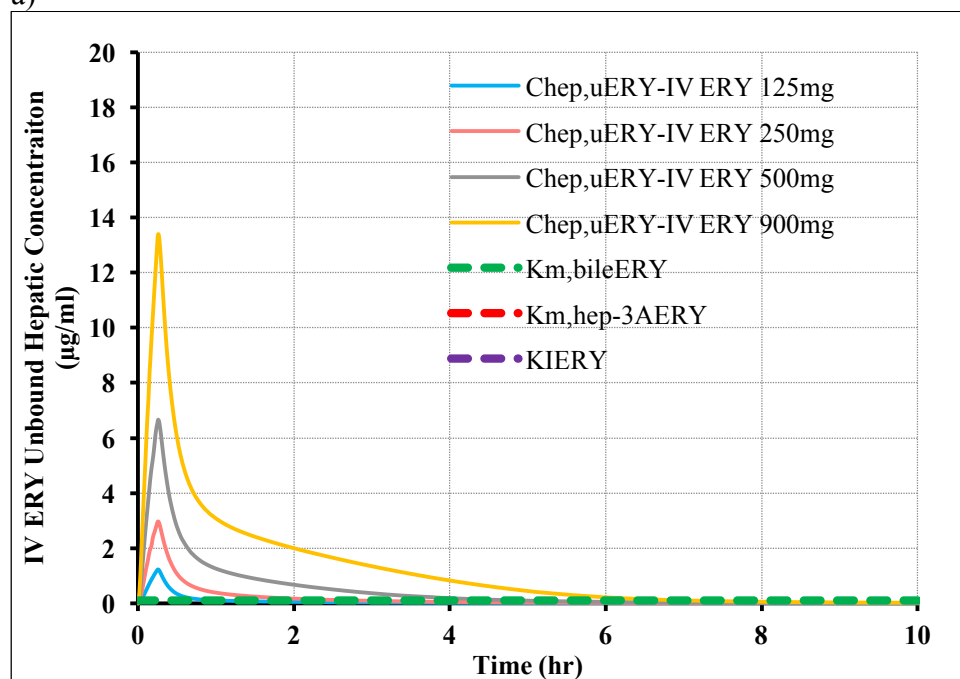
Figure 7.11 Model-predicted and observed total (unbound + bound) ERY clearances versus dose.

Overall, predictive performance checks using exposure metrics in several clinical studies and using clearances in study 611 suggest that the semi-PBPK model for IV ERY predicts the observed data well, confirming the validity of this model and model parameters.

7.3.5.2 Model Predictions

Model predicted ERY unbound hepatic concentrations after various IV single dose relative to $K_{m,bile}^{ERY}$, $K_{m,hep-3A}^{ERY}$ and K_I^{ERY} are plotted in **Figure 7.12a-b**. It is clearly demonstrated in **Figure 7.12b** that biliary excretion of ERY is saturated even under the lowest dose, with $c_{hep,u}^{ERY}$ above $K_{m,bile}^{ERY}$ for 1 hour, and at the highest dose (900 mg), it is saturated up to 7 hours. However, CYP3A metabolism is not saturated across doses, with $c_{hep,u}^{ERY}$ less than $K_{m,hep-3A}^{ERY}$ throughout the entire profiles ($K_{m,hep-3A}^{ERY}$ was not marked in **Figure 7.12a**). MBI of CYP3A is also minor, as even $c_{max,hep,u}^{ERY}$ at 900 mg dose is still less than half of K_I^{ERY} (K_I^{ERY} was not marked in **Figure 7.12a**). To compare hepatic concentration – time profiles across doses, low doses (125 mg and 250 mg) demonstrate apparently linear terminal phase, while high doses (500 mg and 900 mg) show a plateau before linear decline, confirming the existence of saturation in hepatic clearance. IV ERY GW (serosa) concentrations were not plotted, because it is assumed that only ERY in GW mucosa can inhibit GW CYP3A metabolism of MDZ (details discussed in **Chapter 8**).

a)



b)

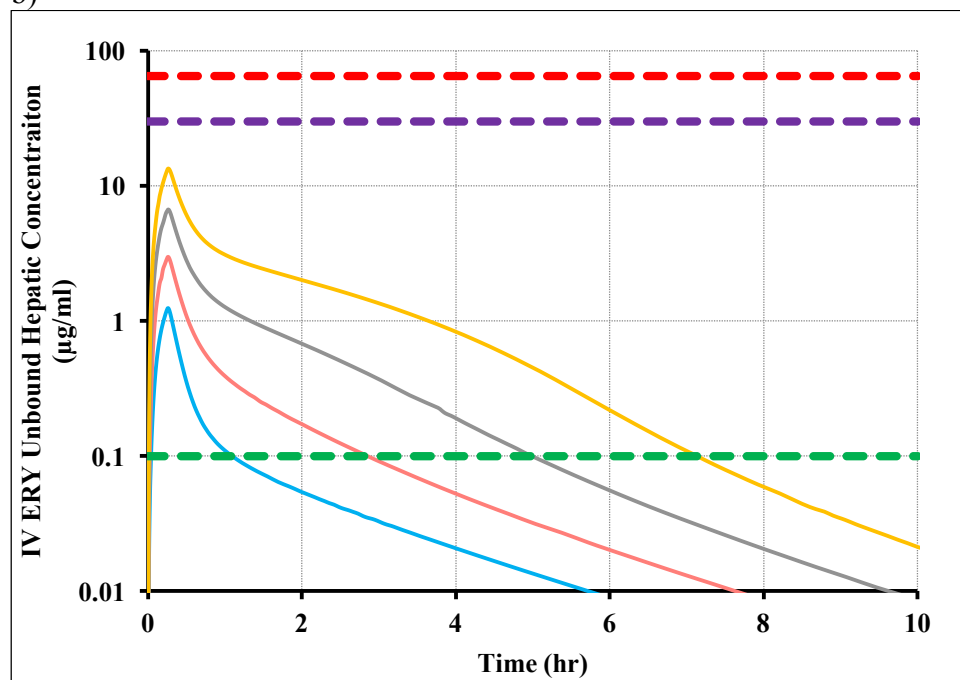


Figure 7.12 Model-predicted unbound hepatic ERY concentrations after various IV dose over 15-min infusion relative to $K_{m,bile}^{ERY}$, $K_{m,hep-3A}^{ERY}$ and K_I^{ERY} on Cartesian and semi-log scales.

Furthermore, model-predicted contribution of different elimination pathways (fraction relative to total clearance for unbound ERY) are plotted against IV ERY dose in **Figure 7.13**. After IV ERY, hepatic clearance is the predominant elimination pathway across doses, although its contribution decreases a bit, from 0.94 to 0.85, with increasing ERY dose from 125 mg to 900 mg. Predicted f_e^{ERY} agrees well with observed f_e^{ERY} , showing an increasing trend with dose. Hepatic clearance consists of CYP3A metabolism and biliary excretion, the contribution of which relative to total clearance represent as $f_{\text{hep-3A}}^{\text{ERY}}$ and $f_{\text{hep-bile}}^{\text{ERY}}$. Since ERY biliary excretion is a high affinity ($K_{m,\text{bile}}^{\text{ERY}} = 0.1 \mu\text{g/ml}$) and low capacity ($v_{\text{max,bile}}^{\text{ERY}} = 10 \mu\text{g/min/kg}$) pathway, its contribution significantly reduces with dose ($f_{\text{hep-bile}}^{\text{ERY}}$ at 125 mg and 900 mg ERY dose are 0.68 and 0.33, respectively), due to its saturation at higher ERY doses. However, CYP3A metabolism is a low affinity ($K_{m,\text{hep-3A}}^{\text{ERY}} = 64.6 \mu\text{g/ml}$) but high capacity pathway ($v_{\text{max,hep-3A}}^{\text{ERY}} = 900 \mu\text{g/min/kg}$), which is not saturated even at the highest dose, so that more drugs shift to CYP3A pathway to get eliminated, and its contribution almost doubles (from 0.27 to 0.52) with increasing dose. From **Figure 7.13**., an obvious elimination shift is observed from biliary excretion to CYP3A metabolism, and when ERY IV dose is about 500 mg, the two parallel hepatic elimination pathways contribute almost the same to ERY's total clearance after IV administration (~0.43 for each pathway). Although biliary excretion is saturated to a large extent at the highest dose, total $f_{\text{hep}}^{\text{ERY}}$ only decreases slightly, due to the increase contribution of CYP3A metabolism.

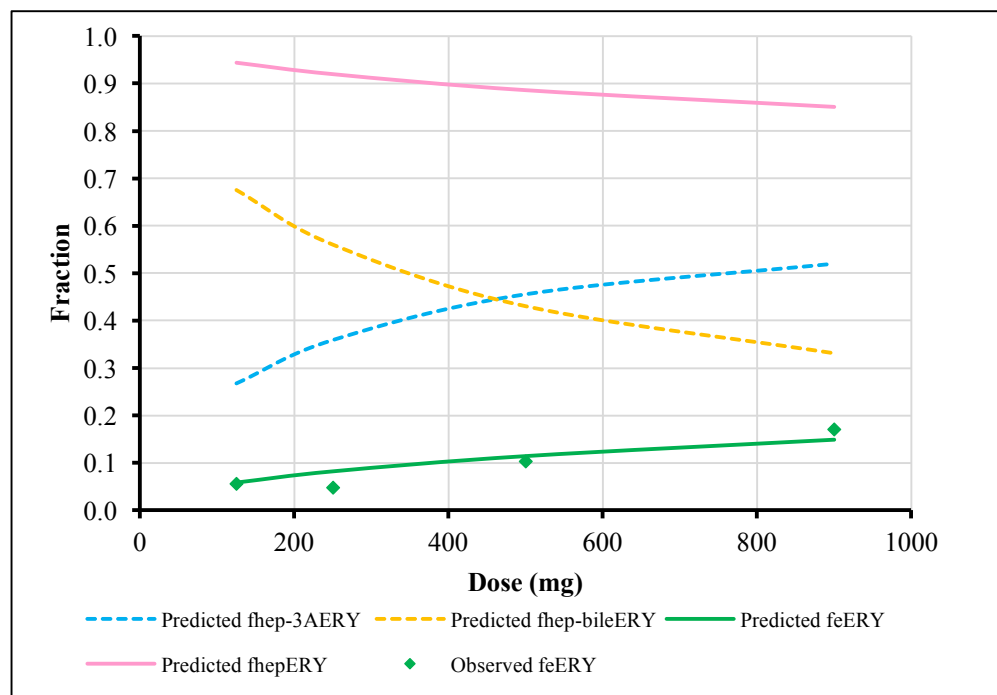


Figure 7.13 Model predicted contribution of different elimination pathways after various IV ERY dose in study 611.

Intrinsic clearance of biliary excretion and hepatic CYP3A metabolism vs. time were simulated by the model, as showed in **Figure 7.14a-b**. Without any saturation or inactivation, $CL_{int,bile}^{ERY}$ is ~7-fold of $CL_{int,hep-3A}^{ERY}$, in consistent with the predominant contribution of biliary excretion to overall clearance at the lowest dose (**Figure 7.13**). Since $K_{m,bile}^{ERY}$ is as low as 0.1 $\mu\text{g/ml}$, $CL_{int,bile}^{ERY}$ drastically decreases to around 0 - 10ml/min/kg, due to saturation, yet quickly recovers back to baseline within 10 hours, given the short pseudo steady-state $t_{1/2}$ of ERY. With respect to $CL_{int,hep-3A}^{ERY}$, it drops slightly at the beginning, followed by an extended decrease lasting for more than 10 hours. The initial drop is primarily due to marginal saturation of CYP3A enzyme, while the prolonged suppression of $CL_{int,hep-3A}^{ERY}$ is actually attributed to auto-inhibition by ERY. Since only single ERY dose is administered, the effect of auto-inhibition is not substantial, but the 900 mg dose still produced ~ 40% sustained inhibition on CYP3A level. The

impact of CYP3A auto-inhibition will be discussed in detail in **sections 7.3.5 and 7.3.6**.

Additionally, unbound ERY hepatic extraction ratio ($ER_{\text{hep,u}}^{\text{ERY}}$) vs. time was calculated by its physiological definition: (inflow concentration – outflow concentration) / inflow concentration, shown in equation 7.25.

$$ER_{\text{hep,u}}^{\text{ERY}} = \frac{[f_{\text{HA}} \cdot c_{\text{B,u}}^{\text{ERY}} + (1-f_{\text{HA}}) \cdot c_{\text{PV,u}}^{\text{ERY}}] - c_{\text{hep,u}}^{\text{ERY}} / K_{\text{p,hep,u}}^{\text{ERY}}}{f_{\text{HA}} \cdot c_{\text{B,u}}^{\text{ERY}} + (1-f_{\text{HA}}) \cdot c_{\text{PV,u}}^{\text{ERY}}} \quad (7.25)$$

As presented in **Figure 7.14c**, even in presence of saturation and auto-inhibition, $ER_{\text{hep,u}}^{\text{ERY}}$ is still relatively high across doses (mostly > 0.7), which is in consistent with literature that $CL_{\text{hep,u}}^{\text{ERY}}$ is similar to hepatic blood flow (98.6 L/hr) (Barre et al., 1987), indicating its high hepatic extraction ratio as unbound drug. For all the four doses, $ER_{\text{hep,u}}^{\text{ERY}}$ – time profiles demonstrate similar patterns, with $ER_{\text{hep,u}}^{\text{ERY}}$ rapidly decreases to different levels due to various extent of saturation, and then quickly recovers. However, $ER_{\text{hep,u}}^{\text{ERY}}$ cannot get back to baseline level ($ER_{\text{hep,u}}^{\text{ERY}} = 1$) within 10 hours, because of the maintained CYP3A auto-inhibition.

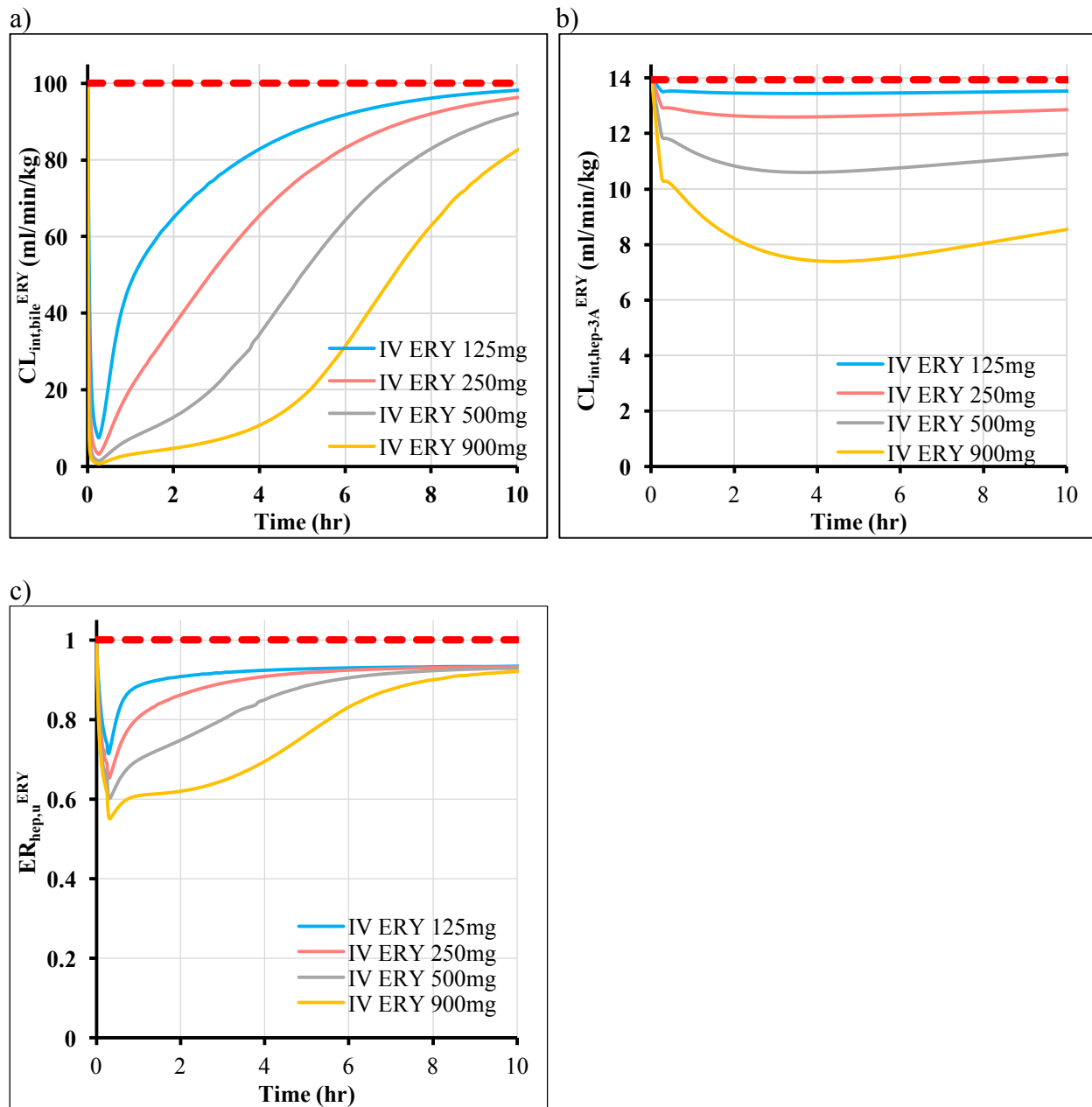


Figure 7.14 Time course of intrinsic hepatic clearances and hepatic extraction ratio at different doses in study 611.

7.3.6 ERY semi-PBPK model after single/repeat- PO doses (ERY base enteric-coated tablet formulation)

7.3.6.1 Predictive performance check

In PO ERY semi-PBPK model, all the parameters were originally assumed to be the same as IV model. However, the predicted ERY concentrations were consistently lower than observed levels from study 20 (**Figure 7.15**), and the observed terminal slopes were apparently over-estimated, especially at 1000 mg dose. Since ERY was only administered orally in study 620, and no IV ERY information available in this study, $v_{\max, \text{hep-3A}}^{\text{ERY}}$ and $v_{\max, \text{bile}}^{\text{ERY}}$ were re-optimized based on visual inspection of predictive performance after both single and repeat- PO EC doses across studies, and $v_{\max, \text{hep-3A}}^{\text{ERY}}$ and $v_{\max, \text{bile}}^{\text{ERY}}$ were finally adjusted to be 800 $\mu\text{g}/\text{min}/\text{kg}$ and 0.5 $\mu\text{g}/\text{min}/\text{kg}$, respectively. $v_{\max, \text{hep-3A}}^{\text{ERY}}$ is very close to $v_{\max, \text{hep-3A}}^{\text{ERY}}$ after IV ERY, while $v_{\max, \text{bile}}^{\text{ERY}}$ after PO EC ERY is 1/20 of the value used in IV ERY model. Schuetz et al. (1995) have determined the variation of P-gp protein in 41 human livers (only 10 of them were from normal adults) by Western blot. They didn't specify the overall P-gp protein variation in normal human livers, but stated that variation of P-gp was 4.5-fold in 6 normal males, and 7.8-fold in 4 normal females. Given the large variations of P-gp expression in very limited number of subjects, it is possible to presume a 20-fold difference in P-gp expression in two different studies, with varied subject demographics (*i.e.*, age and gender).

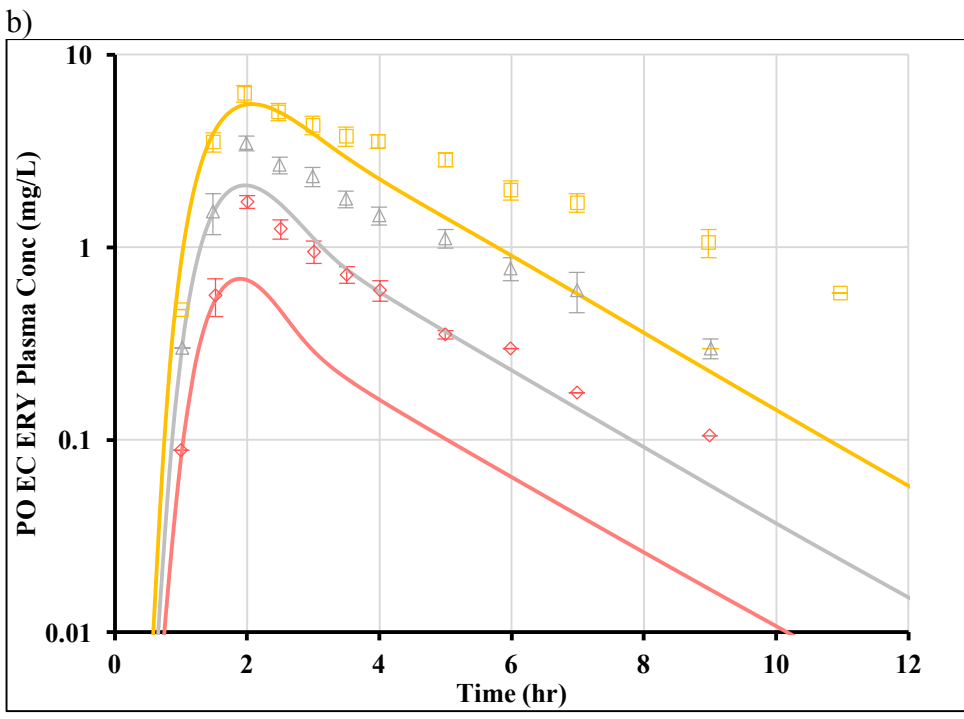
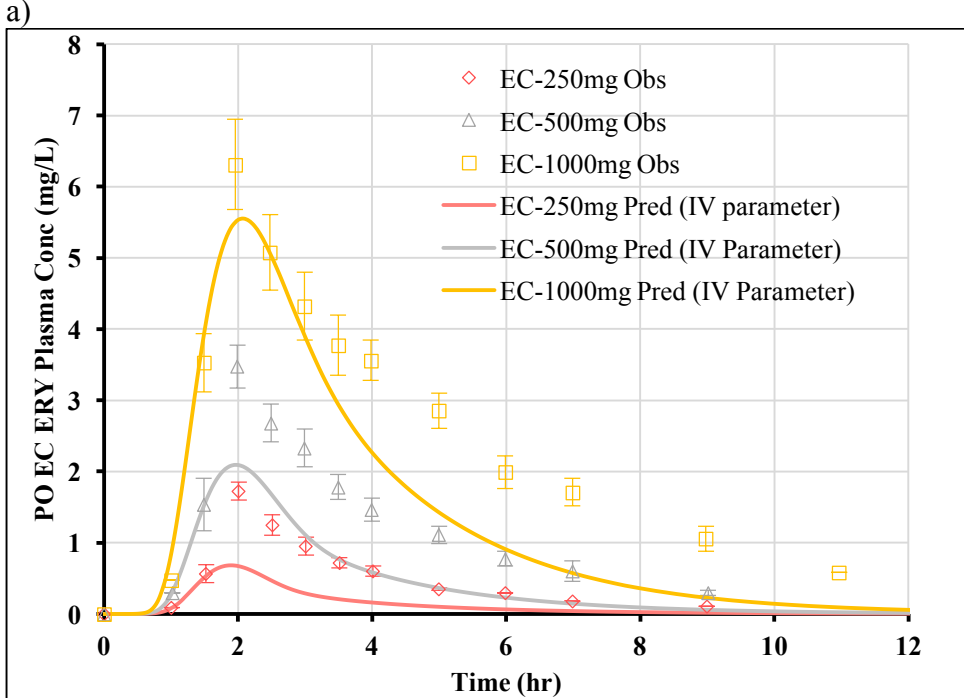
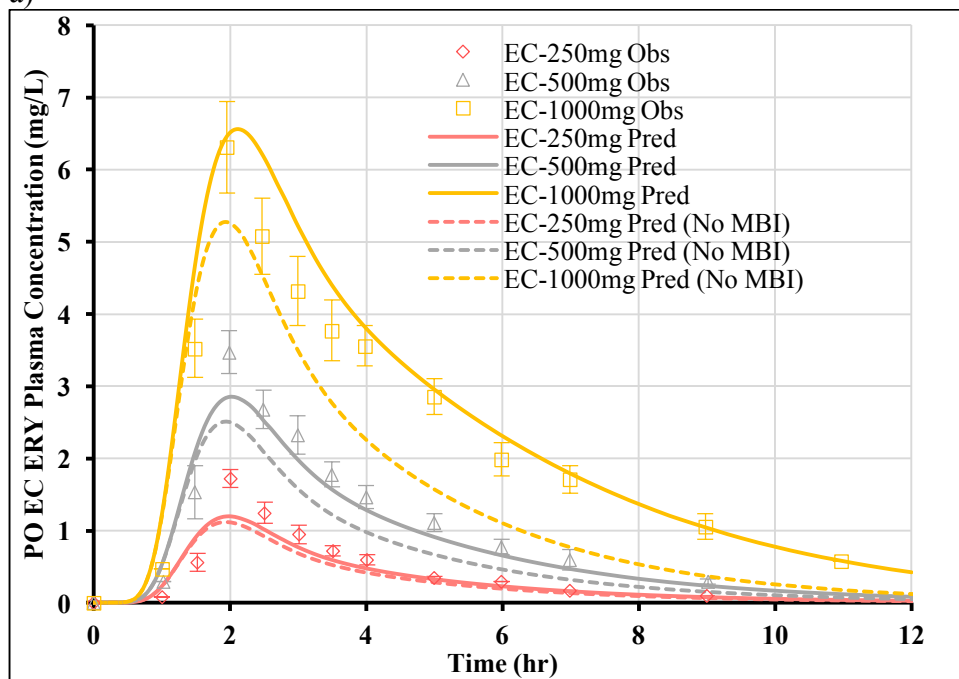


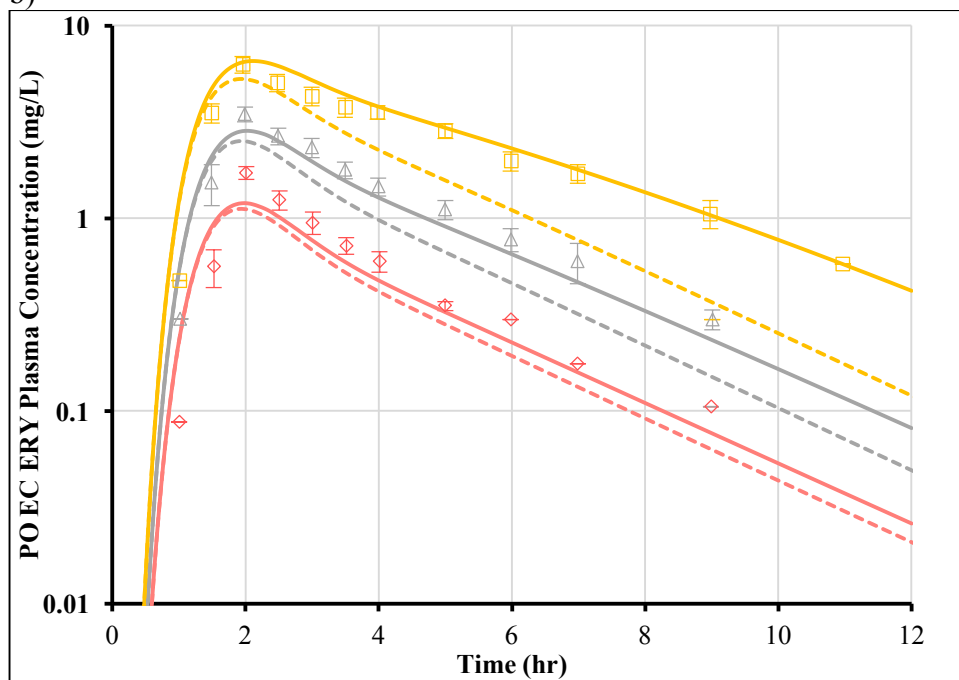
Figure 7.15 Observed and model-predicted ERY PK profiles after PO EC administration in study 620 (Cartesian and semi-log scales).
The solid lines are predicted PK profiles. The symbols and bars are observed means and SD values (if available). All parameters in PO EC ERY model were used the same values as IV ERY model.

After changing $v_{\max, \text{hep-3A}}^{\text{ERY}}$ and $v_{\max, \text{bile}}^{\text{ERY}}$, the adjusted PBPK model was used to predict PO EC ERY PK profiles after both single and multiple doses in studies 620, 623, 626 and 629. To demonstrate the importance of incorporating auto-inhibition of GW and hepatic CYP3A by ERY, predicted PK profiles in absence/presence of ERY auto-inhibition are both showed in **Figure 16a-d**, and exposure metrics are summarized in **Table 7.7** and **Table 7.8**. From **Figure 16** and **Table 7.8**, PBPK model without auto-inhibition (“No MBI” model) slightly underestimates ERY concentrations after single dose in study 620, and significantly underestimates ERY concentrations after repeat- doses, with predicted accumulation ratio at the last administered dose (R_{last}) for all three repeat- doses studies less than half of observed. After including auto- inhibition (“MBI” model), the PBPK model predicts ERY PK profiles reasonably well after both single- and repeat- doses, with deviations of AUC^{ERY} and c_{\max}^{ERY} , as well as accumulation ratio of AUC^{ERY} and c_{\max}^{ERY} , all less than 2-fold (ranged from -50% to 100%) of observed, except for study 629 (shown in **Table 7.7**).

a)



b)



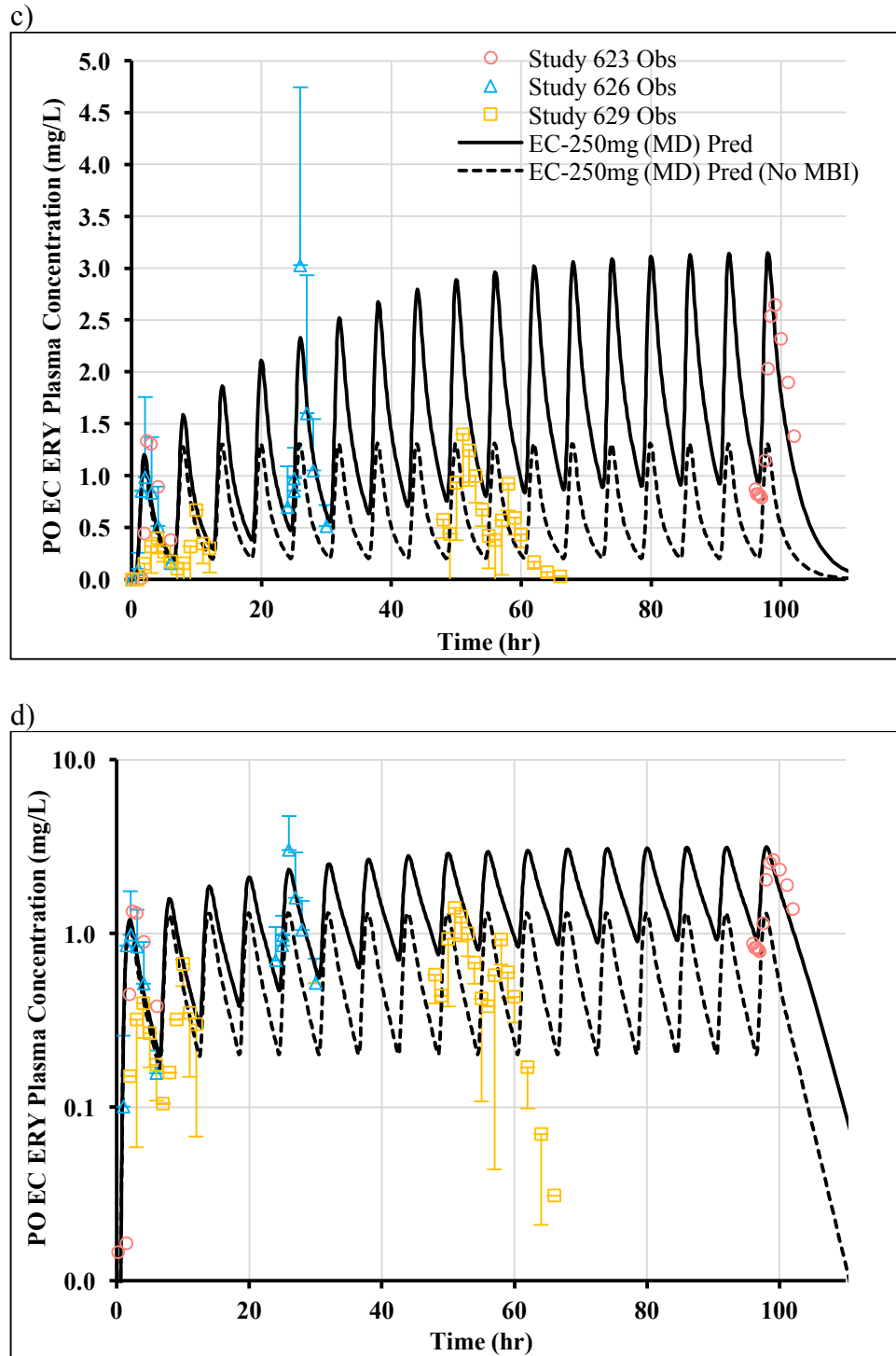


Figure 7.16 Observed and model-predicted ERY PK profiles after PO EC administration. a-b) PK profiles after 250 mg, 500 mg or 1000 mg single PO EC ERY in study 620 (Cartesian and semi-log plots) c-d) PK profiles after PO EC ERY 250 mg q6h for 17 doses (study 623), or 5 doses (study 626), or 10 doses (study 629) (Cartesian and semi-log plots). The solid lines are predicted PK profiles using PBPK model with auto-inhibition. The dash lines are predicted PK profiles using PBPK model without auto-inhibition (No MBI). The symbols and bars are observed means and SD values (if available).

For study 629, “MBI” model significantly over-estimates ERY PK profiles after both single and repeat- doses. Due to the large variation of systemic exposure for EC formulation (see **section 7.3.1**), $F_{\text{abs}}^{\text{ERY}}(\text{EC})$ was changed from 0.88 to 0.50 in study 629, which is within the 3.8-fold inter-study variability of PO ERY EC systemic exposure. After adjusting $F_{\text{abs}}^{\text{ERY}}(\text{EC})$ (**Figure 7.17**), the adjusted PBPK (“MBI”) model adequately captures PK profile of ERY in study 629 after the first two doses and the last dose, although some discrepancy in t_{max} is found, which can be easily improved by tweaking $k_{\text{GL}}^{\text{ERY}}$ further. The current model under-estimates ERY concentrations after the 9th dose, and observed data actually showed higher ERY levels after the 9th dose than the 10th dose, which cannot be reasonably explained. Since no discussion regarding this was provided in the literature, this phenomenon is considered as an artefact due to study error, and is ignored in visual predictive check. Deviations of AUC^{ERY} and $c_{\text{max}}^{\text{ERY}}$, as well as accumulation ratio of AUC^{ERY} and $c_{\text{max}}^{\text{ERY}}$, are also less than 2-fold of observed in study 629 after adjustment. All adjusted parameter values are presented in **Table 7.9**.

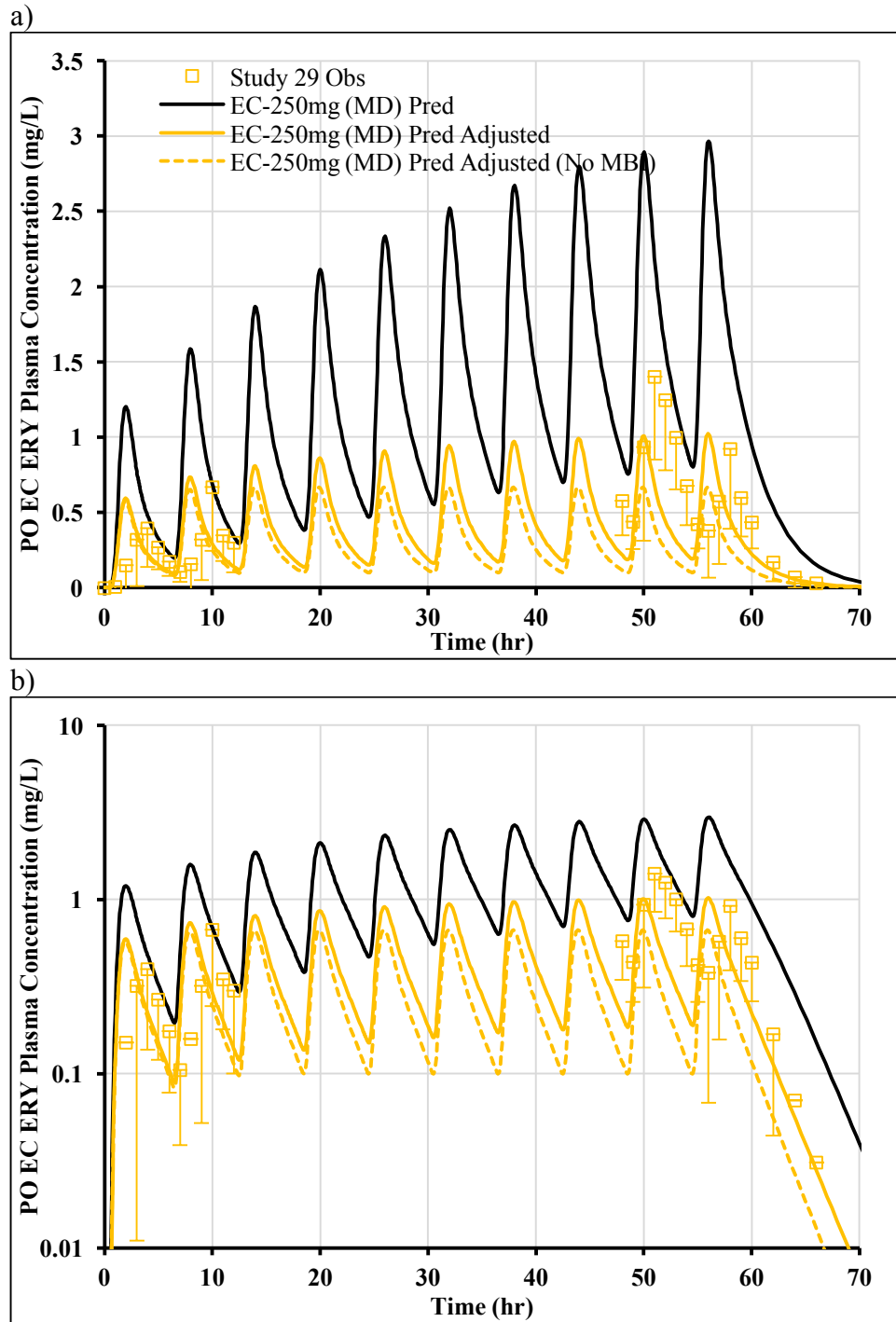


Figure 7.17 Observed and model-predicted ERY PK profiles after PO EC administration in study 629 (Cartesian and semi-log plots).

The black solid line represents predicted PK profile using original F_{abs}^{ERY} (EC) ($F_{abs}^{ERY} = 0.88$).
 The yellow solid line represents predicted PK profile using adjusted F_{abs}^{ERY} (EC) ($F_{abs}^{ERY} = 0.50$).
 The yellow dash line represents predicted PK profile using adjusted F_{abs}^{ERY} (EC) ($F_{abs}^{ERY} = 0.50$) by “No MBI” model. The symbols and bars are observed means and SD values (if available).

Table 7.7 Comparison of reported and semi-PBPK (“MBI”) model-predicted PO EC ERY plasma exposure metrics and accumulation ratios using PO ERY model (study 620, 623, 626) and adjusted model (study 629) parameters.

Deviations greater than 2-fold were marked as bold. ($v_{\max, \text{hep-3A}}^{\text{ERY}} = 800 \mu\text{g}/\text{min}/\text{kg}$; $v_{\max, \text{bile}}^{\text{ERY}} = 0.5 \mu\text{g}/\text{min}/\text{kg}$)

Study ID	Formulation	Dosing Regimen	Observed	Observed	Observed	Observed	Predicted	Predicted	Predicted	Predicted	Deviation	Deviation	Deviation	Deviation
			$^1\text{AUC}^{\text{ERY}}$ (mg/L•hr)	c_{\max}^{ERY} (mg/L)	R_{last} (AUC _{0-τ})	R_{last} (c _{max})	$^1\text{AUC}^{\text{ERY}}$ (mg/L•hr)	c_{\max}^{ERY} (mg/L)	R_{last} (AUC _{0-τ})	R_{last} (c _{max})	AUC ^{ERY} (%)	c_{\max}^{ERY} (%)	R_{last} (AUC _{0-τ} , %)	R_{last} (c _{max} , %)
620	Capsules of EC pellets	250mg SD	4.43	1.72			3.79	1.20			-14%	-30%		
620	Capsules of EC pellets	500mg SD	11.24	3.47			9.88	2.86			-12%	-18%		
620	Capsules of EC pellets	1000mg SD	26.88	6.31			29.19	6.55			9%	4%		
623	Capsules of EC pellets	250mg SD	3.80	1.74	2.84	1.65	3.16	1.20	3.54	2.62	-17%	-31%	25%	59%
623	Capsules of EC pellets	250mg q6h for 17 doses	10.80	2.87			11.19	3.15			4%	10%		
626	Capsules of EC pellets	250mg SD	3.02	0.98	2.62	3.09	3.16	1.20	2.38	1.94	5%	23%	-9%	-37%
626	Capsules of EC pellets	250mg q6h for 5 doses	7.92	3.03			7.51	2.33			-5%	-23%		
629	EC pellets	250mg SD	1.23	0.40	2.52	2.30	3.16	1.20	3.26	2.47	157%	200%	29%	7%
629	EC pellets	250mg q6h for 10 doses	3.45	0.92			10.30	2.97			199%	222%		
629	EC pellets	250mg SD (Adjust $F_{\text{abs}}^{\text{ERY}}$)	1.23	0.40	2.52	2.30	1.53	0.59	2.02	1.72	24%	48%	-20%	-25%
629	EC pellets	250mg q6h for 10 doses (Adjust $F_{\text{abs}}^{\text{ERY}}$)	3.45	0.92			3.09	1.02			-10%	11%		

¹ For Study 620, AUC_{0-∞}^{ERY} was summarized; for other studies, AUC_{0-τ}^{ERY} was summarized.

Table 7.8 Comparison of reported and semi-PBPK (“MBI” or “No MBI”) model-predicted accumulation ratio of $AUC_{0-\tau}$ after PO ERY EC or SS formulation.

Study ID	Formulation	Dosing Regimen	Observed R_{last} ($AUC_{0-\tau}$)	Predicted R_{last}		Deviation R_{last}	
				(MBI) ($AUC_{0-\tau}$)	(No MBI) ($AUC_{0-\tau}$)	(MBI) ($AUC_{0-\tau}$, %)	(No MBI) ($AUC_{0-\tau}$, %)
623	Capsules of EC pellets	250mg q6h for 17 doses	2.84	3.54	1.26	25%	-56%
626	Capsules of EC pellets	250mg q6h for 5 doses	2.62	2.38	1.26	-9%	-52%
629	EC pellets	250mg q6h for 10 doses	2.52	3.26	1.26	29%	-50%
629	EC pellets	250mg q6h for 10 doses (Adjust F_{abs}^{ERY})	2.52	2.02	1.26	-20%	-50%
615	SS capsules	250mg q6h for 5 doses	2.76	1.93	1.3	-30%	-53%
626	SS capsules	250mg q6h for 5 doses	3.75	1.93	1.3	-48%	-65%
627	SS film-coated tablet	250mg q6h for 9 doses	2.86	2.28	1.3	-20%	-55%
625	SS	1000mg q12h for 7 doses	0.96	3.15	1.03	230%	8%

Table 7.9 Adjusted semi-PBPK ERY model parameters.

Parameter	Definition	Value	Source
$V_{max, hep-3A}^{ERY}$ ($\mu\text{g}/\text{min}/\text{kg}$)	Capacity of hepatic CYP3A to metabolize ERY	800	Value used in PO ERY PBPK model optimized by PO EC and SS clinical studies
$V_{max, bile}^{ERY}$ ($\mu\text{g}/\text{min}/\text{kg}$)	Capacity of ERY biliary excretion	0.50	Value used in PO ERY PBPK model optimized by PO EC and SS clinical studies
F_{abs}^{ERY} (EC)	Fraction of ERY EC absorbed from gut lumen	0.50	Value used in study 629, based on visual predictive check.

7.3.6.2 Model Predictions

Model predicted $F_{\text{oral}}^{\text{ERY}}$, $F_{\text{abs}}^{\text{ERY}}$, $F_{\text{hep}}^{\text{ERY}}$ and $F_{\text{GI}}^{\text{ERY}}$ are plotted against PO EC ERY dose in **Figure 7.18**. $F_{\text{abs}}^{\text{ERY}}$ (EC) was set as 0.88, and unchanged with dose. To calculate $F_{\text{oral}}^{\text{ERY}}$, unbound blood AUC after 125 mg, 250 mg, 500 mg and 1000 mg IV ERY and PO EC ERY were simulated using IV and PO EC ERY semi-PBPK model, respectively. $V_{\text{max,hep-3A}}^{\text{ERY}}$ and $V_{\text{max,bile}}^{\text{ERY}}$ in IV ERY model were also set at 800 and 0.5 $\mu\text{g}/\text{min}/\text{kg}$, to avoid the influence of different hepatic clearance on systemic exposure. $F_{\text{oral}}^{\text{ERY}}$ was roughly estimated by the method introduced in **section 7.3.3**, in which the corresponding IV dose that produces the same $\text{AUC}_{0-\infty,\text{u}}^{\text{ERY}}$ as 125 mg/250 mg/500 mg/1000 mg PO EC ERY ($\text{Dose}_{\text{IV}}^{\text{ERY}}$) was predicted using a power model that could capture dose proportionality of IV ERY $\text{AUC}_{0-\infty,\text{u}}^{\text{ERY}}$ vs. $\text{Dose}_{\text{IV}}^{\text{ERY}}$ ($\text{AUC}_{0-\infty,\text{u}}^{\text{ERY}} = 0.0108 \cdot (\text{Dose}_{\text{IV}}^{\text{ERY}})^{1.0919}$). $\text{Dose}_{\text{IV}}^{\text{ERY}}$ was then divided by the corresponding PO EC ERY dose (125mg, 250 mg, 500 mg or 1000 mg) to come up with $F_{\text{oral}}^{\text{ERY}}$ estimation. Afterwards, $\text{ER}_{\text{GI}}^{\text{ERY}}$ was estimated by calculating the ratio of dose of ERY metabolized by GW metabolism (predicted by semi-PBPK model) and dose of ERY absorbed into GW (calculated by $F_{\text{abs}}^{\text{ERY}} \cdot \text{Dose}_{\text{PO}}^{\text{ERY}}$). $F_{\text{GI}}^{\text{ERY}}$ and $F_{\text{hep}}^{\text{ERY}}$ at each ERY dose were then derived by methods used in **Chapter 3, section 3.2.3.1**. From **Figure 7.18**, $F_{\text{oral}}^{\text{ERY}}$, $F_{\text{GI}}^{\text{ERY}}$ and $F_{\text{hep}}^{\text{ERY}}$ are all increased with PO EC ERY dose. Since $\text{ER}_{\text{GI}}^{\text{ERY}}$ is very low, $F_{\text{GI}}^{\text{ERY}}$ only slightly increases with ERY dose (93% at 125 mg and 97% at 1000mg), primarily caused by MBI on GW CYP3A. EC ERY has low-to-intermediate $\text{ER}_{\text{hep}}^{\text{ERY}}$ across doses, and its value at 1000 mg (27%) almost drops to half of that at 125 mg (49%), resulting in a 50% increase in $F_{\text{hep}}^{\text{ERY}}$ at the highest simulated dose compared to the lowest dose (51% at 125 mg vs. 73% at 1000 mg). This is due to saturable biliary excretion and MBI on hepatic CYP3A at the highest simulated dose. $F_{\text{oral}}^{\text{ERY}}$ is the multiplication of $F_{\text{abs}}^{\text{ERY}}$, $F_{\text{GI}}^{\text{ERY}}$ and $F_{\text{hep}}^{\text{ERY}}$, and as only a slight change with dose for $F_{\text{GI}}^{\text{ERY}}$ and constant with

dose for F_{abs}^{ERY} are observed, F_{oral}^{ERY} dose-dependency almost mimics F_{hep}^{ERY} dose-dependency, with a 50% increase at 1000 mg (62%) from 125 mg dose (41%). Our estimated F_{oral}^{ERY} across doses are higher than literature reported values (18%-45% (Somogyi et al., 1995)), probably because F_{oral}^{ERY} reported in literature was calculated by the traditional method, which is to take the ratio of total ERY (unbound + bound) $AUC_{0-\infty}^{ERY}$ after PO and IV administration, corrected by corresponding dose, assuming ERY follows linear PK. Given several nonlinear sources of ERY PK after both IV and PO administration, it is not feasible to use traditional method to estimate F_{oral}^{ERY} , and the F_{oral}^{ERY} we estimated (assuming same unbound AUC value produces the same extent of nonlinearity) is specifically for unbound ERY. Due to higher unbound plasma concentration after IV than the same dose of PO ERY, a larger fraction unbound is expected after IV ERY, therefore, F_{oral}^{ERY} for total ERY is expected to be smaller than unbound F_{oral}^{ERY} .

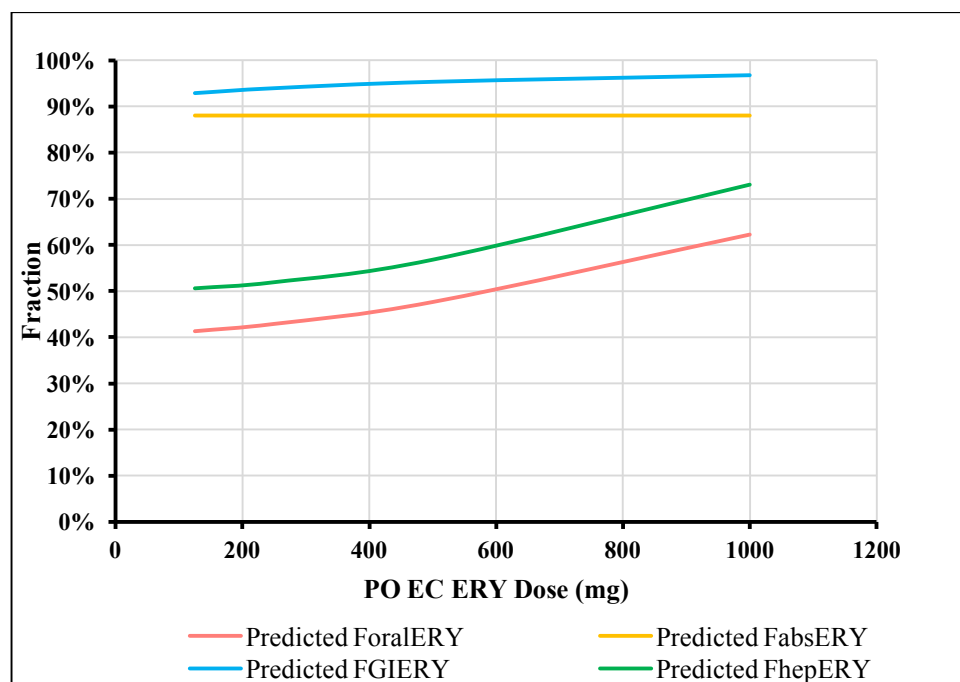


Figure 7.18 Model - predicted F_{oral}^{ERY} and different contribution of F_{oral}^{ERY} (F_{abs}^{ERY} , F_{hep}^{ERY} and F_{GI}^{ERY}) versus PO EC ERY dose (125 mg, 250 mg, 500 mg, 1000 mg).

Model predicted ERY unbound hepatic and GW mucosa concentrations after various PO EC single dose relative to $K_{m,bile}^{ERY}$, $K_{m,hep-3A}^{ERY}$ ($K_{m,GW-3A}^{ERY}$) and K_I^{ERY} are plotted in **Figure 7.19a-d**. It is clearly demonstrated in **Figure 7.19a-b** that biliary excretion of ERY is saturated even at the lowest dose, with $c_{hep,u}^{ERY}$ above $K_{m,bile}^{ERY}$ for ~2 hours, and at the highest dose (1000 mg), it is saturated more than 10 hours. However, CYP3A metabolism is not saturated across doses, with $c_{hep,u}^{ERY}$ less than $K_{m,hep-3A}^{ERY}$ throughout the entire profiles. MBI of CYP3A is also minor, as even $c_{max,hep,u}^{ERY}$ at 1000 mg dose is only 1/3 of K_I^{ERY} . To compare hepatic concentration – time profiles across doses, terminal phases after all single doses appear to be linear and parallel with each other, probably because saturation of biliary excretion mostly occurs before pseudo steady-state, which is difficult to tell from absorption/distribution phases. With respect to GW mucosa concentrations, $c_{max,GW-M,u}^{ERY}$ at 1000 mg dose exceeds K_I^{ERY} for ~0.5 hour, while GW CYP3A metabolism is also not saturated across doses, with $c_{GW-M,u}^{ERY}$ less than $K_{m,GW-3A}^{ERY}$ (assumed to be the same as $K_{m,GW-3A}^{ERY}$) throughout the entire profiles. To compare GW mucosa concentration – time profiles across doses, terminal phase after all single doses appear to be linear and parallel with each other, and decline much faster than hepatic unbound concentrations. This is because in our semi-PBPK model, PO ERY can only be unidirectional carried from GW mucosa to GW serosa, so that drug cannot enter GW mucosa via vascular blood stream (systemically). Therefore, no pseudo steady-state is reached between plasma and GW mucosa, and the terminal phase of GW mucosa concentration is determined by k_{GL}^{ERY} (0.06 min^{-1}), which is much larger than the derived k_e (0.006 min^{-1}) from ~2 hours-plasma $t_{1/2}$. GW mucosa concentrations peak higher and earlier than hepatic concentrations, owing to different inflow and outflow rate of drug transfer in the two tissues. Full simulations of dose-dependent MBI on hepatic and GW CYP3A levels by PO EC ERY will be presented and

discussed in Chapter 8.

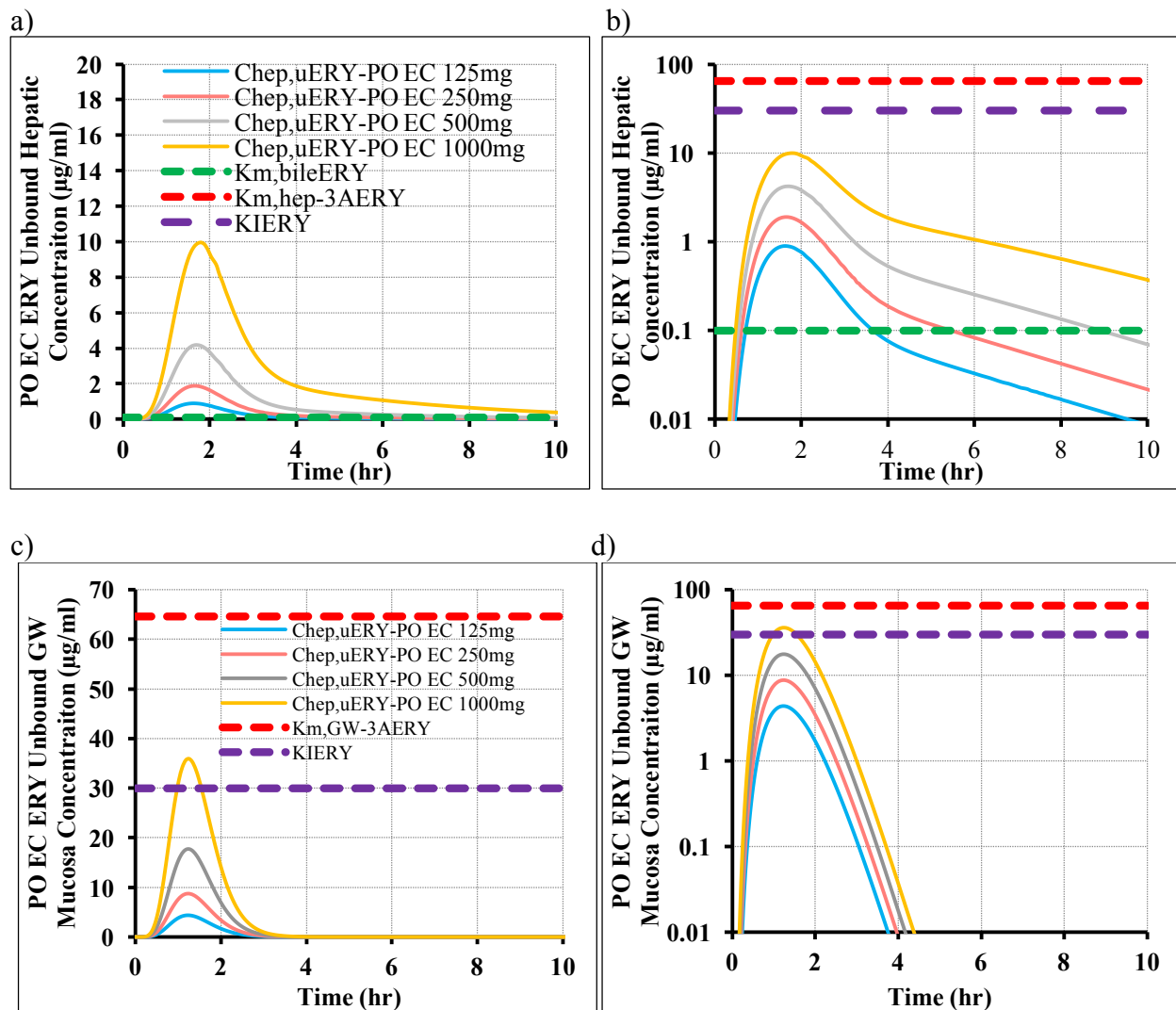


Figure 7.19 Model-predicted unbound ERY concentrations in liver and GW mucosa after 125mg, 250mg, 500mg, 1000mg single PO EC ERY dose relative to $K_{m,bile}^{ERY}$, $K_{m,hep-3A}^{ERY}$ ($K_{m,GW-3A}^{ERY}$) and K_I^{ERY} .

a-b) Unbound ERY hepatic concentration – time profiles (Cartesian and semi-log plots) relative to $K_{m,bile}^{ERY}$, $K_{m,hep-3A}^{ERY}$ and K_I^{ERY} . c-d) Unbound ERY GW mucosa concentration – time profiles (Cartesian and semi-log plots) relative to $K_{m,GW-3A}^{ERY}$ and K_I^{ERY} .

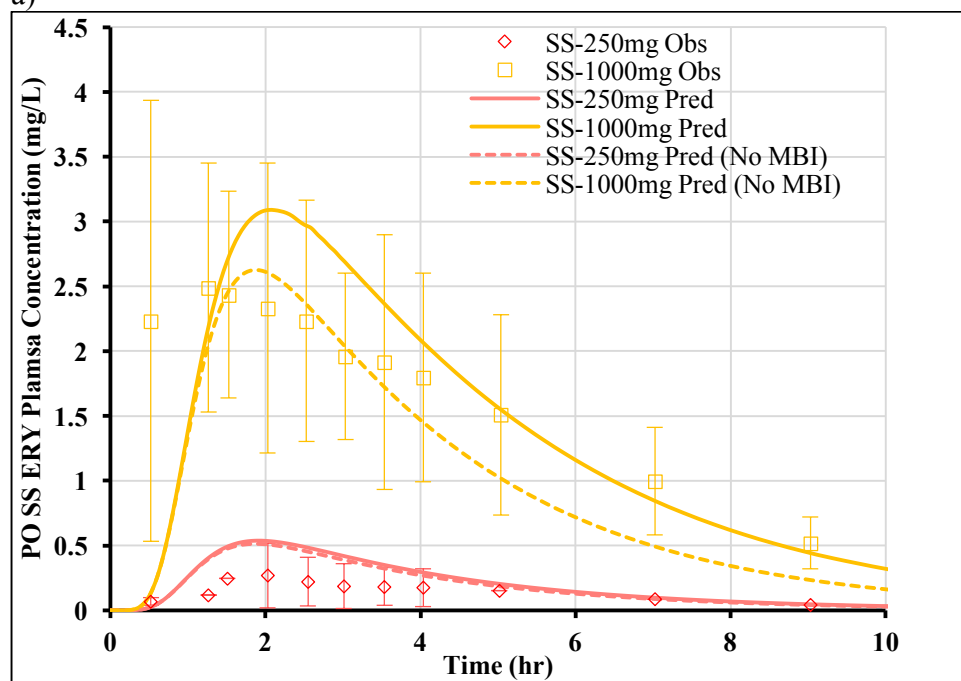
7.3.7 ERY semi-PBPK model after single/repeat- PO doses (ERY stearate salt tablet formulation)

7.3.7.1 Predictive performance check

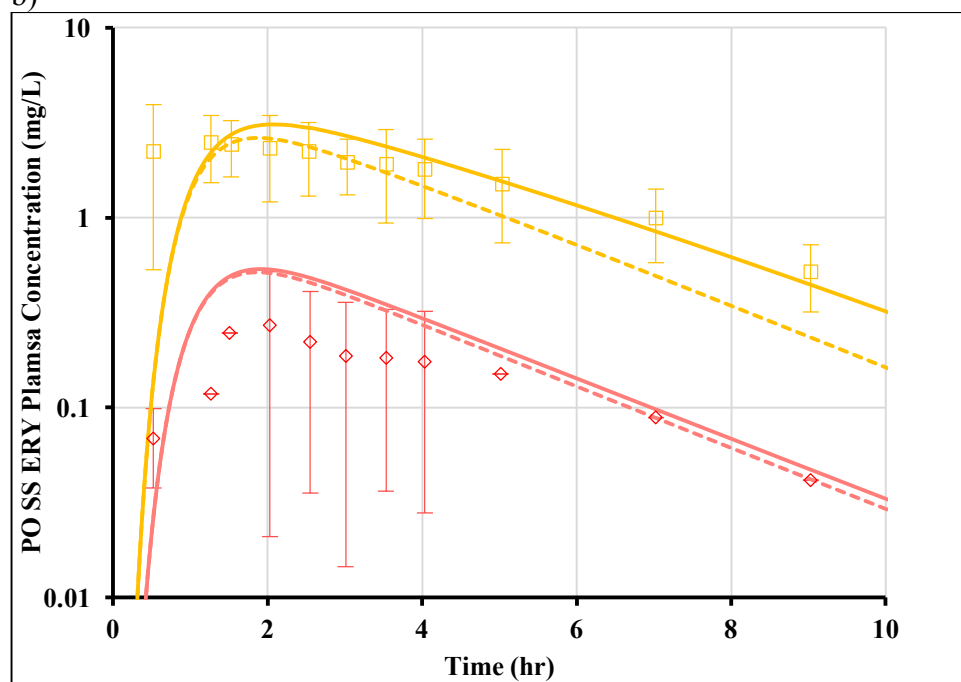
The same $v_{\max, \text{hep-3A}}^{\text{ERY}}$ (800 $\mu\text{g}/\text{min}/\text{kg}$) and $v_{\max, \text{bile}}^{\text{ERY}}$ (0.5 $\mu\text{g}/\text{min}/\text{kg}$) as PO EC ERY model were used in semi-PBPK model for PO SS ERY, to predict its PK profiles after both single- and repeat- doses in studies 604, 615, 626, 627 and 625. PO SS ERY was administered as 250 mg q6h in study 615, 626 and 627, and in study 625, 1000 mg PO SS ERY was given q12h. To demonstrate the importance of incorporating auto-inhibition of GW and hepatic CYP3A by ERY, predicted PK profiles in absence/presence ERY auto-inhibition are both showed in **Figure 7.20a-f**, and exposure metrics are summarized in **Table 7.8** and **Table 7.10**. From **Figure 7.20** and **Table 7.8**, PBPK model without auto-inhibition (“No MBI” model) slightly under-estimates ERY concentrations after single dose in study 604, and significantly underestimates ERY concentrations after multiple doses, with predicted accumulation ratio at the last administration dose (R_{last}) for all four multiple doses studies less than half of observed, except for study 625. After including CYP3A auto-inhibition (“MBI” model), the PBPK model predicts ERY PK profiles reasonably well after both single and repeat- doses, with deviations of AUC^{ERY} and c_{\max}^{ERY} , as well as accumulation ratio of AUC^{ERY} and c_{\max}^{ERY} , all less than 2-fold (ranged from - 50% to 100%) of observed, except for deviation (%) of repeated dose c_{\max}^{ERY} in study 627 and R_{last} in study 629 (shown in **Table 7.10**). In study 604, predicted PK profiles after single 250 mg and 1000 mg SS ERY didn’t match with observed perfectly, but given large SD of observed data (not a crossover study), the predicted profiles well-capture the terminal phase and balance the absorption delay of the two doses (observed profile after 250 mg demonstrated a delay in rising phase, while profiles after 1000 mg didn’t), with deviation of exposure metrics and accumulation

within predefined requirement. For study 627, c_{\max}^{ERY} after multiple is largely under-estimated, however, since c_{\max}^{ERY} after single dose is also under-estimated (to a less extent) and there were large SDs of observed data, the model predictions are still considered acceptable. Regarding study 625, no accumulation was demonstrated from observed profiles, while MBI model predicts a 2-fold accumulation ratio in AUC. For this study, “No MBI” model actually provides better estimation of observed accumulation ratios. This could be explained as ERY in this study has higher K_I^{ERY} or lower $k_{\text{inact}}^{\text{ERY}}$ (K_I^{ERY} ranged from 1-80 mg/L *in-vitro*, but used as 30 mg/L in the model; $k_{\text{inact}}^{\text{ERY}}$ ranged from 0.017 – 0.066 min^{-1} *in-vitro*, but used as 0.0375 min^{-1} in the model) and/or shorter k_{deg} (k_{deg} ranged from 8×10^{-5} and 1.15×10^{-3} min^{-1} *in-vitro*, but used as 8×10^{-3} min^{-1} in the model) than other studies.

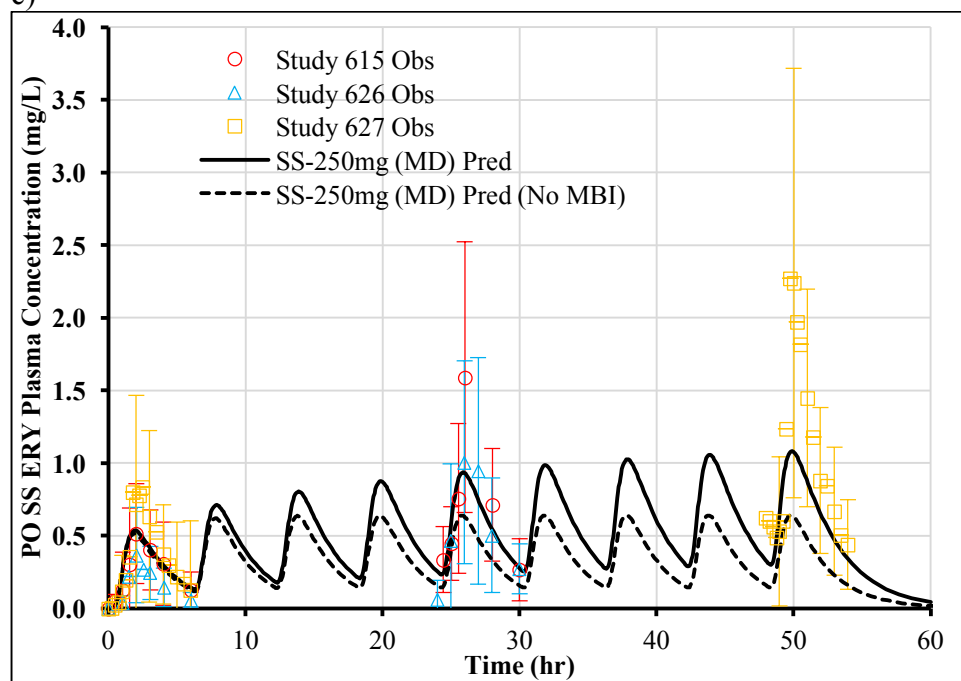
a)



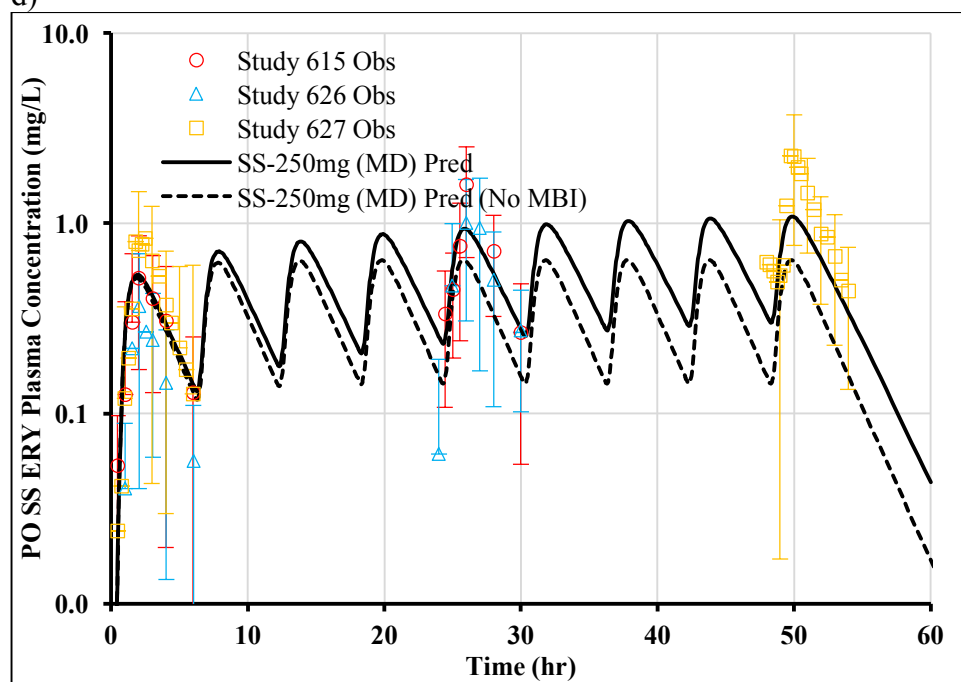
b)



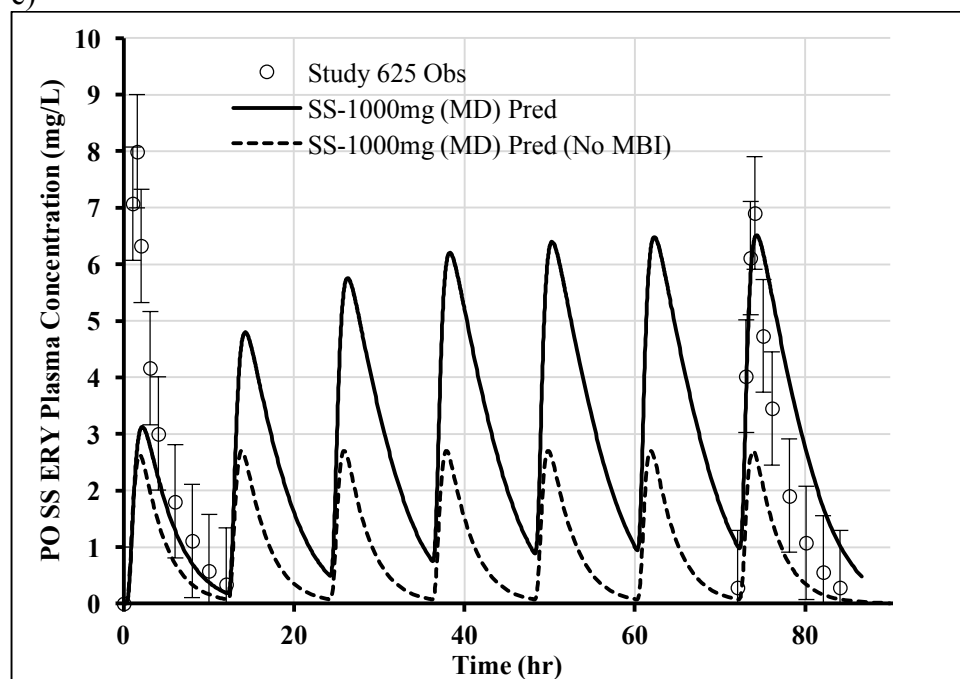
c)



d)



e)



f)

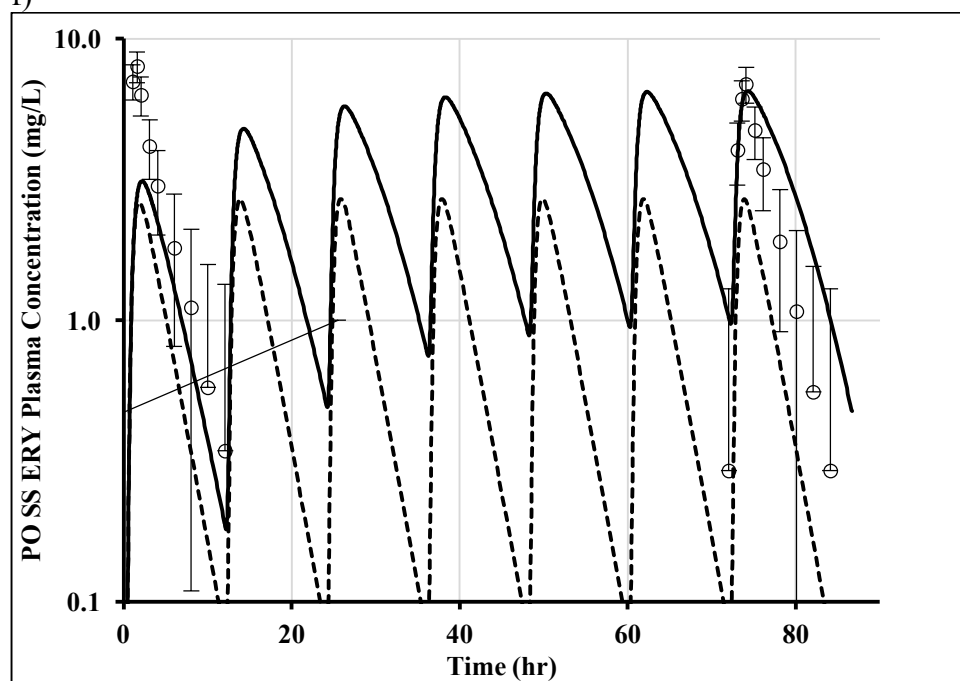


Figure 7.20 Observed and model-predicted ERY PK profiles after PO SS administration. a-b) PK profiles after 250 mg or 1000 mg single PO SS ERY in study 604 (Cartesian and semi-log plots) c-d) PK profiles after PO SS ERY 250 mg q6h for 5 doses (study 615 and 626), or 9 doses (study 627) (Cartesian and semi-log plots). e-f) PK profiles after PO SS ERY 1000 mg q12h for 7 doses (study 625) (Cartesian and semi-log plots). The solid lines are predicted PK profiles using PBPK model with auto-inhibition. The dash lines are predicted PK profiles using PBPK model without auto-inhibition (No MBI). The symbols and bars are observed means and SD values (if available).

Table 7.10 Comparison of reported and semi-PBPK (“MBI”) model-predicted PO SS ERY plasma exposure metrics and accumulation ratios using PO ERY model parameters.

Deviations greater than 2-fold were marked as bold. ($v_{\max, \text{hep-3A}}^{\text{ERY}} = 800 \mu\text{g}/\text{min}/\text{kg}$; $v_{\max, \text{bile}}^{\text{ERY}} = 0.5 \mu\text{g}/\text{min}/\text{kg}$)

Study ID	Formulation	Dosing Regimen	Observed *AUC ^{ERY} (mg/L•hr)	Observed c _{max} ^{ERY} (mg/L)	Observed R _{last} (AUC _{0-τ})	Observed R _{last} (c _{max})	Predicted *AUC ^{ERY} (mg/L•hr)	Predicted c _{max} ^{ERY} (mg/L)	Predicted R _{last} (AUC _{0-τ})	Predicted R _{last} (c _{max})	Deviation AUC ^{ERY} (%)	Deviation c _{max} ^{ERY} (%)	Deviation R _{last} (AUC _{0-τ}) (%)	Deviation R _{last} (c _{max}) (%)
604	SS film-coated tablet	250mg SD	1.36	0.27			2.17	0.54			59%	98%		
604	SS film-coated tablet	1000mg SD	16.15	2.49			14.94	3.09			-7%	24%		
615	SS capsules	250mg SD	1.61	0.51	2.76	3.12	1.78	0.54	1.93	1.75	10%	5%	-30%	-44%
615	SS capsules	250mg q6h for 5 doses	4.44	1.59			3.44	0.94			-23%	-41%		
626	SS capsules	250mg SD	0.92	0.37	3.75	2.70	1.78	0.54	1.93	1.75	93%	45%	-48%	-35%
626	SS capsules	250mg q6h for 5 doses	3.45	1.00			3.44	0.94			0%	-6%		
627	SS film-coated tablet	250mg SD	2.19	0.80	2.86	2.84	1.78	0.54	2.28	2.02	-19%	-33%	-20%	-29%
627	SS film-coated tablet	250mg q6h for 9 doses	6.26	2.27			4.06	1.08			-35%	-52%		
625	SS	1000mg SD	30.27	7.99	0.96	0.86	14.47	3.09	3.15	2.20	-52%	-61%	230%	155%
625	SS	1000mg q12h for 7 doses	28.93	6.90			45.58	6.79			58%	-2%		

¹ For Study 604, AUC_{0-∞}^{ERY} was summarized; for other studies, AUC_{0-τ}^{ERY} was summarized.

7.3.7.2 Model Predictions

Model predicted $F_{\text{oral}}^{\text{ERY}}$, $F_{\text{abs}}^{\text{ERY}}$, $F_{\text{hep}}^{\text{ERY}}$ and $F_{\text{GI}}^{\text{ERY}}$ are plotted against PO SS ERY dose in **Figure 7.21**. $F_{\text{abs}}^{\text{ERY}}$ (SS) was set as 0.59, and unchanged with dose. To calculate $F_{\text{oral}}^{\text{ERY}}$, unbound blood AUC after 125 mg, 250 mg, 500 mg and 1000 mg IV ERY and PO EC ERY were simulated using IV and PO SS ERY semi-PBPK model, respectively. $v_{\text{max,hep-3A}}^{\text{ERY}}$ and $v_{\text{max,bile}}^{\text{ERY}}$ in IV ERY model were also set at 800 and 0.5 $\mu\text{g}/\text{min}/\text{kg}$, to avoid the influence of different hepatic clearance on systemic exposure. $F_{\text{oral}}^{\text{ERY}}$ was roughly estimated by the method introduced in **section 7.3.3**, in which the corresponding IV dose that produces the same $\text{AUC}_{0-\infty,\text{u}}^{\text{ERY}}$ as 125 mg/250 mg/500 mg/1000 mg PO SS ERY ($\text{Dose}_{\text{IV}}^{\text{ERY}}$) was predicted using a power model that could capture dose proportionality of IV ERY $\text{AUC}_{0-\infty,\text{u}}^{\text{ERY}}$ vs. $\text{Dose}_{\text{IV}}^{\text{ERY}}$ ($\text{AUC}_{0-\infty,\text{u}}^{\text{ERY}} = 0.0108 \cdot (\text{Dose}_{\text{IV}}^{\text{ERY}})^{1.0919}$). $\text{Dose}_{\text{IV}}^{\text{ERY}}$ was then divided by the corresponding PO SS ERY dose (125mg, 250 mg, 500 mg or 1000 mg) to come up with $F_{\text{oral}}^{\text{ERY}}$ estimation. Afterwards, $\text{ER}_{\text{GI}}^{\text{ERY}}$ was estimated by calculating the ratio of dose of ERY metabolized by GW metabolism (predicted by PBPK model) and dose of ERY absorbed into GW (calculated by $F_{\text{abs}}^{\text{ERY}} \cdot \text{Dose}_{\text{PO}}^{\text{ERY}}$). $F_{\text{GI}}^{\text{ERY}}$ and $F_{\text{hep}}^{\text{ERY}}$ at each ERY dose were then derived by methods used in **Chapter 3, section 3.2.3.1**. From **Figure 7.21**, $F_{\text{oral}}^{\text{ERY}}$, $F_{\text{GI}}^{\text{ERY}}$ and $F_{\text{hep}}^{\text{ERY}}$ are all increased with PO EC ERY dose. Since $\text{ER}_{\text{GI}}^{\text{ERY}}$ is very low, and MBI on GW CYP3A is less than EC formulation -due to lower $F_{\text{abs}}^{\text{ERY}}$ for SS-, $F_{\text{GI}}^{\text{ERY}}$ is almost constant with dose (91%-92%). SS ERY has intermediate $\text{ER}_{\text{hep}}^{\text{ERY}}$ across doses (50% at 125 mg and 40% at 1000 mg), resulting in slightly higher $F_{\text{hep}}^{\text{ERY}}$ at 1000 mg (60%) than at 125 mg (50%). Compared with EC formulation, SS ERY has similar $F_{\text{hep}}^{\text{ERY}}$ after 125 mg, but lower $F_{\text{hep}}^{\text{ERY}}$ after 1000 mg, because less saturation in biliary excretion and less auto-inhibition on hepatic CYP3A occurs after SS formulation, due to lower hepatic ERY concentration (see **Figure 7.22**). Primarily because of

lower F_{abs}^{ERY} (SS), F_{oral}^{ERY} (SS) is less than F_{oral}^{ERY} (EC) across doses, but F_{oral}^{ERY} (SS) has less dose-dependency, ranging from 27% at the lowest to 33% at the highest simulated dose.

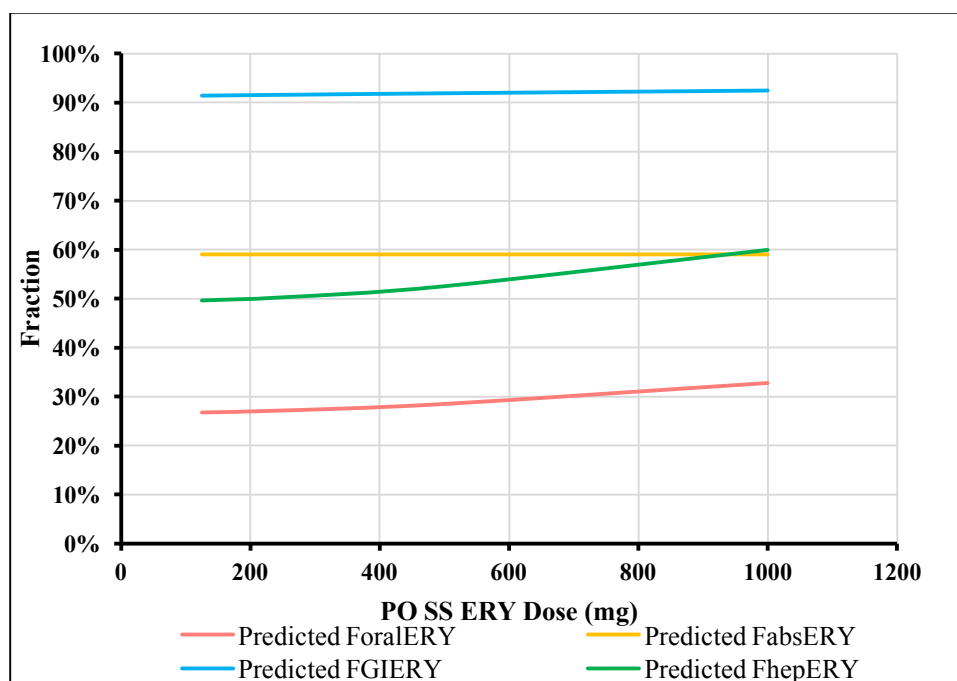


Figure 7.21 Model - predicted F_{oral}^{ERY} and different contribution of F_{oral}^{ERY} (F_{abs}^{ERY} , F_{hep}^{ERY} and F_{GI}^{ERY}) versus PO SS ERY dose (125 mg, 250 mg, 500 mg, 1000 mg).

Model predicted ERY unbound hepatic and GW mucosa concentrations after various PO SS single dose relative to $K_{m,bile}^{ERY}$, $K_{m,hep-3A}^{ERY}$ ($K_{m,GW-3A}^{ERY}$) and K_I^{ERY} are plotted in **Figure 7.22a-d**. It is clearly demonstrated in **Figure 7.22a-b** that biliary excretion of ERY is saturated even at the lowest dose, with $c_{hep,u}^{ERY}$ above $K_{m,bile}^{ERY}$ for ~3 hours, and at the highest dose (1000 mg), it is saturated up to 10 hours. CYP3A metabolism and MBI are almost linear, due to much lower $c_{hep,u}^{ERY}$ than $K_{m,hep-3A}^{ERY}$ and K_I^{ERY} throughout the entire profiles. To compare hepatic concentration – time profiles across doses, terminal phase after all single doses appear to be linear and parallel with each other. With respect to GW mucosa concentrations, $c_{GW-M,u}^{ERY}$ is less than $K_{m,GW-3A}^{ERY}$ and K_I^{ERY} throughout the entire profiles, reflecting negligible GW CYP3A saturation and MBI. To compare GW mucosa concentration – time profiles across doses,

terminal phase after all single doses appear to be linear and parallel with each other, and decline much faster than hepatic unbound concentrations. This is because in our semi-PBPK model, PO ERY can only be unidirectional carried from GW mucosa to GW serosa, and drug cannot enter GW mucosa via vascular blood stream (systemically). Therefore, no pseudo steady-state is reached in GW mucosa concentrations, and the terminal phase of GW mucosa concentration is determined by k_{GL}^{ERY} (0.018 min^{-1}), which is larger than the derived k_e (0.006 min^{-1}) from ~ 2 hours-plasma $t_{1/2}$. GW mucosa concentrations peak higher and earlier than hepatic concentrations, owing to different inflow and outflow rate of drug transfer in the two organs.

To compare hepatic and GW mucosa concentration after different ERY PO formulations, SS consistently has lower concentrations than EC at the same ERY dose (base equivalent), due to lower F_{abs}^{ERY} after SS. Terminal decline of GW mucosa concentrations after SS is shallower than that after EC, because rate constant that determined permeating into GW mucosa (k_{GL}^{ERY}) for SS is slower than EC in their respective semi-PBPK models. Full simulations of dose-dependent MBI on hepatic and GW CYP3A levels by PO SS ERY will be presented and discussed in **Chapter 8**.

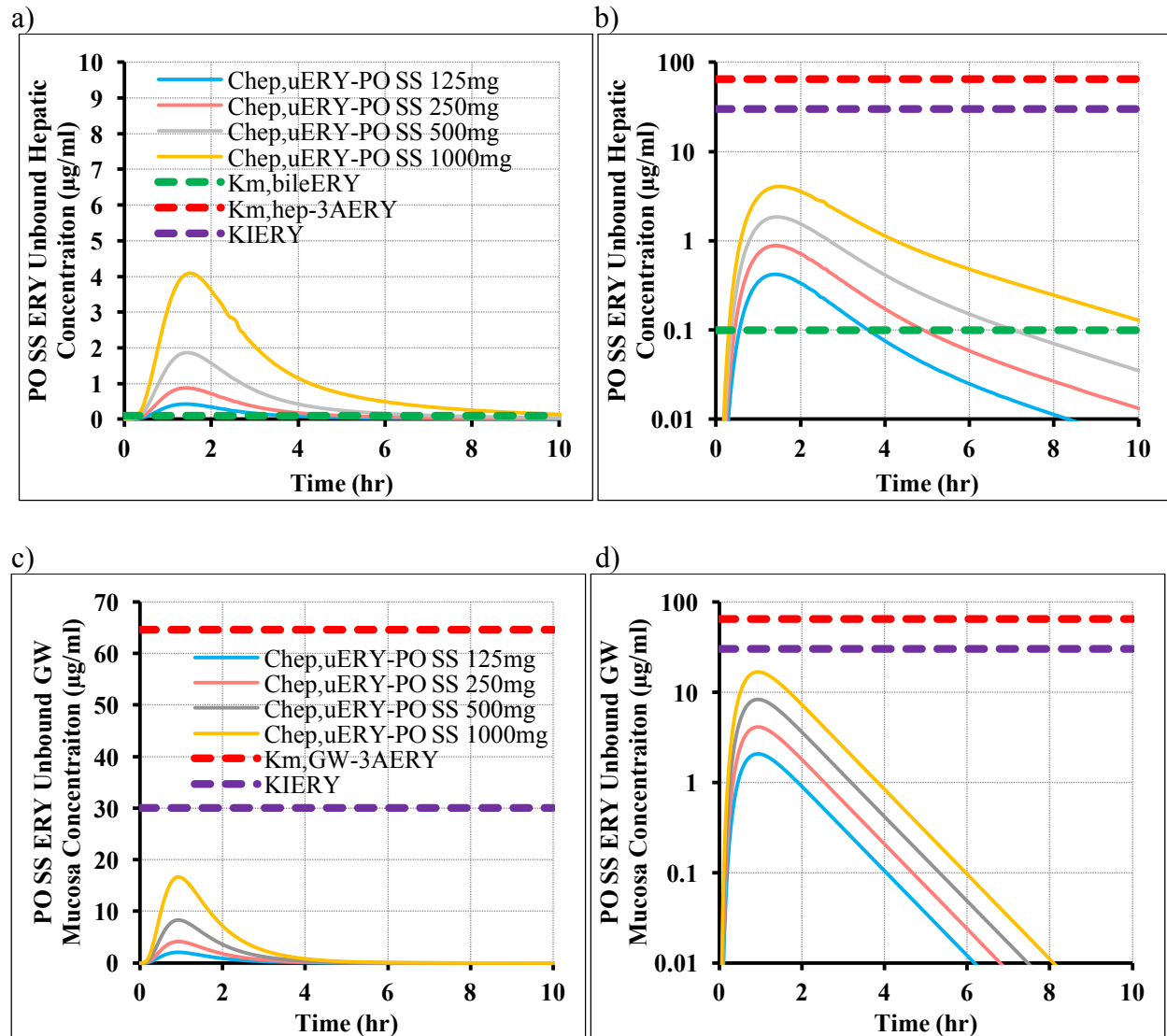


Figure 7.22 Model-predicted unbound ERY concentrations in liver and GW mucosa after 125mg, 250mg, 500mg, 1000mg single PO EC ERY dose relative to $K_{m,bile}^{ERY}$, $K_{m,hep-3A}^{ERY}$ ($K_{m,GW-3A}^{ERY}$) and K_I^{ERY} .

a-b) Unbound ERY hepatic concentration – time profiles (Cartesian and semi-log plots) relative to $K_{m,bile}^{ERY}$, $K_{m,hep-3A}^{ERY}$ and K_I^{ERY} . c-d) Unbound ERY GW mucosa concentration – time profiles (Cartesian and semi-log plots) relative to $K_{m,GW-3A}^{ERY}$ and K_I^{ERY} .

7.4 Conclusions

ERY semi-PBPK models were developed to describe its clinical PK after IV and PO administration, with several nonlinear PK processes incorporated. In IV ERY model, saturable plasma protein binding was described by a sigmoidal/linear model; hepatic CYP3A metabolism and biliary excretion were characterized by two Michaelis-Menten equations; saturable tubular reabsorption was captured by an empirical hyperbolic model. ERY PO semi-PBPK model was specifically developed in EC and SS formulations. All nonlinear PK processes in IV model also exist in PO ERY semi-PBPK model, except for saturable tubular reabsorption. GW metabolism was described by a Michaelis-Menten equation after PO ERY. In both IV and PO ERY models, auto-inhibition on its own hepatic/GW CYP3A activity was considered to better predict ERY plasma PK profiles, especially after repeat-doses. IV semi-PBPK model was validated by several clinical PK studies of ERY after single dose, and PO semi-PBPK models for EC and SS were validated by both SAD studies and repeat-doses studies. After parameter optimization, plasma concentration – time profiles, exposure metrics, available clearances ($CL_{ren,p}^{ERY}$, $CL_{nonren,p}^{ERY}$, $CL_{total,p}^{ERY}$) and accumulation ratios at the last dose can be mostly predicted well by the models, with auto-inhibition incorporated. However, if auto-inhibition was not considered, observed accumulation ratios of exposure metrics were consistently underestimated. Additional simulations using IV ERY model show that biliary excretion is easily saturated across clinical relevant doses, while CYP3A metabolism is almost not saturated. Auto-inhibition on hepatic CYP3A after single dose is limited, but keeps for a long time. At the lowest simulated ERY dose (125 mg), biliary excretion is the predominant elimination pathway, while with increasing dose, more drugs shift to CYP3A metabolism pathway to get cleared, and at the highest simulated IV dose (900 mg), CYP3A metabolism becomes the major elimination route. $CL_{int,bile}^{ERY}$, $CL_{int,hep-}$

F_{3A}^{ERY} and ER_{hep}^{ERY} vs. time profiles are affected by both saturation in biliary excretion and auto-inhibition on hepatic CYP3A. Additional simulations using PO ERY model show that EC formulation has moderate dose-dependent absorption due to saturable hepatobiliary (but not GW) extraction and auto-MBI on CYP3A. SS formulation exhibits less dose-dependent absorption than EC, due to relatively low hepatic/GW concentrations. F_{oral}^{ERY} (EC) is higher than F_{oral}^{ERY} (SS), primarily because of difference in fraction absorbed into GW. For both formulations, GW mucosa concentrations peak higher and earlier, but decline faster than hepatic concentrations - suggesting that the magnitude and time course of metabolic CYP3A inhibition by ERY in GW and liver are different and formulation-dependent. MDZ and ERY DDI model will be developed in the future based on this model.

CHAPTER 8

8 SEMI-PBPK MODELING OF METABOLIC INHIBITION BETWEEN IV/PO ERY AND IV/PO MDZ

8.1 Background and Objectives

8.1.1 Available DDI studies

As mentioned in **Chapter 7**, two studies (study 28 and 603) were finally chosen to validate for MDZ and ERY DDI semi-PBPK model: in study 28, interaction between ERY and MDZ was investigated in two double-blind, randomized, crossover studies. In the first study, 12 healthy (3 males, 9 females) volunteers were given 500 mg ERY TID as EC formulation or placebo for 1 week, and PO MDZ (15 mg) was administered on the 6th day (2 hours) after the 2nd dose of ERY or placebo. In the second study, IV MDZ (0.05 mg/kg) was given to 6 of the same subjects after similar ERY/placebo pretreatment. Plasma concentrations of MDZ in absence/presence of ERY were measured in both studies, and a single ERY plasma concentration at the time point when MDZ was administered was provided. Thus, study 28 was used to validate the DDI model for IV/PO MDZ and PO EC ERY.

In study 603, 12 healthy male volunteers participated in the randomized, 4 × 4 Latin square design study. The PK of PO MDZ was assessed under four conditions: (1) EM0: PO MDZ (5 mg) single dose without ERY (2) EM2: ERY SS 200 mg QID for 2 days + PO MDZ (2.5 mg) single

dose on day 2 (3) EM4: ERY SS 200 mg QID for 4 days + PO MDZ (2.5 mg) single dose on day 4 (4) EM7: ERY SS 200 mg QID for 7 days + PO MDZ (2.5 mg) single dose on day 7. MDZ was administered one hour after the 1st dose of ERY for EM2, EM4, EM7 on day 2, 4, or 7, respectively. This study was used to validate the time course of DDI between PO MDZ and PO SS ERY after different ERY treatment periods, which specifically helps confirming the MBI inhibitory parameters of ERY.

After comprehensive literature search, no IV ERY and MDZ DDI studies could be found; thus, MDZ and IV ERY DDI PBPK model could not be validated.

The reported MDZ PK profiles and exposure metrics in absence/presence of repeat- PO ERY doses were compared with model-predicted profiles/exposure metrics, in order to qualify the model.

8.1.2 ERY MBI information and simulation strategies

ERY is a mechanism-based (MBI) CYP3AI with low $F_{\text{oral}}^{\text{ERY}}$ (18% - 45%) (Somogyi et al., 1995), primarily hepatically metabolized and excreted into bile with a short $t_{1/2}$ (1.5-2 hours) (Austin et al., 1980). After IV administration, hepatic CYP3A metabolism is assumed to be the only elimination pathway for MDZ, thus the magnitude and time course of DDI are expected to be determined by ERY unbound hepatic concentration over time, relative to K_i^{ERY} , as well as the endogenous synthesis and degradation rates of hepatic CYP3A. After PO administration, MDZ is subject to both GW and hepatic metabolism pre-systemically, as well as systemic hepatic metabolism. Hence, the unbound ERY concentration – time profiles in both GW mucosa and liver, relative to K_i^{ERY} , as well as endogenous synthesis and degradation rates of hepatic and GW CYP3A activity, govern the magnitude and time course of ERY inhibition. Owing to the low-intermediate $F_{\text{oral}}^{\text{ERY}}$ after different PO formulations (~60% after 1,000 mg EC ERY and ~30%

after 1,000 mg SS ERY), the hepatic ERY concentration after IV administration are expected to be greater than after PO formulations, leading to more inhibition on MDZ hepatic metabolism after IV ERY. After PO MDZ, both hepatic and GW metabolism (as ERY reaches the enterocytes from the gut lumen) can be inhibited, and GW mucosa concentrations after PO ERY are consistently higher than that after IV ERY (= 0), leading to greater GW CYP3A inhibition after PO ERY. Albeit the short plasma $t_{1/2}$ of ERY, the duration of the DDI is expected to be prolonged, because as a MBI, the duration of metabolic inhibition is determined by turn-over kinetics of CYP3A rather than the PK of ERY. Meanwhile, maximal magnitude of DDI should occur when hepatic or GW CYP3A activity achieves its nadir, rather than the time when tissue concentration peak.

In addition, the impact of route of administration for either MDZ or ERY is also affected by dose/dosing interval of ERY (dose-dependent) and administration time interval between MDZ and ERY (time-dependent). Simulations were performed to assess dose- and time-dependency of route difference in DDI by varying IV/PO ERY doses and dosing intervals after different administration time prior to simulated doses of IV/PO MDZ. Sensitivity analysis was also performed on PK/MBI parameters in the DDI semi-PBPK model, to identify pivotal parameters that determine MDZ or ERY exposure metrics.

Finally, hypothetical CYP3AI and CYP3A substrates were created, based on ERY and MDZ semi-PBPK models, to assess the impact of F_{oral} for a CYP3A MBI, and GW and hepatic metabolism for a CYP3A substrate on the magnitude and time course of route-dependent DDI.

8.1.3 Objectives

The major objectives of the chapter were to:

- a. Develop a semi-PBPK DDI model between MDZ and ERY, to describe IV/PO MDZ PK

profiles in presence of IV/PO (single-/repeat- doses) ERY.

- b. Validate the model using MDZ plasma concentration-time profiles and plasma exposures in presence of PO repeat- doses of ERY in clinical DDI studies.
- c. Identify pivotal PK/MBI parameters that determine MDZ plasma exposure metrics in presence of ERY, and ERY hepatic/GW mucosa exposure metrics after single and repeat- doses by sensitivity analysis.
- d. Assess the impact of route of administration for MDZ and ERY on the magnitude and time course of their metabolic DDI after various administration time intervals between the two drugs.
- e. Assess the impact of route of administration for MDZ and ERY on the magnitude and time course of their metabolic DDI after various single- and repeat- dosing regimens of ERY.
- f. Explore route-dependent DDI between MDZ and a hypothetical CYP3A MBI with higher F_{oral} (than ERY) and between two hypothetical CYP3A substrates with GW or hepatic metabolism removed or reduced and ERY.
- g. Predict profiles of ERY concentrations and relative CYP3A activity in GW and liver for all simulations for a better mechanistic understanding.

8.2 Methods

8.2.1 Development of MDZ-ERY DDI PBPK model

8.2.1.1 DDI PBPK model/model parameters

A semi-PBPK model for IV/PO MDZ in presence of IV/PO ERY was built based on the reported *in-vitro* metabolic inhibitory information and the previously developed MDZ semi-

PBPK and ERY semi-PBPK models (**Figure 8.1**). Metabolic inhibition parameters, along with previously discussed MDZ (as initial parameters) and ERY semi-PBPK model parameters are summarized in **Table 8.1**.

Table 8.1 MDZ and ERY initial semi-PBPK DDI model parameters.

Parameter	Definition	Value	Source
Physiological parameters			
V_{GL} (ml/kg)	Volume of gut lumen	3.57	Assumed to be 250ml (FDA, 2012)
V_{GW} (ml/kg)	Volume of GW	33.6	Calculated by equation (4.6), assumed to be the surface of gut lumen cylinder
V_{PV} (ml/kg)	Volume of portal vein	0.97	Unknown methods (Ito et al., 2003)
V_{hep} (ml/kg)	Volume of liver	22.5	Calculated by equation (4.7) and (4.8)
Q_{villi} (ml/min/kg)	Villous blood flow	4.30	<i>In-vivo</i> experiment (Yang et al., 2007)
Q_{hep} (ml/min/kg)	Hepatic blood flow	21.4	<i>In-vivo</i> experiment (Tsunoda et al., 1999)
f_{HA}	Fraction of hepatic artery to total hepatic blood flow	0.25	(Eipel et al., 2010) (Q_{HA} was calculated as $f_{HA} \cdot Q_{hep}$; Q_{PV} was calculated as $(1-f_{HA}) \cdot Q_{hep}$)
f_{PV}	Fraction of the components of portal vein that contain drug	1.00	A correction factor that can be adjusted according to simulation results.
f_{villi}	IVIVE scaling factor and IIV adjusting factor	2.2	Optimized with data from study 21
ERY PK Parameters (Systemic disposition)			
$V_{B,u}^{ERY}$ (mL/kg)	Unbound volume of central compartment	479	See Appendices G
$V_{P,u}^{ERY}$ (mL/kg)	Unbound volume of peripheral compartment	1853	See Appendices G
$Q_{2,u}^{ERY}$ (ml/min/kg)	Inter-compartmental clearance	34.1	See Appendices G
$CL_{ren,u,min}^{ERY}$ (ml/min/kg)	Minimal unbound renal clearance after IV ERY	0.5	Optimized by empiric hyperbolic model
$CL_{ren,u,max}^{ERY}$ (ml/min/kg)	Maximal unbound renal clearance after IV ERY	3.5	Optimized by empiric hyperbolic model
ED_{50}^{ERY} (mg)	Dose of IV ERY that requires to produce 50% tubular reabsorption	475	Optimized by empiric hyperbolic model
$CL_{ren,u-PO}^{ERY}$ (ml/min/kg)	ERY unbound renal clearance after PO ERY	2.65	Average of CL_{ren}^{ERY} reported at 250, 500, 1000mg dose (Josefsson et al., 1982) (corrected by average f_u^{ERY} and $B:P^{ERY}$)
$V_{max,hep-3A}^{ERY}$ (μ g/min/kg)	Capacity of hepatic CYP3A to metabolize ERY	800	Value used in PO ERY PBPK model optimized by PO EC and SS clinical studies
$K_{m,hep-3A}^{ERY}$ (μ g/ml)	Affinity of hepatic CYP3A to metabolize ERY	64.6	<i>In-vitro</i> study (88 μ M) (Riley & Howbrook, 1998)
$V_{max,bile}^{ERY}$ (μ g/min/kg)	Capacity of ERY biliary excretion	0.5	Value used in PO ERY PBPK model optimized by PO EC and SS clinical studies
$K_{m,bile}^{ERY}$ (μ g/ml)	Affinity to drug transporter that is responsible for biliary excretion	0.1	Optimized by regimen 2 in study 611(Austin et al., 1980)

$K_{p,hep,u}^{ERY}$	liver-to-blood partition coefficient of unbound drug	2.71	(Ahmad, 2007)
$K_{p,GW,u}^{MDZ}$	GW-to-blood partition coefficient of unbound drug	2.71	Assumed to be the same as $K_{p,hep,u}^{ERY}$
$B:P^{ERY}$	Blood-to-plasma partitioning ratio	0.85	(Ahmad, 2007)
B_{max} (mg/L)	Binding capacity to AAG	8.15	See section 7.3.2 (11.1 μ M)
$K_{b,50}$ (mg/L)	Binding affinity to AAG	2.14	See section 7.3.2 (2.92 μ M)
n	Hill coefficient of AAG binding	1.32	See section 7.3.2
m	Slope of non-specific binding	0.265	See section 7.3.2
ERY PK Parameters (Oral Absorption)			
F_{abs}^{ERY} (EC)	Fraction of ERY EC absorbed from gut lumen	0.88	Estimated from study 624 (Somogyi et al., 1995)
k_{GL}^{ERY} (min ⁻¹) (EC)	Absorption rate constant of EC from last transit compartment to GW	0.06	Assume to be k_a^{ERY} in study 620 (Josefsson et al., 1982)
F_{abs}^{ERY} (SS)	Fraction of ERY SS absorbed from gut lumen	0.59	Relative bioavailability between EC and SS in study 620 (Josefsson et al., 1982)
k_{GL}^{ERY} (min ⁻¹) (SS)	Absorption rate constant of SS from last transit compartment to GW	0.018	Assume to be k_a^{ERY} in study 618 (Iliopoulou et al., 1982)
ERY PK Parameters (Auto-inhibition model on CYP3A)			
k_{deg} (min ⁻¹)	CYP3A degradation rate constant	0.0008	Optimized between $t_{1/2}$ of 10 -144 hours (Rowland Yeo et al., 2011; Wang, 2010; Yang et al., 2008) ($t_{1/2}$ = 14 hours)
k_{inact}^{ERY} (min ⁻¹)	ERY maximum rate of inactivation on CYP3A	0.0375	²⁶
K_I^{ERY} (mg/L)	ERY inhibitory potency on CYP3A	30	Optimized between 1 - 80 mg/L (1.48 – 109 μ M) (Ito et al., 2003a; McConn et al., 2004; Rowland Yeo et al., 2011; Xu et al., 2009; Yamano et al., 2001; Yates et al., 2012; Zhang et al., 2009; Zhang et al., 2010; Zhao et al., 2005)
MDZ PK Parameters			
V_B^{MDZ} (ml/kg)	Volume of systemic blood compartment	140.4	See Appendices C
V_{P1}^{MDZ} (ml/kg)	Volume of shallow peripheral compartment	313.7	See Appendices C
V_{P2}^{MDZ} (ml/kg)	Volume of deep peripheral compartment	531.4	See Appendices C
Q_2^{MDZ} (min ⁻¹)	Inter-compartmental clearance between central and peripheral cpt-1	55.27	See Appendices C
Q_3^{MDZ} (min ⁻¹)	Inter-compartmental clearance between central and peripheral cpt-2	7.25	See Appendices C
f_u^{MDZ}	Fraction unbound of MDZ	0.03	Assume to be the same in plasma and hepatocytes (Gandhi et al., 2012)
$f_{u,GW-M}^{MDZ}$	Fraction unbound at mucosal side of intestinal epithelium	1.0	Assumed to be negligible bound
$V_{max,GW}^{MDZ}$ (ng/min/kg)	GW CYP3A capacity to metabolize MDZ	3357.6	<i>In-vitro</i> experiment (Thummel et al., 1996)
$K_{m,GW}^{MDZ}$ (ng/ml)	GW CYP3A affinity of metabolizing MDZ	1173	<i>In-vitro</i> experiment (Thummel et al., 1996) (3.6 μ M)
$V_{max,hep}^{MDZ}$ (ng/min/kg)	Hepatic CYP3A capacity to metabolize MDZ	305067	<i>In-vivo</i> experiment, calculated from equation (5.7-5.8), using data from study 21
$K_{m,hep}$ (ng/ml)	Hepatic CYP3A affinity of metabolizing MDZ	880	<i>In-vitro</i> experiment (Thummel et al., 1996) (2.7 μ M)
$K_{p,GW}^{MDZ}$	GW-to-blood partition coefficient	1.12	Scaled from rat K_p (Björkman et al., 2001)
$K_{p,hep}^{MDZ}$	Liver-to-blood partition coefficient	1.09	Scaled from rat K_p (Björkman et al., 2001)

$B:P^{MDZ}$	Blood-to-plasma partitioning ratio	0.86	(Ervin & Houston, 1994)
$k_{GL}^{MDZ} (min^{-1})$	Absorption rate constant from gut lumen to GW	0.05	<i>In-vivo</i> experiment (Johnson et al., 2002; Kato et al., 2008), assumed to be k_a^{MDZ}
$k_T (min^{-1})$	Transit rate from mucosal to serosal side of intestinal epithelium	0.13	Assumed, calculated from Q_{villi}/V_{GW}
F_{abs}^{MDZ}	Fraction of MDZ absorbed from gut lumen	100%	BCS Class 1 drug (Wu & Benet, 2005)
DDI Parameters (MBI)			
$k_{deg} (min^{-1})$	CYP3A degradation rate constant	0.0008	Same as ERY auto-inhibition model, see above
$k_{inact}^{ERY} (min^{-1})$	ERY maximum rate of inactivation on CYP3A	0.0375	Same as ERY auto-inhibition model, see above
$K_I^{ERY} (mg/L)$	ERY inhibitory potency on CYP3A	30	Same as ERY auto-inhibition model, see above

¹ Different values were used in IV ERY semi-PBPK model ($v_{max, hep-3A}^{ERY} = 900 \mu g/min/kg$, $v_{max, bile}^{ERY} = 10 \mu g/min/kg$)

² Parameter value was adjusted in study 629.

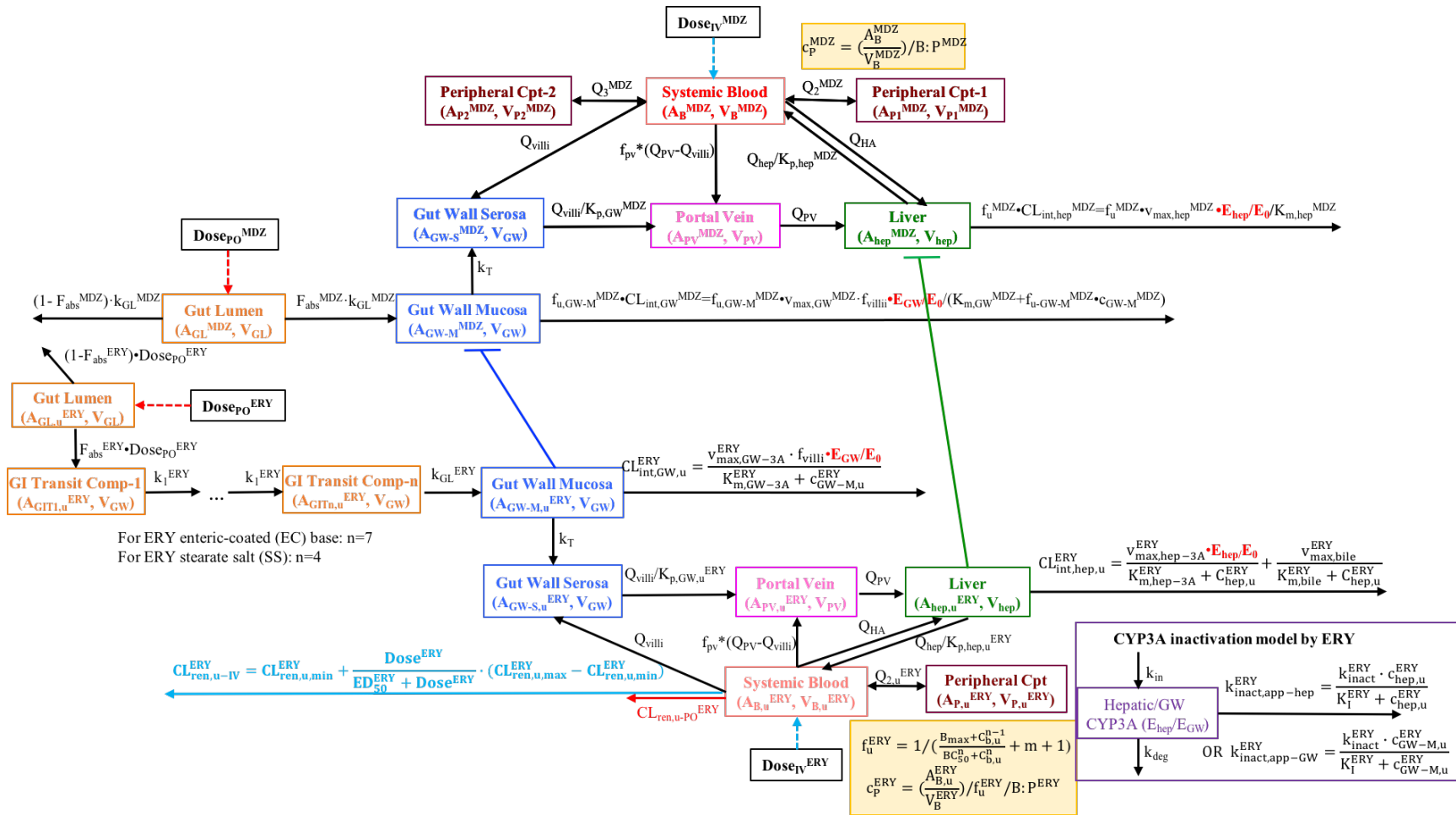


Figure 8.1 Semi-PBPK model scheme of MDZ in presence of ERY.

8.2.1.2 MBI Model

In presence of IV/PO ERY, unbound ERY in liver and GW mucosa irreversibly binds to CYP3A and results in MBI on hepatic/GW CYP3A metabolism. As a result, both CYP3A activity, *i.e.*, $v_{\max, \text{hep}}^{\text{MDZ}}$ and $v_{\max, \text{GW}}^{\text{MDZ}}$, are decreased relative to their baseline ($E_{\text{GW}}(t)/E_0$ and $E_{\text{hep}}(t)/E_0$), respectively, and $E_{\text{GW}}(t)$ and $E_{\text{hep}}(t)$ changed over time can be described by equation (8.1) and (8.2):

$$\frac{dE_{\text{GW}}(t)}{dt} = k_{\text{in}} - E_{\text{GW}} \cdot k_{\text{deg}} - E_{\text{GW}} \cdot \left(\frac{k_{\text{inact}}^{\text{ERY}} \cdot c_{\text{GW-M,u}}^{\text{ERY}}}{K_{\text{I,hep}}^{\text{ERY}} + c_{\text{GW-M,u}}^{\text{ERY}}} \right)$$

when $t = 0$, $E_{\text{GW}}(0) = 1$ (8.1)

$$\frac{dE_{\text{hep}}(t)}{dt} = k_{\text{in}} - E_{\text{hep}} \cdot k_{\text{deg}} - E_{\text{hep}} \cdot \left(\frac{k_{\text{inact}}^{\text{ERY}} \cdot c_{\text{hep,u}}^{\text{ERY}}}{K_{\text{I,hep}}^{\text{ERY}} + c_{\text{hep,u}}^{\text{ERY}}} \right)$$

when $t = 0$, $E_{\text{hep}}(0) = 1$ (8.2)

8.2.1.3 Inhibition of GW metabolism: FLZ vs. ERY

It is assumed that ERY enters GW mucosa from gut lumen only; therefore, only PO (but not IV) ERY causes inhibition of GW metabolism on MDZ and itself. This is different from the assumption made in FLZ semi-PBPK model, where both IV and PO FLZ can cause GW metabolic inhibition. This major difference between FLZ and ERY is mainly due to their different PK and physicochemical properties:

FLZ is a BCS class 1 drug (Charoo et al., 2014), with a high apical-to-basolateral apparent permeability measured in Caco-2 cells ($P_{\text{app A-B}}^{\text{FLZ}} = 29.8 \times 10^{-6} \text{cm/s}$ (Yee, 1997)), albeit a low-moderate log P value ($\log P = 0.5$ (Salerno et al., 2010)). It has not been shown to be a potent substrate for any GI uptake transporters, thus, the high GI permeability is mainly due to passive diffusion. FLZ also has low plasma protein binding, with f_u^{FLZ} value of 0.88 (Humphrey et al.,

1985), allowing more free drug available to cross intestinal epithelial membrane from the vascular serosal space. More importantly, study 103 (Ahonen et al., 1997), a clinical DDI study between PO MDZ and IV/PO FLZ demonstrated a 47% decrease in ER_{GI}^{MDZ} in presence of IV FLZ, based on quantitative meta-analysis in **Chapter 3**, confirming its inhibitory effect on GW metabolism of MDZ after IV administration of FLZ.

On the other hand, ERY is a BCS class 3 drug, and a potent P-gp substrate. It was reported by Nožinić *et al.* (Nožini et al., 2010) that $P_{app\ A-B}^{ERY}$ and $P_{app\ B-A}^{ERY}$ in Caco-2 cells were 0.9 ± 0.2 nm/s and 63.8 ± 3.3 nm/s, respectively, demonstrating its poor GI permeability due to P-gp efflux. After adding 10 μ M P-gp inhibitor (CY-P, full name not mentioned) (Yee, 1997), $P_{app\ A-B}^{ERY}$ was measured to be 3.73 nm/s, suggesting its low-moderate permeability even in absence of P-gp (predicted cLog P value = 0.8 (Erythromycin Scifinder Report)). It is also reasonable to assume that even if some ERY could reach the enterocyte from the basolateral side, P-gp at the apical side would efficiently remove intracellular ERY out of the GW. Moreover, ERY has relatively low f_u^{ERY} (~0.3 at most clinical relevant concentrations), so that less free drug is available in blood to leave the vascular space and penetrate into the enterocyte from the serosal side. No IV ERY and MDZ DDI studies are available to clinically confirm this conclusion. As a consequence, we assume that ERY can only enter GW mucosa from gut lumen, but not via the GI vascular space, and only PO ERY can inhibit GW metabolism of PO MDZ.

The corresponding differential equations for hepatic and GW mucosa mass transfer of MDZ were expressed as equations (8.3) and (8.4):

$$\frac{dA_{hep}^{MDZ}(t)}{dt} = c_B^{MDZ} \cdot Q_{HA} + c_{PV}^{MDZ} \cdot Q_{PV} - \left(\frac{C_{hep}^{MDZ}}{K_{p,hep}^{MDZ}} \right) \cdot Q_{hep} - c_{hep}^{MDZ} \cdot f_u^{MDZ} \cdot v_{max,hep}^{MDZ} \cdot \frac{E_{hep}}{E_0} / K_{m,hep}^{MDZ}$$

$$\text{when } t = 0, A_{\text{hep}}^{\text{MDZ}}(0) = 0 \quad (8.3)$$

$$\frac{dA_{\text{GW-M}}^{\text{MDZ}}(t)}{dt} = c_{\text{GL}}^{\text{MDZ}} \cdot V_{\text{GL}} \cdot F_{\text{abs}}^{\text{MDZ}} \cdot k_{\text{GL}}^{\text{MDZ}} - c_{\text{GW-M}}^{\text{MDZ}} \cdot V_{\text{GW}} \cdot k_{\text{T}} - f_{\text{u,GW-M}}^{\text{MDZ}} \cdot c_{\text{GW-M}}^{\text{MDZ}} \cdot f_{\text{villi}} \cdot v_{\text{max,GW}}^{\text{MDZ}} \cdot \frac{E_{\text{GW}}}{E_0} / (K_{\text{m,GW}}^{\text{MDZ}} + f_{\text{u,GW-M}}^{\text{MDZ}} \cdot c_{\text{GW-M}}^{\text{MDZ}})$$

$$\text{when } t = 0, A_{\text{GW-M}}^{\text{MDZ}}(0) = 0 \quad (8.4)$$

Besides the assumptions mentioned in **Chapter 5** and **Chapter 7**, two additional assumptions were made during the DDI modeling processes, which were:

- 1) ERY can only enter GW mucosa from the gut lumen, therefore, only PO (but not IV) ERY causes inhibition of GW metabolism on MDZ and itself.
- 2) The MBI by ERY on MDZ and its own metabolism (auto-inhibition) share the same $K_{\text{I}}^{\text{ERY}}$ and $k_{\text{inact}}^{\text{ERY}}$ in the liver and GW mucosa.

8.2.2 Model qualification and predictions

Model-simulated MDZ plasma concentration-time profiles in absence/presence of ERY were compared with reported profiles from study 28 and 603 to assess model validity by predictive visual check and exposure metrics comparison. Since some parameters (i.e., $v_{\text{max,hep}}^{\text{MDZ}}$, $F_{\text{abs}}^{\text{ERY}}$ (EC), $k_{\text{GL}}^{\text{MDZ}}$ and f_{villi}) were optimized in different MDZ and ERY DDI, a more stringent acceptance criterion: predicted exposure metrics are $\pm 30\%$ of observed, was used to assess performance of MDZ and ERY DDI semi-PBPK model. Plasma ERY GW mucosa and liver concentrations, as well as relative GW and hepatic CYP3A activity levels were also simulated, to better interpret observed metabolic DDI between the two drugs. All M&S were implemented in Simbiology (MATLAB, 2015a).

8.2.3 Sensitivity Analyses

Sensitivity analyses were performed to provide information about specific parameters that the model predictions are most sensitive to. Parameters (*i.e.*, k_{deg} , K_I^{ERY} , k_{inact}^{ERY} , $v_{max,hep-3A}^{ERY}$, $v_{max,bile}^{ERY}$ and $K_{m,bile}^{ERY}$) that were highly variable /uncertain were selected for perspective sensitivity analyses. Considering high reported variability of these parameters, their values were increased and decreased by 5-fold relative to their original values (overall-fold change in values = 25 - fold), as showed in **Table 8.2**.

As the purpose of a sensitivity analysis is to identify pivotal parameters in determining DDI magnitude, and facilitate parameter optimization for the MDZ and ERY DDI model, the ERY unbound concentration – and relative CYP3A activity – time profiles in the liver and GW mucosa were simulated under the dosing regimens of ERY in the two DDI studies (study 28 and 603): 500 mg TID for 7 days (EC), and 200 mg (base equivalent) QID for 2, 4, and 7 days (SS). MDZ plasma concentration – time profiles were also simulated according to the dosing regimen in two DDI studies: 0.05 mg/kg IV bolus (as 2 min injection) or 15 mg PO MDZ was administered 2 hours after 2nd dose of EC ERY on the 6th day (study 28); 2.5 mg PO MDZ was administered 1 hour after 1st dose of SS ERY on day 2, 4, and 7 (study 603). AUC for all simulated profiles were estimated, and the sensitivity to each parameter was assessed by dividing the respective exposure metrics simulated at the upper limit by that simulated at the lower limit (-fold change). As to MDZ, plasma $AUC_{0-\infty}$ was calculated; as to ERY, hepatic/GW mucosa AUC_{0-t} after single and repeat- ERY (EC/SS) doses were both calculated; as to relative hepatic/GW CYP3A activity, difference between AUC_{0-t} in absence and presence of MBI after single- and repeat-doses of ERY (EC/SS) (inhibited AUC_{0-t}) were both calculated. For $v_{max,hep-3A}^{ERY}$ and $v_{max,bile}^{ERY}$, sensitivity analyses were conducted by varying their values used in PO

ERY semi-PBPK model.

Table 8.2 Values of parameters used in sensitivity analysis.

Parameter Name	Base Value	Lower/Upper Sensitivity Limits -fold change = 25
k_{deg} (min^{-1})	0.0008	0.00016; 0.004
K_I^{ERY} (mg/L)	30	6; 150
K_{inact}^{ERY} (min^{-1})	0.0375	0.0075; 0.1875
$V_{max,hep-3A}^{ERY}$ ($\mu\text{g}/\text{min}/\text{kg}$)	800	160; 4000
$V_{max,bile}^{ERY}$ ($\mu\text{g}/\text{min}/\text{kg}$)	0.5	0.1; 2.5
$K_{m,bile}^{ERY}$ ($\mu\text{g}/\text{ml}$)	0.1	0.02; 0.5

8.2.4 Simulations of route-dependent DDI with various administration time intervals

To investigate the impact of route difference for ERY and MDZ at different administration time intervals between the two drugs, as well as to explore the magnitude and duration of ERY inhibition, the final validated semi-PBPK DDI model between MDZ and ERY (using PO ERY model parameters) was employed to simulate MDZ PK profiles in presence of 1,000 mg IV (as 15min infusion, and PO (EC/SS) ERY, and MDZ administered after 0, 0.5, 1, 2, 5, 10, 20, 50, 100 hours as 1 mg IV MDZ or 3 mg PO MDZ dose. The simulated DDI dosing scheme is illustrated in **Figure 8.2**. The (inhibited/uninhibited) $AUC_{0-\infty}^{MDZ}$ ratio, F_{oral}^{MDZ} , ER_{hep}^{MDZ} and ER_{GI}^{MDZ} in presence of ERY for each scenario were calculated to assess the extent of inhibition. The 1,000 mg ERY dose was selected because it is the most commonly used daily (base-equivalent) total dose of ERY (Arbor Pharmaceuticals, 2013). ERY unbound GW mucosa and hepatic concentrations, as well as relative GW and hepatic CYP3A levels were also simulated, to better interpret observed metabolic DDI between the two drugs.

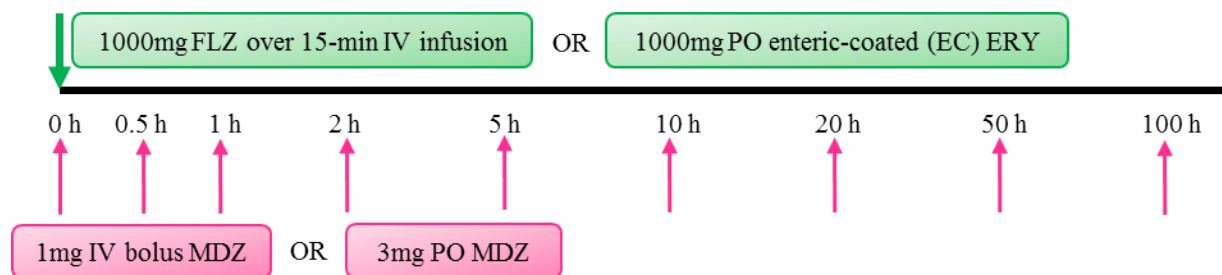


Figure 8.2 Simulated DDI dosing scheme between ERY and MDZ.

8.2.5 Assessment of linearity of MBI by ERY

According to **Chapter 7**, the apparent inactivation rate constant ($k_{\text{inact,app}}$) of ERY on hepatic/GW CYP3A is a function of $k_{\text{inact}}^{\text{ERY}}$, K_I^{ERY} , and unbound ERY concentration in liver and GW mucosa, respectively (equation 7.22 and 7.23). If $c_{\text{GW-M,u}}^{\text{ERY}}$ or $c_{\text{hep,u}}^{\text{ERY}}$ are much smaller than K_I^{ERY} , $k_{\text{inact,app}}^{\text{ERY}}$ is almost proportional to the unbound ERY concentration, indicating as “linear” MBI. If $c_{\text{GW-M,u}}^{\text{ERY}}$ or $c_{\text{hep,u}}^{\text{ERY}}$ is much greater than K_I^{ERY} , $k_{\text{inact,app}}^{\text{ERY}}$ is maxed out, and remains as $k_{\text{inact}}^{\text{ERY}}$, suggesting “nonlinear” (saturable) MBI. The assessment of linearity of MBI is a way to compare ERY tissue concentrations relative to their inhibitory potency, and evaluate how efficiently does ERY inhibit CYP3A.

$$k_{\text{inact,app-hep}}^{\text{ERY}} = \frac{k_{\text{inact}}^{\text{ERY}} \times c_{\text{hep,u}}^{\text{ERY}}}{K_I^{\text{ERY}} + c_{\text{hep,u}}^{\text{ERY}}} \quad (7.22)$$

$$k_{\text{inact,app-GW}}^{\text{ERY}} = \frac{k_{\text{inact}}^{\text{ERY}} \times c_{\text{GW-M,u}}^{\text{ERY}}}{K_I^{\text{ERY}} + c_{\text{GW-M,u}}^{\text{ERY}}} \quad (7.23)$$

$k_{\text{inact,app}}^{\text{ERY}}$ simulated at 1,000 mg IV 15min-infusion ERY or PO (EC/SS) ERY were plotted against ERY unbound tissue concentration, to assess MBI linearity.

8.2.6 Simulations of route-dependent DDI with various single doses of ERY

To investigate the impact of single dose of ERY on the route-dependent DDI between the two drugs, MDZ $\text{AUC}_{0-\infty}$ after 1 mg IV or 3 mg PO administration concurrent with (*i.e.*,

administration time interval = 0) a series of SAD of ERY (namely, 100 mg, 200 mg, 500 mg, 1,000 mg, 2,000 mg, 4,000 mg, 10,000 mg) administered either as 15-min IV infusion or PO EC were simulated. PO SS was not simulated because the major PK difference between the two formulations were F_{abs}^{ERY} , and by increasing administered dose of SS, SS is expected to produce similar results with EC.

AUCR of MDZ for each scenario was calculated, and ERY route difference was assessed to be the ratio of MDZ AUCR by PO (EC) ERY and that by IV ERY. Unbound ERY concentration- and relative CYP3A activity-time profiles in the liver and GW mucosa were also simulated to better interpret the observed dose-dependent route-differences.

8.2.7 Simulations of route-dependent DDI with different dosing intervals of ERY

To investigate impact of PO ERY dosing interval (same daily dose = 1,000 mg) on the route-dependent DDI between the two drugs, as well as to compare ERY inhibition after single- and repeat- doses of PO ERY, MDZ $AUC_{0-\infty}$ were predicted after 1 mg IV or 3 mg PO administration in presence of 250 mg/500 mg/1,000 mg PO (EC/SS) SD ERY, or 250 mg PO (EC/SS) ERY QID, 500 mg PO (EC/SS) ERY BID, and 1,000 mg PO (EC/SS) ERY QD for 5 days (steady-state was achieved for all three multiple dosing regimens). IV/PO MDZ was administered 2-hours after SD ERY, or 2-hours after the 1st dose of EC/SS ERY on the 5th day (steady-state was achieved).

The (inhibited/uninhibited) $AUC_{0-\infty}$ ratio of MDZ for each scenario was calculated, and ERY unbound concentration - and relative CYP3A activity-time profiles in the liver and GW mucosa were simulated, to better interpret observed dosing interval – dependent route difference. Accumulation ratio of ERY concentrations and inhibition ratio of CYP3A after single and repeat- PO (EC/SS) doses for ERY were also predicted.

8.2.8 Simulation of route-dependent DDI between CYP3A substrates and CYP3AIs

ERY is a relatively low- F_{oral} and short $t_{1/2}$ MBI, which are two important PK properties (and are different from FLZ). Thus, a relatively higher – F_{oral} MBI (3AIX4) was created based on the ERY semi-PBPK model, by increasing $F_{\text{abs}}^{\text{ERY}}$ (EC) from 0.88 to 1.0. To avoid changing other PK properties of ERY, hepatic and GW metabolism of ERY were not modified. As a MBI, the duration of inhibition is affected by the turn-over kinetics of CYP3A rather than the PK of inhibitor, as a consequence, influence of changing $t_{1/2}^{\text{ERY}}$ was not investigated further.

As discussed in **Chapter 6**, route difference of IV/PO MDZ is primarily due to existence of pre-systemic hepatic/GW metabolism after PO (but not IV) MDZ, and IV/PO FLZ demonstrated DDI difference when simultaneously administered with PO MDZ, mainly because of different FLZ GW concentrations. Hence, a CYP3A substrate without GW metabolism (3ASX1) was derived from MDZ PBPK model, by setting f_{villi} , the parameter to adjust GW CYP3A activity, to 0. Actually, based on the quantitative meta-analysis in **Chapter 3**, $ER_{\text{GI}}^{\text{MDZ}}$ has very large inter-study variability, and the derived $ER_{\text{GI}}^{\text{MDZ}}$ in study 11 (Krishna et al., 2009) was 0, proving the clinical relevance of making this hypothetical CYP3A substrate.

Furthermore, a second CYP3A substrate (3ASX2) was generated by setting f_{villi} to 0 (no GW metabolism), along with decreasing $v_{\text{max,hep}}^{\text{MDZ}}$ by 5-fold (limited hepatic metabolism), to create a high F_{oral} ($F_{\text{oral}} = 89\%$) CYP3A substrate with limited first pass effect.

All other PBPK parameters, including metabolic inhibitory potency and IV/PO doses, for the three hypothetical drugs remained unchanged from their original drugs, and changes were summarized in **Table 8.3**.

Table 8.3 Parameter modifications for hypothetical drugs, based on ERY and MDZ individual semi-PBPK models.

(MDZ and ERY initial model parameters were used.)

CYP3AI	F _{oral}	t _{1/2}	Mechanism of DDI	Change
ERY	~60% (EC); ~30% (SS)	~2 hrs	MBI	-
3AIX4	71%	~2 hrs	MBI	Change F _{abs} ^{ERY} from 0.88 to 1.0
CYP3A Substrate	F _{oral}	ER _{hep}	ER _{GI}	Change
MDZ	0.28	0.40 (t _{1/2} : ~2.5 hrs)	0.52	-
3ASX1	0.60	0.40 (t _{1/2} : ~2.5 hrs)	0	Change f _{villi} from 2.2 to 0.0.
3ASX2	0.89	0.11 (t _{1/2} : ~9 hrs)	0	Change v _{max,hep} ^{MDZ} from 305067 µg/min/kg to 61013.4 µg/min/kg and change f _{villi} from 2.2 to 0.0.

The route impact on metabolic DDI between MDZ (IV: 1 mg, PO: 3 mg) and 3AIX4 (1,000 mg IV-15min-infusion and PO) and between 3ASX1/2 (same dose as MDZ) and ERY (1,000 mg IV-15min-infusion and PO EC) were investigated by simulating the -fold AUC_{0-∞}^{substrate} increase by CYP3AI at varying time intervals between single-dose substrate and CYP3AI administration (same strategy as **Figure 8.2**). 3AIX4 GW mucosa and liver concentrations, as well as relative GW and hepatic CYP3A activity were also simulated, to better interpret observed metabolic DDI between MDZ and 3AIX4.

8.3 Results and Discussion

8.3.1 Model evaluation

8.3.1.1 Predictive performance check

8.3.1.1.1 Study 28

The observed and model-predicted IV MDZ PK profiles in absence of ERY in study 28 are shown in **Figure 8.3** (using parameter values from **Table 8.1**), and exposure metrics are summarized in **Table 8.4**. From **Figure 8.3**, the predicted terminal slope appears steeper than the

observed slope, resulting in under-estimation of MDZ $AUC_{0-\infty}$ by 35%. Thus, $v_{\max, \text{hep}}^{\text{MDZ}}$ was optimized based on visual inspection of the terminal slope, and a value of 170,000 ng/min/kg was finally chosen to simulate MDZ PK profiles in study 28. This adjustment is within the 4.2-fold inter-study variability of $CL_{\text{int, hep}}^{\text{MDZ}}$, as characterized in **Chapter 3, section 3.3.3.1**. After changing $v_{\max, \text{hep}}^{\text{MDZ}}$, the adjusted PBPK model predicts IV MDZ PK profile in absence of ERY reasonably well (shown in **Figure 8.4**), and the prediction of $AUC_{0-\infty}^{\text{MDZ}}$ is more accurate (see **Table 8.4**).

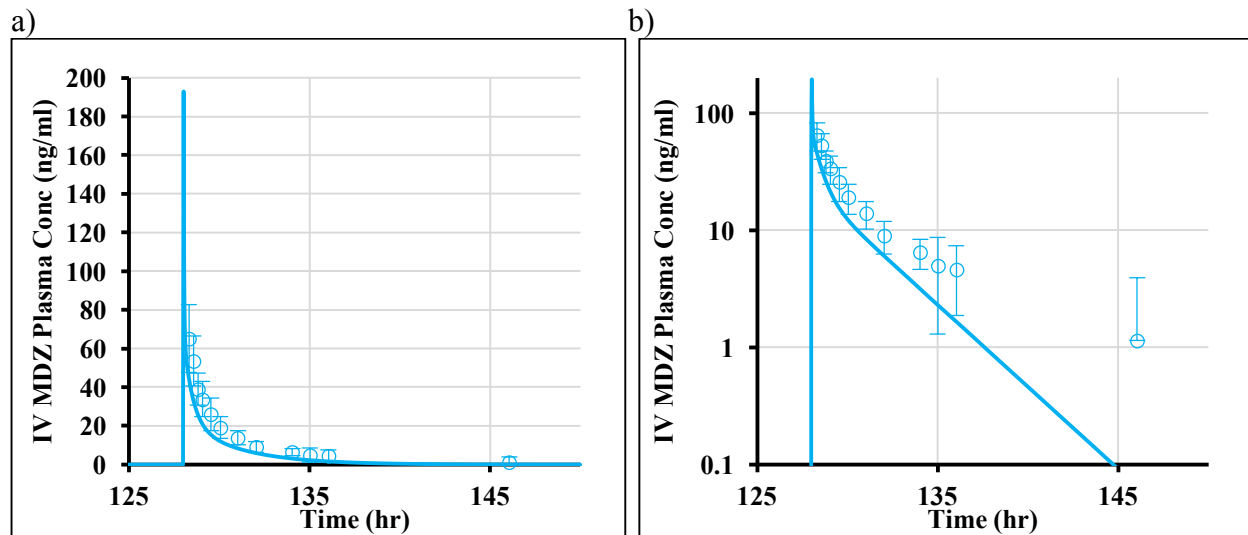


Figure 8.3 Observed and model-predicted MDZ PK profiles after 0.05 mg/kg IV injection over 2 min (Cartesian and semi-log scales) ($v_{\max, \text{hep}}^{\text{MDZ}} = 305067 \mu\text{g}/\text{min}/\text{kg}$).
The solid lines are the predicted PK profiles. The symbols and bars are observed means and SD values (if available). Time is relative to initial ERY/placebo dose.

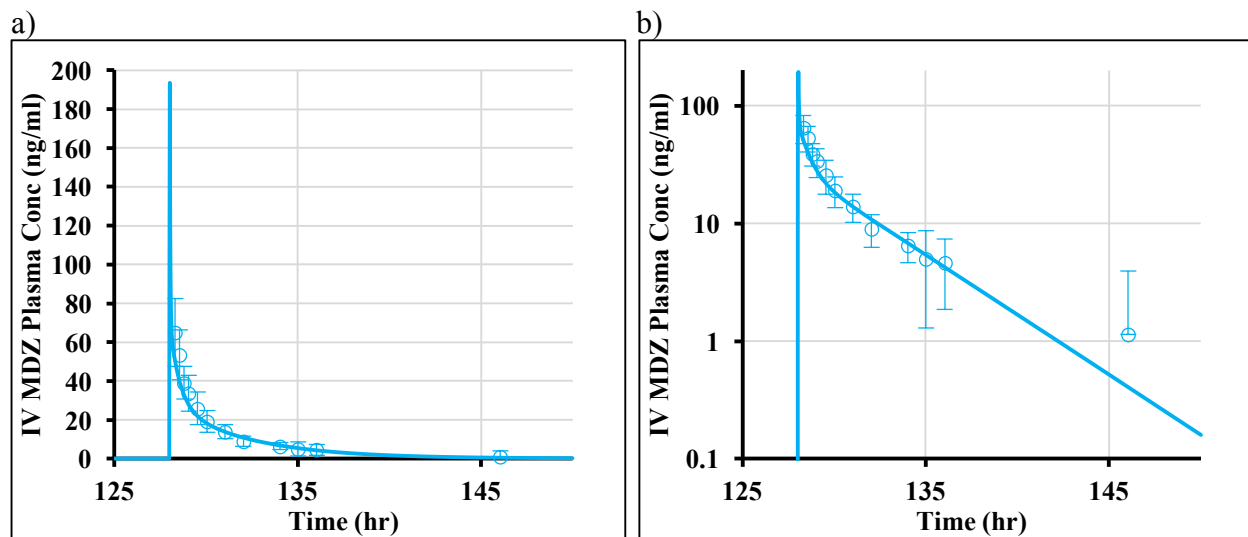


Figure 8.4 Observed and model-predicted MDZ PK profiles after 0.05 mg/kg IV injection over 2 min (Cartesian and semi-log scales) ($v_{\max, \text{hep}}^{\text{MDZ}} = 170,000 \mu\text{g}/\text{min}/\text{kg}$).
The solid lines are the predicted PK profiles. The symbols and bars are observed means and SD values (if available). Time is relative to initial ERY/placebo dose.

Table 8.4 Comparison of reported and semi-PBPK model-predicted MDZ plasma exposure metrics and F_{oral} in the absence and presence of PO (EC/SS) ERY, as well as (inhibited/uninhibited) $AUC_{0-\infty}^{MDZ}$ ratio using PO ERY semi-PBPK model parameters ($v_{max,hep-3A}^{ERY} = 800 \mu\text{g}/\text{min}/\text{kg}$, $v_{max,bile}^{ERY} = 0.5 \mu\text{g}/\text{min}/\text{kg}$) with adjustments in study 28 and 603 (see Table 8.5)

Study ID	MDZ	ERY	Observed					Predicted					Deviation (%)					
			$AUC_{0-\infty}$ (ng/ml·hr)	C_{max} (ng/ml)	t_{max} after MDZ (hr)	F_{oral}	AUCR	$AUC_{0-\infty}$ (ng/ml·hr)	C_{max} (ng/ml)	t_{max} after MDZ (hr)	F_{oral}	AUCR	$AUC_{0-\infty}$ (ng/ml·hr)	C_{max} (ng/ml)	t_{max} after MDZ (hr)	F_{oral}	AUCR	
28	IV: 0.05mg/kg		148	65	0.32	0.33	97	193	0.03	0.37								
28	IV: 0.05mg/kg (Adjust $v_{max,hep-3A}^{MDZ}$)		148	65	0.32		147	194	0.03								14%	
28	PO: 15mg		232	48	1.52		280	82	0.73									
28	PO: 15mg (Adjust $v_{max,hep-3A}^{MDZ}, k_{GL}^{MDZ}$)		232	48	1.52		261	64	0.86									
28	IV: 0.05mg/kg (Adjust $v_{max,hep-3A}^{MDZ}$)	500mg EC TID for 7 days	290	78	0.34	0.91	1.96	676	194	0.03	0.73	2.26	133%				-20%	16%
28	IV: 0.05mg/kg (Adjust $v_{max,hep-3A}^{MDZ}, F_{abs}^{ERY}$)	500mg EC TID for 7 days	290	78	0.34		5.44	332	194	0.03		4.45	14%					-18%
28	PO: 15mg (Adjust $v_{max,hep-3A}^{MDZ}, k_{GL}^{MDZ}, F_{abs}^{ERY}$)	500mg EC TID for 7 days	1264	163	1.06			1161	147	1.10			-8%	-10%	4%			
603	PO: 5mg		42	9	1.38			43	17	0.66			3%	97%	-52%			
603	PO: 5mg (Adjust $v_{max,hep-3A}^{MDZ}, k_{GL}^{MDZ}, f_{villi}$)		42	9	1.38			43	10	0.85			1%	17%	-39%			
603	PO: 5mg (Adjust $v_{max,hep-3A}^{MDZ}, k_{GL}^{MDZ}, f_{villi}$)	200mg SS QID for 2 days	99	17	1.93		2.36	110	20	1.97		2.58	10%	18%	2%		9%	
603	PO: 5mg (Adjust $v_{max,hep-3A}^{MDZ}, k_{GL}^{MDZ}, f_{villi}$)	200mg SS QID for 4 days	146	23	2.05		3.45	128	22	1.98		3.02	-12%	-4%	-3%		-12%	
603	PO: 5mg (Adjust $v_{max,hep-3A}^{MDZ}, k_{GL}^{MDZ}, f_{villi}$)	200mg SS QID for 7 days	141	21	2.11		3.35	130	22	1.98		3.06	-8%	2%	-6%		-9%	

After adjusting $v_{\max, \text{hep}}^{\text{MDZ}}$, the observed and model-predicted PO MDZ PK profiles in absence of ERY in study 28 are shown in **Figure 8.5** with exposure metrics summarized in **Table 8.4**. From **Figure 8.5** and **Table 8.4**, the predicted c_{\max} is significantly overestimated, with t_{\max} underestimated, indicating that a slower than current absorption rate constant ($k_{\text{GL}}^{\text{MDZ}}$) should be used. The current $k_{\text{GL}}^{\text{MDZ}}$ (0.05 min^{-1}) was estimated for a PO dose of 3 mg MDZ, whereas in study 28, 15 mg PO MDZ was administered, possibly resulting in slower absorption rate due to solubility/dissolution limited-absorption. Thus, $k_{\text{GL}}^{\text{MDZ}}$ was optimized based on visual inspection of c_{\max} and t_{\max} of PO MDZ profiles in study 28, and a value of 0.03 min^{-1} was finally chosen. After adjusting $v_{\max, \text{hep}}^{\text{MDZ}}$ and $k_{\text{GL}}^{\text{MDZ}}$, the adjusted PBPK model improves the predictions of PO MDZ PK profile and exposure metrics in absence of ERY (shown in **Figure 8.6** and **Table 8.4**). Although greater than 30% deviations are still observed in c_{\max} and t_{\max} , $\text{AUC}_{0-\infty}$ is well predicted, and semi-PBPK DDI model using the adjusted $k_{\text{GL}}^{\text{MDZ}}$ (0.03 min^{-1}) also captures MDZ profiles in presence of ERY well (discussed later), confirming the necessity of parameter adjustment.

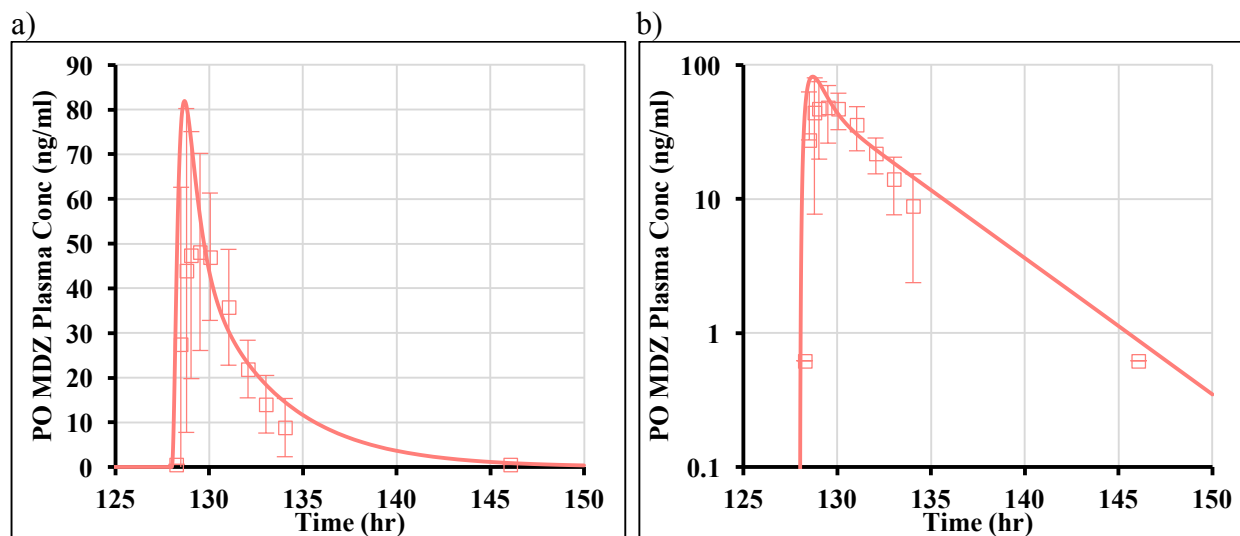


Figure 8.5 Observed and model-predicted MDZ PK profiles after 15 mg PO MDZ (Cartesian and semi-log scales) ($v_{\max, \text{hep}}^{\text{MDZ}} = 170,000 \mu\text{g}/\text{min}/\text{kg}$, $k_{\text{GL}}^{\text{MDZ}} = 0.05 \text{ min}^{-1}$). The solid lines are the predicted PK profiles. The symbols and bars are observed means and SD values (if available). Time is relative to initial ERY/placebo dose.

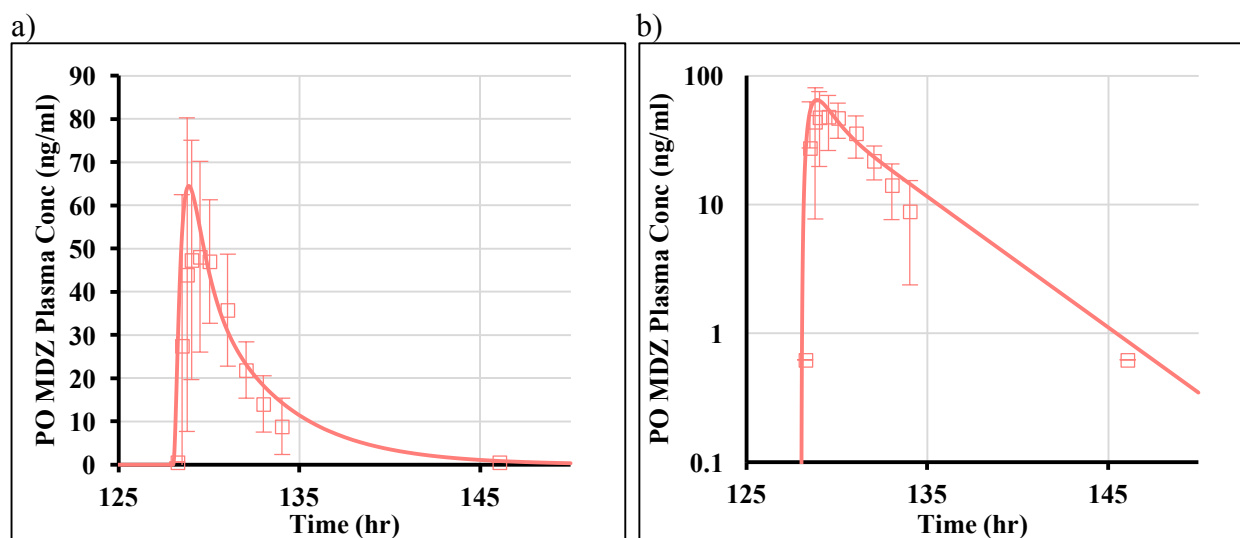


Figure 8.6 Observed and model-predicted MDZ PK profiles after 15 mg PO MDZ (Cartesian and semi-log scales) ($v_{\max, \text{hep}}^{\text{MDZ}} = 170,000 \mu\text{g}/\text{min}/\text{kg}$, $k_{\text{GL}}^{\text{MDZ}} = 0.03 \text{ min}^{-1}$). The solid lines are the predicted PK profiles. The symbols and bars are observed means and SD values (if available). Time is relative to initial ERY/placebo dose.

After adjusting $v_{\max, \text{hep}}^{\text{MDZ}}$, the observed and model-predicted IV MDZ PK profiles in presence of ERY in study 28 are shown in **Figure 8.7** with exposure metrics summarized in **Table 8.4**. From **Figure 8.7 and Table 8.4**, the predicted terminal slope is apparently shallower than the observed slope, resulting in over-estimation of MDZ $\text{AUC}_{0-\infty}$ (in presence of ERY) by 133%. Since MDZ $\text{AUC}_{0-\infty}$ in absence of ERY is well captured by the model parameters, this significant over-estimation is due to over-prediction of ERY's inhibition. Although no ERY PK profiles were provided in study 28, it was reported that when MDZ was administered, ERY plasma concentration was measured to be 3.0 ± 0.7 mg/L. ERY plasma concentration – time profile was then simulated and presented in **Figure 8.8a**, and when MDZ is given, the predicted ERY plasma level is 8.7 mg/L, much higher than the reported value. Due to the large variation of systemic exposure for EC formulation (see **section 7.3.1**), $F_{\text{abs}}^{\text{ERY}}(\text{EC})$ was changed from 0.88 to 0.50 for study 28, which is within the 3.8-fold inter-study variability of PO ERY EC systemic exposure. After adjusting $F_{\text{abs}}^{\text{ERY}}(\text{EC})$ (**Figure 8.8b**), the ERY plasma level is predicted to be 3.2 mg/L, very close to the observed value, and observed IV MDZ PK profile in presence of EC ERY is characterized well by the adjusted PBPK model (shown in **Figure 8.9 and Table 8.4**), with exposure metrics ($\text{AUC}_{0-\infty}$, c_{\max} , t_{\max}), F_{oral} and AUCR all within 30%.

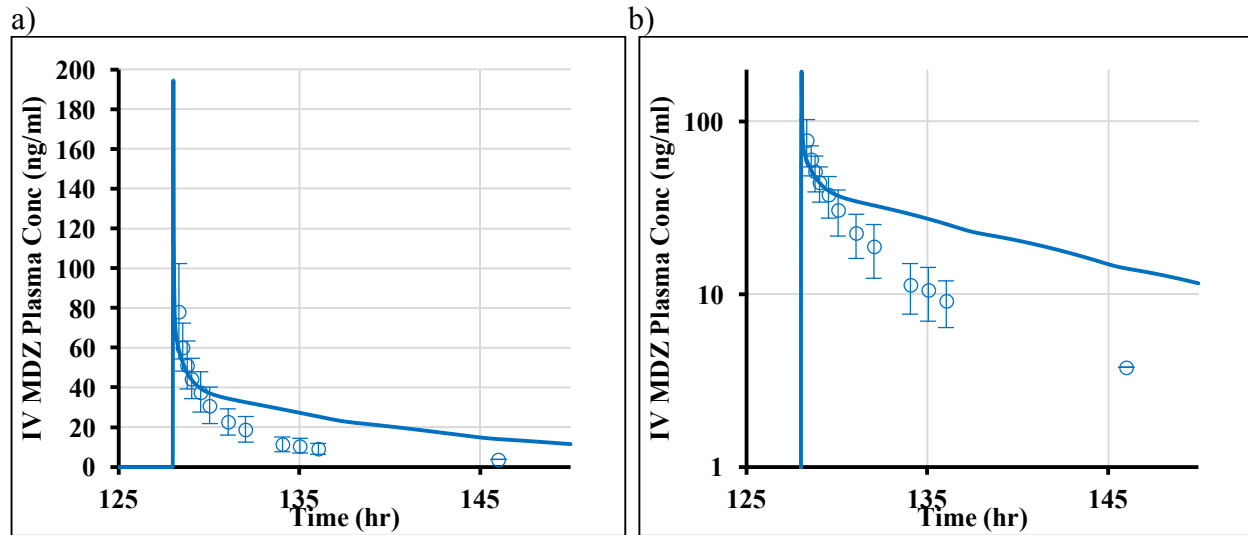


Figure 8.7 Observed and model-predicted IV MDZ (0.05mg/kg) PK profiles in presence of EC ERY (500 mg TID for 7 days, IV MDZ was administered 2 hours after the 2nd ERY dose on the 6th day) on Cartesian and semi-log scales.

($v_{\max, \text{hep}}^{\text{MDZ}} = 170,000 \mu\text{g}/\text{min}/\text{kg}$, $F_{\text{abs}}^{\text{ERY}}(\text{EC}) = 0.88$). The solid lines are the predicted PK profiles. The symbols and bars are observed means and SD values (if available). Time is relative to initial ERY/placebo dose.

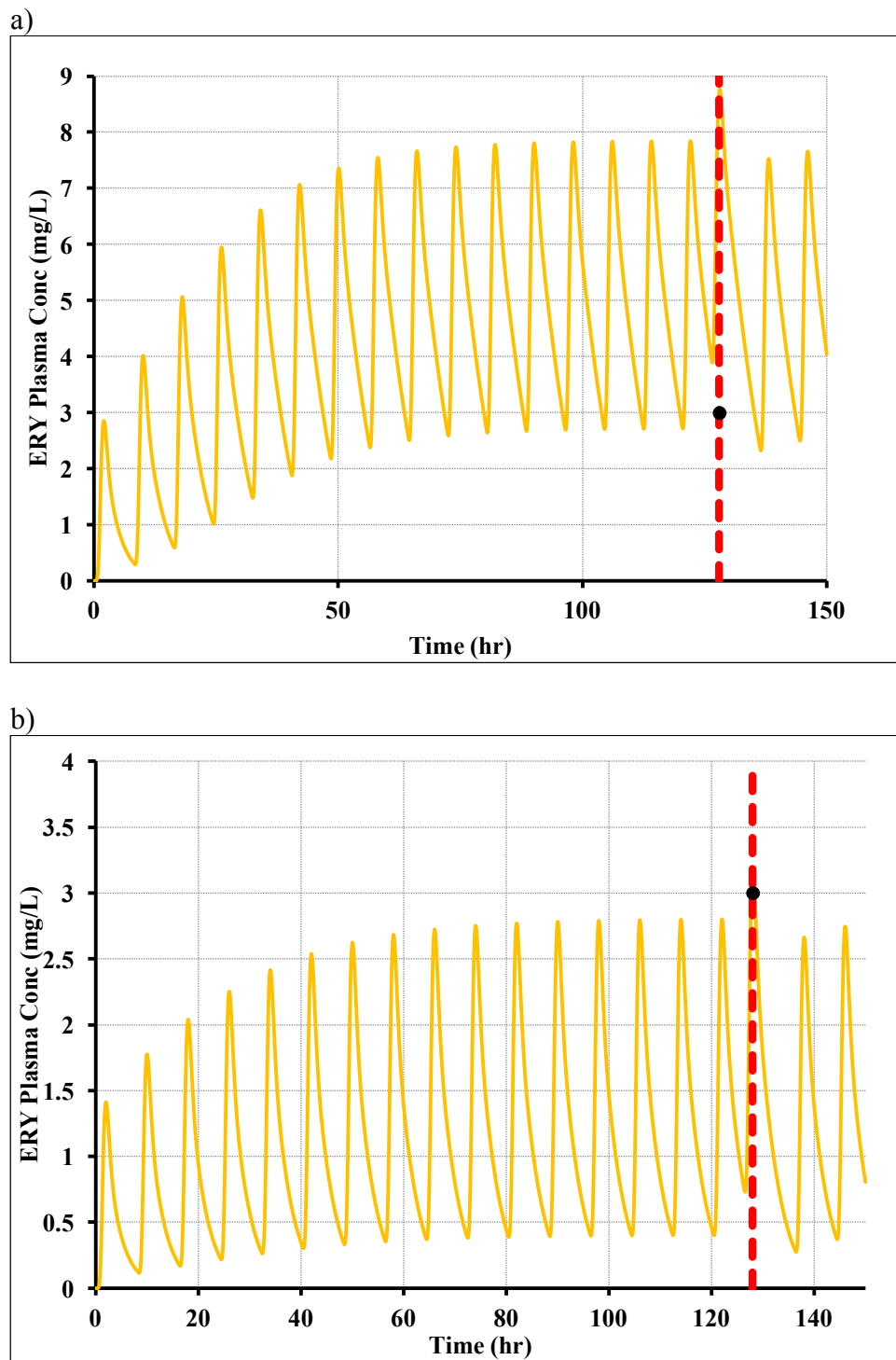


Figure 8.8 Semi-PBPK model-predicted ERY plasma concentration – time profile.

Red dash line represents the time when IV MDZ was administered. a) $F_{\text{abs}}^{\text{ERY}}(\text{EC}) = 0.88$. b) $F_{\text{abs}}^{\text{ERY}}(\text{EC}) = 0.50$. Reported ERY plasma level at the time MDZ was given was 3.0 ± 0.7 mg/L (indicated as black dot).

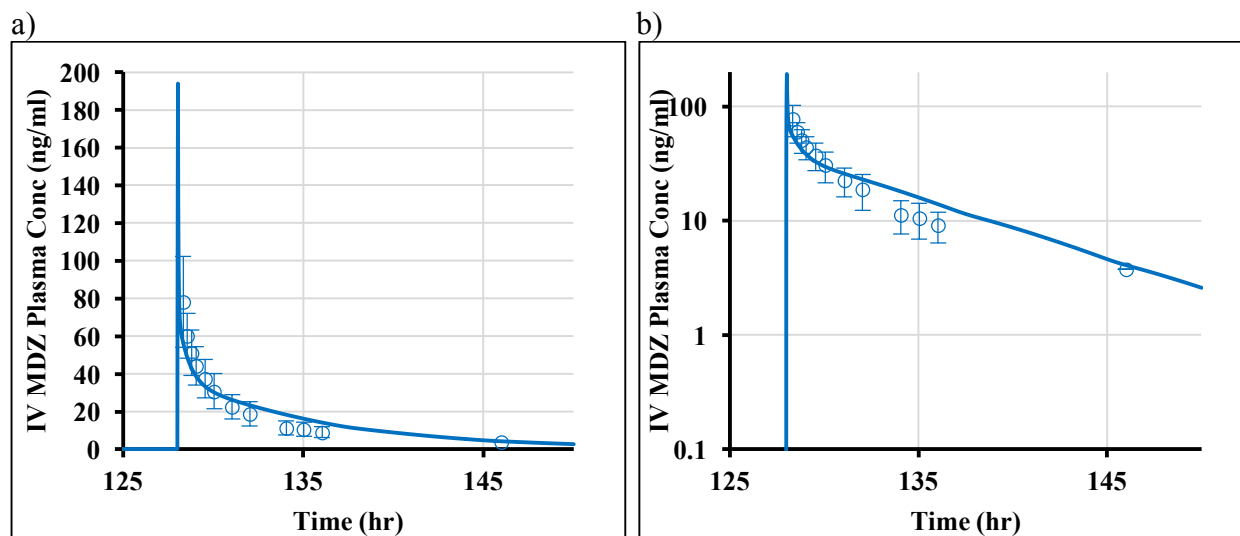


Figure 8.9 Observed and model-predicted IV MDZ (0.05mg/kg) PK profiles in presence of EC ERY (500mg TID for 7 days, IV MDZ was administered 2 hours after the 2nd ERY dose on the 6th day) on Cartesian and semi-log scales.

($v_{\max, \text{hep}}^{\text{MDZ}} = 170,000 \mu\text{g}/\text{min}/\text{kg}$, $F_{\text{abs}}^{\text{ERY}}(\text{EC}) = 0.50$). The solid lines are the predicted PK profiles. The symbols and bars are observed means and SD values (if available). Time is relative to initial ERY/placebo dose.

Since only hepatic metabolic inhibition occurs after IV MDZ, unbound blood/hepatic concentration of ERY as well as relative hepatic CYP3A activity in presence of hepatic CYP3A inhibition by ERY were simulated by semi-PBPK DDI model using adjusted parameters (**Figure 8.10**). ERY unbound hepatic concentration reaches steady-state after 9 doses, and accumulation ratio at steady-state is ~ 4.5 -fold. Throughout the entire profile, $c_{\text{hep,u}}^{\text{ERY}}$ is above $K_{\text{m,bile}}^{\text{ERY}}$, but much lower than $K_{\text{I}}^{\text{ERY}}$ and $K_{\text{m,hep-3A}}^{\text{ERY}}$, suggesting its apparently linear PK (biliary excretion is a minor elimination pathway in PO ERY PBPK model) at the current dosing regimen, and “linear” MBI. Concentrations in the liver are much higher than blood, due to high liver-to-blood partition coefficient ($K_{\text{p,hep,u}}^{\text{ERY}} = 2.71$). When MDZ is administered (indicated as the red dashed line), relative hepatic CYP3A activity reaches the nadir of steady state, and fluctuates between 33% - 46% afterwards.

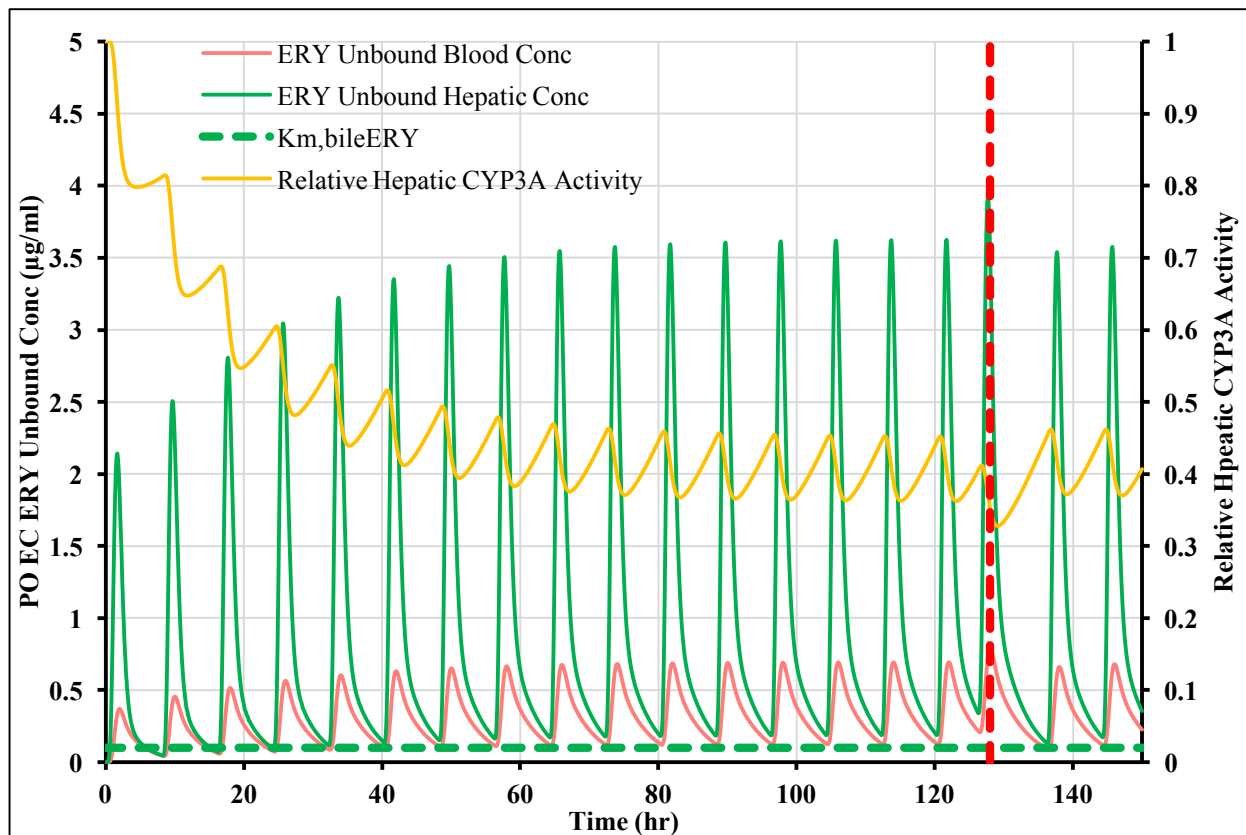
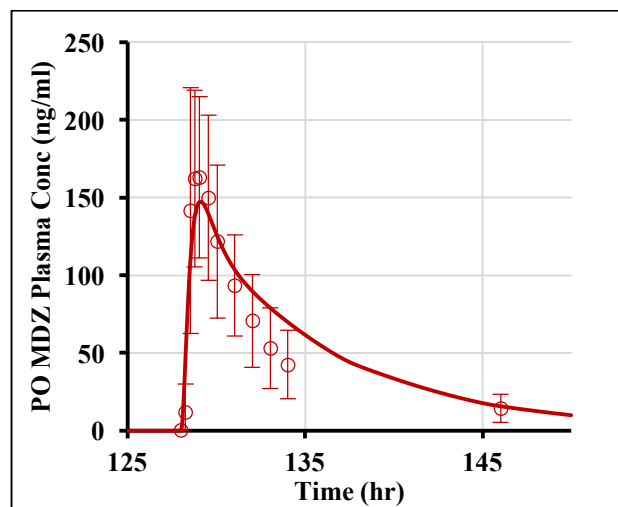


Figure 8.10 Semi-PBPK model - predicted unbound hepatic and blood concentration – time profiles for ERY and relative hepatic CYP3A activity for study 28.

ERY was administered as 500 mg EC TID for 7 days, and MDZ was administered 2 hours after the 2nd EC dose on day 6 (2nd EC dose on day 6 was given 2-hours before scheduled). Red dashed line represents the time when IV MDZ was administered. Time is relative to initial ERY/placebo dose.

After adjusting $v_{\max, \text{hep}}^{\text{MDZ}}$, $k_{\text{GL}}^{\text{MDZ}}$ and $F_{\text{abs}}^{\text{ERY}}(\text{EC})$, the reported PO MDZ PK profile in presence of ERY (**Figure 8.11**) is well captured by the adjusted PBPK model, with exposure metrics ($\text{AUC}_{0-\infty}$, c_{max} , t_{max}), F_{oral} and AUCR all within 30% of observed (**Table 8.4**), confirming the validity of model and final model parameters.

a)



b)

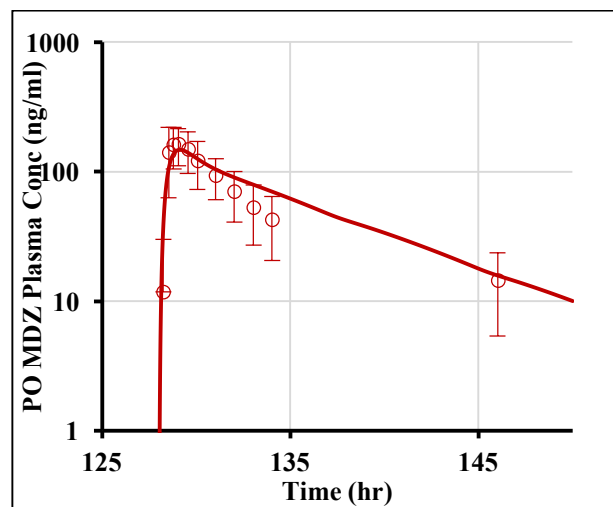


Figure 8.11 Observed and model-predicted PK profiles after 15 mg PO MDZ in presence of EC ERY (500 mg TID for 7 days; PO MDZ was administered 2 hours after the 2nd ERY dose on the 6th day) on Cartesian and semi-log scales.

($v_{\max, \text{hep}}^{\text{MDZ}} = 170,000 \mu\text{g}/\text{min}/\text{kg}$, $k_{\text{GL}}^{\text{MDZ}} = 0.03 \text{ min}^{-1}$, $F_{\text{abs}}^{\text{ERY}}(\text{EC}) = 0.50$). The solid lines are the predicted PK profiles. The symbols and bars are observed means and SD values (if available). Time is relative to initial ERY/placebo dose.

After PO MDZ, both GW and hepatic CYP3A are inhibited by ERY. Unbound hepatic ERY concentration and relative hepatic CYP3A activity are the same as **Figure 8.10**. With respect to ERY GW mucosa concentrations (**Figure 8.12**), no accumulation is observed due to its rapid loss (quick transfer to GW serosa compartment) and minor contribution to ERY's pre-systemic metabolism (<10%). The peak ERY GW mucosa concentration (~10 mg/L) is much higher than its hepatic concentration, resulting in faster inactivation of CYP3A in GW, and greater maximal GW CYP3A inhibition (inhibited by 72%). However, due to the rapid drop of $c_{\text{GW-M,u}}^{\text{ERY}}$,

fluctuation of GW CYP3A (25% - 48%) is larger than hepatic CYP3A, and when MDZ is administered, GW CYP3A reaches its nadir (25% of original).

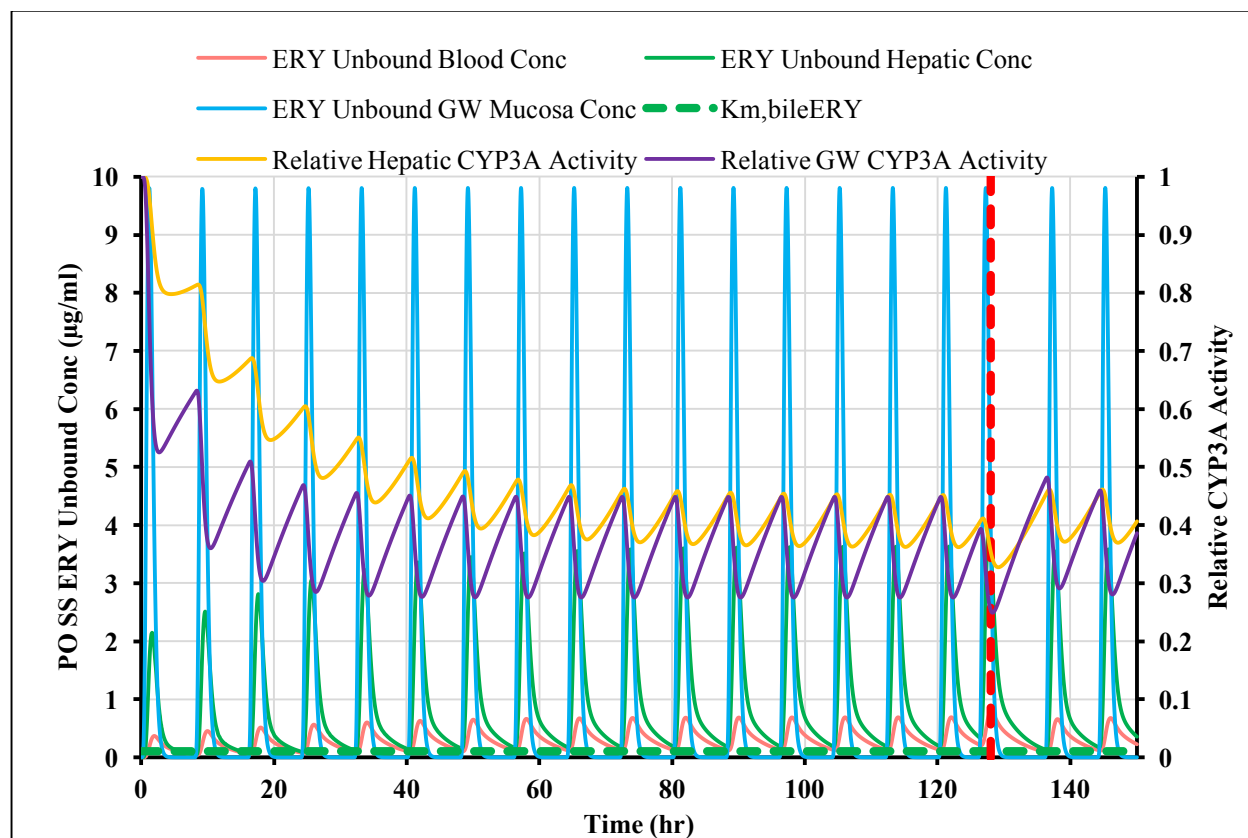


Figure 8.12 Semi-PBPK model-predicted ERY unbound hepatic/GW mucosa/blood concentration – time profiles and relative hepatic/GW CYP3A activity for study 28.

ERY was administered as 500 mg EC TID for 7 days, and MDZ was administered 2 hours after the 2nd EC dose on day 6 (2nd EC dose on day 6 was given 2-hours before scheduled). Red dashed line represents the time when PO MDZ was administered.

8.3.1.1.2 Study 603

For study 603, all model parameters were originally assumed to be the values in **Table 8.1**. The reported and model-predicted PO MDZ PK profiles in absence of ERY are shown in **Figure 8.13** and exposure metrics are summarized in **Table 8.4**. After visual inspection of PK profiles and exposure metrics, the model over-estimates the terminal slope and c_{\max} of MDZ PK profile; thus, $v_{\max, \text{hep}}^{\text{MDZ}}$ and $k_{\text{GL}}^{\text{MDZ}}$ were optimized to 170,000 $\mu\text{g}/\text{min}/\text{kg}$ and 0.03 min^{-1} , explained as inter-individual variability of hepatic CYP3A and possible solubility/dissolution-limited absorption in study 603 (5 mg MDZ dose was administered). f_{villi} was also adjusted (to 5.0) to better characterize the observed MDZ PK profile, attributed to inter-individual variability of GW CYP3A activity. After optimizing $v_{\max, \text{hep}}^{\text{MDZ}}$, $k_{\text{GL}}^{\text{MDZ}}$ and f_{villi} , the adjusted PBPK model predicts PO MDZ PK profile and exposure metrics ($\text{AUC}_{0-\infty}$, c_{\max} , t_{\max}) well (shown in **Figure 8.14** and **Table 8.4**). All adjusted PBPK parameters for study 28 and 603 are summarized in **Table 8.5**.

Table 8.5 Adjusted semi-PBPK DDI (MDZ+ERY) model parameters for study 28 and 603.

Parameter	Definition	Value	Source
$v_{\max, \text{hep}}^{\text{MDZ}}$ (ng/min/kg)	Hepatic CYP3A capacity to metabolize MDZ	170,000	Value used for study 28 and 603 based on terminal slope optimization
$k_{\text{GL}}^{\text{MDZ}}$ (min^{-1})	Absorption rate constant from gut lumen to GW	0.03	Value used for study 28 and 603 due to presumably solubility/dissolution limited absorption
$F_{\text{abs}}^{\text{ERY}}$ (EC)	Fraction of ERY EC absorbed from gut lumen	0.50	Value used for study 28 based on reported ERY plasma level
f_{villi}	IVIVE scaling factor and IIV adjusting factor	5.0	Value used for study 603 based on observed PO MDZ PK profile

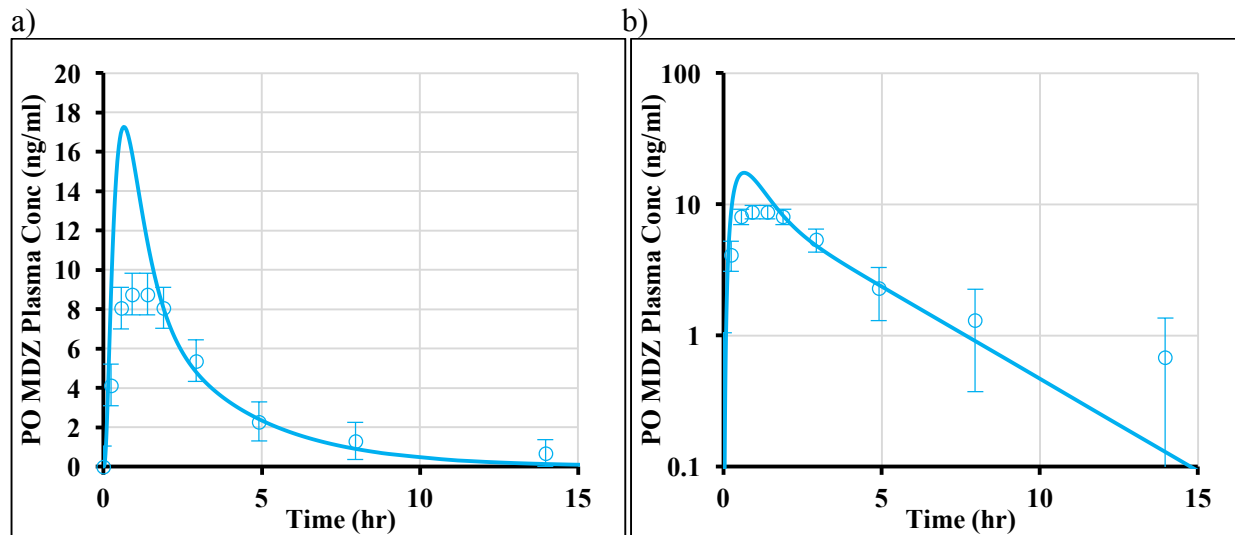


Figure 8.13 Observed and model-predicted MDZ PK profiles after 5 mg PO administration (Cartesian and semi-log scales) ($v_{\max, \text{hep}}^{\text{MDZ}} = 305,067 \mu\text{g}/\text{min}/\text{kg}$, $k_{\text{GL}}^{\text{MDZ}} = 0.05 \text{ min}^{-1}$, $f_{\text{villi}} = 2.2$).

The solid lines are the predicted PK profiles. The symbols and bars are observed means and SD values (if available).

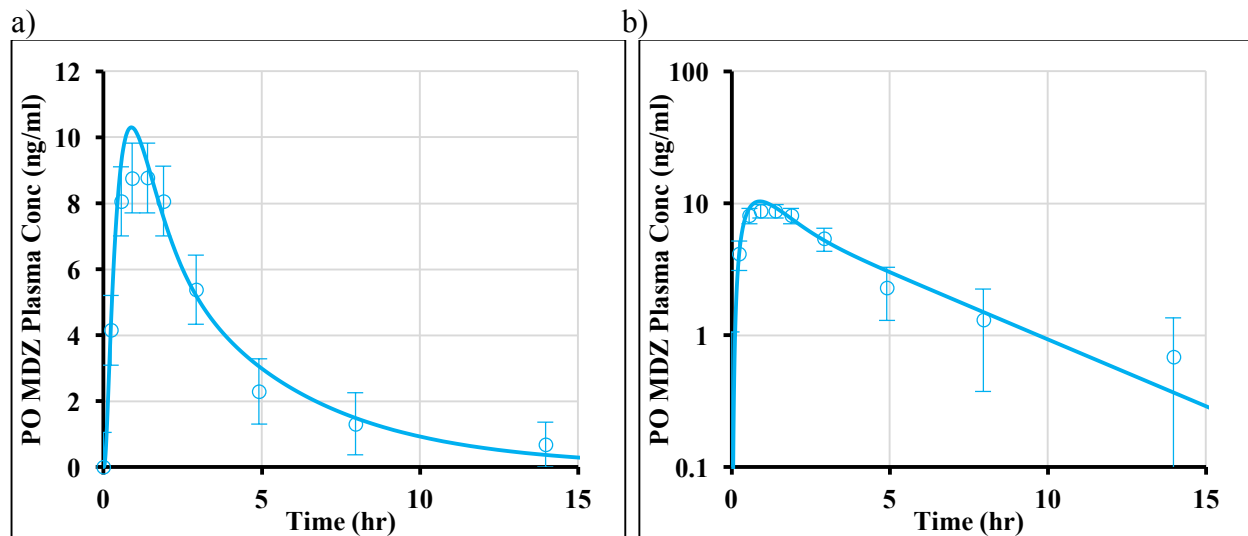


Figure 8.14 Observed and model-predicted MDZ PK profiles after 5 mg PO administration (Cartesian and semi-log scales) ($v_{\max, \text{hep}}^{\text{MDZ}} = 170,000 \mu\text{g}/\text{min}/\text{kg}$, $k_{\text{GL}}^{\text{MDZ}} = 0.03 \text{ min}^{-1}$, $f_{\text{villi}} = 5.0$).

The solid lines are the predicted PK profiles. The symbols and bars are observed means and SD values (if available).

After adjusting $v_{\max, \text{hep}}^{\text{MDZ}}$, $k_{\text{GL}}^{\text{MDZ}}$ and f_{villi} , model-predicted PO MDZ PK profiles in presence of 2 days/4 days/7days ERY are all well captured by the adjusted PBPK model parameters (**Figure 8.15**), with exposure metrics ($\text{AUC}_{0-\infty}$, c_{\max} , t_{\max}), F_{oral} and AUCR all within 30% of observed (**Table 8.4**), confirming the validity of model and final model parameters, especially the MBI parameters.

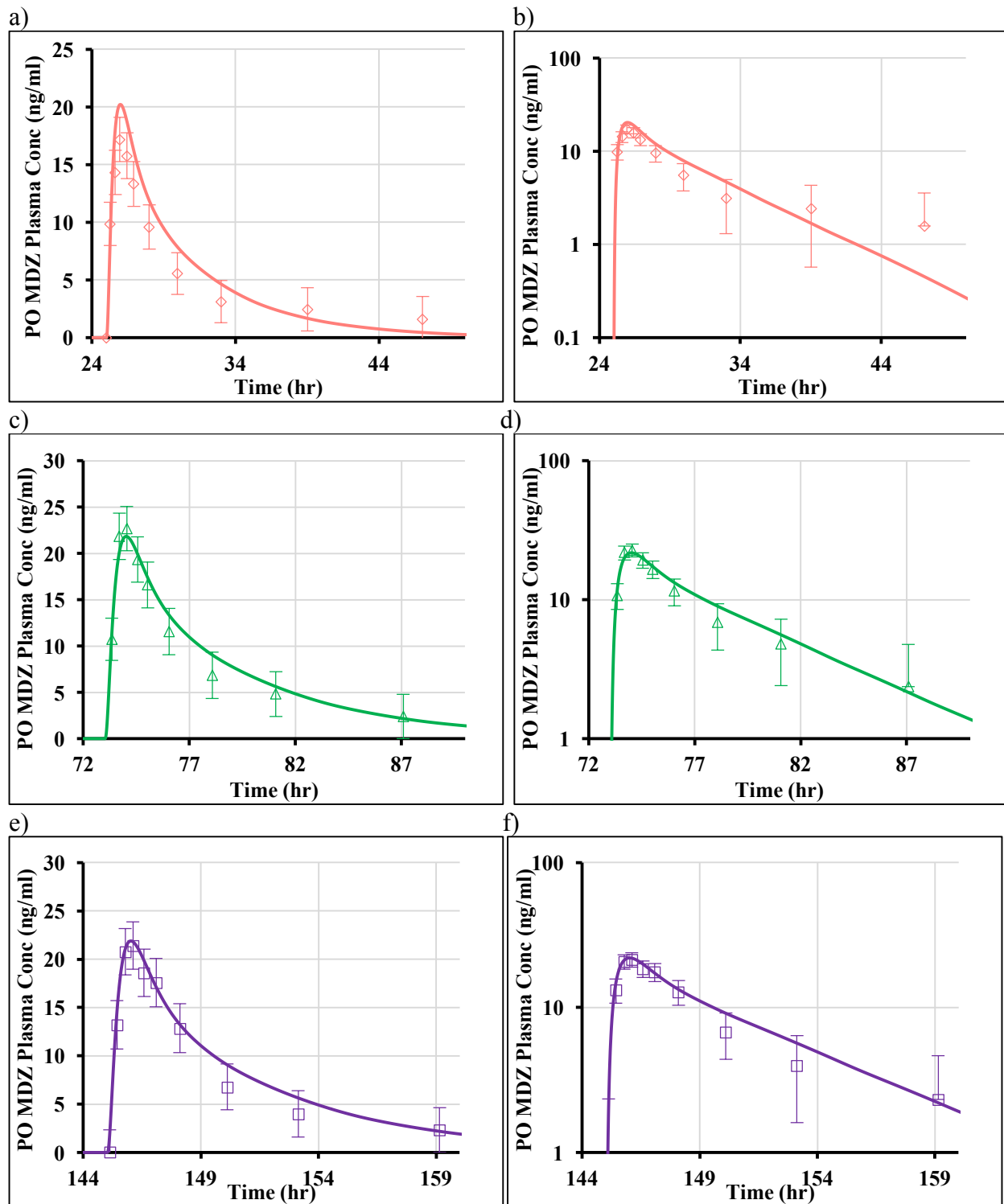


Figure 8.15 Observed and model-predicted 2.5 mg PO MDZ PK profiles (profiles scaled to 5 mg MDZ dose) in presence of SS ERY (200mg QID for 2, 4 or 7 days).

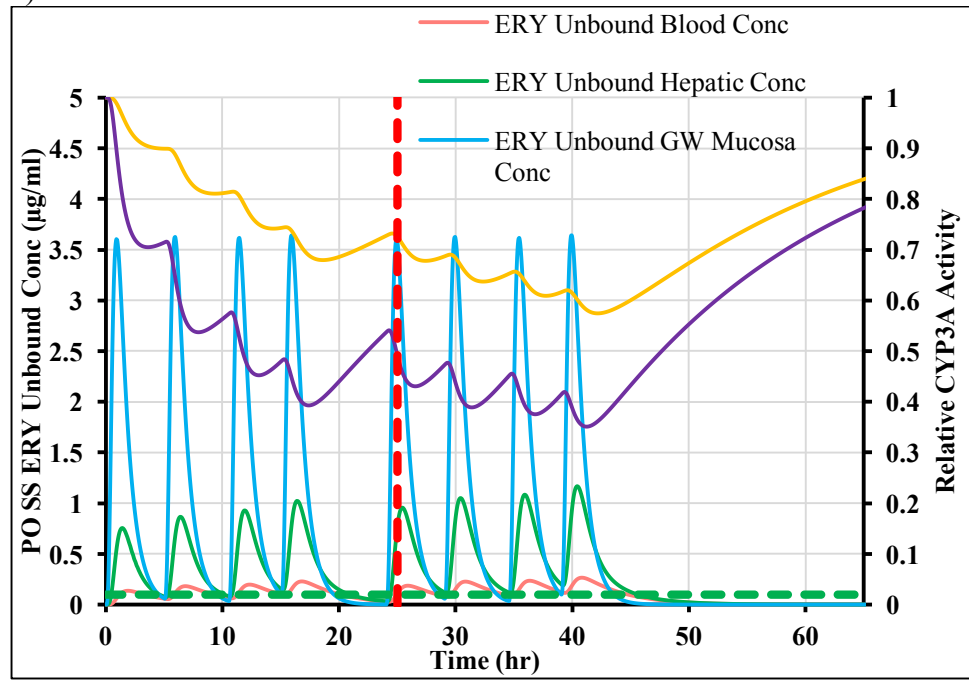
($v_{\max, \text{hep}}^{\text{MDZ}} = 170,000 \mu\text{g}/\text{min}/\text{kg}$, $k_{\text{GL}}^{\text{MDZ}} = 0.03 \text{ min}^{-1}$, $f_{\text{villi}} = 5.0$). a-b) MDZ administered 1-hour after the 1st ERY dose on 2nd day (Cartesian and semi-log scales). c-d) MDZ administered 1-hour after the 1st ERY dose on 4th day (Cartesian and semi-log scales). e-f) MDZ administered

1-hour after the 1st ERY dose on 7th day (Cartesian and semi-log scales). The solid lines are the predicted PK profiles. The symbols and bars are observed means and SD values (if available). Time is relative to initial ERY/placebo dose.

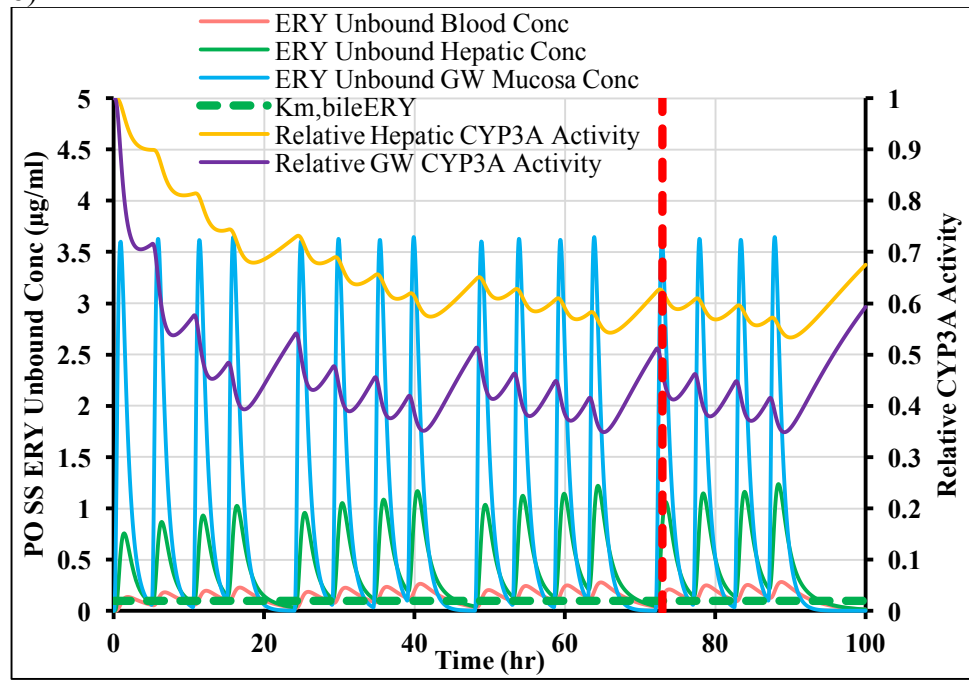
Unbound ERY blood/hepatic/GW mucosa concentrations for ERY, as well as relative hepatic/GW CYP3A activity were simulated by the final semi-PBPK DDI model using adjusted parameters (**Figure 8.16**). ERY was administered as SS formulation 200 mg QID for 2 days (**Figure 8.16a**), 4 days (**Figure 8.16b**) and 7 days (**Figure 8.16c**), and 2.5 mg MDZ was administered 1 hour after the 1st dose of ERY on day 2, day 4 and day 7 (indicated as red dashed line). Throughout the entire profile, $c_{\text{hep,u}}^{\text{ERY}}$ is above $K_{\text{m,bile}}^{\text{ERY}}$, but much lower than $K_{\text{I}}^{\text{ERY}}$ and $K_{\text{m,hep-3A}}^{\text{ERY}}$, confirming its apparently linear PK (biliary excretion is a minor elimination pathway) at the current dosing regimen, and “linear” MBI. With respect to ERY GW mucosa concentration, no accumulation is observed due to its rapid decline (quick transfer to GW serosa compartment) and minor contribution to ERY’s pre-systemic metabolism (<10%). Peak ERY GW mucosa concentration (~3.5 mg/L) is much higher than hepatic concentration, resulting in faster inactivation of CYP3A in GW, and greater maximal CYP3A inhibition (inhibited by 65%) than hepatic CYP3A inhibition (inhibited by 47%). Relative GW CYP3A level reaches steady-state almost on day 2, so there is no difference regarding GW CYP3A inhibition among day 2, 4 or 7. However, hepatic CYP3A level reaches steady-state on day 4, and when MDZ is administered on day 2, the nadir of hepatic CYP3A level within 6-hours of MDZ administration (first ERY dosing interval after MDZ administration) is 68%, compared with 58% when MDZ is administered on day 4 and 7. As a result, the different observed MDZ AUCR after various time course of ERY SS administration (EM2: AUCR = 2.4; EM4 and EM7: AUCR = 3.4) is primarily due to different hepatic metabolic inhibition between 2 days of SS and 4 or 7 days of SS. There

is no difference between metabolic inhibition by 4 days SS and 7 days SS. Concentrations in the liver and GW mucosa are much higher than blood, due to high liver-to-blood and GW-to-blood partition coefficients ($K_{p,hep,u}^{ERY} = 2.71, K_{GW,u}^{ERY} = 2.71$).

a)



b)



c)

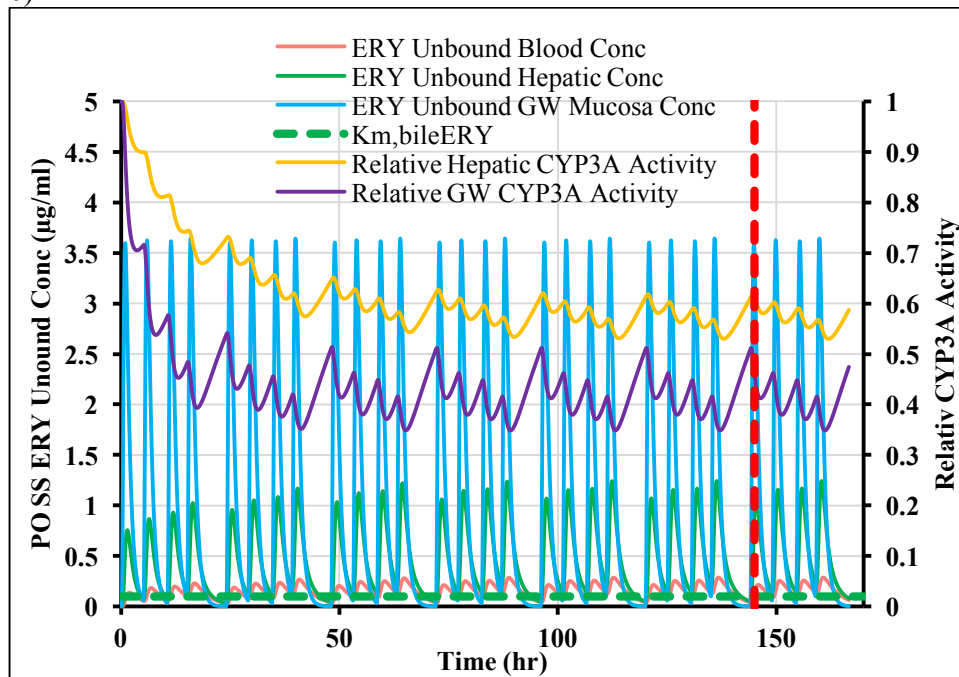


Figure 8.16 Semi-PBPK model predicted ERY unbound hepatic/GW mucosa/blood concentration – time profiles and relative hepatic/GW CYP3A activity in study 603.

a) ERY was administered as 200 mg SS QID for 2 days, and MDZ was administered 1-hour after the 1st SS dose on day 2. b) ERY was administered as 200 mg SS QID for 4 days, and MDZ was administered 1-hour after the 1st SS dose on day 4. c) ERY was administered as 200 mg SS QID for 7 days, and MDZ was administered 1-hour after the 1st SS dose on day 7. Red dashed line represents the time when PO MDZ was administered.

8.3.1.2 Sensitivity analysis

The -fold change in MDZ plasma $AUC_{0-\infty}$, GW/hepatic CYP3A inhibited $AUC_{0-\tau}$ and GW/hepatic ERY $AUC_{0-\tau}$ after single- and repeat- doses were calculated by dividing AUC simulated at the upper limit by that simulated at the lower limit. **Table 8.6** summarizes the results of this sensitivity analysis under dosing regimen of study 28, and **Table 8.7** summarizes sensitivity analysis under dosing regimen of study 603. A greater than 2-fold or less than 0.5-fold change was highlighted in bold, indicating the corresponding exposure is sensitive to that parameter. All sensitivity analysis plots are presented in **Appendices K** (for study 28) and **L** (for study 603).

For study 28, $AUC_{0-\infty}$ for both IV and PO MDZ are substantially affected by k_{deg} , K_I^{ERY} , k_{inact}^{ERY} and $v_{max,hep}^{ERY}$, due to their impact on hepatic/GW CYP3A activity after multiple ERY EC doses. The AUCR of PO MDZ is changed more than AUCR of IV MDZ, because besides systemic hepatic metabolism, pre-systemic GW and hepatic metabolism are also inhibited by ERY. With respect to the -fold change in inhibited $AUC_{0-\tau}^{CYP3A}$, k_{deg} alters $AUC_{0-\tau}^{CYP3A}$ to a greater extent after repeat- ERY doses than after single dose, because after repeat- doses, the natural recovery (without considering MBI) of CYP3A activity, dependent on k_{in} (numerically equal to k_{deg}) and k_{deg} , is more essential to determine CYP3A activity than after single ERY dose. However, K_I^{ERY} , k_{inact}^{ERY} and $v_{max,hep}^{ERY}$ influence $AUC_{0-\tau}^{CYP3A}$ after single-dose more than repeat- doses, because all the three parameters affect MBI of ERY. After multiple ERY doses for 7 days, CYP3A inhibition has reached steady-state, while after single dose, a lower K_I^{ERY} , a higher k_{inact}^{ERY} or a smaller $v_{max,hep}^{ERY}$ can all shorten the time required to reach steady-state (**Figure K.10**, **Figure K.16**, **Figure K.22**), resulting in larger inhibited $AUC_{0-\tau}^{CYP3A}$ after single ERY dose. Hepatic CYP3A is affected more than GW CYP3A, due to the more rapid ERY GW

mucosa concentration decline than hepatic concentration decline. With respect to ERY hepatic and GW mucosa concentration, k_{deg} can only affect hepatic $AUC_{0-\infty}^{ERY}$ after multiple dosing (but not single dose). K_I^{ERY} , k_{inact}^{ERY} and $v_{max,hep}^{ERY}$ influence hepatic $AUC_{0-\infty}^{ERY}$ after both single- and repeat- doses, and $AUC_{0-\infty}^{ERY}$ after repeat- EC doses is affected more than after single dose (**Figure K.12, Figure K.18, Figure K.24**). This is because for MBI, there is a delay between maximal inhibition (hepatic CYP3A nadir) and c_{max} of hepatic ERY concentration; when CYP3A achieves its nadir (within the first dosing interval), hepatic ERY concentration has already dropped to the terminal phase of its concentration profile, which won't have much influence on its hepatic AUC. After multiple dosing, hepatic CYP3A level is consistently low, affecting the entire hepatic ERY PK profile, and a greater extent of AUC influence should be observed. No influence on GW mucosa concentration is found after either single or multiple doses, due to its rapid decline (quick transfer to GW serosa compartment) and minor contribution to ERY's pre-systemic metabolism (<10%). $AUC_{0-\infty}^{CYP3A}$ is consistently more sensitive to k_{deg} , K_I^{ERY} , k_{inact}^{ERY} and $v_{max,hep}^{ERY}$ than $AUC_{0-\infty}^{ERY}$, due to the slow degradation $t_{1/2}$ of CYP3A (~14 hours) and the fast plasma elimination $t_{1/2}$ of ERY (~2 hours). Since biliary excretion in the PO ERY semi-PBPK model is not a major route of elimination, neither $v_{max,bile}^{ERY}$ nor $K_{m,bile}^{ERY}$ has significant influence on any exposure metrics.

Table 8.6 Sensitivity analysis heat-map results for semi-PBPK MDZ and ERY EC DDI model under dosing regimen in study 28.

(PO EC ERY 500 mg TID for 7 days; IV (0.05 mg/kg) or PO (15 mg) MDZ was administered 2 hours after the 2nd EC dose on the 6th day)

(More solid green indicates smaller value; more solid red indicates larger value)

ERY+MDZ Sensitivity Analysis		-Fold change in inhibited AUC_{τ}^{CYP3A} after single ERY dose		-Fold change in $AUC_{\tau,u}^{ERY}$ after single ERY dose	
Parameter		GW CYP3A	Hepatic CYP3A	$C_{GW-M,u}^{ERY}$	$C_{hep,u}^{ERY}$
k_{deg}		0.54	0.55	1.00	0.97
K_I^{ERY}		0.16	0.06	0.96	0.55
k_{inact}^{ERY}		7.98	20.34	1.06	2.21
$v_{max,hep-3A}^{ERY}$		1.00	0.11	1.00	0.06
$v_{max,bile}^{ERY}$		1.00	0.86	1.00	0.80
$K_{m,bile}^{ERY}$		1.00	1.02	1.00	1.04
	-Fold change in plasma $AUC_{0-\infty}^{MDZ}$	-Fold change in inhibited AUC_{τ}^{CYP3A} CYP3A after repeat- ERY dose		-Fold change in $AUC_{\tau,u}^{ERY}$ after repeat- ERY dose	
Parameter	IV MDZ PO MDZ	GW CYP3A	Hepatic CYP3A	$C_{GW-M,u}^{ERY}$	$C_{hep,u}^{ERY}$
k_{deg}	0.09 0.05	0.29	0.14	0.95	0.11
K_I^{ERY}	0.12 0.07	0.37	0.15	0.96	0.13
k_{inact}^{ERY}	9.85 19.85	3.18	7.15	1.05	9.48
$v_{max,hep-3A}^{ERY}$	0.21 0.17	1.00	0.18	1.00	0.02
$v_{max,bile}^{ERY}$	0.75 0.73	1.00	0.79	1.00	0.57
$K_{m,bile}^{ERY}$	1.03 1.03	1.00	1.02	1.00	1.06

In study 603, repeat- SS ERY was administered for different time courses, and sensitivity analyses were conducted after different duration of pretreated SS. $AUC_{0-\infty}$ of PO MDZ is also substantially affected by k_{deg} , K_I^{ERY} , k_{inact}^{ERY} and $v_{max,hep}^{ERY}$, and with increasing duration of SS ERY treatment, the extent of influence becomes larger. There is no significant difference between $AUC_{0-\infty}$ after 4 days and 7 days SS, because inhibition of ERY on GW and hepatic CYP3A reach steady-state on day 4. Some influence (*i.e.* K_I^{ERY} , k_{inact}^{ERY} , $v_{max,bile}^{ERY}$) on $AUC_{0-\infty}^{MDZ}$ is slightly larger after 4 days SS than 7 days, because the sensitivity analysis for MDZ administered on day 2, 4, and 7 was simulated simultaneously, and the slightly higher impact on day 4 is due to minor carry-over effect of MDZ administered on day 2. The carry-over effect is mostly negligible, given the 2-day washout period and the short MDZ $t_{1/2}$ (6 hours without inhibition), and the sensitivity analysis results should be almost the same after 4 days SS and 7 days SS. Inhibited $AUC_{0-\tau}^{CYP3A}$ and $AUC_{0-\tau}^{ERY}$ are also affected by k_{deg} , K_I^{ERY} , k_{inact}^{ERY} and $v_{max,hep}^{ERY}$. Neither

$V_{\max, \text{bile}}^{\text{ERY}}$ nor $K_{\text{m}, \text{bile}}^{\text{ERY}}$ has significant influence on any exposure metrics.

Table 8.7 Sensitivity analysis heat-map results for semi-PBPK MDZ and ERY SS DDI model under dosing regimen in study 603.

(PO SS ERY 200 mg QID for 7 days; PO 5 mg MDZ was administered 1 hours after the 1st SS dose on the 2nd/4th/7th day)

(More solid green indicates smaller value; more solid red indicates larger value)

ERY+MDZ Sensitivity Analysis		-Fold change in inhibited AUC_{CYP3A} after single ERY dose		-Fold change in $AUC_{\text{su}}^{\text{ERY}}$ after single ERY dose	
Parameter		GW CYP3A	Hepatic CYP3A	$C_{\text{GW-M,u}}^{\text{ERY}}$	$C_{\text{hep,u}}^{\text{ERY}}$
$k_{\text{deg}}^{\text{ERY}}$		0.69	0.71	1.00	0.99
$K_{\text{I}}^{\text{ERY}}$		0.09	0.05	1.00	0.80
$k_{\text{inact}}^{\text{ERY}}$		12.63	23.16	1.00	1.27
$V_{\max, \text{hep-3A}}^{\text{ERY}}$		1.00	0.11	1.00	0.08
$V_{\max, \text{bile}}^{\text{ERY}}$		1.00	0.77	1.00	0.72
$K_{\text{m}, \text{bile}}^{\text{ERY}}$		1.00	1.04	1.00	1.05
-Fold change in plasma $AUC_{\infty}^{\text{MDZ}}$ administered on day 2		-Fold change in inhibited AUC_{CYP3A} CYP3A after repeat-ERY dose (2 days)		-Fold change in $AUC_{\text{su}}^{\text{ERY}}$ after repeat-ERY dose (2 days)	
Parameter	PO MDZ	GW CYP3A	Hepatic CYP3A	$C_{\text{GW-M,u}}^{\text{ERY}}$	$C_{\text{hep,u}}^{\text{ERY}}$
$k_{\text{deg}}^{\text{ERY}}$	0.30	0.26	0.15	1.00	0.63
$K_{\text{I}}^{\text{ERY}}$	0.13	0.22	0.07	1.00	0.24
$k_{\text{inact}}^{\text{ERY}}$	9.32	4.85	14.54	1.00	4.89
$V_{\max, \text{hep-3A}}^{\text{ERY}}$	0.43	1.00	0.10	1.00	0.04
$V_{\max, \text{bile}}^{\text{ERY}}$	0.89	1.00	0.70	1.00	0.62
$K_{\text{m}, \text{bile}}^{\text{ERY}}$	1.02	1.00	1.06	1.00	1.08
-Fold change in plasma $AUC_{\infty}^{\text{MDZ}}$ administered on day 4		-Fold change in inhibited AUC_{CYP3A} CYP3A after repeat-ERY dose (4 days)		-Fold change in $AUC_{\text{su}}^{\text{ERY}}$ after repeat-ERY dose (4 days)	
Parameter	PO MDZ	GW CYP3A	Hepatic CYP3A	$C_{\text{GW-M,u}}^{\text{ERY}}$	$C_{\text{hep,u}}^{\text{ERY}}$
$k_{\text{deg}}^{\text{ERY}}$	0.12	0.23	0.08	1.00	0.22
$K_{\text{I}}^{\text{ERY}}$	0.10	0.27	0.09	1.00	0.19
$k_{\text{inact}}^{\text{ERY}}$	12.62	4.05	11.23	1.00	6.44
$V_{\max, \text{hep-3A}}^{\text{ERY}}$	0.39	1.00	0.12	1.00	0.03
$V_{\max, \text{bile}}^{\text{ERY}}$	0.85	1.00	0.68	1.00	0.58
$K_{\text{m}, \text{bile}}^{\text{ERY}}$	1.03	1.00	1.06	1.00	1.09
-Fold change in plasma $AUC_{\infty}^{\text{MDZ}}$ administered on day 7		-Fold change in inhibited AUC_{CYP3A} CYP3A after repeat-ERY dose (7 days)		-Fold change in $AUC_{\text{su}}^{\text{ERY}}$ after repeat-ERY dose (7 days)	
Parameter	PO MDZ	GW CYP3A	Hepatic CYP3A	$C_{\text{GW-M,u}}^{\text{ERY}}$	$C_{\text{hep,u}}^{\text{ERY}}$
$k_{\text{deg}}^{\text{ERY}}$	0.09	0.23	0.08	1.00	0.15
$K_{\text{I}}^{\text{ERY}}$	0.11	0.27	0.10	1.00	0.18
$k_{\text{inact}}^{\text{ERY}}$	12.39	4.01	10.95	1.00	6.50
$V_{\max, \text{hep-3A}}^{\text{ERY}}$	0.39	1.00	0.12	1.00	0.03
$V_{\max, \text{bile}}^{\text{ERY}}$	0.84	1.00	0.68	1.00	0.57
$K_{\text{m}, \text{bile}}^{\text{ERY}}$	1.03	1.00	1.06	1.00	1.09

8.3.2 Model Predictions

8.3.2.1 Simulation of route-dependent DDI between MDZ and ERY after various administration time intervals

AUCR for each scenario was calculated to assess the extent of inhibition, and is plotted against administration interval time shown in **Figure 8.17** (same dose IV ERY vs. PO EC ERY) and **Figure 8.18** (same dose IV ERY vs. PO SS ERY). ERY unbound hepatic/GW mucosa concentration – time profiles and relative hepatic/GW CYP3A activity were simulated to better interpret **Figure 8.17** and **Figure 8.18** (**Figure 8.19**: comparing IV ERY and PO EC ERY; **Figure 8.20**: comparing IV ERY and PO SS ERY).

For IV MDZ, ERY causes more inhibition after IV than after PO (EC and SS) administration, due to ERY's relatively low F_{oral} (EC: ~60%; SS: ~30%) and higher unbound (peak) hepatic concentrations after IV than after PO administration (**Figure 8.19a**, **Figure 8.20a**). Although $t_{max,hep}^{ERY}$ after IV administration is different from that after PO administration, **Figure 8.19b** and **Figure 8.20b** clearly demonstrate that IV ERY produces more inhibition on hepatic CYP3A throughout the entire profile than PO ERY, and the difference between IV and PO SS ERY is larger than the difference between IV and PO EC ERY, due to the lower F_{oral}^{ERY} after SS formulation. The peak DDI magnitude is achieved when MDZ is dosed ~5 hours after ERY (when hepatic CYP3A activity level achieves its nadir), which is much later than the time for ERY to reach its hepatic peak concentration (0.3 hour after IV, 1.7 hours after PO EC, and 1.4 hours after PO SS ERY). This is because for MBI, ERY hepatic concentrations directly affects inactivation rate of CYP3A in the liver, but it still takes time for the existing CYP3A to be inactivated; thus, there is a lag time between peak of ERY hepatic concentration and nadir of hepatic CYP3A activity.

For PO MDZ, when simultaneously administered with MDZ, ERY still shows more inhibition after IV than after PO (EC and SS) administration, while the inhibition by PO ERY gradually exceeds (for EC) or equals (SS) the one by IV ERY over time. This is primarily because ERY is assumed to enter the GW mucosa from the gut lumen only; since its high plasma protein binding and low lipophilicity prevent serosal GW access (see **section 8.2.1**); therefore, only PO (but not IV) ERY causes inhibition of GW metabolism (**Figure 8.19c-d, Figure 8.20c-d**). However, because there is a lag time for ERY to enter GW mucosa (represented by several transit compartments), when the two drugs are dosed simultaneously, their DDI still mainly reflects DDI in hepatic CYP3A, which is the reason why IV ERY still won over PO ERY at the beginning. Maximal DDI magnitude for EC exceeds IV ERY, whereas that for SS only matches with IV ERY, because the hepatic CYP3A inhibition difference between SS and IV ERY is larger than that between EC and IV ERY, and only EC can easily surpass IV ERY with GW CYP3A inhibition. The peak DDI magnitude is achieved when MDZ is dosed ~2-5 hours later than ERY (when GW/hepatic CYP3A activity levels achieves their nadirs), which is much later than the time for ERY to reach its hepatic/GW peak concentration. Despite ERY's short plasma/pseudo steady-state elimination $t_{1/2}$ (~2 hours.), its metabolic DDI with MDZ lasts about 4 days - regardless of route of administration, because the recovery of CYP3A activity mainly depends on the degradation $t_{1/2}$ of CYP3A (~ 14 hours).

With respect to route difference for MDZ, due to its pre-systemic hepatic and GW metabolism, PO MDZ is consistently more sensitive to metabolic inhibition than IV MDZ, regardless of ERY route.

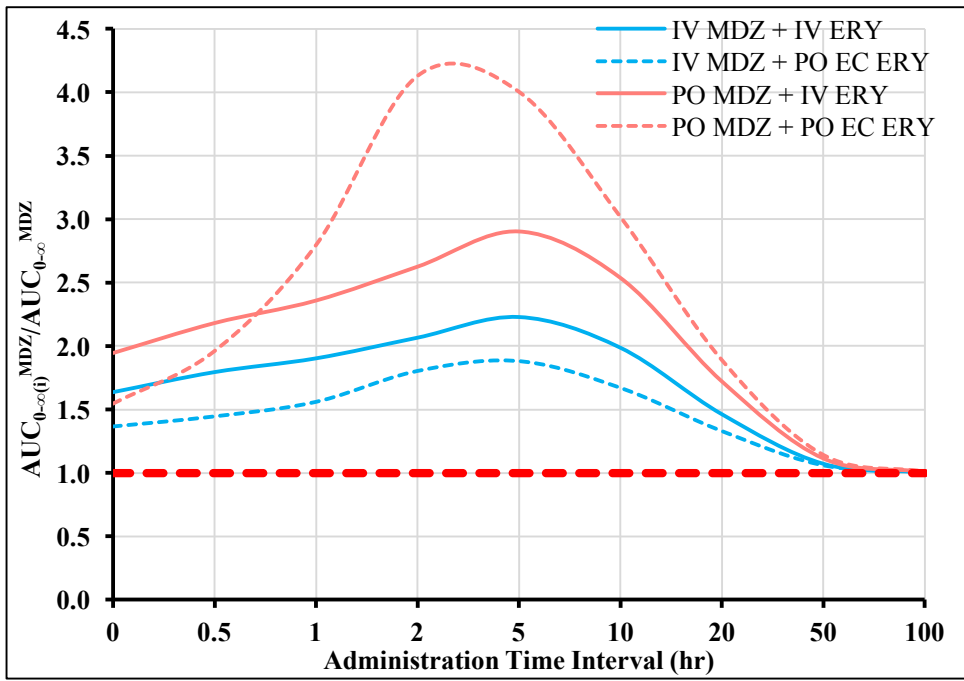


Figure 8.17 MDZ AUCR by 1,000 mg ERY IV (as 15-min infusion) or PO (EC) administration followed by MDZ (IV: 1 mg; PO 3 mg) at various time intervals. Red dash line indicates no inhibition on MDZ exposure.

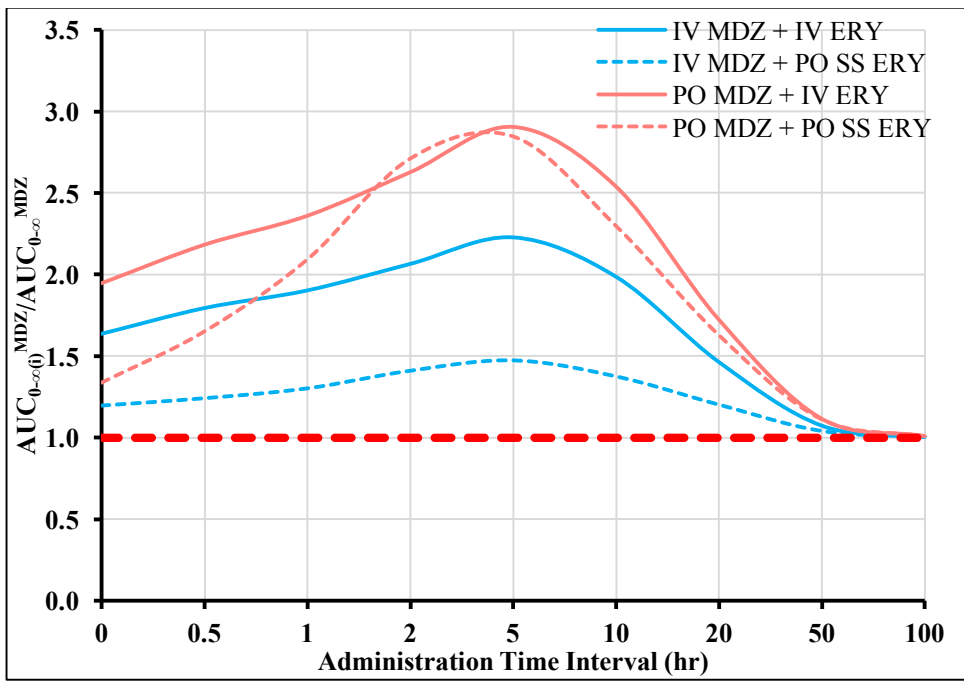


Figure 8.18 MDZ AUCR by 1,000 mg ERY IV (as 15-min infusion) or PO (SS) administration followed by MDZ (IV: 1 mg; PO 3 mg) at various time intervals. Red dash line indicates no inhibition on MDZ exposure.

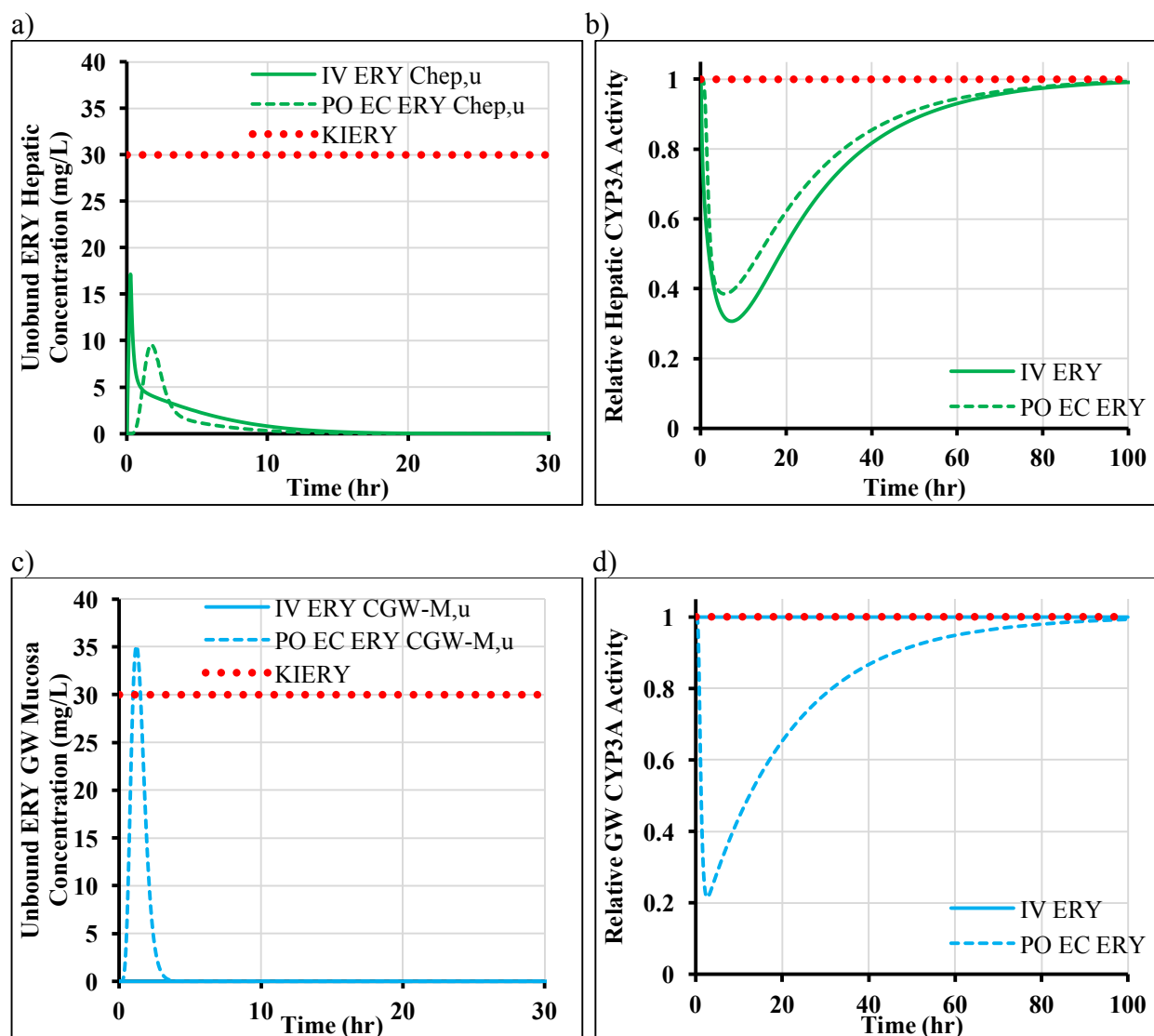


Figure 8.19 Plots of unbound hepatic/GW concentrations for ERY and relative CYP3A activity profiles after a single dose of ERY (1,000 mg; IV: 15-min infusion, PO: EC).

a) ERY unbound hepatic concentration – time profiles. b) Relative hepatic CYP3A activity in presence of ERY. c) ERY unbound GW concentration – time profiles. d) Relative GW CYP3A activity in presence of ERY. Dash lines in a) and c) represent K_I^{ERY} . Dash lines in b) and d) represent no change in hepatic and GW CYP3A activity.

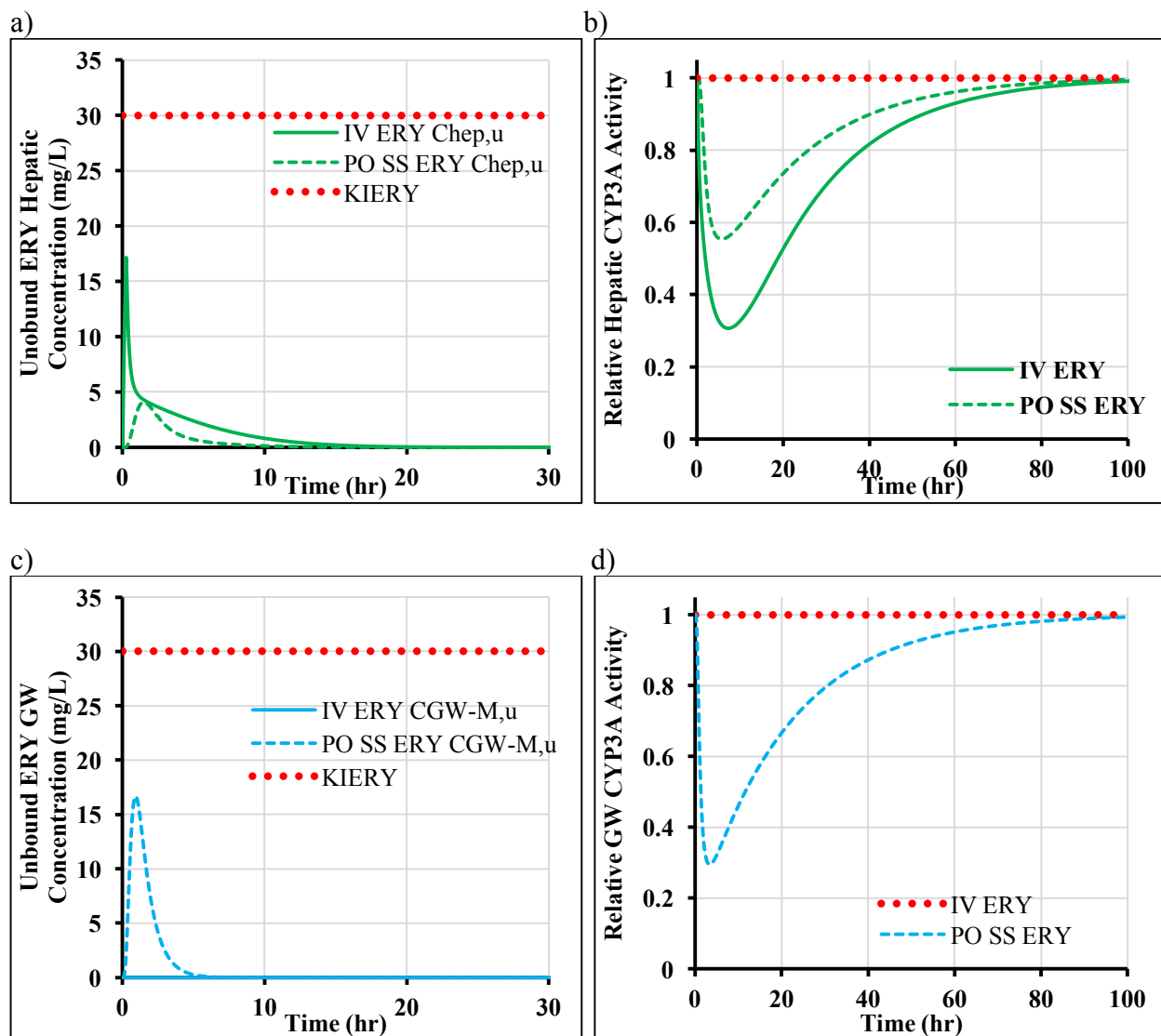


Figure 8.20 Plots of unbound hepatic/GW concentrations for ERY and relative CYP3A activity profiles after a single dose of ERY (1,000 mg; IV: 15-min infusion, PO: SS). a) ERY unbound hepatic concentration – time profiles. b) Relative hepatic CYP3A activity in presence of ERY. c) ERY unbound GW concentration – time profiles. d) Relative GW CYP3A activity in presence of ERY. Dash lines in a) and c) represent K_1^{ERY} . Dash lines in b) and d) represent no change in hepatic and GW CYP3A activity.

$F_{\text{oral}}^{\text{MDZ}}$ (**Figure 8.21**), $ER_{\text{GI}}^{\text{MDZ}}$ and $ER_{\text{hep}}^{\text{MDZ}}$ in presence of different routes of ERY, as well as (inhibited/uninhibited) ratio of $ER_{\text{GI}}^{\text{MDZ}}$ and $ER_{\text{hep}}^{\text{MDZ}}$ (**Figure 8.22**) are plotted against administration time interval (ERY followed by MDZ) between the two drugs.

$ER_{\text{GI}}^{\text{MDZ}}$ in absence/presence of ERY was estimated by calculating the ratio of dose of MDZ metabolized by GW metabolism (predicted by PBPK model) and total dose of MDZ absorbed into GW mucosa (calculated by $F_{\text{abs}}^{\text{MDZ}} \cdot \text{Dose}_{\text{PO}}^{\text{MDZ}}$). $ER_{\text{hep}}^{\text{MDZ}}$ in absence/presence of ERY was calculated by $CL_{\text{hep}}^{\text{MDZ}}$ divided by Q_{hep} , and $CL_{\text{hep}}^{\text{MDZ}}$ was derived from $\text{Dose}_{\text{IV}}^{\text{MDZ}}$ and $AUC_{\text{IV}}^{\text{MDZ}}$, assuming that hepatic clearance is the only elimination route of IV MDZ.

$F_{\text{oral}}^{\text{MDZ}}$ in absence of ERY is 28%, and both routes of ERY can increase $F_{\text{oral}}^{\text{MDZ}}$ but to different extent. When concurrently administered with MDZ (administration time interval = 0), IV ERY increases $F_{\text{oral}}^{\text{MDZ}}$ a little more than PO (EC/SS) ERY, because there is a lag time for ERY to enter the GW mucosa after PO administration, and at zero time interval, the increase in $F_{\text{oral}}^{\text{MDZ}}$ is mainly due to pre-systemic/systemic hepatic metabolic inhibition after PO MDZ. With MDZ dosed further apart from ERY, PO (EC/SS) ERY inhibites GW metabolism of MDZ, thus a more profound increase in $F_{\text{oral}}^{\text{MDZ}}$ is observed after PO ERY than IV ERY. PO ERY can raise $F_{\text{oral}}^{\text{MDZ}}$ up to 63% and 54% for EC and SS formulations, respectively, and IV ERY only elevates $F_{\text{oral}}^{\text{MDZ}}$ up to 36%. The maximal increase is achieved after ~2-5 hours, when hepatic/GW CYP3A levels achieve their nadir. The duration of $F_{\text{oral}}^{\text{MDZ}}$ increase by both routes of ERY are up to 50 hours, reflecting the slow recovery of CYP3A activity levels.

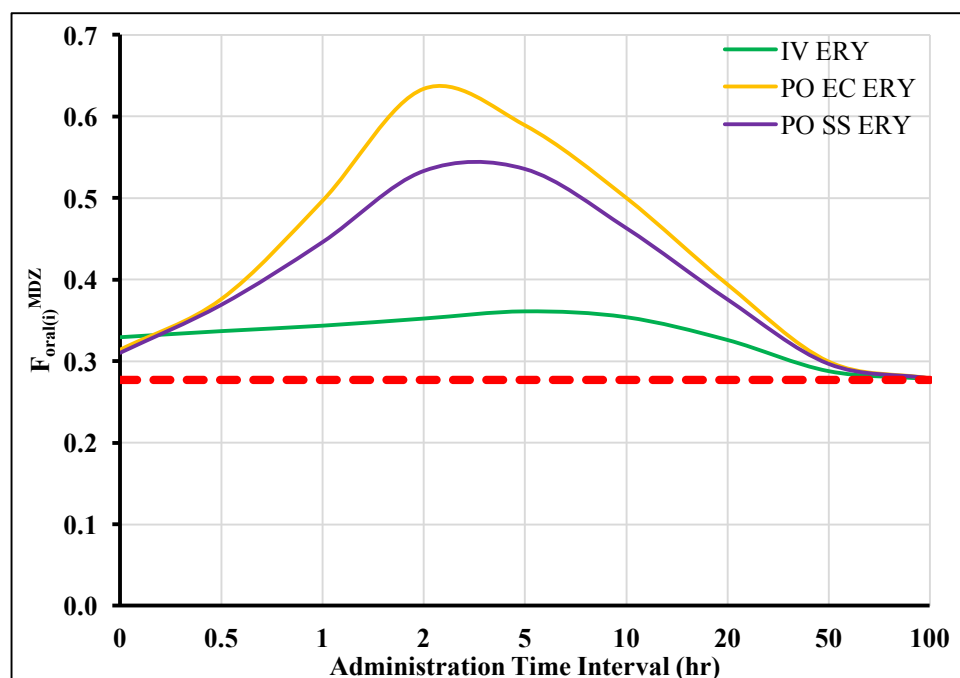


Figure 8.21 $F_{\text{oral}}^{\text{MDZ}}$ in presence of ERY (1,000 mg; IV: 15-min infusion, PO: EC/SS) administered at various time intervals before 1 mg IV/3 mg PO MDZ. Red dash line indicates $F_{\text{oral}}^{\text{MDZ}}$ without ERY.

$ER_{\text{GI}}^{\text{MDZ}}$ and $ER_{\text{hep}}^{\text{MDZ}}$, without ERY, are 52% and 40%, respectively, translating to intermediate hepatic/GW extraction ratios. Only PO ERY reduces $ER_{\text{GI}}^{\text{MDZ}}$, and due to the lag time of ERY GW mucosa absorption, very little inhibition on $ER_{\text{GI}}^{\text{MDZ}}$ is observed when the two drugs are administered simultaneously. With MDZ dosed further apart from ERY, the inhibition on $ER_{\text{GI}}^{\text{MDZ}}$ is more profound, and the lowest $ER_{\text{GI}(i)}^{\text{MDZ}}$ is 0.2 (60% inhibition) after EC ERY, and 0.25 (50% inhibition) after SS ERY. Due to the fast transit of ERY from GW mucosa to serosa compartment, the inhibition on GW metabolism fades away more quickly than that on hepatic metabolism. Both IV and PO (EC/SS) ERY inhibit $ER_{\text{hep}}^{\text{MDZ}}$, and the order of DDI magnitude depends on the order of F_{oral} (IV > PO EC > PO SS). For the two PO ERY formulations, when they are simultaneously administered with MDZ, more inhibition on hepatic metabolism (27% for EC; 18% for SS) is observed than GW metabolism (4% for both

formulations), because hepatic ERY concentration can inhibit both pre-systemic and systemic MDZ hepatic metabolism, while only pre-systemic GW ERY (in GW mucosa) inhibits MDZ GW metabolism. Maximum DDI on ER_{hep}^{MDZ} occurs at ~5 hours, when hepatic CYP3A activity achieves its nadir, and lowest ER_{hep}^{MDZ} is 0.18 (inhibited by 55%), 0.21 (inhibited by 47%), 0.27 (inhibited by 32%) after IV, PO EC and PO SS ERY, respectively.

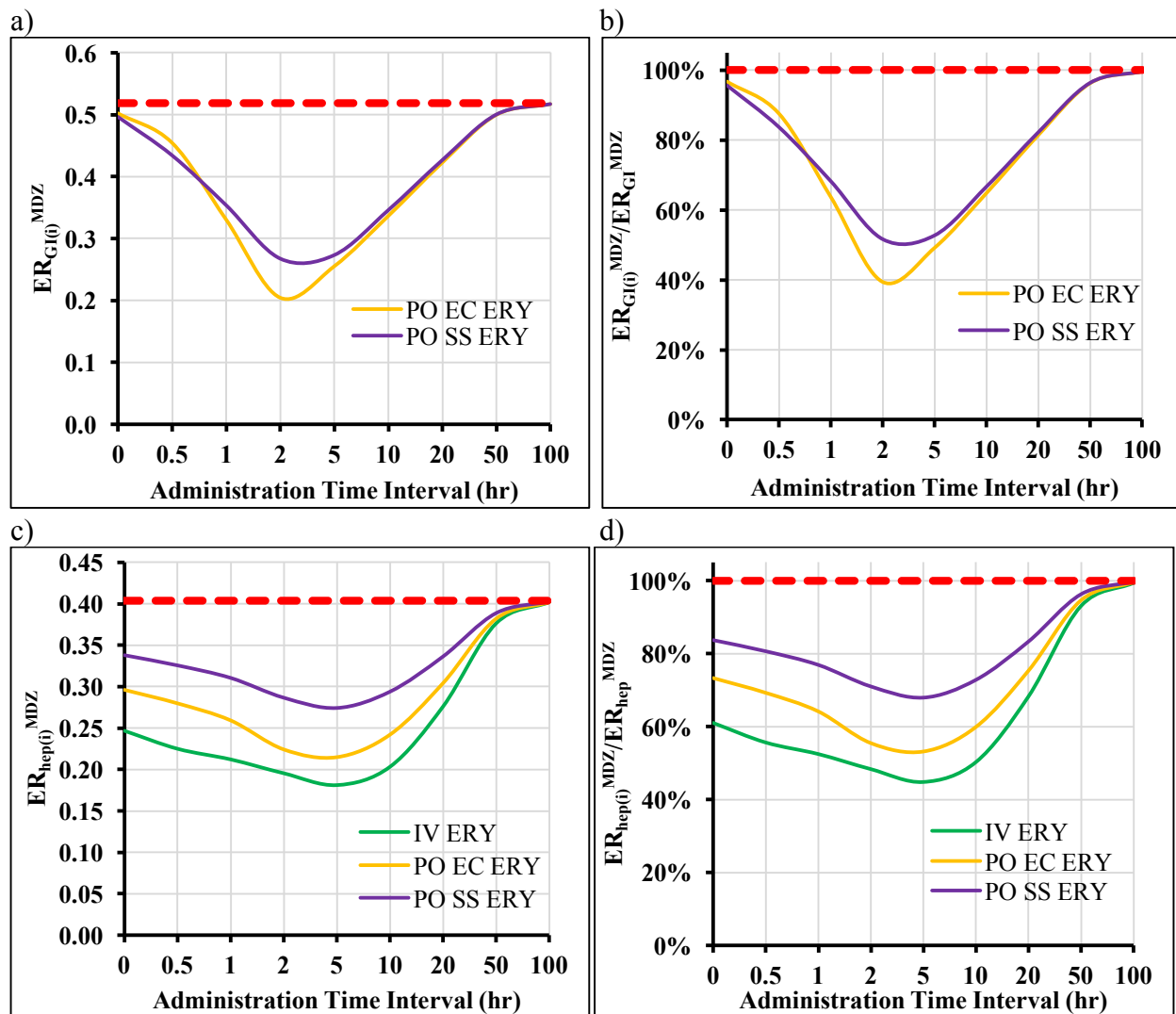


Figure 8.22 Hepatic/GW extraction ratio of MDZ in presence of ERY (1,000 mg; IV: 15-min infusion, PO: EC/SS) administered at various time intervals before 1 mg IV/3 mg PO MDZ.

a) ER_{GI}^{MDZ} in presence of ERY b). (Inhibited/uninhibited) ER_{GI}^{MDZ} ratio in presence of ERY. c) ER_{hep}^{MDZ} in presence of ERY d). (Inhibited/uninhibited) ER_{hep}^{MDZ} ratio in presence of ERY. Red dash lines in a) and c) indicate ER_{GI}^{MDZ} and ER_{hep}^{MDZ} without ERY. Red dash lines in b) and d) indicate no inhibition on ER_{GI}^{MDZ} and ER_{hep}^{MDZ} (ratio = 1).

8.3.2.2 Linearity of MBI by ERY

To assess MBI linearity, $k_{\text{inact,app}}^{\text{ERY}}$ profiles were simulated at 1,000 mg IV-15min-infusion ERY or PO (EC/SS) ERY and plotted against ERY unbound tissue concentration in **Figure 8.23**. Except for GW mucosa concentration after PO EC ERY, all other concentrations at the sites of DDI are below K_I^{ERY} , leading to apparent linear MBI ($k_{\text{inact,app}}^{\text{ERY}}$ is proportional to c_u^{ERY}). In addition, regardless of ERY routes and interaction sites (*i.e.*, liver or GW), $k_{\text{inact,app}}^{\text{ERY}}$ is much below $k_{\text{inact}}^{\text{ERY}}$, indicating that MBI is not maxed out in all scenarios.

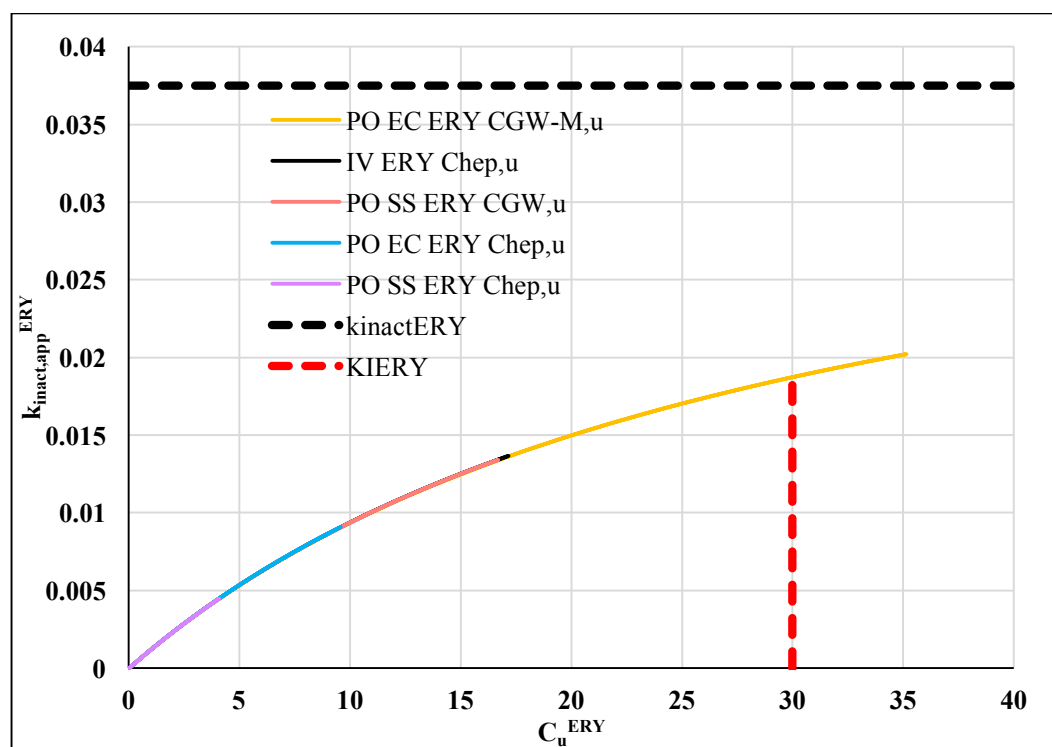


Figure 8.23 Relationship between apparent inactivation rate constant of ERY ($k_{\text{inact,app}}^{\text{ERY}}$) and unbound ERY tissue (liver or GW) concentrations after 1,000 mg ERY (IV 15min-infusion, PO: EC/SS).

Red dashed line represents K_I^{ERY} , and black dashed line represents $k_{\text{inact}}^{\text{ERY}}$.

8.3.2.3 Simulations of route-dependent DDI with various single doses of ERY

To compare the impact of ERY route of administration on DDI after various ERY single doses, the ratios of MDZ AUCR in presence of PO EC ERY and IV ERY are plotted against ERY single dose (**Figure 8.24**). To contrast with the MDZ - FLZ dose-dependency results, simulations were conducted when MDZ and ERY are dosed simultaneously.

Hepatic CYP3A activity levels vs. time after IV ERY, hepatic and GW CYP3A activity levels vs. time after PO EC ERY (**Figure 8.25**) were also plotted to better interpret dose-dependency of ERY on route difference.

Regardless of MDZ route of administration, the ERY dose-dependency on DDI route difference is similar. At the lowest ERY dose (100 mg), there is no IV/PO (EC) ERY route difference, while with increasing doses, PO EC ERY produces a lower MDZ AUC increase than IV ERY, and the largest ERY route difference is observed at a dose of 2,000 mg ($AUCR_{MDZ}^{PO-EC ERY}/AUCR_{MDZ}^{IV-ERY} = 0.7$). For doses above 2,000 mg, the route difference between IV and PO EC ERY gradually declines, and at the largest simulated dose (10,000 mg), $AUCR_{MDZ}^{PO-EC ERY}/AUCR_{MDZ}^{IV-ERY}$ is 0.75. When the two drugs are simultaneously administered, due to the lag time for ERY to enter GW mucosa, their DDI mainly reflects metabolic inhibition in hepatic CYP3A metabolism, which is the reason that the route difference for ERY is similar for both IV and PO MDZ. **Figure 8.25b, d, f** illustrates that IV ERY doesn't have any delay in inhibition of hepatic CYP3A, whereas PO ERY has ~0.2 hour delay in GW metabolic inhibition, and ~0.5 hour delay in hepatic metabolic inhibition. Hepatic inhibition lasts longer than GW inhibition. When MDZ is concurrently administered with ERY, CYP3AI inhibition at the early time (0-6 hours) is very important to the overall AUCR of MDZ, since MDZ concentration peaks immediately after IV administration and within 1 hour after PO administration. At very low

doses, both IV and PO ERY lead to trivial inhibition on hepatic CYP3A, while at very high doses, both routes largely inhibit hepatic CYP3A, reducing their route difference. It is at the middle dose (~2,000 mg), above clinically relevant doses, unbound hepatic concentration of ERY is close to K_I^{ERY} , and the hepatic concentration difference of ERY translates into largest hepatic CYP3A inhibition difference. Unbound hepatic/GW mucosa ERY concentrations and relative CYP3A activity in liver and GW were simulated for the 10,000 mg ERY dose (**Figure 8.26**), in comparison with 1,000 mg ERY dose. From **Figure 8.26a - b**, unbound hepatic concentrations of ERY after both routes are greater than K_I^{ERY} for more than 30 hours, translating into similar inhibition on hepatic CYP3A after IV and PO EC ERY (**Figure 8.26e**). Unbound GW mucosa ERY concentrations at 10,000 mg PO EC dose are above K_I^{ERY} for ~5 hours, driving a large GW CYP3A inhibition difference compared with IV ERY (**Figure 8.26c-d and f**). However, when MDZ is concurrently dosed with ERY, GW CYP3A inhibition is only marginal, due to its absorption delay.

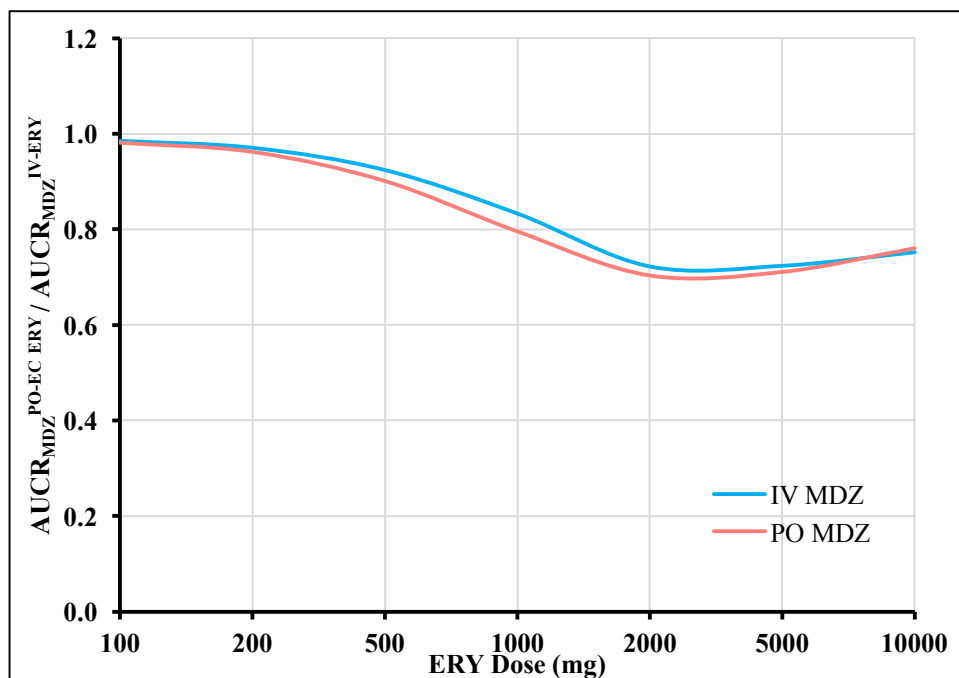


Figure 8.24 Ratio of MDZ AUCR by ERY (IV: 15-min infusion, PO: EC) after various ERY single dose.

(MDZ was simultaneously administered with ERY).

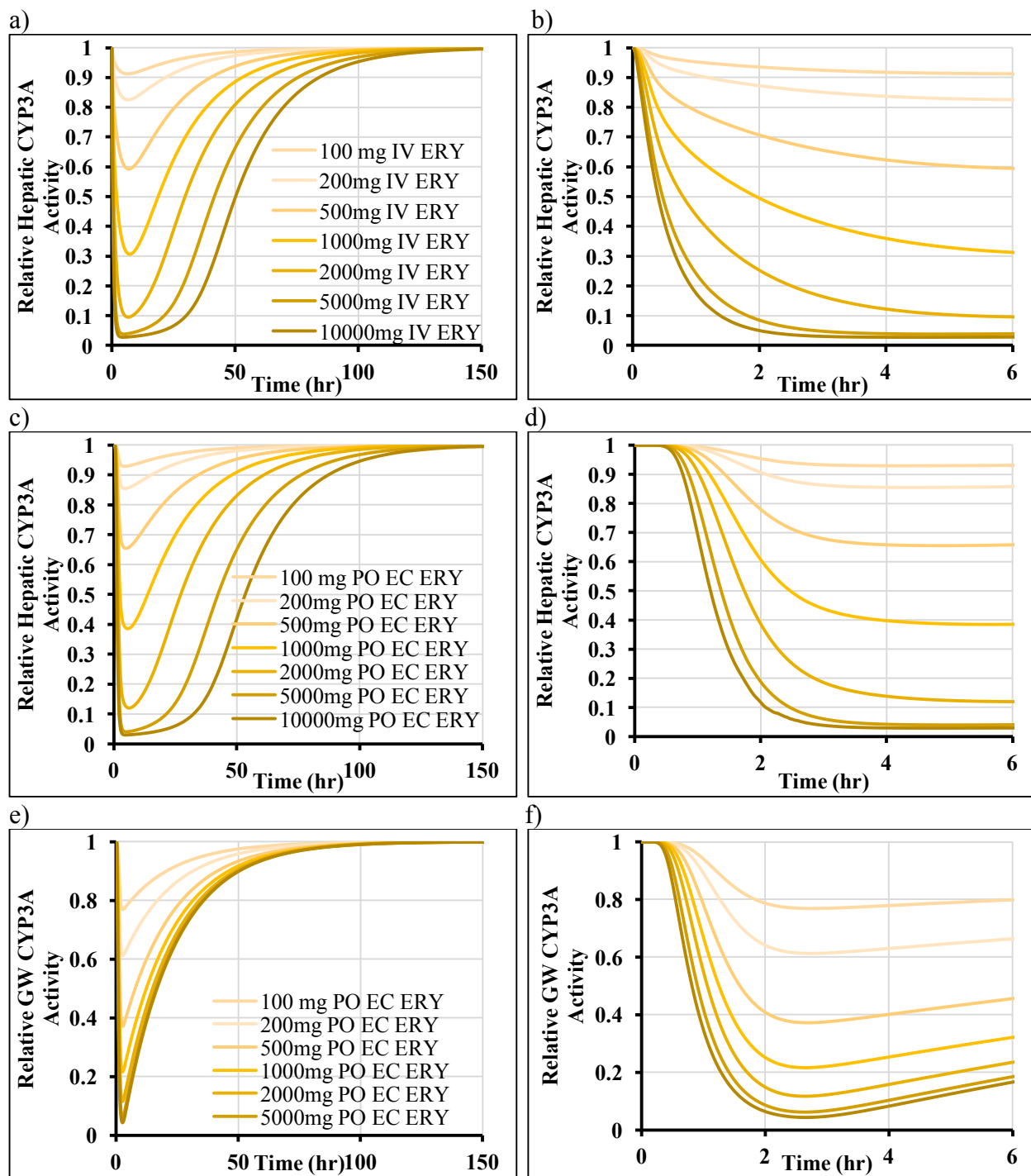


Figure 8.25 Relative CYP3A activity after various single doses of IV 15min infusion or PO EC ERY.

a) Relative hepatic CYP3A activity levels vs. time after IV ERY (0-150 hours). b) Relative hepatic CYP3A activity levels vs. time after IV ERY (0-6 hours) c) Relative hepatic CYP3A activity levels vs. time after PO EC ERY (0-150 hours) d) Relative hepatic CYP3A activity levels vs. time after PO EC ERY (0-6 hours) e) Relative GW CYP3A activity levels vs. time after PO EC ERY (0-150 hours) f) Relative GW CYP3A activity levels vs. time after PO EC ERY (0-6 hours)

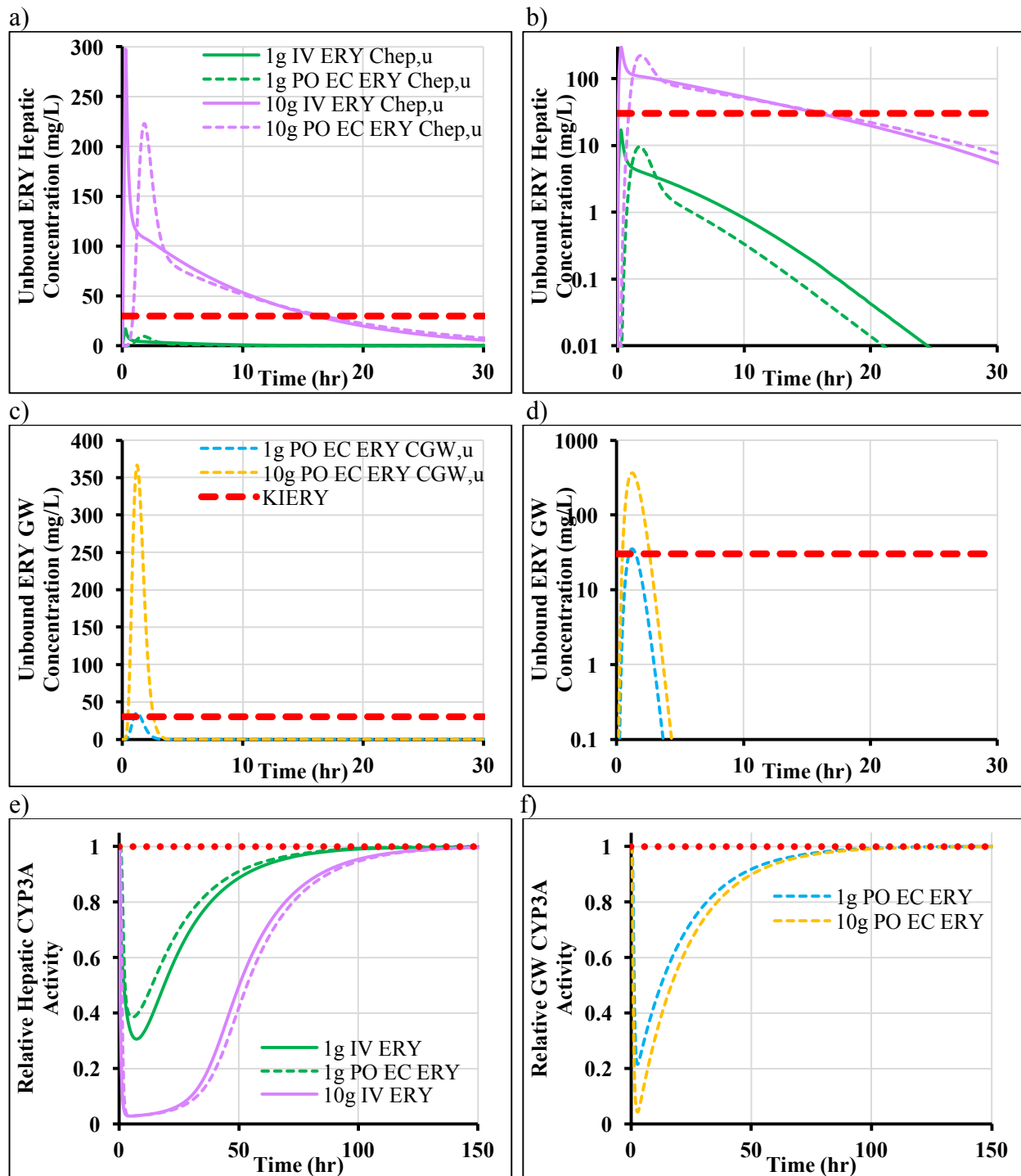


Figure 8.26 Plots of ERY unbound concentrations and relative CYP3A activity after 10,000 mg and 1,000 mg ERY (IV: 15min infusion, PO: EC).

a) ERY unbound hepatic concentration – time profiles (Cartesian plot). b) ERY unbound hepatic concentration – time profiles (Semi-log plot). c) ERY unbound GW mucosa concentration – time profiles (Cartesian plot). d) ERY unbound GW mucosa concentration – time profiles (Semi-log plot). e) Relative hepatic CYP3A activity in presence of ERY. f) Relative GW CYP3A activity in presence of ERY.

8.3.2.4 Simulations of route-dependent DDI with different ERY dosing intervals

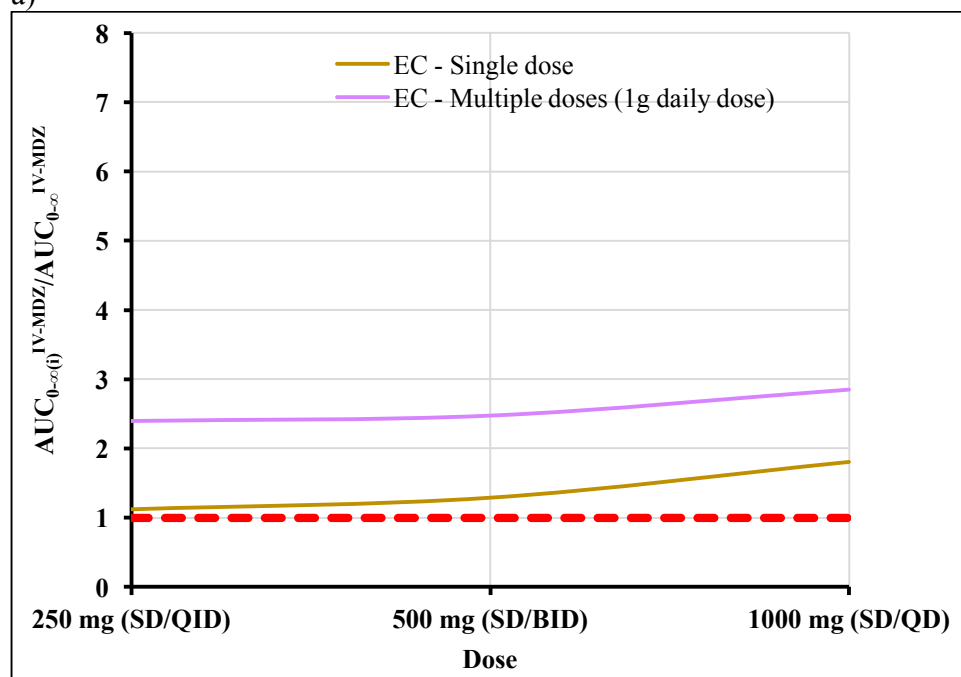
The (inhibited/uninhibited) MDZ AUCR in presence of PO EC ERY is plotted against different ERY dosing regimens: 250 mg/500 mg/1,000 mg single dose (SD) or 250mg QID/500mg BID/1,000 mg QD (same daily dose) multiple doses (MD) in **Figure 8.27**. ERY unbound hepatic/GW mucosa concentrations after the three multiple dosing regimens were also simulated and plotted in **Figure 8.28** and relative hepatic/GW activity in presence of single-/repeat- doses PO EC ERY are showed in **Figure 8.29**.

After ERY PO EC single dose, 1,000 mg SD increases IV MDZ AUC 38% more than 250 mg SD (AUCR = 1.8 after 1,000 mg SD; AUCR = 1.3 after 250 mg SD), due to higher ERY unbound hepatic concentrations and stronger inhibition of hepatic CYP3A metabolism after 1,000 mg SD (shown in **Figure 8.28a** and **Figure 8.29a** (dashed lines)). After PO MDZ, 1,000 mg SD PO EC produces 2.6-fold higher AUC increase than 250 mg SD EC (AUCR = 4.1 after 1,000 mg SD; AUCR = 1.6 after 250 mg SD) due to higher unbound ERY concentration and lower CYP3A level in liver and GW at 1,000 mg SD (shown in **Figure 8.28b** and **Figure 8.29b** (dashed lines)). Repeat- doses of EC ERY gives rise to higher AUCR than single-dose EC ERY at all the three repeat- dosing regimens; because both hepatic and GW CYP3A levels are considerably lower after repeat- EC doses than single dose (**Figure 8.29**). However, given same daily dose of 1,000 mg, 1,000 mg QD of EC ERY only induces a 17% and 36% higher AUCR than 250 mg QID for IV and PO MDZ, respectively. As shown in **Figure 8.29**, CYP3A activity levels in presence of 1,000 mg QD ERY has the lowest nadir, but the largest fluctuation, compared to the other two regimens. After MDZ administration (indicated as black dashed line in **Figure 8.29**), 1,000 mg QD can inhibit MDZ hepatic/GW metabolism to the greatest extent at the beginning, but the inhibitory effect quickly fades away, whereas 250 mg QID regimen yields

less fluctuating hepatic/GW CYP3A levels, so that the inhibitory effect is sustained for a longer time; thus, eventually, no significant difference in AUCR is found among the three multiple dosing regimens.

The accumulation ratio for ERY unbound hepatic/GW mucosa $AUC_{0-\infty}^{ERY}$ and inhibited hepatic/GW $AUC_{0-\infty}^{CYP3A}$ are plotted for different multiple dosing regimens in **Figure 8.30**. From **Figure 8.30**, inhibited hepatic and GW $AUC_{0-\infty}^{CYP3A}$ both have more accumulation than hepatic and GW mucosa $AUC_{0-\infty}^{ERY}$ for all the three regimens, because ERY hepatic/GW mucosa concentrations have much shorter elimination $t_{1/2}$ than hepatic and GW CYP3A (~14 hours). ERY hepatic elimination $t_{1/2}$ is the same as plasma/pseudo steady-state $t_{1/2}$ (~2 hours), and ERY GW mucosa $t_{1/2}$ is even shorter than hepatic concentrations, due to the rapid transit of ERY to the GW serosa, and there is no accumulation on ERY GW mucosa concentration for all the multiple dosing regimens.

a)



b)

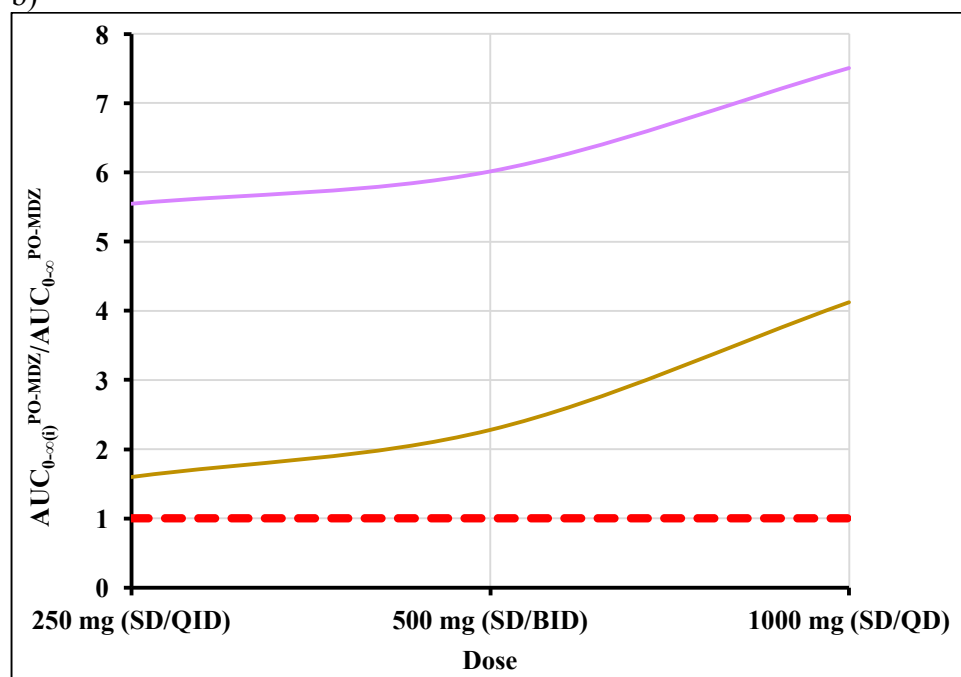


Figure 8.27 AUCR of MDZ in presence of single dose PO EC ERY 250 mg/500 mg/1,000 mg or multiple doses PO EC ERY 250 mg QID/500 mg BID/1,000 mg QD (same daily dose).

a) 1 mg IV MDZ was administered 2 hours after SD EC, or 2 hours after the 1st dose of EC on the 5th day. b) 3 mg PO MDZ was administered 2 hours after SD EC, or 2 hours after the 1st dose of EC on the 5th day. Red dashed lines represent no increase in MDZ AUC.

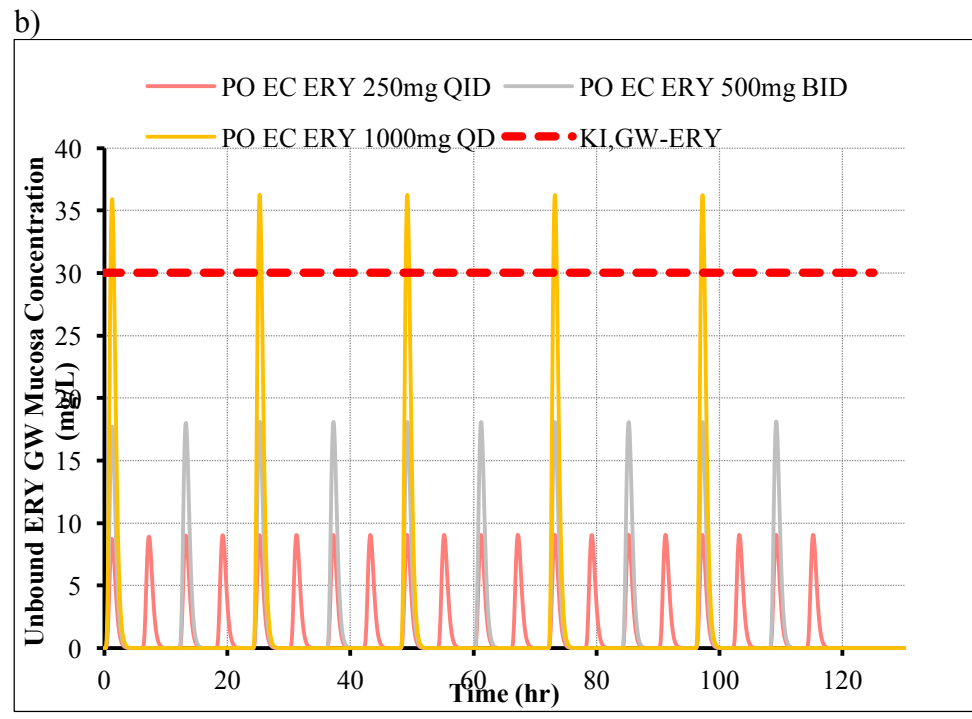
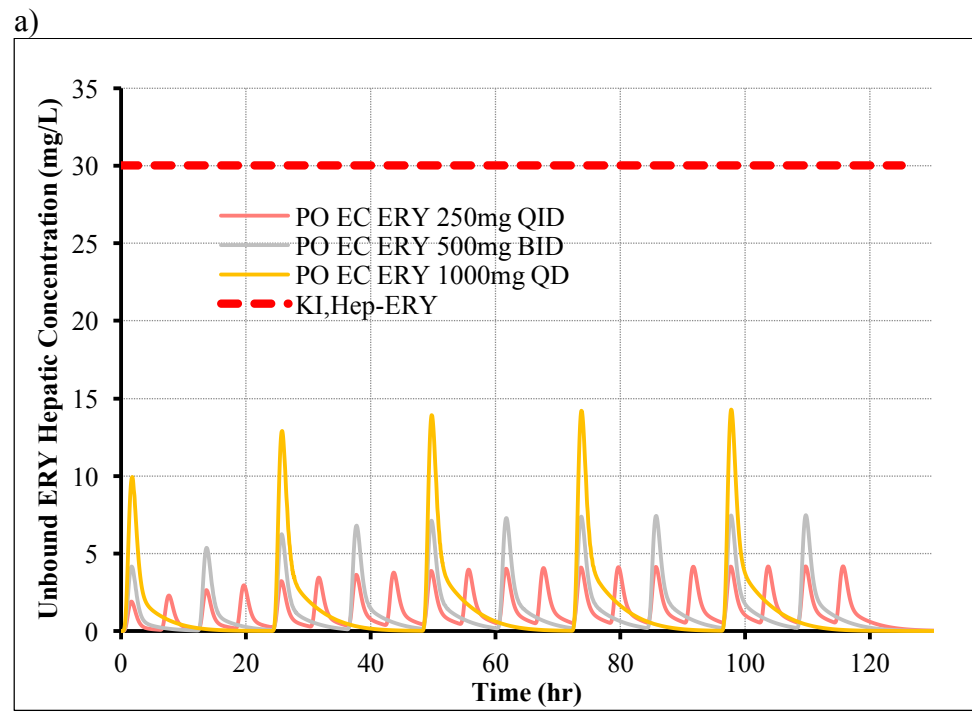


Figure 8.28 Unbound ERY concentration after PO EC 250 mg QID, 500 mg BID and 1,000 mg QD.

a) Unbound ERY hepatic concentration over time b) Unbound ERY GW mucosa concentration over time. Red dashed lines represent K_i^{ERY} .

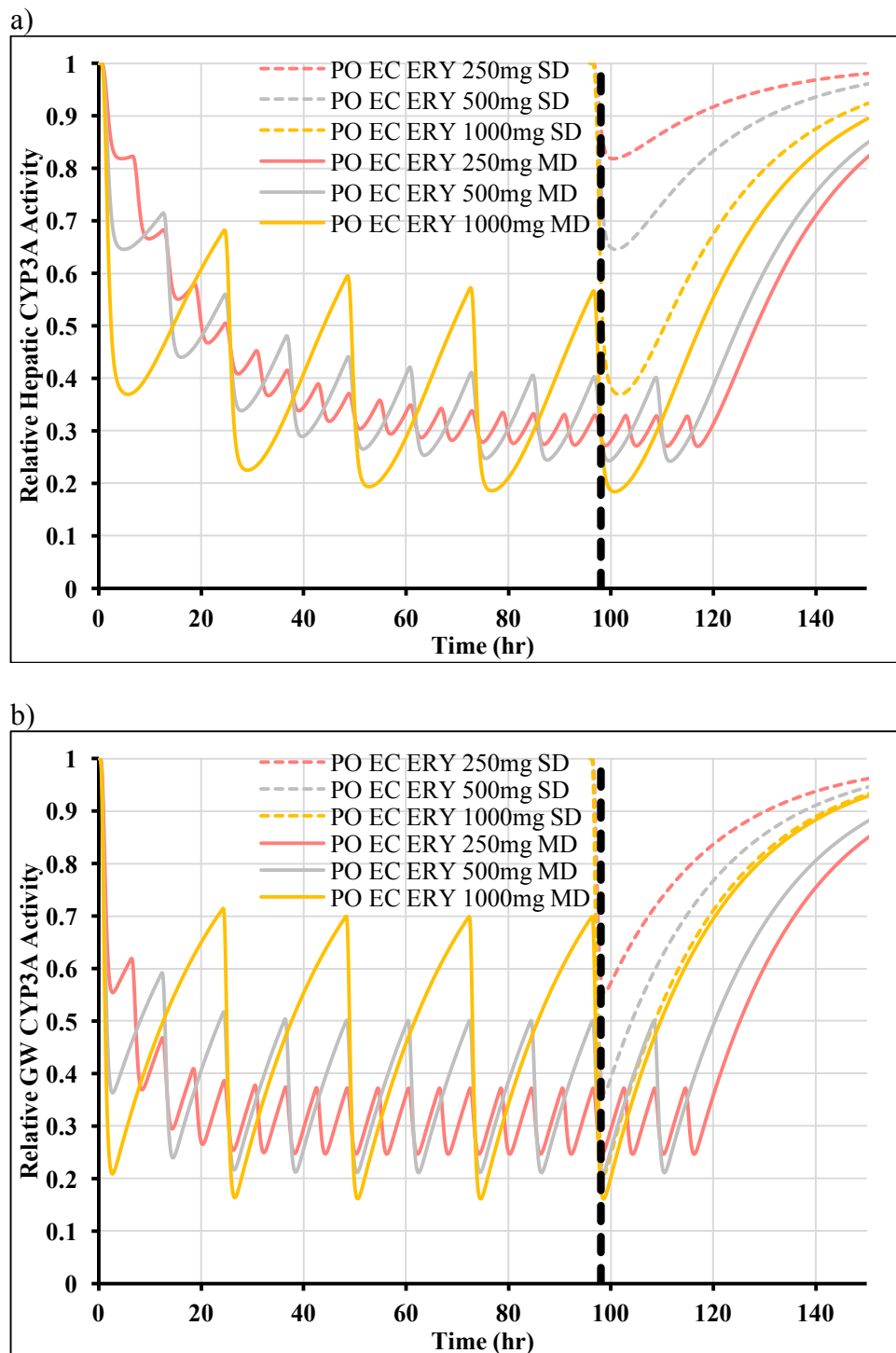


Figure 8.29 Relative CYP3A activity after PO EC ERY single dose (250 mg / 500 mg/ 1,000 mg) or multiple doses (250 mg QID/ 500 mg BID/ 1,000mg QD).

a) Relative hepatic CYP3A activity. B) Relative GW CYP3A activity. Black dashed lines represent the time when MDZ was administered.

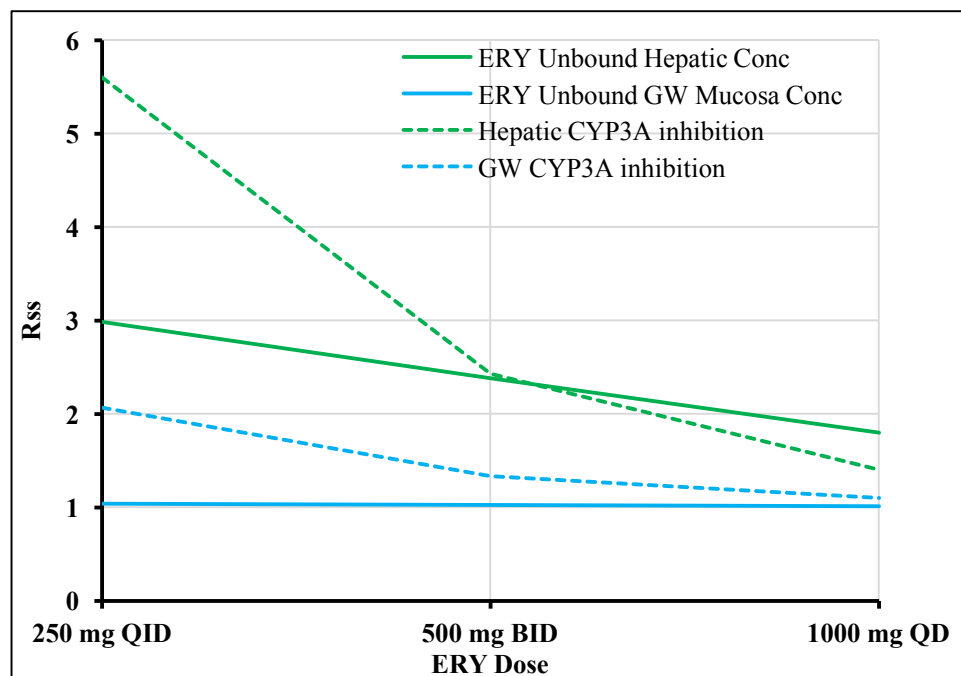
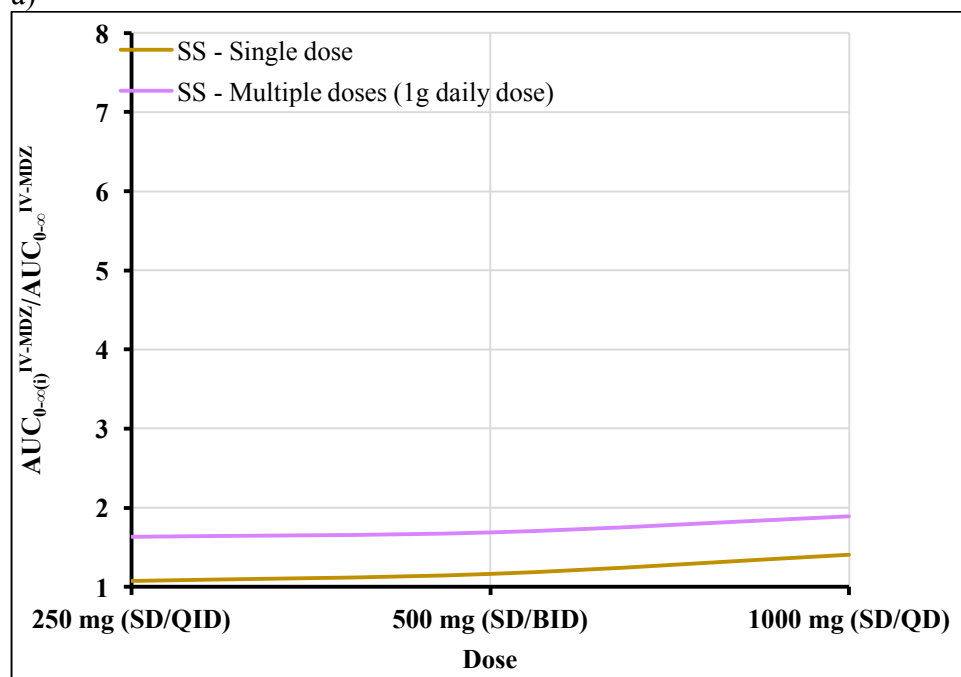


Figure 8.30 (Steady-state) accumulation ratio (R_{ss}) of ERY unbound hepatic/GW mucosa concentration, and inhibited hepatic/GW CYP3A after 250 mg QID / 500 mg BID / 1,000 mg QD PO EC ERY.

The (inhibited/uninhibited) MDZ AUCR in presence of PO SS ERY is plotted against ERY dosing regimen: 250 mg/500 mg/1,000 mg single dose (SD) or 250mg QID/500mg BID/1,000 mg QD (same daily dose) multiple doses (MD) in **Figure 8.31**. ERY unbound hepatic/GW mucosa concentrations after the three multiple dosing regimens were also simulated and plotted in **Figure 8.32** and relative hepatic/GW activity in presence of single-/repeat- doses PO EC ERY are showed in **Figure 8.33**. Similar as EC formulation, 1,000 mg SD SS increase IV MDZ AUC 31% more than 250 mg SD (AUCR = 1.4 after 1,000 mg SD; AUCR = 1.1 after 250 mg SD), due to higher ERY unbound hepatic concentration and stronger inhibition on hepatic CYP3A metabolism after 1,000 mg SD (shown in **Figure 8.32a** and **Figure 8.33a** (dashed lines)). After PO MDZ, 1,000 mg SD PO EC produces a 2-fold higher AUC increase than 250 mg SD EC (AUCR = 2.7 after 1,000 mg SD; AUCR = 1.4 after 250 mg SD) due to higher unbound ERY concentration and lower CYP3A level in liver and GW at 1,000 mg SD (shown in **Figure 8.32b** and **Figure 8.33b** (dashed lines)). Multiple doses SS ERY gives rise to higher AUCR than single dose SS ERY at all the three multiple dosing regimens, because hepatic and GW CYP3A levels are considerably lower after multiple SS doses than single dose (**Figure 8.32**). However, given same daily dose of 1,000 mg, 1,000 mg QD of SS ERY causes only 16% and 23% higher AUCR than 250 mg QID for IV and PO MDZ, respectively. Due to lower F_{oral} than EC, SS ERY has lower hepatic and GW mucosa concentration (**Figure 8.32**) and less inhibition on CYP3A (**Figure 8.33**) compared with EC, but the accumulation ratio (**Figure 8.34**) calculated for ERY unbound hepatic/GW mucosa $AUC_{0-\infty}^{\text{ERY}}$ and inhibited hepatic/GW $AUC_{0-\infty}^{\text{CYP3A}}$ exhibit the same trend for different dosing regimens as EC formulation.

a)



b)

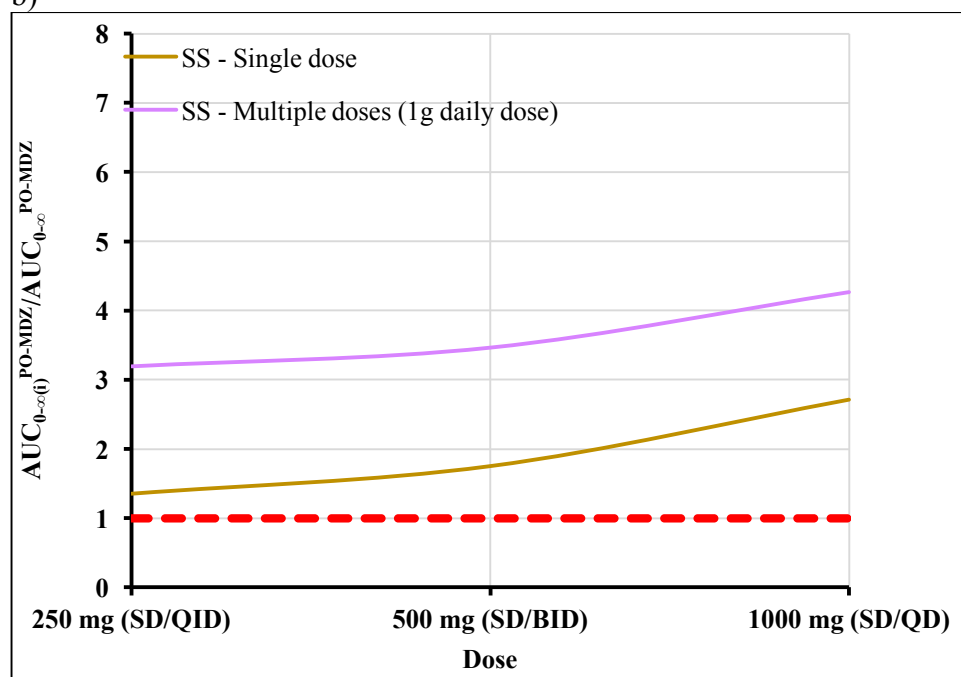


Figure 8.31 AUCR of MDZ in presence of single dose PO SS ERY 250 mg/500 mg/1,000 mg or multiple doses PO SS ERY 250 mg QID/500 mg BID/1,000 mg QD (same daily dose).

a) 1 mg IV MDZ was administered 2 hours after SD SS, or 2 hours after the 1st dose of SS on the 5th day. b) 3 mg PO MDZ was administered 2 hours after SD SS, or 2 hours after the 1st dose of SS on the 5th day. Red dashes lines represent no increase in MDZ AUC.

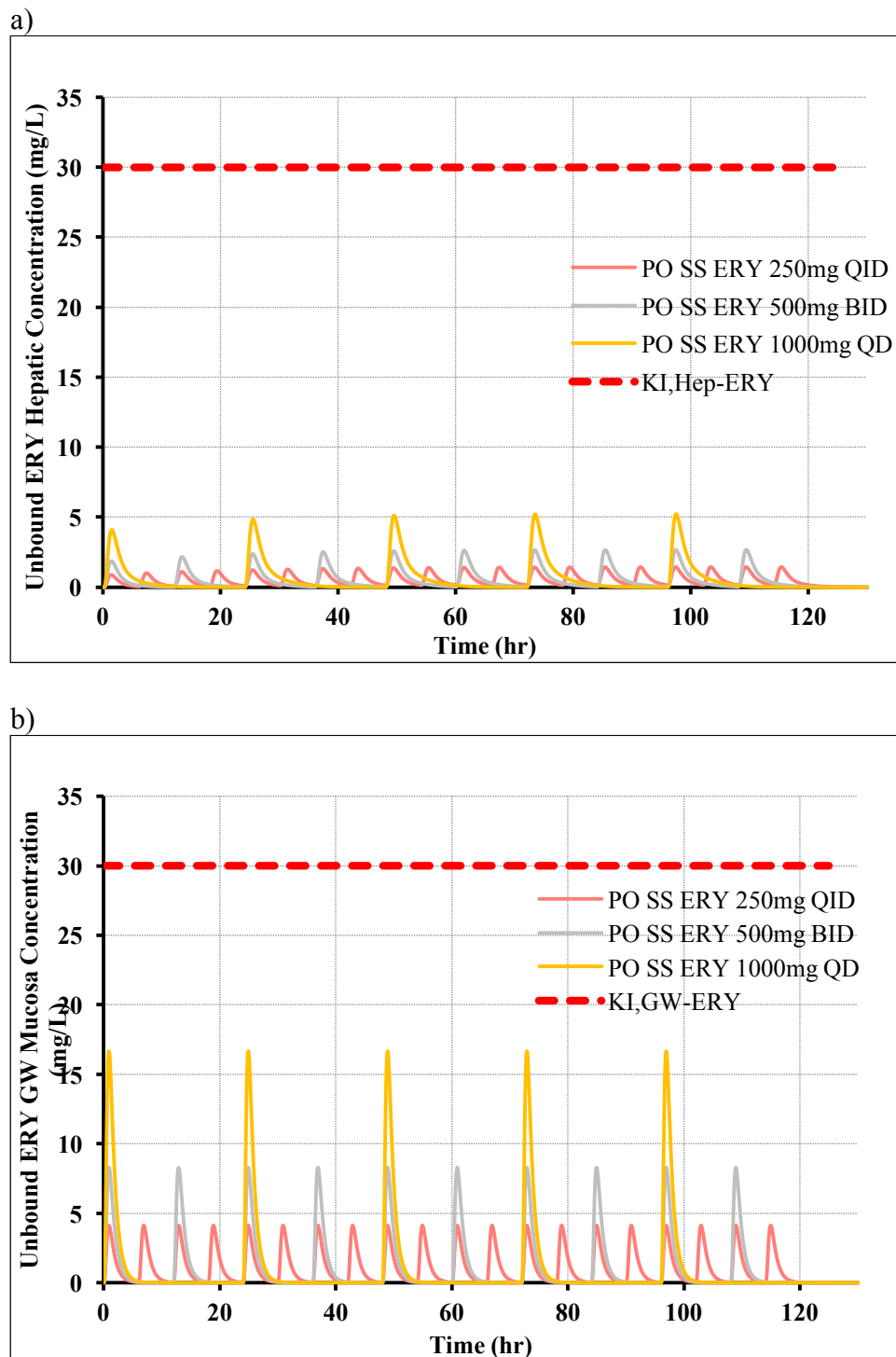


Figure 8.32 Unbound ERY concentration after PO SS 250 mg QID, 500 mg BID and 1,000 mg QD.

a) Unbound ERY hepatic concentration over time b) Unbound ERY GW mucosa concentration over time. Red dashed lines represent K_{I}^{ERY} .

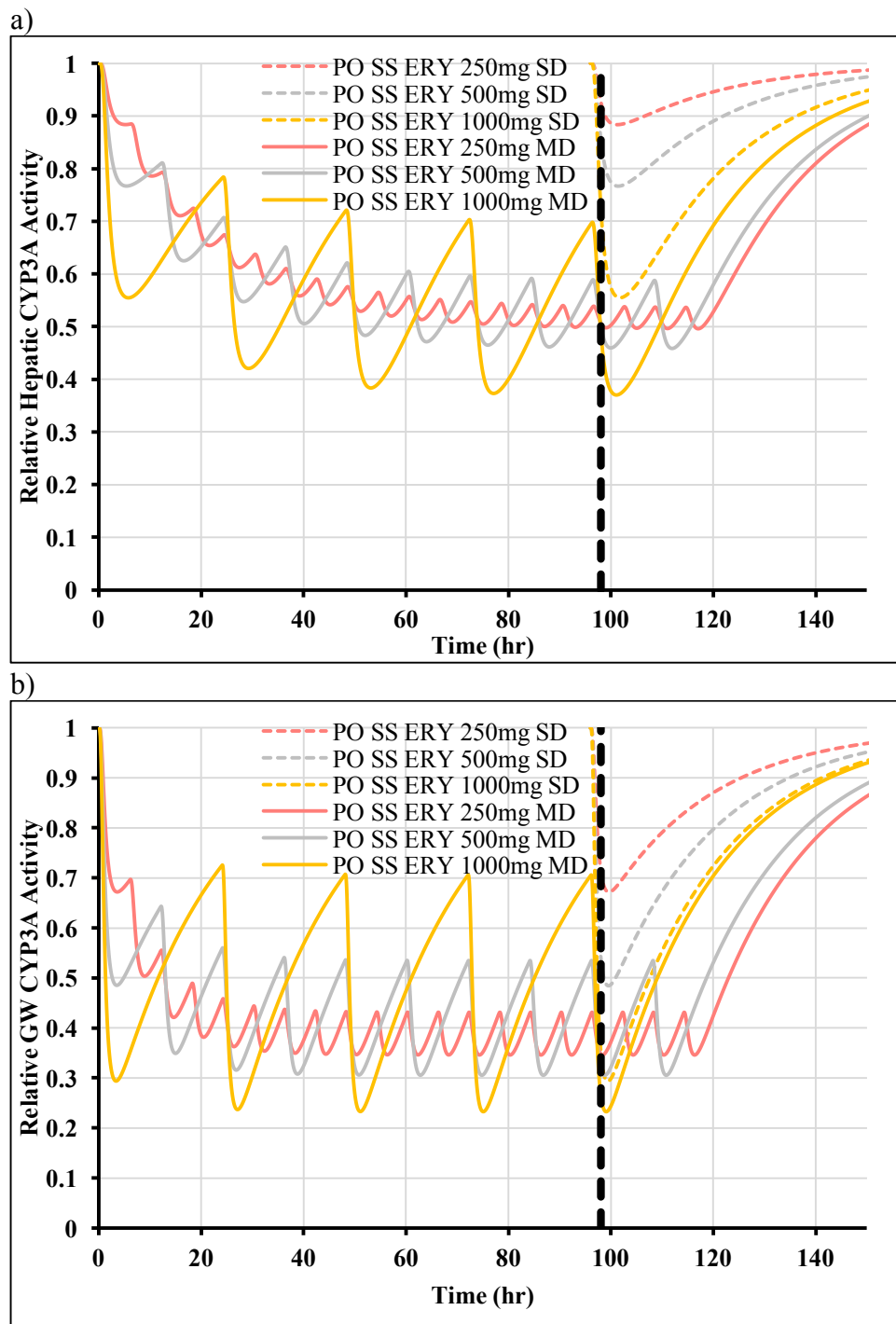


Figure 8.33 Relative CYP3A activity after PO SS ERY single dose (250 mg / 500 mg/ 1,000 mg) or multiple doses (250 mg QID/ 500 mg BID/ 1,000mg QD).

a) Relative hepatic CYP3A activity. B) Relative GW CYP3A activity. Black dashed lines represent the time when MDZ was administered.

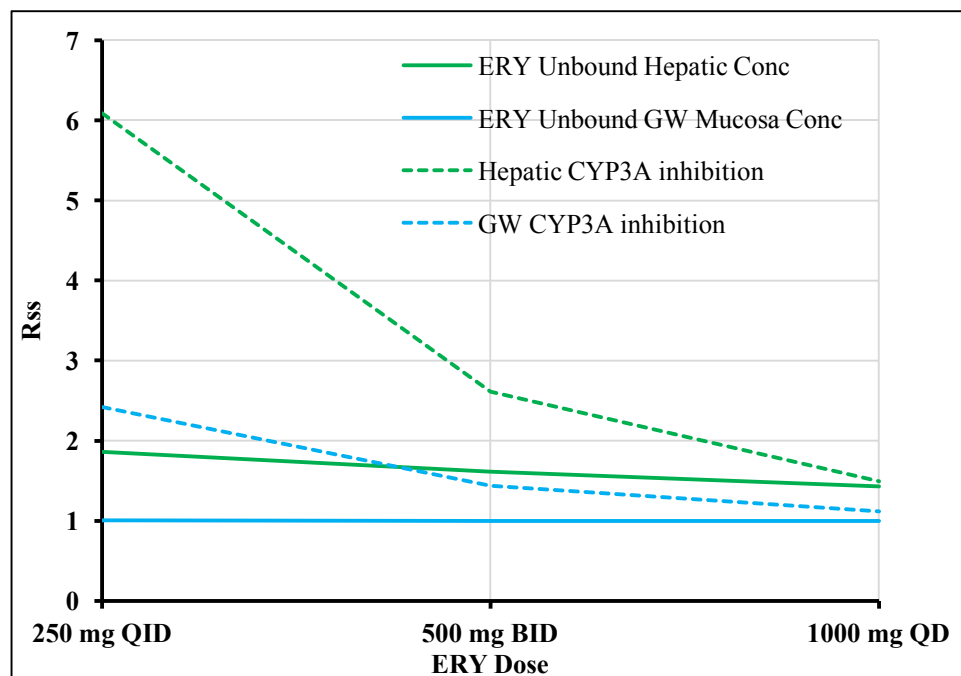


Figure 8.34 (Steady-state) accumulation ratio (R_{ss}) of ERY unbound hepatic/GW mucosa concentration, and inhibited hepatic/GW CYP3A after 250 mg QID / 500 mg BID / 1,000 mg QD PO SS ERY.

8.3.2.5 Simulation of route-dependent DDI between MDZ and hypothetical CYP3AI and between hypothetical CYP3A substrates and ERY

8.3.2.5.1 Route-dependent DDI between MDZ and 3AIX4

To change ERY to a higher F_{oral} CYP3AI (3AIX4), $F_{\text{abs}}^{\text{ERY}}$ was increased from 0.88 to 1.0, while hepatic and GW pre-systemic metabolism of ERY were kept unchanged from ERY.

MDZ AUC in presence of IV/PO 3AIX4 with different administration time intervals were simulated, and AUCR of MDZ for each scenario is plotted against administration interval time as shown in **Figure 8.35**. Plots of 3AIX4 concentrations and corresponding relative CYP3A levels in GW and liver were simulated (**Figure 8.36**), based on the dosing regimen of 1,000 mg IV (15-min infusion) or PO 3AIX4. For 3AIX4, F_{oral} is higher than ERY, but because of its hepatic first-pass metabolism, it is still only 71%, leading to slightly less hepatic CYP3A inhibition after PO than IV administration (maximal DDI: 2.1- vs. 2.2-fold). However, since GW inhibition only occurs when both MDZ and 3AIX4 are dosed PO, the DDI magnitude after PO 3AIX4 is much higher than IV 3AIX4 (maximal DDI: 4.7- vs. 2.9-fold), when PO MDZ is administered more than 1 hour after 3AIX4. Although 3AIX4 has a short plasma $t_{1/2}$ (~ 2 hours), the DDI lasts for about 4 days, as the MBI duration depends strongly on synthesis and degradation rates of CYP3A activity. Maximal DDI magnitude happens when hepatic or GW CYP3A level achieves its nadir (~2-5 hours).

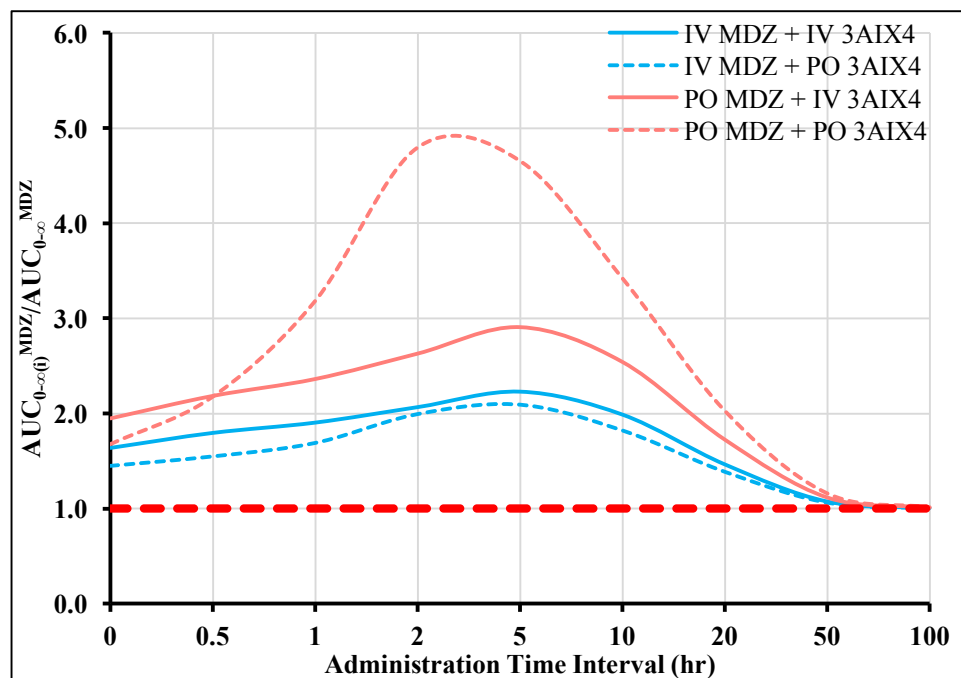


Figure 8.35 MDZ AUCR by 3AIX4 (1,000 mg; IV: 15-min infusion, or PO) administered at various time intervals before 1 mg IV/3 mg PO MDZ.
Red dash line indicates no inhibition on MDZ exposure.

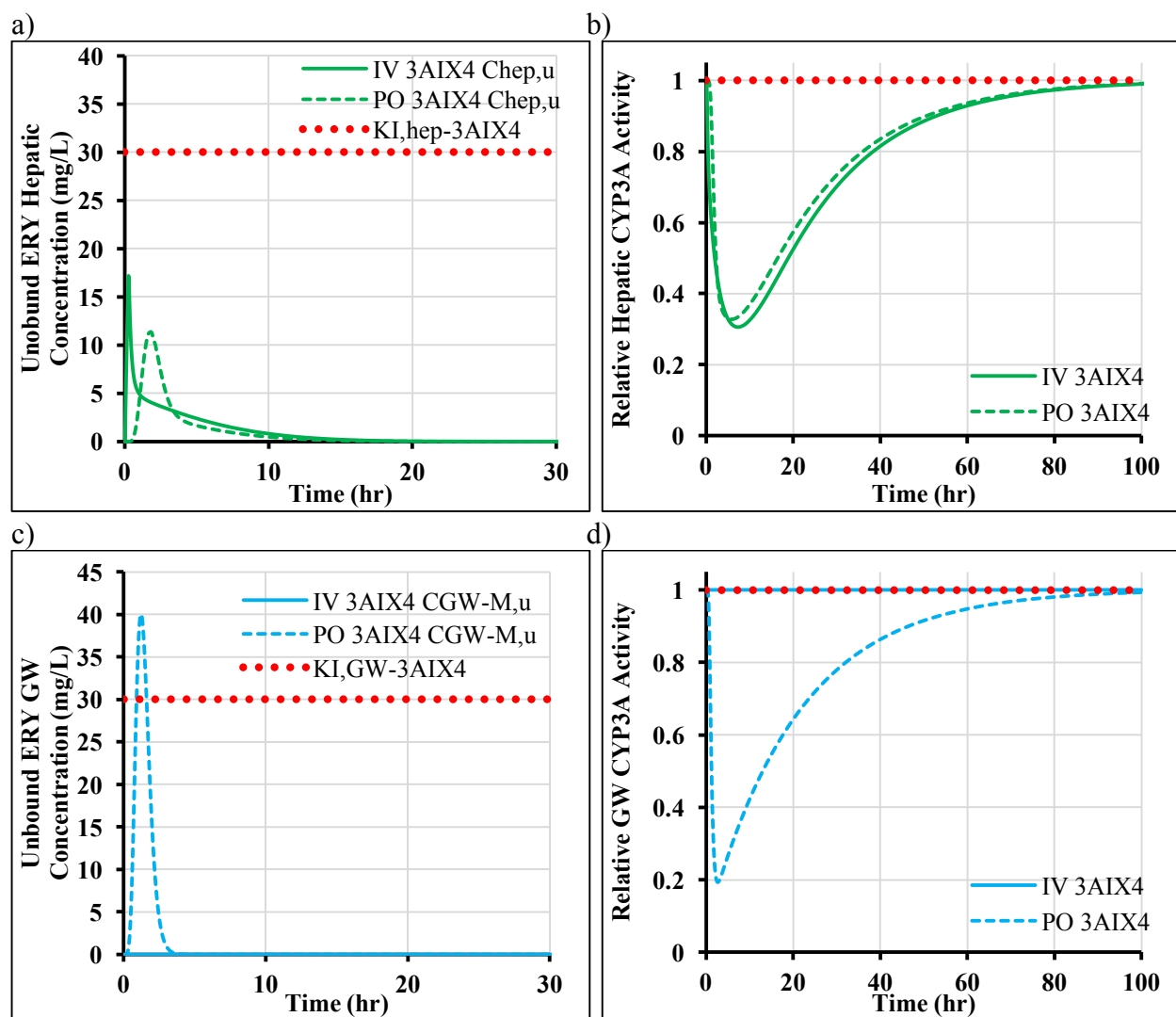


Figure 8.36 Plots of 3AIX4 unbound concentrations and relative CYP3A activity under 1,000 mg IV 15-min infusion or PO 3AIX4.

a) 3AIX4 unbound hepatic concentration – time profiles. b) Relative hepatic CYP3A activity in presence of 3AIX4. c) 3AIX4 unbound GW mucosa concentration – time profiles. d) Relative GW CYP3A activity in presence of 3AIX4. Dash lines in a) and c) represent K_I^{3AIX4} value. Dash lines in b) and d) represent no change in hepatic and GW CYP3A activity.

8.3.2.5.2 Route-dependent DDI between 3ASX1/2 and ERY

Subsequently, two CYP3A substrate (3ASX1: no GW metabolism; 3ASX2: no GW metabolism and decreased hepatic metabolism) were derived from MDZ PBPK model. 3ASX1/2 AUC in presence of 1,000 mg IV 15min infusion or PO (EC) ERY with different administration time intervals were simulated, and AUCR of 3ASX1/2 for each scenario is plotted against administration interval time as shown in **Figure 8.37** and **Figure 8.38**.

From **Figure 8.37**, PO 3ASX1 is consistently more sensitive to metabolic inhibition than after IV administration, because 3ASX still has pre-systemic hepatic metabolism after PO administration. However, the impact of the ERY administration route is the same regardless of 3ASX1 route, as the metabolic DDI is limited to hepatic metabolism of 3ASX1 (but no GW metabolism).

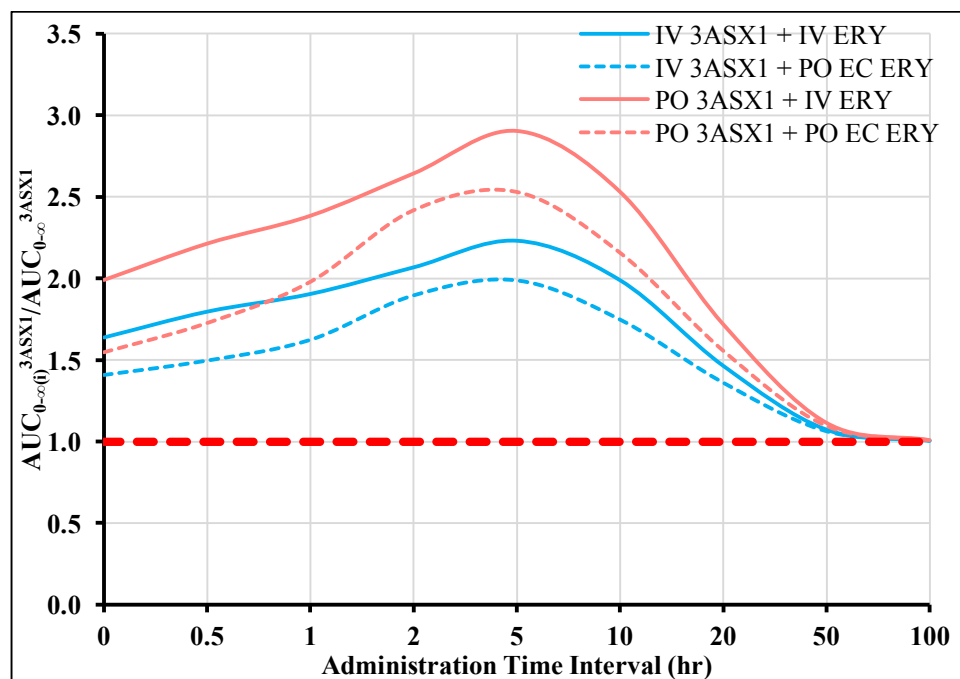


Figure 8.37 3ASX1 AUCR by 1,000 mg ERY (IV: 15-min infusion or PO) administered at various time intervals before (1 mg IV/3 mg PO) 3ASX1. Red dash line indicates no inhibition on 3ASX1 exposure.

From **Figure 8.38**, no clinical significant IV-PO route difference (<10%) of 3ASX2 is observed, due to limited pre-systemic hepatic extraction ($ER_{\text{hep}}^{3\text{ASX}2} = 0.11$) and no GW. To compare **Figure 8.37** and **Figure 8.38**, maximal DDI between PO 3ASX2 and ERY is smaller than maximal DDI between PO 3ASX1 and ERY, because 3ASX1 has lower F_{oral} than 3ASX2, and more potential to increase F_{oral} in presence of ERY. Furthermore, AUCR of 3ASX2 are fairly constant when 3ASX2 is dosed less or equal than 5 hours apart from ERY (difference < 10%), while AUCR of 3ASX1 when ERY is simultaneously dosed is ~50% less than AUCR when ERY is dosed 5 hours before 3ASX1 (maximal DDI). The smaller impact of administration time interval for 3ASX2 is because 3ASX2 has a longer plasma $t_{1/2}$, and even if inhibitory effect of ERY has a delay due to its mechanism-based inhibitory characteristics, the terminal phase of 3ASX2's PK profile is still significantly inhibited, resulting in similar DDI magnitude as delayed administration of 3ASX2 from ERY.

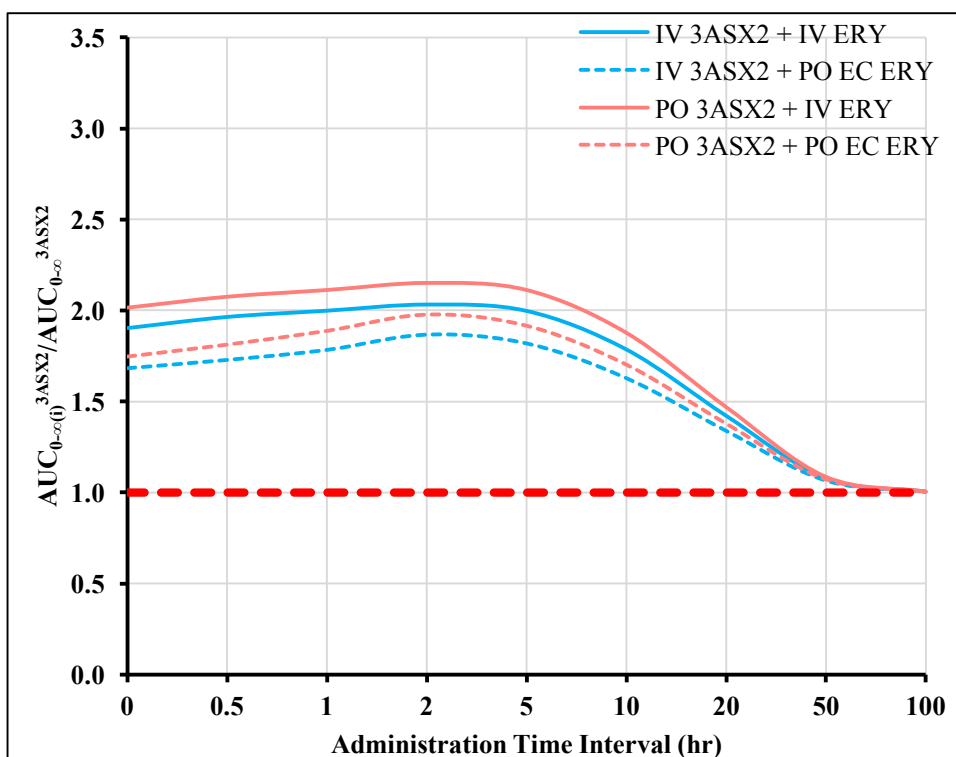


Figure 8.38 3ASX2 AUCR by 1,000 mg ERY (IV: 15-min infusion or PO) administered at various time intervals before (1 mg IV/3 mg PO) 3ASX2.

Red dash line indicates no inhibition on 3ASX2 exposure.

8.4 Conclusions

A semi-PBPK DDI model was developed to describe IV/PO MDZ PK profiles in presence of IV/PO (single-/repeat- doses) ERY. The model was validated against available reported MDZ plasma concentration – time profiles and exposure metrics from two DDI studies, in which IV/PO MDZ was co-administered with repeat- doses of PO ERY as EC or SS tablets; no IV ERY-MDZ DDI information was publically available.

After optimizing model parameters ($v_{\max, \text{hep}}^{\text{MDZ}}$, $k_{\text{GL}}^{\text{MDZ}}$ and $F_{\text{abs}}^{\text{ERY}}$ for study 28; $v_{\max, \text{hep}}^{\text{MDZ}}$, $k_{\text{GL}}^{\text{MDZ}}$ and f_{villi} for study 603) based on MDZ PK profiles without ERY, the DDI model captures MDZ PK profiles in presence of ERY well, with deviations (%) of exposure metrics, $F_{\text{oral}}^{\text{MDZ}}$ and MDZ AUCR less than $\pm 30\%$ in most scenarios, confirming the validity of model and final

model parameters. Formal parameter sensitivity analyses were conducted for 6 uncertain model parameters; k_{deg} , K_I^{ERY} , k_{inact}^{ERY} and $v_{max,hep-3A}^{ERY}$ are identified as pivotal parameters, that affect both MDZ systemic exposure metrics, and hepatic/GW CYP3A inhibition profiles.

Simulations with the validated semi-PBPK-DDI model was performed to predict the DDI magnitude and time course for ERY (IV vs. PO) followed by MDZ (IV vs. PO) at various time intervals: 1) For IV MDZ, ERY causes more inhibition after IV than after PO (EC/SS) administration, due to ERY's relatively low F_{oral} (EC: ~60%; SS: ~30%) and higher unbound hepatic concentrations after IV than after PO administration. 2) For PO MDZ, although ERY still shows more inhibition after IV than after PO (simultaneous!) co-administration with MDZ, the inhibition by PO ERY gradually exceeds (for EC) or equals (SS) the one by IV ERY over time. This is primarily because ERY is assumed to enter the GW mucosa from the gut lumen only, due to its high plasma protein binding and low lipophilicity preventing serosal GW access; therefore, only PO (but not IV) ERY is assumed to cause inhibition of GW metabolism. 3) Regardless of the ERY route, PO MDZ is more sensitive to metabolic inhibition than IV MDZ. 4) Overall, the maximal DDI occurred when hepatic/GW CYP3A activity achieve their nadir, and the DDI duration exceeds the plasma/tissue $t_{1/2}$ of ERY - due to the slow recovery of CYP3A activity, which depends on endogenous CYP3A synthesis and degradation rates.

Regarding MBI linearity, ERY unbound hepatic and GW mucosa concentrations at 1,000 mg for both routes remain mostly below K_I^{ERY} , suggesting "linear" MBI at this dose. To compare ERY route differences across doses, a series of single ERY doses were simulated simultaneously administered with IV/PO MDZ. Regardless of MDZ route of administration, the dose-dependency of ERY on DDI route difference is similar. Only slight ERY route differences are observed at the lowest and the highest single ERY dose, and the largest ERY route difference

(DDI: PO EC ERY < IV ERY) is observed at an intermediate ERY dose of 2000 mg when ERY unbound hepatic/GW concentration is close to K_I^{ERY} .

The impact of PO (EC/SS) ERY dosing interval (same daily dose) after multiple doses (for 5 days) on route difference is also assessed, and it is shown that dosing interval only has only marginal (<20%) impact on route difference when MDZ is administered intravenously; when MDZ is administered orally, 1000 mg QD can produce slightly (~20-30%) more MDZ AUC increase than 250 mg QID regimen.

A high F_{oral} MBI CYP3AI (3AIX4) and two CYP3A substrates (3ASX1/2) were also simulated to generalize the conclusions above. For DDI between MDZ and 3AIX4, marginal IV/PO route difference of 3AIX4 is observed after IV MDZ. However, since GW inhibition only occurred when both MDZ and 3AIX4 are dosed PO, the DDI magnitude after PO 3AIX4 is much higher than IV 3AIX4, when PO MDZ is administered more than 1 hour after 3AIX4. For DDI between 3ASX1 and ERY, PO 3ASX1 is still inhibited more than IV 3ASX1, but the route effects of ERY are the same no matter how 3ASX1 is given. For DDI between 3ASX2 and ERY, marginal route difference of 3ASX2 is observed, due to its limited hepatic first-pass metabolism (low ER_{hep}^{3ASX2}).

CHAPTER 9

9 OVERALL CONCLUSIONS, LIMITATIONS AND FUTURE DIRECTIONS

9.1 Overall Conclusions

The focus of the project was to use PBPK modeling in order to predict metabolic DDI for different routes of administration (IV vs. PO) for a prototypical CYP3A substrate, MDZ, and two prototypical CYP3AIs (FLZ and ERY), along with other, derived hypothetical CYP3A substrates and inhibitors. The ultimate goal is to generalize the obtained results and to identify key *in-vitro* and *in-vivo* substrate and inhibitor properties (*e.g.*, F_{oral} , terminal $t_{1/2}$, contribution of gut wall and hepatic metabolism to overall first-pass extraction and CL_{tot} , inhibitory mechanism and potency) as well as physiological characteristics (*e.g.*, hepatic and gut wall CYP3A expression and turn-over kinetics) that are likely to impact significantly the magnitude and time course of the DDI, depending on the respective route of administration of substrate and/or inhibitor. As a result, generalized decision trees were proposed -using pivotal information about clinical PK/ADME/*in-vitro* DDI substrate and inhibitor properties- to assess the likelihood (and particular circumstances, *e.g.*, timing of inhibitor relative to substrate administration) of clinically significant route differences in DDI magnitude between IV and PO administered substrate and/or inhibitor.

9.1.1 Substrate properties

Figure 9.1 illustrates the impact of administration route (IV vs. PO) of the victim drug on its metabolic inhibitory DDI. First, the contribution of CYP3A metabolism to overall systemic/pre-systemic clearance of victim drug needs to be evaluated, in order to determine whether a CYP3A DDI is likely clinically significant or not. Once the victim drug is confirmed to be a CYP3A substrate, and CYP3A metabolism has been found to be a major ($f_m^{\text{CYP3A}} > 20\%$) elimination pathway (typically assessed from information integrating *in vitro/in vivo* ADME and DDI studies with prototypical CYP3AI), the impact of its route of administration (IV vs. PO) on DDI depends on whether it is subject to significant pre-systemic GW/hepatic CYP3A first-pass metabolism:

If the victim drug is a high F_{oral} drug, or a low F_{oral} drug due to poor GI solubility or poor GI permeability (rather than pre-systemic CYP3A-mediated first-pass effects), the metabolic inhibition will likely be similar for the IV or PO route. Previous M&S for 3ASX2 confirmed this proposed rule for a high F_{oral} victim drug. However, even the victim drug has high F_{oral} or low F_{oral} not due to first-pass metabolism, its unbound hepatic and GW concentration – time profiles after the IV and PO routes of administration are not exactly the same, and in some circumstances, the concentration difference in hepatocytes and enterocytes may still lead to minor route differences in DDI, especially for competitive or non-competitive metabolic inhibition.

If the victim drug has extensive CYP3A-mediated GW and/or hepatic pre-systemic metabolism, it is expected to be more sensitive to metabolic inhibition after PO than after IV administration, because besides the inhibition of systemic clearance (decreasing CL_{tot}), the pre-systemic first-pass metabolism is also inhibited (increasing F_{oral}) by CYP3AIs, resulting in a greater increase in systemic exposure after PO than after IV administration. The extent of route difference between IV and PO routes is dependent on the ER_{hep} of the victim drug: the higher ER_{hep} a victim drug has, the

larger DDI route difference is expected between IV and PO administration ($PO > IV$). Previous M&S for MDZ and 3ASX1 confirmed this proposed rule for a victim drug with low-intermediate F_{oral} .

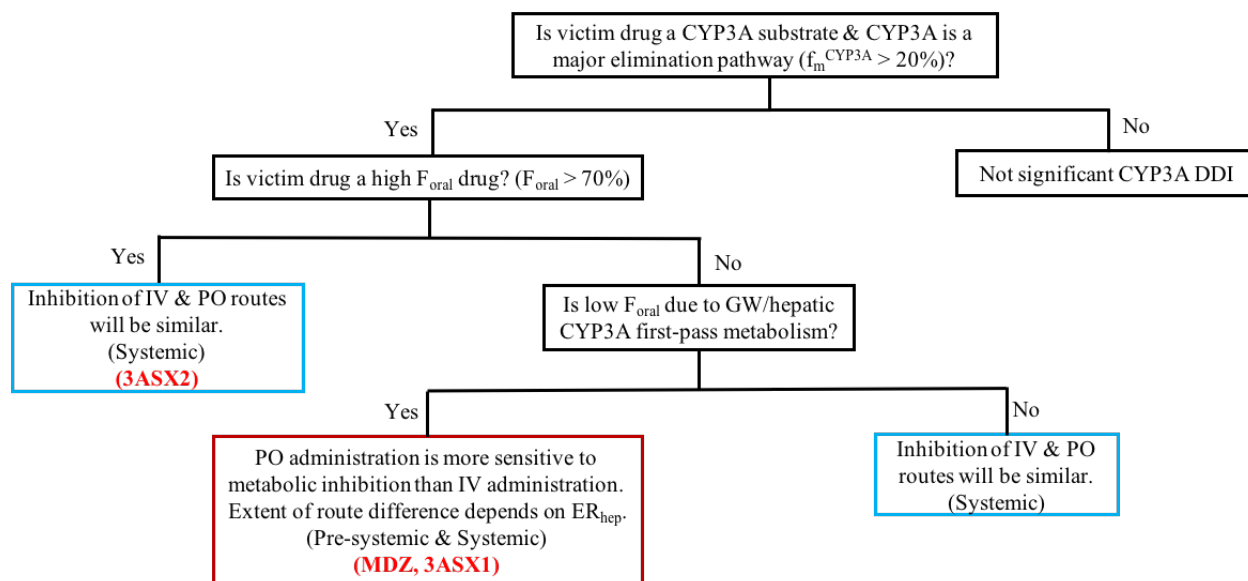


Figure 9.1 Proposed decision tree to determine the impact of route of administration (IV/PO) on the metabolic inhibitory DDI for the victim drug.

9.1.2 CYP3AI properties

With respect to the perpetrator drug, F_{oral} and inhibitory mechanism are two important determinants of the magnitude and time course of its route difference. Therefore, two decision trees are proposed in **Figure 9.2** and **Figure 9.3**, to predict the the likely route of administration difference in DDI under different F_{oral} and inhibitory mechanism of perpetrator drugs:

First, to follow the decision tree in **Figure 9.2**, the perpetrator drug has to be identified as a potential CYP3AI, in order to produce any clinical significant CYP3A-mediated DDI, typically by *in-vitro* studies that are extrapolated *in vivo* and/or *in-vivo* DDI studies with a prototypical CYP3A substrate. Subsequently, confirmed CYP3AI are divided into two categories based on their F_{oral} (high/not-high), using 70% as a proposed cut-off. For a high F_{oral} CYP3AI, if victim drug doesn't

have substantial pre-systemic GW metabolism (IV victim, or PO victim with no GW CYP3A metabolism), only marginal IV/PO route differences are expected. This is because for high F_{oral} CYP3AI, their hepatic concentration – time profiles after IV and PO administration are similar, while their GW concentration – time profiles could be quite different, as shown in previous simulations for FLZ, 3AIX2 and 3AIX4 (see **Chapter 6**). M&S for IV MDZ and FLZ, IV MDZ and 3AIX2, IV MDZ and 3AIX4, IV/PO 3ASX1 and FLZ, IV/PO 3ASX2 and FLZ, IV/PO 3ASX2 and 3AIX2 confirmed this proposed rule.

On the other hand, if victim drug has extensive pre-systemic GW metabolism (after PO administration), PO CYP3AI produces more inhibition than IV CYP3AI, but the duration of the route difference depends on the DDI mechanism and whether the IV inhibitor can inhibit GW metabolism, i.e., has access to the enterocyte from the vascular side. Although it is typically difficult to definitively determine whether the IV inhibitor can inhibit GW metabolism or not (for a conclusive determination, a prototypical victim drug subject to GW metabolism, such as MDZ, needs to be chosen, and a DDI study between both IV and PO substrate and the IV inhibitor needs to be conducted), extrapolations can be made based on available *in vitro/in vivo* PK, BCS classification and physicochemical properties of the inhibitor:

For a BCS class 1 CYP3AI with little plasma protein binding, such as FLZ and 3AIX2, the CYP3AI can enter enterocytes through both apical/GI luminal and basolateral/vascular sides. Hence, any IV-PO route difference for the inhibitor can only occur when the perpetrator drug is simultaneously dosed with PO victim drug, as the resulting GW concentration of CYP3AI and its GW inhibition of CYP3A are higher after PO than after IV administration only during its oral absorption phase. With increasing separation of victim drug from perpetrator drug administration (administered when CYP3AI's systemic distribution has achieved its pseudo steady-state),

no/marginal CYP3AI route difference is expected. Previous M&S for PO MDZ and FLZ, PO MDZ and 3AIX2 confirmed this proposed rule (see **Chapter 6**). However, the magnitude and time course of the route difference is also affected by dosing regimen (*i.e.*, dose, infusion time) of the CYP3AI, as well as the $t_{1/2}$ of the CYP3AI relative to $t_{1/2}$ of the substrate. In the simulations for the MDZ-FLZ DDI, 400 mg of FLZ gave rise to the largest route difference (~62%), while the lowest (40 mg) or highest (4,000 mg) simulated FLZ dose could not bring about a clinically significant DDI route difference (change in AUCR < 20%), due to their much lower (40 mg) or much higher (4,000 mg) hepatic/GW FLZ concentrations than corresponding K_i^{FLZ} . In addition, previous simulations were performed when IV FLZ was administered as 1-hour infusion, and different infusion times affect the c_{max} and t_{max} of hepatic and GW concentration – time profiles of FLZ after IV administration, potentially leading to a route difference. Furthermore, DDI simulations between 3ASX2, a long $t_{1/2}$ CYP3A substrate, and 3AIX2, a short $t_{1/2}$ FLZ-derived CYP3AI demonstrated a smaller DDI than FLZ's inhibition on 3ASX2 (see **Chapter 6**), suggesting that altering $t_{1/2}$ for CYP3AI may affect both the magnitude and duration of DDI.

For a BCS class 3 CYP3AI with high plasma protein binding, such as 3AIX4 (a ERY-like drug), a sustained IV-PO route difference for CYP3AI is expected, even if the victim drug is dosed further apart from the perpetrator drug. As opposed to FLZ and its derivatives discussed above, ERY and 3AIX4 can access the enterocyte via GI luminal/apical side, *i.e.*, after PO administration, only, and no pseudo steady-state can be achieved between (systemic) plasma and GW mucosa. Hence, a continuous IV-PO route difference for 3AIX4 can be expected regarding the metabolic inhibition on GW metabolism (see **Chapter 8**).

Moreover, the duration and peak time of any DDI route difference are also governed by mechanism of inhibition, which will be discussed in **Figure 9.3**. As a consequence, multiple circumstances of route difference may be observed clinically, for different modes of inhibition.

For a low F_{oral} CYP3AI, if victim drug doesn't have substantial pre-systemic GW metabolism (IV victim, or PO victim without GW CYP3A metabolism), greater inhibition is expected after IV than after PO CYP3AI – assuming that PO and IV doses are identical. This is due to lower hepatic concentrations and less hepatic CYP3A inhibition after PO administration, given its low F_{oral} . It is assumed that the low F_{oral} of the inhibitor is not due to GW/hepatic first pass metabolism. Previous M&S for IV MDZ and ERY, IV MDZ and 3AIX1, IV MDZ and 3AIX3, IV/PO 3ASX1 and ERY, IV/PO 3ASX2 and ERY validated this proposed rule.

However, if a drug has a low F_{oral} , its clinical PO dose is usually increased to match systemic exposures after IV administration. Therefore, it may not be appropriate to compare route difference at the same clinical IV and PO inhibitor dose, when it has a low F_{oral} .

On the other hand, if the victim drug has extensive GW metabolism (after PO administration), the impact of inhibitor route of administration is difficult to predict, as it depends on the concentration – time profiles of CYP3AI in GW and liver relative to their corresponding potency values (K_i). The route difference of MBI CYP3AI can also be influenced by k_{inact} and enzyme kinetics (natural synthesis/degradation rate constants). In the previous M&S, IV administration of 3AIX1 and IV 3AIX3 produce more inhibition of PO MDZ than after PO administration; IV ERY produces a similar maximal inhibition on PO MDZ as PO (SS) ERY, but less maximal inhibition than PO (EC) ERY. This inconsistency is due to different dosing regimen (*i.e.*, dose, dosing interval, formulation, administration time interval between victim and perpetrator), PK/physicochemical properties (F_{oral} , terminal $t_{1/2}$, permeability, fraction unbound in plasma) and

inhibition mechanism (MBI or non/-competitive) and potency of the CYP3AI, and have to be considered on a case-by-case basis.

Another interesting finding is the DDI time course between 3ASX2 and ERY: Prolonging the plasma (elimination) $t_{1/2}$ of the CYP3A substrate can reduce the impact of administration time interval between victim and perpetrator, if perpetrator drug is a MBI. This is because even if the inhibitory effect of MBI is delayed relative to its tissue concentration, there is still a significant alteration of the terminal phase of the PK profile for a victim drug with long elimination $t_{1/2}$, resulting in similar DDI magnitude after delayed administration of victim drug relative to perpetrator drug administration. This prolongation of $t_{1/2}$ for the victim drug also reduces the DDI route difference for ERY, especially after PO 3ASX2, because the inhibition/reduction of its CL_{tot} contributes more to the DDI magnitude than the increase in its F_{oral} ; as a consequence, the magnitude of inhibitor route difference becomes similar after IV and PO 3ASX2.

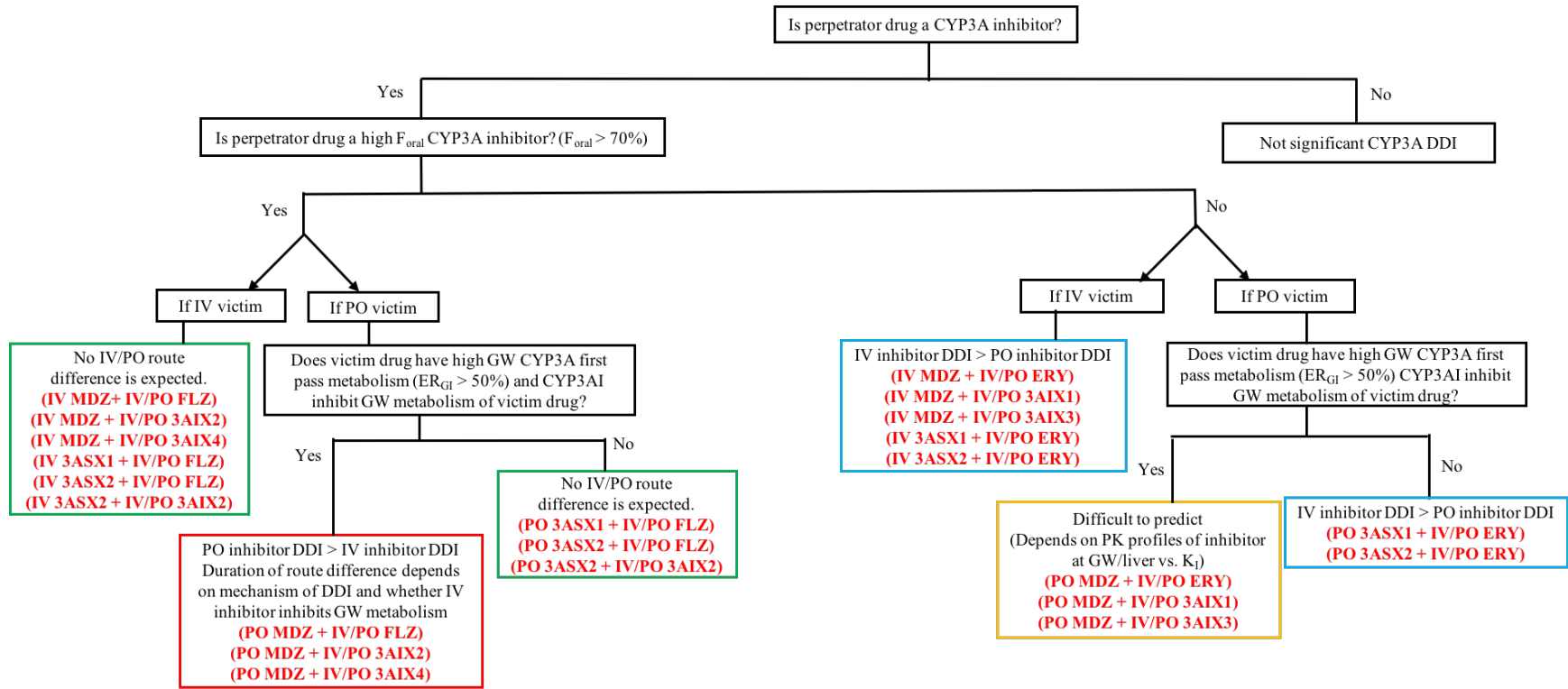


Figure 9.2 Proposed decision tree to determine the impact of route of administration (IV/PO) on the DDI for perpetrator drug (based on F_{oral}).

Figure 9.3 outlines the the difference between reversible (non-/competitive) inhibitors and irreversible inhibitors (MBI):

If the perpetrator drug is a non-/competitive CYP3AI, the peak and duration of its DDI are determined by its oral absorption rate and, for a given inhibitory potency (K_i), by its hepatic and/or GW concentration-time profiles. The plasma $t_{1/2}$ of either the victim or the perpetrator may also affect the time course of the DDI.

If the perpetrator drug is a MBI CYP3AI, besides its inhibitory hepatic and/or GW concentration-time profiles, the peak and duration of DDI are also determined by the endogenous turn-over kinetics of CYP3A. Maximum inhibition occurs when GW/hepatic CYP3A activities achieve their nadir (which is delayed from their respective peak concentrations), and the DDI duration depends on hepatic/GW $t_{1/2}^{CYP3A}$ (k_{deg}); if the plasma/hepatic/GW concentration $t_{1/2}$ of the perpetrator drug is shorter than $t_{1/2}^{CYP3A}$ (most likely scenario, although it is possible that the CYP3AI $t_{1/2}$ can be longer than $t_{1/2}^{CYP3A}$, *e.g.*, after extended-release/long acting dosage forms, resulting in flip-flop PK). In addition, the $t_{1/2}$ of victim drug may also affect the time course of DDI route difference as discussed above.

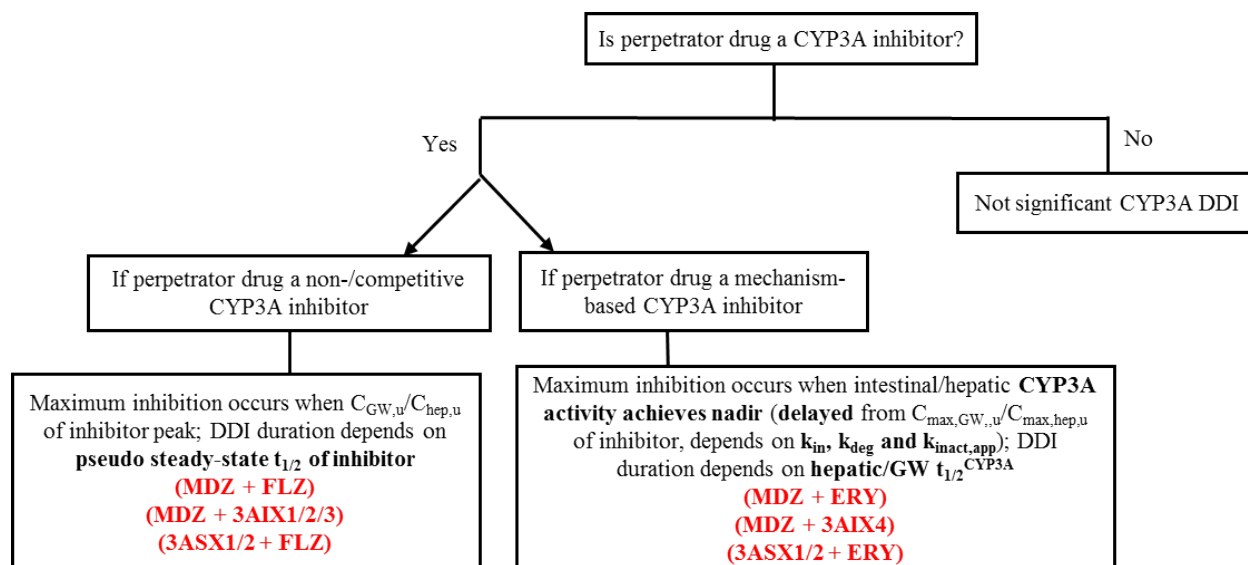


Figure 9.3 Proposed decision tree to determine the impact of route of administration (IV/PO) on the DDI for perpetrator drug (based on mechanism of inhibition)

Overall, this research project allows the identification of key substrate and inhibitor properties, likely to contribute to route of administration (IV vs. PO) differences in DDI magnitude and time course:

For a CYP3A substrate, its F_{oral} , ER_{hep} and ER_{GW} are the three main properties that determine DDI route differences after CYP3A inhibition.

For a CYP3AI, its F_{oral} and whether IV CYP3AI inhibits GW metabolism are the two key determinants for DDI route differences for inhibition of CYP3A substrates.

For example, for a low ER_{hep} CYP3A substrate/investigational drug without GW metabolism, if a pharmaceutical company had conducted a DDI study between their investigational drug after PO administration and a prototypical CYP3AI, they could extrapolate these results to IV administration of their drug with CYP3AI, and potentially avoid a prospective DDI study with their drug after IV administration CYP3AI. On the other hand, for a high ER_{hep} CYP3A substrate and/or a victim drug subject to both intermediate-to-high ER_{hep} and/or ER_{GW} metabolism, even if the pharmaceutical

company had conducted DDI study between PO substrate and CYP3AI and observed a clinically significant DDI, it would be still necessary to prospectively assess the DDI between IV substrate and CYP3AI as well, because IV substrate is expected to be much less sensitive to the metabolic inhibition than PO substrate. However, if the original PO substrate DDI study had demonstrated no clinically significant DDI, it is unlikely that IV substrate administration would result in a clinically significant DDI.

Overall, this M&S approach can be leveraged prospectively in clinical drug development and regulatory decision-making by allowing extrapolation of a DDI from an available to a different route of administration and by helping decide whether a designated clinical DDI study may be necessary for a new/different route in order to support adequate product labeling recommendations.

9.2 Limitations and Future Directions

In this M&S research project, no random sources of variability (*i.e.*, inter-study variability, inter-individual variability, residual error) on parameters were incorporated in the PBPK model; as a consequence, some parameters (*i.e.*, $v_{\max, \text{hep}}^{\text{MDZ}}$, f_{villi} , $k_{\text{GL}}^{\text{MDZ}}$, $v_{\max, \text{hep}}^{\text{ERY}}$, $v_{\max, \text{bile}}^{\text{ERY}}$, $F_{\text{abs}}^{\text{ERY}}$) had to be adjusted for the validation from specific studies, in order to better characterize the respective observed PK profiles. These parameter adjustments were supported by findings from the model-independent analysis in **Chapter 3** and **Chapter 7, section 7.3.1** (meta-analysis of MDZ and ERY), consistent with mechanistic reasoning, supported by the results of the sensitivity analyses and kept to a minimum. Full-fledged Monte Carlo simulations (MCS) could be performed to incorporate statistical distributions for each/some parameters. However, due to the large number of parameters ($n = 63$) used in the semi-PBPK models and the unknown underlying distributions for most parameters, MCS were not used in this research.

There are no individual clinical DDI studies that reported MDZ profiles after both IV and PO MDZ in presence of both IV and PO CYP3AI. FLZ is the only CYP3AI with a DDI study available where both IV and PO CYP3AI had been concomitantly administered with PO MDZ, assessing the impact of route of administration of FLZ in the same study. As to ERY, only PO ERY was used in the reported ERY - MDZ clinical DDI studies. Therefore, no DDI study results could be used to validate the IV FLZ and IV MDZ DDI model, or the IV ERY and IV/PO MDZ DDI model. In the DDI modeling development for ERY, the key assumption that only PO ERY (but not IV ERY) can inhibit GW metabolism of PO MDZ was made based on the PK and physicochemical properties of ERY.

Regarding model validation/qualification, besides visual inspection of predicted plasma concentration –time profiles for the drugs of interest, exposure metrics (*i.e.*, AUC, c_{max} and t_{max}) of plasma PK profiles were calculated to compare with observed. If the same original parameters were used across all validation studies (FLZ, ERY individual semi-PBPK models), an empiric acceptance criterion of 0.5 – 2 fold of observed was used for the exposure metrics. If parameters were adjusted from the initial/original model parameters to account for inter-study differences (based on preliminary meta-analysis of the variability of certain parameters (MDZ individual, MDZ-FLZ DDI, MDZ-ERY DDI semi-PBPK models)), a tighter acceptance criterion of within \pm 30% of observed was used instead.

The clinical significance of the PBPK-model predicted DDIs (expressed as change in AUCR of substrate drug), however, depends not only on exposure changes in plasma parent drug, but also any metabolite exposure changes (if they contribute to safety and/or efficacy), other known patient covariates that may affect substrate and/or CYP3AI PK, *e.g.*, renal function for FLZ, inter-individual (random) variability as well as therapeutic windows for parent substrate

drug/metabolites and overall risk benefit analysis.

Prospectively, these semi-PBPK DDI models can be extended to CYP3A inducers in order to investigate the impact of administration routes for DME inducers on DDI magnitude and time course. Also, important patient intrinsic/extrinsic factors (*e.g.*, age, gender, pharmacogenetics, *etc.*) can be included by modifying model parameters (*e.g.*, enzyme expression levels, renal clearance, *etc.*) accordingly. In addition, DDI route of administration differences for victim/perpetrator drugs with metabolic inhibition of other DME, such as CYP2D6, can be assessed using a similar strategy. Finally, PBPK models for other routes of administration (*e.g.*, intramuscular injection, transdermal penetration, pulmonary inhalation) can also be developed to assess their impact on DDI.

LIST OF REFERENCES

- Abboud, B., Hachem, J.E., Yazbeck, T., & Doumit, C. (2009). Hepatic portal venous gas: Physiopathology, etiology, prognosis and treatment. *World J Gastroenterol*, 15(29), 3585-3590.
- Agrawal, Abha. (2009). Medication errors: prevention using information technology systems. *Br J Clin Pharmacol*, 67(6), 681-686.
- Ahmad, A. M. (2007). Recent advances in pharmacokinetic modeling. *Biopharm Drug Dispos*, 28(3), 135-143.
- Ahonen, J., Olkkola, K. T., & Neuvonen, P. J. (1997). Effect of route of administration of fluconazole on the interaction between fluconazole and midazolam. *Eur J Clin Pharmacol*, 51(5), 415-419.
- Andersin, R. (1991). Solubility and acid-base behaviour of midazolam in media of different pH, studied by ultraviolet spectrophotometry with multicomponent software. *J Pharm Biomed Anal*, 9(6), 451-5.
- Arbor Pharmaceuticals. (2013). Erythromycin Stearate Tablets, USP Film-coated Tablets. FDA Drug Label.
- Argenio, D. Z. D', Schumitzky, A., & Wang, X. (2009). *ADAPT 5 User's Guide: Pharmacokinetic/Pharmacodynamic Systems Analysis Software*.
- Austin, K. L., Mather, L. E., Philpot, C. R., & McDonald, P. J. (1980). Intersubject and dose-related variability after intravenous administration of erythromycin. *Br J Clin Pharmacol*, 10(3), 273-279.
- Barre, J., Mallat, a, Rosenbaum, J., Deforges, L., Houin, G., Dhumeaux, D., & Tillement, J. P. (1987). Pharmacokinetics of erythromycin in patients with severe cirrhosis. Respective influence of decreased serum binding and impaired liver metabolic capacity. *Br J Clin Pharmacol*, 23, 753-757.
- Baxter Healthcare Corporation. Midazolam Hydrochloride – Injection FDA Label. Retrieved from <http://www.rxlist.com/midazolam-injection-drug.htm>
- Benardi, M. De, Feletti, F., Gazzani, G., & Fregnan, G. B. (1988). Human pharmacokinetics of erythromycin propionate-N-acetylcysteine. *Inter J Clin Pharm Ther*, 26(9), 444-447.
- Birkett, D.J., Robson, R.A., Grgurinovich, N., & Tonkin, A. (1990). Single oral dose pharmacokinetics of erythromycin and roxithromycin and the effects of chronic dosing. *Ther Drug Monit* 12, 65-71.
- Björkman, S., Wada, D. R., Berling, B. M., & Benoni, G. (2001). Prediction of the disposition of midazolam in surgical patients by a physiologically based pharmacokinetic model. *J Pharm Sci*, 90(9), 1226-41.
- Brammer, K. W., Coakley, A. J., Jezequel, S. G., & Tarbit, M. H. (1991). The disposition and

metabolism of [^{14}C]fluconazole in humans. *Drug Metab Dispos*, **19**(4), 764–7.

Cao, Y., & Jusko, W. J. (2012). Applications of minimal physiologically-based pharmacokinetic models. *J Pharmacokinet Pharmacodyn*, **39**(6), 711–23.

Carls, A., Jedamzik, J., Witt, L., & Hohmann, N. (2014). Systemic exposure of topical erythromycin in comparison to oral administration and the effect on cytochrome P450 3A4 activity. *Br J Clin Pharmacol*, **78**(6), 1433–30.

Carrasco-Portugal, M. D. C., & Flores-Murrieta, F. J. (2007). Gender differences in the oral pharmacokinetics of fluconazole. *Clin Drug Investig*, **27**(12), 851–5.

Charoo, N., Cristofolletti, R., Graham, A., Lartey, P., Dressman, J., et al. (2014). Biowaiver monograph for immediate-release solid oral dosage forms: Fluconazole. *J Pharm Sci*, **103**(12), 3843–3858.

Chelvan, P., Hamilton-Miller, J. M., & Brumfitt, W. (1979). Biliary excretion of erythromycin after parenteral administration. *Br J Clin Pharmacol*, **8**(3), 233–235.

Chien, J. Y., Lucksiri, A., Ernest, C. S., Gorski, J. C., Wrighton, S. A., & Hall, S. D. (2006). Stochastic prediction of CYP3A-mediated inhibition of midazolam clearance by ketoconazole. *Drug Metab Dispos*, **34**(7), 1208–19.

Classen, D., Pestotnik, S., Evans, S., Lloyd, J., Burke, J. (1997). Adverse drug events in hospitalized patients. Excess length of stay, extra costs, and attributable mortality. *JAMA*, **277**(4), 301–6.

Daly, A. K. (2006). Significance of the minor cytochrome P450 3A isoforms. *Clin Pharmacokinet*, **45**(1), 13–31.

Danan, G., Descatoire, V., & Pessayre, D. (1981). Self-Induction by erythromycin of its own transformation into a metabolite forming an inactive complex with reduced cytochrome P-450. *J Pharmacol Exp Therapeut*, **218**(2), 509–14.

Delafuente, J. C. (2003). Understanding and preventing drug interactions in elderly patients. *Crit Rev Oncol Hematol*, **48**(2), 133–143.

Dette, G. A., & Knothe, H. (1986). The binding protein of erythromycin in human serum. *Biochem Pharmacol*, **35**(6), 959–966.

Dette, G. A., Knothe, H., & Herrmann, G. (1982). Erythromycin binding to human serum. *Biochem Pharmacol*, **31**(6), 1081–1087.

Dhillon, S., & Kostrzewski, A.J. Clinical Pharmacokinetics. (2006) 1st edition. Chapter 1. Basic pharmacokinetics.

Drug Interactions & Labeling Drug Development and Drug Interactions Table of Substrates, Inhibitors and Inducers. Retrieved from <http://www.fda.gov/drugs/developmentapprovalprocess/developmentresources/druginteractionslabeling/ucm093664.htm>

DrugBank Erythromycin (DB00199). Retrieved from <http://www.drugbank.ca/drugs/DB00199>

DrugBank Fluconazole (DB00196). Retrieved from <http://pubs.acs.org/doi/abs/10.1021/jc4010257>

Dundee, J. W., Halliday, N. J., Loughran, P. G., & Harper, K. W. (1985). The influence of age on the onset of anaesthesia with midazolam. *Anaesthesia*, **40**(5), 441–3.

Eipel, C., Abshagen, K., & Vollmar, B. (2010). Regulation of hepatic blood flow: the hepatic arterial buffer response revisited. *World J Gastroenterol*, **16**(48), 6046–57.

Ervine, C. M., & Houston, J. B. (1994). Disposition of azole antifungal agents. III. Binding of fluconazole and other azoles in rat liver. *Pharm Res*, **11**(7), 961–5.

ERY Scifinder Report. Retrieved from <https://scifinder-cas-org.proxy.library.vcu.edu/scifinder/view/scifinder/scifinderExplore.jsf>

Erythromycin (Systemic). Lexi.com. Retrieved from https://online.lexi.com/lco/action/doc/retrieve/docid/patch_f/1831759

European Medicines Agency. Guideline on the Investigation of Drug Interactions. (2012) Retrieved from http://www.ema.europa.eu/docs/en_GB/document_library/Scientific_guideline/2012/07/WC500129606.pdf

FAERS Reporting by Patient Outcomes by Year. (2015). Retrieved from <http://www.fda.gov/Drugs/GuidanceComplianceRegulatoryInformation/Surveillance/AdverseDrugEffects/ucm070461.htm>

FDA. Guidance for industry. Drug interaction studies - study design, data analysis, implications for dosing, and labeling recommendations. (2012). Retrieved from <http://www.fda.gov/downloads/drugs/guidancecomplianceregulatoryinformation/guidances/ucm292362.pdf>

Fenneteau, F., Poulin, P., & Nekka, F. (2010). Physiologically based predictions of the impact of inhibition of intestinal and hepatic metabolism on human pharmacokinetics of CYP3A substrates. *J Pharm Sci*, **99**(1), 486–514.

Fetzner, L., Burhenne, J., Weiss, J., Völker, M., Unger, M., Mikus, G., & Haefeli, W. E. (2011). Daily honey consumption does not change CYP3A activity in humans. *J Clin Pharmacol*, **51**(8), 1223–32.

Fleischer, A. C., Muhletaler, C. A., & James, A. E. (1981). Sonographic assessment of the bowel

- wall. *Am J Roentgenol*, **136**(5), 887–91.
- Frassetto, L.A., Poon, S., Tsourounis C., Valera, C., Benet, L.Z. (2007). Effect of uptake and efflux transporter inhibition on erythromycin breath test results. *Clin Pharmacol Ther*, **81**(6), 828-832.
- Fluconazole. Lexi.com. Retrieved from https://online.lexi.com/lco/action/doc/retrieve/docid/patch_f/6918
- Frechen, S., Junge, L., Saari, T. I., Suleiman, A. A., Fuhr, U., et al. (2013). A semiphysiological population pharmacokinetic model for dynamic inhibition of liver and gut wall cytochrome P450 3A by voriconazole. *Clin Pharmacokinet*, **52**(9), 763–81.
- Furberg, C. D., & Pitt, B. (2001). Withdrawal of cerivastatin from the world market. *Curr Control Trials Cardiovasc Med*, **2**(5), 205–207.
- Galetin, A., Ito, K., Hallifax, D., & Houston, J. B. (2005). CYP3A4 substrate selection and substitution in the prediction of potential drug-drug interactions. *J Pharmacol Exp Ther*, **314**(1), 180–90.
- Gandhi, A. S., Guo, T., Shah, P., Moorthy, B., Chow, D. S.-L., Hu, M., & Ghose, R. (2012). CYP3A-dependent drug metabolism is reduced in bacterial inflammation in mice. *Br J Pharmacol*, **166**(7), 2176–87.
- Garg, V., Chandorkar, G., Farmer, H. F., Smith, F., Alves, K., & van Heeswijk, R. P. G. (2012). Effect of telaprevir on the pharmacokinetics of midazolam and digoxin. *J Clin Pharmacol*, **52**(10), 1566–73.
- Gibbs, M. A., Thummel, K. E., Shen, D. D., & Kunze, K. L. (1999). Inhibition of cytochrome P-450 3A (CYP3A) in human intestinal and liver microsomes: comparison of Ki values and impact of CYP3A5 expression. *Drug Metab Dispos*, **27**(2), 180–7.
- Gorski, J. C., Jones, D. R., Haehner-Daniels, B. D., Hamman, M. A., O'Mara, E. M., & Hall, S. D. (1998). The contribution of intestinal and hepatic CYP3A to the interaction between midazolam and clarithromycin. *Clin Pharmacol Thera*, **64**(2), 133–43.
- Hall, K. W., Nightingale, C. H., Gibaldi, M., Nelson, E., Bates, T. R., & DiSanto, A.R. (1982). Pharmacokinetics of erythromycin in normal and alcoholic liver disease subjects. *J Clin Pharmacol*, **22**(7), 321–325.
- Heinemann, A., Wischhusen, F., Püschel, K., & Rogiers, X. (1999). Standard liver volume in the Caucasian population. *Liver Transplant Surg*, **5**(5), 366–8.
- Heizmann, P., Eckert, M., & Ziegler, W. H. (1983). Pharmacokinetics and Bioavailability of Midazolam in Man. *Br J Pharmacol*, **16**, 43S–49S.
- Hospira. (2013). Erythromycin TM Lactobionate for Injection. FDA Drug Label

- Huang, S.-M., & Rowland, M. (2012). The role of physiologically based pharmacokinetic modeling in regulatory review. *Clin Pharmacol Ther*, **91**(3), 542–9.
- Humphrey, M. J., Jevons, S., & Tarbit, M. H. (1985). Pharmacokinetic evaluation of UK-49,858, a metabolically stable triazole antifungal drug, in animals and humans. *Antimicrob Agents and Chemother*, **28**(5), 648–53.
- Hyland, R., Osborne, T., Payne, A., Kempshall, S., Logan, Y. R., Ezzeddine, K., & Jones, B. (2009). In vitro and in vivo glucuronidation of midazolam in humans. *Br J Clin Pharmacol*, **67**(4), 445–54.
- Iliopoulou, A., Aldhous, M. E., Johnston, A. & Turner, P. (1982). Pharmacokinetic interaction between theophylline and erythromycin. *Br J Clin Pharm*, **14**, 495–499.
- Inhibition of Enzyme Activity, class handout. Retrieved from <http://www.csun.edu/~hcchm001/5enzyme.pdf>
- Isoherranen, N., Ludington, S. R., Givens, R. C., Lamba, J. K., Paine, M. F et al. (2008). The influence of CYP3A5 expression on the extent of hepatic CYP3A inhibition is substrate-dependent: an in vitro-in vivo evaluation. *Drug Metab Dispos*, **36**(1), 146–54.
- Ito, K., Ogihara, K., Kanamitsu, S. I., & Itoh, T. (2003). Prediction of the in vivo interaction between midazolam and macrolides based on in vitro studies using human liver microsomes. *Drug Metab Dispos*, **31**(7), 945–954.
- Janardan, S. K., Lown, K. S., Schmiedlin-Ren, P., Thummel, K. E., & Watkins, P. B. (1996). Selective expression of CYP3A5 and not CYP3A4 in human blood. *Pharmacogenet*, **6**, 379–385.
- Johnson, J. A., & Boothman, J. L. (1995). Drug-related morbidity and mortality. A cost-of-illness model. *Arch Intern Med*, **155**, 1949–56.
- Johnson, T. N., Rostami-Hodjegan, A., Goddard, J. M., Tanner, M. S., & Tucker, G. T. (2002). Contribution of midazolam and its 1-hydroxy metabolite to preoperative sedation in children: a pharmacokinetic-pharmacodynamic analysis. *Br J Anaesth*, **89**(3), 428–37.
- Jonge, H. de, Loor, H. de, Yves, V., & Kuypers, D. R. (2013). Impact of CYP3A5 genotype on tacrolimus versus midazolam clearance in renal transplant recipients : new insights in CYP3A5-mediated drug metabolism. *Pharmacogenomics*, **14**(12), 1467–1480.
- Josefsson, K., Bergan, T., & Magni, L. (1982). Dose-related pharmacokinetics after oral administration of a new formulation of erythromycin base. *Br J Clin Pharm*, **13**(9), 685–691.
- Jovanovid, D., Kilibarda, V., Vu, S., Srnid, D., Vehabovid, M., & Potogija, N. (2005). A randomized , open-label pharmacokinetic comparison of two oral formulations of fluconazole 150 mg in healthy adult volunteers. *Clin Ther*, **27**(10), 1588–95.

- Kan, M. K., & Hopkins, G. B. (1979). Measurement of liver volume by emission computed tomography. *J Nucl Med* :, **20**(6), 514–20.
- Kato, M., Shitara, Y., Sato, H., Yoshisue, K., Hirano, M., Ikeda, T., & Sugiyama, Y. (2008). The quantitative prediction of CYP-mediated drug interaction by physiologically based pharmacokinetic modeling. *Pharm Res*, **25**(8), 1891–901.
- Kharasch, E. D., Walker, A., Hoffer, C., & Sheffels, P. (2004). Intravenous and oral alfentanil as in vivo probes for hepatic and first-pass cytochrome P450 3A activity: noninvasive assessment by use of pupillary miosis. *Clin Pharmacol Ther*, **76**(5), 452–66.
- Kharasch, E. D., Walker, A., Hoffer, C., & Sheffels, P. (2005). Sensitivity of intravenous and oral alfentanil and pupillary miosis as minimally invasive and noninvasive probes for hepatic and first-pass CYP3A activity. *J Clin Pharm*, **45**(10), 1187–1197.
- Kirby, B. J., Collier, A. C., Kharasch, E. D., Whittington, D., Thummel, K. E., & Unadkat, J. D. (2011). Complex drug interactions of HIV protease inhibitors 1: inactivation, induction, and inhibition of cytochrome P450 3A by ritonavir or nelfinavir. *Drug Metab Dispos*, **39**(6), 1070–8.
- Klieber, S., Hugla, S., Ngo, R., Arabeyre-Fabre, Fabre, G., et al. (2008). Contribution of the N-glucuronidation pathway to the overall in vitro metabolic clearance of midazolam in humans. *Drug Metab Dispos*, **36**(5), 851–62.
- Krishna, G., Moton, A., Ma, L., Savant, I., Martinho, M., Seiberling, M., & McLeod, J. (2009). Effects of oral posaconazole on the pharmacokinetic properties of oral and intravenous midazolam: a phase I, randomized, open-label, crossover study in healthy volunteers. *Clin Ther*, **31**(2), 286–98.
- Kupferschmidt, H. H., Ha, H. R., Ziegler, W. H., Meier, P. J., & Krähenbühl, S. (1995). Interaction between grapefruit juice and midazolam in humans. *Clin Pharmacol Ther*, **58**(1), 20–8.
- Kurnik, D., Wood, A. J. J., & Wilkinson, G. R. (2006). The erythromycin breath test reflects P-glycoprotein function independently of cytochrome P450 3A activity. *Clin Pharmacol Ther*, **80**(3), 228–234.
- Lappin, G., Kuhnz, W., Jochemsen, R., Kneer, J., Garner, R. C. (2006). Use of microdosing to predict pharmacokinetics at the therapeutic dose: Experience with 5 drugs. *Clin Pharm Ther*, **80**(3), 203–215.
- Larrey, D., Funck-Brentano, C., Breil, P., Vitaux, J., Theodore, C., Babany, G., & Pessayre, D. (1983). Effects of erythromycin on hepatic drug-metabolizing enzymes in humans. *Biochem Pharmacol*, **32**(6), 1063–8.
- Lazarou, J., Pomeranz, B. H., & Corey, P. N. (1998). Incidence of adverse drug reactions in hospitalized patients: a meta-analysis of prospective studies. *Jama*, **279**(15), 1200–1205.

- Leape, L., Bates, D., Cullen, D., Cooper, J., Demonaco, H., et al. (1995). Systems analysis of adverse drug events. *JAMA : The Journal of the American Medical Association*, **274**(1), 35–43.
- Lin, X., Skolnik, S., Chen, X., & Wang, J. (2011). Attenuation of intestinal absorption by major efflux transporters: Quantitative tools and strategies using a Caco-2 model. *Drug Metab Dispos*, **39**(2), 265–274.
- Lindenberg, M., Kopp, S., & Dressman, J. B. (2004). Classification of orally administered drugs on the World Health Organization Model list of Essential Medicines according to the biopharmaceutics classification system. *Eur J Pharm Biopharm* :, **58**(2), 265–78.
- Link, B., Haschke, M., Grignaschi, N., Bodmer, M., Aschmann, Y. Z., Wenk, M., & Krähenbühl, S. (2008). Pharmacokinetics of intravenous and oral midazolam in plasma and saliva in humans: usefulness of saliva as matrix for CYP3A phenotyping. *Br J Clin Pharmacol*, **66**(4), 473–84.
- Lown, K., Kolars, J., Thummel, K., Barnett, J., Kunze, K., Wrighton, S., & Watkins, P. (1994). Interpatient heterogeneity in expression of CYP3A4 and CYP3A5 in small bowel. *Drug Metab Dispos*, **22**(6), 947–955.
- Malmberg, A.S. (1979). Effect of food on absorption of erythromycin. A study of two derivatives, the stearate and the base. *J Antimicrob Chemother*, **5**, 591–599.
- Mandema, J. W., Tuk, B., van Steveninck, A. L., Breimer, D. D., Cohen, A. F., & Danhof, M. (1992). Pharmacokinetic-pharmacodynamic modeling of the central nervous system effects of midazolam and its main metabolite alpha-hydroxymidazolam in healthy volunteers. *Clin Pharmacol Ther*, **51**(6), 715–28.
- Mannisto, P. T., Taskinen, J., Ottoila, P., Solkinen, A., Vuorela, A., & Nykanen, S. (1988). Fate of single oral doses of ERY acistrate, ERY stearate and pelleted ERY base analysed by mass-spectrometry in plasma of healthy human volunteers. *J Antimicrob Chemother*, **21**(Suppl. D), 33–43.
- Mather, L. E., Austin, K. L., Philpot, C. R., & McDonald, P. J. (1981). Absorption and bioavailability of oral erythromycin. *Br J Clin Pharmacol*, **12**(2), 131–140.
- McConn, D. J., Lin, Y. S., Allen, K., Kunze, K. L., & Thummel, K. E. (2004). Differences in the inhibition of cytochromes P450 3A4 and 3A5 by metabolite-inhibitor complex-forming drugs. *Drug Metab Dispos*, **32**(10), 1083–1091.
- McDonald, P. J., Mather, L. E., & Story, M. J. (1977). Studies on absorption of a newly developed enteric-coated erythromycin base. *J Clin Pharm*, **17**(10 Pt 1), 601–606.
- Midazolam SciFinder Report. Retrieved from <https://scifinder-cas-org.proxy.library.vcu.edu/scifinder/view/scifinder/scifinderExplore.jsf>
- Miao, J., Jin, Y., Marunde, R. L., Kim, S., Quinney, Hall, S. D., et al. (2009). Association of

- genotypes of the CYP3A cluster with midazolam disposition in vivo. *Pharmacogenomics J*, **9**, 319–326.
- Michalets, E. L., & Williams, C. R. (2000). Drug interactions with cisapride. *Clin Pharmacokinet*, **39**(1), 49–75.
- Miglioli, P.A., Pivetta, P., Strazzabosco, M., Orlando, R., Okolicsanyi, L., & Palatini, P. (1990). Effect of age on single- and multiple-dose pharmacokinetics of erythromycin. *Eur J Clin Pharmacol*, **39**, 161–164.
- Mirošević Skvrce, N., Macolić Šarinić, V., Mucalo, I., Krnić, D., Božina, N., & Tomić, S. (2011). Adverse drug reactions caused by drug-drug interactions reported to Croatian Agency for Medicinal Products and Medical Devices: a retrospective observational study. *Croat Med J*, **52**(5), 604–614.
- Moura, CS, Acurcio, FA, Belo, NO. (2009) Drug-drug interactions associated with length of stay and cost of hospitalization. *J Pharm Pharm Sci*, **12**(3), 266-272.
- Novel drug approval for 2015. Retrieved from <http://www.fda.gov/Drugs/DevelopmentApprovalProcess/DrugInnovation/ucm430302.htm>
- Nožini, D., Mili, A., & Mikac, L. (2010). Assessment of macrolide transport using PAMPA , Caco-2 and MDCKII-hMDR1 assays. *Croat Chem Acta*, **83**(3), 323–331.
- Okudaira, T., Kotegawa, T., Imai, H., Tsutsumi, K., Nakano, S., & Ohashi, K. (2007). Effect of the treatment period with erythromycin on cytochrome P450 3A activity in humans. *J Clin Pharmacol*, **47**, 871–876.
- Olkkola, K. T., Ahonen, J., & Neuvonen, P. J. (1996). The effects of the systemic antimycotics, itraconazole and fluconazole, on the pharmacokinetics and pharmacodynamics of intravenous and oral midazolam. *Anesth Analg*, **82**(3), 511–6.
- Olkkola, K. T., Aranko, K., Luurila, H., Hiller, A., Saarnivaara, L., Himberg, J. J., & Neuvonen, P. J. (1993). A potentially hazardous interaction between erythromycin and midazolam. *Clin Pharm Ther*, **53**(3), 298–305.
- Ozawa, S., Soyama, A., Saeki, M., Fukushima-Uesaka, H., Sawada, J.-I., et al. (2004). Ethnic differences in genetic polymorphisms of CYP2D6, CYP2C19, CYP3As and MDR1/ABCB1. *Drug Metab Pharmacokinet*, **19**(2), 83–95.
- Paine, M. F., Khalighi, M., Fisher, J. M., Shen, D. D., Thummel, K. E., et al. (1997). Characterization of interintestinal and intrainestinal variations in human CYP3A-dependent metabolism. *J Pharmacol Exp Ther*, **283**, 1552–1562.
- Palkama, V. J., Ahonen, J., Neuvonen, P. J., & Olkkola, K. T. (1999). Effect of saquinavir on the pharmacokinetics and pharmacodynamics of oral and intravenous midazolam. *Clin*

Pharmacol Ther, **66**(1), 33–9.

- Palkama, V. J., Isohanni, M. H., Neuvonen, P. J., & Olkkola, K. T. (1998). The effect of intravenous and oral fluconazole on the pharmacokinetics and pharmacodynamics of intravenous alfentanil. *Anesth Analg*, **87**(1), 190–4.
- Parsons, R. L., & David, J. A. (1980). Pharmacokinetics of intravenous erythromycin lactobionate. *Int Met Res*, **8**(Supplement (2)), 15–23.
- Pfizer. (2011). DIFLUCAN (Fluconazole Tablets) (Fluconazole Injection - for intravenous infusion only) (Fluconazole for Oral Suspension). FDA Drug Label.
- Plevry, B. (2005). Pharmacodynamic and pharmacokinetic drug interactions. *Anaesthesia*, **6**(4), 129–133.
- Porta, V., Chang, K. H., & Storpirtis, S. (2005). Evaluation of the bioequivalence of capsules containing 150 mg of fluconazole. *Int J Pharm*, **288**(1), 81–6.
- Quinney, S. K., Zhang, X., Lucksiri, A., Gorski, J. C., Li, L., & Hall, S. D. (2010). Physiologically based pharmacokinetic model of mechanism-based inhibition of CYP3A by clarithromycin. *Drug Metab Dispos*, **38**(2), 241–248.
- Ranbaxy Pharmaceuticals Inc. (2013). Midazolam Hydrochloride - Syrup. FDA Drug Label. Retrieved from <http://www.rxlist.com/midazolam-hydrochloride-syrup-drug.htm>
- Raschetti, R., Morgutti, M., Menniti-Ippolito, F., Belisari, A., Rossignoli, A., Longhini, P., & La Guidara, C. (1999). Suspected adverse drug events requiring emergency department visits or hospital admissions. *Eur J Clin Pharm*, **54**(12), 959–963.
- Ray, S. Pramanik, J. Bhattacharyya, M. & Todi, S. (2010). Prospective observational evaluation of incidences and implications of drug-drug interactions induced adverse drug reactions in critically III patients. *Indian J Pharm Sci*, **72**(6), 787-792.
- Riley, R. J., & Howbrook, D. (1998). In vitro analysis of the activity of the major human hepatic CYP enzyme (CYP3A4) using [N-Methyl-¹⁴C]-erythromycin. *J Pharm and Toxicol Methods*, **38**(97), 189–193.
- Ripa, S., Ferrante, L., & Prenna, M. (1993). Pharmacokinetics of fluconazole in normal volunteers. *Chemotherapy*, **39**(1), 6–12.
- Rivory, L. P., Slaviero, K. a, Hoskins, J. M., & Clarke, S. J. (2001). The erythromycin breath test for the prediction of drug clearance. *Clin Pharmacokinet*, **40**(3), 151–158.
- Rowland Yeo, K., Walsky, R. L., Jamei, M., Rostami-Hodjegan, A., & Tucker, G. T. (2011). Prediction of time-dependent CYP3A4 drug-drug interactions by physiologically based pharmacokinetic modelling: Impact of inactivation parameters and enzyme turnover. *Eur J Pharma Sci*, **43**(3), 160–173.

- Rowland, M., & Tozer, T. N. (2011). *Clin Pharmacokinetics and Pharmacodynamics* (4th ed.). Wolters Kluwer Health/Lippincott Williams & Wilkins.
- Saari, T. I., Laine, K., Leino, K., Valtonen, M., Neuvonen, P. J., & Olkkola, K. T. (2006). Effect of voriconazole on the pharmacokinetics and pharmacodynamics of intravenous and oral midazolam. *Clin Pharmacol Ther*, **79**(4), 362–70.
- Salerno, C., Carlucci, A. M., & Bregni, C. (2010). Study of in vitro drug release and percutaneous absorption of fluconazole from topical dosage forms. *AAPS Pharm Sci Tech*, **11**(2), 986–93.
- Schuetz, E. G., Furuya, K. N., & Schuetz, J. D. (1995). Interindividual variation in expression of P-glycoprotein in normal human liver and secondary hepatic neoplasms. *J Pharma Exp Ther*, **275**(2), 1011–1018.
- Schuetz, E. G., Yasuda, K., Arimori, K., & Schuetz, J. D. (1998). Human MDR1 and mouse mdr1a P-glycoprotein alter the cellular retention and disposition of erythromycin, but not of retinoic acid or benzo(a)pyrene. *Arch Biochem Biophys*, **350**(2), 340–347.
- Seldane (Rxlist). Retrieved from <http://www.rxlist.com/seldane-drug.htm>
- Shirasaka, Y., Chang, S., Grubb, M. F., Peng, C., Thummel, K. E., Isoherranen, N., & Rodrigues, A. D. (2013). Effect of CYP3A5 expression on the inhibition of CYP3A-catalyzed drug metabolism : impact on modeling CYP3A-mediated drug- drug interactions. *Drug Metab Dispos*, **41**, 1566–1574.
- Sobue, S., Tan, K., Shaw, L., Layton, G., & Hust, R. (2004). Comparison of the pharmacokinetics of fosfluconazole and fluconazole after single intravenous administration of fosfluconazole in healthy Japanese and Caucasian volunteers. *Eur J Clin Pharmacol*, **60**(4), 247–53.
- Somogyi, Andrew A.; Bochner, Felix; Hetzel, David; Williams, D. B. (1995). Evaluation of the intestinal absorption of erythromycin in man: absolute bioavailability and comparison with enteric coated erythromycin. *Pharm Res*, **12**(1), 149–154.
- Suarez, A. F., Aires, B., & Ellis, R. Erythromycin Report. Ministry of Health, Labour and Welfare
- Sultana, J., Cutroneo, P & Trifiro, G. (2013). Clinical and economic burden of adverse drug reactions. *J Pharmacol Pharmacother*. **4**(Suppl1), S73-S77.
- Sun, H., Frassetto, L.A., Huang, Y., & Benet, L. Z. (2010). Hepatic clearance, but not gut availability, of erythromycin is altered in patients with end-stage renal disease. *Clin Pharmacol Ther*, **87**(4), 465–472.
- Tatsunami, S., Yago, N., & Hosoe, M. (1981). Kinetics of suicide substrates. Steady-state treatments and computer-aided exact solutions. *Biochim Biophys Acta*, **662**, 226–35.

- Thummel, K. E., O'Shea, D., Paine, M. F., Shen, D. D., Kunze, K. L., Perkins, J. D., & Wilkinson, G. R. (1996). Oral first-pass elimination of midazolam involves both gastrointestinal and hepatic CYP3A-mediated metabolism. *Clin Pharmacol Ther*, **59**(5), 491–502.
- Tolle-Sander, S., Rautio, J., Wring, S., Polli, J. W., & Polli, J. E. (2003). Midazolam exhibits characteristics of a highly permeable P-glycoprotein substrate. *Pharm Res*, **20**(5), 757–64.
- Triggs, E. J., & Ashley, J. J. (1978). Oral administration of erythromycin stearate: effect of dosage form on plasma levels. *Med J Aust*, **2**, 121–123.
- Tsunoda, S. M., Velez, R. L., von Moltke, L. L., & Greenblatt, D. J. (1999). Differentiation of intestinal and hepatic cytochrome P450 3A activity with use of midazolam as an in vivo probe: effect of ketoconazole. *Clin Pharmacol Ther*, **66**(5), 461–71.
- Vieira, M. L. T., Zhao, P., Berglund, E. G., Reynolds, K. S., Zhang, L., Lesko, L. J., & Huang, S.-M. (2012). Predicting drug interaction potential with a physiologically based pharmacokinetic model: a case study of telithromycin, a time-dependent CYP3A inhibitor. *Clin Pharmacol Ther*, **91**(4), 700–8.
- von Moltke, L. L., Greenblatt, D. J., Schmider, J., Duan, S. X., Wright, C. E., Harmatz, J. S., & Shader, R. I. (1996). Midazolam hydroxylation by human liver microsomes in vitro: inhibition by fluoxetine, norfluoxetine, and by azole antifungal agents. *J Clin Pharmacol*, **36**(9), 783–91.
- Wagner, C., Ping, Z., Pan, Y., Hsu, V., Grillo, J., et al. (2015) Application of Physiologically Based Pharmacokinetic (PBPK) Modeling to Support Dose Selection: Report of an FDA Public Workshop on PBPK. *CPT Pharmacometrics Syst Pharmacol*, **4**, 226-230.
- Wandel, C., Witte, J. S., Hall, J. M., Stein, C. M., Wood, A. J., & Wilkinson, G. R. (2000). CYP3A activity in African American and European American men: population differences and functional effect of the CYP3A4*1B5'-promoter region polymorphism. *Clin Pharmacol Ther*, **68**(1), 82–91.
- Wang, Y. H. (2010). Confidence assessment of the Simcyp time-based approach and a static mathematical model in predicting clinical drug-drug interactions for mechanism-based CYP3A inhibitors. *Drug Metabo Dispos*, **38**(7), 1094–1104.
- Washton, H. (1989). Review of fluconazole: a new triazole antifungal agent. *Diagn Microbiol Infect Dis*, **12**(4 Suppl), 229S–233S.
- Watkins, P. (1997). The barrier function of CYP3A4 and P-glycoprotein in the small bowel. *Adv Drug Deliv Rev*, **27**(2-3), 161–170.
- Williams, J. A., Ring, B. J., Cantrell, V. E., Jones, D. R., Wrighton, S. A., et al. (2002). Comparative metabolic capabilities of CYP3A4, CYP3A5, and CYP3A7. *Drug Metab Dispos*, **30**(8), 883–891.

- Won C. S., Oberlies N. H. & Paine M. F. (2013). Influence of dietary substances on intestinal drug metabolism and transport. *Curr Drug Metab*, **11**(9), 778–92.
- World Health Organization. (2005). Proposal to waive in vivo bioequivalence requirements for the WHO model list of essential medicines immediate release, solid oral dose forms, 1–45.
- Wu, C.Y., & Benet, L. Z. (2005). Predicting drug disposition via application of BCS: transport/absorption/ elimination interplay and development of a biopharmaceutics drug disposition classification system. *Pharm Res*, **22**(1), 11–23.
- Xu, L., Chen, Y., Pan, Y., Skiles, G. L., & Shou, M. (2009). Prediction of human drug-drug interactions from time-dependent inactivation of CYP3A4 in primary hepatocytes using a population-based simulator. *Drug Metab Dispos*, **37**(12), 2330–2339.
- Yakatan, G. J., Rasmussen, C. E., Feis, P. J., & Wallen, S. (1985). Bioinequivalence of erythromycin ethylsuccinate and enteric-coated erythromycin pellets following multiple oral doses. *J Clin Pharmacol*, **25**(1), 36–42.
- Yamano, K., Yamamoto, K., Katashima, M., Kotaki, H., Iga, T., et al. (2001). Prediction of midazolam-CYP3A inhibitors interaction in the human liver from in vivo/in vitro absorption, distribution, and metabolism data. *Drug Metab Dispos*, **29**(4 Pt 1), 443–452.
- Yang, J., Atkins, W. M., Isoherranen, N., Paine, M. F., & Thummel, K. E. (2012). Evidence of CYP3A allosterism in vivo: analysis of interaction between fluconazole and midazolam. *Clin Pharmacol Ther*, **91**(3), 442–9.
- Yang, J., Jamei, M., Yeo, K. R., Tucker, G. T., & Rostami-Hodjegan, A. (2005). Kinetic values for mechanism-based enzyme inhibition: Assessing the bias introduced by the conventional experimental protocol. *Eur J Pharm Sci*, **26**(3-4), 334–340.
- Yang, J., Jamei, M., Yeo, K. R., Tucker, G. T., & Rostami-Hodjegan, A. (2007). Prediction of intestinal first-pass drug metabolism. *Curr Drug Metab*, **8**(7), 676–84.
- Yang, J., Liao, M., Shou, M., Jamei, M., Yeo, K. R., Tucker, G. T., & Rostami-Hodjegan, A. (2008). Cytochrome p450 turnover: regulation of synthesis and degradation, methods for determining rates, and implications for the prediction of drug interactions. *Curr Drug Metab*, **9**(5), 384–394.
- Yates, P., Eng, H., Di, L., & Obach, R. S. (2012). Statistical Methods for Analysis of time-dependent inhibition of cytochrome P450 enzymes ABSTRACT: *Pharmacology*, **40**(12), 2289–2296.
- Yeates, R. A., Zimmermann, T., Laufen, H., Albrecht, M., & Wildfeuer, A. (1995). Comparative pharmacokinetics of fluconazole and of itraconazole in Japanese and in German subjects. *Inter J Clin Pharmacol Ther*, **33**(3), 131–5.
- Yee, S. (1997). In vitro permeability across caco-2 cells (colonic) can predict in vivo (small intestinal) absorption in man-fact or myth. *Pharm Res*, **14**(6), 763–6.

- Yu, K., Cho, J., Jang, I., Hong, K., Chung, J., Shin, S., et al. (2004). Pharmacogenetics and genomics effect of the CYP3A5 genotype on the pharmacokinetics of intravenous midazolam during inhibited and induced metabolic states. *Clin Pharmacol Ther*, **76**(2), 104–112.
- Zhang, X. (2007). Prediction of mechanism-based inhibition of CYP3A by single and multiple inhibitors. *Ph.D Dissertation*, Purdue University
- Zhang, X., Galinsky, R. E., Kimura, R. E., Quinney, S. K., Jones, D. R., & Hall, S. D. (2010). Inhibition of CYP3A by erythromycin : in vitro-in vivo correlation in rats. *Drug Metab Dispos*, **38**(1), 61-72.
- Zhang, X., Jones, D. R., & Hall, S. D. (2009). Prediction of the effect of erythromycin, diltiazem, and their metabolites, alone and in combination, on CYP3A4 inhibition. *Drug Metab Dispos*, **37**(1), 150–160.
- Zhang, X., Quinney, S. K., Gorski, J. C., Jones, D. R., & Hall, S. D. (2009). Semiphysiologically based pharmacokinetic models for the inhibition of midazolam clearance by diltiazem and its major metabolite. *Drug Metab Dispos*, **37**(8), 1587–97.
- Zhao, P., Kunze, K. L., & Lee, C. A. (2005). Evaluation of time-dependent inactivation of CYP3A in cryopreserved human hepatocytes. *Drug Metab Dispos*, **33**(6), 853–861.
- Zhao, P., Zhang, L., Grillo, J. a, Liu, Q., Huang, S.-M. et al. (2011). Applications of physiologically based pharmacokinetic (PBPK) modeling and simulation during regulatory review. *Clin Pharmacol Ther*, **89**(2), 259–67.
- Zimmermann, T., Yeates, R. a, Laufen, H., Pfaff, G., & Wildfeuer, A. (1994). Influence of concomitant food intake on the oral absorption of two triazole antifungal agents, itraconazole and fluconazole. *Eur J Clin Pharmacol*, **46**(2), 147–50.
- Zimmermann, T., Yeates, R. A., Laufen, H., Scharpf, F., Leitold, M., & Wilderfeuer, A. (1996). Influence of the antibiotics erythromycin and azithromycin on the pharmacokinetics and pharmacodynamics of midazolam. *Drug Res.*, **46**(1), 213–17.

APPENDICES

A. MDZ META-ANALYSIS

A.1 Summary of MDZ meta-analysis after IV administration in absence of CYP3A1

Study ID	MDZ Dosing regimen		MDZ exposure metrics		MDZ secondary PK parameters							
	MDZ Route	Dose [mg/kg]	AUC _{IV} ^{MDZ} [µg/L*hrs]	SD of AUC _{IV} ^{MDZ} [µg/L*hrs]	CL _{tot,p} ^{MDZ} [ml/min/kg]	CL _{tot,b} ^{MDZ} [ml/min/kg]	F _{oral} ^{MDZ} [%]	Q _{hep} [ml/min/kg]	ER _{hep} [%]	ER _{presys} [%]	ER _{GI} [%]	CL _{int,hep} ^{MDZ} [mg/min/kg]
1	IV	0.025	73.8	31.7	5.6	6.6	26%	21.4	31%	74%	63%	9.5
8	IV	0.050	216.3	58.5	3.9	4.5	32%	21.4	21%	68%	60%	5.7
11	IV	0.005	11.6	3.5	7.7	8.9	59%	21.4	42%	41%	-1%	15.3
11	IV	0.005	12.1	3.5	7.3	8.5	53%	21.4	40%	47%	12%	14.2
16	IV	0.050	119.0	43.0	7.0	8.1	42%	21.4	38%	58%	33%	13.1
17	IV	0.029	63.4	18.7	7.5	8.7	31%	21.4	41%	69%	48%	14.8
18	IV	0.050	109.2	52.5	6.6	6.6 ¹	34%	21.4	26%	66%	54%	8.8
20	IV	0.013	36.2	10.4	5.9	5.9 ¹	31%	21.4	28%	69%	57%	8.2
21	IV	0.014	29.2	7.2	8.2	9.5	26%	21.4	45%	76%	56%	17.2
22	IV	0.014	28.4	4.0	7.9	7.9 ¹	25%	21.4	37%	75%	61%	12.6
23	IV	0.007	23.4	13.0	4.7	4.7 ¹	29%	21.4	22%	71%	62%	6.1
25	IV	0.050	151.0	40.0	5.5	6.4	32%	21.4	30%	68%	54%	9.2
26	IV	0.050	95.8		8.7	10.1	38%	21.4	47%	62%	37%	19.2
28	IV	0.050	106.8		7.8	9.1	28%	21.4	42%	72%	52%	15.7
30	IV	0.071	199.0	16.0	6.0	7.0	24%	21.4	33%	76%	65%	10.3
201	IV	0.100	219.9		7.6	8.8	24%	21.4	41%	76%	59%	12.2
202	IV	0.013	45.6		4.9	4.9 ^a	26%	21.4	23%	74%	66%	6.3
203	IV	0.030	80.7	5.9	6.2	7.2	27%	21.4	34%	73%	59%	8.7
204	IV	0.029	125.8	83.7-268.7	3.8	4.4	22%	21.4	21%	78%	73%	4.6
158 ²	IV	0.013	52.1	11.4	4.2	4.9		21.4	23%			5.2
		0.013	48.9	10.1								
		0.013	48.0	12.9								

¹ AUC were estimated using blood concentrations, thus CL_{tot,b} was calculated.

² AUC of IV MDZ in CYP3A*1*1, CYP3A5*1*X and CYP3A5*X*X populations were provided, and an average AUC among three populations was calculated to generate secondary PK parameters.

Study ID	1'-OH-MDZ										4-OH-MDZ			
	c_{max}^{met}	SD of c_{max}^{met}	t_{max}^{met}	Range of t_{max}^{met}	AUC_{IV}^{met}	SD of AUC_{IV}^{met}	MR_{IV}	SD of MR_{IV}	$CL_{tot,p}^{met}/f^{met}$	F_{oral}^{met}	AUC	SD of AUC	MR_{IV}	SD of MR_{IV}
	[ng/ml]	[ng/ml]	[h]	[h]	[μ g/L*hrs]	[μ g/L*hrs]			[ml/min/kg]	[%]	[ml/min/kg]	[%]		[ml/min/kg]
1														
8														
11														
11														
16	3.7	1.2	0.5	0.25-1.5	22.61	8.3	0.18	0.07	36.9	0.92				
17														
18														
20														
21														
22														
23														
25	3.8	0.9	0.8	0.25-1.5	16.1	3.2	0.10	0.04	51.8	0.81				
26														
28														
30	6.9	0.7	0.5	0.17	24.5	3.8	0.12	0.01	48.6	0.78				
201					27.8		0.12		59.9	0.65				
202					5.8	1.8	0.12	0.04	38.3	0.77				
203	2.8	0.4			9.4	1.8	0.11	0.02	52.7	1.00				
204	3.5	1.7-6.5	2.2	1.8-4.2	14.7	8.9-21.6	0.11	0.05	32.4	1.03	1.90	1.5-2.5	0.015	0.003
158				CYP3A5 *1*1	4.6	1.1	0.08	0.02	47.5		0.75	0.21	0.010	0.004
				CYP3A5 *1*X	8.7	1.6	0.17	0.06	25.1		1.03	0.27	0.020	0.005
				CYP3A5 *X*X	8.1	3.0	0.15	0.05	27.0		1.30	0.44	0.027	0.006

Study ID	Study Design			Demographics				
	Sample size	Cross-over (Yes=1, No=0)	Infusion time [h]	Age [yrs]	Weight (M: Male; F: Female) [kg]	Gender M/F	Race	Contraceptive (Yes=1, No=0)
1	8	1	0.50			8/0		
8	3	1	0.50	20-40		2/1		
11	12	1	0.50	42.8	80.6	11/1	White	0
11								
16	12	1	0.03	25.5	69	6/6		1
17	9	0		26	77.5 for M, 59.7 for F	6/3	White	0
18	16	1	0.50	20-40	78 for M, 65 for F	8/8	M: 6 White+2 Hispanic; F: 6 White+1 Black+ 1 Asian	1
20	16	1		33	78	5/11	14 White+1 Asian+1 African American	1
21	12	1		24	70	6/6		0
22	10	1		27	74	5/5		0
23	24	1	0.03					
25	10	1	0.03	23-29	65-100	10/0		
26	12	1	0.03	19-25	57-85	7/5		1
28	6	0	0.03	20-22	56-70	2/4		1
30	8	1		25	70	8/0		
201	8	1	0.25	22	69	4/4		
202	20	1		31.5	83 for M; 70 for F	10/10		
203	20	1	0.5	21-34	67	10/10		
204	8	1		21-46	70	8/0		
158	19	1		24	76	6/13	African American	

Study ID	Sample analysis			Comments
	Sample time points [h]	Assay method	LLOQ ng/ml	
1	0, 0.25, 0.5, 0.75, 1, 1.5, 2, 3, 4, 6, 8, 10, 12, 24	GC-MS		Sample size is small. IV 16h below LLOQ, large AUC variability
8	0.5, 0.75, 1, 1.5, 2, 4, 8, 12	LC-MS	0.25	
11	0, 0.5, 1, 2, 3, 4, 8, 12, 24	LC-MS	0.1	
11				IV 5h under LLOQ, 1'-OH-MDZ above LLOQ
16	0, 0.25, 0.5, 1, 1.5, 2, 3, 4, 5, 6, 7, 8, 10, 12, 18	HPLC	2	
17	0, 0.25, 0.5, 0.75, 1, 1.5, 2, 2.5, 3, 4, 5, 6, 8	HPLC		
18	0.083, 0.25, 0.5, 0.75, 1, 1.5, 2, 2.5, 3, 4, 5, 6, 8, 10, 12, 24	GC-MS	0.25	
20	Many	UPLC-MS	0.1	
21	0, 0.25, 0.5, 0.75, 1, 1.5, 2, 3, 4, 5, 6, 7, 8	LC-MS	0.1	
22	0.25, 0.5, 0.75, 1, 1.5, 2, 2.5, 3, 4, 5, 6, 7, 8, 9	LC-MS	0.125	MDZ given together with Alfitanil
23	0, 0.167, 0.24, 0.33, 0.5, 0.75, 1, 2, 4, 6, 8, 10, 12, 24	LC-MS	0.1	No information of volunteer, MDZ given together with digoxin
25	0, 0.25, 0.5, 1, 1.5, 2, 3, 4, 6, 8, 12, 24	HPLC	2	1ng/ml for 1'-OH-MDZ, not known if under LLOQ
26	0, 0.25, 0.5, 1, 1.5, 2, 3, 4, 5, 6, 7, 17	GC	0.1	
28	0, 0.25, 0.5, 0.75, 1, 2, 3, 4, 5, 6, 7, 8, 18	GC		CL is provided instead of AUC
30	0, 0.083, 0.167, 0.333, 0.667, 1, 1.5, 2, 2.5, 3.5, 5, 7, 9, 24	HPLC	1	CL is provided instead of AUC
201	0, 0.085, 0.167, 0.25, 0.583, 0.75, 1, 1.5, 2, 2.5, 3, 4, 5, 6, 8	GLC	1	All above LLOQ
202	0, 0.083, 0.25, 0.5, 1, 2, 3, 4, 5, 6	GC-MS	0.3	
203	0.25, 0.5, 0.67, 0.83, 1, 1.25, 1.5, 2, 3, 4, 6, 8	LC-MS	0.5	Contraceptive included. Given together with sugar cream, AUC _{0-8h}
204	0, 0.083, 0.167, 0.33, 0.5, 0.67, 1.5, 2, 4, 6, 8, 10, 12	LC-MS	0.05	Nonsmoker
158	0, 0.083, 0.167, 0.25, 0.75, 1, 2, 3, 4, 6, 8, 10, 12	GC-MS	0.1	

A.2 Summary of MDZ meta-analysis after PO administration in absence of inhibitors

Study ID	MDZ dosing regimen		MDZ exposure metrics				MDZ secondary PK parameters		1'-OH-MDZ							
	MDZ Route	Dose [mg/kg]	AUC _{PO} ^{MDZ} [µg/L*hrs]	SD of AUC _{PO} ^{MDZ} [µg/L*hrs]	c _{max} ^{MDZ} [ng/ml]	SD of c _{max} ^{MDZ} [ng/ml]	CL _{tot,p} ^{MDZ} /F _{oral} ^{MDZ} [mg/min/kg]	CL _{tot,b} ^{MDZ} /F _{oral} ^{MDZ} [mg/min/kg]	c _{max} ^{met} [ng/ml]	SD of c _{max} ^{met} [ng/ml]	t _{max} ^{met} [h]	Range of t _{max} ^{met} [h]	AUC _{PO} ^{met} [µg/L*hrs]	SD of AUC _{PO} ^{met} [µg/L*hrs]	MR _{PO}	SD of MR _{PO}
1	PO	0.075	57.1	22.3	20.8	5.8	21.9	25.5								
8	PO	0.050	69.0	15.7	15.8	2.8	12.1	14.0								
11	PO	0.025	31.9	12.4	7.0	2.2	13.1	15.2								
11	PO	0.025	30.1	11.7	6.6	1.7	13.8	16.1								
16	PO	0.109	108.0	59.3	26.9	8.6	16.8	19.5	8.7	1.9	1.5	1-3	45.4	15.1	0.4	0.1
17	PO	0.086	58.2	31.1	19.1	8.1	24.5	28.5								
18	PO	0.056	41.3	18.1	8.8		19.4	19.4								
20	PO	0.026	22.7	9.4			18.8	18.8								
21	PO	0.043	21.3	10.3	8.8	4.5	33.5	39.0								
22	PO	0.041	20.9	4.2	9.1	2.4	32.3	32.3								
23	PO	0.027	27.4	8.0	7.7	2.1	16.2	16.2	3.1	1.6	10.2	4.6	10.2	4.6	0.4	0.2
25	PO	0.094	91.0	30.0	24.1	7.2	17.2	20.0	8.2	2.7	1	0.5-2.0	24.4	5.7	0.3	0.1
26	PO	0.107	78.0	24.0	28.0	9.0	22.9	26.6								
28	PO	0.244	200.0	16.7	70.0	9.0	20.3	23.6								
30	PO	0.214	143.0	26.0			25.0	29.0	29.6	5.2	0.6	0.2	57.2	9.6	0.4	0.0
201	PO	0.109	45.3 ³		25.0	5.0	40.0	46.5	12.0	2.0	0.8	0.1	19.7		0.4	0.0
202	PO	0.027	23.9 ³				18.6	18.6					8.9	3.1	0.4	0.1
203	PO	0.060	44.3	7.5	24.6	7.6	22.5	26.4	12.2	4.9			18.8	7.0	0.4	0.2
204	PO	0.107	102.9	64-163.7	63.1	25.9-80.2	17.4		36.9	15-52.6	5.8	1.8-21.8	56.6	30.7-91.9	0.5	
103	PO	0.104	113.0	16.4	37.4	3.9	15.4	24.8	14.7	1.5			41.2	5.1	0.4	0.4

³ AUC_{PO}^{MDZ} was calculated by apparent total clearance (CL_{tot,p}^{MDZ}/F_{oral}^{MDZ}).

Study ID	1'-OH-MDZ secondary PK parameters						4-OH-MDZ exposure metrics			
	$CL_{tot}^{met}/F_{oral}^{met}$	AUC_{sys}^{met}	AUC_{presys}^{met}	AUC_{hep}^{met}	$AUC_{presys-hep}^{met}$	$AUC_{presys-GI}^{met}$	AUC_{PO}^{met}	SD of AUC_{PO}^{met}	MR_{PO}	SD of MR_{PO}
	[ml/min/kg]	[μ g/L*hrs]	[μ g/L*hrs]	[μ g/L*hrs]	[μ g/L*hrs]	[μ g/L*hrs]	[μ g/L*hrs]	[μ g/L*hrs]		
1										
8										
11										
11										
16	39.9	20.5	24.8	30.2	9.7	15.2				
17										
18										
20										
21										
22										
23	43.6									
25	64.0	9.7	14.7	13.0	3.3	11.4				
26										
28										
30	62.4	17.6	39.6	24.2	6.6	33.0				
201	92.0	7.3	12.4	11.1	3.9	8.6				
202	49.8	3.0	5.9	3.9	0.9	5.0				
203	52.8	5.2	13.7	7.2	2.0	11.6				
204	31.5	12.0	44.6	14.5	2.5	42.1	6.3	5.4-9.8	0.06	0.01
103	42.1									

Study ID	Study design						
	Sample size	Crossover (Yes=1, No=0)	Age [yrs]	Weight M: Male; F: Female [kg]	Gender M: Male; F: Female M/F	Race	Contraceptive (Yes=1, No=0)
1	12	1					
8	3	1	20-40		2/1		
11	12	1	42.8	80.6	11/1	White	0
11							
16	12	1	25.5	69	6/6		1
17	9	0	26	77.5 for M, 59.7 for F	6/3	White	0
18	16	1	20-40	78 for M, 65 for F	8/8	M: 6 White+2 Hispanic; F: 6 White+1 Black+ 1 Asian	1
20							1
21	12	1	24	70	6/6		0
22	10	1	27	74	5/5		0
23	23	1					
25	10	1	23-29	65-100	10/0		
26	12	1	19-25	57-85	7/5		1
28	12	0	18-29	50-73	3/9		1
30	8	1	25	70	8/0		
201	8	1	22	69	4/4		
202							
203	20	1	21-34	67	10/10		
204	8	1	21-46	70	10/0		
103	9	1	19-25	52-92	5/4		

Study ID	Sample Analysis		Comments
	Sample time points [h]	Assay method LLOQ [ng/ml]	
1	before, 0.25, 0.5, 0.75, 1, 1.5, 2, 3, 4, 6, 8, 10, 12, 24		Sample size is small. IV 16h below LLOQ, large AUC variability
8	0.5, 0.75, 1, 1.5, 2, 4, 8, 12, 24	LC-MS 0.25	
11	before, 0.5, 1, 2, 3, 4, 8, 12, 24	LC-MS 0.1	IV 5h under LLOQ, 1'-OH-MDZ above LLOQ
11			
16	before, 0.5, 1, 1.5, 2, 3, 4, 5, 6, 7, 8, 10, 12, 18	HPLC 2	MDZ given together with Alfitanil No information of volunteer, MDZ given together with digoxin 1ng/ml for 1'-OH-MDZ, not known if under LLOQ
17	0, 0.25, 0.5, 0.75, 1, 1.5, 2, 2.5, 3, 4, 5, 6, 8, 12, 24	HPLC	
18	0.083, 0.25, 0.5, 0.75, 1, 1.5, 2, 2.5, 3, 4, 5, 6, 8, 10, 12, 24	GC-MS 0.25	CL is provided instead of AUC CL is provided instead of AUC All above LLOQ
20			
21	0, 0.25, 0.5, 0.75, 1, 1.5, 2, 3, 4, 5, 6, 7, 8	LC-MS 0.1	Contraceptive included. Given together with sugar cream, AUC _{0-8h} Nonsmoker
22	0.25, 0.5, 0.75, 1, 1.5, 2, 2.5, 3, 4, 5, 6, 7, 8, 9	LC-MS 0.125	
23	0, 0.25, 0.5, 0.75, 1, 1.5, 2, 4, 6, 8, 10, 12, 24	LC-MS 0.1	
25	0, 0.5, 1, 1.5, 2, 3, 4, 6, 8, 12, 24	HPLC 5	
26	0, 0.5, 1, 1.5, 2, 3, 4, 5, 6, 7, 17	GC 0.1	
28	0, 0.25, 0.5, 0.75, 1, 2, 3, 4, 5, 6, 18	GC	
30	0, 0.083, 0.167, 0.333, 0.667, 1, 1.5, 2, 2.5, 3, 5, 5, 7, 9, 24	HPLC 1	
201	0, 0.085, 0.167, 0.25, 0.583, 0.75, 1, 1.5, 2, 2.5, 3, 4, 5, 6, 8	1	
202	0, 0.25, 0.5, 1, 2, 3, 4, 5, 6		
203	0, 0.16, 0.33, 0.5, 0.75, 1, 1.5, 2, 3, 4, 5, 6	LC-MS 1.61	
204	0, 0.167, 0.33, 0.5, 0.67, 1.5, 2, 3, 4, 6, 8, 10, 12	LC-MS 0.05	
103	before, 0.5, 1, 1.5, 2, 3, 4, 5, 6, 7, 17	HPLC 1	

A.3 Summary of MDZ meta-analysis after IV administration in presence of CYP3AI

Study ID	MDZ dosing regimen		Inhibitor				MDZ exposure metrics	
	MDZ Route	Dose [mg/kg]	Name	Category	Route	Dose	AUC _{PO} ^{MDZ} [µg/L*hrs]	SD of AUC _{PO} ^{MDZ} [µg/L*hrs]
1	IV	0.025	Telithromycin	ABX	PO	Day 2-7: 800mg QD	159.0	57.2
8	IV	0.050	Diltiazem	DTZ	PO	Day 1-6: 120mg BID	372.0	58.0
11	IV	0.005	Posaconazole	Azole	PO	Day 1-7: 200mg BID	51.3	22.1
		0.005	Posaconazole	Azole	PO	Day 1-7: 400mg BID	72.3	33.3
11	IV	0.005	Ketoconazole	Azole	PO	Day 1-7: 400mg BID	95.2	25.7
16	IV	0.050	Saquinavir	PI	PO	Day 1-5: 1200mg TID	296.0	133.0
17	IV	0.029	Ketoconazole	Azole	PO	Day 1-2: 200mg BID	300.0	104.0
18	IV	0.050	Clarithromycin	ABX	PO	Day 2-8: 500mg BID	300.1	102.3
20	IV	0.013	Ritonavir	PI	PO	Day 3-17: 400mg BID	120.0	23.6
	IV	0.013	Nelfinavir	PI	PO	Day 3-17: 400mg BID	66.3	22.0
21	IV	0.014	Fluconazole	Azole	PO	SD: 100mg	37.0	9.2
		0.014	Fluconazole	Azole	PO	SD: 200mg	42.5	10.1
		0.014	Fluconazole	Azole	PO	SD: 400mg	56.6	17.4
22	IV	0.014	Troleandomycin	ABX	PO	SD: 500mg	132.0	46.0
	IV	0.014	Grapefruit juice	GFJ	PO	Day 1: 8oz; Day 2:3oz (double strength)	35.5	17.4
23	IV	0.007	Telaprevir	PI	PO	Day 8-23: 750mg BID	115.0	38.4
25	IV	0.050	Voriconazole	Azole	PO	Day 1-2: 200mg BID	534.0	88.0
26	IV	0.050	Itraconazole	Azole	PO	Day 1-6: 200mg QD	308.6	
		0.050	Fluconazole	Azole	PO	Day 1: 400mg qd; Day 2-6: 200mg QD	193.8	
28	IV	0.050	Erythromycin	ABX	PO	Day 1-7: 500mg TID	231.5	
30	IV	0.071	Grapefruit juice	GFJ	PO	SD: 200ml	207.0	15.0
158	IV	0.013	Fluconazole	Azole	PO	SD: 400mg	74.0	195.5
		0.013	Fluconazole	Azole	PO	SD: 400mg	85.3	224.8
		0.13	Fluconazole	Azole	PO	SD: 400mg	100.4	186.3

ABX: antibiotics; DTZ: diltiazem; PI: proteinase inhibitor; GFJ: grape fruit juice

Study ID	MDZ secondary PK paramters							
	CL _{tot,p} ^{MDZ} [mg/min/kg]	CL _{tot,b} ^{MDZ} [mg/min/kg]	F _{oral} ^{MDZ} [%]	Q _{hep} [ml/min/kg]	ER _{hep} ^{MDZ} [%]	ER _{presys} ^{MDZ} [%]	ER _{GI} ^{MDZ} [%]	CL _{int,hep} ^{MDZ} [ml/min/kg]
1	2.6	3.0	74%	21.4	14%	26%	13%	3.6
8	2.2	2.6	74%	21.4	12%	26%	15%	3.0
11	1.6	1.9	62%	21.4	9%	38%	32%	2.1
	1.2	1.3	46%	21.4	6%	54%	50%	1.4
11	0.9	1.0	48%	21.4	5%	52%	49%	1.1
16	2.8	3.3	87%	21.4	15%	13%	-3%	3.9
17	1.6	1.8	80%	21.4	9%	20%	13%	2.0
18	2.4	2.4	86%	21.4	9%	14%	5%	2.6
20	1.8	1.8	78%	21.4	8%	22%	15%	1.9
	3.2	3.2	58%	21.4	15%	42%	31%	3.8
21	6.4	6.4	42%	21.4	30%	58%	41%	9.2
	5.6	5.6	55%	21.4	26%	45%	25%	7.6
	4.2	4.2	62%	21.4	20%	38%	23%	5.2
22	1.7	1.7	85%	21.4	8%	15%	7%	1.9
	6.3	6.3	37%	21.4	30%	63%	47%	9.0
23	1.0	1.0	80%	21.4	5%	20%	16%	1.0
25	1.6	1.8	85%	21.4	8%	15%	7%	2.0
26	2.7	3.1	87%	21.4	15%	13%	-2%	3.7
	4.3	5.0	73%	21.4	23%	27%	4%	6.5
28	3.6	4.2	78%	21.4	20%	22%	3%	5.2
30	5.8	6.7	35%	21.4	31%	65%	49%	9.7
158	3.0	3.4						

Study ID	1'-OH-MDZ										4-OH-MDZ			
	c_{max}^{met} [ng/ml]	SD of c_{max}^{met} [ng/ml]	t_{max}^{met} [h]	Range of t_{max} [h]	AUC_{IV}^{met} [µg/L*hrs]	SD of AUC_{IV}^{met} [µg/L*hrs]	MR_{IV}	SD of MR_{IV}	$CL_{tot,p}^{met}/f^{met}$ [ml/min/kg]	F_{oral}^{met} [%]	AUC_{IV}^{met} [µg/L*hrs]	SD of AUC_{IV}^{met} [µg/L*hrs]	MR_{IV}	SD of MR_{IV}
1														
8														
11														
11														
16	2.1	1.2	0.5	0.25-3	23.68	14.80	0.08	0.05	35.19	0.87				
17														
18														
20														
21														
22														
23														
25	3.1	1.2	2	1.0-3.0	27.0	13.1	0.0	0.0	30.9	1.20				
26														
28														
30	8.2	1.4	0.48	0.13	26.1	3.9	0.1	0.0	45.6	0.95				
158				CYP3A5 *1*1	5.7	0.8	0.1	0.0	38.7		1.64	0.48	0.02	0.006
				CYP3A5*1*X	10.6	3.2	0.1	0.0	20.8		2.39	0.75	0.03	0.004
				CYP3A5*X*X	10.5	3.1	0.1	0.0	20.8		3.62	0.82	0.04	0.005

Study ID	Study design			Demographics			
	Sample size	Crossover (Yes=1, No=0)	Infusion time [h]	Age [yrs]	Weight M: Male; F: Female [kg]	Gender M: Male; F: Female M/F	Race
1		1	0.50			12/0	
8	3	1	0.50	20-40		2/1	
11	12	1	0.50	42.8	80.6	11/1	White
11							
16	12	1	0.03	25.5	69	6/6	
17	9	0		26	77.5 for M, 59.7 for F	6/3	White
18	16	1	0.50	20-40	78 for M, 65 for F	8/8	M: 6 White+2 Hispanic; F: 6 White+1 Black+ 1 Asian
20							
21	12	1		24	70	6/6	
22	10	1		27	74	5/5	
23	22		0.03				
25	10	1	0.03	23-29	65-100	10/0	
26	12	1	0.03	19-25	57-85	7/5	
28	6	0	0.03	20-22	56-70		
30	8	1		25	70	8/0	
158	19	1		24	76	6/13	African American

Study ID	Sample Analysis			Comments
	Sample time points [h]	Assay method	LLOQ [ng/ml]	
1	0, 0.25, 0.5, 0.75, 1, 1.5, 2, 3, 4, 6, 8, 10, 12, 24, 34, 48	GC-MS		Sample size is small.
8	0,0.5,0.75,1,1.5,2,4,8,12	LC-MS	0.25	
11	0,0.5,1,2,3,4,8,12,24	LC-MS	0.1	
11				Long duration of Midazolam, may cause auto-induction of CYP3A. IV 12h under LLOQ
16	0,0.25,0.5,1,1.5,2,3,4,5,6,7,8,10,12,18	HPLC	2	
17	0,0.25,0.5,0.75,1,1.5,2,2.5,3,4,5,6,8	HPLC		
18	0.083, 0.25, 0.5,0.75,1,1.5,2,2.5,3,4,5,6,8,10,12,24	GC-MS	0.25	
20				
21	0,0.25,0.5,0.75,1,1.5,2,3,4,5,6,7,8	LC-MS	0.1	Inhibitor single dose
22	0.25,0.5,0.75,1,1.5,2,2.5,3,4,5,6,7,8,9,10,12	LC-MS	0.125	MDZ give together with Alfitanil
23	0,0.167,0.24,0.33,0.5,0.75,1,2,4,6,8,10,12,24	LC-MS	0.1	No information of volunteer, MDZ given together with digoxin contraceptive steroids were used; CL is provided, instead of AUC
25	0,0.25,0.5,1,1.5,2,3,4,6,8,12,24	HPLC	5	
26	0,0.5,1,1.5,2,3,4,5,6,7,17	GC	0.1	
28	0,0.25,0.5,0.75,1,2,3,4,5,6,7,8,18	GC		CL is provided, instead of AUC
30	0,0.083,0.167,0.333,0.667,1,1.5,2,2.5,3.5,5,7,9,24	HPLC	1	Single dose of inhibitor
158	0,0.083,0.167,0.25,0.75,1,2,3,4,6,8,10,12	GC-MS	0.1	

A.4 Summary of MDZ meta-analysis after PO administration in presence of CYP3A4

Study ID	MDZ dose regimen		Inhibitor				MDZ exposure metrics			
	MDZ Route	Dose [mg/kg]	Name	Category	Route	Dose	AUC _{PO} ^{MDZ} [µg/L*hrs]	SD of AUC _{PO} ^{MDZ} [µg/L*hrs]	c _{max} ^{MDZ} [ng/ml]	SD of c _{max} ^{MDZ} [ng/ml]
1	PO	0.075	Telithromycin	ABX	PO	Day 2-7: 800mg QD	354.0	145.1	54.6	15.8
8	PO	0.050	Diltiazem	DTZ	PO	Day 1-6: 120mg BID	276.7	33.3	41.3	14.0
11	PO	0.025	Posaconazole	Azole	PO	Day 1-7: 200mg BID	159.0	54.1	15.4	3.1
		0.025	Posaconazole	Azole	PO	Day 1-7: 400mg BID	168.0	42.0	16.3	3.6
11	PO	0.025	Ketoconazole	Azole	PO	Day 1-7: 400mg BID	230.0	34.5	18.1	2.0
16	PO	0.109	Saquinavir	PI	PO	Day 1-5: 1200mg TID	559.0	258.0	63.2	16.3
17	PO	0.086	Ketoconazole	Azole	PO	Day 1-2: 200mg TID	719.0	181.0	81.0	28.9
18	PO	0.056	Clarithromycin	ABX	PO	Day 2-8: 500mg BID	289.0	120.4	34.4	
20	PO	0.026	Ritonavir	PI	PO	Day 3-17: 400mg BID	188.0	33.0		
		0.026	Nelfinavir	PI	PO	Day 3-17: 400mg BID	77.4	51.5		
21	PO	0.043	Fluconazole	Azole	PO	SD: 100mg	46.1	13.0	15.6	6.1
		0.043	Fluconazole	Azole	PO	SD: 200mg	70.7	20.2	19.0	7.9
		0.043	Fluconazole	Azole	PO	SD: 400mg	105.0	30.0	24.9	8.1
22	PO	0.041	Troleandomycin	ABX	PO	SD: 500mg	338.0	95.0	35.5	14.9
	PO	0.041	Grapefruit juice	GFJ	PO	Day 1: 8oz; Day 2:3oz (double strength)	39.5	6.4	15.6	4.2
23	PO	0.027	Telaprevir	PI	PO	Day 8-23: 750mg BID	369.0	116.0	22.3	6.5
25	PO	0.094	Voriconazole	Azole	PO	Day 1-2: 200mg BID	855.0	104.0	86.6	26.2
26	PO (Day 6)	0.107	Itraconazole	Azole	PO	Day 1-6: 200mg QD	578.0	142.0	88.0	15.0
	PO (Day-6)	0.110	Fluconazole	Azole	PO	Day 1: 400mg QD; Day 2-6: 200mg QD	313.0	117.0	61.0	16.0
28	PO	0.244	Erythromycin	ABX	PO	Day 1-7: 500mg TID	883.3	116.7	189.0	16.0
30	PO	0.214	Grapefruit juice	GFJ	PO	SD: 200ml	217.0	31.0	189.0	16.0
103	PO	0.104	Fluconazole	Azole	IV	SD: 400mg	389.0	37.2	66.8	8.0
	PO	0.104	Fluconazole	Azole	PO	SD: 400mg	421.0	42.1	85.9	9.8

Study ID	1'-OH-MDZ exposure metrics							1'-OH-MDZ secondary PK parameters			
	c _{max} ^{met} [ng/ml]	SD of c _{max} ^{met} [ng/ml]	t _{max} ^{met} [h]	Range of t _{max} ^{met} [h]	AUC _{PO} ^{met} [µg/L*hrs]	SD of AUC _{PO} ^{met} [µg/L*hrs]	MR _{PO}	SD of MR _{PO}	CL _{tot,p} ^{met} /F ^{met} /F _{oral} ^{met} [ml/min/kg]	AUC _{sys} ^{met} [µg/L*hrs]	AUC _{presys} ^{met} [µg/L*hrs]
1											
8											
11											

11											
16	5.4	1.8	2	1-4	44.72	22.36	0.08	0.04	40.51	44.7	0.0
17											
18											
20											
21											
22											
23	0.42	0.18			6.2	4.5	0.0	0.0	71.5		
25	7.7	3.8	1	0.5-6.0	60.8	22.1	0.1	0.0	25.7	43.2	17.6
26											
28											
30	29.6	5.3	1.27	0.26	74.6	14.6	0.3	0.0	47.9	27.4	47.2
103	11.9	1.7			61.8	8.0	0.2	0.2	28.1		
	13.3	1.9			64.3	9.7	0.2	0.2	27.0		

Study ID	1'-OH-MDZ			Study design		Demographics			
	AUC _{hep} ^{met} [µg/L*hrs]	AUC _{presys-hep} ^{met} [µg/L*hrs]	AUC _{presys-GI} ^{met} [µg/L*hrs]	Sample size	Crossover (Yes=1, No=0)	Age [yrs]	Weight M: Male; F: Female [kg]	Gender M: Male; F: Female M/F	Race
1				3	1				
8				3	1	20-40		2/1	

11				12	1	42.8	80.6	11/1	White
11									
16	51.3	6.6	-6.6	12	1	25.5	69	6/6	
17				9	0	26	77.5 for M, 59.7 for F	6/3	White
18				16	1	20-40	78 for M, 65 for F	8/8	M: 6 White+2 Hispanic; F: 6 White+1 Black+ 1 Asian
20									
21				12	1	24	70	6/6	
22				10	1	27	74	5/5	
23				21					
25	46.6	3.3	14.2	10	1	23-29	65-100	10/0	
26				12	1	29	72	7/5	
28				12	0	18-29	50-73	3/9	
30	37.1	9.8	37.5	8	1	25	70	8/0	
103				9	1	19-25	52-92	5/4	

Sample Analysis				
Study ID	Sample time points [h]	Assay method	LLOQ [ng/ml]	Comments
1	0, 0.25, 0.5, 0.75, 1, 1.5, 2, 3, 4, 6, 8, 10, 12, 24 (day1,6)	GC-MS		
8	0,0.5,0.75,1,1.5,2,4,8,12,24	LC-MS	0.25	Sample size is small.

11	0,0.5,1,2,3,4,8,12,24	LC-MS	0.1	
11				
16	0,0.5,1,1.5,2,3,4,5,6,7,8,10,12,18	HPLC	2	
17	0,0.25,0.5,0.75,1,1.5,2,2.5,3,4,5,6,8	HPLC		
18	0.083, 0.25, 0.5,0.75,1,1.5,2,2.5,3,4,5,6,8,10,12,24	GC-MS	0.25	
20				
21	0,0.25,0.5,0.75,1,1.5,2,3,4,5,6,7,8	LC-MS	0.1	Inhibitor single dose
22	0.25,0.5,0.75,1,1.5,2,2.5,3,4,5,6,7,8,9,10,12	LC-MS	0.125	MDZ give together with Alfitanil
23	0,0.25,0.5,0.75,1,1.5,2,4,6,8,10,12,24	LC-MS	0.1	No information of volunteer, MDZ given together with digoxin
25	0,0.5,1,1.5,2,3,4,6,8,12,24	HPLC	5	
26	0,0.5,0.75,1,1.5,2,2.5,3,4,6,8	LC-MS	0.25	Cocktail administration
28	0,0.25,0.5,0.75,1,2,3,4,5,6,18	GC		CL is provided, instead of AUC
30	0,0.083,0.167,0.333,0.667,1,1.5,2,2.5,3.5,5,7,9,24	HPLC	1	Single dose of inhibitor
103	before, 0.5,1,1.5,2,3,4,5,6,7,17	HPLC	1	1 woman uses oral contraceptive

B. SENSITIVITY ANALYSIS OF FLZ

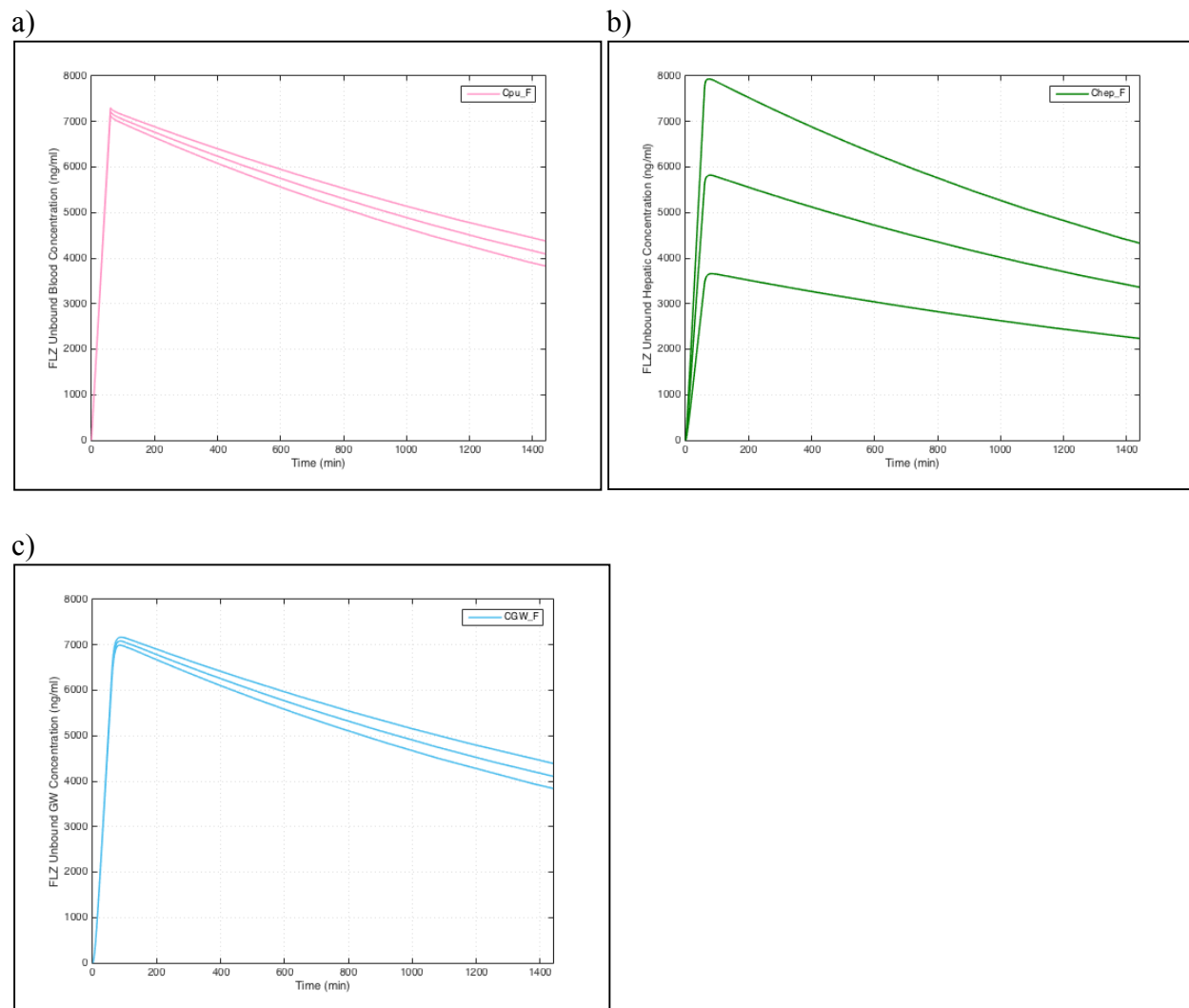


Figure B.1 Sensitivity analysis of FLZ concentrations after IV administration to the change in f_{pv} . a) FLZ unbound blood concentration – time profile (top line: $f_{pv} = 0.0$; middle line: $f_{pv} = 0.5$; bottom line: $f_{pv} = 1.0$) b) FLZ unbound hepatic concentration – time profile (top line: $f_{pv} = 1.0$; middle line: $f_{pv} = 0.5$; bottom line: $f_{pv} = 0.0$) c) FLZ unbound GW concentration – time profile (top line: $f_{pv} = 0.0$; middle line: $f_{pv} = 0.5$; bottom line: $f_{pv} = 1.0$)

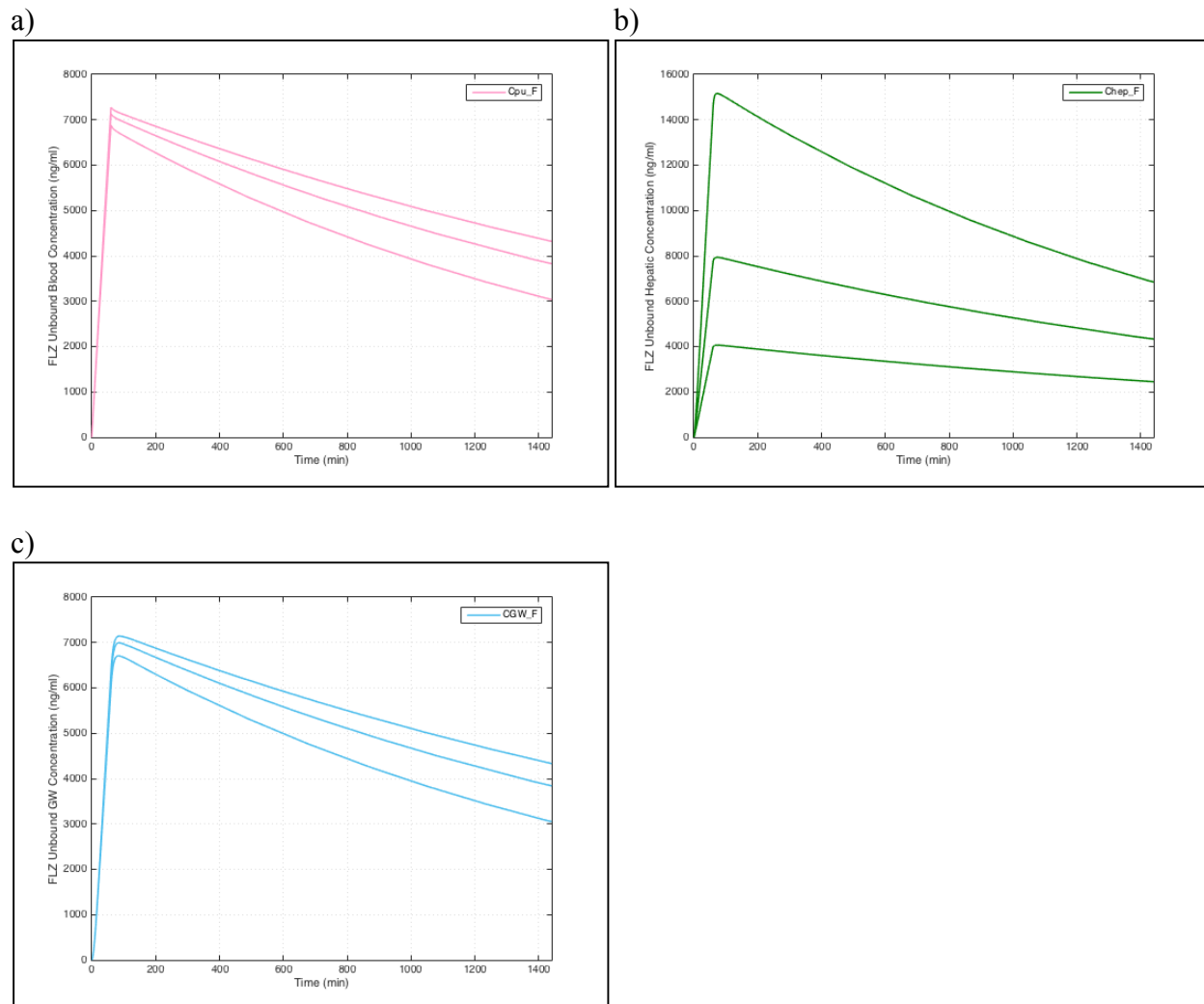


Figure B.2 Sensitivity analysis of FLZ concentrations after IV administration to the change in $K_{p,hep}^{FLZ}$. a) FLZ unbound blood concentration – time profile (top line: $K_{p,hep}^{FLZ} = 0.5$; middle line: $K_{p,hep}^{FLZ} = 1.0$; bottom line: $K_{p,hep}^{FLZ} = 2.0$) b) FLZ unbound hepatic concentration – time profile (top line: $K_{p,hep}^{FLZ} = 2.0$; middle line: $K_{p,hep}^{FLZ} = 1.0$; bottom line: $K_{p,hep}^{FLZ} = 0.5$) c) FLZ unbound GW concentration – time profile (top line: $K_{p,hep}^{FLZ} = 0.5$; middle line: $K_{p,hep}^{FLZ} = 1.0$; bottom line: $K_{p,hep}^{FLZ} = 2.0$)

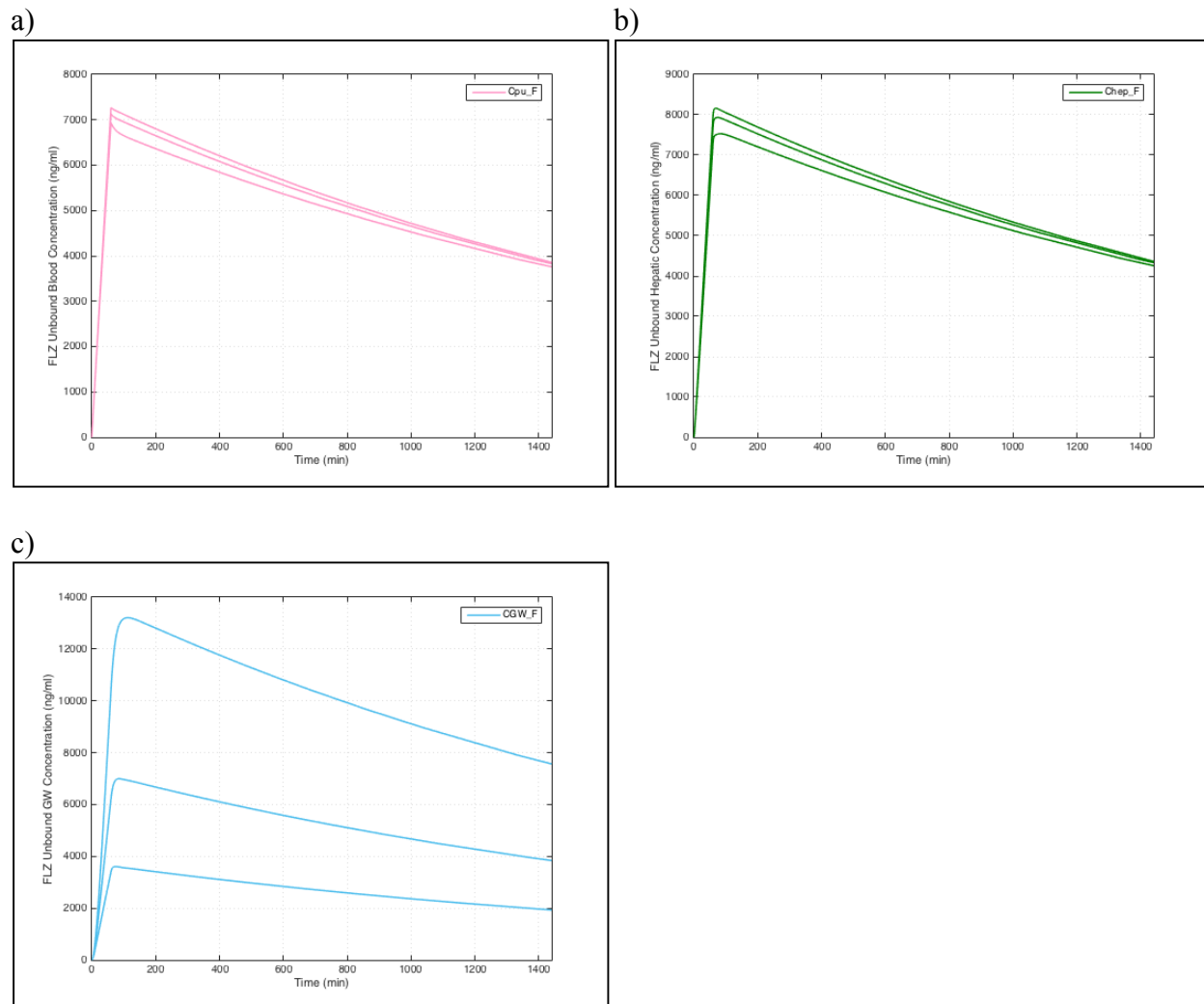


Figure B.3 Sensitivity analysis of FLZ concentrations after IV administration to the change in $K_{p,GW}^{FLZ}$. a) FLZ unbound blood concentration – time profile ($K_{p,GW}^{FLZ} = 0.5$; middle line: $K_{p,GW}^{FLZ} = 1.0$; bottom line: $K_{p,GW}^{FLZ} = 2.0$) b) FLZ unbound hepatic concentration – time profile (top line: $K_{p,GW}^{FLZ} = 0.5$; middle line: $K_{p,GW}^{FLZ} = 1.0$; bottom line: $K_{p,GW}^{FLZ} = 2.0$) c) FLZ unbound GW concentration – time profile (top line: $K_{p,GW}^{FLZ} = 2.0$; middle line: $K_{p,GW}^{FLZ} = 1.0$; bottom line: $K_{p,GW}^{FLZ} = 0.5$)

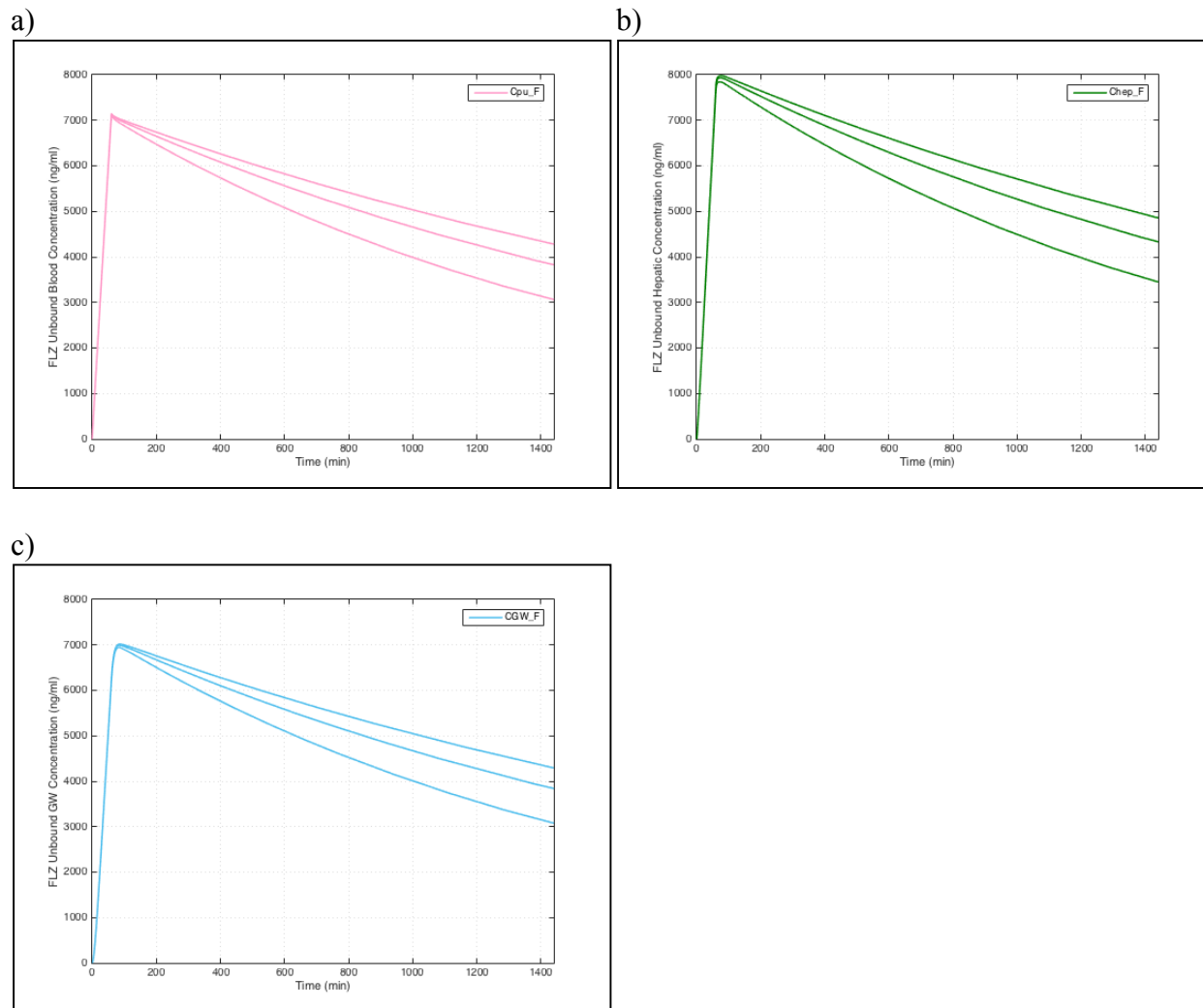


Figure B.4 Sensitivity analysis of FLZ concentrations after IV administration to the change in $CL_{int,hep}^{FLZ}$. a) FLZ unbound blood concentration – time profile (top line: $CL_{int,hep}^{FLZ} = 0.05$; middle line: $CL_{int,hep}^{FLZ} = 0.1$; bottom line: $CL_{int,hep}^{FLZ} = 0.2$) b) FLZ unbound hepatic concentration – time profile (top line: $CL_{int,hep}^{FLZ} = 0.05$; middle line: $CL_{int,hep}^{FLZ} = 0.1$; bottom line: $CL_{int,hep}^{FLZ} = 0.2$) c) FLZ unbound GW concentration – time profile (top line: $CL_{int,hep}^{FLZ} = 0.05$; middle line: $CL_{int,hep}^{FLZ} = 0.1$; bottom line: $CL_{int,hep}^{FLZ} = 0.2$)

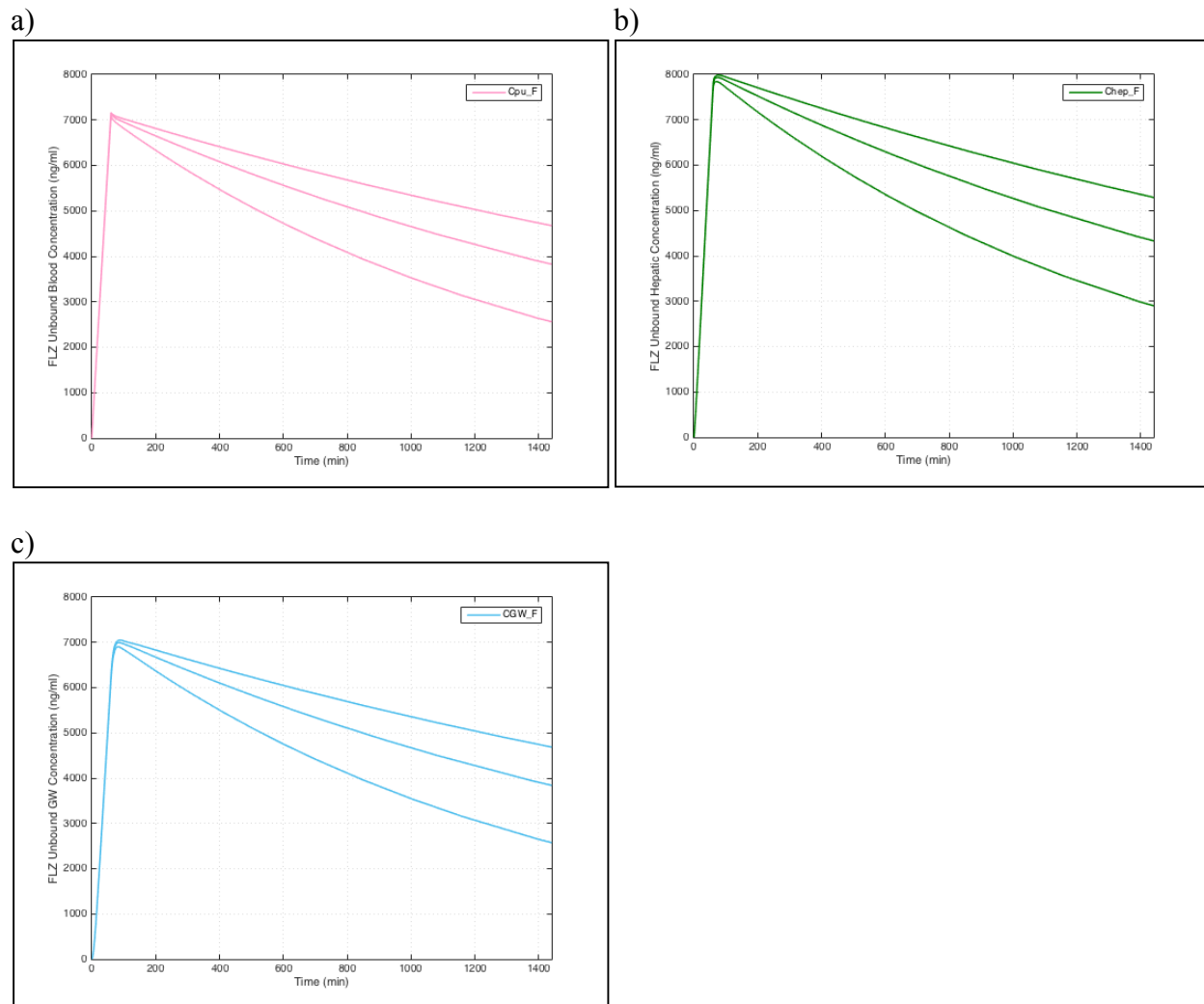


Figure B.5 Sensitivity analysis of FLZ concentrations after IV administration to the change in CL_{ren}^{FLZ} . a) FLZ unbound blood concentration – time profile (top line: $CL_{ren}^{FLZ} = 0.1$; middle line: $CL_{ren}^{FLZ} = 0.2$; bottom line: $CL_{ren}^{FLZ} = 0.4$) b) FLZ unbound hepatic concentration – time profile (top line: $CL_{ren}^{FLZ} = 0.1$; middle line: $CL_{ren}^{FLZ} = 0.2$; bottom line: $CL_{ren}^{FLZ} = 0.4$) c) FLZ unbound GW concentration – time profile (top line: $CL_{ren}^{FLZ} = 0.1$; middle line: $CL_{ren}^{FLZ} = 0.2$; bottom line: $CL_{ren}^{FLZ} = 0.4$)

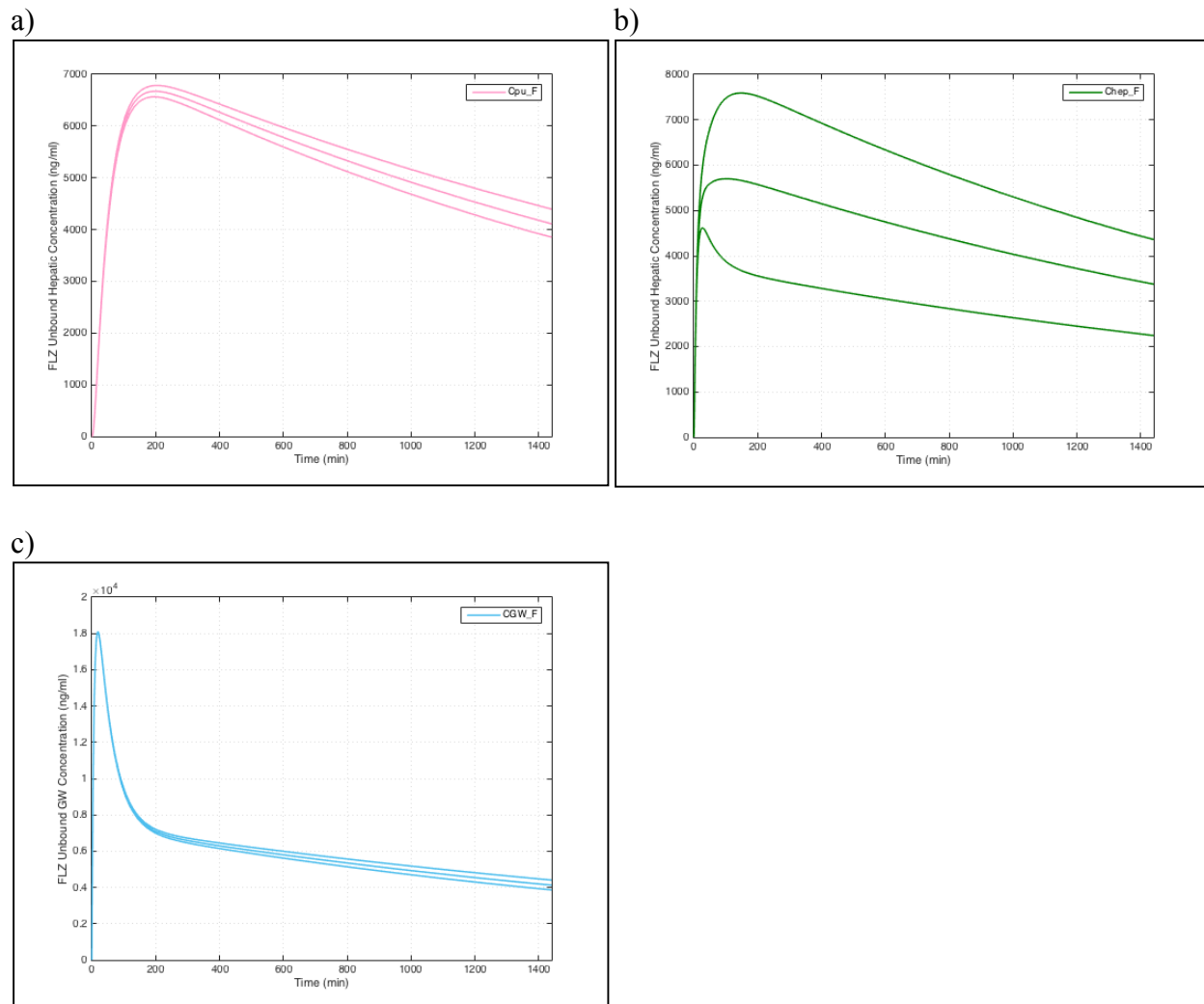


Figure B.6 Sensitivity analysis of FLZ concentrations after PO administration to the change in f_{pv} . a) FLZ unbound blood concentration – time profile (top line: $f_{pv} = 0.0$; middle line: $f_{pv} = 0.5$; bottom line: $f_{pv} = 1.0$) b) FLZ unbound hepatic concentration – time profile (top line: $f_{pv} = 1.0$; middle line: $f_{pv} = 0.5$; bottom line: $f_{pv} = 0.0$) c) FLZ unbound GW concentration – time profile (top line: $f_{pv} = 0.0$; middle line: $f_{pv} = 0.5$; bottom line: $f_{pv} = 1.0$)

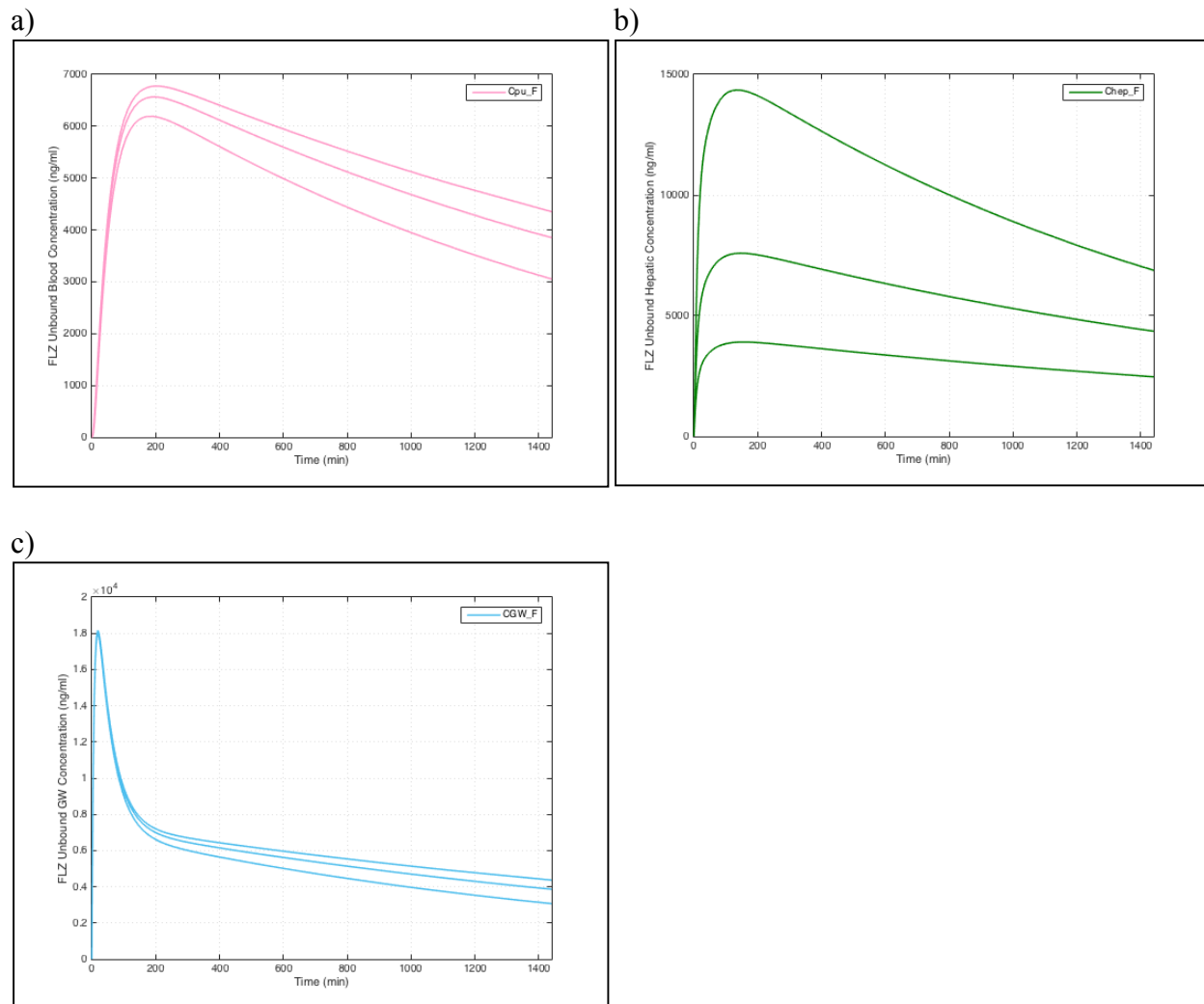


Figure B.7 Sensitivity analysis of FLZ concentrations after PO administration to the change in $K_{p,hep}^{FLZ}$. a) FLZ unbound blood concentration – time profile (top line: $K_{p,hep}^{FLZ} = 0.5$; middle line: $K_{p,hep}^{FLZ} = 1.0$; bottom line: $K_{p,hep}^{FLZ} = 2.0$) b) FLZ unbound hepatic concentration – time profile (top line: $K_{p,hep}^{FLZ} = 2.0$; middle line: $K_{p,hep}^{FLZ} = 1.0$; bottom line: $K_{p,hep}^{FLZ} = 0.5$) c) FLZ unbound GW concentration – time profile (top line: $K_{p,hep}^{FLZ} = 0.5$; middle line: $K_{p,hep}^{FLZ} = 1.0$; bottom line: $K_{p,hep}^{FLZ} = 2.0$)

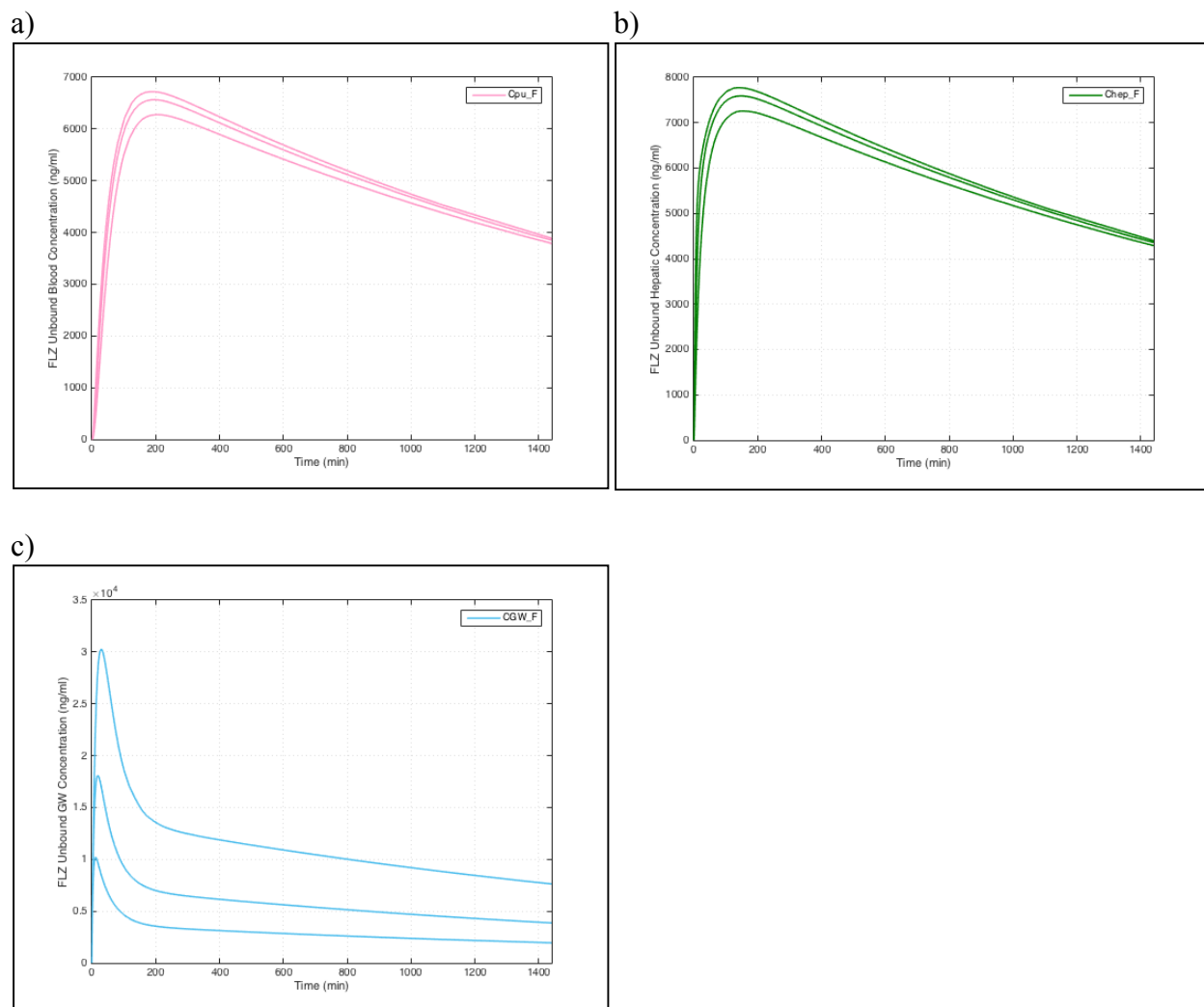


Figure B.8 Sensitivity analysis of FLZ concentrations after PO administration to the change in $K_{p,GW}^{FLZ}$. a) FLZ unbound blood concentration – time profile (top line: $K_{p,GW}^{FLZ} = 0.5$; middle line: $K_{p,GW}^{FLZ} = 1.0$; bottom line: $K_{p,GW}^{FLZ} = 2.0$) b) FLZ unbound hepatic concentration – time profile (top line: $K_{p,GW}^{FLZ} = 0.5$; middle line: $K_{p,GW}^{FLZ} = 1.0$; bottom line: $K_{p,GW}^{FLZ} = 2.0$) c) FLZ unbound GW concentration – time profile (top line: $K_{p,GW}^{FLZ} = 2.0$; middle line: $K_{p,GW}^{FLZ} = 1.0$; bottom line: $K_{p,GW}^{FLZ} = 0.5$)

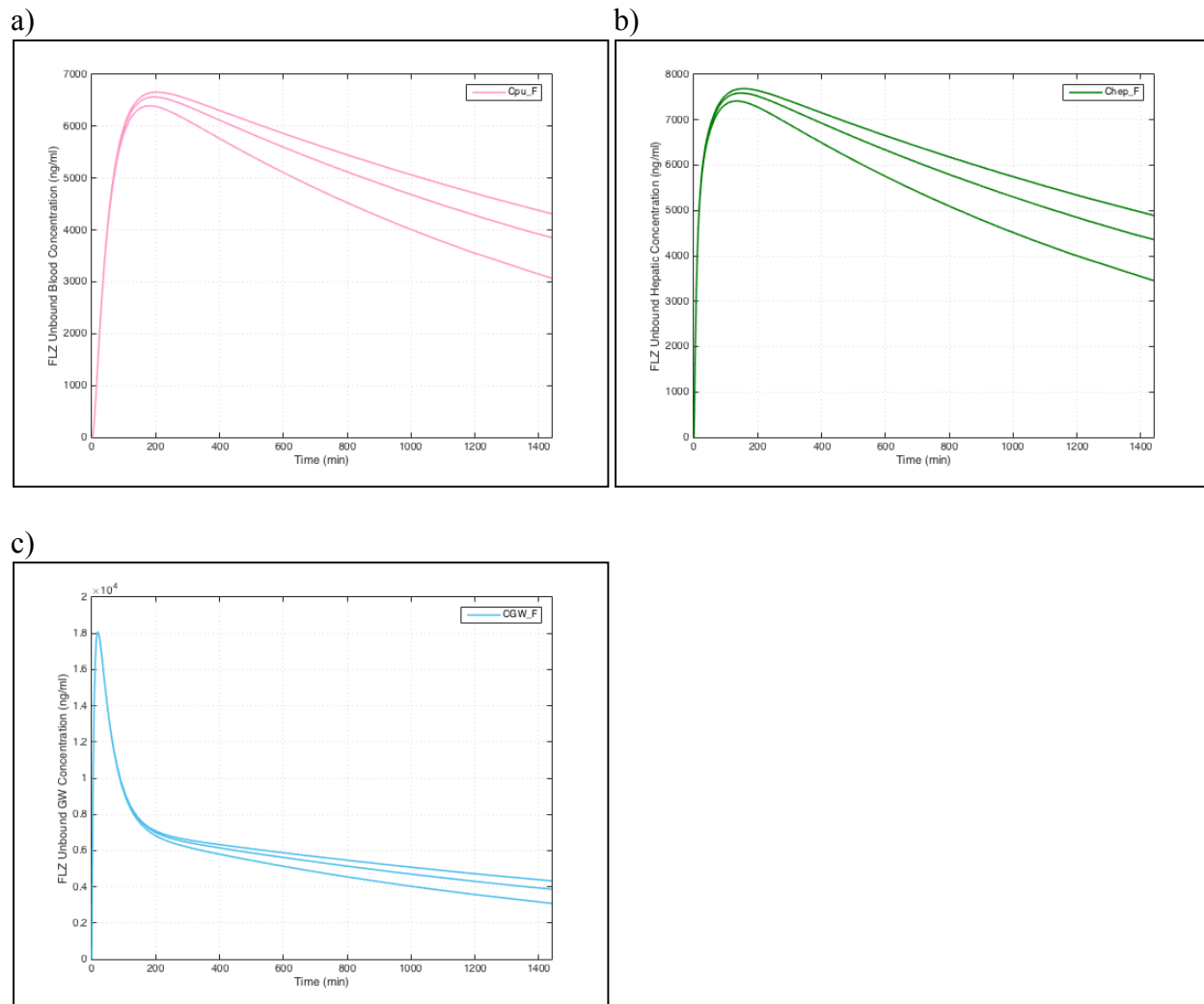


Figure B.9 Sensitivity analysis of FLZ concentrations after PO administration to the change in $CL_{int,hep}^{FLZ}$. a) FLZ unbound blood concentration – time profile (top line: $CL_{int,hep}^{FLZ} = 0.05$; middle line: $CL_{int,hep}^{FLZ} = 0.1$; bottom line: $CL_{int,hep}^{FLZ} = 0.2$) b) FLZ unbound hepatic concentration – time profile (top line: $CL_{int,hep}^{FLZ} = 0.05$; middle line: $CL_{int,hep}^{FLZ} = 0.1$; bottom line: $CL_{int,hep}^{FLZ} = 0.2$) c) FLZ unbound GW concentration – time profile (top line: $CL_{int,hep}^{FLZ} = 0.05$; middle line: $CL_{int,hep}^{FLZ} = 0.1$; bottom line: $CL_{int,hep}^{FLZ} = 0.2$)

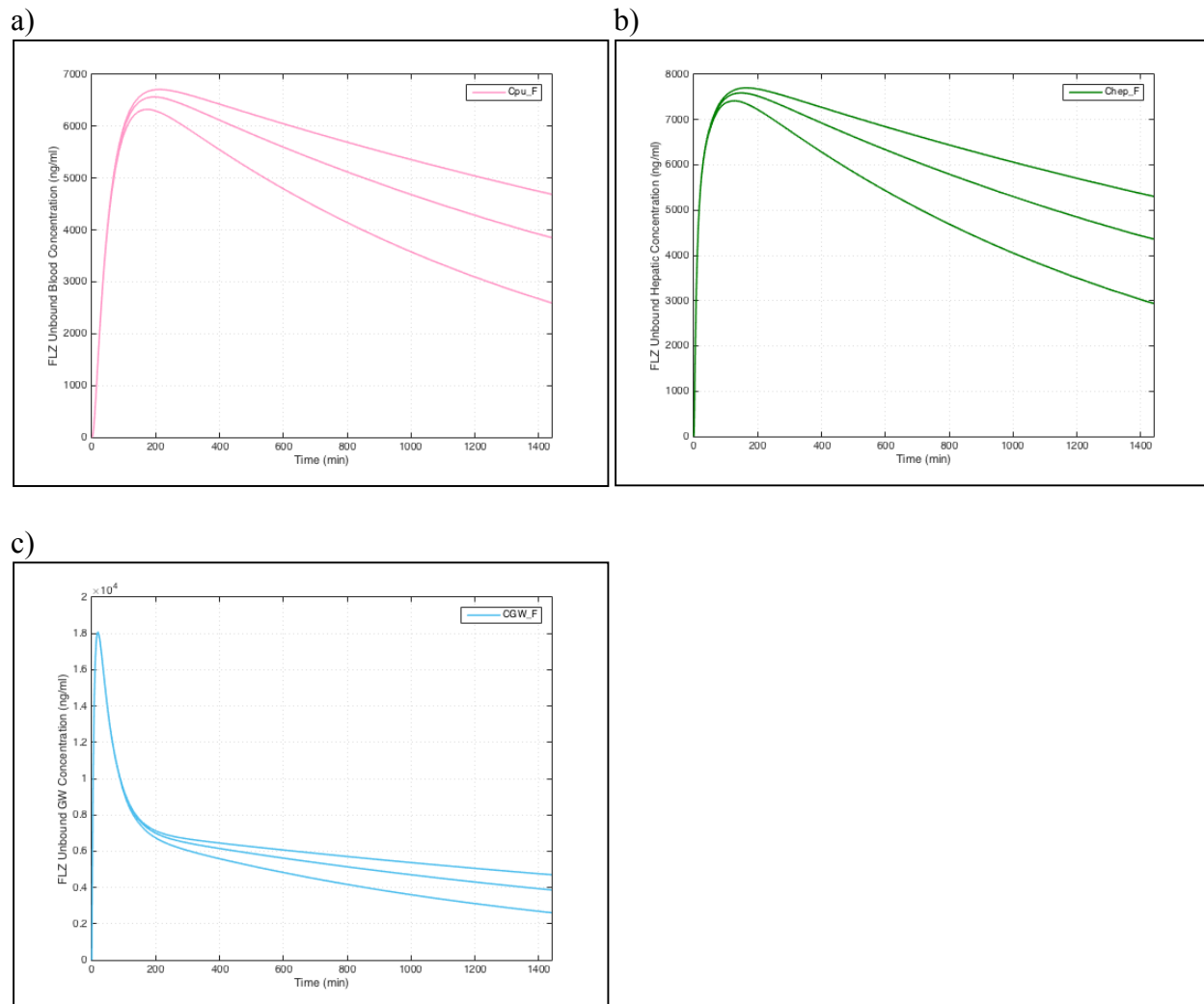


Figure B.10 Sensitivity analysis of FLZ concentrations after PO administration to the change in CL_{ren}^{FLZ} . a) FLZ unbound blood concentration – time profile (top line: $CL_{ren}^{FLZ} = 0.1$; middle line: $CL_{ren}^{FLZ} = 0.2$; bottom line: $CL_{ren}^{FLZ} = 0.4$) b) FLZ unbound hepatic concentration – time profile (top line: $CL_{ren}^{FLZ} = 0.1$; middle line: $CL_{ren}^{FLZ} = 0.2$; bottom line: $CL_{ren}^{FLZ} = 0.4$) c) FLZ unbound GW concentration – time profile (top line: $CL_{ren}^{FLZ} = 0.1$; middle line: $CL_{ren}^{FLZ} = 0.2$; bottom line: $CL_{ren}^{FLZ} = 0.4$)

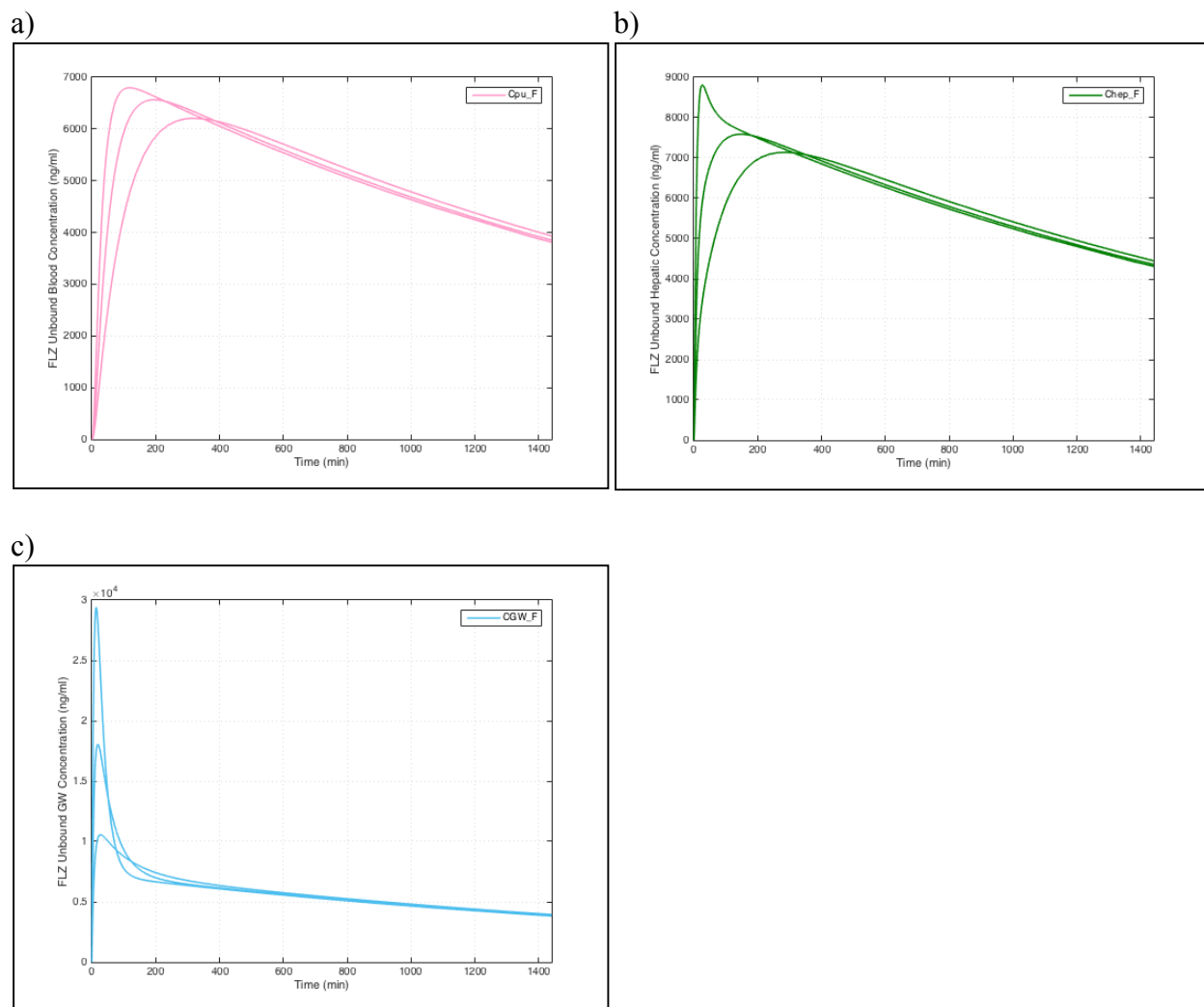


Figure B.11 Sensitivity analysis of FLZ concentrations after PO administration to the change in k_{GL}^{FLZ} . a) FLZ unbound blood concentration – time profile (line with lowest c_{max}^{FLZ} : $k_{GL}^{FLZ} = 0.0106$; line with middle c_{max}^{FLZ} : $k_{GL}^{FLZ} = 0.0213$; line with highest c_{max}^{FLZ} : $k_{GL}^{FLZ} = 0.0426$) b) FLZ unbound hepatic concentration – time profile (line with lowest c_{max}^{FLZ} : $k_{GL}^{FLZ} = 0.0106$; line with middle c_{max}^{FLZ} : $k_{GL}^{FLZ} = 0.0213$; line with highest c_{max}^{FLZ} : $k_{GL}^{FLZ} = 0.0426$) c) FLZ unbound GW concentration – time profile (line with lowest c_{max}^{FLZ} : $k_{GL}^{FLZ} = 0.0106$; line with middle c_{max}^{FLZ} : $k_{GL}^{FLZ} = 0.0213$; line with highest c_{max}^{FLZ} : $k_{GL}^{FLZ} = 0.0426$)

C. ESTIMATION OF V_B^{MDZ} , V_{P1}^{MDZ} , V_{P2}^{MDZ} , Q_2^{MDZ} AND Q_3^{MDZ}

In study 21 (Kharasch et al., 2005b), a three-exponents PK profile was clearly demonstrated after IV MDZ (in absence of FLZ), thus three - compartmental body model was applied to fit observed plasma concentrations extracted from this study. To link the parameters estimated from study 21 and our PBPK model, plasma concentrations were converted into blood concentrations, corrected by 0.86 (B:P^{MDZ}) (Chien et al., 2006). The observed blood concentrations were listed in **Table C.1**.

Table C.1 Observed and predicted MDZ blood concentrations after 1mg IV MDZ (data were digitized from study 21).

Time hour	Observed Mean Blood Concentration ng/ml	Predicted Mean Blood Concentration ng/ml
0.02	62.21	62.21
0.08	25.12	25.11
0.20	17.57	17.60
0.48	12.45	12.37
0.95	7.87	7.80
1.05	6.94	7.20
1.14	6.59	6.74
1.24	6.46	6.29
1.49	5.41	5.41
1.75	4.87	4.74
1.99	4.30	4.25
2.48	3.46	3.54
2.98	3.02	2.99
3.99	2.12	2.19
4.99	1.58	1.62
5.99	1.29	1.21
6.98	0.90	0.90
8.00	0.66	0.70
8.99	0.52	0.50

The model estimation was performed by Scientist v2.0 (Micromath®, MO) with Stiff episode. Model control file, statistics reports and diagnostic plots were presented below.

Model control file

```

//MDZ PK model-IV
//Version 2 (using study 21 data)
//
//Aug, 04, 2014
//
//Mengyao Li
//
//Units
//All units for CL and Q are ml/hr/kg
//All units for V is ml/kg
//All units for T is hr
//All units for amount (A) is ng/kg
//All units for blood concentration (C) is ng/ml.
//All units for rate constant is h-1
//
IndVars: T
DepVars: C1
Params: V1, V2, V3, Q2, Q3, CL
//Equations
K12=Q2/V1
K21=Q2/V2
K10=CL/V1
K13=Q3/V1
K31=Q3/V3
C1=A1/V1
C2=A2/V2
C3=A3/V3
//
//PK MODEL
//
//CENTRAL CPT
A1'=-C1*V1*K10+C2*V2*K21-C1*V1*K12+C3*V3*K31-C1*V1*K13
//
//PERIPHERAL CPT 1
//
A2'=C1*V1*k12-C2*V2*k21
//
//PERIPHERAL CPT 2
//
A3'=C1*V1*k13-C3*V3*k31
//
//IC
t=0
A1=14286
A2=0
A3=0

```

.....

Statistical Reports

	Weighted	Unweighted
Sum of squared observations:	5262.59	5262.59
Sum of squared deviations:	0.17	0.17
Standard deviation of data:	0.11	0.11
R-squared:	1.00	1.00
Coefficient of determination:	1.00	1.00
Correlation:	1.00	1.00
Model Selection Criterion:	9.37	9.37

Confidence Intervals:

Parameter Name : V1
 Estimate Value = 140.369988
 Standard Deviation = 1.42923189
 95% Range (Univar) = 137.282320 143.457656
 95% Range (S-Plane) = 134.392515 146.347461

Parameter Name : V2
 Estimate Value = 337.160239
 Standard Deviation = 6.54249323
 95% Range (Univar) = 323.026042 351.294436
 95% Range (S-Plane) = 309.797584 364.522894

Parameter Name : V3
 Estimate Value = 564.986465
 Standard Deviation = 23.7537865
 95% Range (Univar) = 513.669529 616.303401
 95% Range (S-Plane) = 465.641054 664.331876

Parameter Name : Q2
 Estimate Value = 3315.89346
 Standard Deviation = 44.5358636
 95% Range (Univar) = 3219.67958 3412.10734
 95% Range (S-Plane) = 3129.63121 3502.15571

Parameter Name : Q3
 Estimate Value = 434.875188
 Standard Deviation = 19.4748834
 95% Range (Univar) = 392.802260 476.948116
 95% Range (S-Plane) = 353.425425 516.324951

Parameter Name : CL
 Estimate Value = 418.475366
 Standard Deviation = 5.81287833
 95% Range (Univar) = 405.917406 431.033326
 95% Range (S-Plane) = 394.164177 442.786555

.....

Diagnostic Plots

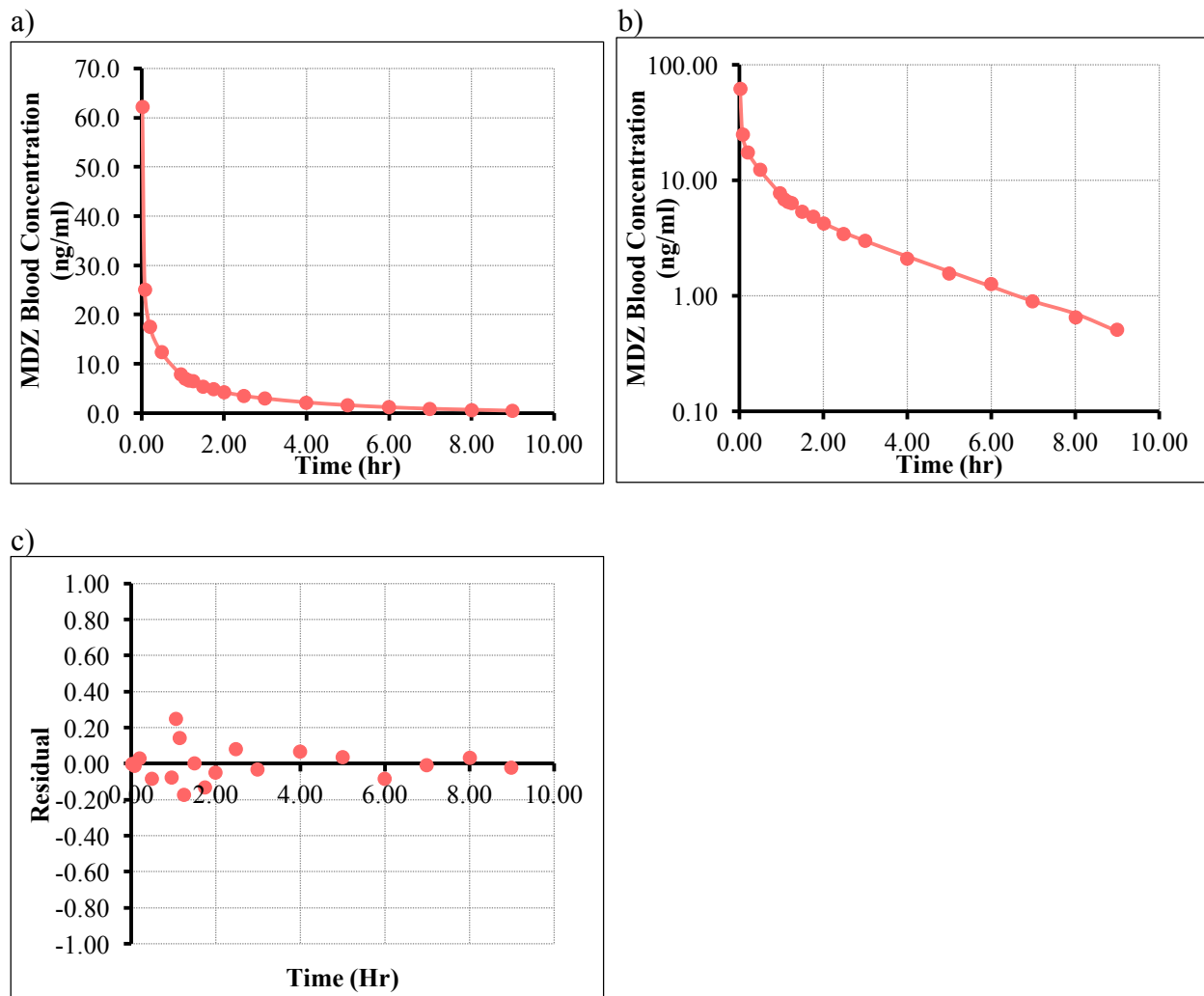


Figure C.1 Diagnostic plots of MDZ 3-compartmental model fit.

a) Observed and predicted MDZ blood concentration – time profiles on Cartesian scale. b) Observed and predicted MDZ blood concentration – time profiles on semi-log scale. c) Relationship between residual and time. Solid lines in a) and b) are predicted profiles. Symbols in a), b) and c) are observed blood concentrations.

As the results showed above, the model can perfectly depict observed data from study 21, and model parameters were precisely predicted. Residuals were evenly spread throughout the x-axle, indicating no systemic bias exists. CL estimated by this compartmental model (418.5ml/hr/kg) matched perfectly with non-compartmental analysis (412.3ml/hr/kg) (Kharasch et al., 2005b). In the semi-PBPK model, physiological volumes of GW, portal vein and liver should be excluded from the estimated V1, V2 or V3. Since estimated V1 was almost identical to total blood volume in normal human body (6-8 L), the three physiological volumes should be subtracted from V2 or V3. Blood flow to liver (Q_{HA}) and portal vein (Q_{PV}) were more rapid than Q_3 (Q_3^{MDZ} , inter-compartmental clearance between central and peripheral cpt-2), suggesting that liver and portal vein were in shallow peripheral compartment, and GW was considered to be in deep peripheral compartment. The final parameters used in our semi-PBPK model were demonstrated in **Table C.2**. Q_2^{MDZ} and Q_3^{MDZ} were not affected by the partition to physiological compartments.

Table C.2 Final systemic distribution parameters used in MDZ semi-PBPK model.

Parameters	Values	Source
V_B^{MDZ} (ml/kg)	140.4	Model estimated V1
V_{P1}^{MDZ} (ml/kg)	313.7	Model estimated $V_2 - K_{p,hep}^{MDZ} \cdot V_{hep} - V_{PV}$
V_{P2}^{MDZ} (ml/kg)	531.4	Model estimated $V_3 - K_{p,GW}^{MDZ} \cdot V_{GW}$
Q_2^{MDZ} (ml/min/kg)	55.27	Model estimated (after unit conversion)
Q_3^{MDZ} (ml/min/kg)	7.25	Model estimated (after unit conversion)

D. SENSITIVITY ANALYSIS OF MDZ

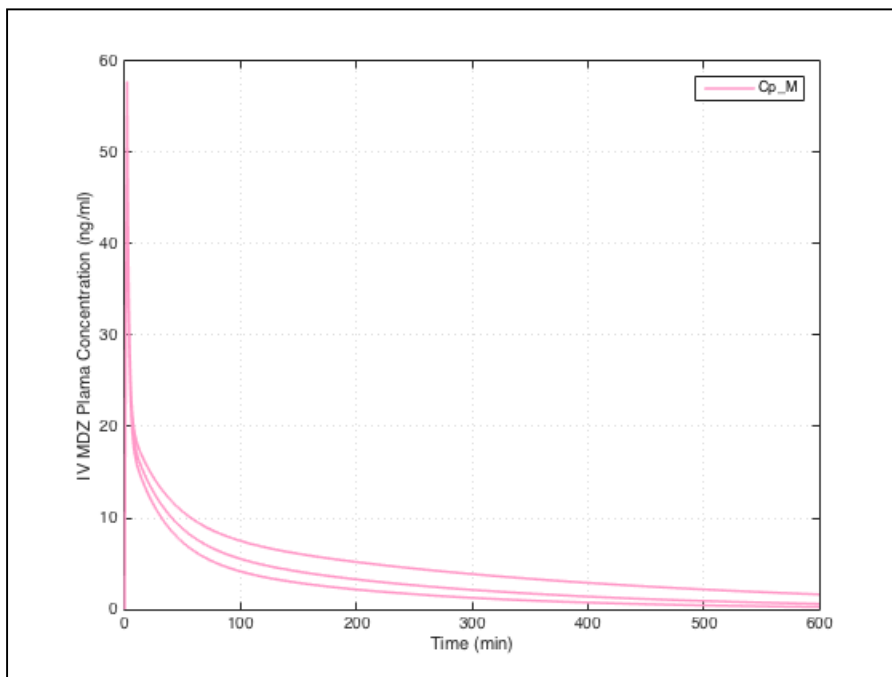


Figure D.1 Sensitivity analysis of MDZ plasma concentrations after IV administration to the change in f_{pv} . (top line: $f_{pv} = 0.0$; middle line: $f_{pv} = 0.5$; bottom line: $f_{pv} = 1.0$)

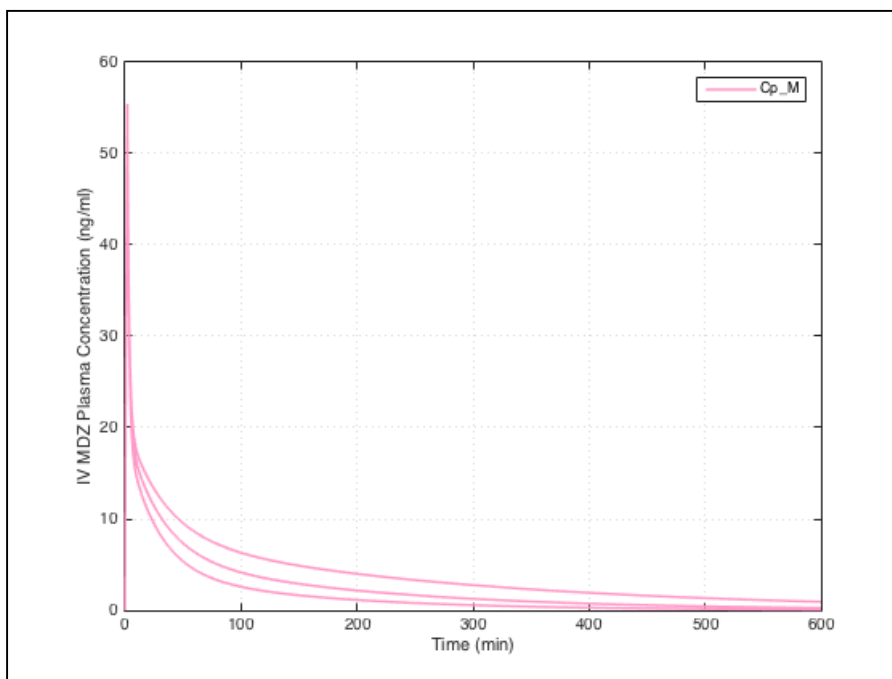


Figure D.2 Sensitivity analysis of MDZ plasma concentrations after IV administration to the change in $v_{\max,hep}^{MDZ}$. (top line: $v_{\max,hep}^{MDZ} = 152534$ ng/min/kg; middle line: $v_{\max,hep}^{MDZ} = 305067$ ng/min/kg; bottom line: $v_{\max,hep}^{MDZ} = 610134$ ng/min/kg)

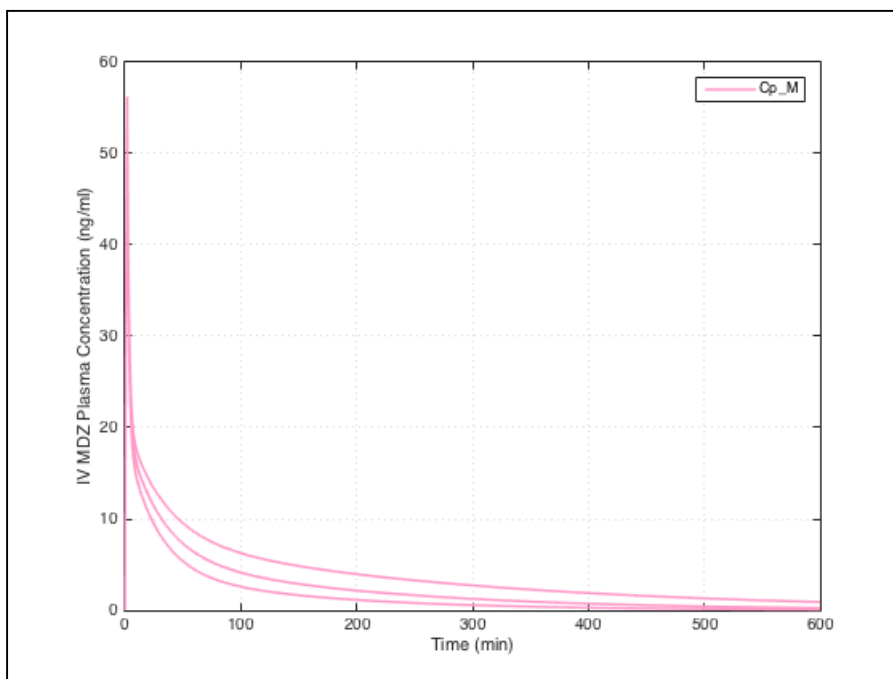


Figure D.3 Sensitivity analysis of MDZ plasma concentrations after IV administration to the change in $K_{p,hep}^{MDZ}$. (top line: $K_{p,hep}^{MDZ} = 0.55$; middle line: $K_{p,hep}^{MDZ} = 1.09$; bottom line: $K_{p,hep}^{MDZ} = 2.18$)

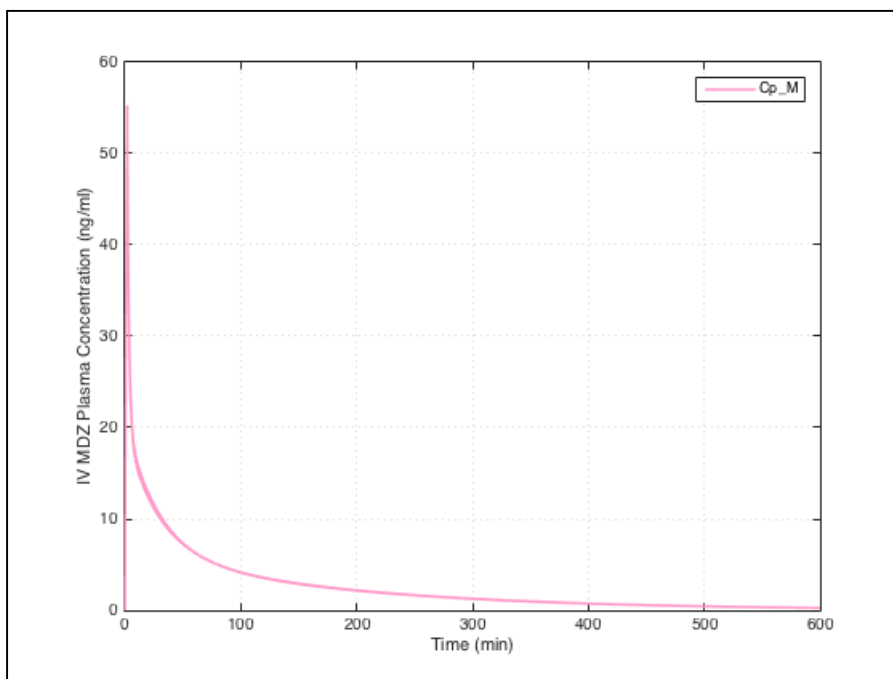


Figure D.4 Sensitivity analysis of MDZ plasma concentrations after IV administration to the change in $K_{p,GW}^{MDZ}$. ($K_{p,GW}^{MDZ} = 0.56/1.12/2.24$ are superimposable).

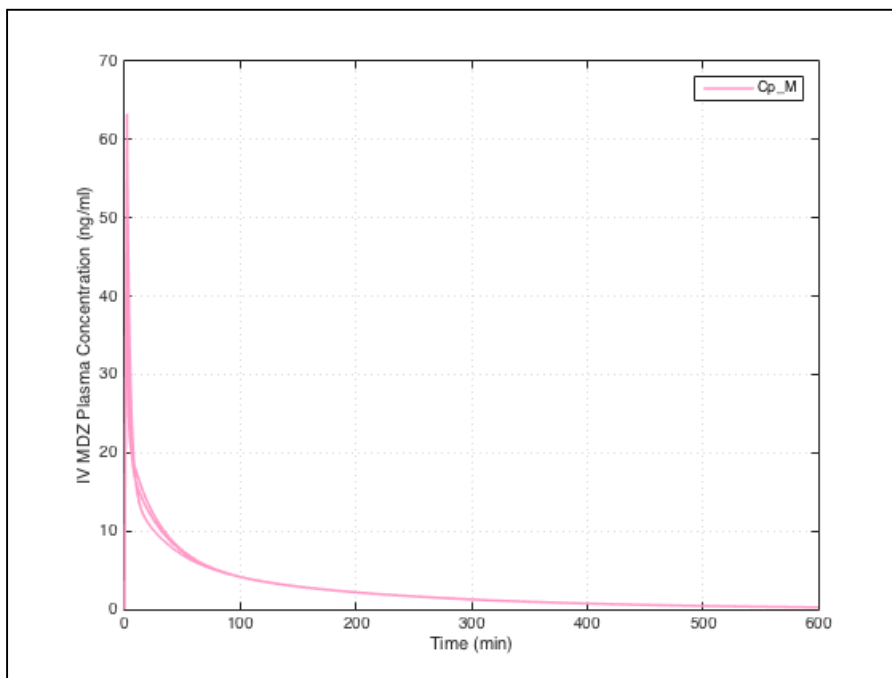


Figure D.5 Sensitivity analysis of MDZ plasma concentrations after IV administration to the change in Q_2^{MDZ} . ($Q_2^{\text{MDZ}} = 27.7/55.3/110.6$ ml/min/kg are superimposable)

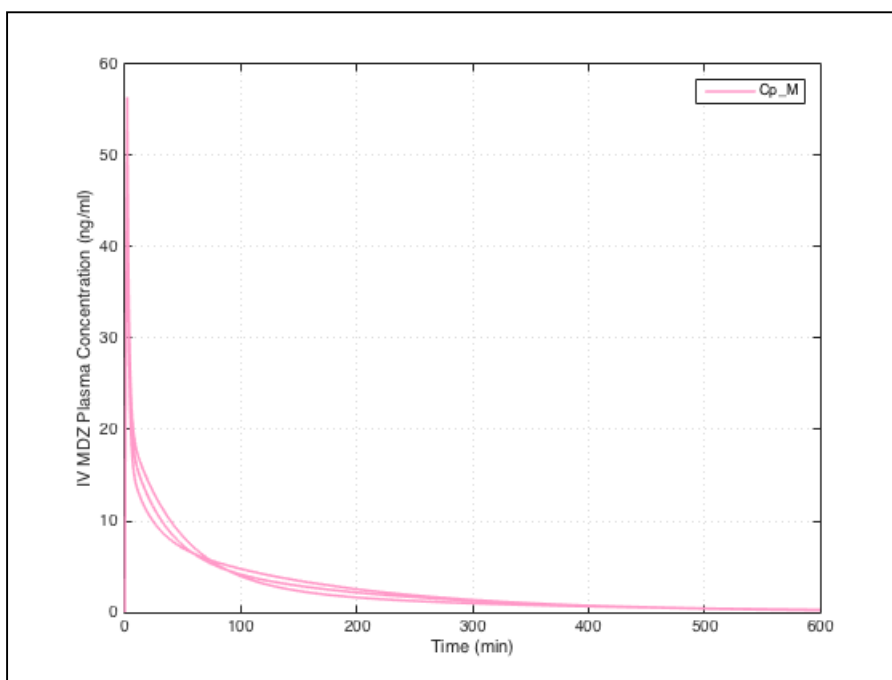


Figure D.6 Sensitivity analysis of MDZ plasma concentrations after IV administration to the change in Q_3^{MDZ} . (line with highest terminal levels: $Q_3^{\text{MDZ}} = 3.63$; line with middle terminal levels: $Q_3^{\text{MDZ}} = 7.25$; line with lowest terminal levels: $Q_3^{\text{MDZ}} = 14.5$)

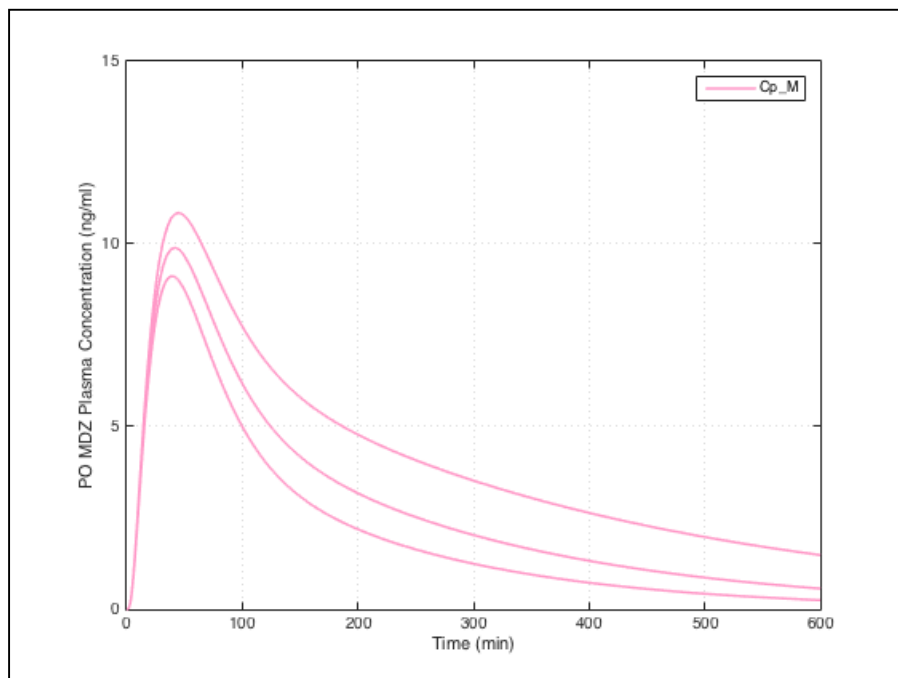


Figure D.7 Sensitivity analysis of MDZ plasma concentrations after PO administration to the change in f_{pv} . (Top line: $f_{pv} = 0.0$; middle line: $f_{pv} = 0.5$; bottom line: $f_{pv} = 1.0$)

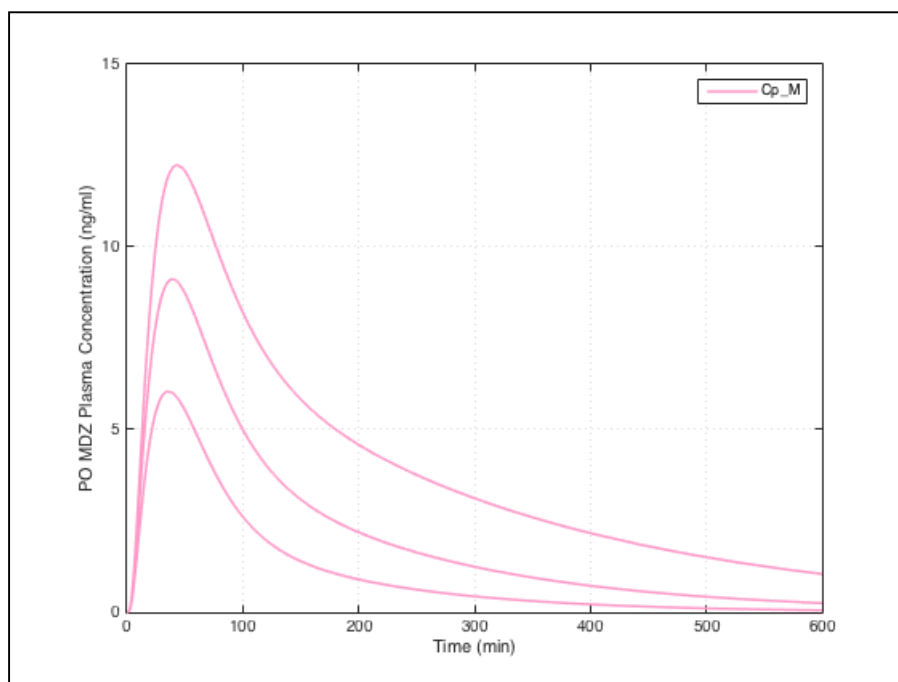


Figure D.8 Sensitivity analysis of MDZ plasma concentrations after PO administration to the change in $v_{\max,hep}^{MDZ}$. (top line: $v_{\max,hep}^{MDZ} = 152534$ ng/min/kg; middle line: $v_{\max,hep}^{MDZ} = 305067$ ng/min/kg; bottom line: $v_{\max,hep}^{MDZ} = 610134$ ng/min/kg)

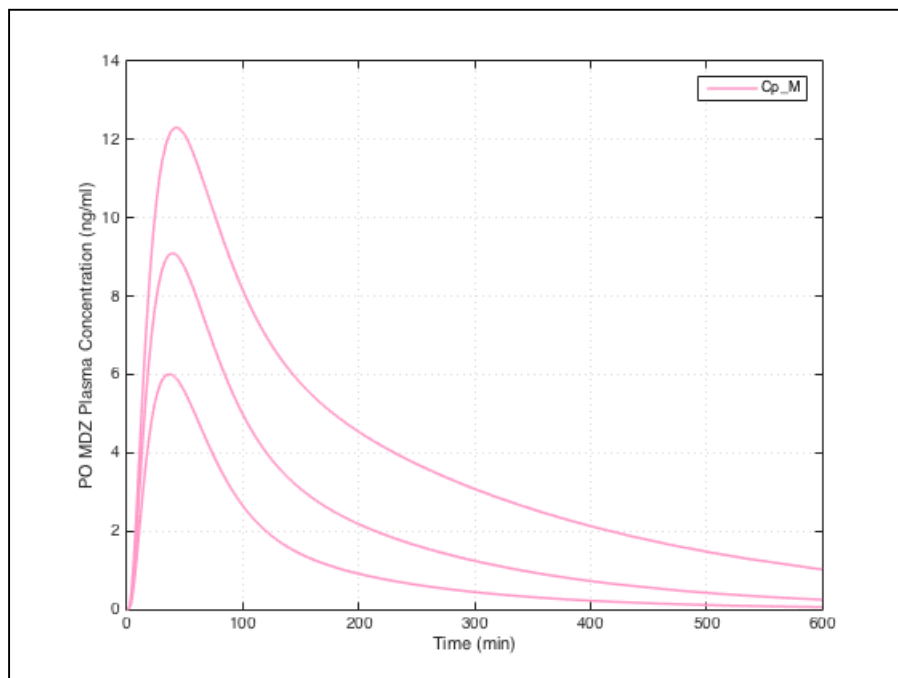


Figure D.9 Sensitivity analysis of MDZ plasma concentrations after PO administration to the change in $K_{p,hep}^{MDZ}$. (top line: $K_{p,hep}^{MDZ} = 0.55$; middle line: $K_{p,hep}^{MDZ} = 1.09$; bottom line: $K_{p,hep}^{MDZ} = 2.18$)

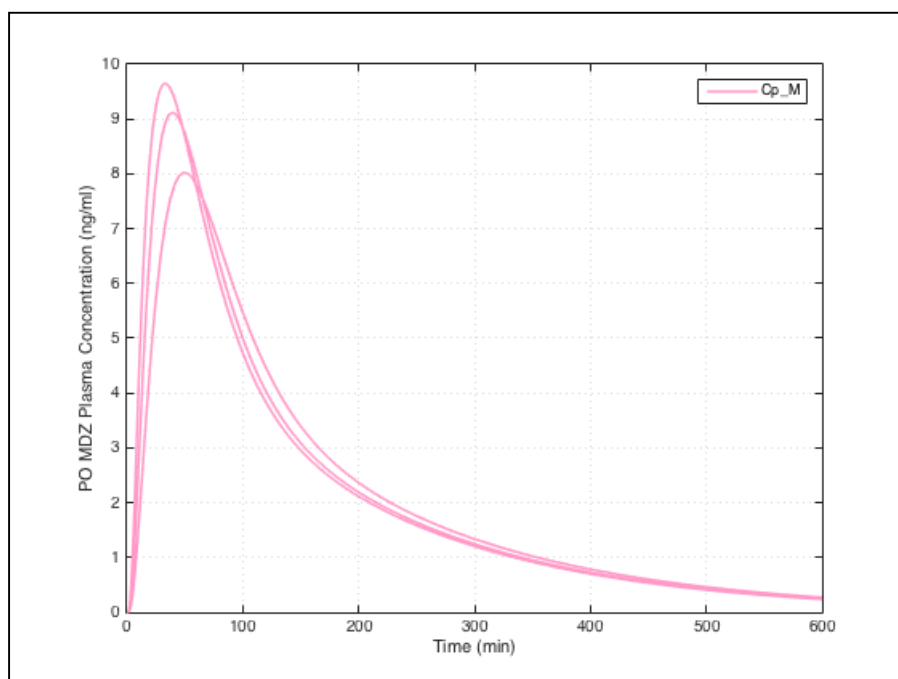


Figure D.10 Sensitivity analysis of MDZ plasma concentrations after PO administration to the change in $K_{p,GW}^{MDZ}$. (line with highest c_{max}^{MDZ} : $K_{p,GW}^{MDZ} = 0.56$; line with middle c_{max}^{MDZ} : $K_{p,GW}^{MDZ} = 1.12$; line with lowest c_{max}^{MDZ} : $K_{p,GW}^{MDZ} = 2.24$)

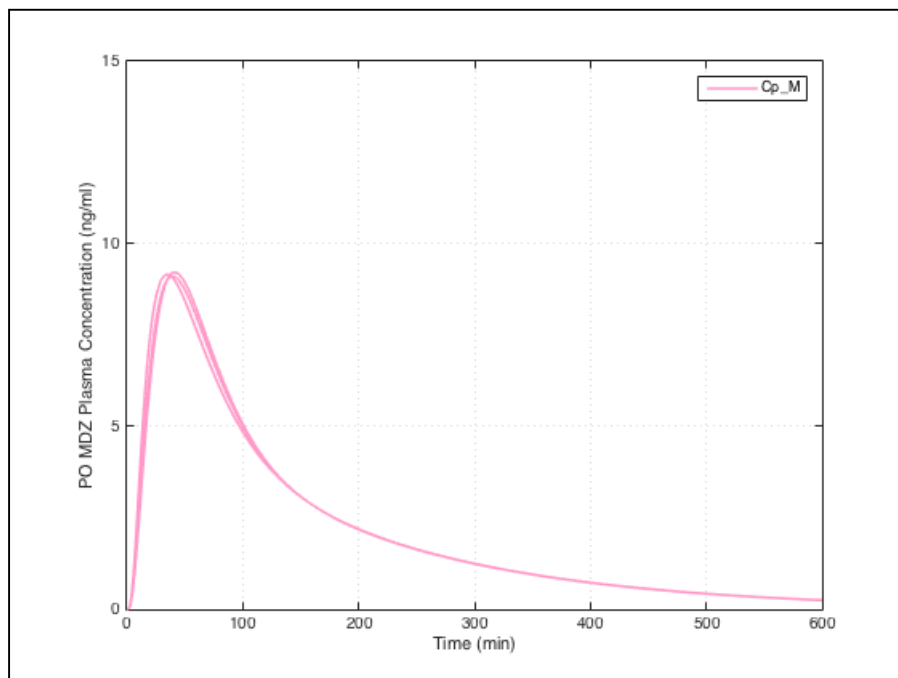


Figure D.11 Sensitivity analysis of MDZ plasma concentrations after PO administration to the change in Q_2^{MDZ} . ($Q_2^{\text{MDZ}} = 27.7/55.3/110.6$ ml/min/kg are superimposable)

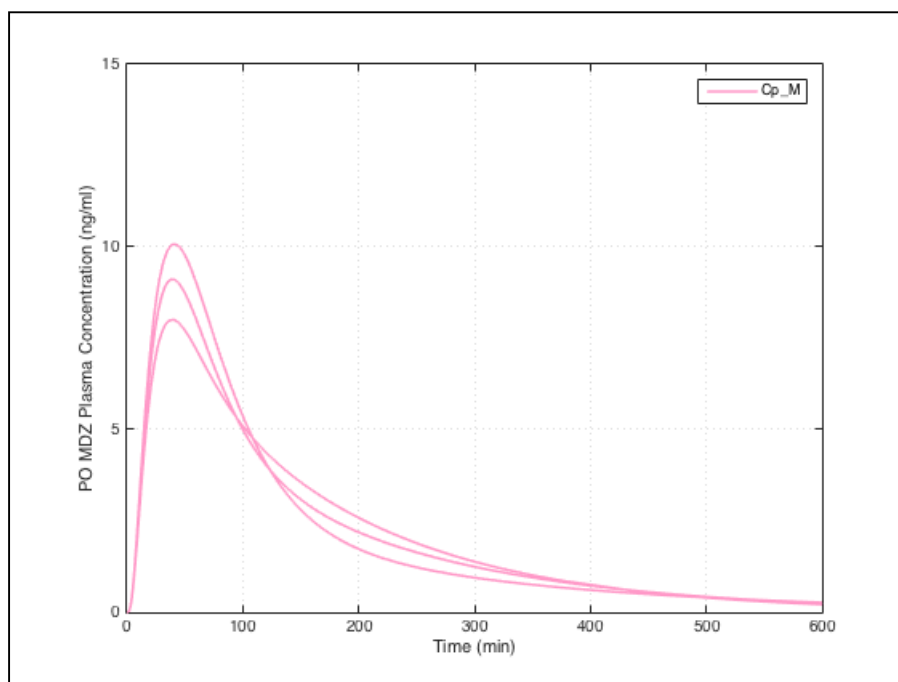


Figure D.12 Sensitivity analysis of MDZ plasma concentrations after PO administration to the change in Q_3^{MDZ} . (line with highest terminal levels: $Q_3^{\text{MDZ}} = 3.63$; line with middle terminal levels: $Q_3^{\text{MDZ}} = 7.25$; line with lowest terminal levels: $Q_3^{\text{MDZ}} = 14.5$)

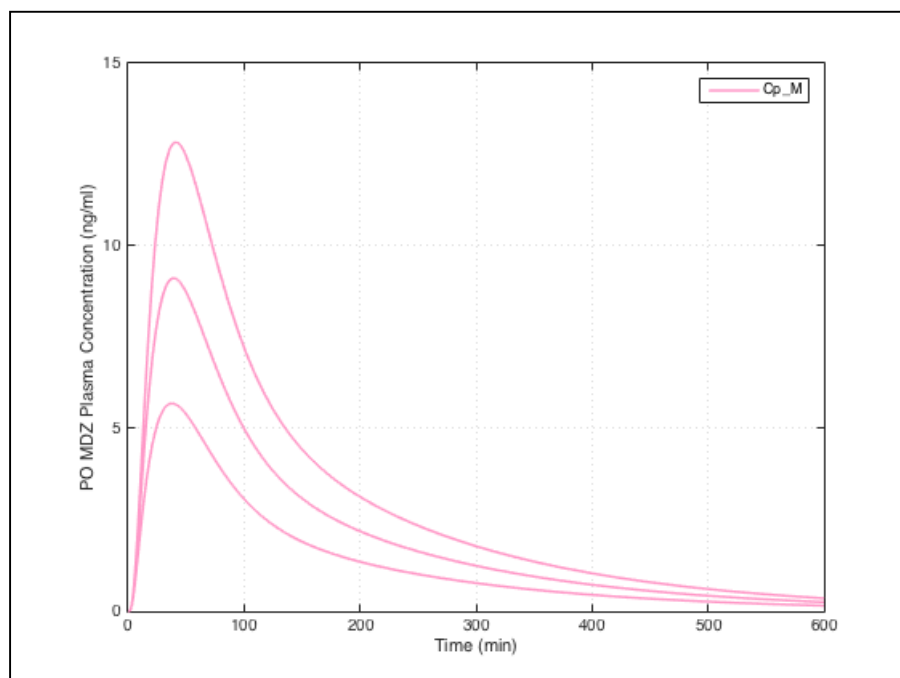


Figure D.13 Sensitivity analysis of MDZ plasma concentrations after PO administration to the change in f_{villi} . (top line: $f_{villi} = 1.1$; middle line: $f_{villi} = 2.2$; bottom line: $f_{villi} = 4.4$)

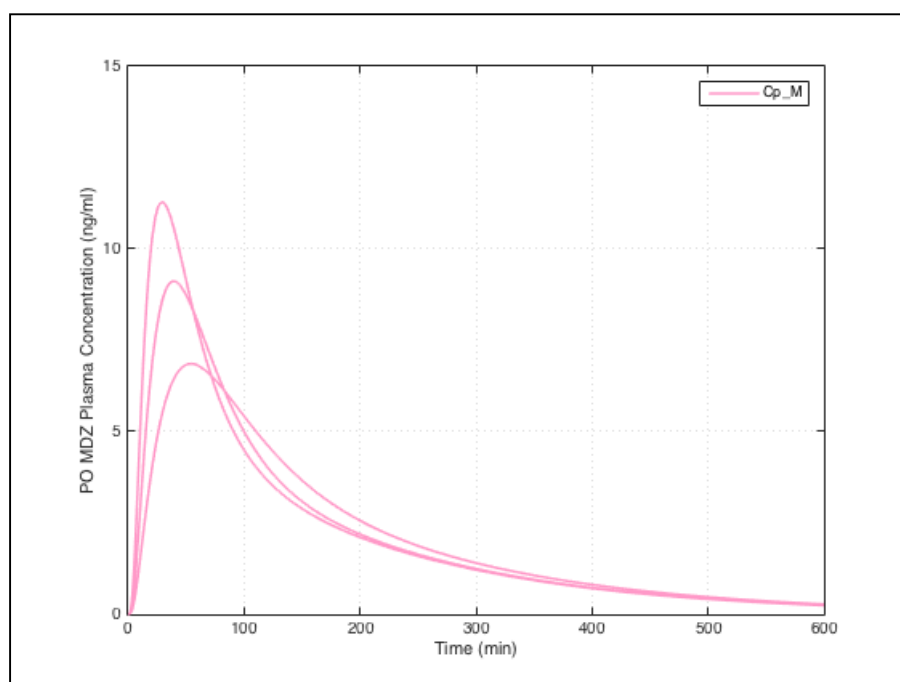


Figure D.14 Sensitivity analysis of MDZ plasma concentrations after PO administration to the change in k_{GL}^{MDZ} . (line with highest c_{max}^{MDZ} : $k_{GL}^{MDZ} = 0.1$; line with middle c_{max}^{MDZ} : $k_{GL}^{MDZ} = 0.05$; line with lowest c_{max}^{MDZ} : $k_{GL}^{MDZ} = 0.025$)

E. SENSITIVITY ANALYSIS OF MDZ IN PRESENCE OF FLZ

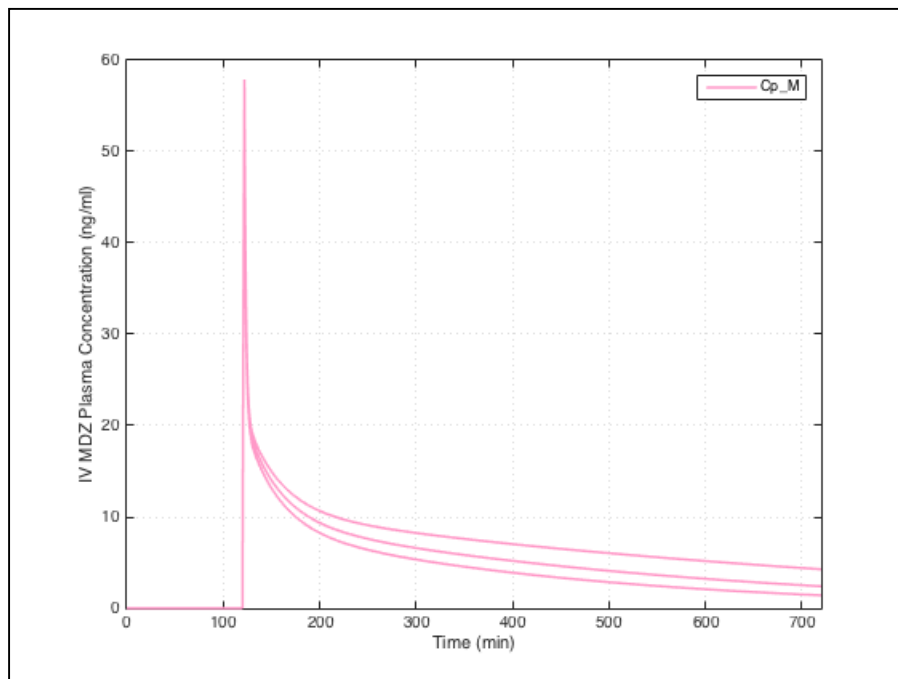


Figure E.1 Sensitivity analysis of IV MDZ plasma concentrations in presence of IV FLZ to the change in f_{pv} . (top line: $f_{pv} = 0.0$; middle line: $f_{pv} = 0.5$; bottom line: $f_{pv} = 1.0$)

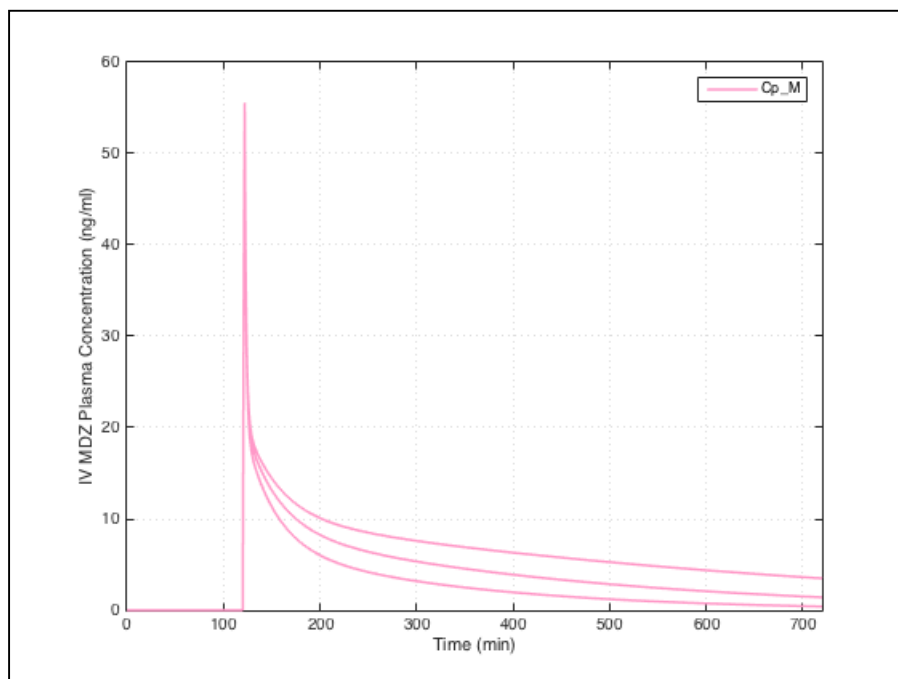


Figure E.2 Sensitivity analysis of IV MDZ plasma concentrations in presence of IV FLZ to the change in $v_{max,hep}^{MDZ}$. (top line: $v_{max,hep}^{MDZ} = 152534$ ng/min/kg; middle line: $v_{max,hep}^{MDZ} = 305067$ ng/min/kg; bottom line: $v_{max,hep}^{MDZ} = 610134$ ng/min/kg)

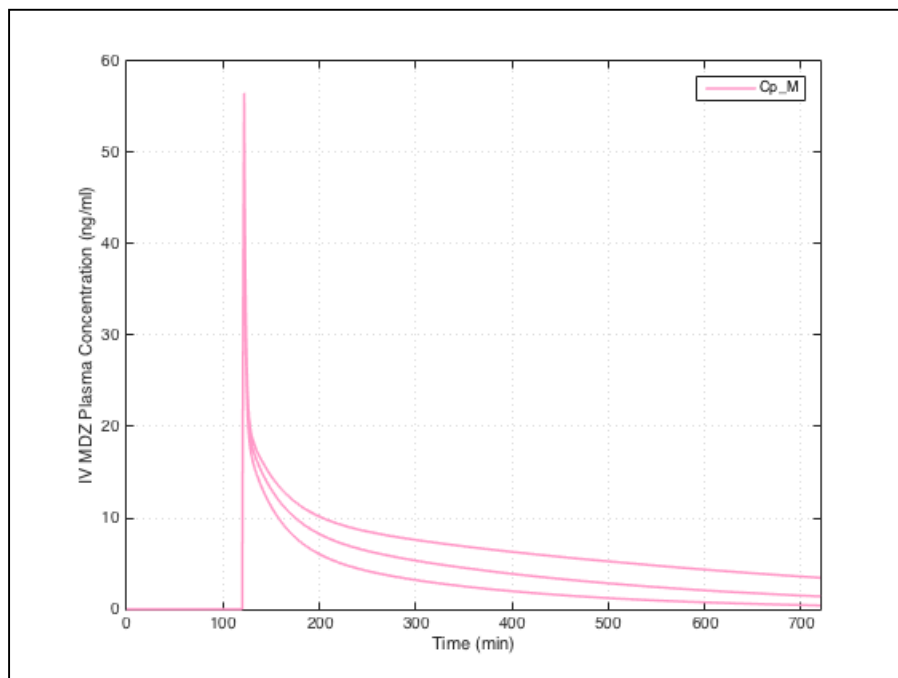


Figure E.3 Sensitivity analysis of IV MDZ plasma concentrations in presence of IV FLZ to the change in $K_{p,hep}^{MDZ}$. (top line: $K_{p,hep}^{MDZ} = 0.55$; middle line: $K_{p,hep}^{MDZ} = 1.09$; bottom line: $K_{p,hep}^{MDZ} = 2.18$)

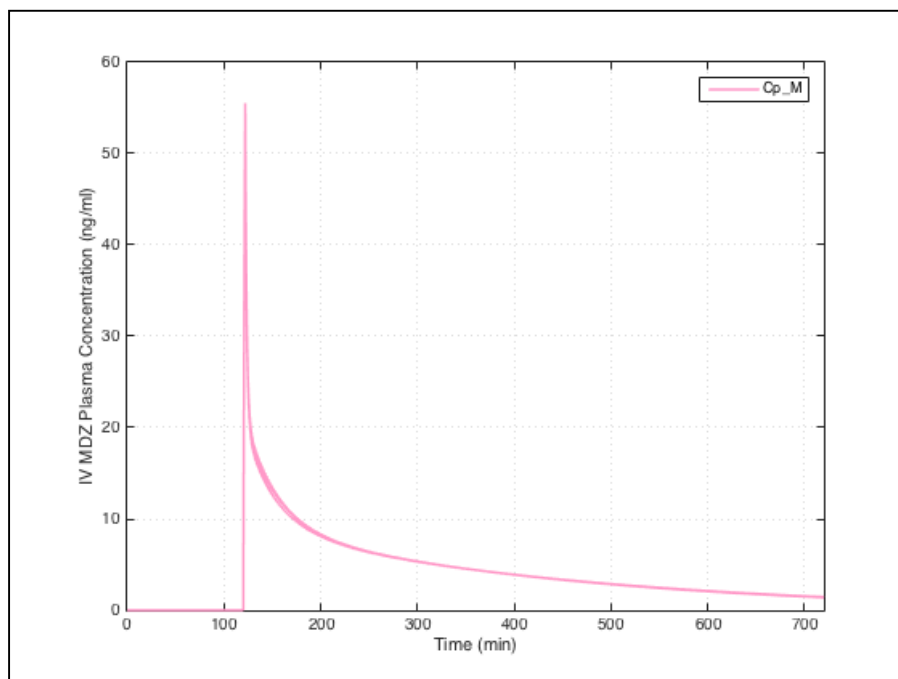


Figure E.4 Sensitivity analysis of IV MDZ plasma concentrations in presence of IV FLZ to the change in $K_{p,GW}^{MDZ}$. ($K_{p,GW}^{MDZ} = 0.56/1.12/2.24$ are superimposable).

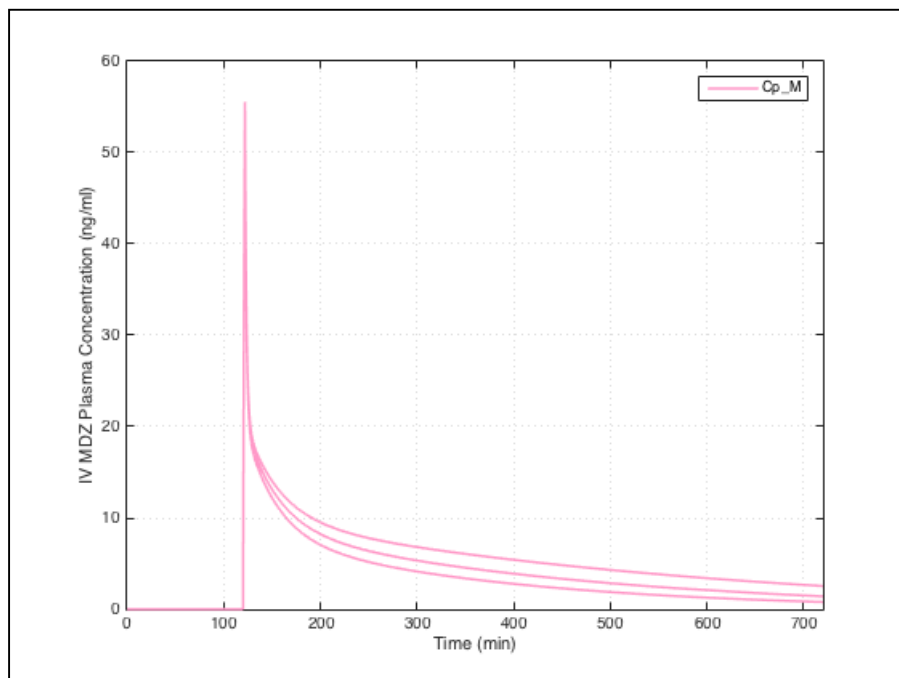


Figure E.5 Sensitivity analysis of IV MDZ plasma concentrations in presence of IV FLZ to the change in $K_{p,hep}^{FLZ}$. (top line: $K_{p,hep}^{MDZ} = 2.0$; middle line: $K_{p,hep}^{MDZ} = 1.0$; bottom line: $K_{p,hep}^{MDZ} = 0.5$)

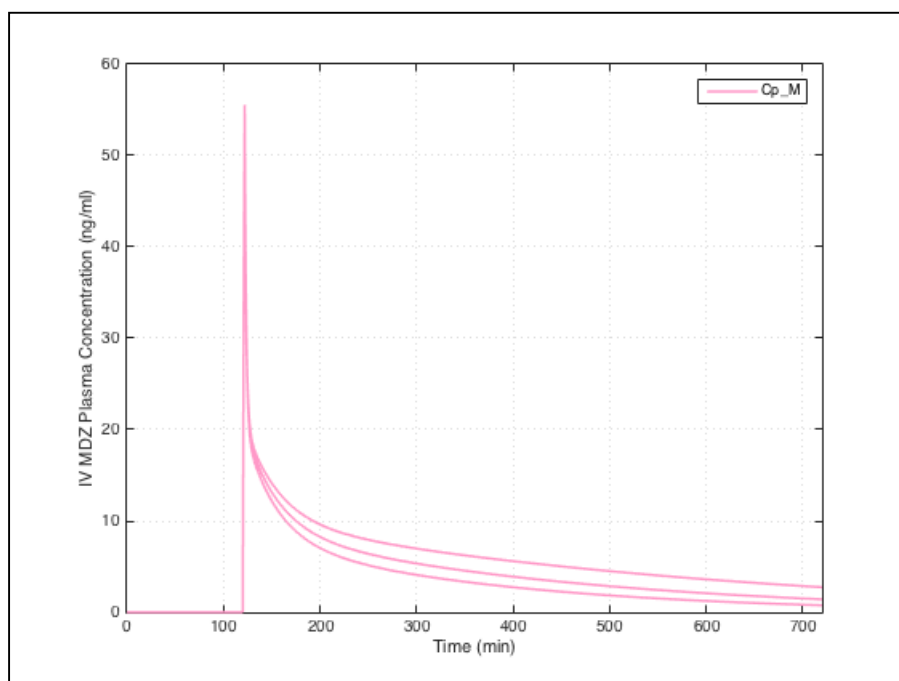


Figure E.6 Sensitivity analysis of IV MDZ plasma concentrations in presence of IV FLZ to the change in $K_{i,hep}^{FLZ}$. (top line: $K_{i,hep}^{MDZ} = 1915$ ng/ml; middle line: $K_{i,hep}^{MDZ} = 3829$ ng/ml; bottom line: $K_{i,hep}^{MDZ} = 7658$ ng/ml)

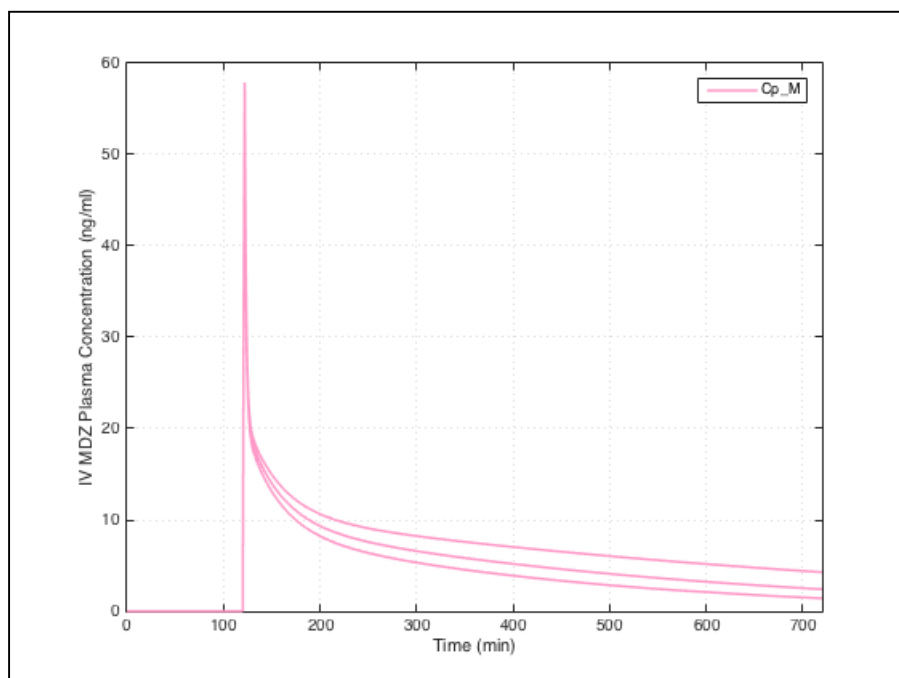


Figure E.7 Sensitivity analysis of IV MDZ plasma concentrations in presence of PO FLZ to the change in f_{pv} . (top line: $f_{pv} = 0.0$; middle line: $f_{pv} = 0.5$; bottom line: $f_{pv} = 1.0$)

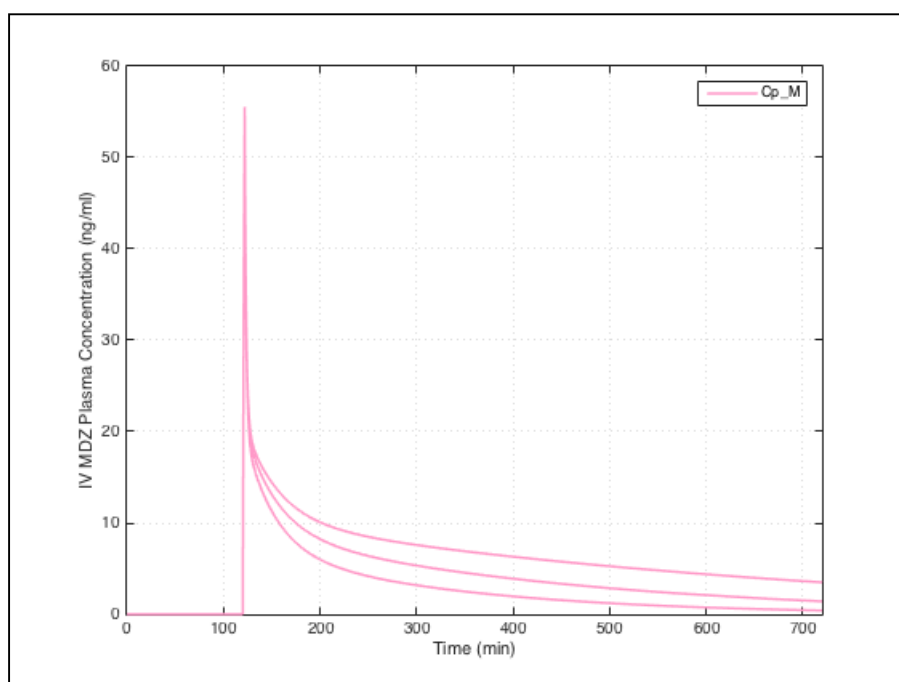


Figure E.8 Sensitivity analysis of IV MDZ plasma concentrations in presence of PO FLZ to the change in $v_{\max, \text{hep}}^{\text{MDZ}}$. (top line: $v_{\max, \text{hep}}^{\text{MDZ}} = 152534 \text{ ng/min/kg}$; middle line: $v_{\max, \text{hep}}^{\text{MDZ}} = 305067 \text{ ng/min/kg}$; bottom line: $v_{\max, \text{hep}}^{\text{MDZ}} = 610134 \text{ ng/min/kg}$)

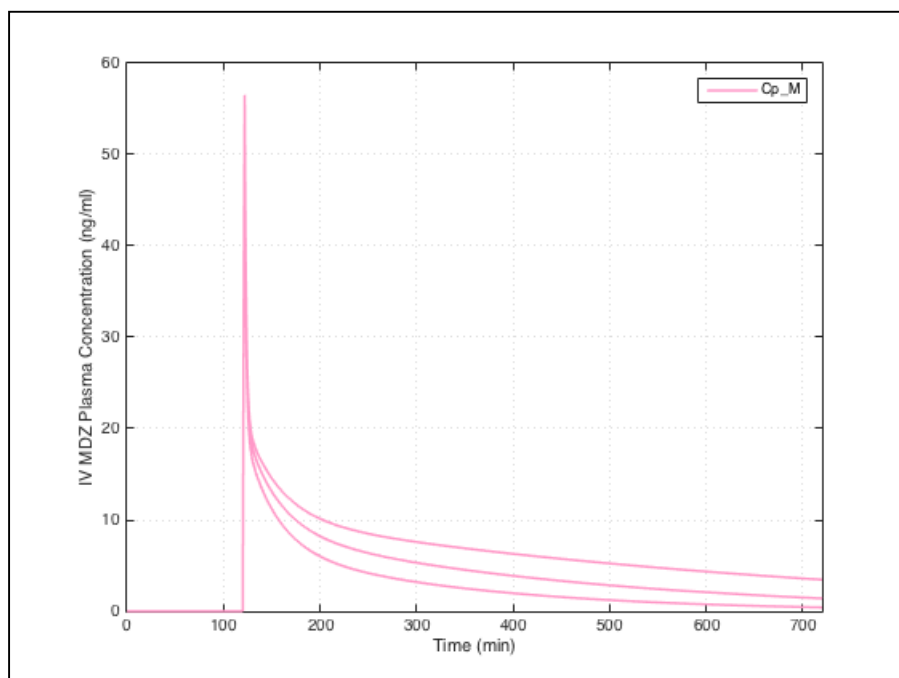


Figure E.9 Sensitivity analysis of IV MDZ plasma concentrations in presence of PO FLZ to the change in $K_{p,hep}^{MDZ}$. (top line: $K_{p,hep}^{MDZ} = 0.55$; middle line: $K_{p,hep}^{MDZ} = 1.09$; bottom line: $K_{p,hep}^{MDZ} = 2.18$)

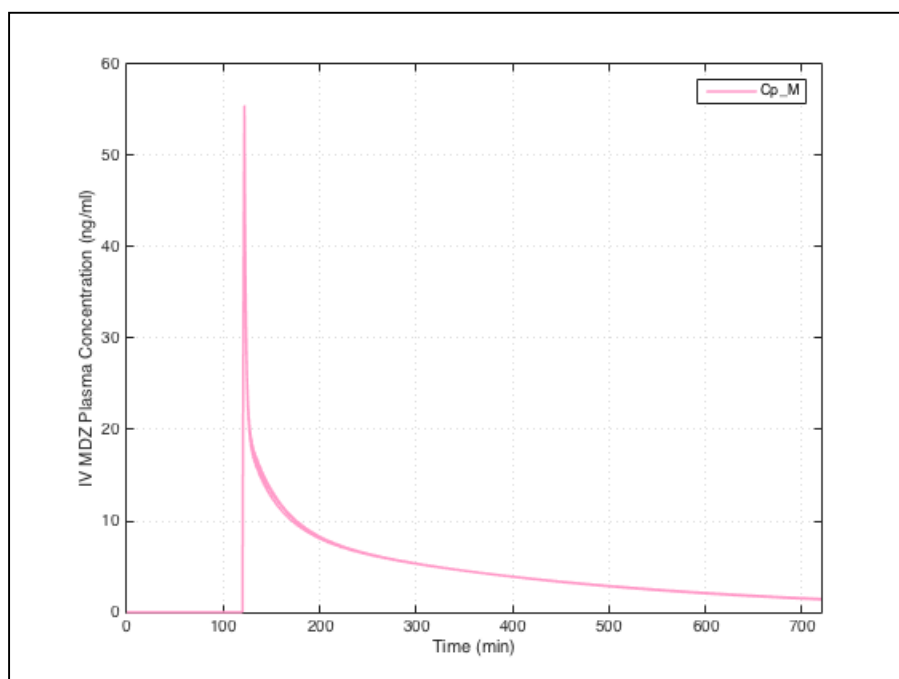


Figure E.10 Sensitivity analysis of IV MDZ plasma concentrations in presence of PO FLZ to the change in $K_{p,GW}^{MDZ}$. ($K_{p,GW}^{MDZ} = 0.56/1.12/2.24$ are superimposable).

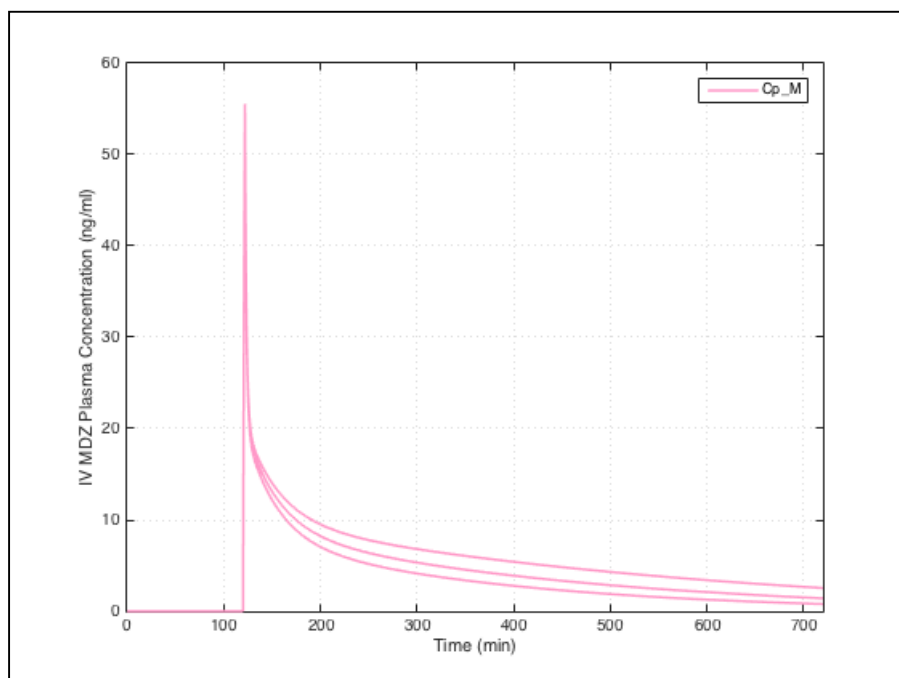


Figure E.11 Sensitivity analysis of IV MDZ plasma concentrations in presence of PO FLZ to the change in $K_{p,hep}^{FLZ}$. (Top line: $K_{p,hep}^{MDZ} = 2.0$; middle line: $K_{p,hep}^{MDZ} = 1.0$; bottom line: $K_{p,hep}^{MDZ} = 0.5$)

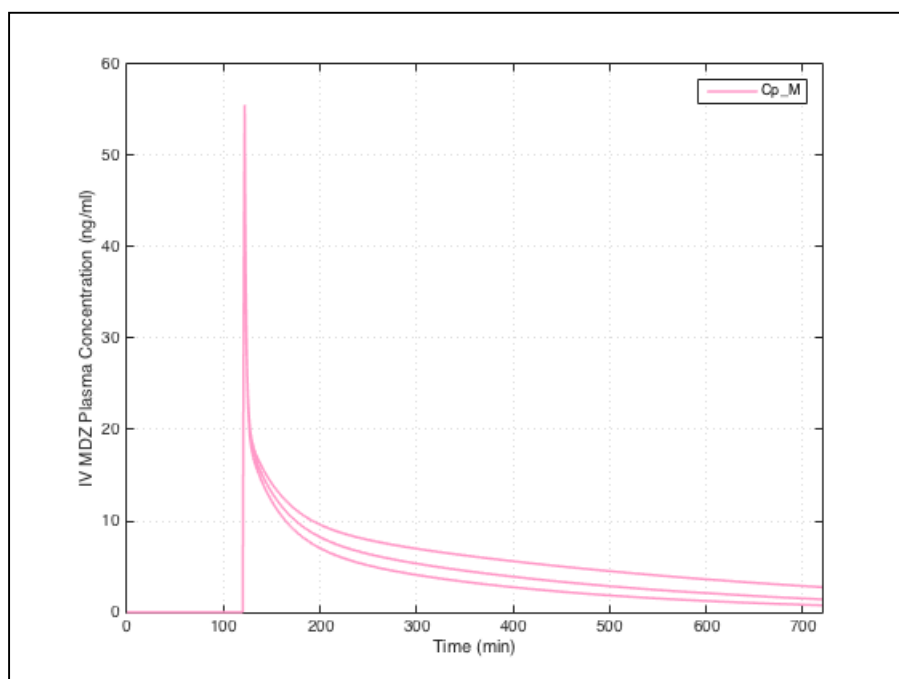


Figure E.12 Sensitivity analysis of IV MDZ plasma concentrations in presence of PO FLZ to the change in $K_{i,hep}^{FLZ}$. (top line: $K_{i,hep}^{MDZ} = 1915$ ng/ml; middle line: $K_{i,hep}^{MDZ} = 3829$ ng/ml; bottom line: $K_{i,hep}^{MDZ} = 7658$ ng/ml)

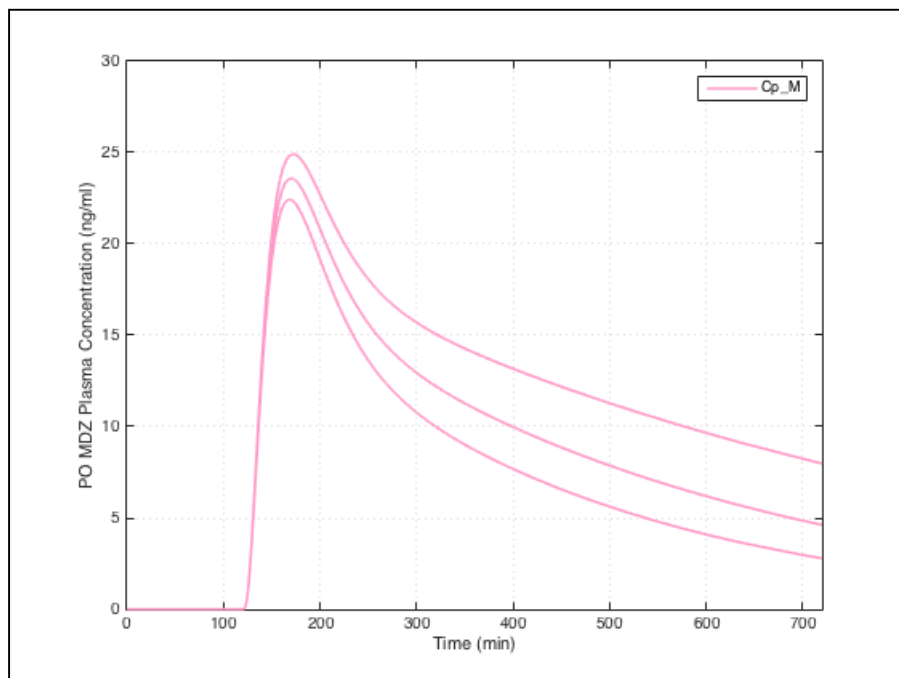


Figure E.13 Sensitivity analysis of PO MDZ plasma concentrations in presence of IV FLZ to the change in f_{pv} . (top line: $f_{pv} = 0.0$; middle line: $f_{pv} = 0.5$; bottom line: $f_{pv} = 1.0$)

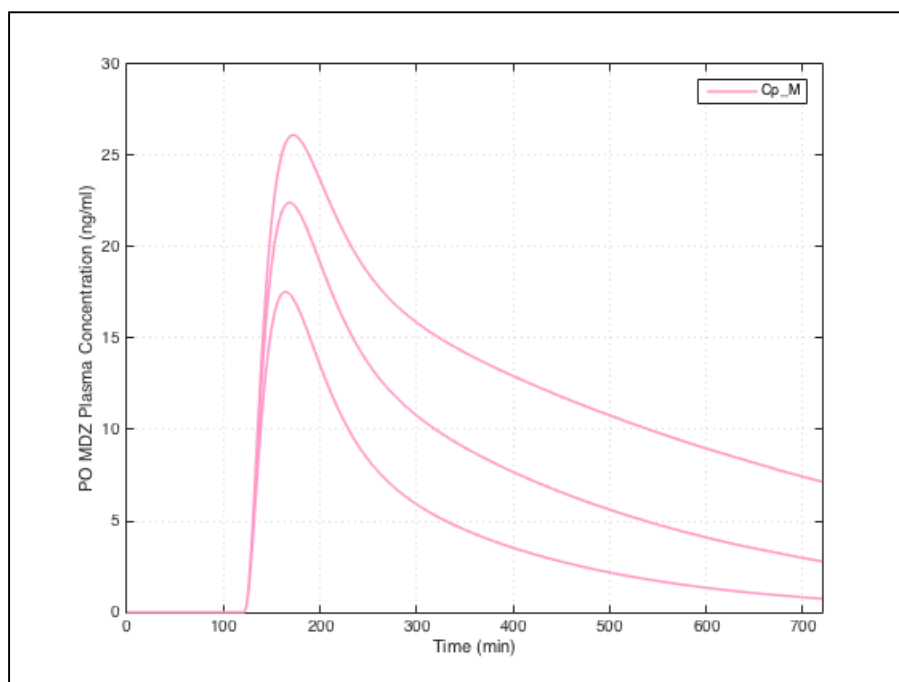


Figure E.14 Sensitivity analysis of PO MDZ plasma concentrations in presence of IV FLZ to the change in $v_{\max, \text{hep}}^{\text{MDZ}}$. (top line: $v_{\max, \text{hep}}^{\text{MDZ}} = 152534 \text{ ng/min/kg}$; middle line: $v_{\max, \text{hep}}^{\text{MDZ}} = 305067 \text{ ng/min/kg}$; bottom line: $v_{\max, \text{hep}}^{\text{MDZ}} = 610134 \text{ ng/min/kg}$)

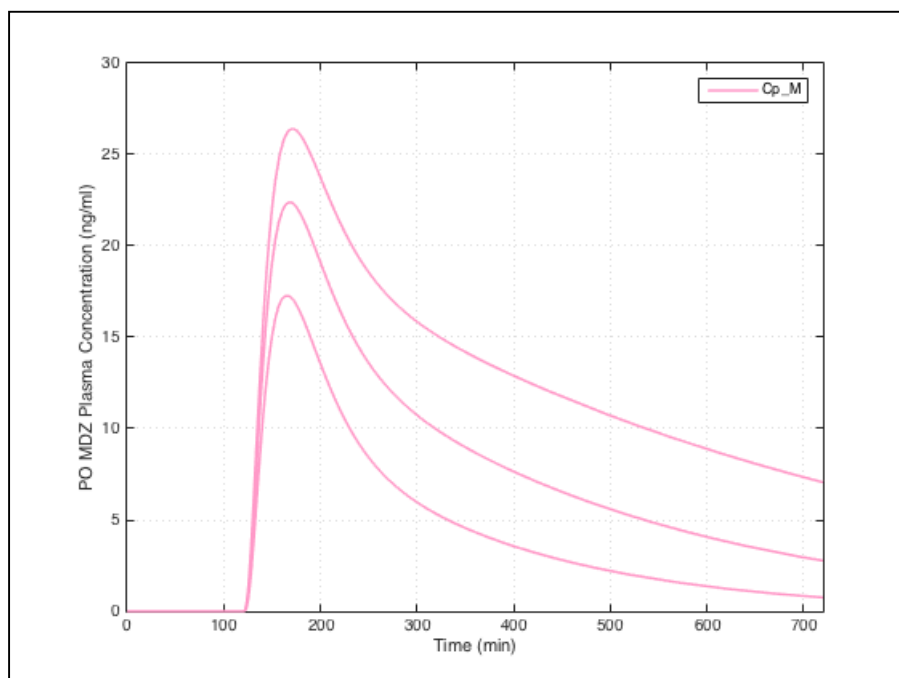


Figure E.15 Sensitivity analysis of PO MDZ plasma concentrations in presence of IV FLZ to the change in $K_{p,hep}^{MDZ}$. (top line: $K_{p,hep}^{MDZ} = 0.55$; middle line: $K_{p,hep}^{MDZ} = 1.09$; bottom line: $K_{p,hep}^{MDZ} = 2.18$)

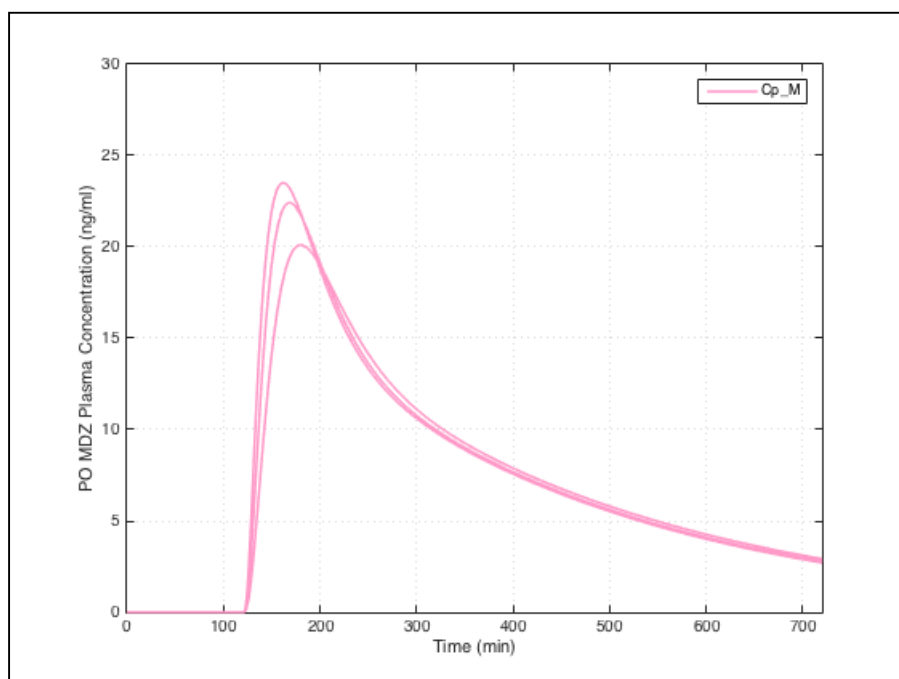


Figure E.16 Sensitivity analysis of PO MDZ plasma concentrations in presence of IV FLZ to the change in $K_{p,GW}^{MDZ}$. (line with highest c_{max}^{MDZ} : $K_{p,GW}^{MDZ} = 0.56$; line with middle c_{max}^{MDZ} : $K_{p,GW}^{MDZ} = 1.12$; line with lowest c_{max}^{MDZ} : $K_{p,GW}^{MDZ} = 2.24$)

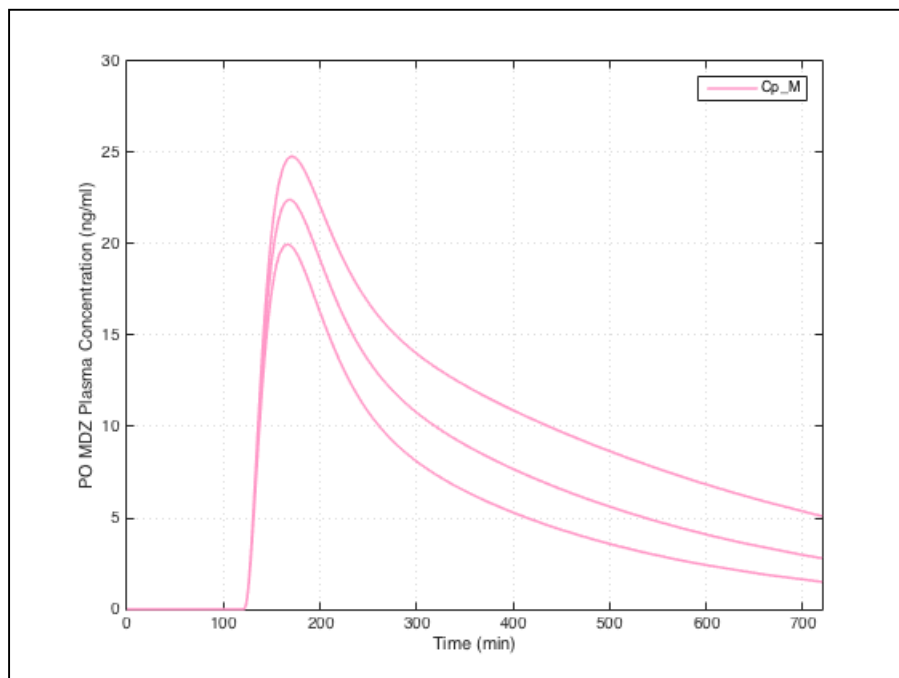


Figure E.17 Sensitivity analysis of PO MDZ plasma concentrations in presence of IV FLZ to the change in $K_{p,hep}^{FLZ}$. (Top line: $K_{p,hep}^{MDZ} = 2.0$; middle line: $K_{p,hep}^{MDZ} = 1.0$; bottom line: $K_{p,hep}^{MDZ} = 0.5$)

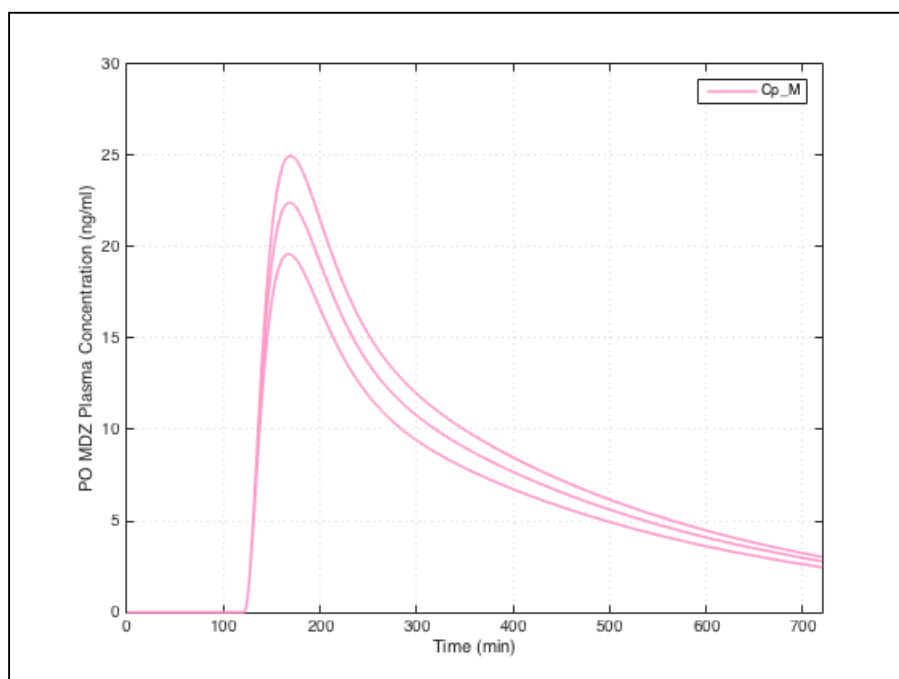


Figure E.18 Sensitivity analysis of PO MDZ plasma concentrations in presence of IV FLZ to the change in $K_{p,GW}^{FLZ}$. (top line: $K_{p,GW}^{FLZ} = 2.0$; middle line: $K_{p,GW}^{FLZ} = 1.0$; bottom line: $K_{p,GW}^{FLZ} = 0.5$)

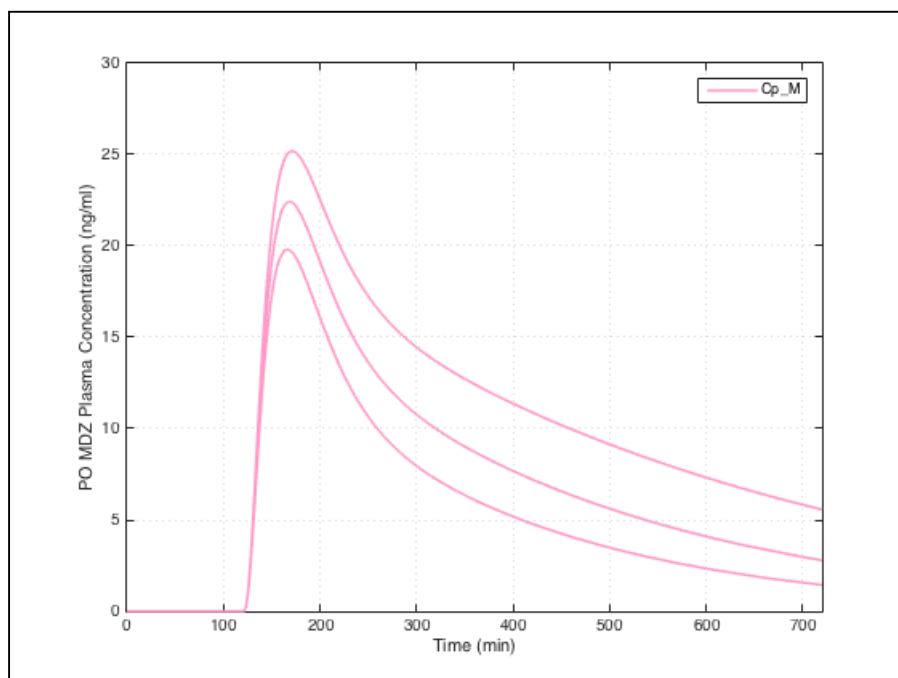


Figure E.19 Sensitivity analysis of PO MDZ plasma concentrations in presence of IV FLZ to the change in $K_{i,hep}^{FLZ}$. (top line: $K_{i,hep}^{MDZ} = 1915$ ng/ml; middle line: $K_{i,hep}^{MDZ} = 3829$ ng/ml; bottom line: $K_{i,hep}^{MDZ} = 7658$ ng/ml)

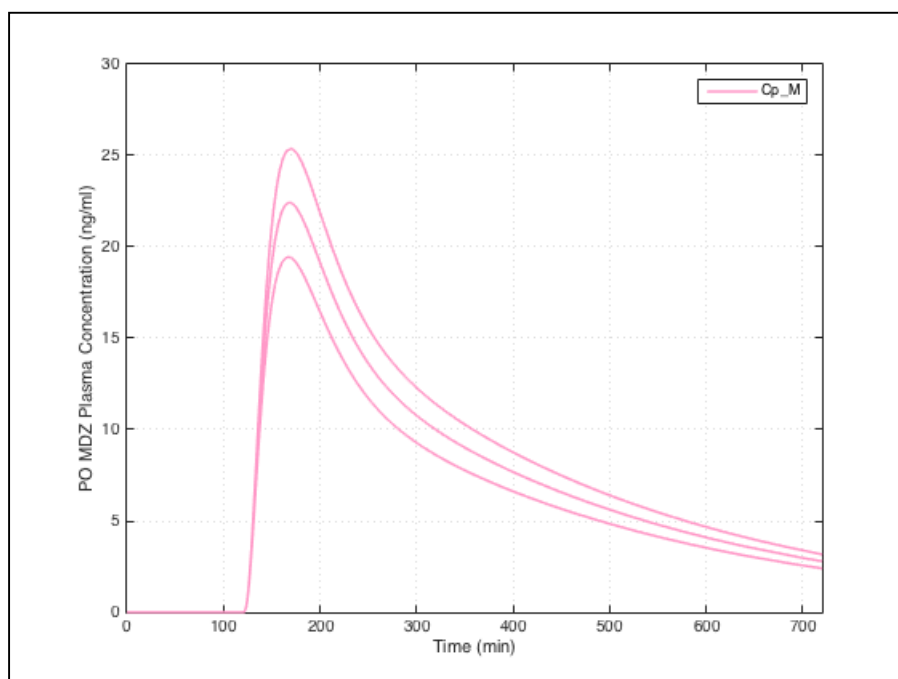


Figure E.20 Sensitivity analysis of PO MDZ plasma concentrations in presence of IV FLZ to the change in $K_{i,GW}^{FLZ}$. (top line: $K_{i,GW}^{MDZ} = 1591$ ng/ml; middle line: $K_{i,GW}^{MDZ} = 3182$ ng/ml; bottom line: $K_{i,GW}^{MDZ} = 6364$ ng/ml)

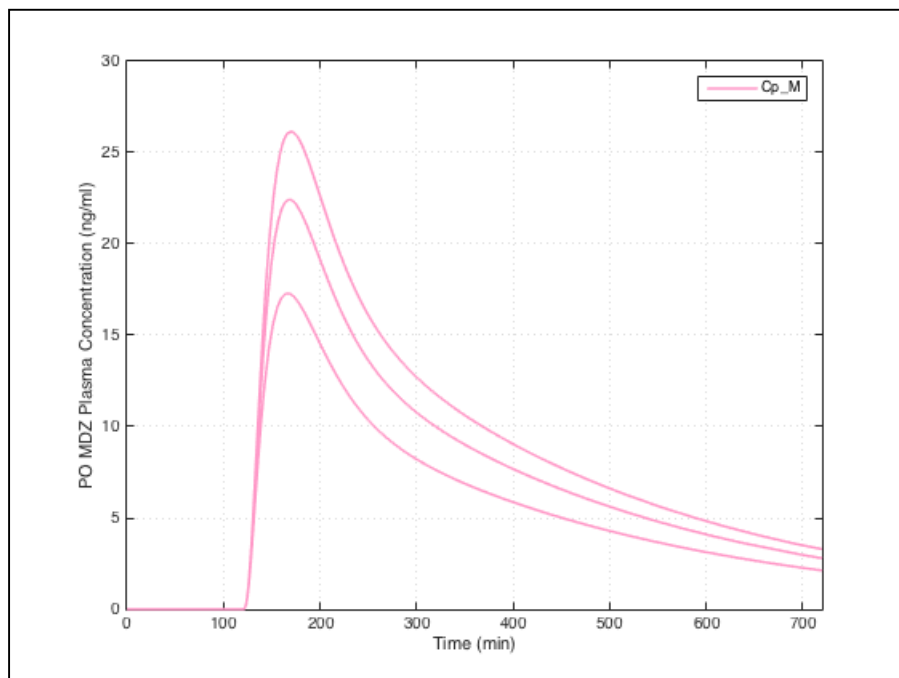


Figure E.21 Sensitivity analysis of PO MDZ plasma concentrations in presence of IV FLZ to the change in f_{villi} . (top line: $f_{villi} = 1.1$; middle line: $f_{villi} = 2.2$; bottom line: $f_{villi} = 4.4$)

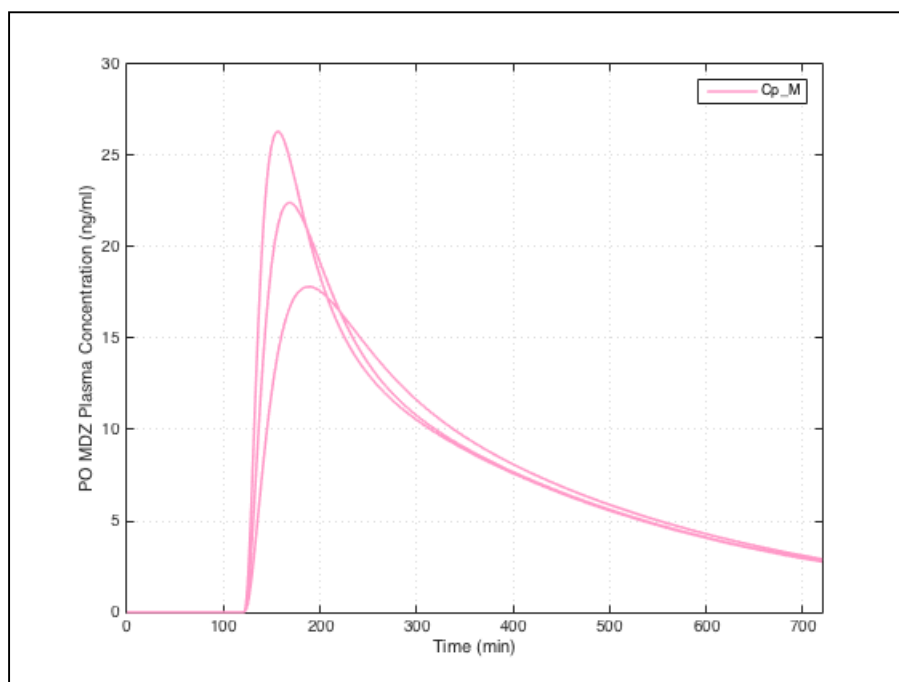


Figure E.22 Sensitivity analysis of PO MDZ plasma concentrations in presence of IV FLZ to the change in k_{GL}^{MDZ} . (line with highest c_{max}^{MDZ} : $k_{GL}^{MDZ} = 0.1$; line with middle c_{max}^{MDZ} : $k_{GL}^{MDZ} = 0.05$; line with lowest c_{max}^{MDZ} : $k_{GL}^{MDZ} = 0.025$)

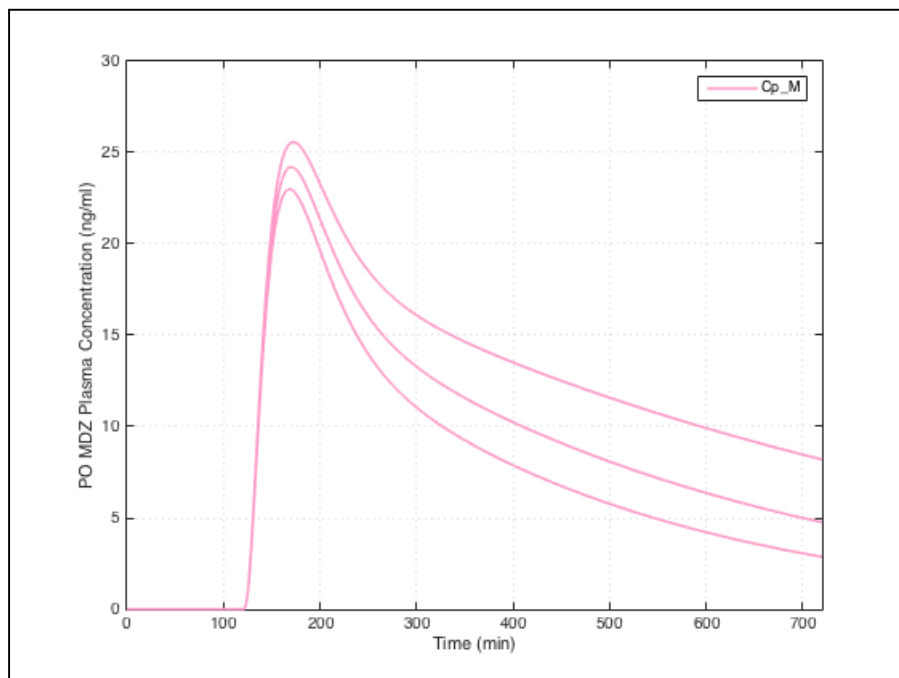


Figure E.23 Sensitivity analysis of PO MDZ plasma concentrations in presence of PO FLZ to the change in f_{pv} . (top line: $f_{pv} = 0.0$; middle line: $f_{pv} = 0.5$; bottom line: $f_{pv} = 1.0$)

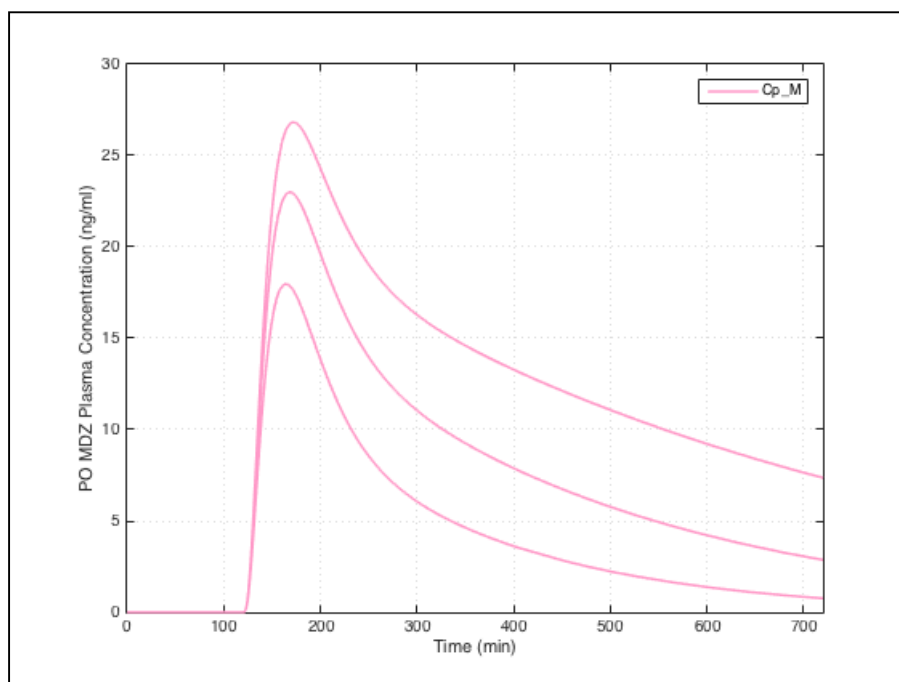


Figure E.24 Sensitivity analysis of PO MDZ plasma concentrations in presence of PO FLZ to the change in $v_{\max, \text{hep}}^{\text{MDZ}}$. (top line: $v_{\max, \text{hep}}^{\text{MDZ}} = 152534$ ng/min/kg; middle line: $v_{\max, \text{hep}}^{\text{MDZ}} = 305067$ ng/min/kg; bottom line: $v_{\max, \text{hep}}^{\text{MDZ}} = 610134$ ng/min/kg)

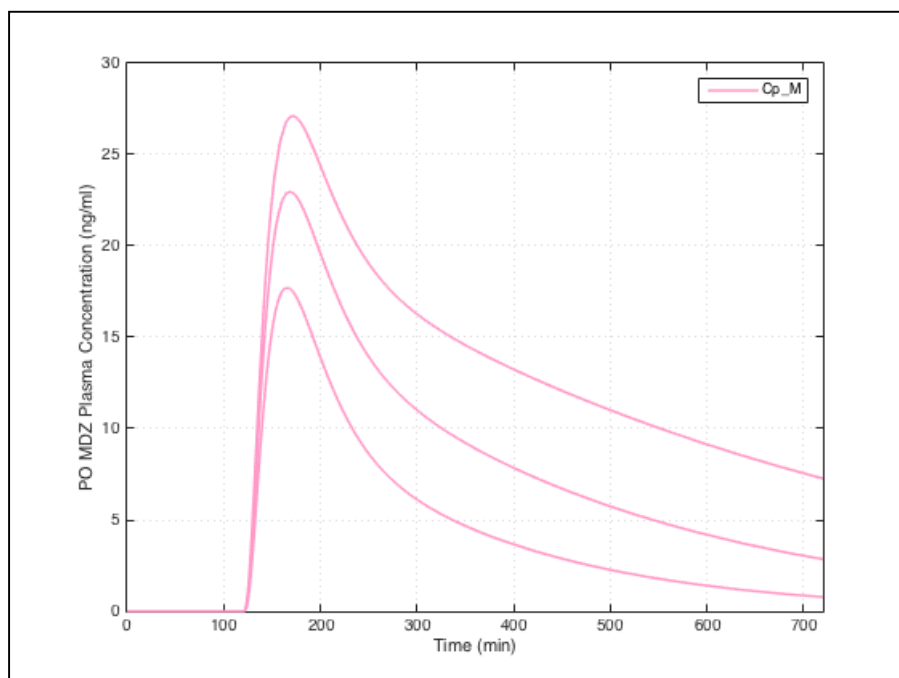


Figure E.25 Sensitivity analysis of PO MDZ plasma concentrations in presence of PO FLZ to the change in $K_{p,hep}^{MDZ}$. (top line: $K_{p,hep}^{MDZ} = 0.55$; middle line: $K_{p,hep}^{MDZ} = 1.09$; bottom line: $K_{p,hep}^{MDZ} = 2.18$)

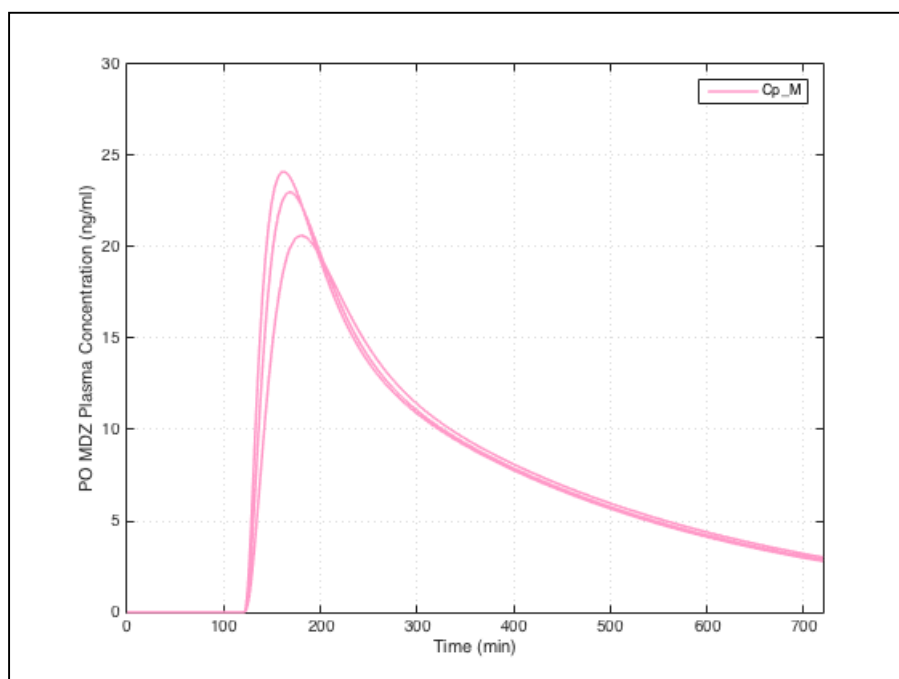


Figure E.26 Sensitivity analysis of PO MDZ plasma concentrations in presence of PO FLZ to the change in $K_{p,GW}^{MDZ}$. (line with highest c_{max}^{MDZ} : $K_{p,GW}^{MDZ} = 0.56$; line with middle c_{max}^{MDZ} : $K_{p,GW}^{MDZ} = 1.12$; line with lowest c_{max}^{MDZ} : $K_{p,GW}^{MDZ} = 2.24$)

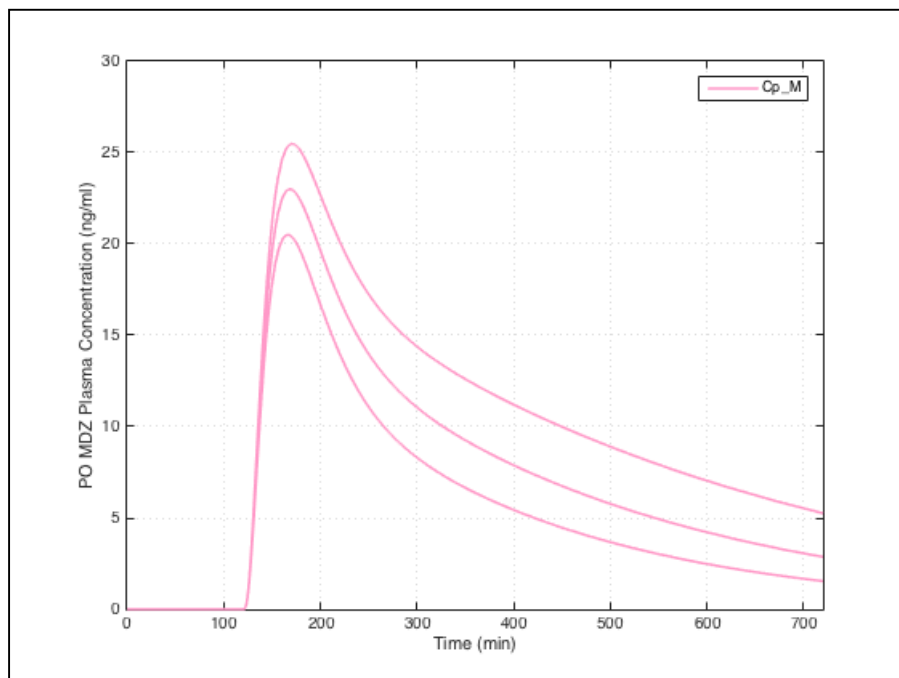


Figure E.27 Sensitivity analysis of PO MDZ plasma concentrations in presence of PO FLZ to the change in $K_{p,hep}^{FLZ}$. (top line: $K_{p,hep}^{MDZ} = 2.0$; middle line: $K_{p,hep}^{MDZ} = 1.0$; bottom line: $K_{p,hep}^{MDZ} = 0.5$)

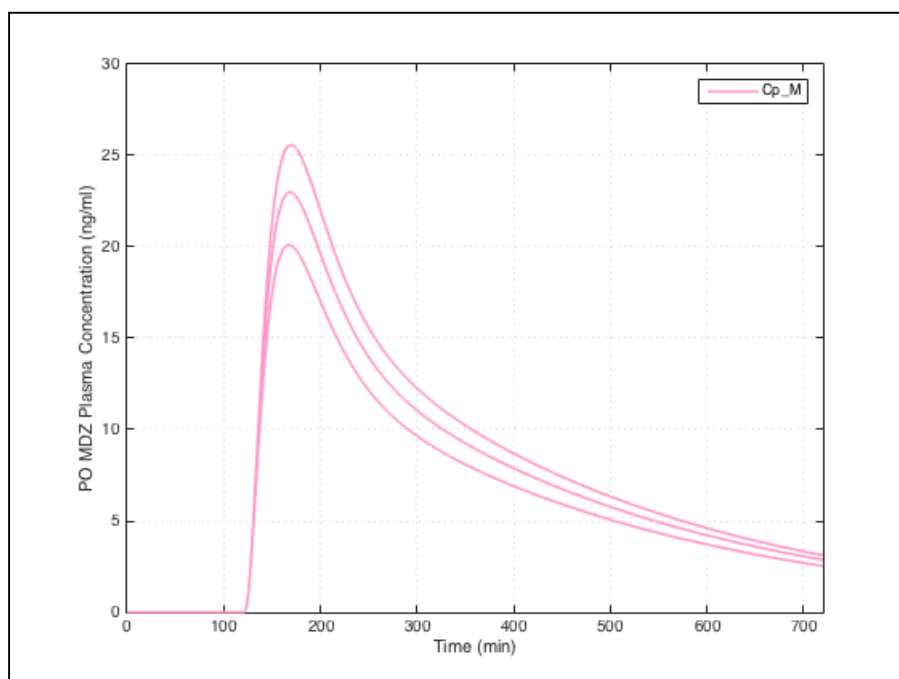


Figure E.28 Sensitivity analysis of PO MDZ plasma concentrations in presence of PO FLZ to the change in $K_{p,GW}^{FLZ}$. (top line: $K_{p,GW}^{FLZ} = 2.0$; middle line: $K_{p,GW}^{FLZ} = 1.0$; bottom line: $K_{p,GW}^{FLZ} = 0.5$)

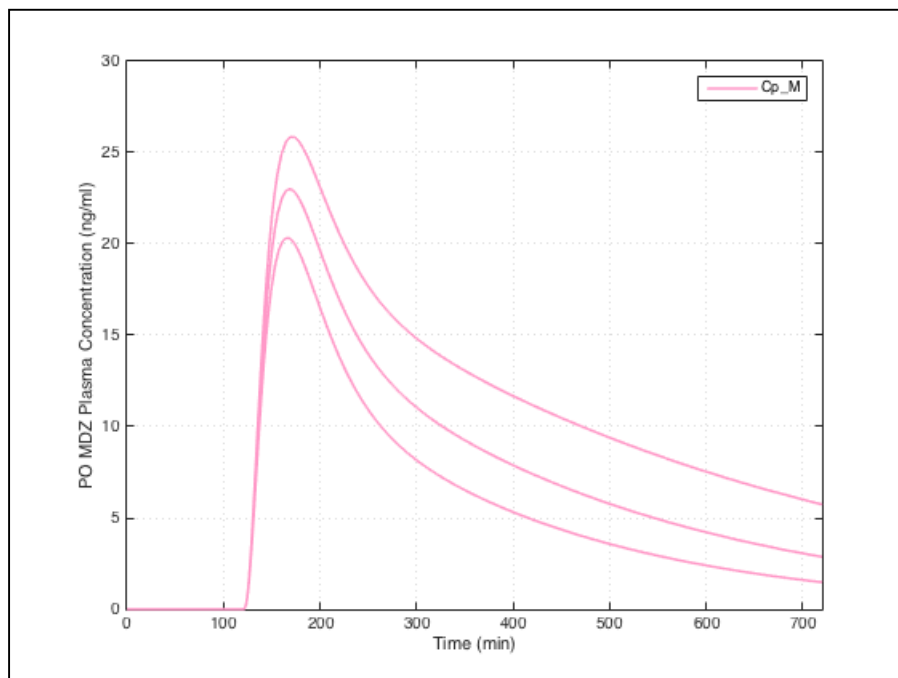


Figure E.29 Sensitivity analysis of PO MDZ plasma concentrations in presence of PO FLZ to the change in $K_{i,hep}^{FLZ}$. (top line: $K_{i,hep}^{MDZ} = 1915$ ng/ml; middle line: $K_{i,hep}^{MDZ} = 3829$ ng/ml; bottom line: $K_{i,hep}^{MDZ} = 7658$ ng/ml)

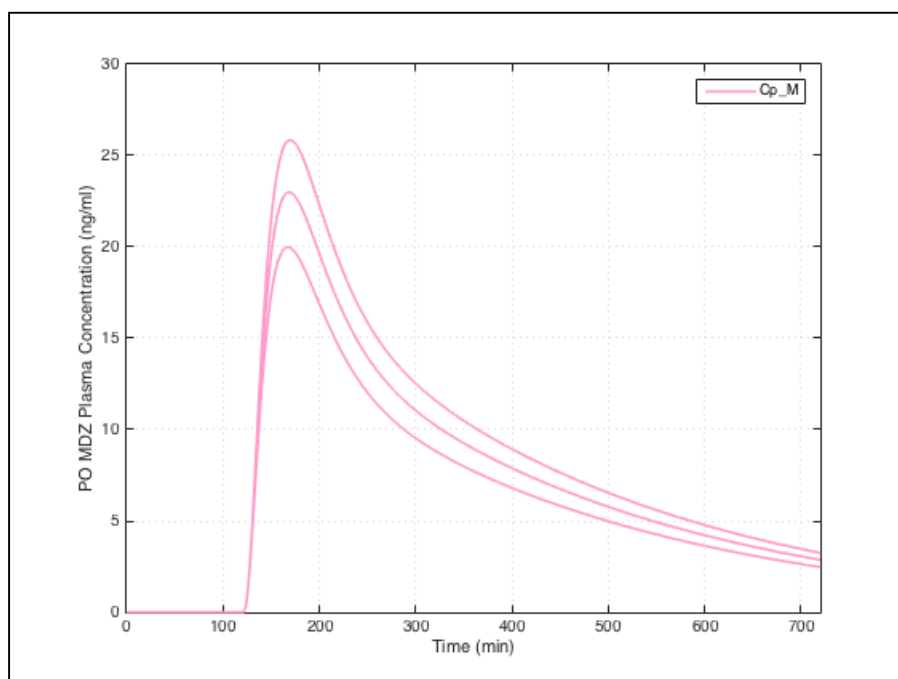


Figure E.30 Sensitivity analysis of PO MDZ plasma concentrations in presence of PO FLZ to the change in $K_{i,GW}^{FLZ}$. (top line: $K_{i,GW}^{MDZ} = 1591$ ng/ml; middle line: $K_{i,GW}^{MDZ} = 3182$ ng/ml; bottom line: $K_{i,GW}^{MDZ} = 6364$ ng/ml)

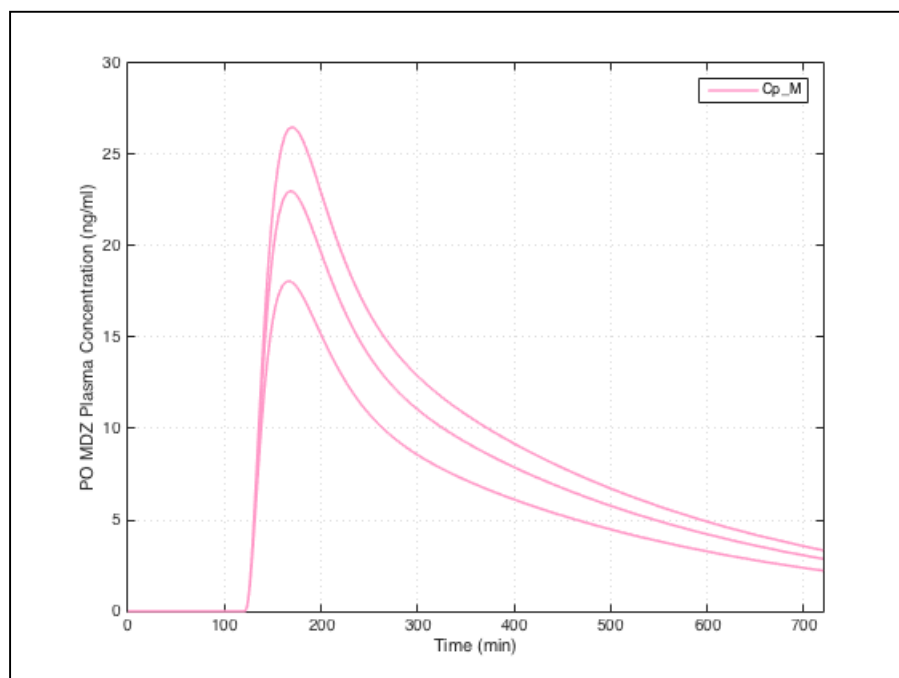


Figure E.31 Sensitivity analysis of PO MDZ plasma concentrations in presence of PO FLZ to the change in f_{villi} . (top line: $f_{villi} = 1.1$; middle line: $f_{villi} = 2.2$; bottom line: $f_{villi} = 4.4$)

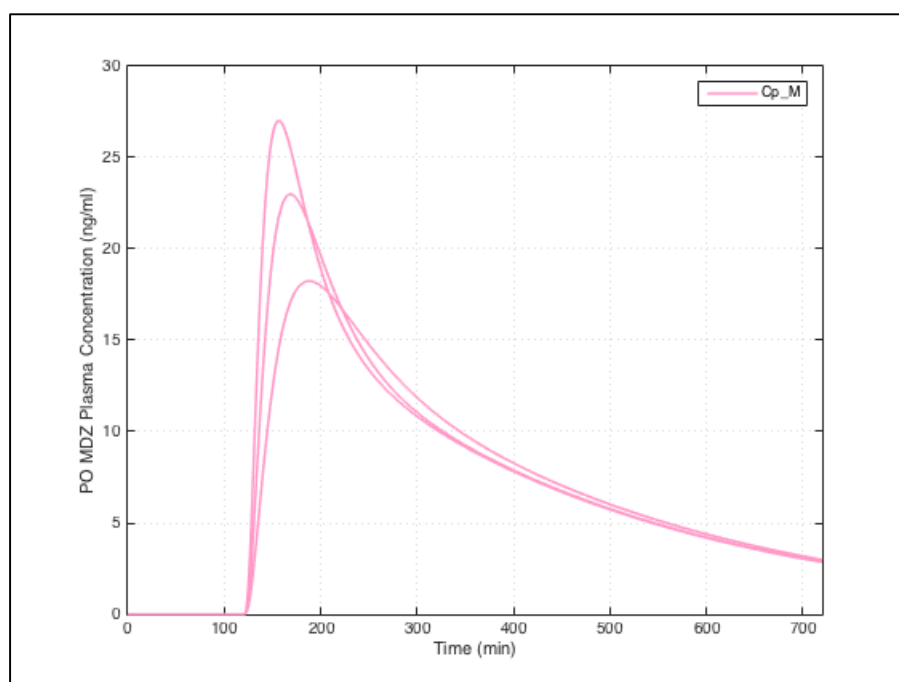


Figure E.32 Sensitivity analysis of PO MDZ plasma concentrations in presence of PO FLZ to the change in k_{GL}^{MDZ} . (line with highest c_{max}^{MDZ} : $k_{GL}^{MDZ} = 0.1$; line with middle c_{max}^{MDZ} : $k_{GL}^{MDZ} = 0.05$; line with lowest c_{max}^{MDZ} : $k_{GL}^{MDZ} = 0.025$)

F. ESTIMATION OF SATURABLE (SPECIFIC) PLASMA PROTEIN BINDING

PARAMETERS OF ERY

F.1. Control profile of hyperbolic binding model (using ADAPT)

```

CC
C-----C
C Enter as Indicated                      C
C--c-----C

NDEqs = 0 ! Enter # of Diff. Eqs.
NSParam = 2 ! Enter # of System Parameters.
NVparam = 0 ! Enter # of Variance Parameters.
NSecPar = 0 ! Enter # of Secondary Parameters.
NSecOut = 0 ! Enter # of Secondary Outputs (not used).
Ieqsol = 3 ! Model type: 1 - DIFFEQ, 2 - AMAT, 3 - OUTPUT only.
Descr = 'ERY Binding Model - Cb-Cu '

CC
C-----C
C Enter Symbol for Each System Parameter (eg. Psym(1)='Kel')    C
C--c-----C
    PSym(1) = 'Bmax'
    PSym(2) = 'BC50'

CC
C-----C
C Enter Output Equations Below {e.g. Y(1) = X(1)/P(2)}    C
C--c-----C

Y(1) = P(1)*t/(P(2)+t)

```

F.2. Control profile of Sigmoidal binding model (using ADAPT)

```

CC
C-----C
C Enter as Indicated                               C
C---c-----C

NDEqs = 0 ! Enter # of Diff. Eqs.
NSParam = 3 ! Enter # of System Parameters.
NVparam = 2 ! Enter # of Variance Parameters.
NSecPar = 0 ! Enter # of Secondary Parameters.
NSecOut = 0 ! Enter # of Secondary Outputs (not used).
Ieqsol = 3 ! Model type: 1 - DIFFEQ, 2 - AMAT, 3 - OUTPUT only.
Descr = 'ERY Binding Model - Cb-Cu--add n '

CC
C-----C
C Enter Symbol for Each System Parameter (eg. Psym(1)='Kel')    C
C---c-----C
    PSym(1) = 'Bmax'
    PSym(2) = 'BC50'
    PSym(3) = 'n'

CC
C-----C
C Enter Output Equations Below {e.g. Y(1) = X(1)/P(2) }    C
C---c-----C

Y(1) = P(1)*(t**P(3))/(P(2)**P(3)+t**P(3))

```


F.3. *In-vitro* total binding data digitized from Detta et al. (Dette et al., 1982)

$C_u(\mu\text{M})$	$C_{\text{bo-total}}(\mu\text{M})$
0.37	0.79
0.50	1.20
0.68	1.81
0.68	1.67
0.93	2.43
1.18	2.67
1.24	3.04
1.43	3.38
1.62	3.72
1.68	4.07
1.80	4.41
2.24	5.09
2.30	5.30
3.12	6.42
3.68	7.55
4.25	8.30
4.44	7.93
9.95	11.87
10.20	12.42
16.76	14.39
17.01	14.59
17.33	14.63

F.4. *In-vitro* non-specific binding data digitized from Detta et al. (Dette et al., 1982)

$C_u(\mu\text{M})$	$C_{\text{bo-ns}}(\mu\text{M})$
0.38	0.10
1.97	0.48
4.33	1.35
10.18	3.28
16.82	4.29

G. ESTIMATION OF $V_{B,U}^{ERY}$, $V_{P,U}^{ERY}$ AND $Q_{2,U}^{ERY}$

In order to estimate PK parameters of unbound ERY in the blood, all measurements from study 611 were digitized and corrected by f_u^{ERY} at corresponding total ERY concentration (using equation (7.24)), and blood-to-plasma partition ratio ($B:P^{ERY} = 0.85$), as shown in equation (G.1)

$$C_{b,u}^{ERY} = C_{p,t}^{ERY} \cdot f_u^{ERY} \cdot B:P^{ERY} \quad (G.1)$$

$C_{b,u}^{ERY}$ is ERY unbound blood concentration and $C_{p,t}^{ERY}$ is ERY total plasma concentration reported in study 611(Austin et al., 1980b). Observed total plasma concentrations and calculated fraction unbound, unbound plasma, unbound blood, and SD of total plasma concentrations at different dose levels were presented in **Table G.1**.

Table G.1 Observed total plasma concentrations and calculated fraction unbound, unbound plasma, unbound blood, and SD of total plasma concentrations at different dose levels.

125mg 15min IV infusion (Regimen 2)

Time (hr)	$C_{p,t}$ (mg/L)	f_u	$C_{p,u}$ (mg/L)	$C_{b,u}$ (mg/L)	SD(mg/L)
0.28	7.26	0.36	2.59	2.20	0.00
0.52	2.38	0.29	0.70	0.59	0.00
0.76	1.47	0.30	0.45	0.38	0.00
1.02	0.99	0.32	0.31	0.27	0.19
1.28	0.87	0.32	0.28	0.24	0.00
1.52	0.67	0.33	0.22	0.19	0.17
1.78	0.61	0.34	0.21	0.17	0.07
2.03	0.64	0.33	0.21	0.18	0.07
2.53	0.50	0.35	0.17	0.15	0.12
3.03	0.36	0.36	0.13	0.11	0.00
3.53	0.29	0.37	0.11	0.09	0.14
4.02	0.21	0.39	0.08	0.07	0.00
4.52	0.14	0.42	0.06	0.05	0.07
5.02	0.11	0.43	0.05	0.04	0.00
6.02	0.05	0.46	0.02	0.02	0.04
7.02	0.02	0.50	0.01	0.01	0.00

250mg 15min IV infusion (Regimen 2)

Time (hr)	C _{p,t} (mg/L)	f _u	C _{p,u} (mg/L)	C _{b,u} (mg/L)	SD(mg/L)
0.28	10.11	0.36	3.67	3.12	3.61
0.52	5.24	0.30	1.57	1.34	1.72
0.75	3.31	0.29	0.96	0.82	0.00
1.00	2.55	0.29	0.74	0.63	0.00
1.29	2.49	0.29	0.73	0.62	1.06
1.52	2.49	0.29	0.73	0.62	0.62
1.78	1.96	0.30	0.58	0.49	0.00
2.03	1.75	0.30	0.52	0.44	0.52
2.53	1.01	0.31	0.32	0.27	0.11
3.02	1.06	0.31	0.33	0.28	0.66
3.54	0.95	0.32	0.30	0.26	0.00
4.02	0.78	0.32	0.25	0.22	0.27
4.53	0.55	0.34	0.19	0.16	0.03
5.02	0.30	0.37	0.11	0.09	0.05
6.00	0.16	0.40	0.07	0.06	0.01
7.07	0.09	0.43	0.04	0.03	0.06

500mg 15min IV infusion (Regimen 2)

Time (hr)	C _{p,t} (mg/L)	f _u	C _{p,u} (mg/L)	C _{b,u} (mg/L)	SD(mg/L)
0.26	17.89	0.48	8.60	7.31	0.00
0.54	7.46	0.32	2.42	2.06	0.00
0.75	5.26	0.30	1.58	1.34	0.00
1.02	3.32	0.29	0.96	0.82	1.03
1.30	3.33	0.29	0.97	0.82	0.00
1.51	2.92	0.29	0.85	0.72	1.25
1.78	3.72	0.29	1.08	0.92	0.00
2.04	2.40	0.29	0.70	0.60	1.21
2.52	2.40	0.29	0.70	0.60	0.82
3.04	2.11	0.29	0.62	0.53	0.00
3.56	2.26	0.29	0.66	0.56	0.61
4.04	2.16	0.29	0.64	0.54	0.78
4.52	1.74	0.30	0.52	0.44	0.63
5.04	1.15	0.31	0.36	0.30	0.32
6.01	0.70	0.33	0.23	0.20	0.36
7.04	0.40	0.36	0.14	0.12	0.00

900mg 15min IV infusion (Regimen 2)

Time (hr)	C _{p,t} (mg/L)	f _u	C _{p,u} (mg/L)	C _{b,u} (mg/L)	SD(mg/L)
0.12	20.85	0.51	10.73	9.12	0.00
0.28	29.61	0.59	17.35	14.75	0.00
0.54	13.77	0.42	5.81	4.94	4.01
0.75	8.15	0.33	2.72	2.31	0.00
1.06	8.90	0.34	3.07	2.61	0.00
1.26	8.91	0.34	3.07	2.61	4.43
1.54	7.16	0.32	2.30	1.95	0.00
1.78	7.17	0.32	2.30	1.95	0.00
2.04	9.33	0.35	3.27	2.78	6.89
2.56	6.03	0.31	1.85	1.58	0.00
3.02	5.78	0.30	1.76	1.50	3.98
3.56	4.35	0.29	1.28	1.09	0.00
4.04	3.50	0.29	1.02	0.87	2.24
4.56	3.43	0.29	1.00	0.85	0.00
5.04	2.42	0.29	0.71	0.60	1.70
6.02	1.91	0.30	0.57	0.48	0.00
7.02	1.50	0.30	0.45	0.39	1.02

250mg 3min IV infusion (Regimen 1)

Time (hr)	C _{p,t} (mg/L)	f _u	C _{p,u} (mg/L)	C _{b,u} (mg/L)	SD(mg/L)
0.11	9.39	0.35	3.31	2.81	3.52
0.25	5.15	0.30	1.54	1.31	1.61
0.50	3.42	0.29	0.99	0.85	0.90
0.76	2.89	0.29	0.84	0.71	0.79
1.02	2.33	0.29	0.68	0.58	0.56
1.26	2.01	0.30	0.59	0.50	0.69
1.50	1.93	0.30	0.57	0.48	0.63
1.75	1.73	0.30	0.52	0.44	0.67
2.01	1.49	0.30	0.45	0.38	0.60
2.49	1.21	0.31	0.37	0.32	0.41
2.99	1.18	0.31	0.37	0.31	0.31
3.50	0.68	0.33	0.23	0.19	0.27
4.02	0.57	0.34	0.19	0.17	0.28
4.51	0.42	0.36	0.15	0.13	0.19
5.01	0.30	0.37	0.11	0.09	0.17
6.00	0.17	0.40	0.07	0.06	0.10
7.01	0.10	0.43	0.04	0.04	0.08

Model estimation was performed by ADAPT 5 (BMSR Biomedical Simulations Resource, available at <https://bmsr.usc.edu/software/adapt/>). Model control file was presented below.

Model Control Profile:

```

CC
C-----C
C Enter as Indicated          C
C---c-----C

NDEqs = 2 ! Enter # of Diff. Eqs.
NSParam = 4 ! Enter # of System Parameters.
NVparam = 2 ! Enter # of Variance Parameters.
NSecPar = 3 ! Enter # of Secondary Parameters.
NSecOut = 0 ! Enter # of Secondary Outputs (not used).
Ieqsol = 1 ! Model type: 1 - DIFFEQ, 2 - AMAT, 3 - OUTPUT only.
Descr = 'ERY IV PK Modeling '

CC
C-----C
C Enter Symbol for Each System Parameter (eg. Psym(1)='Kel')    C
C---c-----C
  Psym(1)='V1'
  Psym(2)='V2'
  Psym(3)='CL'
  Psym(4)='Q'

CC
C-----C
C Enter Symbol for Each Variance Parameter {eg: PVsym(1)='Sigma'}  C
C---c-----C
  PVsym(1)='SDinter'
  PVsym(2)='SDslope'

CC
C-----C
C Enter Symbol for Each Secondary Parameter {eg: PSsym(1)='CLt'}  C
C---c-----C
  PSsym(1)='k10'
  PSsym(2)='k12'
  PSsym(3)='k21'

C-----C
C-----C
C

Return
End

CC
C-----C
C Enter Differential Equations Below {e.g. XP(1) = -P(1)*X(1)}  C
C---c-----C
  XP(1)=-P(3)/P(1)+P(4)/P(1))*X(1)+P(4)/P(2)*X(2)+R(1)
  XP(2)=P(4)/P(1)*X(1)-P(4)/P(2)*X(2)
C-----C
C-----C
C

Return

```

End

CC

C-----C

C Enter Output Equations Below {e.g. $Y(1) = X(1)/P(2)$ } C

C-----C

$$Y(1) = X(1)/P(1)$$

CC

C-----C

C Enter Variance Model Equations Below C

C {e.g. $V(1) = (PV(1) + PV(2)*Y(1))^{**2}$ } C

C-----C

$$V(1) = (PV(1) + PV(2)*Y(1))^{**2}$$

C-----C

C-----C

C

Return

End

.....

The final estimates of central, peripheral compartment volume of distribution and inter-compartmental clearance from the two compartmental model fit ($V_{1,u}$, $V_{2,u}$ and $Q_{2,u}$) were averaged across the four doses in regimen 2, to come up with distribution parameters across doses (shown in **Table G.2**). Parameter estimates from regimen 1 data (250mg ERY 3min IV infusion) were also demonstrated in **Table G.2**, but not included in calculating final $V_{B,u}^{ERY}$, $V_{P,u}^{ERY}$ and $Q_{2,u}^{ERY}$ values in semi-PBPK model, because PK profiles with different infusion time may lead to different parameter estimates.

Table G.2 PK parameters estimated from two-compartmental model fit of unbound blood concentrations in study 611.

Parameters (CV%)	125mg (Regimen 2)	250mg (Regimen 2)	500mg (Regimen 2)	900mg (Regimen 2)	250mg (Regimen 1)	Average of regimen 2
$V_{1,u}$ (ml/kg)	408 (2.5%)	715 (4.0%)	523 (4.2%)	517 (6.3%)	715 (3.7%)	541
$V_{2,u}$ (ml/kg)	1385 (6.2%)	1589 (7.8%)	2812 (13%)	1990 (18%)	2103 (3.6%)	1944
CL_u (ml/min/kg)	22.2 (2.3%)	20.9 (3.7%)	19.5 (7.1%)	15.4 (11%)	25.4 (2.2%)	
$Q_{2,u}$ (ml/min/kg)	26.9 (3.3%)	38.1 (6.9%)	36.9 (5.2%)	34.6 (10%)	75 (2.8%)	34.1

In the semi-PBPK model, physiological volumes of GW, portal vein and liver should be excluded from the estimated $V_{1,u}$ or $V_{2,u}$. Portal vein and liver were presumably included in central compartment, and GW volume was presumably incorporated into peripheral compartment. The final parameters used in ERY semi-PBPK model were demonstrated in **Table G.3**. $Q_{2,u}^{MDZ}$ was not affected by the perfusion to physiological compartments.

Table G.3 Final systemic distribution parameters used in ERY semi-PBPK model.

Parameters	Values	Source
$V_{B,u}^{ERY}$ (ml/kg)	479	Model estimated $V_{1,u} - V_{PV} - K_{p,hep,u}^{ERY} \cdot V_{hep}$
$V_{P,u}^{ERY}$ (ml/kg)	1853	Model estimated $V_{2,u} - K_{p,GW,u}^{ERY} \cdot V_{GW}$
$Q_{2,u}^{ERY}$ (ml/min/kg)	34.1	Model estimated $Q_{2,u}$

H. ERY META-ANALYSIS

H.1. Meta-analysis of IV ERY studies

Study ID	ERY Dosing Regimen			ERY Exposure Metrics		Non-compartmental Analysis Parameters							
	ERY Route	Dose	Formulation	AUC _{IV} ^{ERY}	SD of AUC _{IV} ^{ERY}	f _u ^{ERY}	CL _{ren} ^{ERY}	CL _{tot,p} ^{ERY}	CL _{tot,b} ^{ERY}	CL _{int,hep}	V _{ss} ^{ERY}	t _{1/2} ^{ERY}	MRT ^{ERY}
		[mg]		[mg/L*hrs]	[mg/L*hrs]	%	ml/min/kg	ml/min/kg	ml/min/kg	ml/min/kg	mL/kg	hr	hr
611	IV	250	ERY Lactobionate (Abbott Lab)	9.3			0.8	7±2.5	7.3	11.1	693±190	1.5±0.3	
611	IV	125	ERY Lactobionate (Abbott Lab)	4.6	0.9		0.4	7±1.5	7.8	12.2	493±67	1.3±0.1	
611	IV	250	ERY Lactobionate (Abbott Lab)	10.5	3		0.3	7.2±3.6	8.1	13.1	603±375	1.3±0.2	
611	IV	500	ERY Lactobionate (Abbott Lab)	19.4	3.3		0.6	6.2±1.1	6.6	9.5	1031±167	2.4±0.4	
611	IV	900	ERY Lactobionate (Abbott Lab)	41	23.1		1.1	6.2±2.8	6.0	8.3	1088±377	2.4±0.4	
612	IV	500	ERY Lactobionate (Abbott Lab)			30.5±2.8	1.2	8.9±3.2	9.1	15.7	900±231	1.4±0.4	
613	IV	1000	ERY Lactobionate	41.63	1.79			5.7	6.1	8.4			
616	IV	125		3.58	1.02	27±5	0.5±0.17	8.8±2.2	9.8	18.0	740±190	2.3±1.03	1.41±0.3
617	IV	0.1	ERY powder	0.004	0.003			5.21 (76.4%)	5.5	7.4	1140 (68%)	2.52 (34.6%)	
619	IV	500	ERY lactobionate (Abbott)					9.10	9.6	17.5	770	1.6	
624	IV	240	ERY lactobionate (Abbott)	12.2	4.4			6.42±2.33	6.8	10.0	450±150	1.54	1.19

Study ID	Compartmental Analysis Parameters					Study Design			Demographics					
	No. of Comp	V_1^{ERY}	V_2^{ERY}	k_{10}^{ERY}	k_{12}^{ERY}	k_{21}^{ERY}	Fast	Sample size	Crossover	Infusion time	Age	Weight	Gender	Race
		ml/kg	ml/kg	hr ⁻¹	hr ⁻¹	hr ⁻¹	(Yes=1, No=0)		(Yes=1, No=0)	[min]	[yrs]	[kg]	(M: Male; F: Female) M/F	(AA: African American; C: Caucasian; AP: Asian Pacific)
611	2	260±140	434				1	24	0	3	19.2±1.4	64±9.4	12/12	
611	2	154±28	339				1	5	1	15	19-20	66.98	3/2	
611	2	278±263	325				1	5	1	15	19-20	66.98	3/2	
611	2	263±70	768				1	4	1	15	19-20	68.175	3/1	
611	2	444±414	644				1	3	1	15	19	70.5	2/1	
612	2							6	0	30	24.5±1.6	64±7.2	5/1	
613	2 or 3			0.78	0.49	0.84		6	0	60	21.8±0.31	63.7±2.4		
616							1	12		30	44.8±8.5	75±19.4	6/6	7/2/3 (AA/C/AP)
617							1	30	0	30	18-80		24/6	
619	2	450	320				1	6		60	23-31		2/4	
624	2						0	6	1	30	20-21	60.7	3/3	

Study ID	Sample Analysis			Comments
	Sample time points	Assay method	LLOQ	
	[h]		[ng/ml]	
611	0.125,0.25,0.5,0.75,1,1.25,1.5,1.75,2,2.5,3,3.5,4.5,5,6,7	Bioassay using Sarcina lutea		V ₁ ^{ERY} and CL _{tot,p} ^{ERY} were significantly different between males and females; t _{1/2} ^α and t _{1/2} ^β were provided.
611	0.125,0.25,0.5,0.75,1,1.25,1.5,1.75,2,2.5,3,3.5,4.5,5,6,7	Bioassay using Sarcina lutea		
611	0.125,0.25,0.5,0.75,1,1.25,1.5,1.75,2,2.5,3,3.5,4.5,5,6,7	Bioassay using Sarcina lutea		
611	0.125,0.25,0.5,0.75,1,1.25,1.5,1.75,2,2.5,3,3.5,4.5,5,6,7	Bioassay using Sarcina lutea		
611	0.125,0.25,0.5,0.75,1,1.25,1.5,1.75,2,2.5,3,3.5,4.5,5,6,7	Bioassay using Sarcina lutea		
612	0.1,0.2,0.3,0.4,0.5 during infusion and 0.083, 0.167,0.25,0.5,0.75,1,1.5,2,3,4,6,9,12 after infusion	Bioassay using Sarcina lutea	70	Mean serum AAG levels = 10.3 ± 2.1 μmol/L in normal subjects
613	0.25,0.5,0.75,1,1.5,2,3,4,6,8,12,16,20,24	Bioassay using Sarcina lutea		Not sure if dose of ERY base was 1000 mg or dose of lactobionate was 1000 mg; Didn't mention reported AUC values were AUC _{0-∞} or AUC _{0-t} ; Macro-rate constants (A and B) after 2-compartmental model fit were provided.
616	0.5,1,1.5,2,4,6,8,10,12,14,24	LC-MS	1.5	
617		HPLC-AMS (Accelerator Mass Spectrometry)	0.01	
619	0.25,0.5,0.75,1,1.5,2,2.5,3,4,5,6,7,8,8,10,11,12	Bioassay using Sarcina lutea	100	α and β were provided.
624	0.167,0.33,0.5,0.58,0.67,0.83,1,1.25,1.5,2,2.5,3.5,4.5,5.5,6.5	Bioassay using Micrococcus luteus	100	

H.2. Meta-analysis of PO ERY studies

Study ID	ERY Dosing Regimen			ERY Exposure Metrics					
	ERY Route	Dose	Formulation	AUC _{IV} ^{ERY}	SD of AUC _{IV} ^{ERY}	C _{max} ^{ERY}	SD of C _{max} ^{ERY}	t _{max} ^{ERY}	t _{max} ^{ERY} range
		[mg]		[mg/L*hrs]	[mg/L*hrs]	µg/ml	µg/ml	hr	hr
604	PO	250	SS	1.3		0.371	0.1-0.64	2	1.5-5
604	PO	1000	SS	16.2		3	2.0-3.9	1.38	0.5-4
614	PO	500	SS (Abbott)	5.6	0.4	1.3	0.1	2	
614	PO	500	SS (Abbott)	7.2	0.8	2.8	0.3	1	
614	PO	500mg q8h for 7 days	SS (Abbott)	12.4	1.7	2.9	0.5	1.5	
614	PO	500	ERY base (Lilly)	4.6	0.7	1.2	0.2	4	
614	PO	500	ERY base (Lilly)					Vareid	
614	PO	500mg q8h for 7 days	ERY base (Abbott)	Varied					
615	PO	250mg q6h for 5 doses	SS						
616	PO	250		1.0	0.7	0.45	0.30	0.92	±0.56
617	PO	250	ERY-SS 250 granulate suspension (Abbott)	1.6	0.6	0.72	0.27	0.45	22.30%
618	PO	500mg q8h for 5 days	SS (Erythromcin, Abbott Lab)	7.2	3.6	1.45	0.87		
619	PO	500	EC						
620	PO	250	EC	4.5	1.7	1.9	0.8	1.5-2.5	
620	PO	500	EC	11.2	4.3	3.8	1.4	1.5-2.5	
620	PO	1000	EC	27.2	10.6	6.5	2.9	1.5-2.5	
620	PO	500	SS	7.5	3.4	2.9	1.7	1.5-2.5	
621	PO	500	EC	9.0	5.9	1.5	0.91	6.3	6-8
622	PO	500	SS	8.3	0.8	2	0.3	2	
622	PO	500	SS	7.5	1.2	2.2	0.4	1.5	
622	PO	500	EC	10.6	1.1	1.5	0.5	4	1.5-10
622	PO	500	EC	8.8	1.2	1.5	0.2	5	
623	PO	250	EC	4.7	2.0	1.74	0.9	2.85	0.54
623	PO	250mg q6h for 5 days	EC	10.8	3.4	2.87	0.83	3.11	1
624	PO	271	duodenal solution	5.0	1.3	2.3	0.55	0.25	0.08
624	PO	250	EC	4.1	2.2	1.66	0.79	2.92	0.53
625	PO	1000	SS	29.1	4.7	8	1.3	1.5	0.2
625	PO	1000mg q12h for 4 days		25.1	4.8	6.8	0.7	2	0.2
626	PO	250	SS	1.0	0.3	0.41	0.34	2.1	0.6
626	PO	250	EC	2.9	1.8	1.18	0.73	2.7	1.3
626	PO	250mg q6h for 5 doses	SS	4.1	2.6	1.38	0.87	2.1	0.6
626	PO	250mg, q6h for 5 doses	EC	7.9	2.2	2.59	0.76	2.1	0.3

627	PO	250	SS	2.2	0-5.9	1.1	0-3.3	2.1	1-6
627	PO	250	EC	0.5	0-5.5	0.4	0-2.2	3	1.2-6
627	PO	250mg q6h for 9 doses	SS	5.7	1.6-16.6	2.7	0.6-7.3	2	1.3-3.5
627	PO	250mg q6h for 9 doses	EC	3.5	0.5-11.1	1.4	0.2-4.9	3	0.75-6
628	PO	500	SS	4.7	1.6	1.23	0.37	2.92	0.49
629	PO	250mg q6h for 10 doses	EC						
629	PO	400mg q6h for 10 doses	ERY ethylsuccinate						
630	PO	7.5mg/kg	ERY piopionate capsules	27.7	5.1	4.07	0.29		
630	PO	7.5mg/kg	SS	2.1?	0.43?	2.15?	0.14?		
631	PO	250	ERY acistrate (EA)	1.9	0.4	0.46	0.07	1.3	0.3
631	PO	250	ERY stearate (ES)	4.5	1.0	0.93	0.23	2.6	0.4
631	PO	250	EC	5.8	0.5	1.6	0.1	3.3	0.4
632	PO	500	SS	6.4	2.2	0.66	0.18	2.79	0.56
633	PO	500	SS (Resibion®)	12.2	3.0	3.35	0.85	2.5	0.3
633	PO	500	SS (Erythrocin®)	17.9	4.9	3.86	0.67	2.3	0.4

Study ID	Non-compartmental Analysis Parameters									Compartmental Analysis Parameters				
	f_u^{ERY}	CL_{ren}^{ERY}	$CL_{tot,p}^{ERY}/F_{oral}^{ERY}$	$t_{1/2}^{ERY}$	MRT^{ERY}	F_{oral}^{ERY}	ER_{hep}^{ERY}	F_{hep}^{ERY}	$F_{abs}^{ERY} \cdot F_{GI}^{ERY}$	No. of Comp	k_a^{ERY}	V_1^{ERY}	V_2^{ERY}	k_{21}^{ERY}
	%	ml/min/kg	ml/min/kg	hr	hr	%	%	%	%		h^{-1}	ml/kg	hr^{-1}	
604			92.6	2.25 (1.78-2.72)										
604			17.7	2.79 (2.42-3.16)										
614				1.8										
614				1.2										
614				2.1										
614				2.5							308.2			
614											471.7			
615														
616	27±5			2.86±1.27	1.52±0.56	15±6	46%	50%±10%	33%±30%					
617				2.50 (17.6%)		14%	26%	74%	19%					
618	28±4			2.8	0.6						1.07			
619				2		34.90%	45%	55%	63%					
620	0.65±0.26			2±2						2	3.2±1.3			
620	0.76±0.35			2.5±1.0						2	4.3±2.2			
620	0.63±0.30			3.0±1.7						2	3.2±1.8			
620	0.59±0.24			2.7±2.3						2	2.3±0.7			
621				3.4						2	1		0.163±0.058	
622				2.5										
622				1.9										
622				1.9										
622				1.6										
623				1.53±0.42										
623														
624					2.17±0.46	43%±14%	32%	68%	63%					
624					3.28±0.28	32%±7%	32%	68%	47%					
625				10.7±2.3	2.6±0.3									
625				11.5±1.8	2.3±0.2									
626	0.59±0.51									1	3			
626	0.41±0.11									1	2.2			
626	0.36±0.14									1	1.9			
626	0.40±0.13									1	1.7			

627			
627			
627			
627			
628		1.18±0.19	
629			
629			
630		5.22±0.86	
630		6.61±0.95	
631		2.5±0.6	
631		1.5±0.1	
631		1.5±0.1	
632		1.57±0.33	
633	0.41±0.06	1.43±0.08	
633	0.37±0.05	1.78±0.16	

Study ID	Study Design			Demographics				Sample Analysis			Comments		
	Fast	Sample size	Cross-over	Age	Weight	Gender	Race	Oral contraceptives	Sample time points	Assay method		LLOQ	
	Yes=1, No=0	Yes=1, No=0		[yrs]	[kg]	M/F		Yes = 1, No = 0	[h]			ng/ml	
604		8	0	28±7				9/7	1	0.25,0.5,1,1.5,2,2.5,3,4,6,8	LC-MS	1	Auto-inhibition of ERY clearance
604		8	0	28±7				9/7	1	0.25,0.5,1,1.5,2,2.5,3,4,6,8	LC-MS	1	
614	1	15	1	22-30	66.7 (52-88)	9/6		3 out of 5		0.5,1,1.52,2.5,3,4,6,7.5	Bioassay using Sarcina lutea	200	Food delays the release of drug from the enteric coated tablets, but the absorption is not prevented
614	0	15	1	22-30	66.7 (52-88)	9/6		3 out of 5		0.5,1,1.52,2.5,3,4,6,7.5	Bioassay using Sarcina lutea	200	
614	0	15	1	22-30	66.7 (52-88)	9/6		3 out of 5		0.5,1,1.52,2.5,3,4,6,7.5	Bioassay using Sarcina lutea	200	
614	1	15	1	22-30	66.7 (52-88)	9/6		3 out of 5		0.5,1,1.52,2.5,3,4,6,7.5	Bioassay using Sarcina lutea	200	
614	0	15	1	22-30	66.7 (52-88)	9/6		3 out of 5		0.5,1,1.52,2.5,3,4,6,7.5	Bioassay using Sarcina lutea	200	
614	0	15	1	22-30	66.7 (52-88)	9/6		3 out of 5		0.5,1,1.52,2.5,3,4,6,7.5	Bioassay using Sarcina lutea	200	
615	0	12						12/0		0.5,1,1.5,2,3,4,6	Bioassay using Sarcina lutea		Both single and multiple doses profiles were available
616	1	12		44.8±8.5	75±19.4	6/6	7/2/3 (AA/C/AP)			0.5,1,1.5,2,4,6,8,10,12,14,24	LC-MS	1.47	
617	1	30	0	18-80		24/6					LC-MS	0.01	
618		6		20-32	52-75	2/4				0.167,0.33,0.5,0.75,1,1.5,2,2.5,3,4,6,8,12,24	Bioassay using Sarcina lutea		C_{max}^{ERY} $C_{ss,max}^{ERY}$
619	1	6		23-31		2/4				0.25,0.5,0.75,1,1.5,2,2.5,3,4,5,6,7,8,8,10,11,12	Bioassay using Sarcina lutea	100	
620	1	24	0	26.4 (22-36)	76.7 (63-92)					0.5,1,1.5,2,2.5,3,3.5,4,5,6,7,9,11	Bioassay using Micrococcus luteus	60	k_e^{ERY} was provided
620	1	24	0	26.4 (22-36)	76.7 (63-92)					0.5,1,1.5,2,2.5,3,3.5,4,5,6,7,9,11	Bioassay using Micrococcus luteus	60	

620	1	24	0	26.4 (22-36)	76.7 (63-92)		0.5,1,1.5,2,2.5,3,3.5,4,5,6,7,9,11	Bioassay using Micrococcus luteus	60	
620	1	24	0	26.4 (22-36)	76.7 (63-92)		0.5,1,1.5,2,2.5,3,3.5,4,5,6,7,9,11	Bioassay using Micrococcus luteus	60	
621	1	6		30±1.8	83±11.4		0,1,2,3,4,6,8,10,12,14,16,24	Bioassay using Micrococcus luteus	25	AUC _{0-t} was provided, instead of AUC _{0-∞} ; k _e ^{ERY} was provided; α and β were provided.
622	0	16		25.6 (24-29)		8/8	0.5,1,1.5,2,2.5,3,3.5,4,5,6,7,8,9,10	Bioassay using Micrococcus luteus	100	SS & EC _{max} ^{ERY} were significantly different.
622	0	10		25.6 (24-29)		5/5	0.5,1,1.5,2,2.5,3,3.5,4,5,6,7,8,9,10		100	
622	0	16		25.6 (24-29)		8/8	0.5,1,1.5,2,2.5,3,3.5,4,5,6,7,8,9,10		100	
622	0	10		25.6 (24-29)		5/5	0.5,1,1.5,2,2.5,3,3.5,4,5,6,7,8,9,10		100	
623	0	12		20.8±2.5 (18-28)	70.3±5.3	12/0	0.25,0.5,0.75,1,1.5,2,2.5,3,4,5,6	HPLC-electrochemical detection	100	
623	0	12		20.8±2.5 (18-28)	70.3±5.3	12/0	0.25,0.5,0.75,1,1.5,2,2.5,3,4,5,6		100	
624	0	6	1	20-21	60.7±9.1	3/3	0.1,0.167,0.33,0.5,0.67,0.83,1,1.67,1.33,1.5,1.67,1.83,2,2.25,2.5,2.75,3,4,5,6	Bioassay using Micrococcus luteus	100	F _{oral} ^{ERY} calculation was not corrected.
624	0	6	1	20-21	60.7±9.1	3/3	0.5,1,1.5,2,2.5,3,4,5,6		100	
625	1	8		26-34	56-77	4/4	1,1.5,2,3,4,6,8,10,12	Bioassay using Sarcina lutea		
625	1	8		26-34	56-77	4/4	1,1.5,2,3,4,6,8,10,12			
626	1	10		18-24		13/3	0.5,1,1.5,2,3,4,6	Bioassay using Sarcina lutea	500	
626	1	10		18-24		13/3	0.5,1,1.5,2,3,4,6		500	
626	1	10		18-24		13/3	0.5,1,1.5,2,3,4,6		500	
626	1	10		18-24		13/3	0.5,1,1.5,2,3,4,6		500	
627	60min before meal	32	1		64±9.4	12/12	0.25,0.5,0.75,1,1.25,1.5,1.75,2,2.15,2.5,3,3.5,4,4.5,5,5.5,6 (1st & 9th dose)	Bioassay		

627	30min after meal	32	1		64±9.4	12/12	0.25,0.5,0.75,1,1.25,1.5,1.75,2,2.15,2.5,3,3.5,4,4.5,5,5.5,6 (1st & 9th dose)			
627	60min before meal	32	1		64±9.4	12/12	0.25,0.5,0.75,1,1.25,1.5,1.75,2,2.15,2.5,3,3.5,4,4.5,5,5.5,6 (1st & 9th dose)			
627	30min after meal	32	1		64±9.4	12/12	0.25,0.5,0.75,1,1.25,1.5,1.75,2,2.15,2.5,3,3.5,4,4.5,5,5.5,6 (1st & 9th dose)			
628	1	6	1	20-30		3/3	0.33,0.67,1,1.5,2,4,6,8,12,24	Bacillus subtilis	40	
629	1	24	1	26	76 (61-92)	24/0	1,2,3,4,5,6,7,8,9,10,11,12,48,49,50,51,52,53,54,55,56,67,58,59,60,62,64,66			
629	1	24	1	26	76 (61-92)	24/0	1,2,3,4,5,6,7,8,9,10,11,12,48,49,50,51,52,53,54,55,56,67,58,59,60,62,64,66			
630	1	8	1	28-40	70.5 (62-87)	4/4	1,2,4,8,10,12	Fluorimetric method		Individual data available
630	1	8	1	28-40	70.5 (62-87)	4/4	1,2,4,8,10,12			
631	1	12	1	22±2	64±15	12/0	0.25,0.5,1,1.5,2,3,4,6,8,10	Bacillus subtilis	500	3 phases of studies; check literature for details
631	1	12	1	22±2	64±15	12/0	0.25,0.5,1,1.5,2,3,4,6,8,10		500	
631	1	12	1	22±2	64±15	12/0	0.25,0.5,1,1.5,2,3,4,6,8,10		500	
632	1	12	1	25-51	48-86		0.5,1,2,3,4,6,8,12,24	Microbiological assay		
633	1	6	1	30.7±8.2	60.8±4.1	6/0		Microbiological assay	40	Multiple dose study was also conducted.
633	1	6	1	30.7±8.2	60.8±4.1	6/0		(Sarcinalutea)	40	

I. META-ANALYSIS OF MDZ AND ERY DDI STUDIES

Without ERY, IV											
MDZ Dosing Regimen			MDZ Exposure Metrics					Study Design			
Study ID	MDZ Route	Dose	AUC _{0-∞} ^{MDZ}	SD of AUC _{0-∞} ^{MDZ}	C _{max} ^{MDZ}	SD of C _{max} ^{MDZ}	t _{max} ^{MDZ}	t _{max} ^{MDZ} range	Sample size	Crossover	Fast
		[mg/kg]	[ug/L*hrs]	[ug/L*hrs]	ng/ml	ng/ml	hr	hr		(Yes=1, No=0)	(Yes=1, No=0)
28	IV	0.050	106.8						6	0	1
Without ERY, PO											
Study ID	MDZ Route	Dose	AUC _{0-∞} ^{MDZ}	SD of AUC _{0-∞} ^{MDZ}	C _{max} ^{MDZ}	SD of C _{max} ^{MDZ}	t _{max} ^{MDZ}	t _{max} ^{MDZ} range	Sample size	Crossover	Fast
		[mg/kg]	[ug/L*hrs]	[ug/L*hrs]	ng/ml	ng/ml	hr	hr		(Yes=1, No=0)	Yes=1, No=0)
28	PO	0.244	200.0	16.7	70.0	9.0			12	0	1
601	PO	0.205	173.8	24.7	67.2	11.4	0.5		12	1	1
603	PO	0.078	35.8	7.8	11.0	2.6	15	0.67-2	12	1	Took light breakfast at 7:20am, took ERY at 8am
604	PO	0.00004							16	1	

Without ERY, IV										
Study ID	Demographics					Sample Analysis				Comments
	Age	Weight	Gender	Race	Oral contraceptives	Infusion time	Sample time points	Assay method	LLOQ	
	[yrs]	[kg]	M/F		(Yes = 1, No = 0)	[h]	[h]		ng/ml	
28	20-22	56-70	2/4		2 out of 4	0.03	0,0.25,0.5,0.75,1,2,3,4,5,6,7,8,18	GC		
Without ERY, PO										
Study ID	Demographics					Sample Analysis				Comments
	Age	Weight	Gender	Race	Oral contraceptives	Infusion time	Sample time points	Assay method	LLOQ	
	[yrs]	[kg]	M/F		(Yes = 1, No = 0)	[h]	[h]		ng/ml	
28	18-29	50-73	3/9		2 out of 9		0,0.25,0.5,0.75,1,2,3,4,5,6,18	GC		
601	24-53	49-97	12/0				0.5,1,2,3,4,5,6,8,12,24	GC	2	
603	21-28	54.3-73.4	4/8		4 out of 9		0.33, 0.66, 1, 1.5, 2, 3, 5, 8, 14, 22	HPLC	1	No smoking, no GFJ, SJW, alcohol, caffeine
604	28±7		9/7		1		0.25,0.5,1,1.5,2,2.5,3,4,6,8	UPLC-MS	0.0001	AUC ₂₋₄ was provided; CL _{met} was estimated using partial AUC regression method.

With ERY, IV											
	ERY Dosing Regimen			MDZ Dosing Regimen		MDZ Exposure Metrics					
Study ID	ERY Route	ERY Formulation	ERY Dose	MDZ Route	MDZ Dose	AUC _{0-∞} ^{MDZ}	SD of AUC _{0-∞} ^{MDZ}	C _{max} ^{MDZ}	SD of C _{max} ^{MDZ}	t _{max} ^{MDZ}	t _{max} ^{MDZ} range
					[mg/kg]	[ug/L*hrs]	[ug/L*hrs]	ng/ml	ng/ml	hr	hr
28	PO	EC	Day 1-7: EC 500mg q8h; Day 6 (2h after ERY): MDZ IV 0.05mg/kg	IV	0.050	231.5					
With ERY, PO											
Study ID	ERY Route	ERY Formulation	ERY Dose	MDZ Route	MDZ Dose	AUC _{0-∞} ^{MDZ}	SD of AUC _{0-∞} ^{MDZ}	C _{max} ^{MDZ}	SD of C _{max} ^{MDZ}	t _{max} ^{MDZ}	t _{max} ^{MDZ} range
					[mg/kg]	[ug/L*hrs]	[ug/L*hrs]	ng/ml	ng/ml	hr	hr
28	PO	EC	Day 1-7: EC 500mg q8h; Day 6 (2h after ERY): MDZ IV 15 mg	PO	0.244	883.3	116.7	189.0	16.0		
601	PO		Day 1-5: EC ERY 500mg q8h; Day 5 (1.5h after ERY): MDZ PO 15 mg	PO	0.205	662.7	76.5	182.3	22.9	0.5	
603	PO	SS (Dainippon Pharmaceutical Co)	Day 1-2: SS 200mg q6h; Day 2 (1h after ERY): MDZ PO 2.5mg	PO	0.039	83.1	37.7	20.0	5.9	1.0	0.33-2
603	PO	SS (Dainippon Pharmaceutical Co)	Day 1-4: SS 200mg q6h; Day 4 (1h after ERY): MDZ PO 2.5mg	PO	0.039	118.7	57.0	26.4	8.7	1.0	0.67-2
603	PO	SS (Dainippon Pharmaceutical Co)	Day 1-7: SS 200mg q6h; Day 7 (1h after ERY): MDZ PO 2.5mg	PO	0.039	119.2	50.8	25.8	9.9	1.0	0.33-2
604	PO	SS	Day 1: 3µg MDZ was administered; Day 3 250mg SS was administered 1h before 3µg MDZ	PO	0.00004						
604	PO	SS	Day 1: 3µg MDZ was administered; Day 3 250mg SS was administered 1h before 3µg MDZ	PO	0.00004						

With ERY, IV												
Study ID	Study Design						Sample Analysis				Comments	
	Fast	Sample size	Cross-over	Age	Weight	Gender	Oral contraceptives	Infusion time	Sample time points	Assay method		LLOQ
	Yes=1, No=0		(Yes=1, No=0)	[yrs]	[kg]	M/F		[h]	[h]		ng/ml	
28	1	6	0	20-22	56-70		2 out of 4	0.03	0,0.25,0.5,0.75,1,2,3,4,5,6,7,8,18	GC		ERY concentration available
With ERY, PO												
Study ID		Sample size	Cross-over	Age	Weight	Gender	Oral contraceptives	Infusion time	Sample time points	Assay method	LLOQ	Comments
28	1	12	0	18-29	50-73	3/9	2 out of 9		0,0.25,0.5,0.75,1,2,3,4,5,6,18	GC		ERY concentration available
601	1	12	1	24-53	49-97	4/8	4 out of 9		0.5,1,2,3,4,5,6,8,12,24	GC	2	
603	Took light breakfast at 7:20am, took ERY at 8am	12	1	21-28	54.3-73.4	12/0			0.33, 0.66, 1, 1.5, 2, 3, 5, 8, 14, 22	HPLC	1	No smoking, no GFJ, SJW, alcohol, caffeine; Dose-corrected AUC, c _{max}
603		12	1	21-28	54.3-73.4	12/0			0.33, 0.66, 1, 1.5, 2, 3, 5, 8, 14, 22	HPLC	1	
603		12	1	21-28	54.3-73.4	12/0			0.33, 0.66, 1, 1.5, 2, 3, 5, 8, 14, 22	HPLC	1	
604		8	0	28±7		9/7	1		0.25,0.5,1,1.5,2,2.5,3,4,6,8	UPLC-MS	0.0001	AUC ₂₋₄ was provided; CL _{met} was estimated using partial AUC regression method.
604		8	0	28±7		9/7	1		0.25,0.5,1,1.5,2,2.5,3,4,6,8	UPLC-MS	0.0001	

J. ESTIMATION OF UNBOUND ERY RENAL CLEARANCE AFTER IV ADMINISTRATION

J.1. Assumptions

Assumptions made in $CL_{ren,u-IV}^{ERY}$ estimation were:

- 1) Both glomerular filtration and tubular secretion processes are constant with dose.
- 2) Tubular reabsorption follows Michaelis-Menten kinetics with dose (saturated with increasing dose).
- 3) Maximal $CL_{ren,u-IV}^{ERY}$ is 3.5 ml/min/kg, which is achieved at very high ERY dose, when tubular reabsorption is fully saturated. Therefore,

$$CL_{gl,u}^{ERY} + CL_{ts,u}^{ERY} = 3.5 \text{ ml/min/kg } (CL_{ren,u,max}^{ERY})$$

$CL_{gl,u}^{ERY}$ is unbound glomerular filtration clearance of ERY, $CL_{ts,u}^{ERY}$ is unbound tubular secretion clearance of ERY.

- 4) Minimal $CL_{ren,u-IV}^{ERY}$ is 0.5 ml/min/kg, which is achieved at very low ERY dose, when tubular reabsorption is not saturated and remains a constant. Therefore,

$$CL_{gl,u}^{ERY} + CL_{ts,u}^{ERY} - CL_{ra,u}^{ERY} = 0.5 \text{ ml/min/kg } (CL_{ren,u,min}^{ERY})$$

$CL_{ra,u}^{ERY}$ is unbound tubular reabsorption clearance of ERY.

J.2. Predictability assessment of empirical hyperbolic renal clearance model

In order to assess predictability of empirical hyperbolic renal clearance model, predicted $CL_{ren,u}^{ERY}$ after IV administration were plotted against observed $CL_{ren,u}^{ERY}$ (**Figure J.1**), and deviation (%) at each dose was calculated and presented in **Table J.1**. Observed $CL_{ren,u}^{ERY}$ was transformed from study reported total ERY plasma renal clearance ($CL_{ren,p}^{ERY}$) by dividing average f_u^{ERY} (f_u^{ERY} at $c_{max}^{ERY}/2$) at each dose and $B:P^{ERY}$.

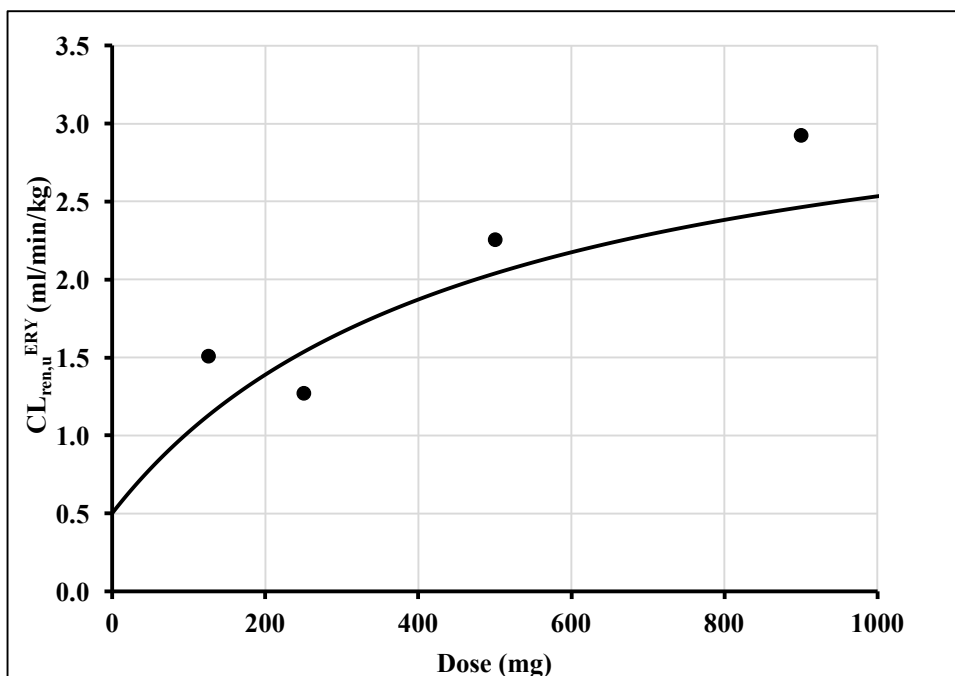


Figure J.1. Predictability assessment of empirical hyperbolic renal clearance model after IV ERY. The symbols represent observed unbound blood renal clearance after various dose of IV ERY in study 611. The line represents predicted unbound blood renal clearance after various dose of IV ERY.

Table J.1 Predictability assessment of empirical hyperbolic renal clearance model after IV ERY.

Dose (mg)	Observed $CL_{ren,u}^{ERY}$ (ml/min/kg)	Predicted $CL_{ren,u}^{ERY}$ (ml/min/kg)	Deviation (%)
125	1.51	1.13	-25%
250	1.27	1.53	21%
500	2.26	2.04	-10%
900	2.93	2.46	-16%

From **Figure J.1** and **Table J.1**, the empirical model successfully balances deviation (%) of predicted values around 0 from observed data, and adequately characterizes the increasing trend of $CL_{ren,u}^{ERY}$ with dose, given the limited available data.

K. SENSITIVITY ANALYSIS OF DDI BETWEEN MDZ AND EC ERY FOR STUDY 28

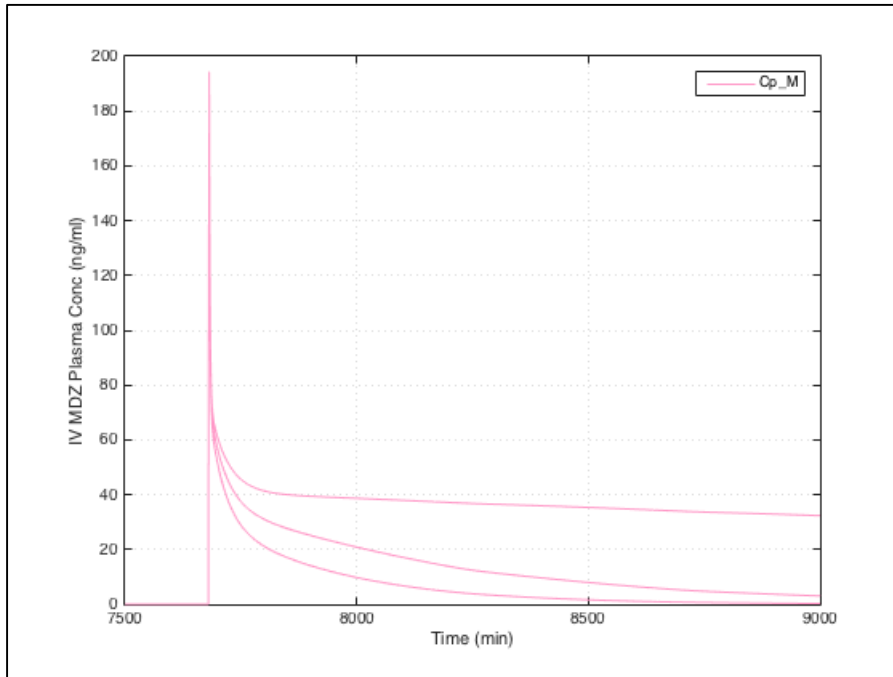


Figure K.1 Sensitivity analysis of IV MDZ plasma concentrations in presence of PO EC ERY to the change in k_{deg} . (top line: $k_{deg} = 0.00016 \text{ min}^{-1}$; middle line: $k_{deg} = 0.0008 \text{ min}^{-1}$; bottom line: $k_{deg} = 0.004 \text{ min}^{-1}$). Time is relative to initial ERY/placebo dose.

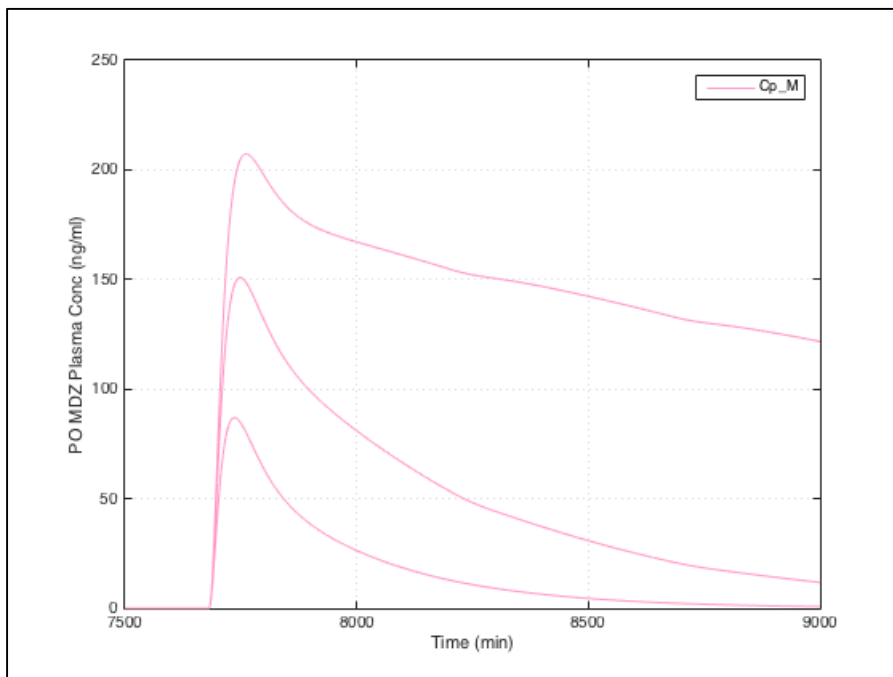


Figure K.2 Sensitivity analysis of PO MDZ plasma concentrations in presence of PO EC ERY to the change in k_{deg} . (top line: $k_{deg} = 0.00016 \text{ min}^{-1}$; middle line: $k_{deg} = 0.0008 \text{ min}^{-1}$; bottom line: $k_{deg} = 0.004 \text{ min}^{-1}$). Time is relative to initial ERY/placebo dose.

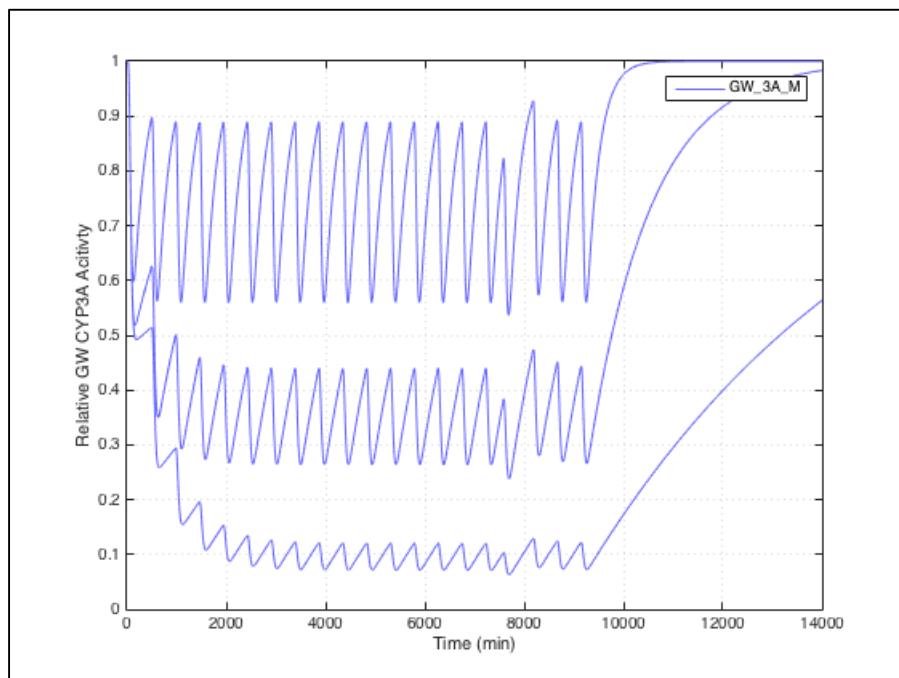


Figure K.3. Sensitivity analysis of relative GW CYP3A activity to the change in k_{deg} . (top line: $k_{deg} = 0.004 \text{ min}^{-1}$; middle line: $k_{deg} = 0.0008 \text{ min}^{-1}$; bottom line: $k_{deg} = 0.00016 \text{ min}^{-1}$)

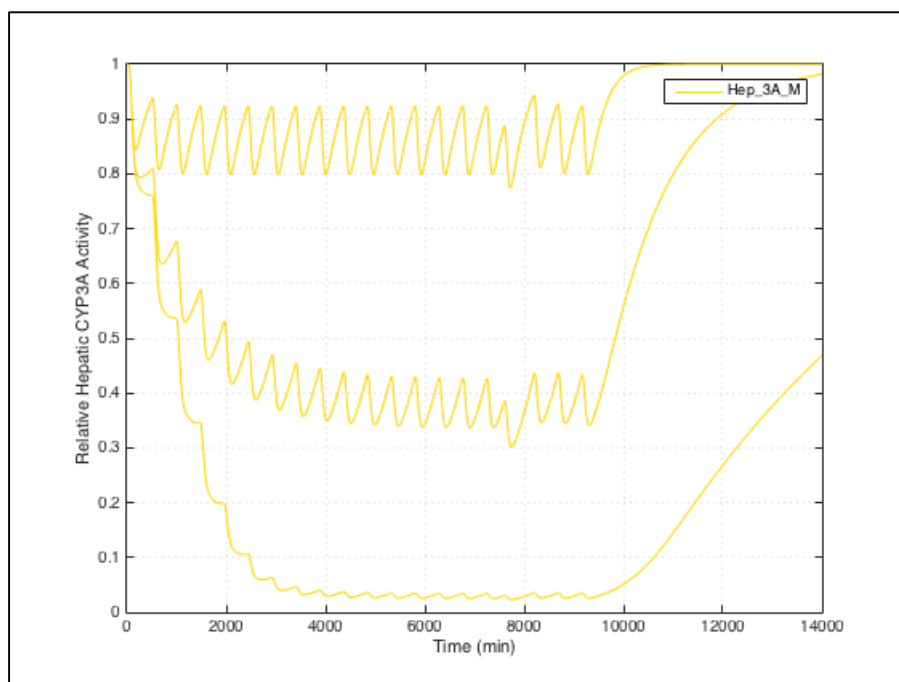


Figure K.4 Sensitivity analysis of relative hepatic CYP3A activity to the change in k_{deg} . (top line: $k_{deg} = 0.004 \text{ min}^{-1}$; middle line: $k_{deg} = 0.0008 \text{ min}^{-1}$; bottom line: $k_{deg} = 0.00016 \text{ min}^{-1}$)

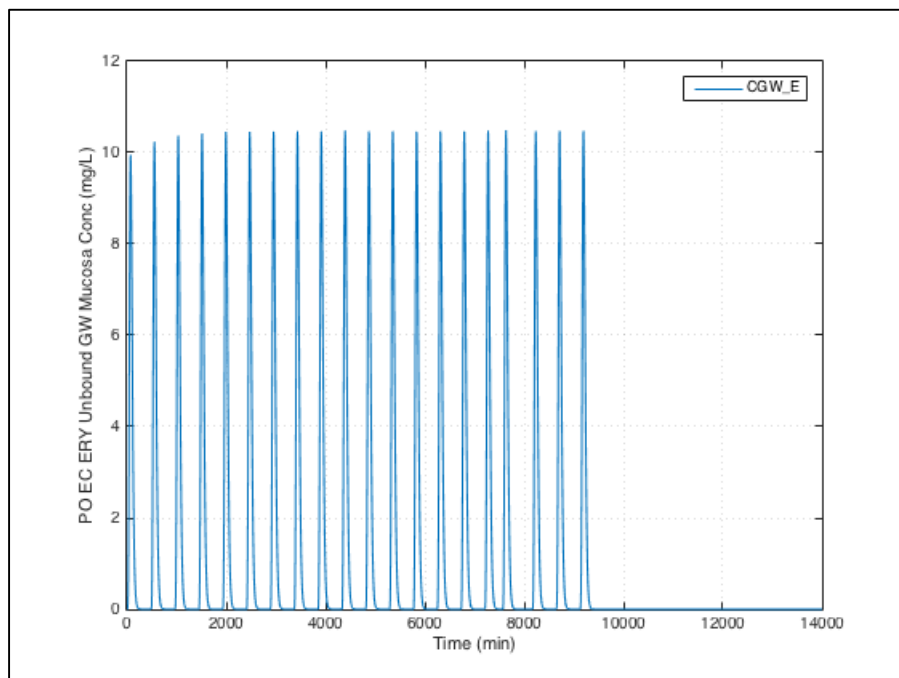


Figure K.5 Sensitivity analysis of ERY unbound GW mucosa concentration to the change in k_{deg} . ($k_{deg} = 0.00016/0.0008/0.004 \text{ min}^{-1}$ are superimposable.)

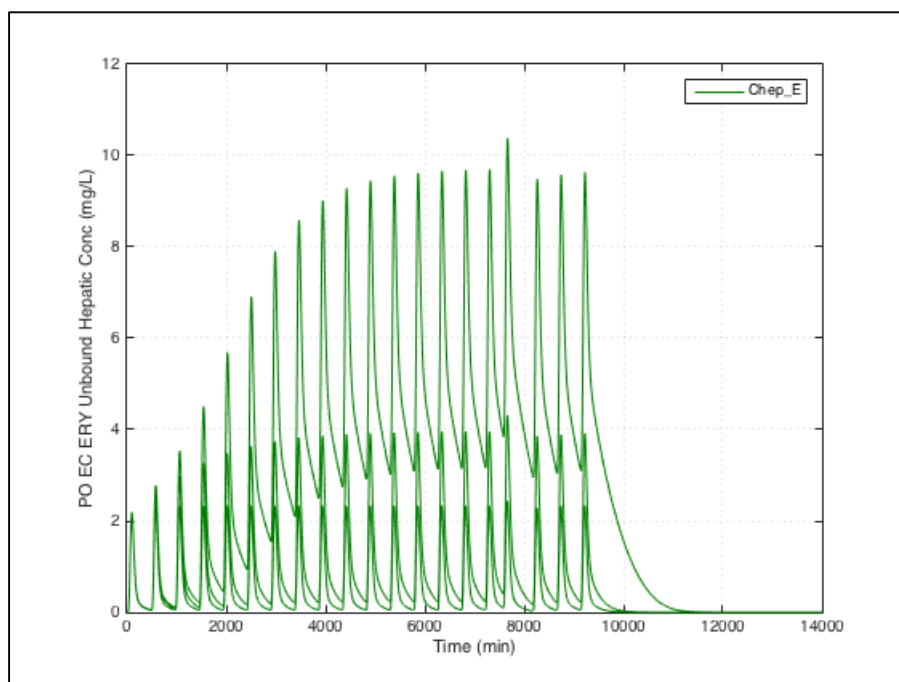


Figure K.6 Sensitivity analysis of ERY unbound hepatic concentration to the change in k_{deg} . (top line: $k_{deg} = 0.00016 \text{ min}^{-1}$; middle line: $k_{deg} = 0.0008 \text{ min}^{-1}$; bottom line: $k_{deg} = 0.004 \text{ min}^{-1}$)

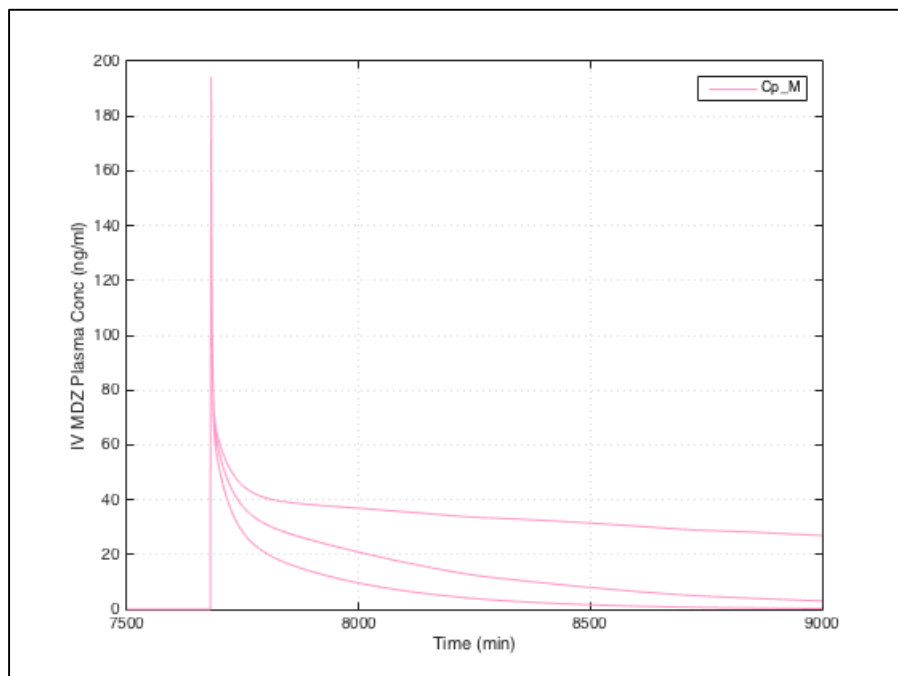


Figure K.7 Sensitivity analysis of IV MDZ plasma concentrations in presence of PO EC ERY to the change in K_I^{ERY} . (top line: $K_I^{ERY} = 6$ mg/L; middle line: $K_I^{ERY} = 30$ mg/L; bottom line: $K_I^{ERY} = 150$ mg/L). Time is relative to initial ERY/placebo dose.

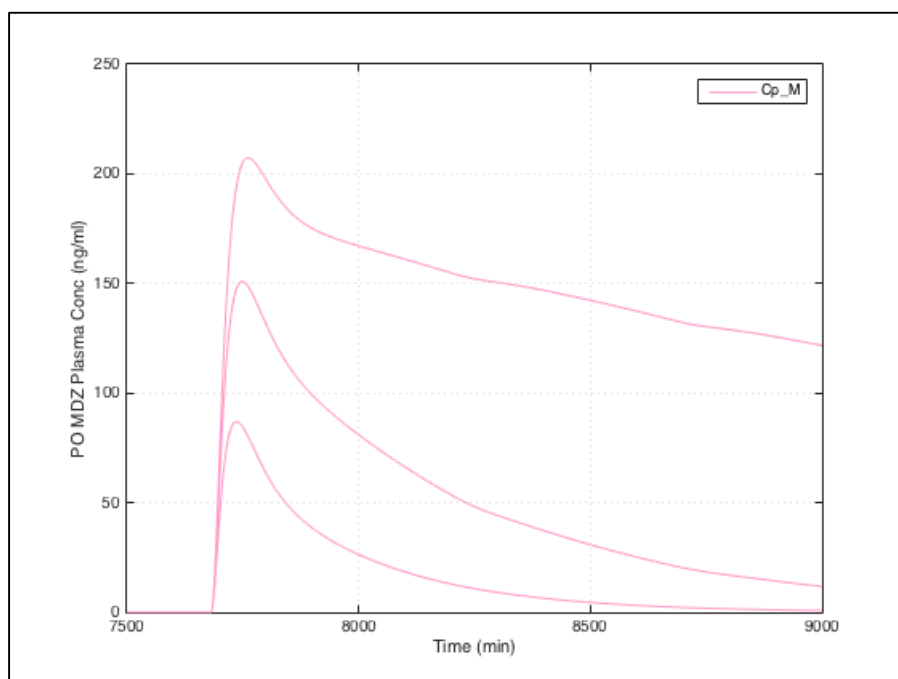


Figure K.8 Sensitivity analysis of PO MDZ plasma concentrations in presence of PO EC ERY to the change in K_I^{ERY} . (top line: $K_I^{ERY} = 6$ mg/L; middle line: $K_I^{ERY} = 30$ mg/L; bottom line: $K_I^{ERY} = 150$ mg/L). Time is relative to initial ERY/placebo dose.

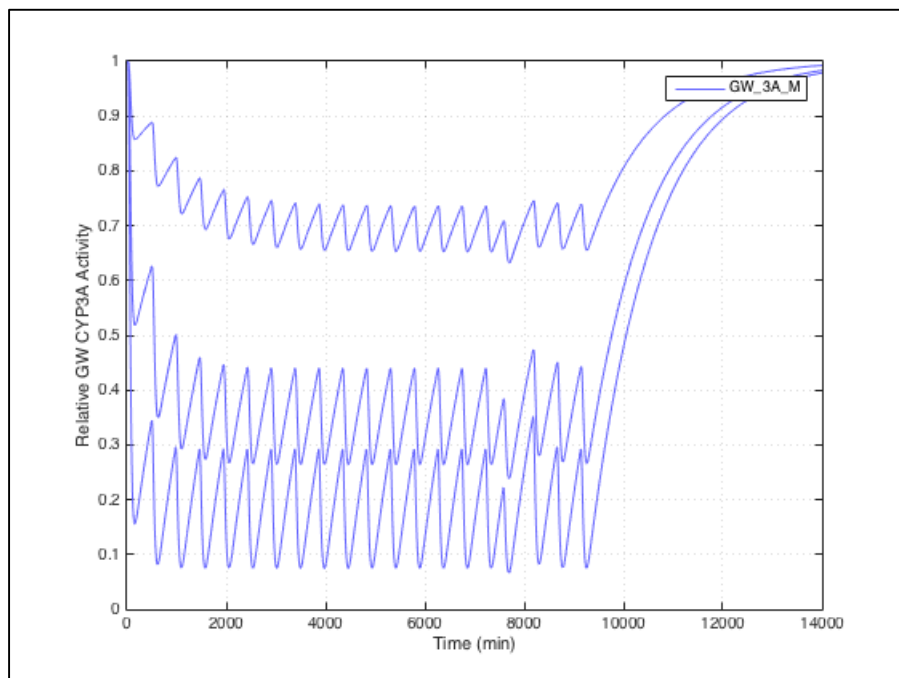


Figure K.9 Sensitivity analysis of relative GW CYP3A activity to the change in K_I^{ERY} . (top line: $K_I^{ERY} = 150$ mg/L; middle line: $K_I^{ERY} = 30$ mg/L; bottom line: $K_I^{ERY} = 6$ mg/L)

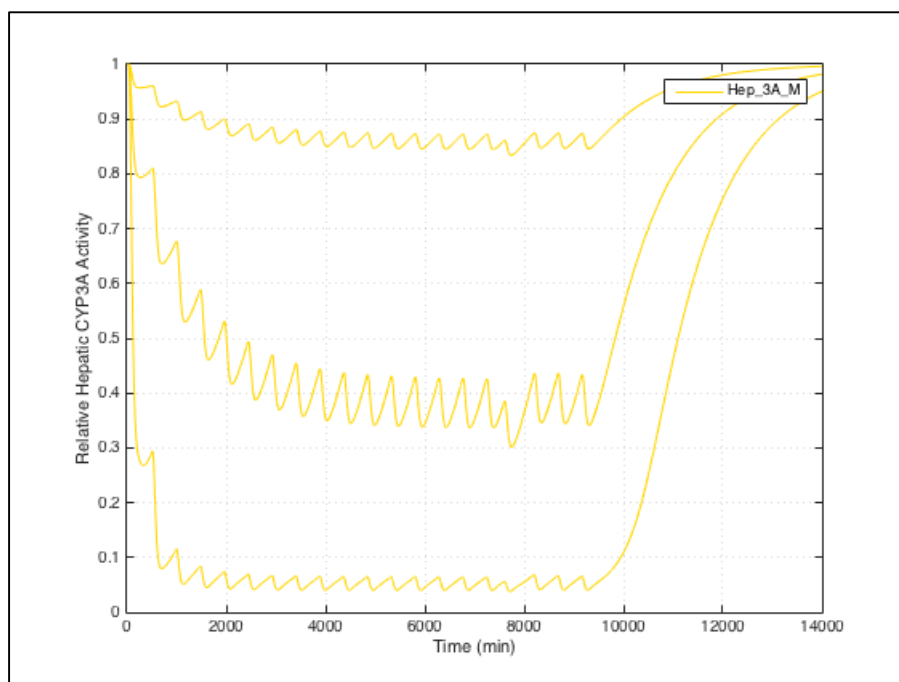


Figure K.10 Sensitivity analysis of relative hepatic CYP3A activity to the change in K_I^{ERY} . (top line: $K_I^{ERY} = 150$ mg/L; middle line: $K_I^{ERY} = 30$ mg/L; bottom line: $K_I^{ERY} = 6$ mg/L)

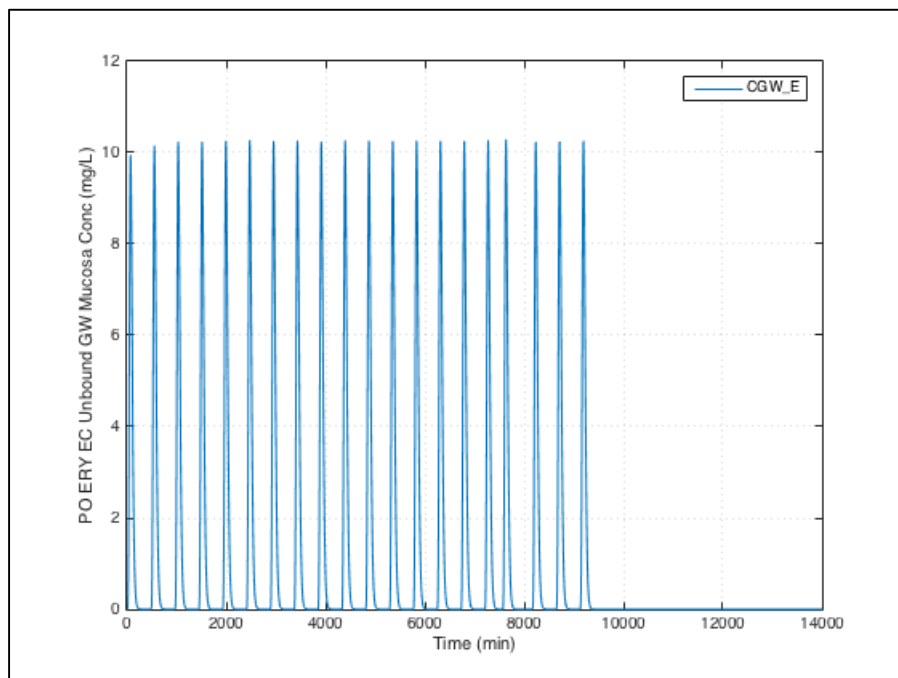


Figure K.11 Sensitivity analysis of ERY unbound GW mucosa concentration to the change in K_I^{ERY} . ($K_I^{ERY} = 6/30/150$ mg/L are superimposable)

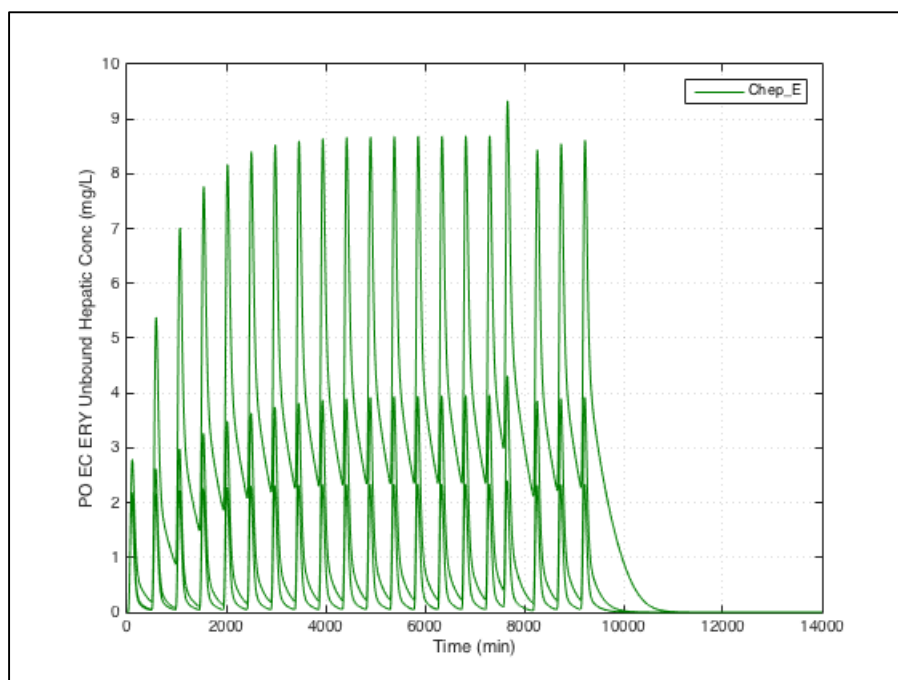


Figure K.12 Sensitivity analysis of ERY unbound hepatic concentration to the change in K_I^{ERY} . (top line: $K_I^{ERY} = 6$ mg/L; middle line: $K_I^{ERY} = 30$ mg/L; bottom line: $K_I^{ERY} = 150$ mg/L)

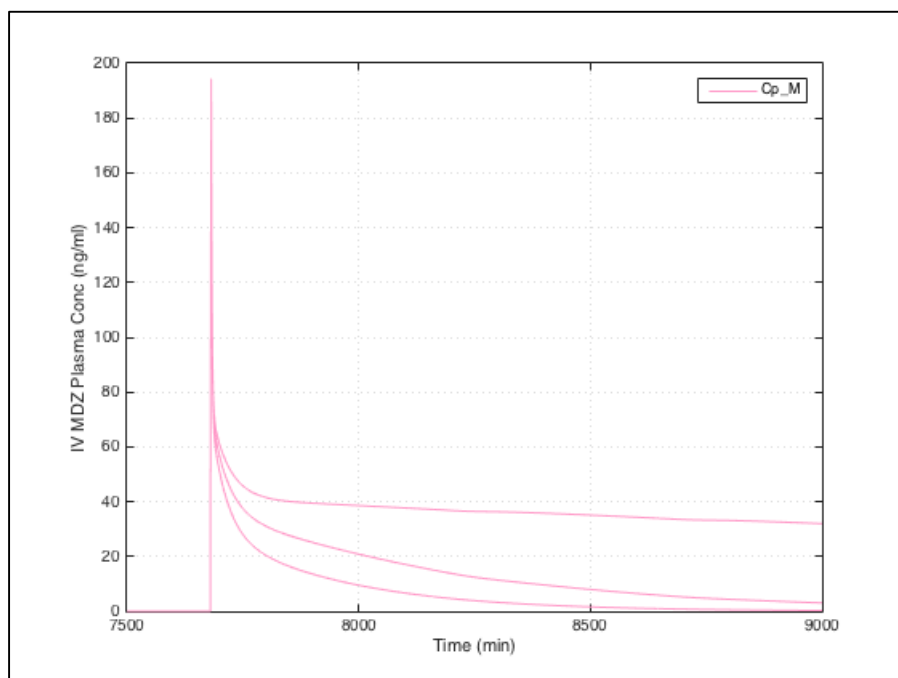


Figure K.13 Sensitivity analysis of IV MDZ plasma concentrations in presence of PO EC ERY to the change in k_{inact}^{ERY} . (top line: $k_{inact}^{ERY} = 0.1875 \text{ min}^{-1}$; middle line: $k_{inact}^{ERY} = 0.0375 \text{ min}^{-1}$; $k_{inact}^{ERY} =$ bottom line: 0.0075 min^{-1}). Time is relative to initial ERY/placebo dose.

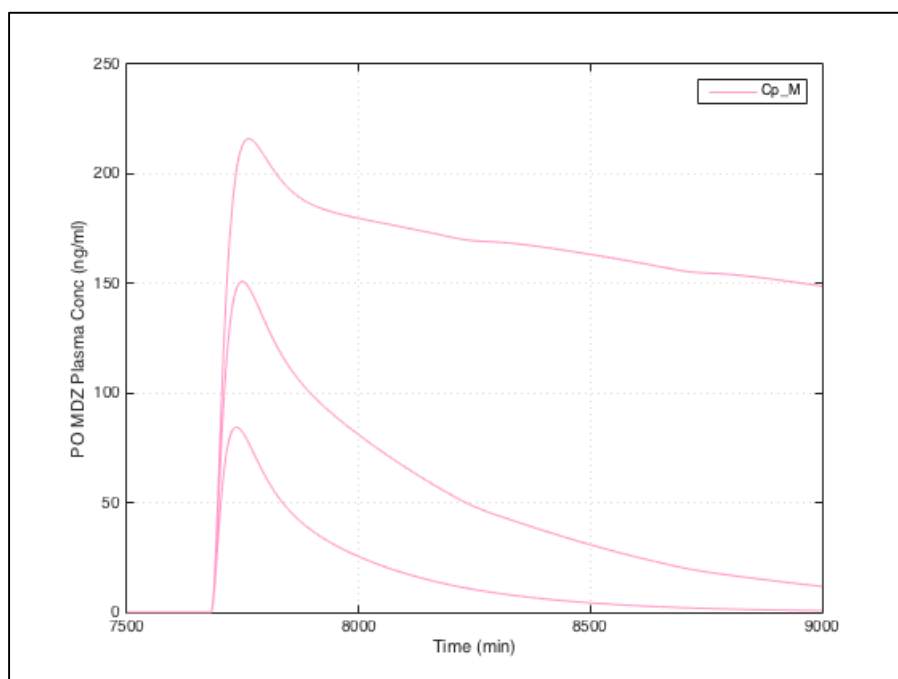


Figure K.14 Sensitivity analysis of PO MDZ plasma concentrations in presence of PO EC ERY to the change in k_{inact}^{ERY} . (top line: $k_{inact}^{ERY} = 0.1875 \text{ min}^{-1}$; middle line: $k_{inact}^{ERY} = 0.0375 \text{ min}^{-1}$; bottom line: $k_{inact}^{ERY} = 0.0075 \text{ min}^{-1}$). Time is relative to initial ERY/placebo dose.

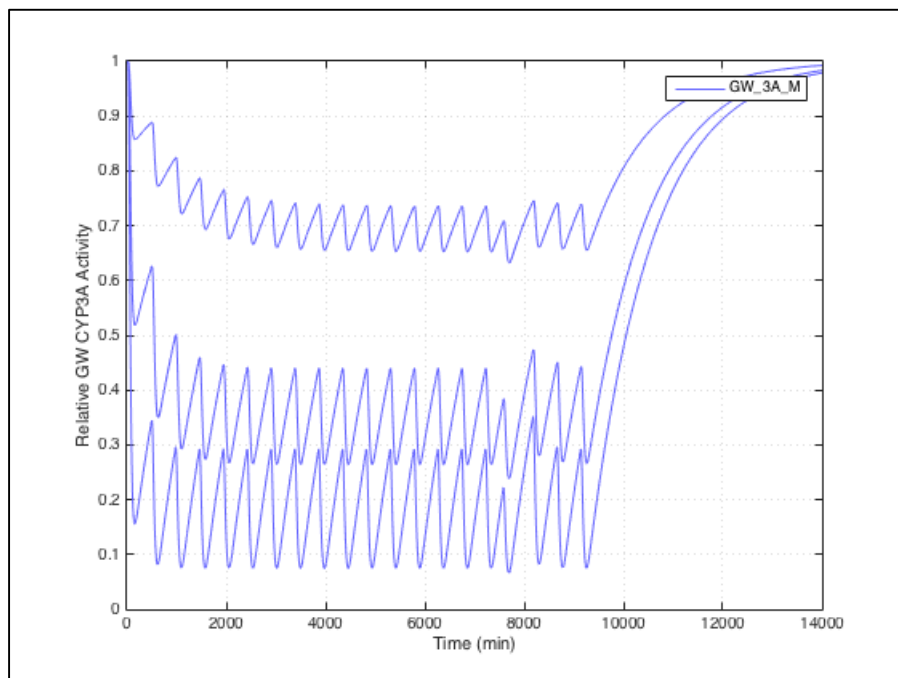


Figure K.15 Sensitivity analysis of relative GW CYP3A activity to the change in $k_{\text{inact}}^{\text{ERY}}$. (top line: $k_{\text{inact}}^{\text{ERY}} = 0.0075 \text{ min}^{-1}$; middle line: $k_{\text{inact}}^{\text{ERY}} = 0.0375 \text{ min}^{-1}$; bottom line: $k_{\text{inact}}^{\text{ERY}} = 0.1875 \text{ min}^{-1}$)

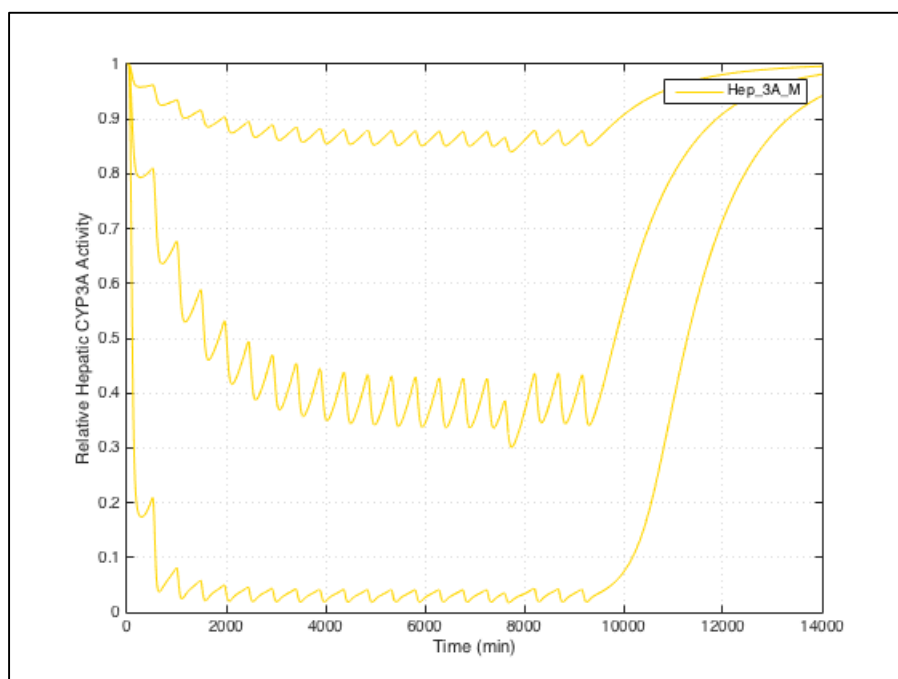


Figure K.16 Sensitivity analysis of relative hepatic CYP3A activity to the change in $k_{\text{inact}}^{\text{ERY}}$. (top line: $k_{\text{inact}}^{\text{ERY}} = 0.0075 \text{ min}^{-1}$; middle line: $k_{\text{inact}}^{\text{ERY}} = 0.0375 \text{ min}^{-1}$; bottom line: $k_{\text{inact}}^{\text{ERY}} = 0.1875 \text{ min}^{-1}$)

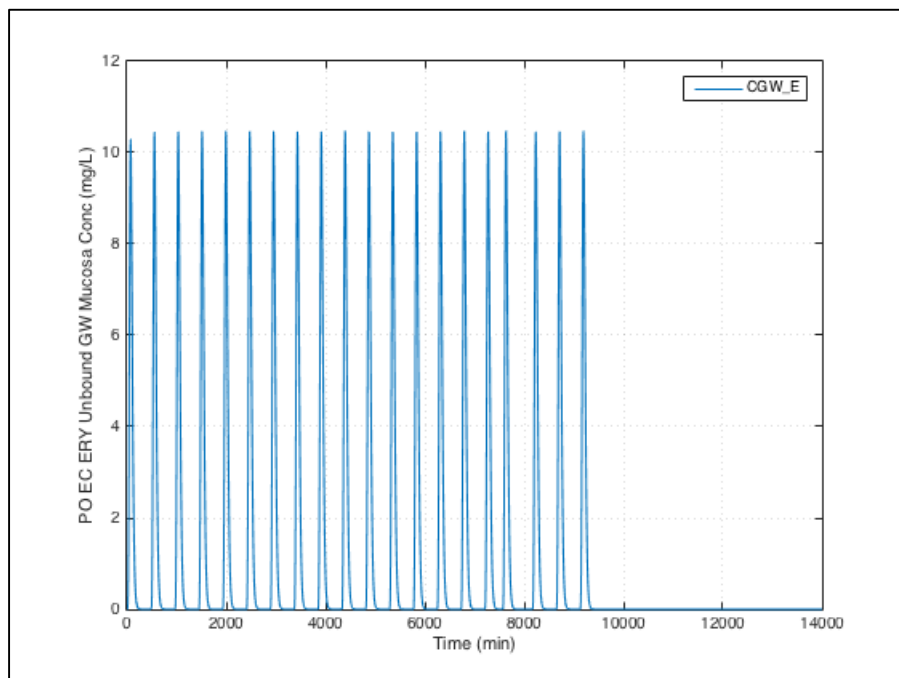


Figure K.17 Sensitivity analysis of ERY unbound GW mucosa concentration to the change in k_{inact}^{ERY} . ($k_{inact}^{ERY} = 0.0075/0.0375/0.1875 \text{ min}^{-1}$ are superimposable)

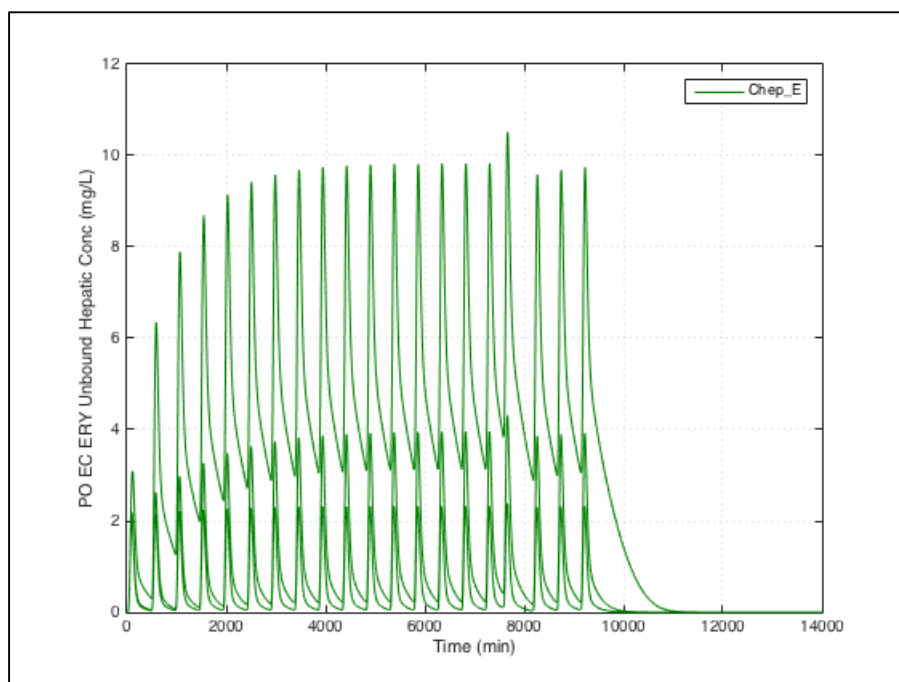


Figure K.18 Sensitivity analysis of ERY unbound hepatic concentration to the change in k_{inact}^{ERY} . (top line: $k_{inact}^{ERY} = 0.1875 \text{ min}^{-1}$; middle line: $k_{inact}^{ERY} = 0.0375 \text{ min}^{-1}$; bottom line: $k_{inact}^{ERY} = 0.0075 \text{ min}^{-1}$)

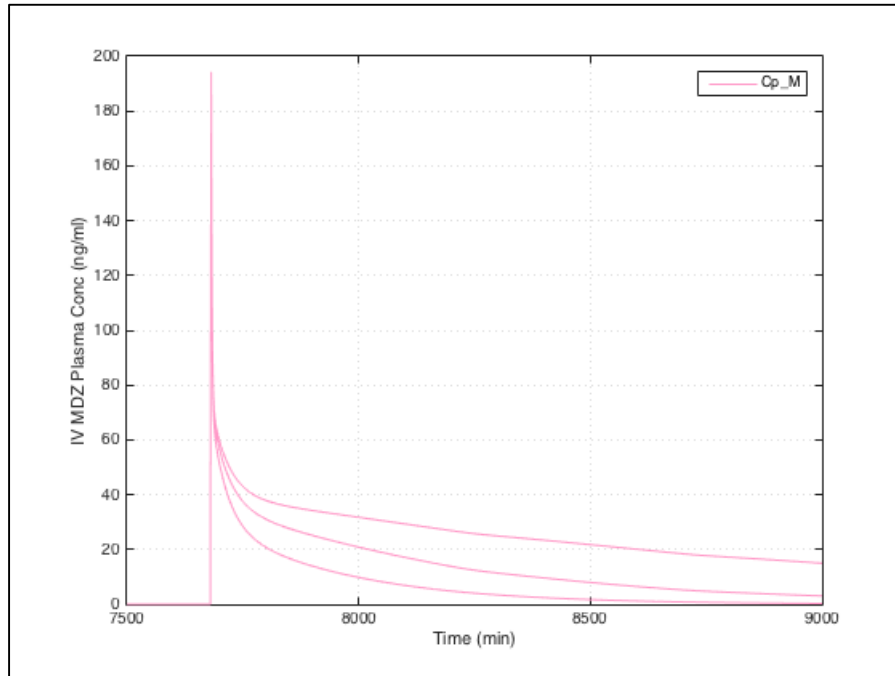


Figure K.19 Sensitivity analysis of IV MDZ plasma concentrations in presence of PO EC ERY to the change in $v_{\max, \text{hep-3A}}^{\text{ERY}}$. (top line: $v_{\max, \text{hep-3A}}^{\text{ERY}} = 160 \mu\text{g}/\text{min}/\text{kg}$; middle line: $v_{\max, \text{hep-3A}}^{\text{ERY}} = 800 \mu\text{g}/\text{min}/\text{kg}$, bottom line: $v_{\max, \text{hep-3A}}^{\text{ERY}} = 4000 \mu\text{g}/\text{min}/\text{kg}$). Time is relative to initial ERY/placebo dose.

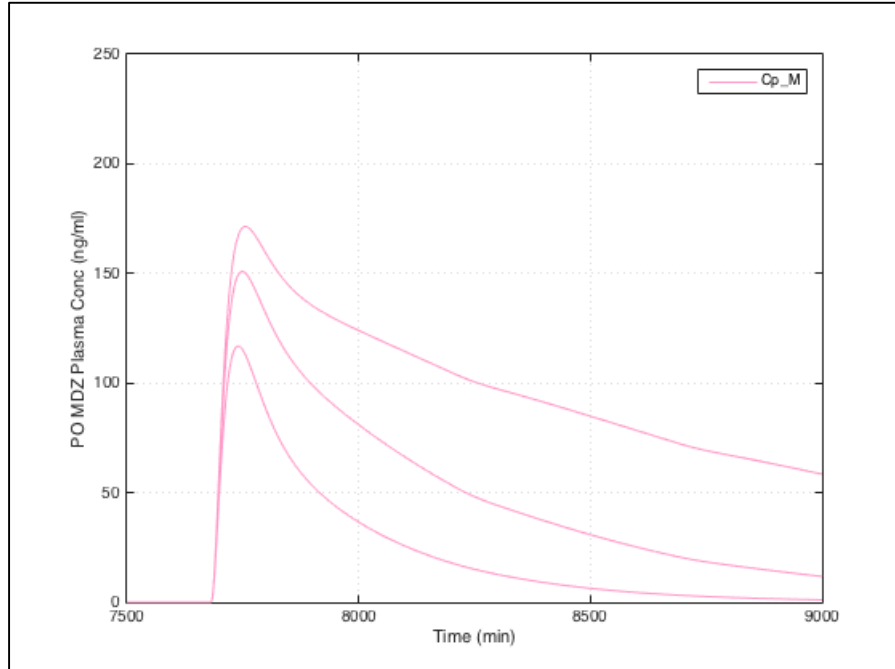


Figure K.20 Sensitivity analysis of PO MDZ plasma concentrations in presence of PO EC ERY to the change in $v_{\max, \text{hep-3A}}^{\text{ERY}}$. (top line: $v_{\max, \text{hep-3A}}^{\text{ERY}} = 160 \mu\text{g}/\text{min}/\text{kg}$; middle line: $v_{\max, \text{hep-3A}}^{\text{ERY}} = 800 \mu\text{g}/\text{min}/\text{kg}$, bottom line: $v_{\max, \text{hep-3A}}^{\text{ERY}} = 4000 \mu\text{g}/\text{min}/\text{kg}$). Time is relative to initial ERY/placebo dose.

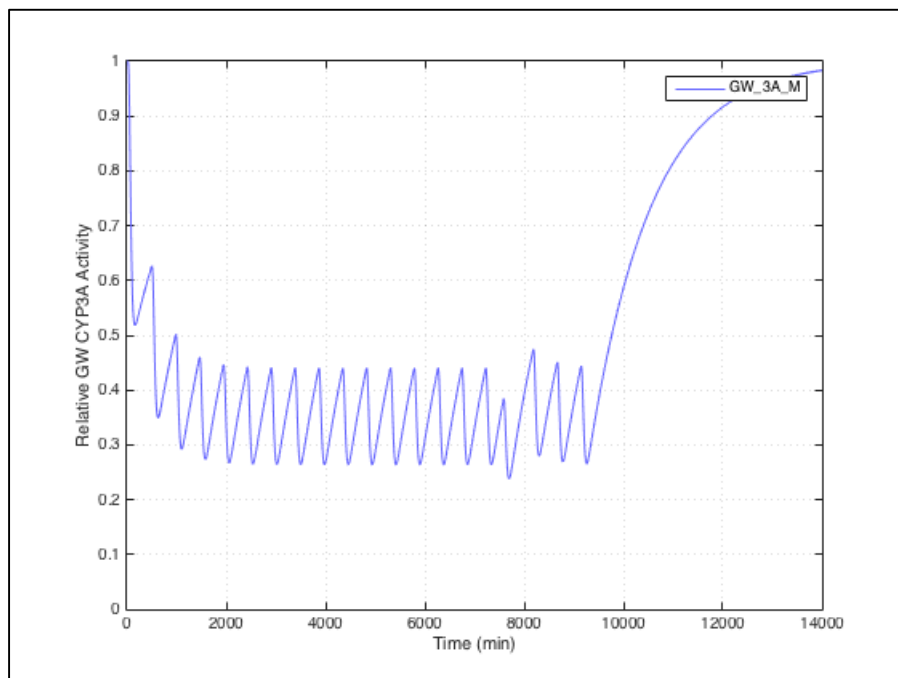


Figure K.21 Sensitivity analysis of relative GW CYP3A activity to the change in $v_{\max, \text{hep-3A}}^{\text{ERY}}$. ($v_{\max, \text{hep-3A}}^{\text{ERY}} = 160/800/4000 \mu\text{g}/\text{min}/\text{kg}$ are superimposable)

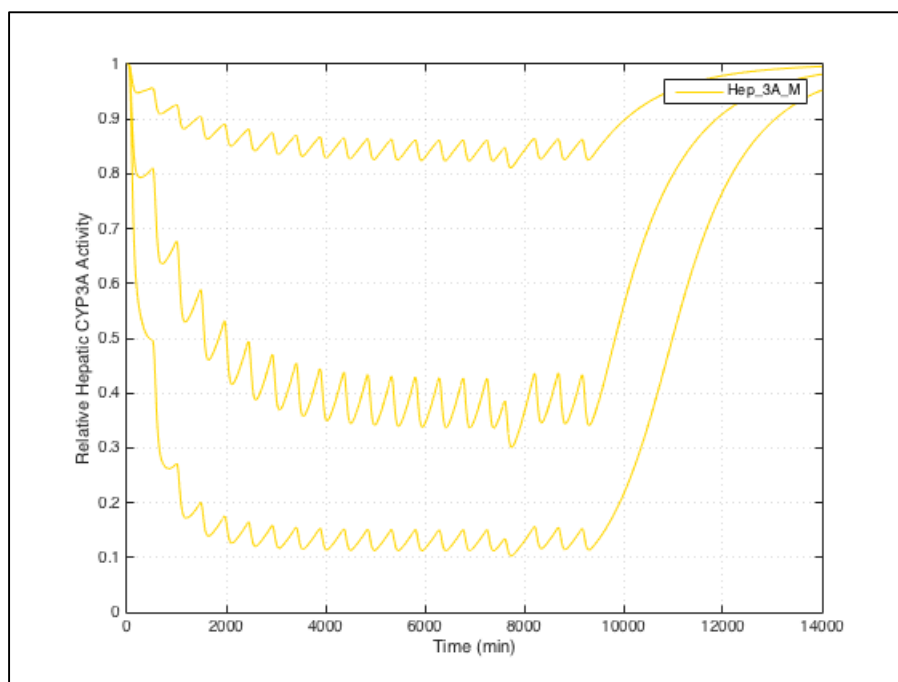


Figure K.22 Sensitivity analysis of relative hepatic CYP3A activity to the change in $v_{\max, \text{hep-3A}}^{\text{ERY}}$. (top line: $v_{\max, \text{hep-3A}}^{\text{ERY}} = 4000 \mu\text{g}/\text{min}/\text{kg}$; middle line: $v_{\max, \text{hep-3A}}^{\text{ERY}} = 800 \mu\text{g}/\text{min}/\text{kg}$; bottom line: $v_{\max, \text{hep-3A}}^{\text{ERY}} = 160 \mu\text{g}/\text{min}/\text{kg}$)

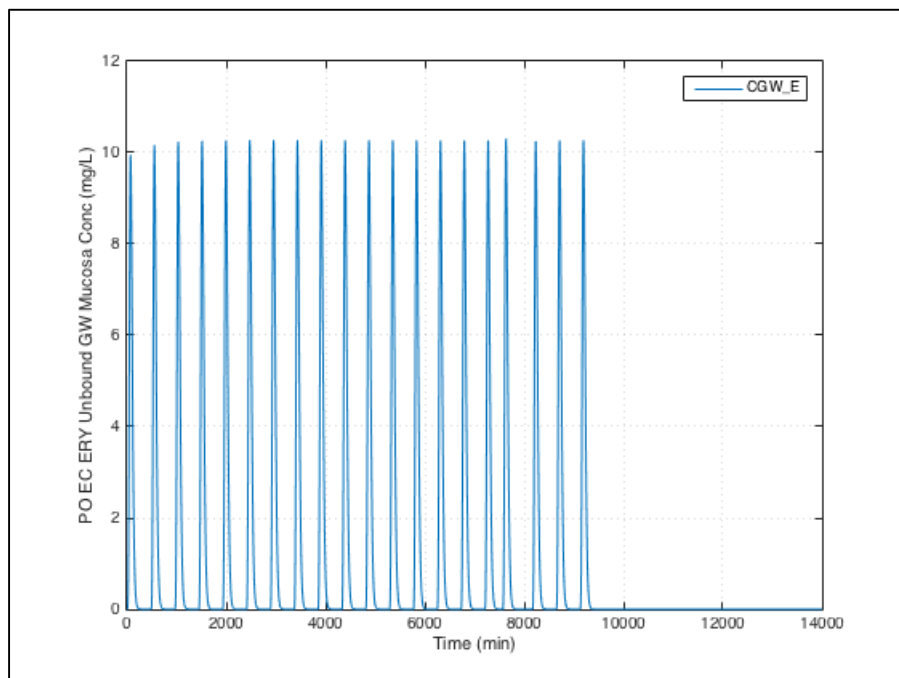


Figure K.23 Sensitivity analysis of ERY unbound GW mucosa concentration to the change in $v_{\max, \text{hep-3A}}^{\text{ERY}}$. ($v_{\max, \text{hep-3A}}^{\text{ERY}} = 160/800/4000 \mu\text{g}/\text{min}/\text{kg}$ are superimposable)

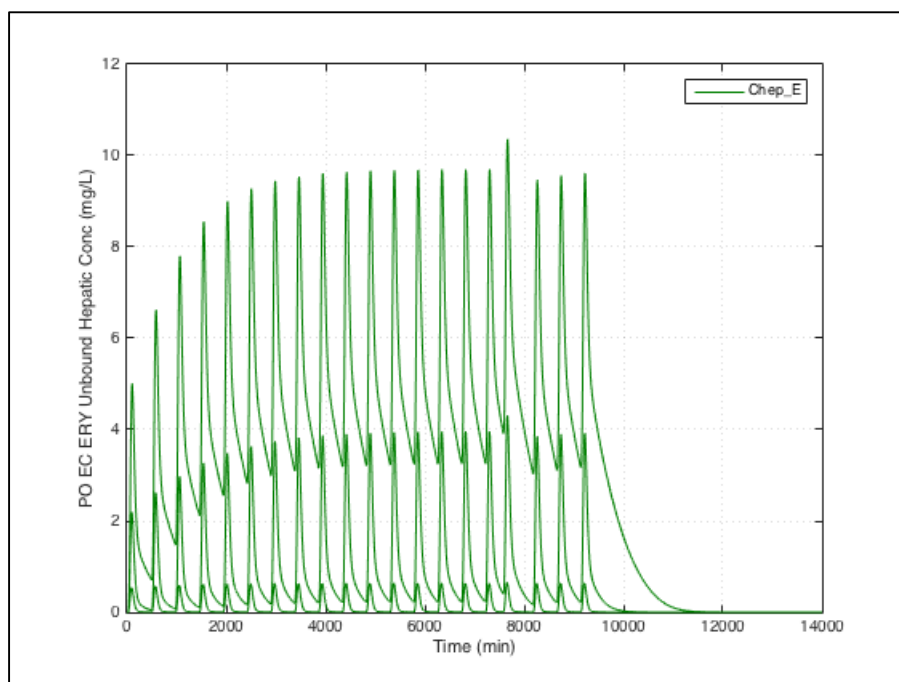


Figure K.24 Sensitivity analysis of ERY unbound hepatic concentration to the change in $v_{\max, \text{hep-3A}}^{\text{ERY}}$. (top line: $v_{\max, \text{hep-3A}}^{\text{ERY}} = 160 \mu\text{g}/\text{min}/\text{kg}$; middle line: $v_{\max, \text{hep-3A}}^{\text{ERY}} = 800 \mu\text{g}/\text{min}/\text{kg}$; bottom line: $v_{\max, \text{hep-3A}}^{\text{ERY}} = 4000 \mu\text{g}/\text{min}/\text{kg}$)

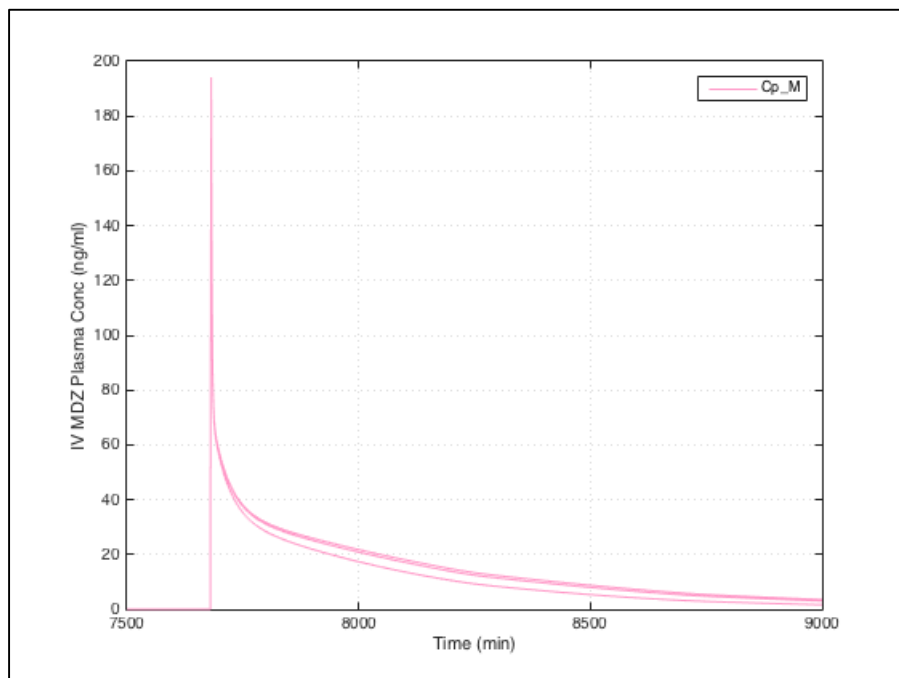


Figure K.25 Sensitivity analysis of IV MDZ plasma concentrations in presence of PO EC ERY to the change in $v_{\max, \text{bile}}^{\text{ERY}}$. (top line: $v_{\max, \text{bile}}^{\text{ERY}} = 0.1 \mu\text{g}/\text{min}/\text{kg}$; middle line: $v_{\max, \text{bile}}^{\text{ERY}} = 0.5 \mu\text{g}/\text{min}/\text{kg}$, bottom line: $v_{\max, \text{bile}}^{\text{ERY}} = 2.5 \mu\text{g}/\text{min}/\text{kg}$). Time is relative to initial ERY/placebo dose.

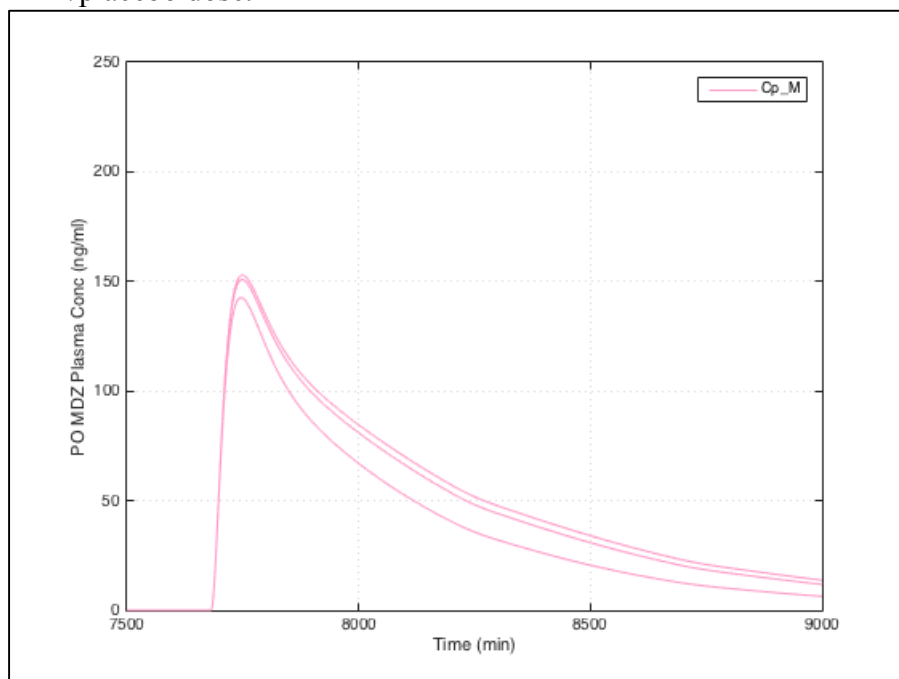


Figure K.26 Sensitivity analysis of PO MDZ plasma concentrations in presence of PO EC ERY to the change in $v_{\max, \text{bile}}^{\text{ERY}}$. (top line: $v_{\max, \text{bile}}^{\text{ERY}} = 0.1 \mu\text{g}/\text{min}/\text{kg}$; middle line: $v_{\max, \text{bile}}^{\text{ERY}} = 0.5 \mu\text{g}/\text{min}/\text{kg}$, bottom line: $v_{\max, \text{bile}}^{\text{ERY}} = 2.5 \mu\text{g}/\text{min}/\text{kg}$). Time is relative to initial ERY/placebo dose.

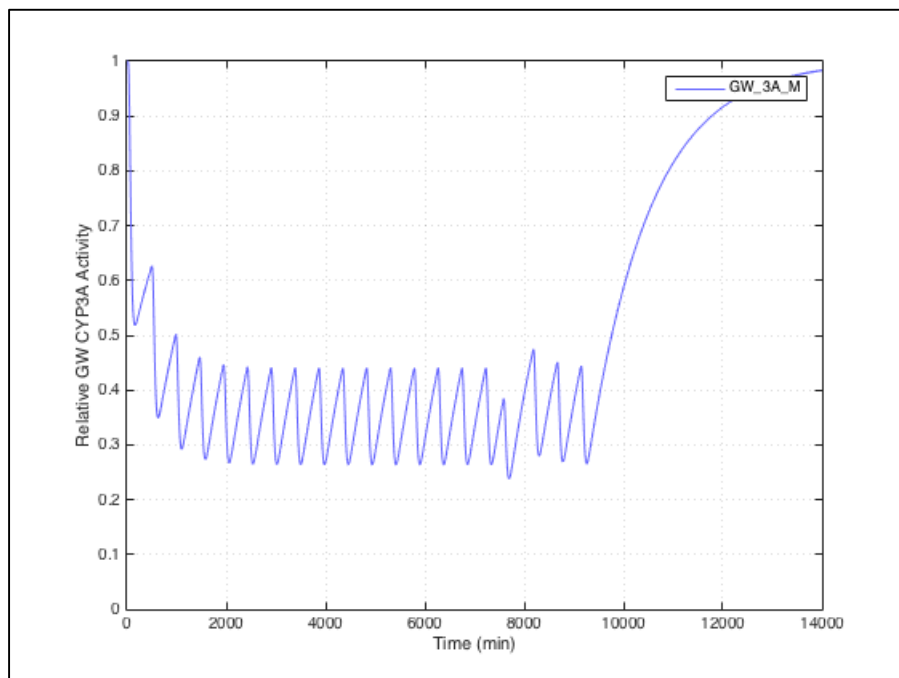


Figure K.27 Sensitivity analysis of relative GW CYP3A activity to the change in $v_{\max,bile}^{ERY}$. ($v_{\max,bile}^{ERY} = 0.1/0.5/2.5 \mu\text{g}/\text{min}/\text{kg}$ are superimposable)

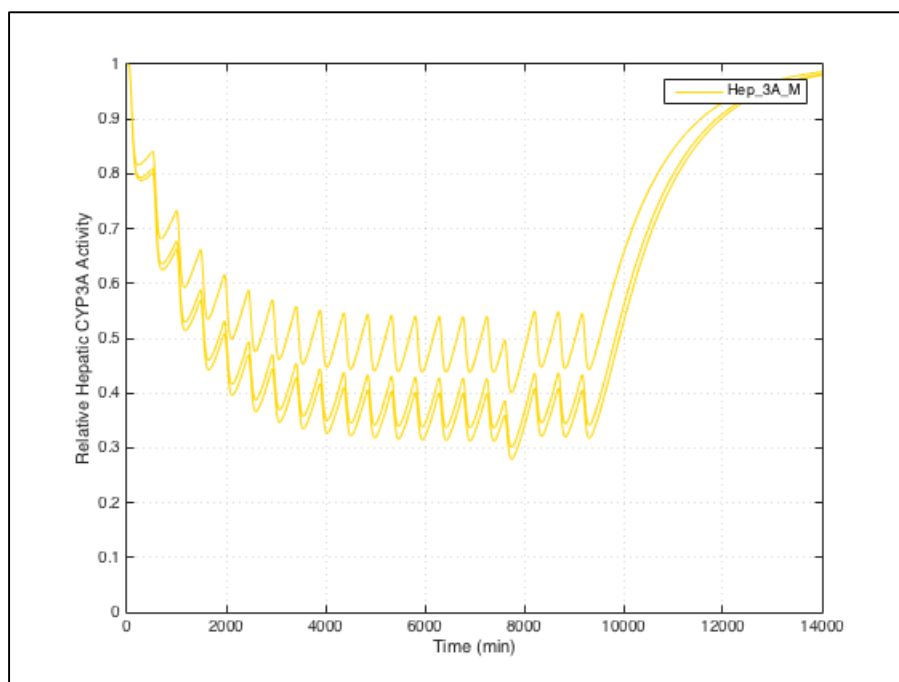


Figure K.28 Sensitivity analysis of relative hepatic CYP3A activity to the change in $v_{\max,bile}^{ERY}$. (top line: $v_{\max,bile}^{ERY} = 2.5 \mu\text{g}/\text{min}/\text{kg}$; middle line: $v_{\max,bile}^{ERY} = 0.5 \mu\text{g}/\text{min}/\text{kg}$; bottom line: $v_{\max,bile}^{ERY} = 0.1 \mu\text{g}/\text{min}/\text{kg}$)

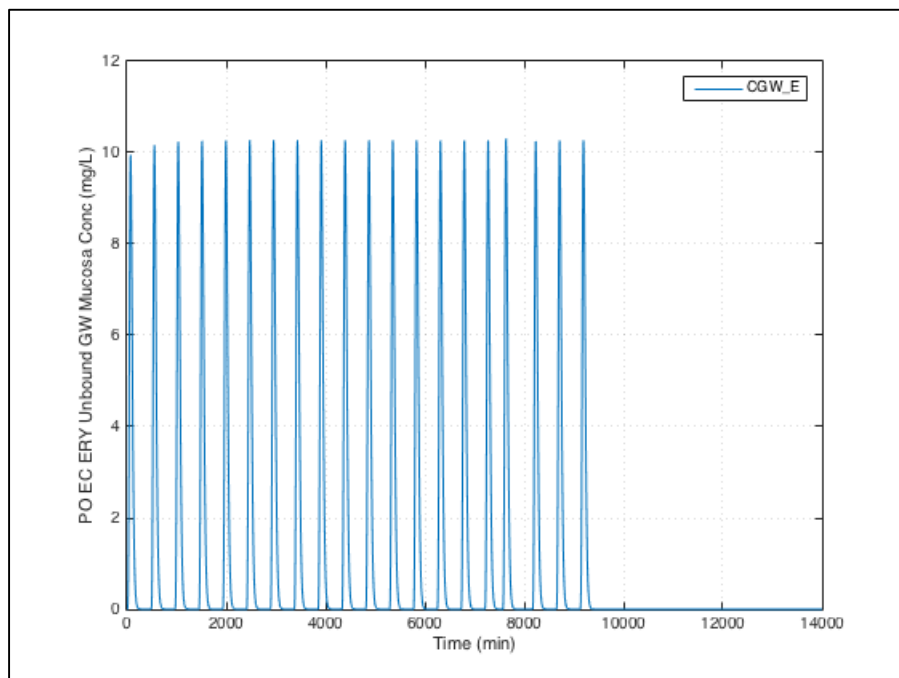


Figure K.29 Sensitivity analysis of ERY unbound GW mucosa concentration to the change in $v_{\max,bile}^{ERY}$. ($v_{\max,bile}^{ERY} = 0.1/0.5/2.5 \mu\text{g}/\text{min}/\text{kg}$ are superimposable)

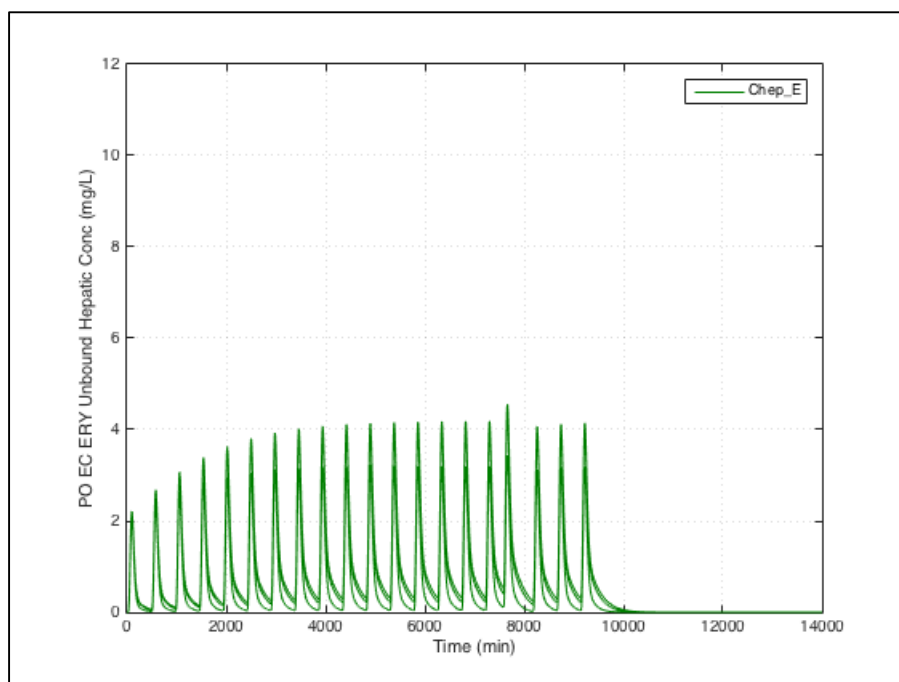


Figure K.30 Sensitivity analysis of ERY unbound hepatic concentration to the change in $v_{\max,bile}^{ERY}$. (top line: $v_{\max,bile}^{ERY} = 0.1 \mu\text{g}/\text{min}/\text{kg}$; middle line: $v_{\max,bile}^{ERY} = 0.5 \mu\text{g}/\text{min}/\text{kg}$; bottom line: $v_{\max,bile}^{ERY} = 2.5 \mu\text{g}/\text{min}/\text{kg}$)

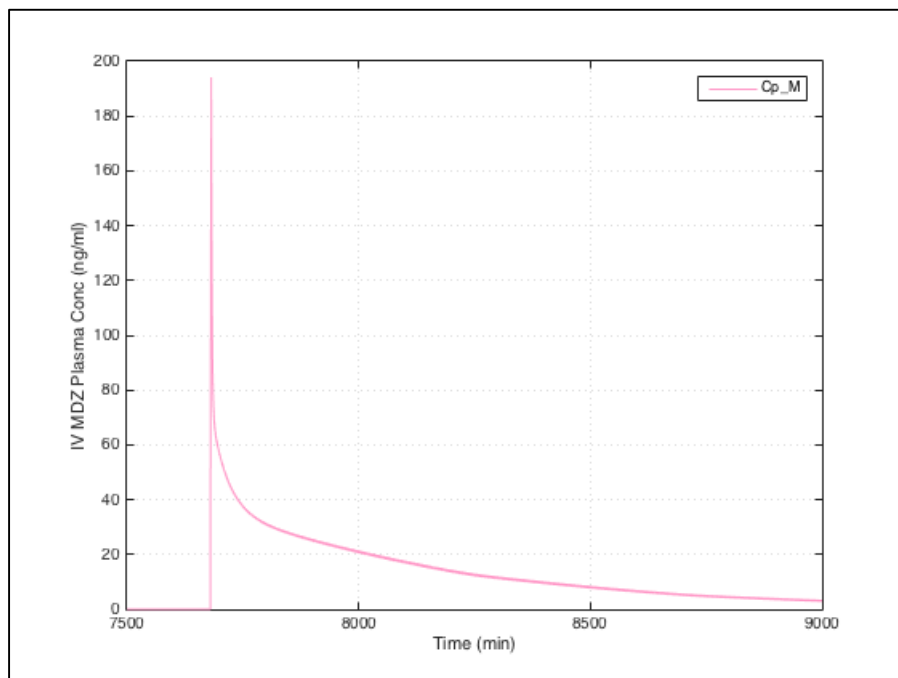


Figure K.31 Sensitivity analysis of IV MDZ plasma concentrations in presence of PO EC ERY to the change in $K_{m,bile}^{ERY}$. ($K_{m,bile}^{ERY} = 0.02/0.1/0.5$ mg/L are superimposable). Time is relative to initial ERY/placebo dose.

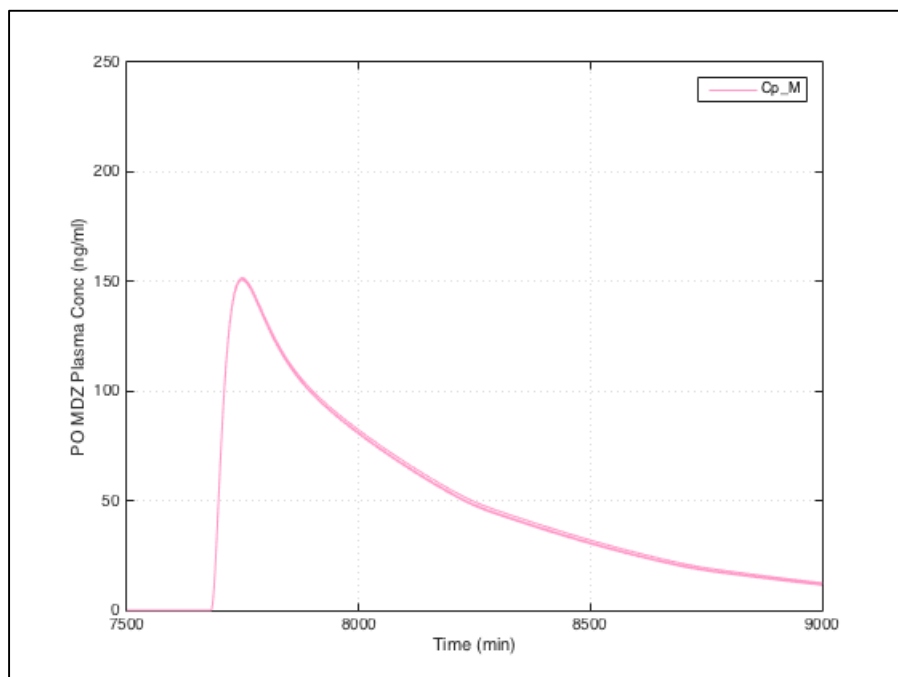


Figure K.32 Sensitivity analysis of PO MDZ plasma concentrations in presence of PO EC ERY to the change in $K_{m,bile}^{ERY}$. ($K_{m,bile}^{ERY} = 0.02/0.1/0.5$ mg/L are superimposable). Time is relative to initial ERY/placebo dose.

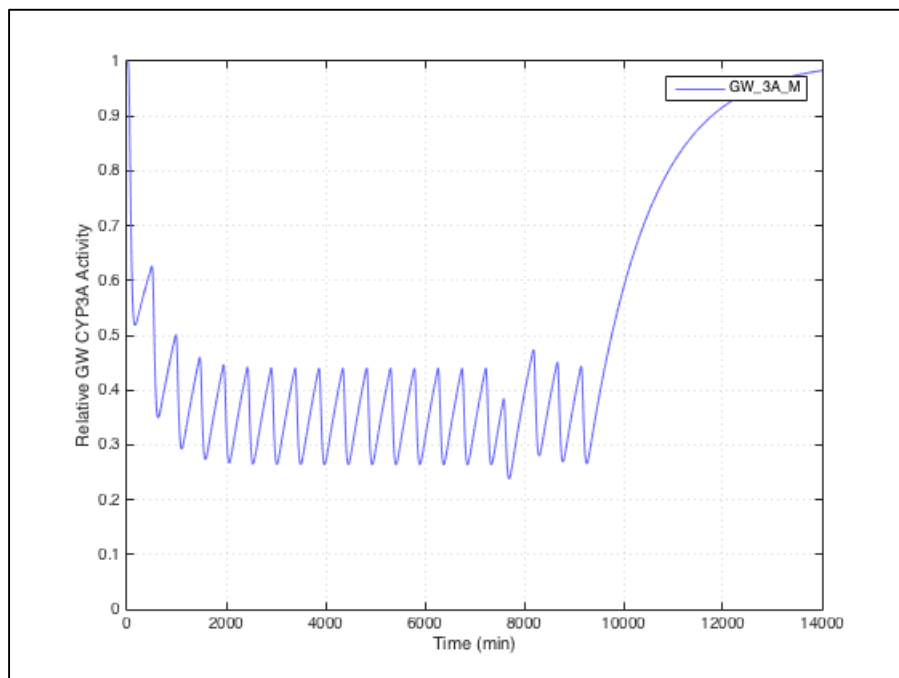


Figure K.33 Sensitivity analysis of relative GW CYP3A activity to the change in $K_{m,bile}^{ERY}$. ($K_{m,bile}^{ERY} = 0.02/0.1/0.5$ mg/L are superimposable)

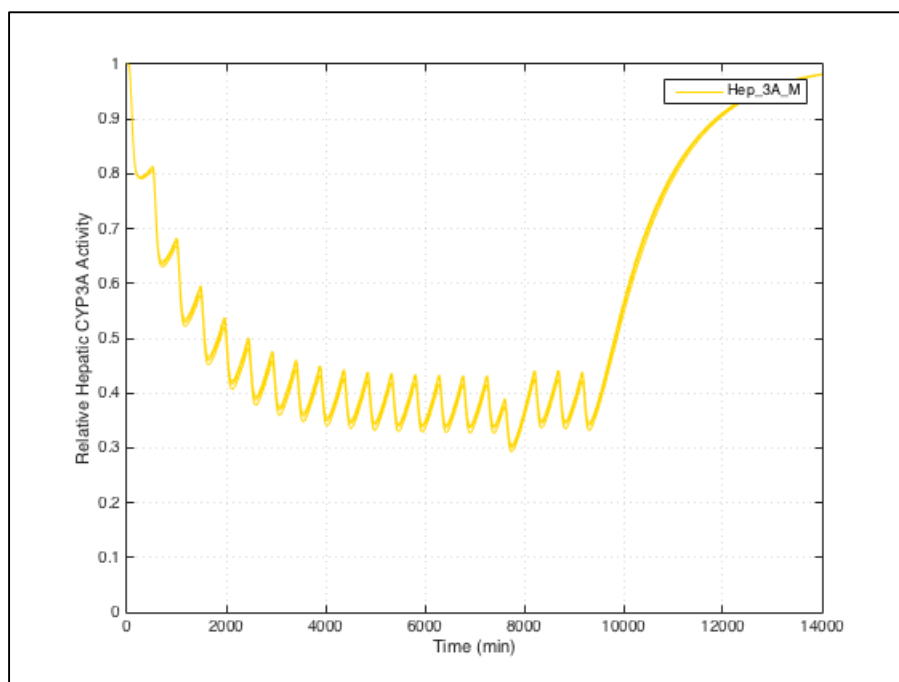


Figure K.34 Sensitivity analysis of relative hepatic CYP3A activity to the change in $K_{m,bile}^{ERY}$. ($K_{m,bile}^{ERY} = 0.02/0.1/0.5$ mg/L are superimposable)

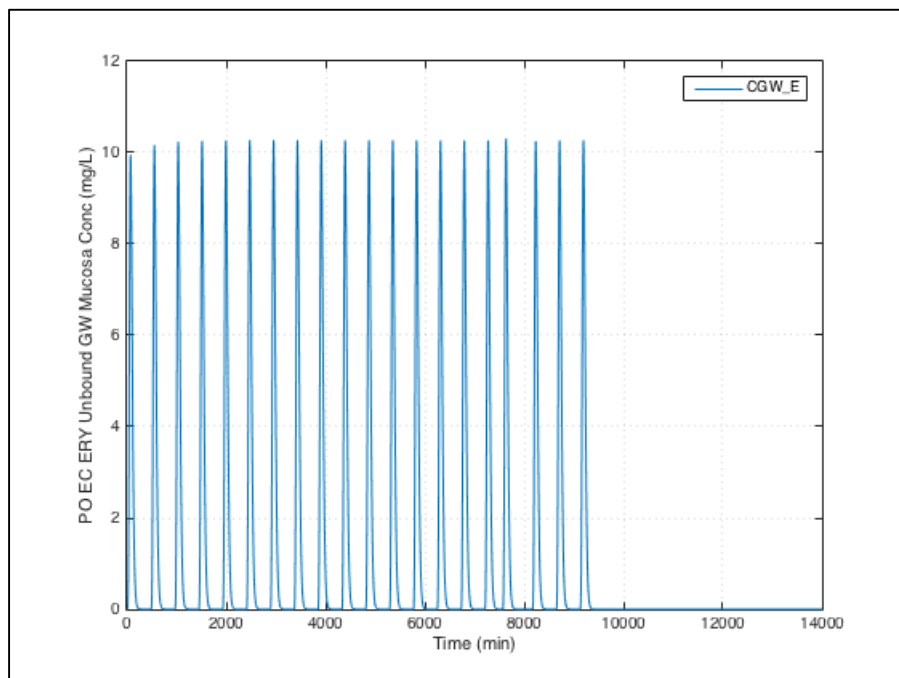


Figure K.35 Sensitivity analysis of ERY unbound GW mucosa concentration to the change in $K_{m,bile}^{ERY}$ ($K_{m,bile}^{ERY} = 0.02/0.1/0.5$ mg/L are superimposable).

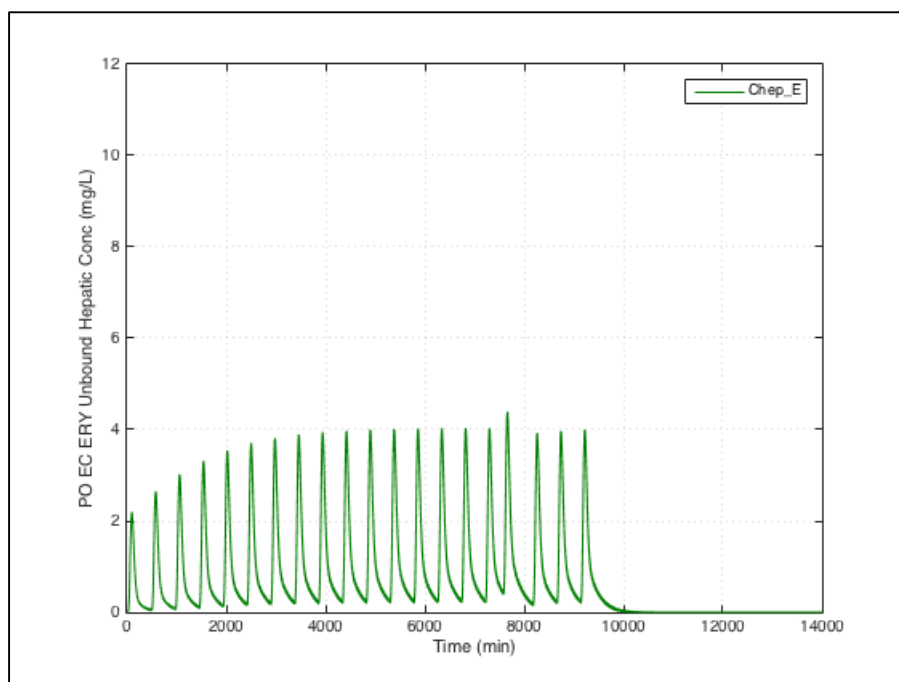


Figure K.36 Sensitivity analysis of ERY unbound hepatic concentration to the change in $K_{m,bile}^{ERY}$ ($K_{m,bile}^{ERY} = 0.02/0.1/0.5$ mg/L are superimposable).

L. SENSITIVITY ANALYSIS OF DDI BETWEEN MDZ AND SS ERY FOR STUDY 603

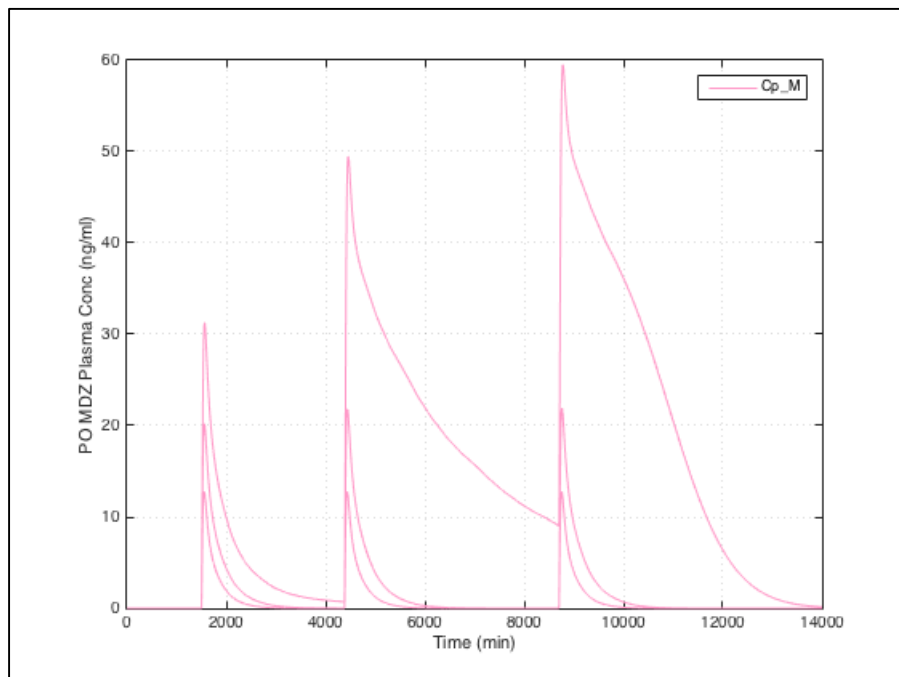


Figure L.1 Sensitivity analysis of PO MDZ (administered on day 2, 4 and 7) plasma concentrations in presence of PO SS ERY to the change in k_{deg} . (top line: $k_{deg} = 0.00016 \text{ min}^{-1}$; middle line: $k_{deg} = 0.0008 \text{ min}^{-1}$; bottom line: $k_{deg} = 0.004 \text{ min}^{-1}$). Time is relative to initial ERY/placebo dose.

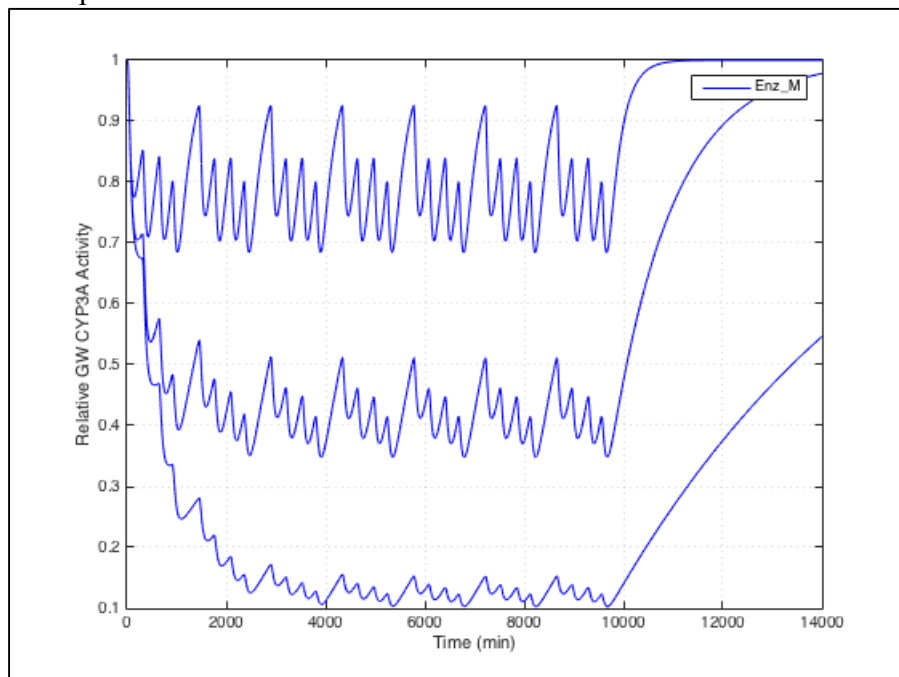


Figure L.2 Sensitivity analysis of relative GW CYP3A activity to the change in k_{deg} . (top line: $k_{deg} = 0.004 \text{ min}^{-1}$; middle line: $k_{deg} = 0.0008 \text{ min}^{-1}$; bottom line: $k_{deg} = 0.00016 \text{ min}^{-1}$)

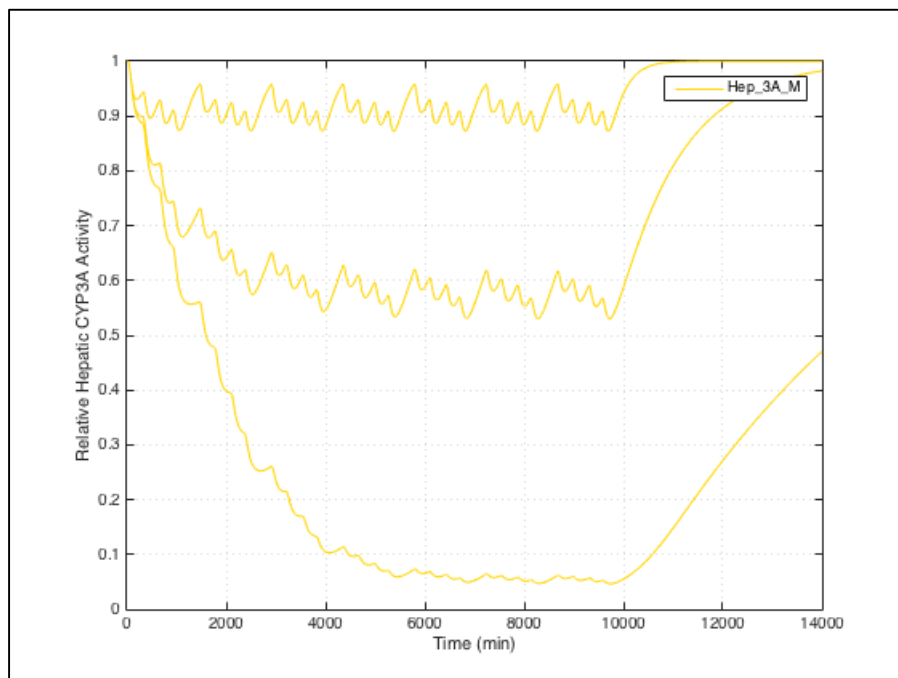


Figure L.3 Sensitivity analysis of relative hepatic CYP3A activity to the change in k_{deg} . (top line: $k_{deg} = 0.004 \text{ min}^{-1}$; middle line: $k_{deg} = 0.0008 \text{ min}^{-1}$; bottom line: $k_{deg} = 0.00016 \text{ min}^{-1}$)

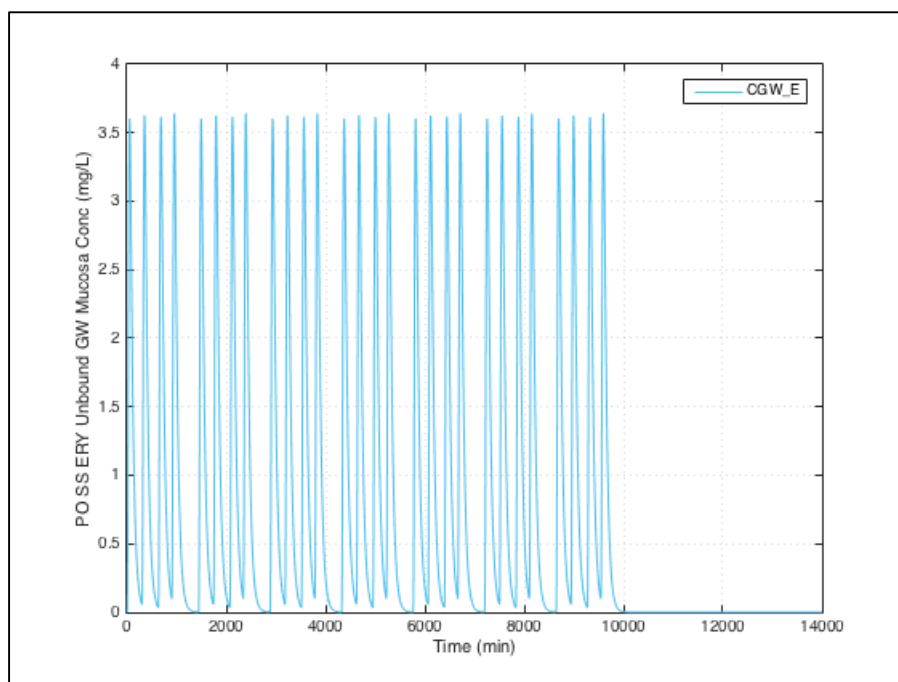


Figure L.4 Sensitivity analysis of ERY unbound GW mucosa concentration to the change in k_{deg} . ($k_{deg} = 0.00016/0.0008/0.004 \text{ min}^{-1}$ are superimposable.)

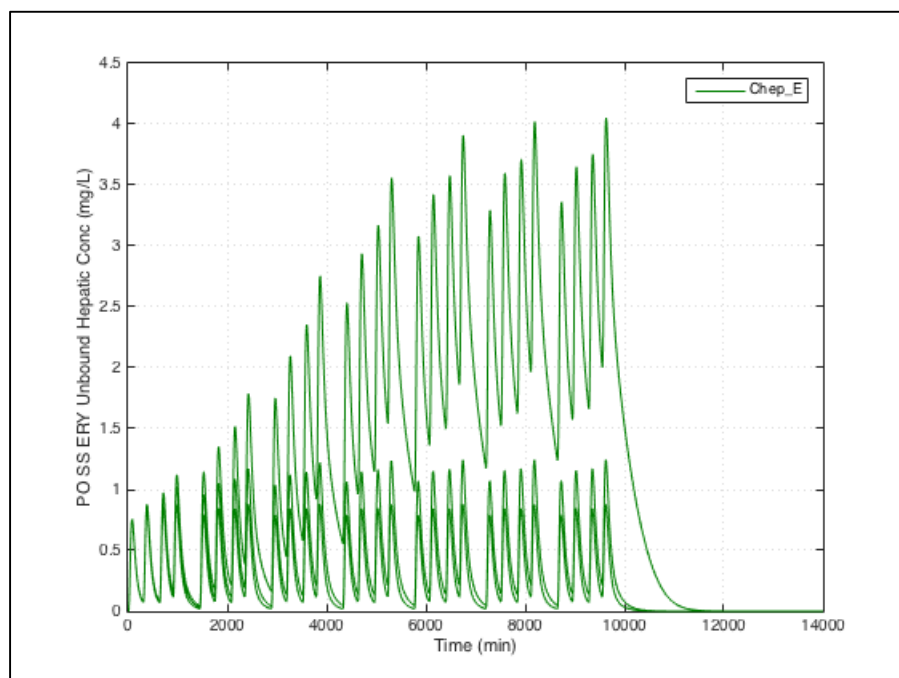


Figure L.5 Sensitivity analysis of ERY unbound hepatic concentration to the change in k_{deg} . (top line: $k_{deg} = 0.00016 \text{ min}^{-1}$; middle line: $k_{deg} = 0.0008 \text{ min}^{-1}$; bottom line: $k_{deg} = 0.004 \text{ min}^{-1}$)

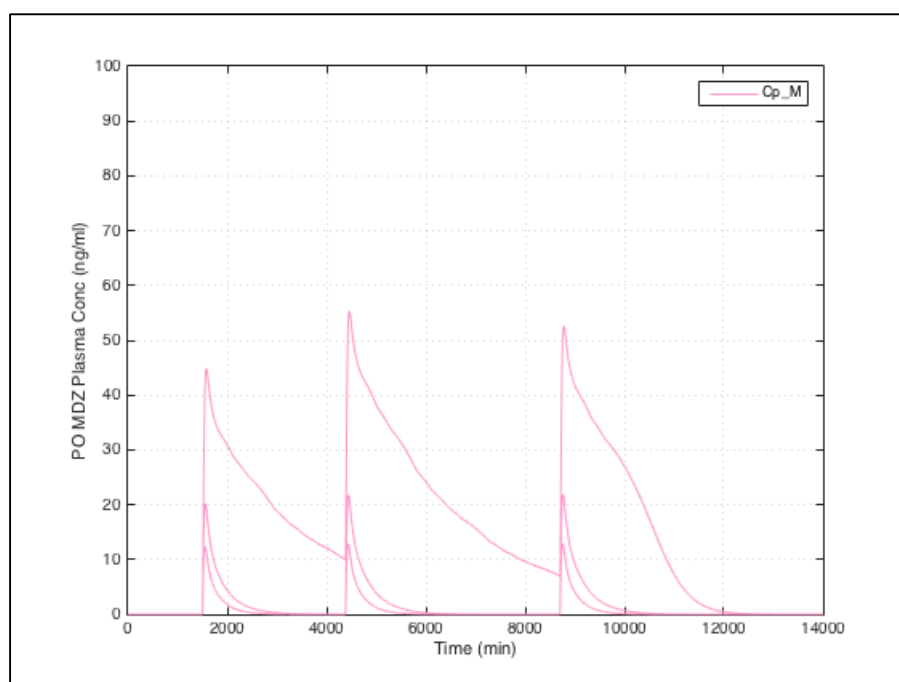


Figure L.6 Sensitivity analysis of PO MDZ (administered on day 2, 4 and 7) plasma concentrations in presence of PO EC ERY to the change in K_I^{ERY} . (top line: $K_I^{ERY} = 6 \text{ mg/L}$; middle line: $K_I^{ERY} = 30 \text{ mg/L}$; bottom line: $K_I^{ERY} = 150 \text{ mg/L}$). Time is relative to initial ERY/placebo dose.

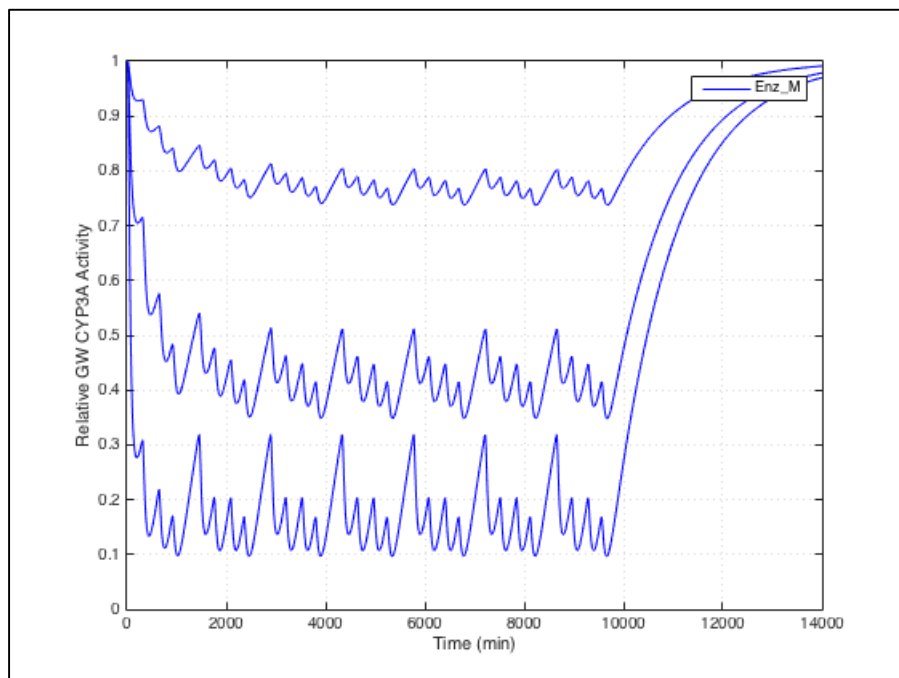


Figure L.7 Sensitivity analysis of relative GW CYP3A activity to the change in K_I^{ERY} . (top line: $K_I^{ERY} = 150$ mg/L; middle line: $K_I^{ERY} = 30$ mg/L; bottom line: $K_I^{ERY} = 6$ mg/L)

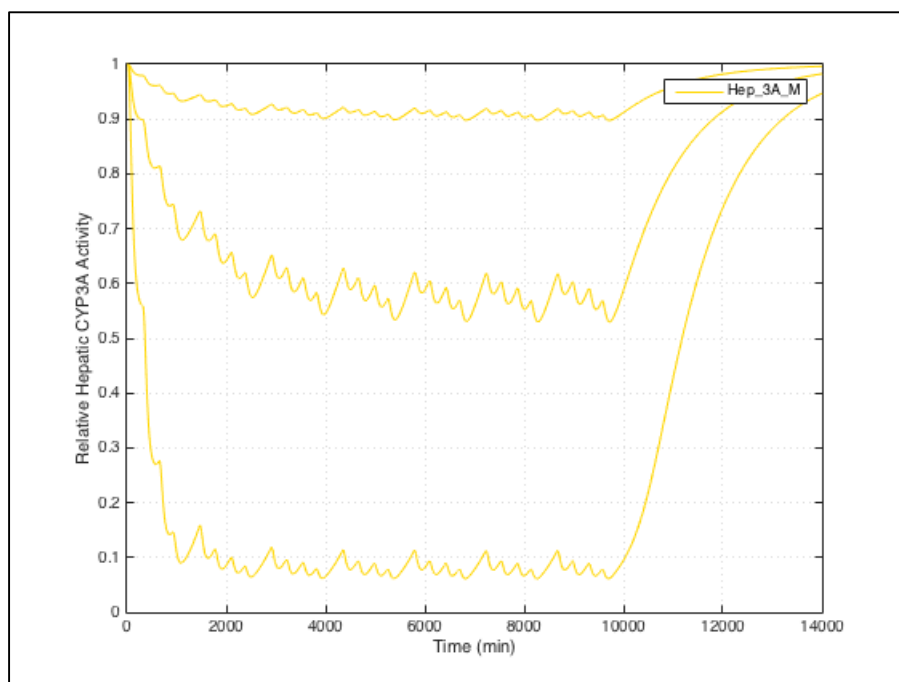


Figure L.8 Sensitivity analysis of relative hepatic CYP3A activity to the change in K_I^{ERY} . (top line: $K_I^{ERY} = 150$ mg/L; middle line: $K_I^{ERY} = 30$ mg/L; bottom line: $K_I^{ERY} = 6$ mg/L)

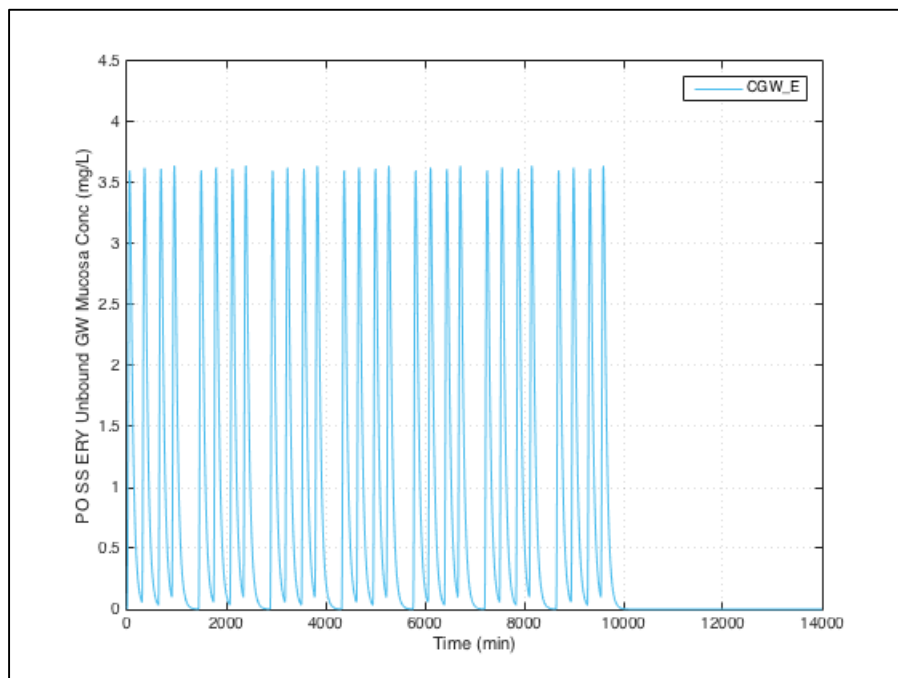


Figure L.9 Sensitivity analysis of ERY unbound GW mucosa concentration to the change in K_I^{ERY} . ($K_I^{ERY} = 6/30/150$ mg/L are superimposable)

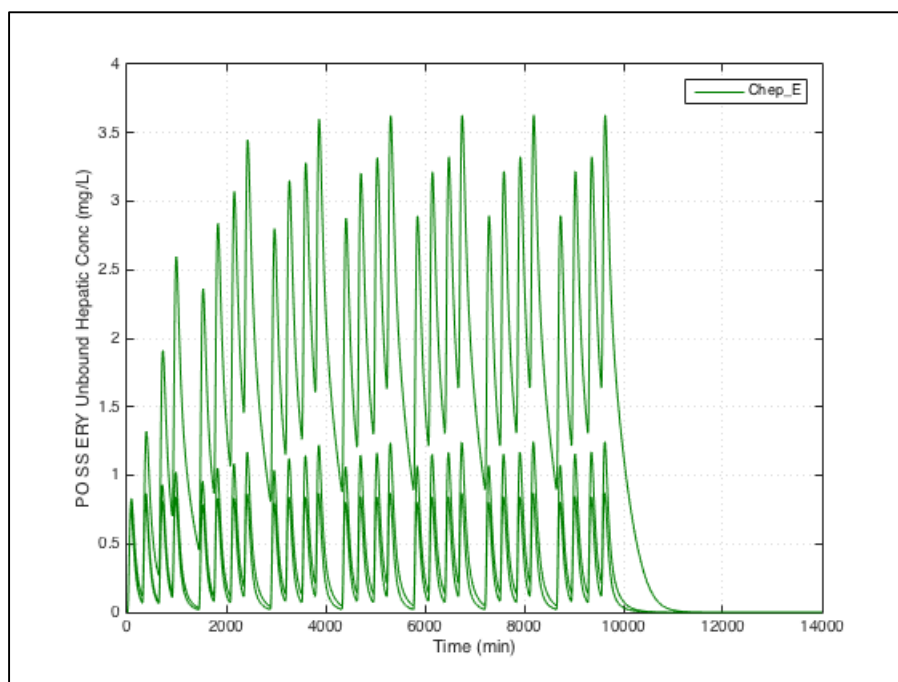


Figure L.10 Sensitivity analysis of ERY unbound hepatic concentration to the change in K_I^{ERY} . (top line: $K_I^{ERY} = 6$ mg/L; middle line: $K_I^{ERY} = 30$ mg/L; bottom line: $K_I^{ERY} = 150$ mg/L)

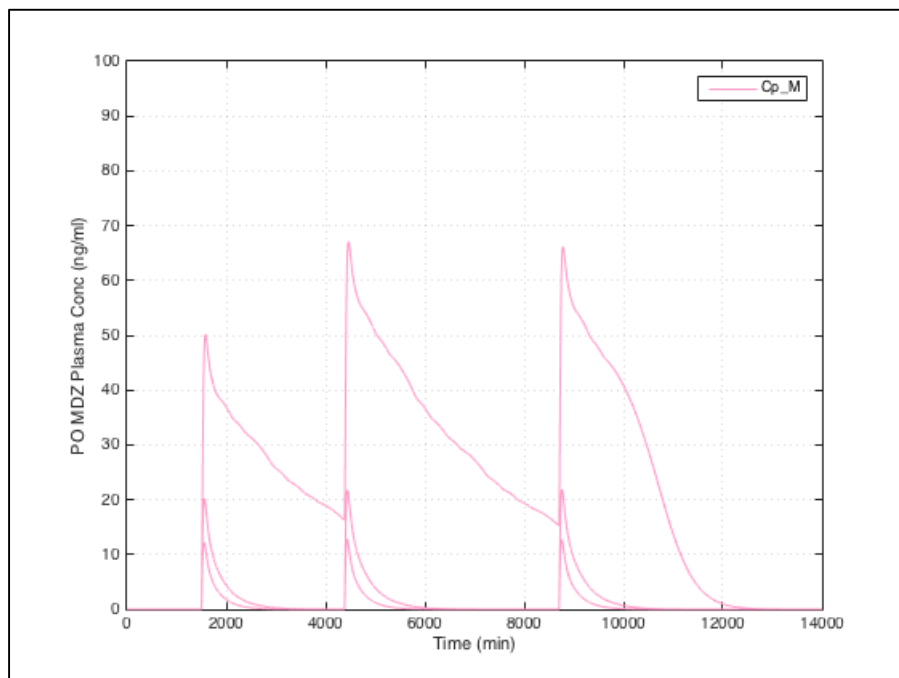


Figure L.11 Sensitivity analysis of PO MDZ (administered on day 2, 4 and 7) plasma concentrations in presence of PO EC ERY to the change in k_{inact}^{ERY} . (top line: $k_{inact}^{ERY} = 0.1875 \text{ min}^{-1}$; middle line: $k_{inact}^{ERY} = 0.0375 \text{ min}^{-1}$; bottom line: $k_{inact}^{ERY} = 0.0075 \text{ min}^{-1}$). Time is relative to initial ERY/placebo dose.

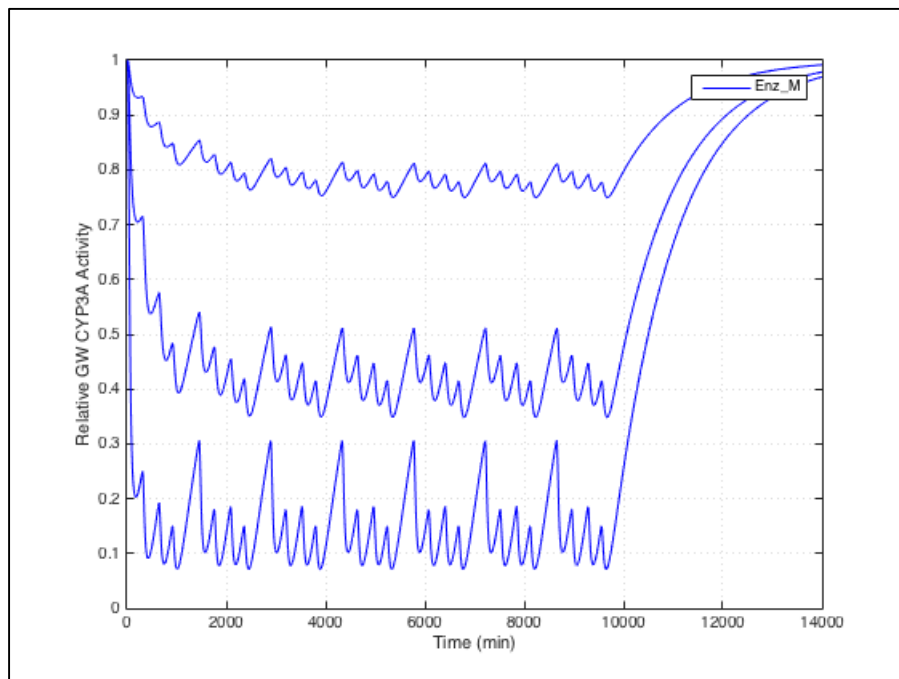


Figure L.12 Sensitivity analysis of relative GW CYP3A activity to the change in k_{inact}^{ERY} . (top line: $k_{inact}^{ERY} = 0.0075 \text{ min}^{-1}$; middle line: $k_{inact}^{ERY} = 0.0375 \text{ min}^{-1}$; bottom line: $k_{inact}^{ERY} = 0.1875 \text{ min}^{-1}$)

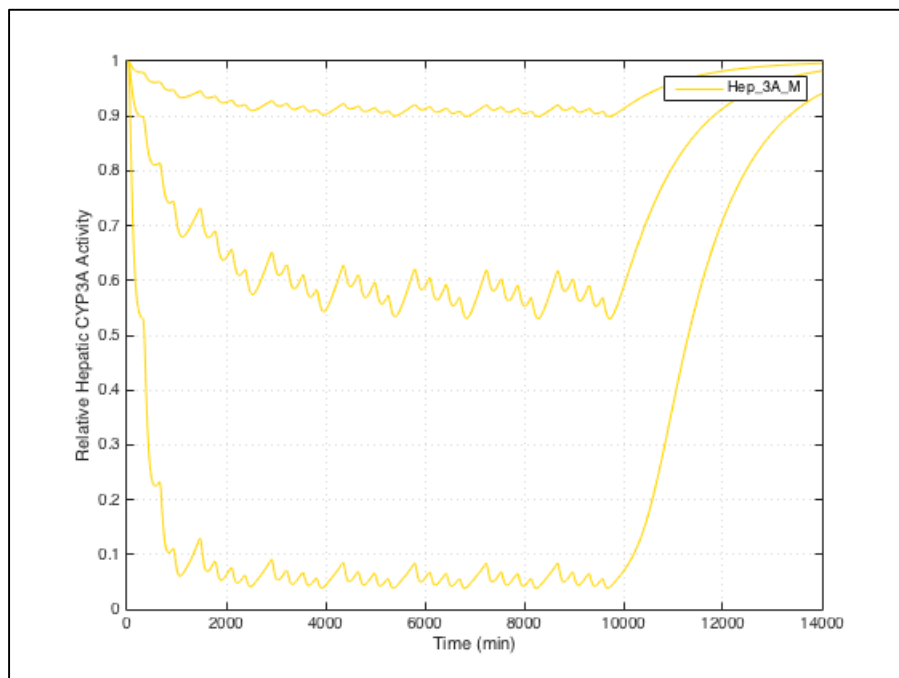


Figure L.13 Sensitivity analysis of relative hepatic CYP3A activity to the change in $k_{\text{inact}}^{\text{ERY}}$. (top line: $k_{\text{inact}}^{\text{ERY}} = 0.0075 \text{ min}^{-1}$; middle line: $k_{\text{inact}}^{\text{ERY}} = 0.0375 \text{ min}^{-1}$; bottom line: $k_{\text{inact}}^{\text{ERY}} = 0.1875 \text{ min}^{-1}$)

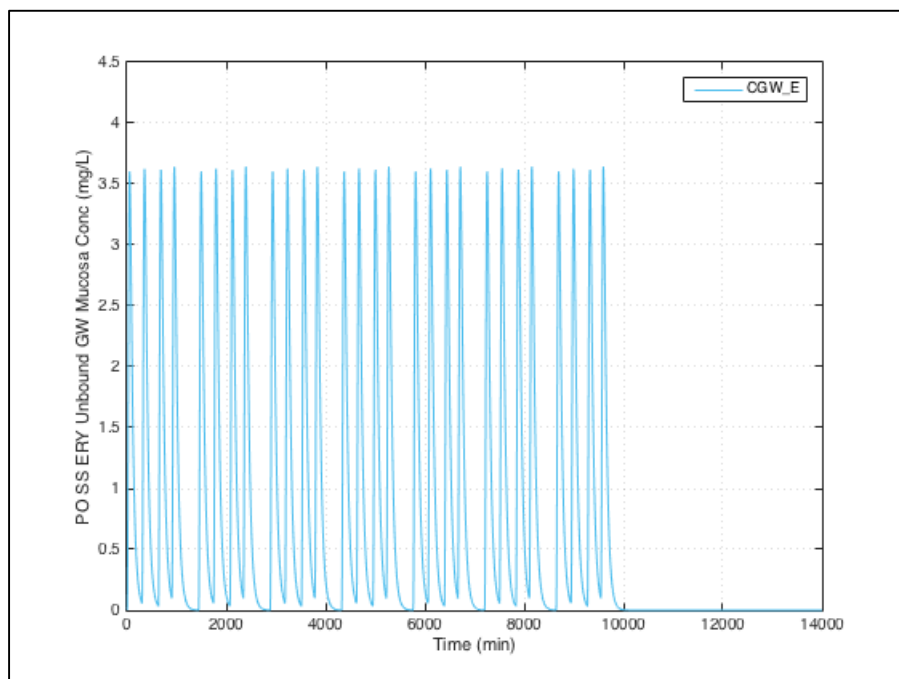


Figure L.14 Sensitivity analysis of ERY unbound GW mucosa concentration to the change in $k_{\text{inact}}^{\text{ERY}}$. ($k_{\text{inact}}^{\text{ERY}} = 0.0075/0.0375/0.1875 \text{ min}^{-1}$ are superimposable)

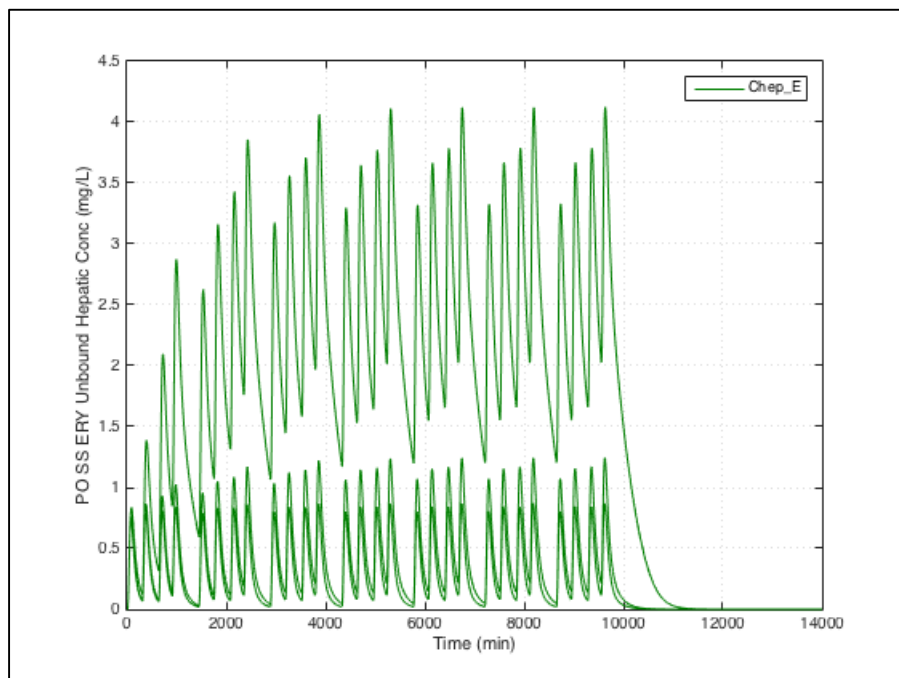


Figure L.15 Sensitivity analysis of ERY unbound hepatic concentration to the change in k_{inact}^{ERY} . (top line: $k_{inact}^{ERY} = 0.1875 \text{ min}^{-1}$; middle line: $k_{inact}^{ERY} = 0.0375 \text{ min}^{-1}$; bottom line: $k_{inact}^{ERY} = 0.0075 \text{ min}^{-1}$)

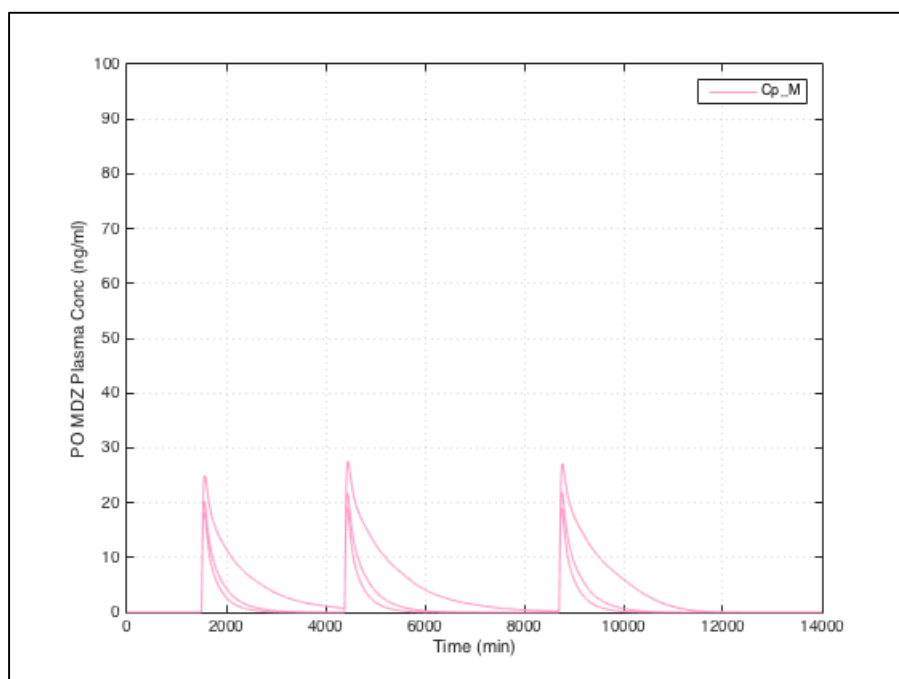


Figure L.16 Sensitivity analysis of PO MDZ (administered on day 2, 4, or 7) plasma concentrations in presence of PO EC ERY to the change in $v_{max,hep-3A}^{ERY}$. (top line: $v_{max,hep-3A}^{ERY} = 160 \text{ µg/min/kg}$; middle line: $v_{max,hep-3A}^{ERY} = 800 \text{ µg/min/kg}$, bottom line: $v_{max,hep-3A}^{ERY} = 4000 \text{ µg/min/kg}$). Time is relative to initial ERY/placebo dose.

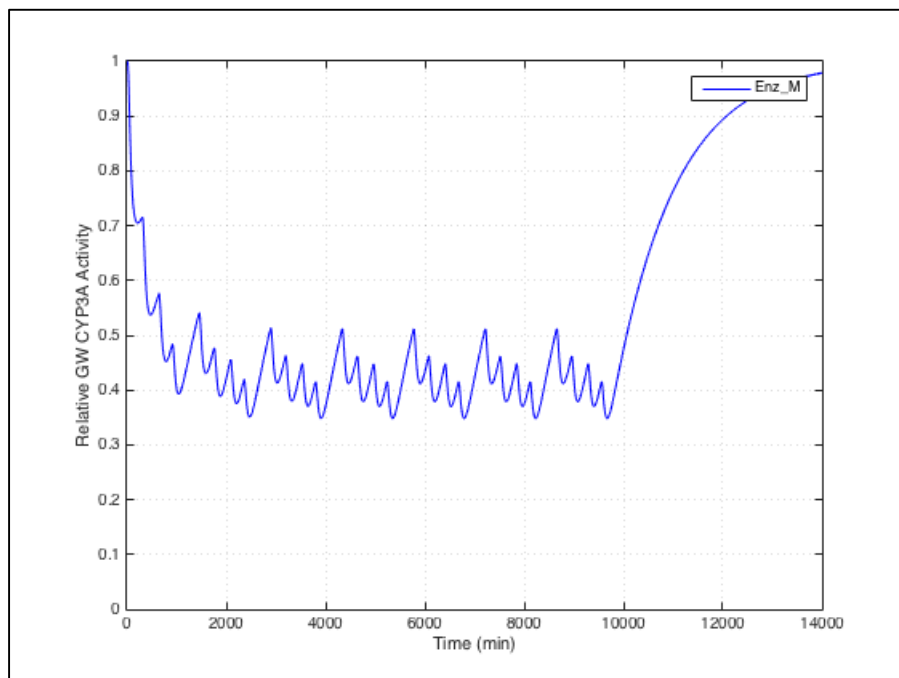


Figure L.17 Sensitivity analysis of relative GW CYP3A activity to the change in $v_{\max, \text{hep-3A}}^{\text{ERY}}$. ($v_{\max, \text{hep-3A}}^{\text{ERY}} = 160/800/4000 \mu\text{g}/\text{min}/\text{kg}$ are superimposable.)

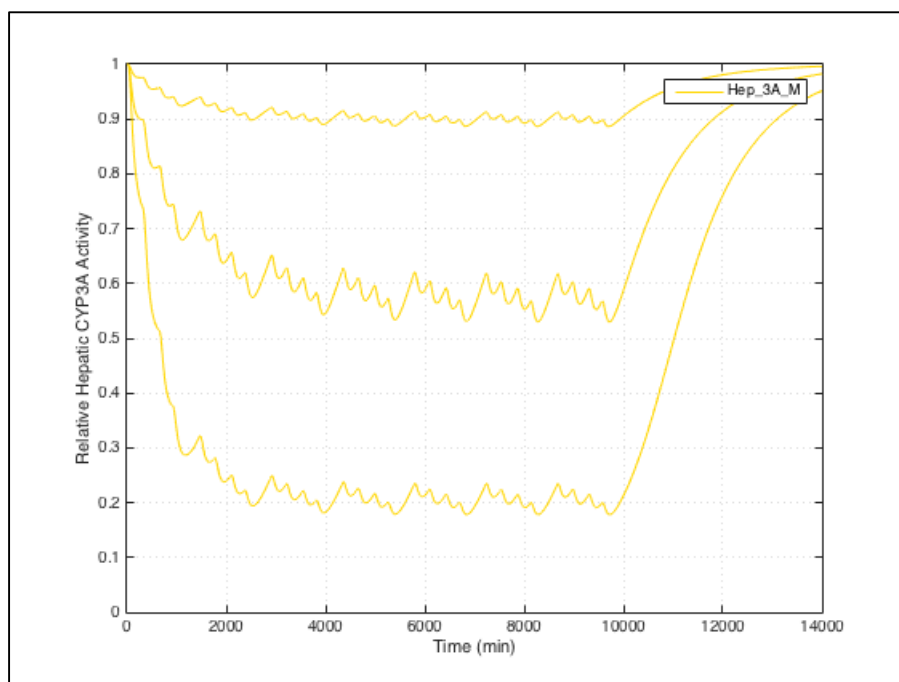


Figure L.18 Sensitivity analysis of relative hepatic CYP3A activity to the change in $v_{\max, \text{hep-3A}}^{\text{ERY}}$. (top line: $v_{\max, \text{hep-3A}}^{\text{ERY}} = 4000 \mu\text{g}/\text{min}/\text{kg}$; middle line: $v_{\max, \text{hep-3A}}^{\text{ERY}} = 800 \mu\text{g}/\text{min}/\text{kg}$; bottom line: $v_{\max, \text{hep-3A}}^{\text{ERY}} = 160 \mu\text{g}/\text{min}/\text{kg}$)

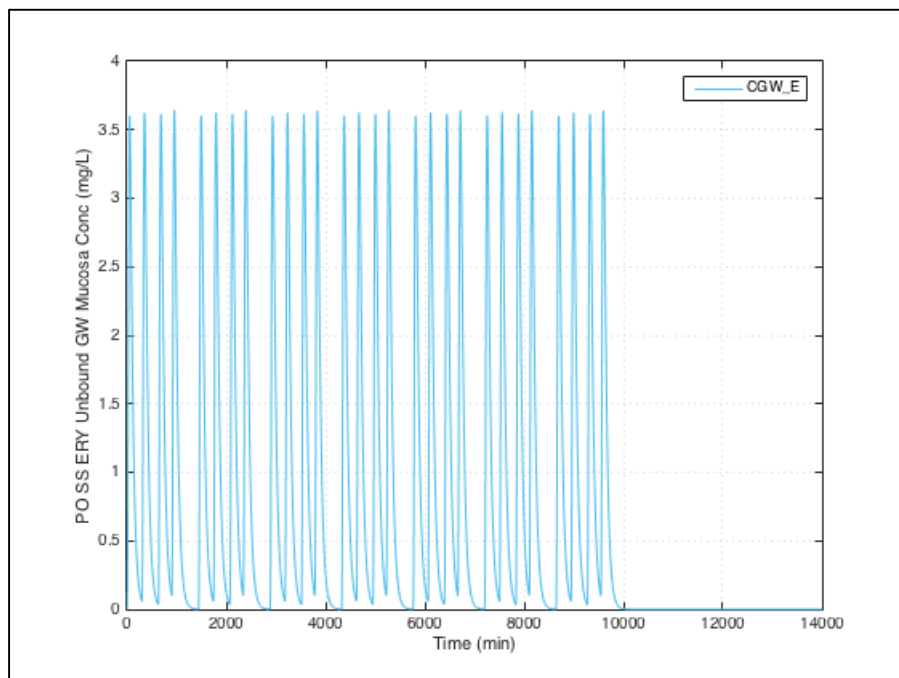


Figure L.19 Sensitivity analysis of ERY unbound GW mucosa concentration to the change in $v_{\max, \text{hep-3A}}^{\text{ERY}}$. ($v_{\max, \text{hep-3A}}^{\text{ERY}} = 160/800/4000 \mu\text{g}/\text{min}/\text{kg}$ are superimposable)

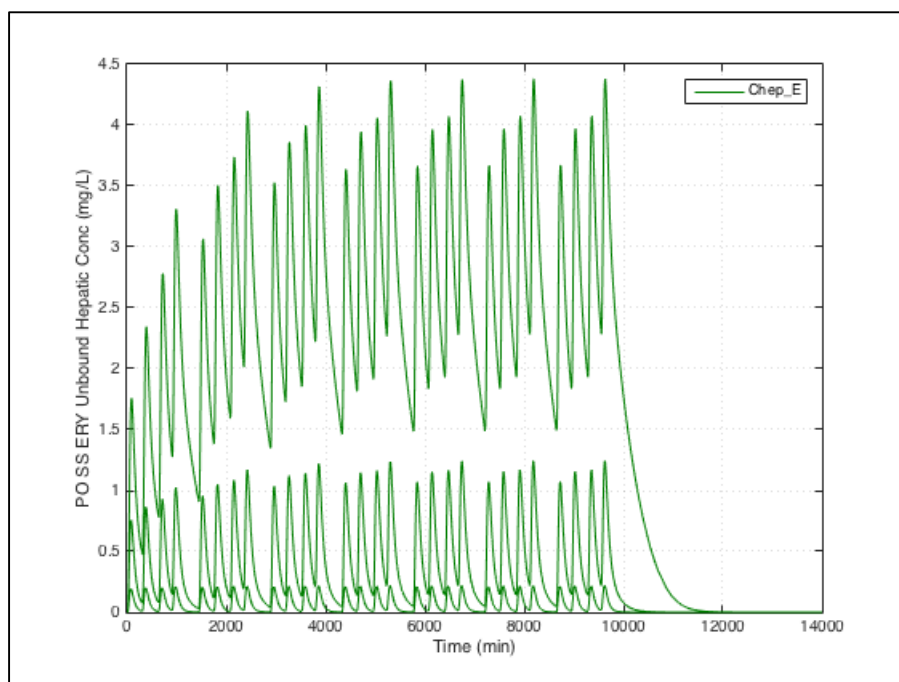


Figure L.20 Sensitivity analysis of ERY unbound hepatic concentration to the change in $v_{\max, \text{hep-3A}}^{\text{ERY}}$. (top line: $v_{\max, \text{hep-3A}}^{\text{ERY}} = 160 \mu\text{g}/\text{min}/\text{kg}$; middle line: $v_{\max, \text{hep-3A}}^{\text{ERY}} = 800 \mu\text{g}/\text{min}/\text{kg}$; bottom line: $v_{\max, \text{hep-3A}}^{\text{ERY}} = 4000 \mu\text{g}/\text{min}/\text{kg}$)

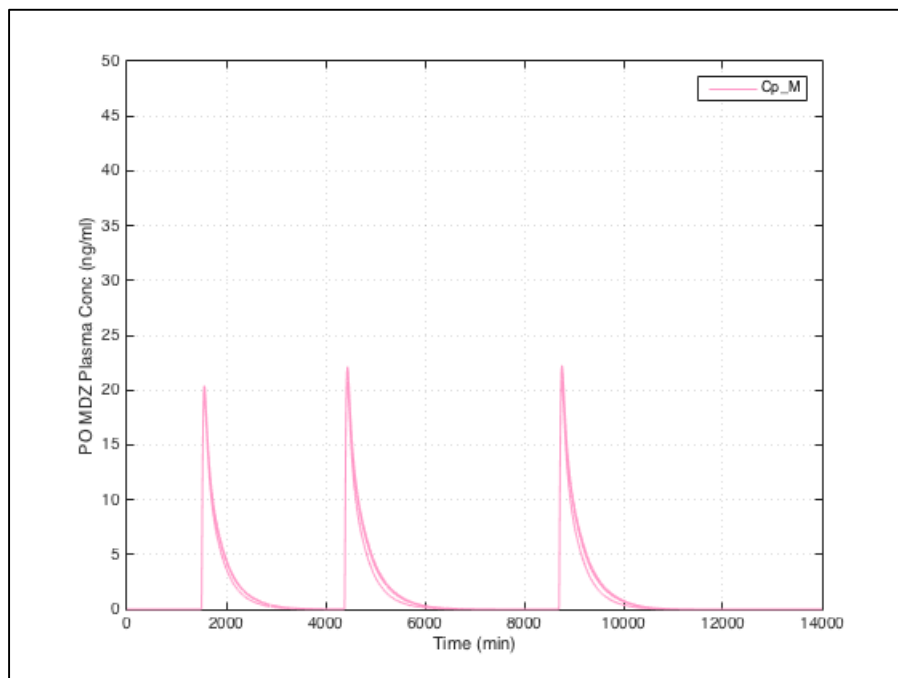


Figure L.21 Sensitivity analysis of IV MDZ plasma concentrations in presence of PO EC ERY to the change in $v_{\max, \text{bile}}^{\text{ERY}}$. (top line: $v_{\max, \text{bile}}^{\text{ERY}} = 0.1 \mu\text{g}/\text{min}/\text{kg}$; middle line: $v_{\max, \text{bile}}^{\text{ERY}} = 0.5 \mu\text{g}/\text{min}/\text{kg}$, bottom line: $v_{\max, \text{bile}}^{\text{ERY}} = 2.5 \mu\text{g}/\text{min}/\text{kg}$). Time is relative to initial ERY/placebo dose.

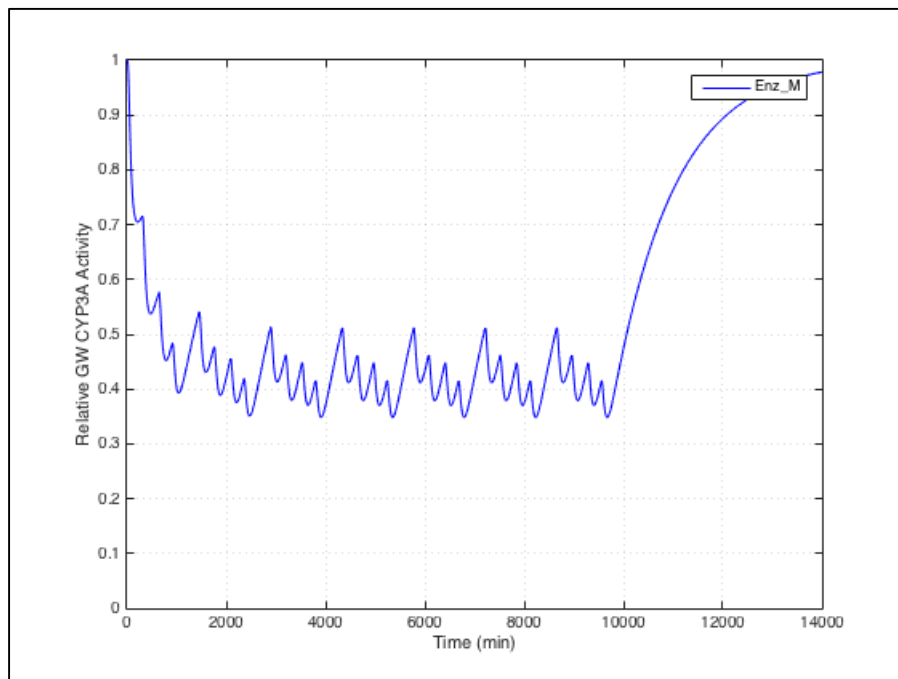


Figure L.12 Sensitivity analysis of relative GW CYP3A activity to the change in $v_{\max, \text{bile}}^{\text{ERY}}$. ($v_{\max, \text{bile}}^{\text{ERY}} = 0.1/0.5/2.5 \mu\text{g}/\text{min}/\text{kg}$ are superimposable)

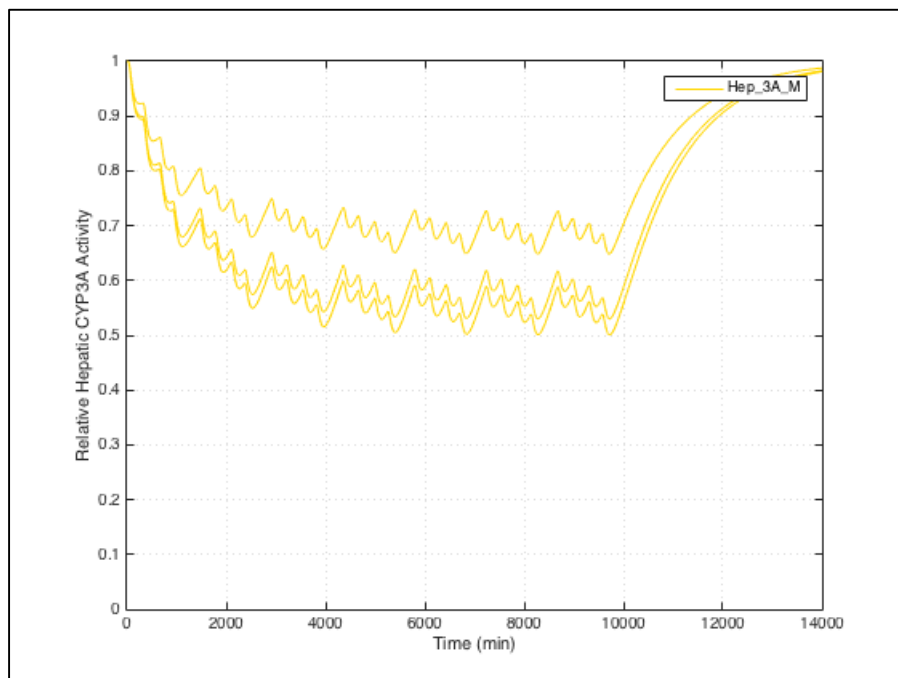


Figure L.23 Sensitivity analysis of relative hepatic CYP3A activity to the change in $v_{\max,bile}^{ERY}$. (Top line: $v_{\max,bile}^{ERY} = 2.5 \mu\text{g}/\text{min}/\text{kg}$; middle line: $v_{\max,bile}^{ERY} = 0.5 \mu\text{g}/\text{min}/\text{kg}$; bottom line: $v_{\max,bile}^{ERY} = 0.1 \mu\text{g}/\text{min}/\text{kg}$)

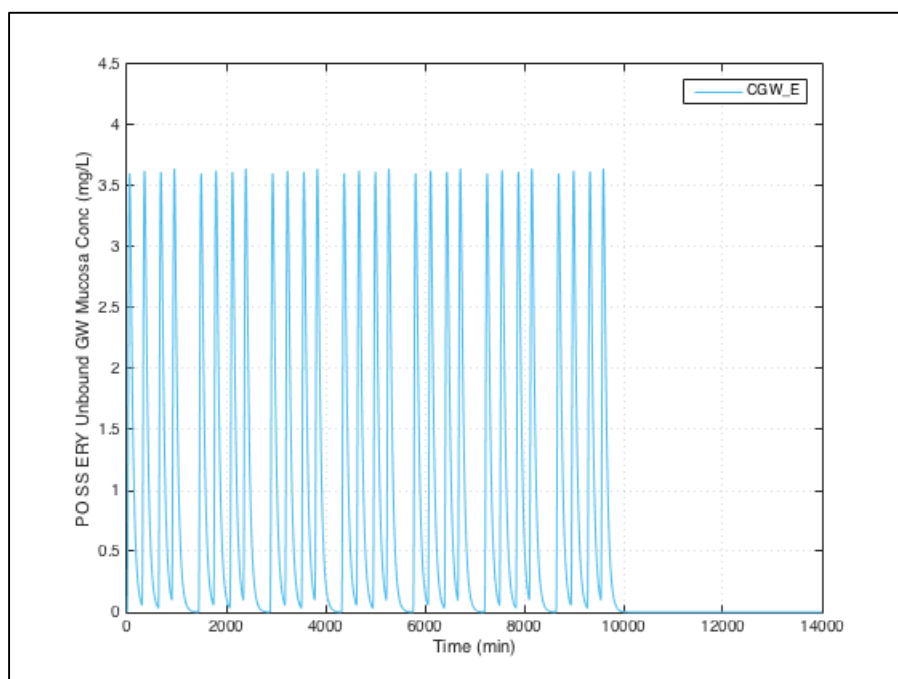


Figure L.24 Sensitivity analysis of ERY unbound GW mucosa concentration to the change in $v_{\max,bile}^{ERY}$. ($v_{\max,bile}^{ERY} = 0.1/0.5/2.5 \mu\text{g}/\text{min}/\text{kg}$ are superimposable)

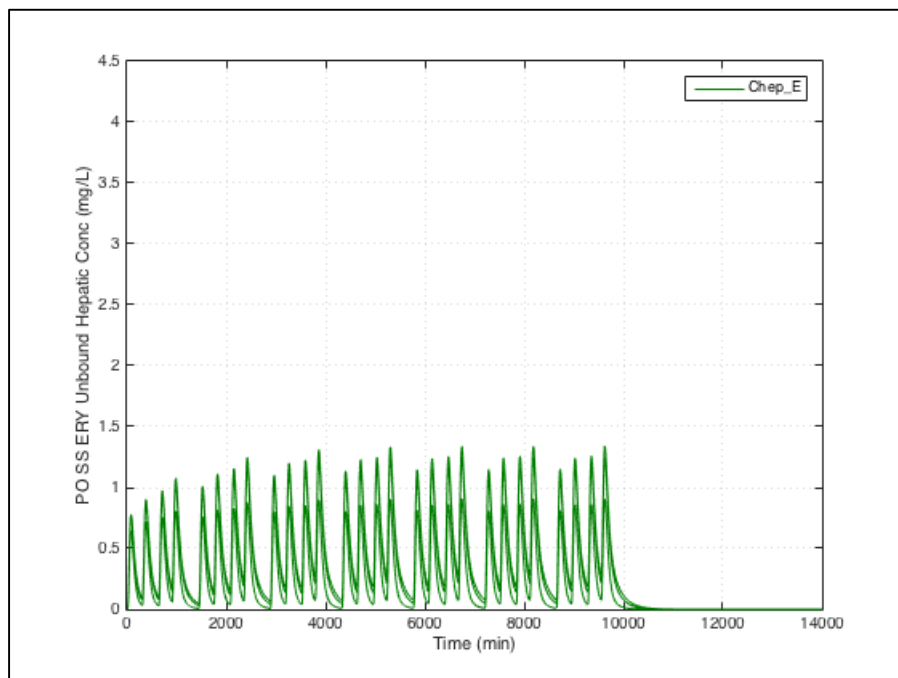


Figure L.25 Sensitivity analysis of ERY unbound hepatic concentration to the change in $v_{\max,bile}^{ERY}$. (top line: $v_{\max,bile}^{ERY} = 0.1 \mu\text{g}/\text{min}/\text{kg}$; middle line: $v_{\max,bile}^{ERY} = 0.5 \mu\text{g}/\text{min}/\text{kg}$; bottom line: $v_{\max,bile}^{ERY} = 2.5 \mu\text{g}/\text{min}/\text{kg}$)

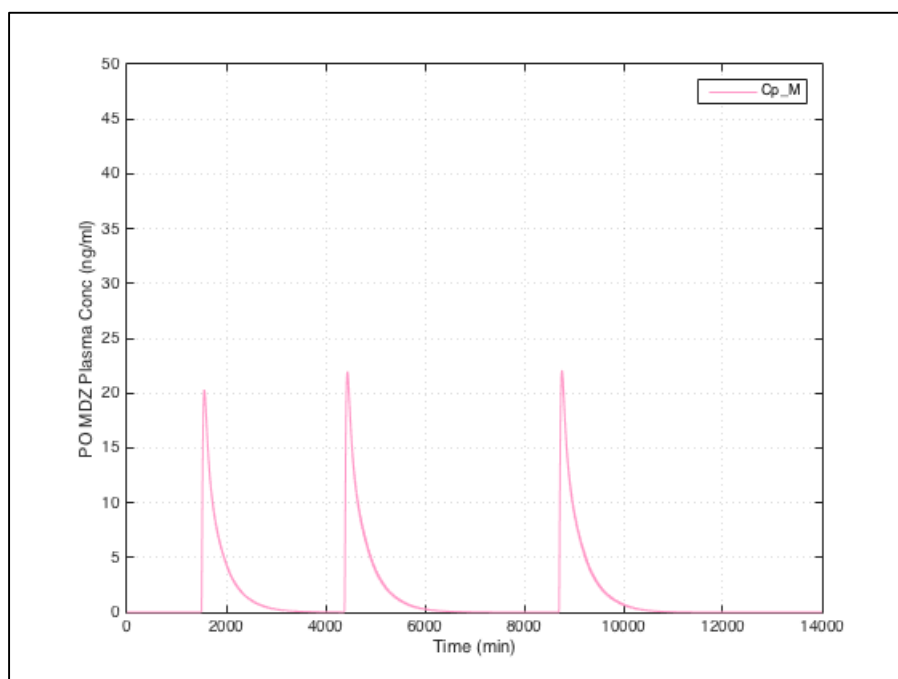


Figure L.26 Sensitivity analysis of PO MDZ (administered on day 2, 4, and 7) plasma concentrations in presence of PO EC ERY to the change in $K_{m,bile}^{ERY}$. ($K_{m,bile}^{ERY} = 0.02/0.1/0.5 \text{ mg}/\text{L}$ are superimposable). Time is relative to initial ERY/placebo dose.

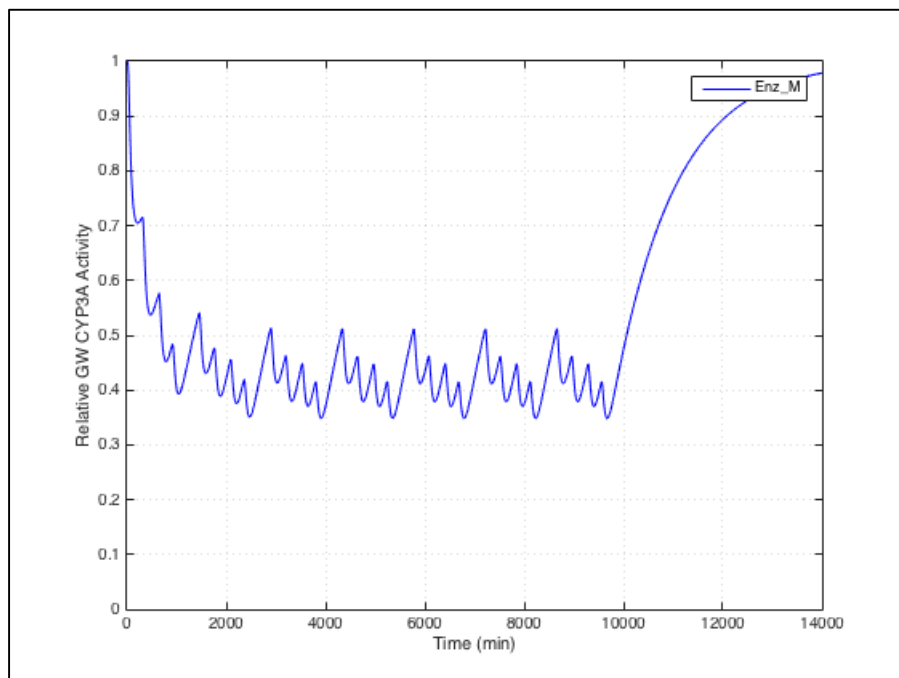


Figure L.27 Sensitivity analysis of relative GW CYP3A activity to the change in $K_{m,bile}^{ERY}$. ($K_{m,bile}^{ERY} = 0.02/0.1/0.5$ mg/L are superimposable)

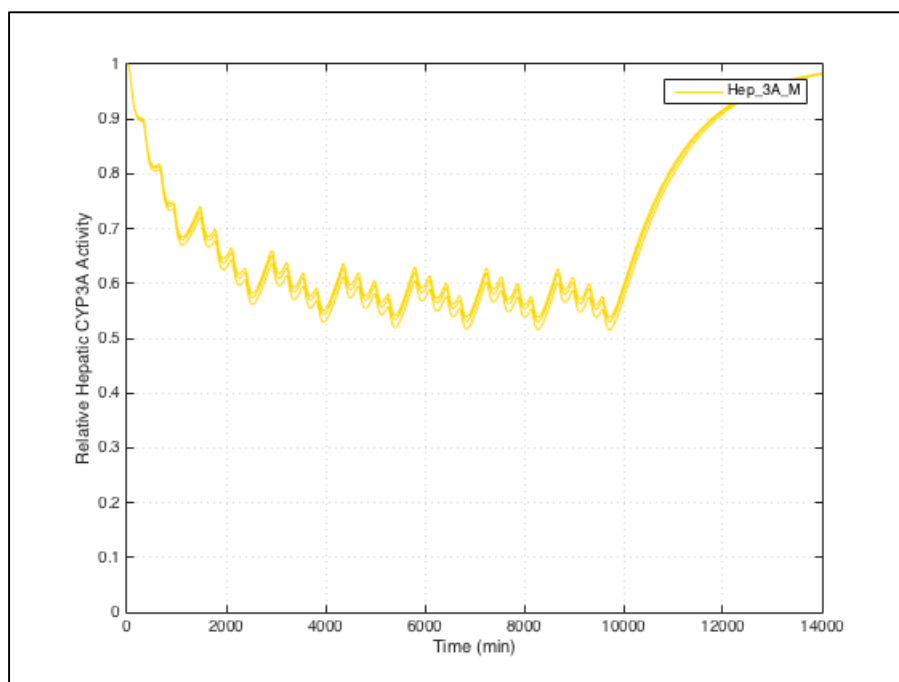


Figure L.28 Sensitivity analysis of relative hepatic CYP3A activity to the change in $K_{m,bile}^{ERY}$. ($K_{m,bile}^{ERY} = 0.02/0.1/0.5$ mg/L are superimposable)

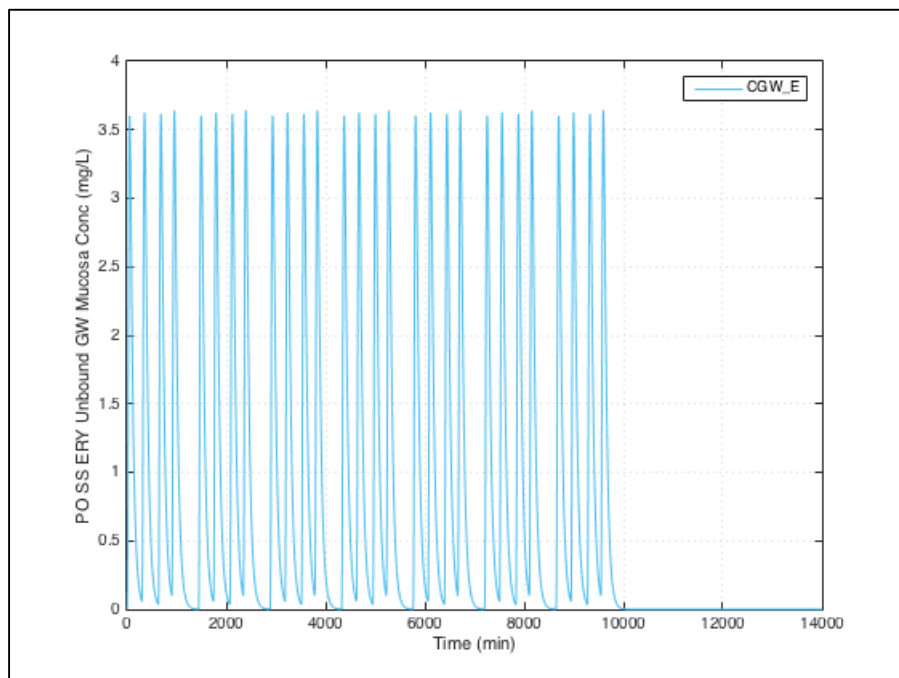


Figure L.29 Sensitivity analysis of ERY unbound GW mucosa concentration to the change in $K_{m,bile}^{ERY}$ ($K_{m,bile}^{ERY} = 0.02/0.1/0.5$ mg/L are superimposable).

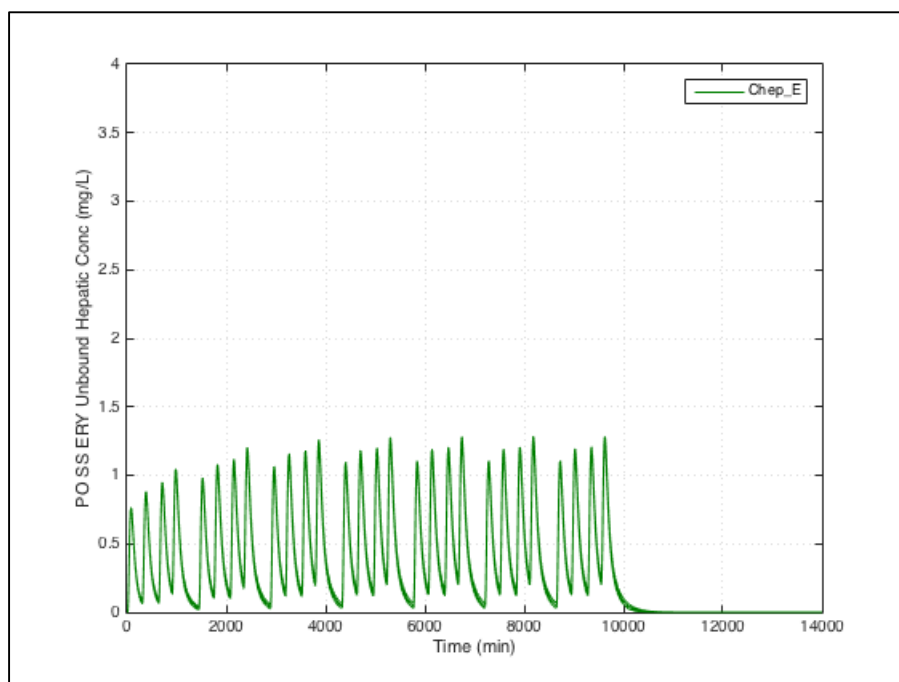


Figure L.30 Sensitivity analysis of ERY unbound hepatic concentration to the change in $K_{m,bile}^{ERY}$ ($K_{m,bile}^{ERY} = 0.02/0.1/0.5$ mg/L are superimposable).

VITA

Mengyao Li was born on July 2nd, 1988 in Tianjin, China and is a citizen of the People's Republic of China (PRC). She graduated from College of Pharmacy, Peking University Health Science Center, Beijing, China, with a bachelor degree in Pharmacy in 2010 and a master degree in Pharmacometrics in 2012. During the fall of 2012, she joined the Ph.D. program at Department of Pharmaceutics, Virginia Commonwealth University (VCU), Richmond, VA, under supervision of Dr. Jürgen Venitz, M.D., Ph.D.

During her tenure as a graduate student at VCU, Mengyao has published five abstracts, and has 2 additional abstracts waiting for acceptance. She presented her research extramurally at American Society of Clinical Pharmacology and Therapeutics (ASCPT 2014, 2015 and 2016) and American Association of Pharmaceutical Scientists (AAPS 2015), in addition to intramural presentations both within the department and School of Pharmacy. During the summer of 2015, she successfully completed a summer internship in Department of Clinical Pharmacology and Pharmacometrics at AbbVie Inc., and has an abstract accepted by The American College of Clinical Pharmacology (AACCP 2016) based on the work there. Since the fall of 2015, she was selected as an Oak Ridge Institute for Science and Education (ORISE) fellow at Office of Clinical Pharmacology, Food and Drug Administration (FDA), and successfully finished two projects in related to PBPK modeling and has two manuscripts in preparation based on the work there.

She received numerous intra- and extramural awards, namely Jyotsa and Mavji Thakker award in 2013, Joseph P. Schwartz Graduate Student Travel award in 2014, NIH Clinical Investigator Training Award in 2014, VCU Graduate School Travel Grant in 2015, Phi Kappa Phi Scholarship in 2015, Graduate Training/Travel Fund in 2015, Pfizer Consumer Healthcare R&D Leading for Innovation Award in 2015, ASCPT Presidential Trainee Award in 2015 and mostly recently Charles T. Rector & Thomas W. Rorrer, Jr. Dean's Award in 2016.

Mengyao served as a mentor task force member for ASCPT since summer 2015, and she was a student co-moderator for 2015 AAPS Annual Meeting. She also previously served as the vice president for AAPS student chapter at VCU (2014-2015) and Pharmaceutics Graduate Student Association (PGSA) at VCU (2014-2015). During 2013-2014, she was the secretary and treasurer for AAPS and PGSA at VCU. She was the treasurer of Sigma Delta Epsilon – Graduate Women in Science, Zeta Chapter in Richmond during 2014-2015. She is currently the member of three professional associations: AAPS, ASCPT and International Society of Pharmacometrics. (ISoP)